

**Illuminating Protein-Targets:  
Design and Synthesis of  
New Optical Imaging Probes for Studies of the  
Cannabinoid Type 2 Receptor and Plectin-1**

Inaugural-Dissertation  
to obtain the academic degree  
Doctor rerum naturalium (Dr. rer. nat.)

Submitted to the Department of Biology, Chemistry, Pharmacy  
of Freie Universität Berlin

by

THAIS GAZZI  
from Porto Alegre, Brazil

December 2020



This work was performed between February 2016 and December 2020 under the direction of Dr. Nazaré in the Department of Medicinal Chemistry, at Leibniz-Forschungsinstitut für Molekulare Pharmakologie (FMP).

Supervisor: DR. MARC NAZARÉ

Second examiner: PROF. DR. MATHIAS CHRISTMANN

Date of oral defense: 23.03.2021

My doctoral degree thesis entitled “Illuminating Protein-Targets: Design and Synthesis of New Optical Imaging Probes for Studies of the Cannabinoid Type 2 Receptor and Plectin-1” has been prepared by myself and is based on my own work; the work from others has been specifically acknowledged in the text. This thesis is submitted to the Department of Biology, Chemistry and Pharmacy of Freie Universität Berlin to obtain the academic degree Doctor rerum naturalium (Dr. rer. nat.) and has not been submitted for any other degree.

Berlin, December 2020





## Acknowledgments

Firstly, I would like to express my gratitude to Dr. Marc Nazaré for giving me the opportunity to conduct my doctoral studies in his research group. Surely, his guidance and constructive insights provided during these years were essential for my growth as a scientist. I enjoyed all the highly interesting topics as well as the many international research partners I was given the chance to work and collaborate with.

I am truly grateful to Prof. Dr. Mathias Christmann for kindly accepting me as his student at the Freie Universität Berlin as well as for all his valuable advice and enlightening suggestions since the beginning of my PhD studies.

I thank all the external collaborators that enabled achievements at both projects presented in this thesis. In special, I would like to thank Dr. Uwe Grether who introduced me to the intriguing world of the endocannabinoid system. Thank you for making me feel welcome in Basel and for trusting my work! Moreover, I am profoundly grateful to Isabelle Kaufmann for her encouragement and the whole Hoffmann La-Roche CB<sub>2</sub>R and MAGL teams for the inexhaustible cooperation and assistance. Likewise, I thank Prof. Dr. Haiyu Hu and her group for the exciting collaboration and for the warm welcome that we received in Beijing. It was a pleasure to exchange not only project-related “tips and tricks”, but also to experience the Chinese rich culture, delicious gastronomy, and disciplined lifestyle. Moreover, I would like to thank Prof. Dr. Björn Meermann for enabling me to conduct ICP-MS experiments at the BAM with the assistance of Sebastian Fassbender and Andreas Schultz for measurements and evaluation of the data.

Actual and former members of the Nazaré Group deserve immense acknowledgments. Thank you all for the helpful discussions and motivation. In particular, I thank both the CB<sub>2</sub>R and DOTA teams: Benjamin Brennecke, Leonard Mach, and Yelena Mostinski for advancing the CB<sub>2</sub>R probes to an unthinkable status as well as Vera Martos for initiating me into DOTA synthesis. I am thankful to Jana Langosch, Sebastian Wilke, and Waldemar Meiser for their help and contribution as internship students. I thank Edgar Specker and Jérôme Paul for executing HR-MS experiments and being always supportive. I also would like to thank Sandra Miksche for her support, especially with handling the HPLC, I learned a lot from you!

I am grateful to Monica Guberman, Yelena Mostinski, Carolina Vinagreiro, Leonard Mach, and Malgorzata Wasinska-Kalwa for the time, patience, and constructive inputs invested while

proofreading this thesis. To Benjamin Brennecke, thank you for kindly translating this thesis abstract section to German, I wouldn't be able to accomplish this task alone!

Endless gratitude belongs to my family in Brazil and my new family in Germany. Thank you for all the love, care, and for believing in my potential. To my Brazilian family, I learned that home is wherever we are together. Thank you for supporting me at every decision and bringing the comfort of home at each new visit. *Saudade* is indeed a work without translation. To my family in Germany, thank you for accepting me so effortlessly and integrating me into your culture with so much love. After 6 years, I feel almost like a Berliner!

# Table of Contents

<b>ABSTRACT</b> .....	<b>1</b>
<b>KURZFASSUNG</b> .....	<b>3</b>
<b>ABBREVIATION LIST</b> .....	<b>5</b>
<b>1. MOTIVATION AND BACKGROUND</b> .....	<b>9</b>
1.1. <b>Molecular Imaging</b> .....	<b>9</b>
1.2. <b>Molecular Imaging Modalities – Overview and Applications</b> .....	<b>11</b>
1.3. <b>Molecular Imaging Probes</b> .....	<b>16</b>
1.4. <b>General Aim of this Thesis</b> .....	<b>21</b>
<b>2. TRACING THE CANNABINOID TYPE 2 RECEPTOR WITH A FLUORESCENT PROBE TOOLBOX</b> .....	<b>23</b>
2.1. <b>Introduction</b> .....	<b>23</b>
2.1.1. <b>G Protein-Coupled Receptors</b> .....	<b>23</b>
2.1.2. <b>Exploring the Cannabinoid Type 2 Receptor (CB<sub>2</sub>R) as a Drug Target</b> .....	<b>26</b>
2.1.3. <b>Imaging Tools to Study the CB<sub>2</sub>R</b> .....	<b>30</b>
2.1.4. <b>Motivation for the Synthesis of a CB<sub>2</sub>R-Selective Fluorescent Ligand and Specific Aims</b> .....	<b>41</b>
2.2. <b>Results</b> .....	<b>42</b>
2.2.1. <b>Recognition Element Selection and Fluorescent Probe Design</b> .....	<b>42</b>
2.2.2. <b>Synthesis of the Recognition Element Scaffolds</b> .....	<b>45</b>
2.2.3. <b>First Approach Towards CB<sub>2</sub>R-Selective Fluorescent Ligands: Probing the R<sup>2</sup>-Position of the Pyrazine Recognition Element as Linker Attachment Point</b> .....	<b>46</b>
2.2.4. <b>Second Approach Towards CB<sub>2</sub>R-Selective Fluorescent Ligands: Probing the R<sup>3</sup>-Position with an Ether Functionality for Linker Attachment</b> .....	<b>51</b>
2.2.5. <b>Small SAR of Unlabeled Ligands: Exploring Alternative Functionalities for Linker Attachment at the R<sup>3</sup>-Position</b> .....	<b>54</b>
2.2.6. <b>Third Approach Towards CB<sub>2</sub>R-Selective Fluorescent Ligands: Probing the R<sup>3</sup>-Position with a Thioether Functionality for Linker Attachment</b> .....	<b>61</b>
2.2.7. <b>Synthesis of Enantiomeric Pure Fluorescent CB<sub>2</sub>R-Probes</b> .....	<b>66</b>

2.2.8.	Applications of Fluorescent Probes labeled with NBD, Alexa 488, and SiR for Detection and Visualization of the CB <sub>2</sub> R .....	73
<b>2.3.</b>	<b>Conclusion and Outlook .....</b>	<b>79</b>
<b>3.</b>	<b>DEVELOPMENT OF A CYCLEN-BASED CLICKABLE PLATFORM FOR PANCREATIC CANCER IMAGING.....</b>	<b>82</b>
<b>3.1.</b>	<b>Introduction.....</b>	<b>82</b>
3.1.1.	Pancreatic Cancer – Current Status and Challenges .....	82
3.1.2.	Plectin-1 as a Biomarker for Pancreatic Cancer .....	84
3.1.3.	Molecular Imaging Probes for Pancreatic Cancer Imaging.....	86
3.1.4.	Exploring the DOTA Scaffold for Multivalent Probe Design .....	89
3.1.5.	Motivation for the Synthesis of Multivalent Cyclen-based Fluorescent Ligands and Specific Aims .....	93
<b>3.2.</b>	<b>Results .....</b>	<b>94</b>
3.2.1.	Design of a Tetrasubstituted Cyclen-based Fluorescent Probe .....	94
3.2.2.	Preparation of Fourfold <i>N</i> -Functionalized Cyclen Building Blocks and Linker Synthesis	96
3.2.3.	Synthesis of Fluorescently Labeled Monovalent Control Probes.....	99
3.2.4.	First Approach Towards Cyclen-based Multivalent Ligands: Probing the R <sup>2</sup> -Substitution with an Amine for Fluorophore Attachment .....	101
3.2.5.	Second Approach Towards Cyclen-based Multivalent Ligands: Probing the R <sup>2</sup> -Substitution with an Azide for Fluorophore Attachment .....	107
3.2.6.	Third Approach Towards Cyclen-based Multivalent Ligands: Probing the R <sup>2</sup> -Substitution with an Alkyne for Fluorophore Attachment.....	110
3.2.7.	Applications of Multivalent Fluorescent Ligands labeled with Cy3 and Cy5.5 for Pancreatic Cancer Detection by Plectin-1 Visualization.....	120
<b>3.3.</b>	<b>Conclusion and Outlook .....</b>	<b>125</b>
<b>4.</b>	<b>CONCLUSION.....</b>	<b>128</b>
<b>5.</b>	<b>EXPERIMENTAL PROCEDURES.....</b>	<b>131</b>
<b>5.1.</b>	<b>General Synthetic Information .....</b>	<b>131</b>
<b>5.2.</b>	<b>To “Tracing the Cannabinoid Type 2 Receptor with a Fluorescent Probe Toolbox”</b>	<b>133</b>

5.2.1. Supplementary Figure .....	133
5.2.2. Supplementary Tables .....	134
5.2.3. Synthesis of Pyrazine Carboxylic Acid <b>2.37</b> .....	137
5.2.4. Synthesis of Picolinic Acid <b>2.42</b> .....	139
5.2.5. Synthesis of Amino Ester Building Blocks .....	143
5.2.6. Synthesis of Pyrazine-based NBD-Labeled Probes.....	155
5.2.7. Synthesis of SAR Compounds.....	166
5.2.8. Synthesis of Racemic NBD-Labeled Probes .....	182
5.2.9. Synthesis of Pyridine-based Enantiomeric Pure Probes .....	199
5.2.10. Pharmacological Assessment of CB <sub>2</sub> R-Agonist Probes and Fluorescence Imaging Experiments.....	203
<b>5.3. To “Development of a DOTA-based Clickable Platform for Pancreatic Cancer Imaging” .....</b>	<b>215</b>
5.3.1. Synthesis of DOTA Building Blocks .....	215
5.3.2. Synthesis of Linker Building Blocks .....	219
5.3.3. Plectin-1 Targeting Peptide Deprotection Procedure .....	227
5.3.4. Synthesis of Monovalent Control Probes .....	227
5.3.5. Synthesis of Tetravalent DOTAM Probe Precursors .....	234
5.3.6. Synthesis of DOTAM-based Probes .....	242
5.3.7. Determination of the Copper Content of final DOTAM probes by ICP-MS Analysis ..	248
5.3.8. Confocal Fluorescence Microscopy using Multivalent DOTAM-based Probes and Controls.....	250
<b>6. REFERENCES.....</b>	<b>251</b>
<b>APPENDIX: NMR-SPECTRA.....</b>	<b>267</b>



## Abstract

Molecular imaging has revolutionized the practice of medicine and patient healthcare. The use of targeted imaging tools have enabled the non-invasive and selective interrogation of biological processes triggering pathology. This approach includes a variety of complementary techniques such as PET, MRI, and optical imaging. In particular, fluorescent probes allow for the synergistic evaluation of the drug, the target, and treatment response in real-time and excellent spatiotemporal resolution. Generally, three main components should be considered for the design of a fluorescent probe: (i) a recognition element (ligand or pharmacophore) that tolerates further chemical functionalization while preserving its affinity and selectivity towards the protein-target, (ii) an appropriate reporter unit (fluorophore), and (iii) a linker that combines these two functionalities. Each of these constituents poses unique challenges for the successful design of a molecular probe as their selection will strongly depend on the imaging technique the probe will be applied to (Chapter 1).

The presented thesis displays a case in which the design, synthesis, and pharmacological characterization of highly specific imaging probes led to the labeling of two relevant drug targets. In both projects, a modular synthesis strategy enabled the assembly of ligand and fluorophore units tailored for specific optical imaging applications.

The first part of this thesis described the development of fluorescent ligands to trace the cannabinoid type 2 receptor (CB<sub>2</sub>R) (Chapter 2). This receptor is known to be strongly up-regulated in pathological conditions correlated with the onset of inflammation and, thus, represents an important protein-target for both therapeutic and diagnostic purposes. Exploiting a preclinical CB<sub>2</sub>R agonist drug as recognition element, investigations on suitable linker length, composition, and placement were conducted. Of particular interest was to avoid detrimental interactions of the linker-reporter construct with the CB<sub>2</sub>R, while providing a linker trajectory that reaches the extracellular space, i.e., outside the receptor binding pocket. This strategy resulted in the generation of a robust platform where binding affinity and selectivity were largely independent of fluorophore attachment.

The second part of this thesis aimed at the synthesis of imaging ligands containing multiple targeting moieties, i.e., multivalent for applications in the early detection of pancreatic cancer (PDAC) (Chapter 3). Here, probe design was based on the fourfold derivatization of the cyclen scaffold to develop a “clickable” platform encompassing three terminal maleimides and one alkyne. This cyclen-based platform enabled the *one-pot* assembly of PDAC-targeted agents which were labeled with two different

cyanine fluorophores. These fluorescent compounds displayed high specificity for the detection of PDAC in cell-based assays in comparison to their respective non-targeted controls.



## Kurzfassung

Molekulare Bildgebung hat die klinische Praxis der Patientenversorgung grundlegend verändert. Der Einsatz zielgerichteter Reportermoleküle hat es ermöglicht, biologische Prozesse als Auslöser von Krankheiten nichtinvasiv und selektiv zu untersuchen. Diese Methodologie vereint eine Reihe komplementärer Verfahren einschließlich PET, MRI und optischer Bildgebung. Insbesondere Fluoreszenz-Sonden ermöglichen die synergistische Bewertung von Medikamenten, Targets, und Therapieansätze in Echtzeit mit ausgezeichneter räumlicher und zeitlicher Auflösung. Im Allgemeinen müssen drei grundlegende Komponenten für das Design einer fluoreszenten Sonde berücksichtigt werden: (i) ein Erkennungselement (Ligand oder Pharmakophor), welches chemische Funktionalisierungen unter Erhaltung seiner Affinität und Selektivität zum Protein-Target toleriert, (ii) eine geeignete Reportereinheit (Fluorophor), und (iii) ein Linker, welcher beide Funktionalitäten verbindet. Jedes dieser Bestandteile stellt spezifische Anforderungen an das erfolgreiche Design einer molekularen Sonde und hängt stark vom Bildgebungsverfahren ab, für das die Sonde eingesetzt werden soll (Kapitel 1).

Die vorliegende Arbeit behandelt das Design, die Synthese und die pharmakologische Charakterisierung hochspezifischer bildgebender Sonden, welche weiterführend zur Untersuchung von zwei pharmakologisch relevanten Targets eingesetzt wurden. In beiden Projekten ermöglichte eine modulare Synthesestrategie die Verknüpfung spezifischer Liganden mit Reportereinheiten, welche jeweils auf spezielle Anwendungen optischer Bildgebung zugeschnitten sind.

Der erste Teil dieser Arbeit beschreibt die Entwicklung fluoreszenter Sonden für die Untersuchung des Cannabinoid Typ 2 Rezeptors (CB<sub>2</sub>R) (Kapitel 2). Die starke Hochregulierung dieses Rezeptors wird mit pathologischen Zuständen assoziiert, die hauptsächlich von Entzündungsprozessen ausgelöst werden. CB<sub>2</sub>R stellt daher ein wichtiges Protein-Target für sowohl therapeutische als auch diagnostische Ansätze dar. Ausgehend von einem präklinischen CB<sub>2</sub>R Agonisten als Erkennungselement wurden geeignete strukturelle Verknüpfungspunkte für einen Linker sowie der Einfluss von Linkeraufbau und -Länge untersucht. Von besonderer Bedeutung war es dabei, eine Linkertrajektorie zu finden, die aus der Bindungstasche des Proteins in die umgebende Matrix reicht und gleichzeitig abträgliche Interaktionen zwischen Linker-Reporter Konstrukt und Rezeptor zu vermeiden. Diese Strategie resultierte in einer robusten synthetischen Plattform, bei der

Bindungsaffinität und –Selektivität überwiegend unbeeinflusst von der Art des angebrachten Farbstoffs sind.

Der zweite Teil der Arbeit befasst sich mit der Synthese fluoreszenter Sonden zur Früherkennung von Bauchspeicheldrüsenkrebs (PDAC), die multivalent mit Targeting-Einheiten versehen sind (Kapitel 3). Das Sondendesign basiert auf einem vierfach derivatisiertem Cyclengerüst zur Entwicklung einer „klickbaren“ Plattform, die aus drei terminalen Maleimid-Funktionalitäten und einem Alkin besteht. Diese cyclenbasierte Plattform ermöglichte die Eintopfsynthese von PDAC zielgerichteten Sonden, welche jeweils mit zwei verschiedenen Cyaninfarbstoffen markiert wurden. Die Sonden wiesen hohe Selektivitäten für die Detektion von PDAC in zellbasierten Assays im Vergleich zu ihren nicht-zielgerichteten Kontrollen auf.

## Abbreviation List

2-AG	2-Arachidonoylglycerol	2,5-DHAP	2,5-Dihydroxyacetophenone
4-DMAP	4-Dimethylaminophthalimide	9-BBN	9-Borabicyclo[3.3.1]nonane
μM	Micromolar (10 <sup>-6</sup> M)	Ac	Acetyl
Acc.	Acceptor	AEA	<i>N</i> -Arachidonoylethanolamide
ACN	Acetonitrile	AlogP	Atomic logP
aq.	Aqueous	Bn	Benzyl
Boc	<i>tert</i> -Butoxycarbonyl	BOP-Cl	Bis(2-oxo-3-oxazolidinyl)phosphinic chloride
BRCA2	Breast cancer type 2 susceptibility protein	BTFFH	Fluoro-dipyrrolidinocarbenium hexafluorophosphate
Bu	Butyl	CA 19-9	Carbohydrate antigen 19-9
cAMP	Cyclic AMP, refers to EC <sub>50</sub> assay	CBD	Cannabidiol
CB <sub>1</sub> R	Cannabinoid type 1 receptor	CB <sub>2</sub> R	Cannabinoid type 2 receptor
Cbz	Carboxybenzyl	CDI	1,1'-Carbonyldiimidazole
cHex	Cyclohexane	CHO	Chinese Hamster Ovary
cRGD	Cyclic RGD	CuAAC	Copper assisted azide-alkyne cycloaddition
Cy	Cyanine fluorophore	Cyclam	1,4,8,11-Tetraazacyclotetradecane
Cyclen	1,4,7,10-Tetraazacyclododecane	Cys	Cysteine
d	Duplet	dba	Dibenzylideneacetone
DBU	1,8-Diazabicyclo[5.4.0]undec-7-ene	DCM	Dichloromethane
DIAD	Diisopropyl azodicarboxylate	DIPEA	Diisopropylethylamine
DMAP	<i>N,N</i> -Dimethylaminopyridine	DMF	Dimethylformamide
DMSO	Dimethyl sulfoxide	DMT	Dimercaptotriazine
DMTMM	4-(4,6-Dimethoxy-1,3,5-triazin-2-yl)-4-methylmorpholin-4-ium chloride	DO3A	Tri- <i>tert</i> -butyl 2,2',2''-(1,4,7,10-tetraazacyclododecane-1,4,7-triyl)triacetate
DOTA	1,4,7,10-Tetraazacyclododecane-1,4,7,10-tetraacetic acid	DOTAM	1,4,7,10-Tetrakis(carbamoylmethyl)-1,4,7,10-tetraazacyclododecane
DOTP	1,4,7,10-Tetraazacyclododecane-1,4,7,10-tetra(methylene phosphonic acid)	DPBS	Dulbecco's phosphate buffered saline
DPC4	Decapentaplegic homolog 4 protein	dppf	1,1'-Ferrocenediyl-bis(diphenylphosphine)
<i>ee</i>	Enantiomeric excess	EC <sub>50</sub>	Half maximal effective concentration

eCB	Endocannabinoid	ECL	Extracellular loop
EDTA	Ethylenediaminetetraacetic acid	eff.	Efficacy
EGFR	Endothelial growth factor receptor	equiv.	Equivalents
ESI	Electrospray ionization	Et	Ethyl
<i>et al.</i>	Et alli (“and others”)	FAAH	Fatty acid amide hydrolase
FACS	Fluorescence-activated cell sorting	FDA	Food and Drug Administration
FDG	Fluorodeoxyglucose	Fmoc	Fluorenylmethoxycarbonyl
GPCR	G protein-coupled receptor	GRK	GPCR kinases
h	Human	HEK	Human Embryonic Kidney
HATU	1-[Bis(dimethylamino)methylene]-1H-1,2,3-triazolo[4,5-b]pyridinium 3-oxid hexafluorophosphate	HBTU	<i>N,N,N',N'</i> -Tetramethyl-O-(1H-benzotriazol-1-yl)uronium hexafluorophosphate
HMDS	Hexamethyldisilazane	HPLC	High-pressure liquid chromatography
HSTU	<i>N,N,N',N'</i> -Tetramethyl-O-( <i>N</i> -succinimidyl)-uronium hexafluorophosphate	HTRF	Homogeneous time-resolved fluorescence
Hz	Hertz (s <sup>-1</sup> )	IC <sub>50</sub>	Half maximal inhibitory concentration
ID	Identification	ICG	Indocyanine green
ICL	Intracellular loop	ICP-MS	Inductively coupled plasma mass spectrometry
<i>i</i> Pr	Isopropyl	<i>J</i>	Coupling constant
<i>K</i> <sub>d</sub>	Equilibrium dissociation constant (M)	<i>K</i> <sub>i</sub>	Inhibitory constant (M)
<i>K</i> <sub>ob</sub>	Observed rate of association (min <sup>-1</sup> )	<i>K</i> <sub>off</sub>	Dissociation constant (min <sup>-1</sup> )
<i>K</i> <sub>on</sub>	Association rate constant (M <sup>-1</sup> min <sup>-1</sup> )	KRAS	Kirsten rat sarcoma gene
LC-MS	Liquid chromatography–mass spectrometry	LDA	Lithiumdiisopropyl amide
LE	Ligand efficiency	m	Mouse
m	Multiplet	M	Molar (mol/L)
MALDI	Matrix-assisted laser desorption/ionization	MAPK	Mitogen-activated protein kinase
<i>m</i> -CPBA	<i>meta</i> -Chloroperoxybenzoic acid	Me	Methyl
Memb.	Membrane	MFI	Mean fluorescence intensity
MPLC	Medium-pressure liquid chromatography	MRI	Magnetic resonance imaging
ms	Milliseconds (10 <sup>-3</sup> s)	n.a.	Not applicable
NAPE-PLD	<i>N</i> -Acylphosphatidylethanolamine phospholipase D	NBD	7-Nitrobenzofurazan

NBS	<i>N</i> -Bromosuccinimide	NCS	Isothiocyanate
n.d.	Not determined	nHep	n-Heptane
NHS	<i>N</i> -Hydroxysuccinimide	NIR	Near-infrared
nm	Nanometer (10 <sup>-9</sup> m)	nM	Nanomolar (10 <sup>-9</sup> M)
NMR	Nuclear magnetic resonance	NOTA	2,2',2''-(1,4,7-Triazonane-1,4,7-triyl)tri-acetic acid
OI	Optical imaging	OP	Optimization
P	Partition coefficient	p53	Tumor protein p53 gene
pAfBPP	Photoaffinity-based protein profiling	PALM	Photoactivated localization microscopy
PAMPA	Parallel artificial membrane permeability assay	PanIN	Pancreatic intraneoplasia
PBS	Phosphate buffered saline	Pd/C	Palladium on charcoal
PDAC	Pancreatic ductal adenocarcinoma	PDB	Protein data bank
PEG	Polyethylene glycol	PET	Positron emission tomography
PFP	Perfluorophenol	PI	Photoacoustic imaging
ppm	Parts per million	PSA	Polar surface area
PTP	Plectin-1 targeting peptide	py.	Pyridine
PyBOP	Benzotriazole-1-yl-oxy-tris-pyrrolidino-phosphonium hexafluorophosphate	q	Quartet
qRT-PCR	Real-time quantitative reverse transcription polymerase chain reaction	quant.	Quantitative
rcf	Relative centrifugal force	R <sub>f</sub>	Retention factor
rpm	Rotations per minute	r.t.	Room temperature
RT	Residence time (min)	s	Singlet
SAR	Structure activity relationship	SERS	Surface-enhanced Raman spectroscopy
SFC	Supercritical fluid chromatography	SiR	Silicon-Rhodamine fluorophore
SNAP	Type of self-labeling protein tag	sol.	Solution
SPAAC	Strain-promoted azide-alkyne cycloaddition	SPECT	Single-photon emission computed tomography
SPIO	Superparamagnetic iron oxide	SST <sub>2</sub> R	Somatostatin type 2 receptor
STED	Stimulated emission depletion	STORM	Stochastic optical reconstruction microscopy
t	Triplet	T	Temperature
T <sub>1</sub>	Longitudinal relaxation	T <sub>2</sub>	Transverse relaxation
T3P	Propanephosphonic acid anhydride	Tacn	1,4,7-Triazonane

TATE	Octreotate, cyclic peptide targeting SST <sub>2</sub> R	TBAF	tetra- <i>N</i> -Butylammonium fluoride
TBTA	Tris(benzyltriazolylmethyl)amine	TBTU	2-(1H-Benzotriazole-1-yl)-1,1,3,3-tetramethylammonium tetrafluoroborate
TETA	2,2',2'',2'''-(1,4,8,11-Tetraazacyclotetradecane-1,4,8,11-tetrayl)tetraacetic acid	TFA	Trifluoroacetic acid
THC	$\Delta^9$ -Tetrahydrocannabinol	THF	Tetrahydrofuran
TOF	Time-of-flight	TR-FRET	Time-resolved fluorescence resonance energy transfer
Ts	Tosyl	UV	Ultraviolet
<i>v</i>	Volume	VEGFR2	Vascular endothelial growth factor receptor 2
vs.	Versus	w	Weight
WT	Wild-type		

# 1. Motivation and Background

## 1.1. Molecular Imaging

In 1665, Robert Hooke described in the essay “*Micrographia*” his observations using a microscope, including compartment-like structures in cork samples – which he termed cells.<sup>[1]</sup> The foundations of modern light microscopy were established 200 years later by Ernst Abbe with the demonstration that the resolution of a focusing light microscope is limited by diffraction.<sup>[2]</sup> In the same decade, Rudolf Virchow founded the field of cellular pathology by correlating the understanding of diseases with cellular abnormalities.<sup>[3]</sup> The emergence of the synthetic fluorescent dye industry<sup>[4]</sup> – in particular, the synthesis and commercialization of fluorescein by Adolf von Bayer in 1871<sup>[5]</sup> – aided Paul Ehrlich in developing his innovative cellular staining techniques,<sup>[6]</sup> which lastly evolved into the magic bullet concept.<sup>[7]</sup> However, it was only after the discovery of the X-ray by Wilhelm Conrad Röntgen in 1895 that the first medical image was generated.<sup>[8]</sup> The image featured Ms. Röntgen hand wearing her wedding ring on the fourth finger. Over the following 125 years, the understanding of the cell, microscopy techniques, and anatomical imaging have vastly improved upon. Nowadays, image acquisition is performed at highly sophisticated instruments in a time-dependent manner with resolutions evolving up the nanometer range.

With the ultimate goal of “seeing for believing”, scientists are motivated to decipher the underlying cellular and molecular mechanisms of action driving both health and disease. Methods to directly *see into cells* or *see into the body* have become essential tools for the study, diagnosis, and monitoring of pathologies. Seeing is, however, not always possible in biology as size, sensitivity, resolution, and additional concerns hamper an accurate investigation. Much research efforts have been directed toward understanding the function of specific genes and proteins, from subcellular compartments to humans, in a high-resolution, non-invasive, time, and costly manner. In the past two decades, the molecular imaging field has grown exponentially as it allows for the visualization, characterization, and tracing of biologic pathways at the cellular and molecular level.<sup>[9]</sup> Traditionally, medical imaging has been exploited for diagnostic purposes, enabling the identification and localization of diseased tissues.

In contrast to solely anatomy-based imaging techniques, molecular imaging has the potential to provide functional characterization of the molecular processes involved in pathology.

Technological advances in imaging modalities i.e. laser, camera, and processing tools have largely impacted health care. The principles of molecular imaging can be now tailored to diverse imaging modalities, including positron emission tomography (PET)<sup>[10]</sup> and single-photon emission computed tomography (SPECT),<sup>[11]</sup> magnetic resonance imaging (MRI),<sup>[12]</sup> ultrasound,<sup>[13]</sup> photoacoustic imaging (PI),<sup>[14]</sup> optical imaging (OI),<sup>[15]</sup> and Raman spectroscopy.<sup>[16]</sup> These technologies differ in spatial and temporal resolution, depth penetration, energy expended for image generation (ionizing or non-ionizing), availability of imaging probes, and the respective detection threshold of probes.<sup>[16b, 17]</sup> As each technology encounters particular limitations and challenges, choosing the appropriate readout strongly depends on the scientific question and specific research aims. At present, molecular imaging applications in medicine range from target validation<sup>[18]</sup> and target engagement studies<sup>[19]</sup> at drug development and pre-clinical stages to precision prevention<sup>[20]</sup> and early diagnosis of diseases<sup>[15b, 21]</sup> up to intraoperative imaging.<sup>[22]</sup>

Besides the unprecedented development of imaging technology, targeted imaging ligands have played a central role in highlighting subcellular components that would be otherwise invisible under anatomical imaging analysis. The discovery and exploitation of imaging agents have evolved from more traditional pharmacological approaches – where advantage was taken from individual natural products and drugs for probe generation – to the current higher throughput methodologies, including phage display, DNA-encoded library screening, and fragment-based approaches.<sup>[23]</sup> These tools can be applied to tackle the biological and chemical space more systematically as they allow, e.g., to study molecular pathways, to thoroughly validate new pharmacological targets, and to transition therapeutics into the human situation. Yet, one major concern in the field is the use of poorly characterized imaging agents which may confound the interpretation of data and misleading biological conclusions about target relevance. Recent publications from both academia and pharmaceutical industry underscore the need for robust and reliable probes that are both chemically and pharmacologically fully characterized.<sup>[24]</sup> Therefore, the evaluation of several parameters, including stability, water solubility, cell permeability, on- and off-target effects, potency, and selectivity is of paramount importance.



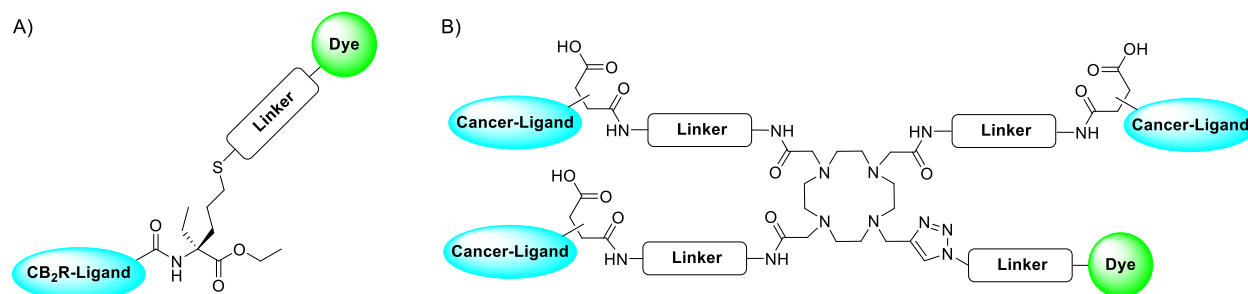


**Figure 1.1. Molecular imaging probe platforms developed in this thesis.** A) CB<sub>2</sub>R-selective fluorescent ligand template and B) multivalent fluorescent agent targeting pancreatic cancer.

The presented thesis illustrates a case in which the design, synthesis, and characterization of highly specific imaging probes led to the labeling of two relevant drug targets: the cannabinoid subtype 2 receptor (CB<sub>2</sub>R) (Figure 1.1.A) and plectin-1 (Figure 1.1.B). Altogether, the fluorescently labeled platforms shown in Figure 1.1. derived from highly versatile precursors which were carefully designed and optimized to suit an array of biologically and pharmacologically relevant investigations. The two following sections give a brief introduction of commonly used molecular imaging modalities as well as highlight the key aspects of probe design and how imaging tools help to circumvent the intrinsic drawbacks of each imaging technique.

## 1.2. Molecular Imaging Modalities – Overview and Applications

X-ray medical imaging has rapidly progressed, becoming the foundation of numerous modern diagnostic imaging procedures, including mammography, tomography, and angiography.<sup>[8]</sup> By the 1950s, the administration of contrast agents containing barium or iodine allowed the identification and treatment of several cancers and pathologies in the gastrointestinal tract and brain. With the emergence of radioactivity, nuclear medicine promptly joined the arsenal of imaging modalities. The two most prominent tests in nuclear medicine today are single-photon emission computed tomography (SPECT) and positron emission tomography (PET) scanning. While SPECT utilizes gamma rays derived from radionuclides, such as <sup>99m</sup>Tc, <sup>123</sup>I, and <sup>111</sup>In, from which 3D images are reconstructed by computer analysis,<sup>[25]</sup> PET is based on the detection of high-energy photon pairs produced during annihilation collision between a positron and an electron as source for readout.<sup>[26]</sup>

Most PET is based on positron-emitting isotopes of  $^{18}\text{F}$ ,  $^{64}\text{Cu}$ , and  $^{68}\text{Ga}$  which have typically short half-lives. Thus, incorporation of such isotopes into PET imaging tracers must occur in a cyclotron near the PET facility for immediate application. Both SPECT and PET techniques share similar strengths and drawbacks as they display unlimited depth penetration and high sensitivity, having the ability to provide detailed metabolic information, but are restricted by low spatial resolution, lack of anatomical information and high costs.

Ultrasound was first used clinically in the 1970s.<sup>[27]</sup> Conversely to X-ray and nuclear medicine which require ionizing radiation, ultrasound is based solely on sound waves.<sup>[28]</sup> In particular, tomographic images are generated by the reflection of sound waves as they pass through tissues. This technique offers high spatial resolution and provides excellent anatomical features for coregistration with molecular information. Despite plenty of targeted imaging agents that have been designed for ultrasound applications, these molecules have often large sizes ( $>250$  nm), which may hamper tissue penetration.<sup>[29]</sup> Therefore, ultrasound is commonly used for noninvasive imaging of the abdomen and pelvis, including imaging the fetus during pregnancy.

Magnetic resonance imaging (MRI) and optical imaging (OI) also evolved during the 1970s.<sup>[30]</sup> Both modalities have the advantage of not requiring ionizing radiation and have considerably impacted the (bio)medical imaging field. The ability of MRI to provide soft tissue discrimination allowed clinicians to obtain earlier diagnoses. MRI images are generated from differences in longitudinal ( $T_1$ ) and transverse ( $T_2$ ) relaxation times of a specific active nucleus, such as  $^1\text{H}$  and  $^{19}\text{F}$ , in different tissues when specific radiofrequency pulse sequences are applied.<sup>[31]</sup> By exploring proton density, perfusion, diffusion, and biochemical contrasts, MRI has the advantages of high spatial resolution and good depth penetration, offering anatomic, physiologic, and metabolic information. The primary limitation of MRI is its low sensitivity, which is partially overcome by longer acquisition times and the use of imaging agents for contrast enhancement. Especially, targeted paramagnetic, e.g., gadolinium(III) complexes and superparamagnetic, e.g., iron oxide nanoparticles (SPIO) contrast agents increase signal contrast in the tissue of interest by disturbing the local magnetic field, either  $T_1$  or  $T_2$ .<sup>[32]</sup> In particular, these agents are indirectly detected by their effect on bulk water molecules and the magnitude of this effect is strongly influenced by their chemical properties.<sup>[33]</sup> Taking advantage of these tunable properties, state-of-art MRI contrast agents are being explored as activatable tools, whose signal is modulated upon physiological changes, e.g., pH, enzymatic activity, and temperature. In the clinics, the vast majority of MRI contrast agents are composed by small, hydrophilic

gadolinium(III)-based complexes.<sup>[34]</sup> The chelating cage has the important role of reducing the inherent toxicity of gadolinium(III) ions and enhancing its excretion of the human body. These tools are primarily indicated for imaging lesions of the central nervous system, with secondary applications bearing liver and angiographic imaging.

Optical imaging (OI) is one of the most successful imaging modalities for preclinical studies, as it allows for real-time monitoring of molecular events in a highly sensitive, throughput, and inexpensive fashion. Recent clinical applications of OI comprise image-guided surgery<sup>[35]</sup> and ophthalmic, cardiovascular, and cancer imaging.<sup>[36]</sup> Particularly for *in vivo* applications, this modality covers a range of techniques which can be divided into bioluminescence and fluorescence imaging. Whilst bioluminescence imaging depends on luciferase expression, an enzyme available in nature and responsible for the glowing of some insects, jellyfish, and bacteria, fluorescence imaging detects light emitted from fluorescent reporters, including organic dyes,<sup>[37]</sup> quantum dots,<sup>[38]</sup> and lanthanides.<sup>[39]</sup> A major advantage of fluorescence imaging is the possibility of multichannel imaging experiments by simultaneously applying multiple fluorophores containing different photophysical properties.<sup>[36]</sup> Fluorescence emissions in the visible region (400–650 nm) usually have limited utility for *in vivo* imaging settings due to attenuation and scattering of light as well as interference caused by autofluorescence from endogenous substances, including cytochromes and hemoglobin. These drawbacks are minimized in the near-infrared (NIR) window (650–900 nm) which enables deeper penetration depths – up to 10 cm.<sup>[40]</sup> In addition, many new technologies and techniques have been developed that allow for combinations of deeper and faster, imaging at a higher resolution. For example, two-photon fluorescence microscopy allows for imaging thick samples, e.g., tissues both *in vitro* and *in vivo* by applying pulsed NIR excitation light.<sup>[41]</sup> The excitation occurs when fluorescent molecules absorb two photons simultaneously, thereby producing higher energy (700–1000 nm). This effect increases penetration depth, while limiting bleaching and phototoxicity. Alternatively, the nonlinear properties of fluorescent molecules, e.g., switching behaviors and on/off states enable to surpass the light diffraction limit.<sup>[42]</sup> The so-called super-resolution or nanoscopy techniques have demonstrated to resolve images in a 10–100 nm resolution range. Current super resolution methods fundamentally differ in the excitation mode of fluorophores and in the detection of emitted photons. Most common approaches for biological imaging are photoactivated localization microscopy (PALM),<sup>[43]</sup> stochastic optical reconstruction microscopy (STORM),<sup>[44]</sup> and stimulated emission depletion (STED).<sup>[45]</sup>

During the 1990s, photoacoustic imaging (PI) emerged as a new non-invasive imaging methodology.<sup>[46]</sup> This technique typically uses short-pulsed electromagnetic radiation as probing energy, while detecting ultrasound generated by photon absorption and thermoelastic expansion. The photoacoustic effect can be either generated by endogenous, e.g., cytochromes and hemoglobin, or exogenous absorbers, e.g., porphyrin-based derivatives. Because ultrasound undergoes considerably less scattering and attenuation in tissue compared with light, PI provides high spatial resolution and deep tissue penetration. Modern photoacoustic devices enable real-time visualization of physiological, morphological, vascular, and molecular details of diseased tissues.<sup>[47]</sup> Such measurements, however, still lack sensitivity in detection and image acquisition.

Raman scattering of light by molecules was first observed by Raman and Krishnan in 1928,<sup>[48]</sup> however, it was only in the late 1990s that this technology has been applied to characterize biological systems.<sup>[49]</sup> Raman spectroscopy explores monochromatic light, from the NIR up to the ultraviolet (UV) range, to generate the Raman scattering effect, i.e., inelastic scattering of photons,<sup>[49]</sup> which is dependent on the vibrational modes associated with chemical bonds within the analyzed sample. During such experiments, each compound displays unique energy levels which it translates to a specific spectrum or Raman fingerprint.<sup>[50]</sup> For example, the Raman spectrum of a cell or tissue can provide detailed information on their chemical composition in a non-invasive manner.<sup>[51]</sup> As spontaneous Raman events are of low-probability, being detected only in a small fraction of the scattered light (circa 1 in  $10^7$ ),<sup>[52]</sup> Raman spectroscopy lacks the required sensitivity for clinical applications.<sup>[53]</sup> To enhance sensitivity and penetration depth, variations of the Raman spectroscopy technique have been developed over the years, allowing for imaging studies to be conducted *in vivo*.<sup>[54]</sup> In particular, surface-enhanced Raman spectroscopy (SERS) explores metal nanoparticles, usually gold or silver, in combination with fluorophores, such as cyanine (Cy) dyes, to increase Raman scattering. This approach enables image acquisition with superior sensitivity over label-free analysis with the possibility of multiplexing, i.e., detecting multiple analytes, thereby improving diagnostic specificity.

Currently, various imaging modalities can be used to access specific molecular targets – certainly, depending on the application, some techniques are better suited than others. Nevertheless, no single modality is perfect and sufficient to provide all the necessary information on the structure and function of a subject. For example, PET displays high sensitivity but poor spatial resolution, MRI has good resolution yet low sensitivity and OI offers real-time images with remarkably high sensitivity and

resolution but has limited penetration depth.<sup>[16b, 17]</sup> The general characteristics of the imaging modalities here described are summarized in Table 1.1. and Figure 1.2.

**Table 1.1. General characteristics and brief comparison of the imaging modalities described here.**<sup>[16b, 17]</sup>

Modality	Type of Radiation	Most Common Contrast Agents	Sensitivity <sup>[a]</sup> (mol/L)	Spatial Resolution <sup>[b]</sup>	Penetration Depth	Clinical Availability	Costs <sup>[c]</sup>	Information provided
<b>SPECT</b>	High-energy $\gamma$ rays	Radioisotopes, such as $^{99m}\text{Tc}$ , $^{111}\text{In}$ , $^{123}\text{I}$ , $^{177}\text{Lu}$	High ( $10^{-10}$ - $10^{-11}$ )	Low (0.5-2 mm)	>500 mm	Yes	High	Metabolic, 3D biodistribution of SPECT tracers
<b>PET</b>	Lower-energy $\gamma$ rays	Radioisotopes, such as $^{18}\text{F}$ , $^{11}\text{C}$ , $^{64}\text{Cu}$ , $^{68}\text{Ga}$ , $^{89}\text{Zr}$	Very high ( $10^{-11}$ - $10^{-12}$ )	Low (1-2 mm)	>500 mm	Yes	Very high	Metabolic, 3D biodistribution of PET tracers
<b>Ultrasound</b>	High-frequency sound	Microbubbles (encapsulated inert gas)	Not fully characterized	Very high (30-800 $\mu\text{m}$ )	10-150 mm	Yes	Moderate	Anatomical information
<b>MRI</b>	Radio waves	$\text{Gd}^{3+}$ and $\text{Mn}^{2+}$ complexes, SPIO, $^{19}\text{F}$ enriched compounds	Low ( $10^{-3}$ - $10^{-5}$ )	High (< 100 $\mu\text{m}$ )	>500 mm	Yes	Very high	3D anatomy, physiological information
<b>OI</b>	Visible to NIR light	Fluorophores, quantum dots, lanthanides	High ( $10^{-9}$ - $10^{-12}$ )	Very high <i>in vitro</i> (10 – 100 nm); Moderate <i>in vivo</i> (1-3 mm)	1-10 mm	Optical guided surgery	Low	Real-time functional information
<b>PI</b>	NIR light	Photosensitizers: NIR dyes, gold nanorods, carbon nanotubes	Not fully characterized	Very high (80-1000 $\mu\text{m}$ )	10 mm	Emerging	Moderate	Functional and anatomical information
<b>Raman SERS</b>	Visible light to near UV	metal nanoparticles with fluorophores	High (comparable to OI) <sup>[d]</sup>	Very high <100 nm	Up to 50 mm	No	Moderate	Functional information, molecular and chemical content

<sup>[a]</sup> Ability to detect the probe relative to the background; <sup>[b]</sup> Measure of the accuracy and detail of graphic displayed in the images; <sup>[c]</sup> This includes the cost of equipment and cost per study; <sup>[d]</sup> Sensitivity limits not determined.

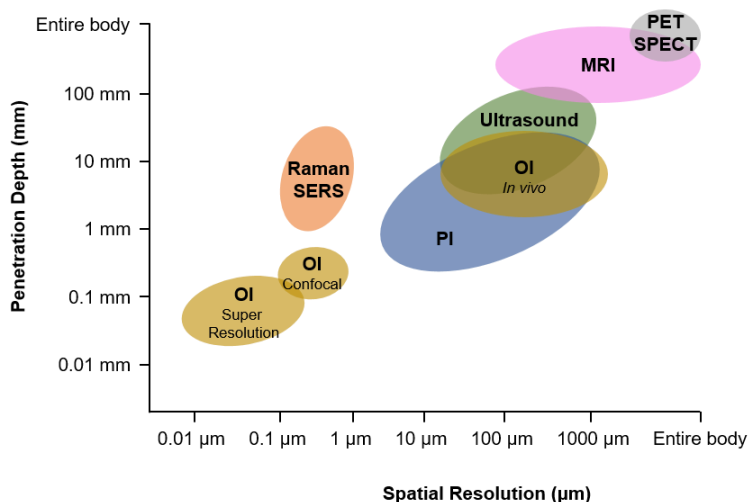


**Figure 1.2. Comparison of the resolution and penetration depth of the discussed imaging modalities.** Usually, resolution decreases as depth increases, rendering modalities such as PET and MRI suitable for imaging whole organs *in vivo* whereas modalities with higher resolution such as OI are best suited for *ex vivo* and *in vitro* imaging at the sub-cellular level.

Amongst all these methodologies, the design of appropriate imaging probes is key to distinguish particular biological mechanisms of action and to reflect this information in the format of images. Therefore, it is presumable that important breakthroughs in the molecular imaging field will be largely due to the interdisciplinary efforts of synthetic chemists, molecular biologists, biomedical and imaging scientists.

### **1.3. Molecular Imaging Probes**

Besides the preferred imaging read-out, molecular imaging relies on the appropriate target or biomarker selection and the generation of reliable targeted imaging ligands. With the advance of genomics and proteomics as well as the increased knowledge on disease etiology, however, target identification has become an extremely faster process than probe development.<sup>[55]</sup> As a consequence, the pathophysiological role of several pharmacological relevant targets remain uncharted due to the lack of appropriate chemical tools. Because of the central role of contrast agents in molecular imaging investigations, the design and validation of these molecules is one of the major research interests within the field.<sup>[17a, 56]</sup>

By definition, imaging probes are thoroughly chemically characterized small molecules of well-defined biological affinity and selectivity which are used to visualize and investigate complex biological systems.<sup>[24a]</sup> The underlying differences between molecular imaging tools and conventional drugs reside in their distinctive application purposes, design strategy, and characterization.<sup>[57]</sup> For example, drugs are intended to treat abnormalities, and thus, may act on multiple targets in a polypharmacological approach to produce the desired clinical benefits. Whereas imaging ligands must be extremely selective to deliver accurate diagnostic information and address specific questions related to functional aspects of the target in the context of the disease – e.g., determining downstream signaling cascades related to specific phenotypes and investigating the mode-of-action of a pharmacophore. In particular, such tools enable the synergistic evaluation of the drug, the target, and the biological response, providing means for scientists and clinicians to identify and elucidate the molecular mechanisms triggering disease. In addition to their clinical applications which include disease diagnoses, assessment of treatment response, and surgery-guided options, imaging agents are

now an important component of drug development.<sup>[18, 23a, 24c]</sup> During early drug discovery research, labeled derivatives are used to determine expression levels of the target and its function, providing information related to biodistribution, pharmacokinetics, target engagement, toxicity, and dose selection of drug candidates.<sup>[58]</sup>

A molecular imaging probe is generally constituted of three main components: (i) a reporter or contrast enhancing unit, (ii) a recognition element (ligand or pharmacophore) that tolerates further chemical functionalization while preserving its affinity and selectivity towards the target, and (iii) a linker that separates these two functionalities (Figure 1.3.).<sup>[59]</sup> Each of these constituents represents unique challenges for the design of a successful probe. The reporter unit produces the signal for imaging purposes and its nature will depend on the application of the probe in a respective imaging modality. Signal agents span from radionuclides for PET and SPECT to magnetic complexes for MRI up to fluorophores for OI, PI, and Raman-based SERS (*see* Table 1.1., Section 1.2.). The recognition element directs the probe to the site of interest and interacts with the target of a particular biological process. Any targeting ligand, such as drugs, natural products, endogenous molecules, peptides, proteins, antibodies and its fragments, can be exploited as recognition element. By connecting the reporter with the recognition element, the linker minimizes the interaction between these two moieties,<sup>[60]</sup> thereby, avoiding detrimental effects of the often bulky and charged signal agent with the target. Importantly, the linker composition has a significant impact on the pharmacology and biodistribution of the probe.<sup>[61]</sup> Thus, the length, flexibility, hydrophilicity, and charges are key features to be considered during linker selection. Another crucial aspect is the linker attachment point at the ligand as choosing the “wrong” position may lead to complete loss in affinity and/or selectivity.<sup>[62]</sup>

In general, the composition of molecular imaging probes can be categorized into three major approaches: the linear, the multivalent, and the multimodal (Figures 1.3. to 1.5.).<sup>[57]</sup> The linear design is probably the most common approach and involves the coupling of the ligand with the reporter unit through a linker (Figure 1.3.A). One example of this labeled ligand class was developed for targeting the somatostatin type 2 receptor (SST<sub>2</sub>R) which is known to be overexpressed in a variety of cancers.<sup>[63]</sup> The cyclic peptide octreotate (TATE, **1.1**, Figure 1.3.B) was selected as recognition element for labeling at the N-terminus with a Sulfo-Cy5 dye (**1.2**, Figure 1.3.C). In a cell-based assay using cancer cells expressing the SST<sub>2</sub>R, compound **1.2** displayed an IC<sub>50</sub> of 106 nM which corresponds to a fivefold decrease in potency when compared to the parent TATE structure (**1.1**: IC<sub>50</sub> of 20 nM).<sup>[64]</sup> Therefore,

this case study demonstrates how the introduction of a signal agent can influence the overall binding properties of the ligand conjugate.

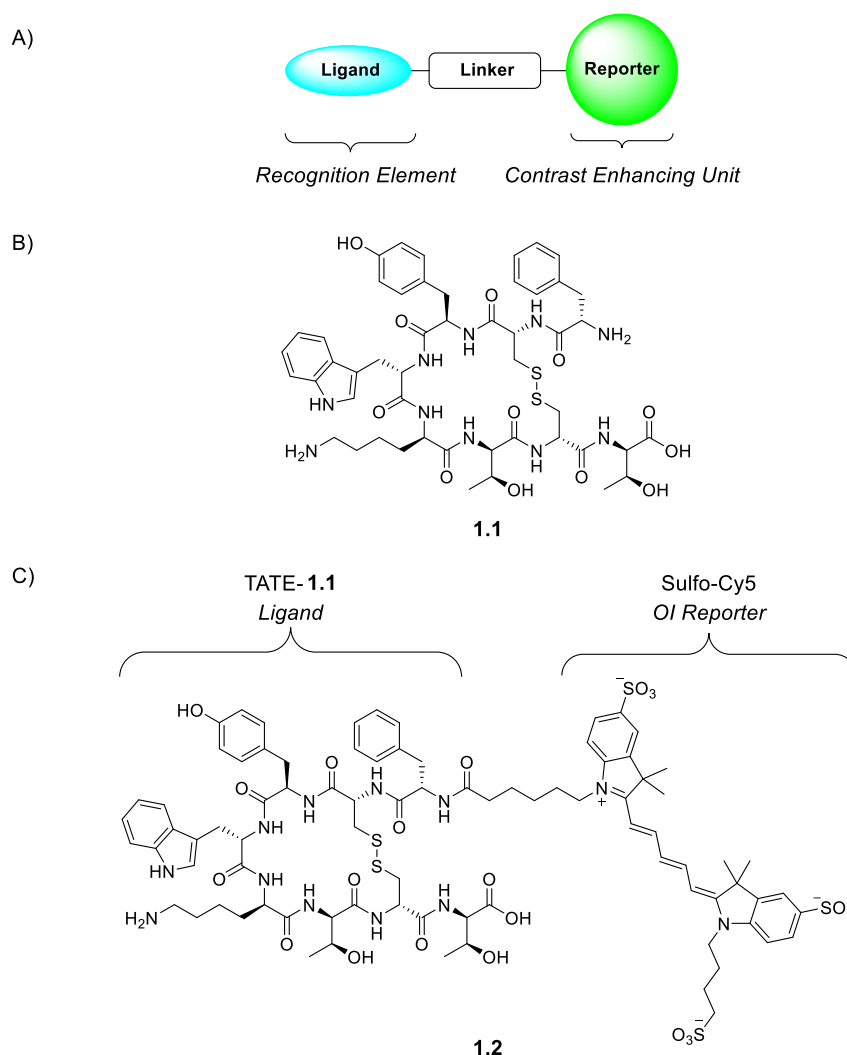


**Figure 1.3. The linear probe design strategy combines the recognition element of choice with the reporter unit through a linker.** A) Schematic representation of this design strategy, B) structure of the recognition element TATE chosen for probe development (**1.1**),<sup>[64]</sup> and C) SSTR<sub>2</sub>R-targeted fluorescent probe **1.2**.<sup>[64]</sup> Modified after K. CHEN *et al.*<sup>[57]</sup>

The combination of multiple ligands via covalent linkage to a template generates multivalency (Figure 1.4.A). Many studies have described the benefits of compound multimerization to enhance target avidity and *in vivo* retention times at the site of interest.<sup>[65]</sup> For this design strategy, a delivery vehicle, such as a nanocapsule, can also function as a linker.<sup>[66]</sup> For example, multiple units of the TATE peptide (**1.1**, Figure 1.3.B) were employed for assembling the SSTR<sub>2</sub>R-targeted liposomal PET tracer **1.3** (Figure 1.4.B).<sup>[67]</sup> The TATE peptides were conjugated via thiol-maleimide Michael- addition type



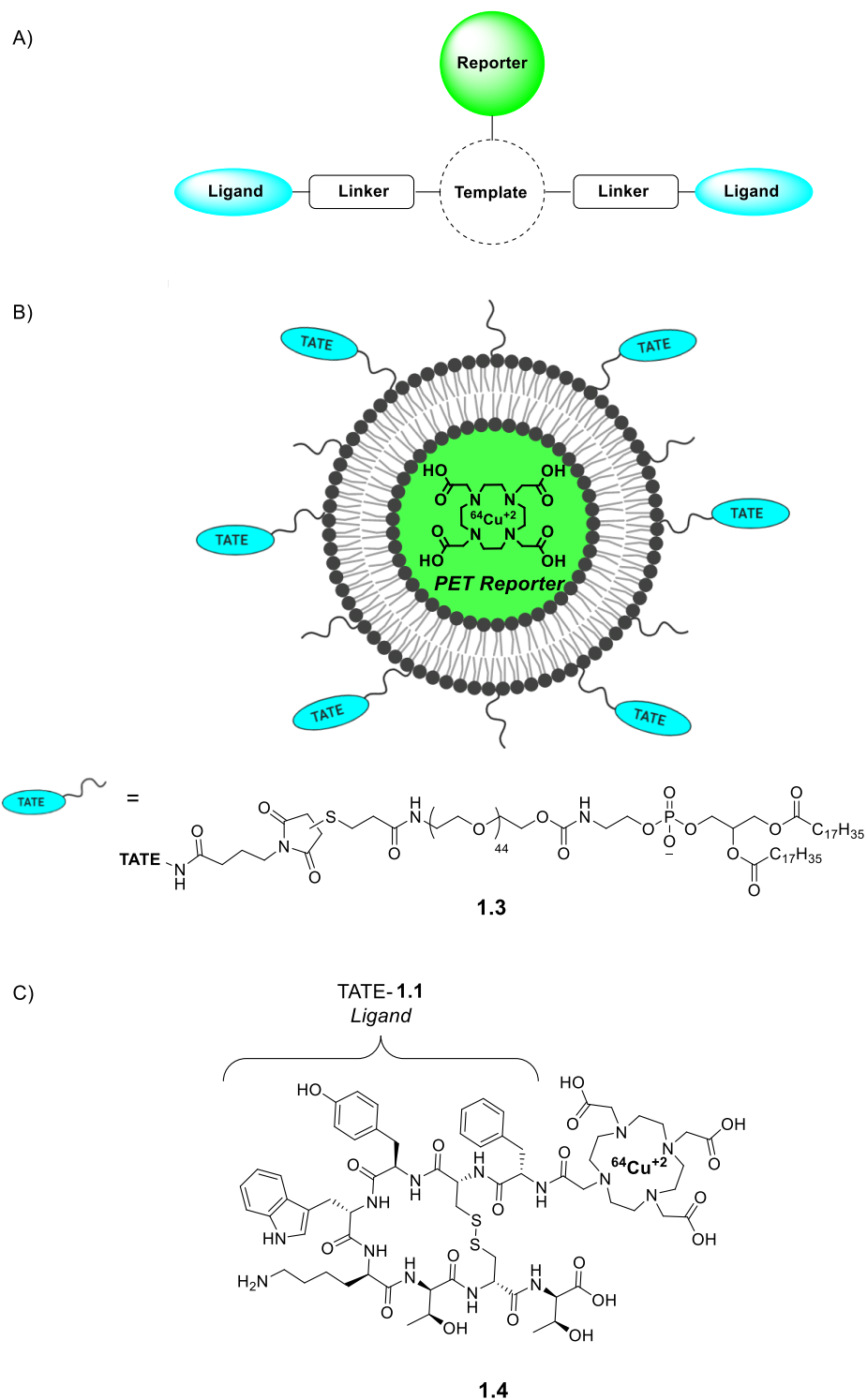


**Figure 1.4. The Multivalent probe design combines multiple recognition elements and the reporter unit via covalent linkage to a template.** A) Schematic representation of this design strategy, B) multivalent somatostatin type 2 receptor-targeted PET tracer **1.3**,<sup>[67]</sup> and C) monovalent SST<sub>2</sub>R-targeted control **1.4**.<sup>[67]</sup> Modified after K. CHEN *et al.*<sup>[57]</sup>

reaction to a PEG-ylated liposomal drug carrier with an encapsulated  $^{64}\text{Cu}$  positron emitter. PET images applying multivalent derivative **1.3** demonstrated very good *in vivo* uptake at the tumor region in comparison to surrounding healthy tissues. Moreover, this uptake was twofold higher than the monovalent TATE-tracer **1.4** (Figure 1.4.C) which was used as control for these PET experiments.<sup>[67]</sup>

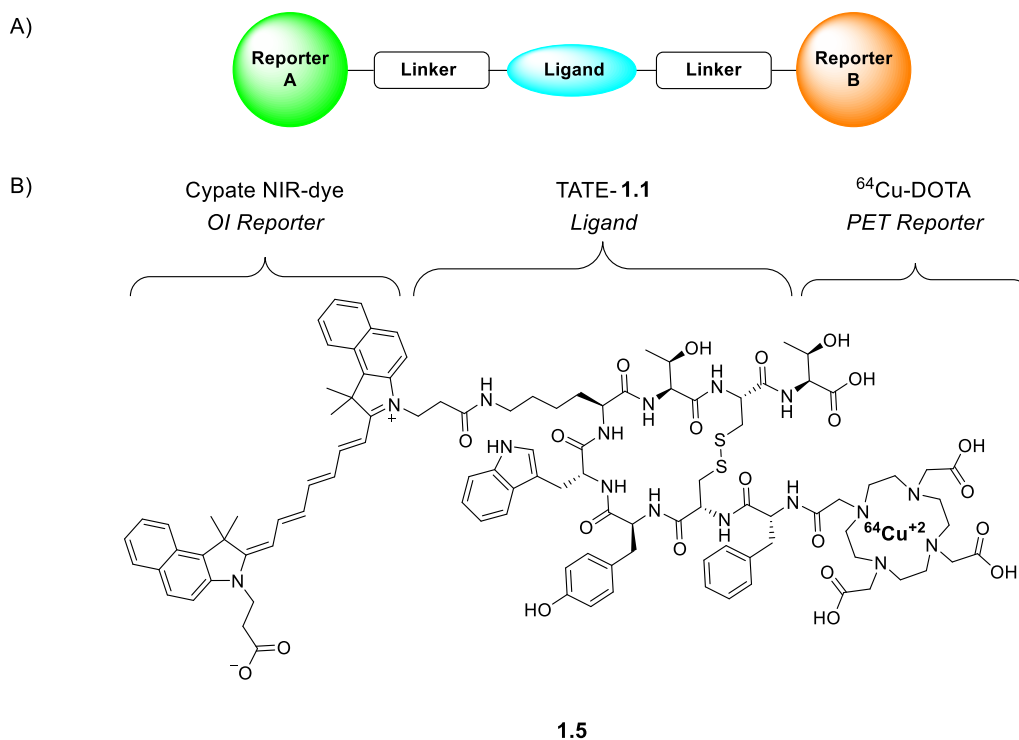


**Figure 1.5. The dual-imaging design combines the recognition element with several reporters to enable complementary imaging read-outs.** A) Schematic representation of this design strategy and B) dual-OI and PET probe **1.5** targeting the SST<sub>2</sub>R.<sup>[68]</sup> Modified after K. CHEN *et al.*<sup>[57]</sup>

Alternatively, the ligand can be conjugated to several reporter units for dual-imaging applications (Figure 1.5.A).<sup>[65b, 69]</sup> Using this concept, the advantages of two imaging modalities are combined, whilst at the same time reducing the disadvantages of both. However, the synthesis of such a compound is an extremely challenging task as it requires a ligand with two amenable positions for conjugating both linker-reporter unit constructs. Each signal agent introduces a large amount of steric bulk to the probe scaffold which can significantly alter the pharmacology and physicochemical properties compared to the unconjugated recognition element. The TATE peptide (**1.1**, Figure 1.3.B) served as starting point for the synthesis of a multimodal OI and PET agent containing a NIR-dye at the side chain of the lysine amino acid and a  $^{64}\text{Cu}$ -DOTA group at the N-terminus (**1.5**, Figure 1.5.B).<sup>[68]</sup> These modifications led to a 19-fold loss in activity towards the SST<sub>2</sub>R when compared to the unlabeled peptide (**1.1**).

The best design approach for probe development will depend on the specific target and imaging modality and to achieve optimal performance, each component of the construct must be thoroughly investigated.<sup>[57]</sup> As illustrated by the TATE-based ligands (Figures 1.3. to 1.5.), the conjugation of the linker and reporter unit affects the structure, physicochemical and pharmacological properties of the recognition element. Therefore, the imaging probe should be considered as a completely new pharmacological entity when compared to the parent ligand and be fully characterized before its use in further studies. Overall, imaging agents should display good solubility and stability in aqueous media in order to avoid unwanted aggregation, be readily available in pure form, and have known cell permeability.<sup>[70]</sup> High-quality probes are pharmacologically well characterized, exhibiting high potency and selectivity profiles. Moreover, such tools need to demonstrate target engagement and, in some cases, even modulate a relevant biochemical pathway in cells. These parameters require experimental characterization not only from cell-free assays but also from multiple cellular test settings and/or whole animal assessment. Evaluation of these properties provides a robust characterization of the imaging ligand and helps to determine their suitability for exploratory biology. In addition, to minimize off-target effects and avoid false conclusions, the use of precisely designed control derivatives with distinct recognition elements and/or inactive analogs is of utmost importance.

#### **1.4. General Aim of this Thesis**

The present thesis aims at the development, characterization, and application of two distinct optical imaging probe platforms. For both projects, a modular synthesis concept was applied to enable recognition element and reporter unit selection tailored for a multitude of imaging investigations and test settings.

The first part of this thesis describes the design, synthesis, and biological *in vitro* evaluation of fluorescent ligands to visualize the cannabinoid type 2 receptor (CB<sub>2</sub>R), a relevant pharmacological target correlated with the onset of inflammation (Chapter 2.). The focus was set on the generation of a CB<sub>2</sub>R-specific fluorescent probe template based on the linear design approach (Figure 1.3.A, Section 1.3.) exploring two small-molecule recognition elements derived from a CB<sub>2</sub>R agonist drug discovery

program from Hofmann La-Roche. In particular, this labeled compound should display high affinity towards human and mouse CB<sub>2</sub>R while retaining selectivity over the cannabinoid type 1 receptor (CB<sub>1</sub>R) subtype. Assisted by molecular modeling studies performed at Hofmann La-Roche by DR. WOLFGANG GUBA, two different attachment sites were investigated at each pharmacophore for linker conjugation (Section 2.1.1.). For both attachment sites, the linker properties were investigated through modifications of its length and composition. Of special interest was to identify a robust linker exit vector pointing towards the extracellular space of the receptor. This design would allow the introduction of diverse fluorescent dyes useful in a broad range of biological applications.

For the second project, the 1,4,7,10-tetraazacyclododecane (cyclen) scaffold was exploited for the design of a multivalent probe template (Figure 1.4., Section 1.3.) targeting plectin-1, a cytoskeleton protein known to be overexpressed in pancreatic cancer (Chapter 3.). A plectin-1 targeting peptide sequence (PTP, NH<sub>2</sub>-KTLLPTPC-COOH) was selected as recognition element and two cyanine dyes, Cy3 and Cy5.5 served as reporter units. A modular synthesis approach was envisioned applying subsequent *click* chemistry reactions, i.e., biocompatible reactions that are simple to perform, provide high conversion rates to the product, and are broad in scope.<sup>[71]</sup> While Michael type addition reaction of cysteines and reactive thiols was planned to introduce three PTP sequences, the cyanine dyes would be attached through amide coupling or Copper-mediated azide alkyne cycloaddition (CuAAC). To evaluate the influence of multiple ligands on pancreatic cancer imaging, monovalent control congeners following the linear design (Figure 1.3.A, Section 1.3.) were additionally synthesized.

## 2. Tracing the Cannabinoid type 2 Receptor with a Fluorescent Probe Toolbox

### 2.1. Introduction

#### 2.1.1. G Protein-Coupled Receptors

G protein-coupled receptors (GPCRs) are key mediators of a wide range of cell signaling processes.<sup>[72]</sup> Due to their therapeutic potential in disease modulation and their chemical tractability as membrane proteins, GPCRs constitute one of the most important druggable human receptor families.<sup>[73]</sup> It is currently estimated that 35% of the approved drugs target GPCRs,<sup>[74]</sup> and these drugs act in diverse therapeutic areas, including neurological, inflammatory, cardiovascular, respiratory, and gastrointestinal disorders.<sup>[75]</sup> Structure-based tools are largely explored for GPCR drug design and lead optimization.<sup>[76]</sup> Recent crystal structures have the ability to reveal the three-dimensional structure of GPCRs, location of bound ligands, and details regarding receptor-ligand interactions.

Generally, GPCRs share a highly conserved structure, consisting of seven transmembrane helices (I to VII) linked by three intracellular loops (ICLs), and three extracellular loops (ECLs)<sup>[77]</sup> (Figure 2.1.). The GPCR superfamily is subdivided into classes based on amino acid sequence homology and common physiological ligands,<sup>[78]</sup> such as neurotransmitters, hormones, cytokines, metabolites, and odorants.<sup>[79]</sup> In particular, the human proteome encompasses five of these subfamilies: rhodopsin (class A), adhesion and secretin (class B), glutamate (class C), as well as frizzled and smoothed (class F).<sup>[80]</sup> Among these, the Rhodopsin family contains the largest number of receptors, including many well-characterized drug targets. An example of this receptor class is the family of cannabinoid receptors, which are the subject of this thesis chapter.

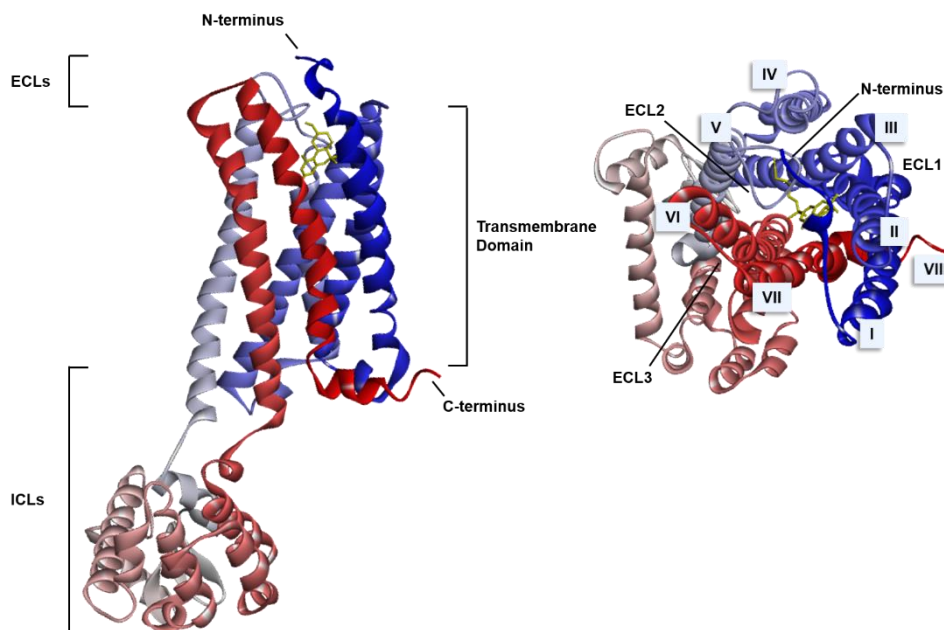


**Figure 2.1. General structure of a GPCR.** Views from within the membrane plane (*left*) and extracellular side (*right*) represent the typical seven-pass transmembrane GPCR architecture. The 3D structure shown is from the active state of the CB<sub>2</sub>R, a representative class A GPCR, co-crystallized in complex with the agonist AM12033 (PDB 6KPF).<sup>[81]</sup> Transmembrane domains are colored from the N-terminus (dark blue) to the C-terminus (dark red). ECLs – extracellular loops, ICLs – intracellular loops.

The activity of a GPCR is defined by its conformational state, which ranges from inactive to multiple active states.<sup>[82]</sup> In the absence of bound ligands, GPCRs exhibit variable basal activities. Upon binding, each ligand displays a characteristic efficacy, i.e., the ability to activate or deactivate its target, which affects their pharmacological properties. According to the inherent efficacy, GPCR modulators are classified as full agonists, partial agonists, antagonists, and inverse agonists (Figure 2.2).<sup>[83]</sup>

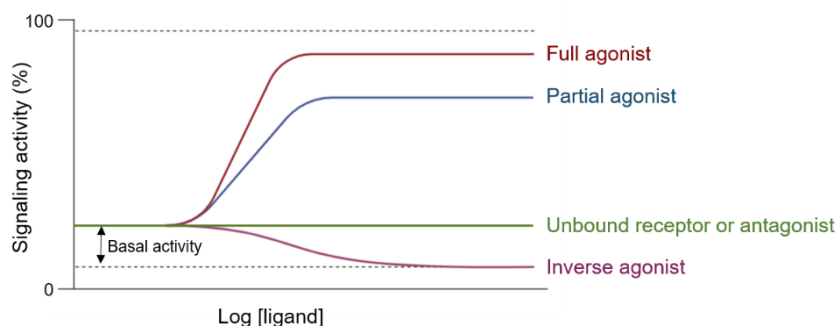


**Figure 2.2. Representative plots of signaling activity versus ligand concentration illustrating different GPCR efficacies.**

In brief, full agonist binding induces conformational changes to an active state of the receptor, maximizing signaling response. Likewise, partial agonists also promote receptor activation but elicit

submaximal stimulation, even at saturating concentrations. Antagonists prevent binding of other modulators without modifying the basal activity of the target. Conversely, inverse agonists shift the receptor conformational equilibrium toward inactive conformations, thereby decreasing the level of activity below that of the unbound receptor.<sup>[83]</sup>

Agonist binding activates the receptor by inducing conformational changes that trigger signal transduction mediated by G proteins, GPCR kinases (GRKs), and arrestins<sup>[84]</sup> (Figure 2.3). Coupling of heterotrimeric G proteins to the receptor generates dissociation of the G $\alpha$  subunit from the G $\beta\gamma$  subunits that regulate different downstream effector proteins, stimulating the production of second messengers such as cyclic AMP (cAMP), calcium, and phospholipases. Activation of the receptor may also promote phosphorylation by GRKs which is followed by coupling to arrestin. Signal transduction mediated by arrestins leads to receptor desensitization and activation of downstream cascades, including mitogen-activated protein kinases (MAPKs) and tyrosine kinases. In addition, arrestin activation stimulates endosomal receptor internalization and subsequent receptor degradation or recycling to the plasma membrane. The signaling modulation through G protein and arrestin pathways varies according to the ligand, and those that preferentially modulate one pathway over the others are referred to as biased ligands.<sup>[85]</sup> Importantly, differences in biased signaling critically affect the therapeutic properties of drugs acting on GPCRs, and offers new mechanisms for reducing side effects.

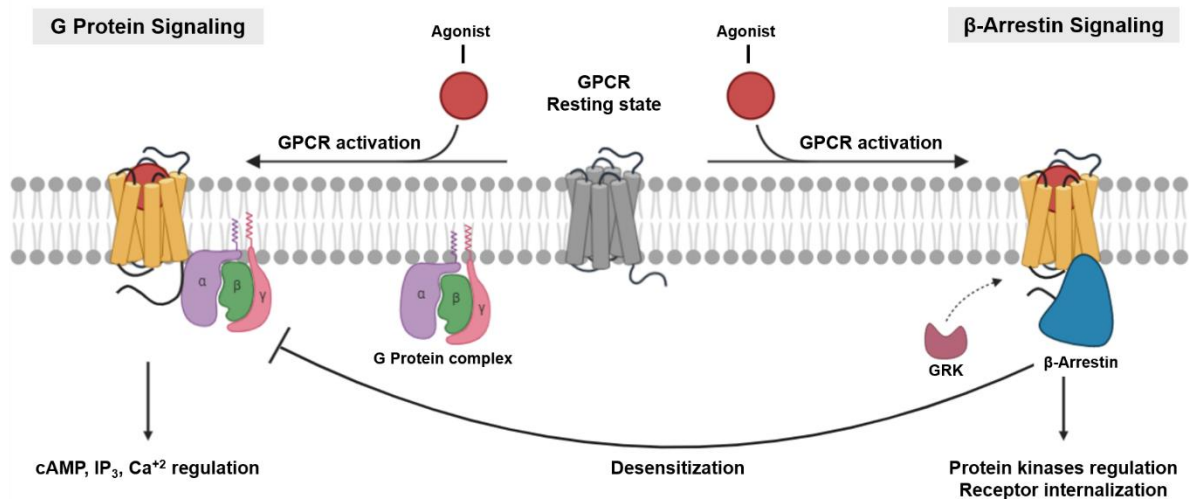


**Figure 2.3. Schematic diagram of GPCR signaling.** Activated GPCRs induce signal transduction through independent signaling pathways via either G proteins (*left*) or GPCR kinases (GRKs) and arrestins (*right*). Modified after D. HILGER *et al.*<sup>[84]</sup>

Despite recent advances in the structural characterization of many GPCRs,<sup>[76]</sup> specific ligand-receptor interactions that drive the essential conformational changes and ultimately result in activation or inhibition of receptor-mediated signaling pathways remain uncharted. Understanding the pharmacology of an unmodified receptor in its native cellular environment and tracing of specific signaling cascades upon modulation is extremely important for the development of new and more efficient drugs. Here, molecular imaging provides diverse opportunities to evaluate the chemical environment and intermolecular interactions of GPCRs.<sup>[86]</sup> In particular, optical imaging (OI)-based techniques applying fluorescent probe modulators enable real-time visualization of protein trafficking and monitoring of many dynamic downstream pathways (*see* Sections 1.2s and 1.3.). Depending on their photophysical properties, fluorescent ligands can be applied to plenty of spectroscopic approaches, including confocal microscopy for high-resolution images, fluorescence activated cell sorting (FACS) for target engagement and selectivity studies, time-resolved fluorescence resonance energy transfer (TR-FRET) for equilibrium and kinetic binding investigations, and automated confocal microscopy for high-throughput screening assays.<sup>[87]</sup>

### 2.1.2. Exploring the Cannabinoid Type 2 Receptor (CB<sub>2</sub>R) as a Drug Target

The therapeutic and psychoactive properties of the plant *Cannabis sativa* have been known for centuries. However, research on cannabis chemistry and pharmacology advanced slowly. Over nearly a century, several unsuccessful attempts were made to isolate in pure form active marijuana constituents and to elucidate its structures.<sup>[88]</sup> The lack of success of former trials could retrospectively be explained by the numerous constituents of cannabis with closely related structures and physico-chemical properties, which hampered their separation.<sup>[89]</sup> In 1964, MECHOULAM and co-workers<sup>[90]</sup> were able to obtain and characterize  $\Delta^9$ -tetrahydrocannabinol (THC, **2.1**), one of the most important active components of the plant (Figure 2.4.A). Since then, THC (**2.1**) has been the subject of many scientific investigations due to its intriguing biological properties.<sup>[91]</sup> In the early 1990s, the endogenous signaling system responsible for the *in vivo* effects of THC (**2.1**) was finally discovered.<sup>[92]</sup>



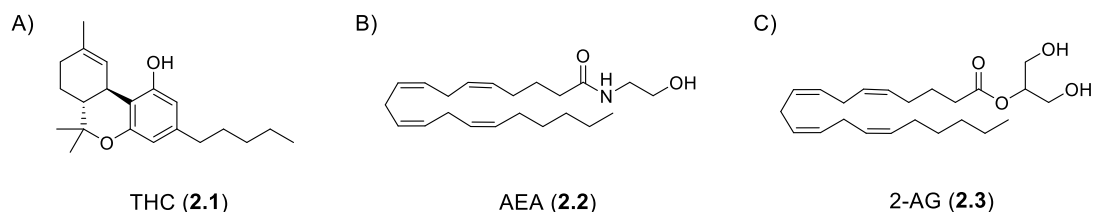


**Figure 2.4. Structures of common plant-derived and endogenous cannabinoids.** A)  $\Delta^9$ -Tetrahydrocannabinol (THC, **2.1**), B) *N*-Arachidonylethanolamide (AEA, **2.2**), and C) 2-Arachidonoylglycerol (2-AG, **2.3**).

The endocannabinoid (eCB) system is a fundamental lipid signaling system present in all vertebrates and responsible for eliciting multiple physiological processes.<sup>[93]</sup> The endogenously synthesized cannabinoids, also named endocannabinoids, cannabinoid receptors, and the enzymes that metabolize endogenous ligands are the main constituents of this system. Among the range of endocannabinoids, the two most well-known lipid-signaling molecules are *N*-arachidonylethanolamide (anandamide, AEA, **2.2**, Figure 2.4.B) and 2-arachidonoylglycerol (2-AG, **2.3**, Figure 2.4.C).<sup>[94]</sup> Unlike most neurotransmitters, such as acetylcholine, dopamine, and serotonin, AEA and 2-AG are not stored in vesicles but are rather synthesized when and where they are needed.<sup>[95]</sup> The biosynthesis of 2-AG (**2.3**) is mainly performed by diacylglycerol lipases and phospholipase C,<sup>[96]</sup> and degraded by monoacylglycerol lipase,<sup>[97]</sup> while AEA (**2.2**) is produced by *N*-acylphosphatidylethanolamine phospholipase D (NAPE-PLD),<sup>[98]</sup> and metabolized by fatty acid amide hydrolase (FAAH).<sup>[99]</sup>

At present only two cannabinoid receptors – cannabinoid type 1 receptor (CB<sub>1</sub>R) and cannabinoid type 2 receptor (CB<sub>2</sub>R) – have been cloned, characterized, and confirmed as key members of the endocannabinoid system.<sup>[92, 100]</sup> Besides the modulation of various intracellular signal transduction cascades via G protein, GRK and arrestin signaling pathways, the eCB receptors are known to undergo ligand dependent biased modulation<sup>[101]</sup> and display interspecies differences.<sup>[102]</sup> Cannabinoid receptors share common features such as structure similarity and signaling mechanisms but largely differ in tissue distribution.<sup>[103]</sup> The CB<sub>1</sub>R is mainly expressed in the central nervous system – being one of the most abundant GPCR in the brain – and to a lesser extent in peripheral tissues.<sup>[104]</sup> Whereas the CB<sub>2</sub>R is found throughout the periphery and is primarily expressed in immune cells, having very low to undetectable expression levels in the central nervous system (CNS) under basal conditions.<sup>[105]</sup> Immediately after their discovery, these receptors have received considerable attention by both academic and industrial settings. The potential of CB<sub>1</sub>R receptors as target for diseases of the CNS and also peripheral disorders has been limited, however, by the psychoactive side effects derived from synthetic ligand antagonists – especially due to reports of severe depression and suicide.<sup>[106]</sup> Because of these unwanted responses, cannabinoid research has shifted the focus to CB<sub>2</sub>R pharmacology. The

strong upregulation of CB<sub>2</sub>R, both in the brain and periphery, occurs only under specific pathological conditions correlated with the pharmacological onset of inflammation.<sup>[107]</sup> Therefore, CB<sub>2</sub>R activation may provide pharmacological benefits to treat a multitude of inflammatory conditions without psychotropic effects derived from CB<sub>1</sub>R modulation. As most of these disorders are not only severely debilitating but also offer limited choices of available treatment. In particular, CB<sub>2</sub>R agonist-driven downstream signaling cascades promote reduction of inflammatory processes by altering microglia phenotype and stimulating the production of anti-inflammatory cytokines.<sup>[108]</sup> There is growing evidence that impairment of CB<sub>2</sub>R signaling in inflammatory conditions is correlated with several pathologies, especially organ and tissue injury.<sup>[109]</sup> Thus, many diseases including kidney, cardiovascular, gastrointestinal, lung, neurodegenerative, and psychiatric diseases, as well as pain and cancer are correlated with an impaired eCB system.<sup>[110]</sup>

There are several distinct compound classes which have been reported to bind cannabinoid receptors.<sup>[111]</sup> Besides endocannabinoids **2.2** and **2.3** (Figure 2.4.B and 2.4.C), classical cannabinoids are based on the chemical structure of THC (**2.1**, Figure 2.4.A), possessing a characteristic tricyclic core, and synthetic cannabinoids encompass structurally diverse compounds, including aminoalkylindoles, diaryl pyrazoles, and bicyclic ligands.<sup>[111]</sup> Due to the sequence similarities between the cannabinoid receptors, a considerable number of cannabinoids are mixed ligands, i.e., not discriminate between particular receptor subtypes. Nevertheless, novel synthetic and classical cannabinoids designed to interact selectively with only one cannabinoid receptor have also been pursued. In particular, pyridines, pyrimidines, indols, quinolones, oxoquinolines, triazines, and other ligand series are selective modulators of the CB<sub>2</sub>R.<sup>[103, 111a, 112]</sup>

The only approved drugs targeting the eCB system to date are plant-derived and semi-synthetic, including medical cannabis as well as the isolated phytocannabinoids THC (**2.1**), cannabidiol (CBD, **2.4**), and their analogs or combinations (Figure 2.5.). Drugs containing dronabinol (**2.1**) and nabilone (**2.5**), synthetic THC analogs, are potent dual CB<sub>1</sub>R/CB<sub>2</sub>R agonists which are administered for the treatment of anorexia, cachexia, and chemotherapy-induced sickness.<sup>[113]</sup> In contrast, CBD (**2.4**) is a partial agonist of both CB<sub>1</sub>R and CB<sub>2</sub>R which is promiscuous to several other targets as well.<sup>[114]</sup> Oral CBD (**2.4**) has been launched for treating two forms of epilepsy: Dravet and Lennox-Gastaut syndromes.<sup>[115]</sup> Moreover, combinations of THC (**2.1**) and CBD (**2.4**) are approved in various countries for spasticity and pain management with clinical trials being evaluated for additional implications, such as Alzheimer's disease.<sup>[116]</sup>

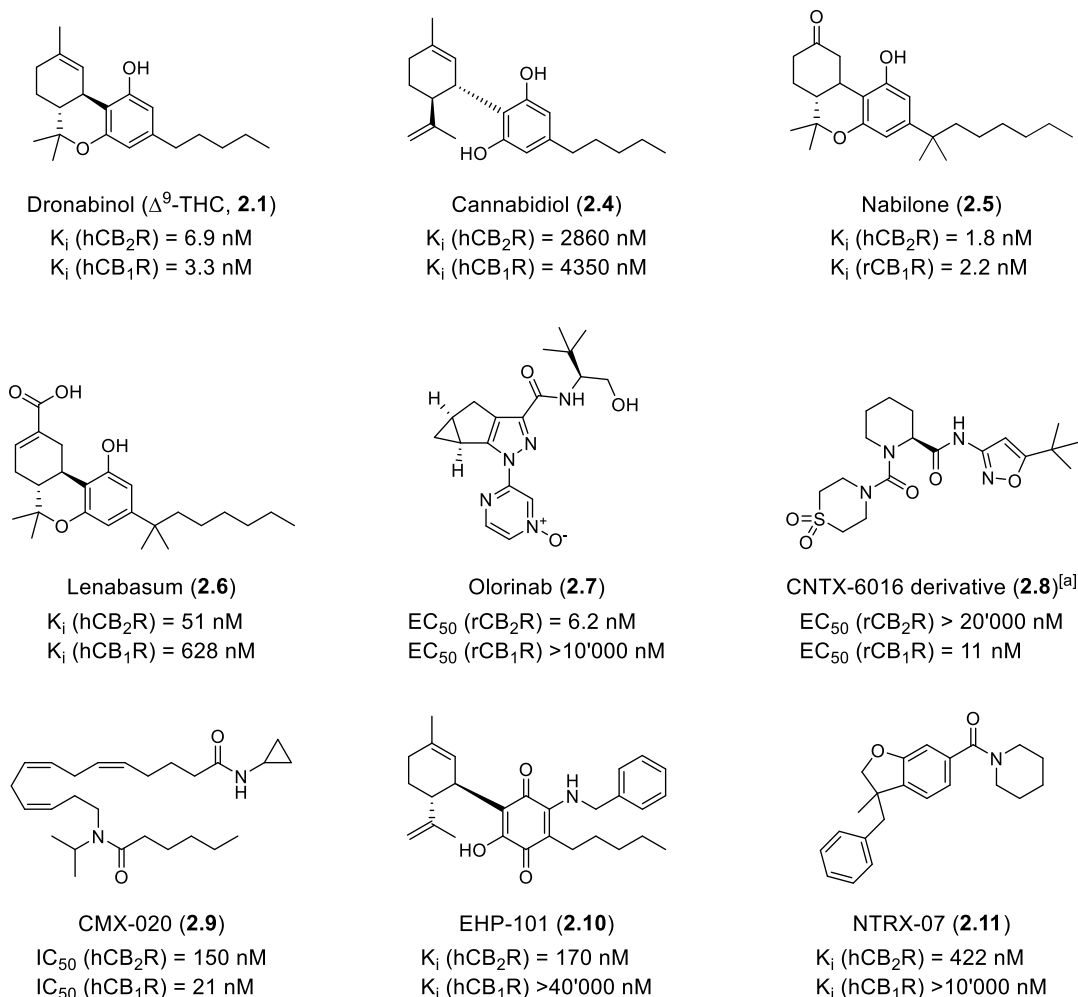


**Figure 2.5. Chemical structure and *in vitro* binding affinity ( $K_i$ ) or functional activity ( $EC_{50}$ ) of CB<sub>2</sub>R agonists which are launched or under active clinical development.**<sup>[113-117]</sup> <sup>[a]</sup> The chemical structure of CNTX-6016 was not disclosed to date, the structure activity relationship (SAR) series of this compound is described on the patent US10112934B2.<sup>[118]</sup> h – human, r – rat.

The most advanced selective CB<sub>2</sub>R agonist under active clinical development are Lenabasum (JBT-101, **2.6**) and Olorinab (APD371, **2.7**) (Figure 2.5.). While Lenabasum (**2.6**) is another phytocannabinoid which is currently in phase III trials for several disorders, including cystic fibrosis, systemic sclerosis, rheumatoid arthritis, and dermatomyositis.<sup>[117a-c]</sup> Olorinab (**2.7**) is a synthetic cannabinoid composed of a tricyclic 3–5–5-fused pyrazole 3-carboxamides template that reached phase II trials for abdominal pain in Crohn's disease and irritable bowel syndrome.<sup>[117d, 117e]</sup>

Numerous selective CB<sub>2</sub>R ligands were active in animal models of, e.g., chronic and inflammatory pain, (neuro)inflammatory conditions, and liver and kidney fibrosis,<sup>[112, 119]</sup> yet only a few drug candidates are currently tested in clinical trials (Figure 2.5., compounds **2.8** to **2.11**). These ligands vary from endocannabinoid-derived (CMX-020, **2.9**) and classical cannabinoid structures (EPH-101, **2.10**)

to more drug-like synthetic cannabinoids (CNTX-6016, **2.8** and NTRX-07, **2.11**) and have been mostly explored for their analgesic and anti-inflammatory properties.<sup>[118, 120]</sup> Despite the promising experimental observations in preclinical settings, most ligands were discontinued in phase II trials due to poor therapeutic efficacy.<sup>[121]</sup> There are many potential factors which contribute to these failures, including (i) the lack of validation of CB<sub>2</sub>R as a therapeutic target for the patient cohort, (ii) the inability to translate preclinical *in vitro* and *in vivo* pharmacology into the clinic, which is probably related to differences across species, (iii) the lack of appropriate chemical and biological tools for dose selection in humans, and (iv) the absence of target engagement studies and information on the compound's mechanisms of action.<sup>[122]</sup> Consequently, there is a tremendous need for the development of novel and well-characterized imaging probes to address CB<sub>2</sub>R questions regarding target validation, engagement, and signaling modulation as well as to enable further drug discovery efforts. Ideally, these tools should have a known pharmacological profile and be devoid of any interspecies difference between rodent and human CB<sub>2</sub>Rs to particularly tackle issues (ii) and (iii).

### 2.1.3. Imaging Tools to Study the CB<sub>2</sub>R

The high potential of CB<sub>2</sub>R as a prime drug target has promoted extensive efforts in drug discovery and clinical research. However, the underlying receptor-ligand interactions and molecular mechanisms driving its activation state are yet to be deciphered. The complexity of CB<sub>2</sub>R as a drug target is twofold. On the one hand, it belongs to the GPCR family and modulates the eCB lipid signaling system which are both biological entities characterized by promiscuous regulation of downstream signaling cascades.<sup>[123]</sup> On the other hand, its intriguing functional selectivity due to the bias against a variety of activation pathways.<sup>[101b]</sup> Together, these features make investigations of physiological responses to changes and pharmacological manipulations on the level of CB<sub>2</sub>R extremely challenging tasks. Therefore, experimental outcomes significantly vary according to the assay's conditions, e.g., applied readout, cell type, receptor density, and ligand of choice.<sup>[124]</sup> As a consequence, tissue and cell-type specific receptor expression profiles remain poorly characterized. In particular, the expression of CB<sub>2</sub>R in non-immune brain cells and at which degree its upregulation occurs in pathology are under current debate.<sup>[101b, 108, 125]</sup>

Because any improvement of CB<sub>2</sub>R agonists as new therapeutics requires a thorough understanding of their molecular and cellular mechanisms of action,<sup>[126]</sup> many research efforts have been directed to the development of new strategies and biological and chemical tools to visualize CB<sub>2</sub>R. The use of recombinant expression systems to label CB<sub>2</sub>R with fluorescent and peptide reporters have enabled initial imaging studies and purification of this receptor.<sup>[127]</sup> Nevertheless, in more pharmacological relevant systems, such as native cells and tissues, CB<sub>2</sub>R is expressed at very low levels, even if the cells are known to be responsive to its activation.<sup>[62a, 128]</sup> Attempts on determining CB<sub>2</sub>R expression profiles have been made applying standard biochemical techniques, such as qRT-PCR<sup>[129]</sup> and immunohistochemistry<sup>[130]</sup> assays. The major drawbacks of these experiments rely on the poor correlation of mRNA levels with functional protein and the absence of sufficiently specific antibodies for both human (h) and rodent (r) CB<sub>2</sub>R which prevents studies at a cellular or sub-cellular level.<sup>[131]</sup>

As discussed in the previous sections, chemical probes targeting the CB<sub>2</sub>R can be applied to determine its pharmacology, distribution, expression levels, occupancy, and follow signaling cascades both *in vitro* and *in vivo*. At present, CB<sub>2</sub>R-selective PET tracers as well as covalent, fluorescent, biotinylated, and photochromic compounds have been reported.<sup>[62a, 132]</sup> This section highlights the advances in the development and applications of these tools.

### 2.1.3.1. Positron Emission Tomography (PET) Tracer

Positron emission tomography (PET) tracers were extensively used to study CB<sub>2</sub>R expression at tissue level.<sup>[133]</sup> This technique, however, lacks the cellular resolution required for many investigations, such as receptor occupancy and tracing internalization events.<sup>[134]</sup> Radioisotope introduction at the recognition element rarely implies significant structural changes, since a connective linker is not required (Figure 2.6.). Thus, the synthesis of radiotracers which are highly selective toward CB<sub>2</sub>R is considerably more straightforward than for other imaging modalities.

One of the first CB<sub>2</sub>R-selective PET tracers developed was based on the thiazole A-836339 (**2.12**), a CB<sub>2</sub>R agonist from the Abbott pipeline (Figure 2.6.).<sup>[135]</sup> The [<sup>11</sup>C]A-836339 analog (**2.13**), however, lacked CB<sub>2</sub>R specificity *in vivo* and displayed low stability.<sup>[136]</sup> More recently the fluorinated derivative **2.14** have been synthesized with promising results in rodents.<sup>[137]</sup> The first reports of a brain penetrant radiotracer to display selective CB<sub>2</sub>R binding explored the oxoquinoline core ([<sup>11</sup>C]NE40, **2.15**, Figure 2.6.).<sup>[138]</sup> Besides promising results in rodents, discrepancies between preclinical and first in human

studies prevent [ $^{11}\text{C}$ ]-tracer **2.15** from further clinical applications.<sup>[139]</sup> In order to improve pharmacological parameters, such as affinity, plasma protein binding, lipophilicity, and half-life, this scaffold has undergone several optimization rounds. However, this probe series has still metabolic and pharmacokinetic issues, including nonspecific binding which limit their use for more relevant *in vivo* studies.

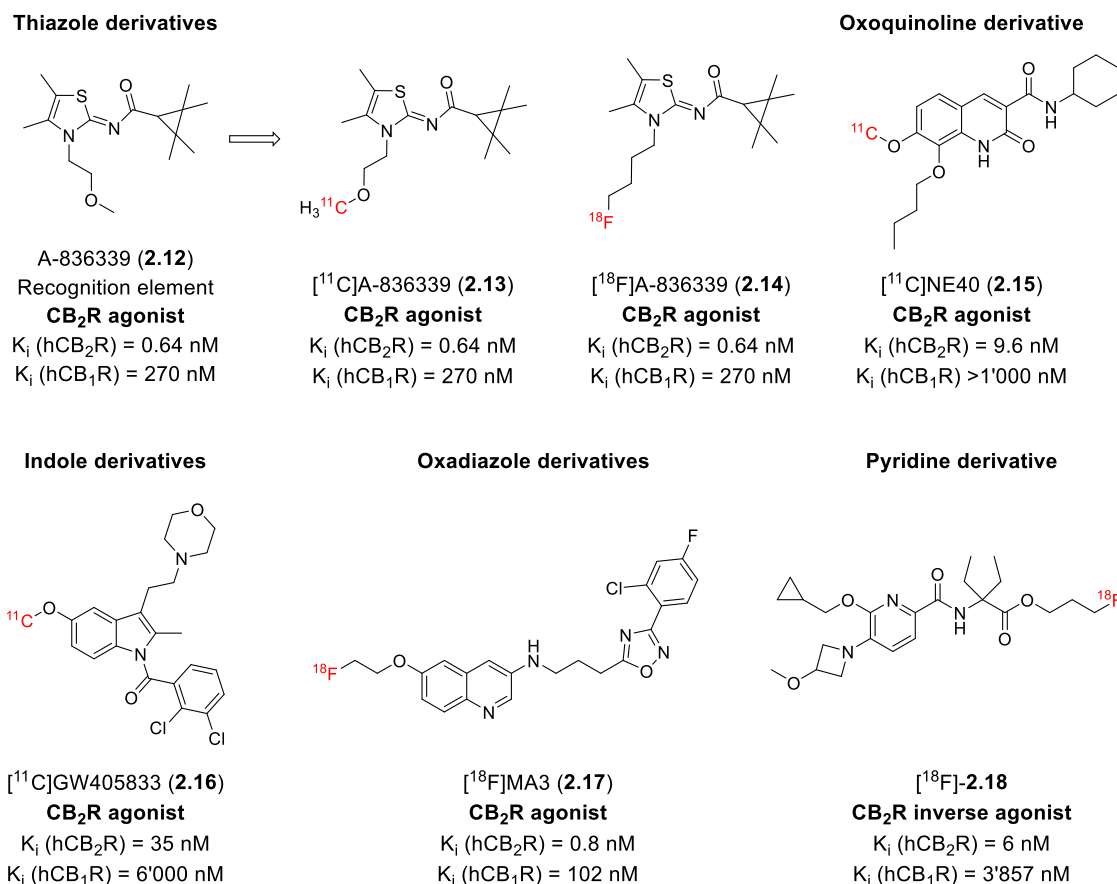


**Figure 2.6. Structures of CB<sub>2</sub>R-selective recognition element and PET tracers.**<sup>[136-138, 140]</sup> These ligands are synthetic cannabinoids which are classified by their functional efficacy at the CB<sub>2</sub>R. Their literature reported binding affinities towards CB<sub>2</sub>R and CB<sub>1</sub>R of the respective nonradioactive analogs is given below each structure. PET reporters are highlighted in red.

Indole derivatives, such as the agonist [ $^{11}\text{C}$ ]GW405833 (**2.16**) was also applied for biodistribution experiments both in rodent and rhesus monkey (Figure 2.6.).<sup>[140a, 140b]</sup> Due to its relatively low binding affinity, slow washout and nonspecific binding, investigations with this ligand are unlikely to advance. Recently oxadiazole and pyridine cores were also exploited for the synthesis of PET tracers targeting the CB<sub>2</sub>R (Figure 2.6.). The [ $^{18}\text{F}$ ]MA3 (**2.17**) have demonstrated promising biodistribution in health mice and stronger brain uptake in comparison to previous tracers, but was unspecific.<sup>[140c, 140d]</sup> From

an extensive structure activity relationship (SAR) on the 2,5,6-substituted pyridine scaffold, a 5-methoxyazetidone derivative was identified with best pharmacological profile.<sup>[141]</sup> Using a fluorinated derivative this analog (<sup>18</sup>F]-**2.18**, Figure 2.6.), imaging experiments using postmortem human spinal cord tissues from a patient with amyotrophic lateral sclerosis and a healthy control showed significant compound uptake at diseased tissues.<sup>[140c]</sup> These promising results indicate that tracer **2.18** will possibly undergo further evaluation in neuroinflammation models.

Up to now, the poor specificity due to highly lipophilic scaffolds, lack of CB<sub>2</sub>R selectivity against CB<sub>1</sub>R, low chemical stability, unfavorable metabolic fate, and low uptake of these radiotracers in preclinical applications have hampered the advance of such tracers into clinical settings and the precise characterization of CB<sub>2</sub>R expression *in vivo*. In addition, the higher costs, safety concerns, radioactive synthesis, storage, and waste management further limit the applicability of PET assays from investigations. Conversely, covalent, fluorescent, and biotinylated imaging ligands are sensitive tools that allow for real-time imaging in living cells with a high degree of spatiotemporal resolution,<sup>[87]</sup> while eliminating radioactive material demand.

### 2.1.3.2. Covalent Probes

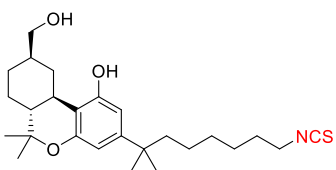
The selective covalent binding to specific amino acids of GPCRs represents a valuable method for elucidating their structure and function, such as binding site mapping and stabilizing the receptor for X-ray crystal structure elucidation.<sup>[142]</sup> Covalent bond formation occurs through two main mechanisms of activation: (i) spontaneously reactive electrophilic moieties, e.g., reactive thiols, isothiocyanates (NCS), halomethylketones, and Michael acceptors or (ii) light activation of a photoaffinity group, e.g., azide, diazirine, and benzophenone. Usually ligands decorated with an electrophilic reactive handle are called covalent probes and react with nucleophilic amino acid side chains, such as serine, cysteine, threonine, while the ones containing a photoaffinity label are denominated photoactivatable probes and are not selective to amino acid types.<sup>[143]</sup>

The MAKRIYANNIS GROUP at the Northeastern University have designed the majority of covalent probes so far described with the ultimate goal to define structural aspects of ligand recognition in hCB<sub>2</sub>R. Initially, this group generated a covalent mixed agonist series by introducing NCS groups at the THC scaffold.<sup>[144]</sup> Despite the lack of selectivity, analog AM841 (**2.19**, Figure 2.7.) has been used to map the CB<sub>2</sub>R binding site<sup>[145]</sup> and to investigate the (patho)physiological role of CB<sub>2</sub>R in

inflammatory disorders in mouse models.<sup>[146]</sup> Based on the CB<sub>2</sub>R inverse agonist SR144528 (**2.20**), the CB<sub>2</sub>R-selective diarylpyrazole AM1336 (**2.21**) was synthesized with a NCS-tag (Figure 2.7.) to enable complementary binding site mapping investigations.<sup>[147]</sup> The same group also explored the THC core to prepare the first photoactivatable probe with selective CB<sub>2</sub>R binding (AM967, **2.22**, Figure 2.7.).<sup>[148]</sup>

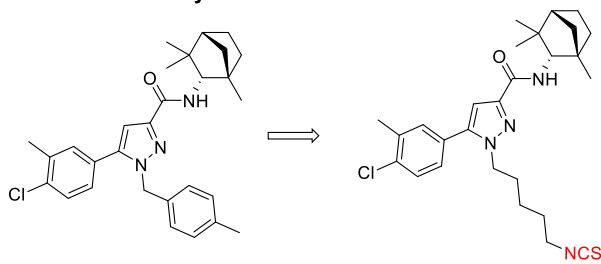
**Covalent probes:**

**Classical cannabinoids**



AM841 (**2.19**)  
**mixed agonist**  
 $K_i$  (hCB<sub>2</sub>R) = 1.5 nM  
 $K_i$  (hCB<sub>1</sub>R) = 9.1 nM

**Synthetic cannabinoids**

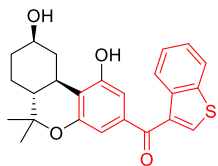


SR144528 (**2.20**)  
 Recognition element  
**CB<sub>2</sub>R inverse agonist**  
 $K_i$  (hCB<sub>2</sub>R) = 0.6 nM  
 $K_i$  (hCB<sub>1</sub>R) = 400 nM

AM1336 (**2.21**)  
**CB<sub>2</sub>R inverse agonist**  
 $K_i$  (hCB<sub>2</sub>R) = 0.5 nM  
 $K_i$  (rCB<sub>1</sub>R) = 5.8 nM

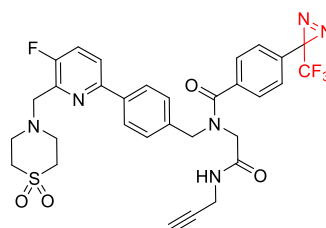
**Photoactivated probes:**

**Classical cannabinoids**



AM967 (**2.22**)  
**CB<sub>2</sub>R agonist**  
 $K_i$  (hCB<sub>2</sub>R) = 125 nM  
 $K_i$  (rCB<sub>1</sub>R) = 1'248 nM

**Synthetic cannabinoids**



LEI121 (**2.23**)  
**CB<sub>2</sub>R inverse agonist**  
 $K_i$  (hCB<sub>2</sub>R) = 63 nM  
 $K_i$  (hCB<sub>1</sub>R) > 10'000 nM

**Figure 2.7. Structures of recognition element and covalent tools to study the CB<sub>2</sub>R.**<sup>[144, 147-149]</sup> These ligands are classified by type of covalent bond formation in covalent and photoactivatable probes and by compound class as classical and synthetic cannabinoids. Their functional efficacy at the CB<sub>2</sub>R and literature reported binding affinities towards CB<sub>2</sub>R and CB<sub>1</sub>R are given below each structure; due to plausible covalent binding this values refer to as “apparent  $K_i$ ’s”. The covalent reactive moiety is highlighted in red.

The major limitation of covalent tools is the lack of a signal agent, which would enable further imaging studies. To overcome detection issues, the VANDER STELT GROUP at the University of Leiden designed a photoactivatable probe containing both a photoaffinity (diazirine) and a biorthogonal (terminal alkyne) ligation handle (LEI121, **2.23**, Figure 2.7.).<sup>[149]</sup> Thereby, enabling covalently trapping of hCB<sub>2</sub>R upon irradiation, followed by *in situ* copper azide-alkyne cycloaddition (CuAAC) conjugation of the



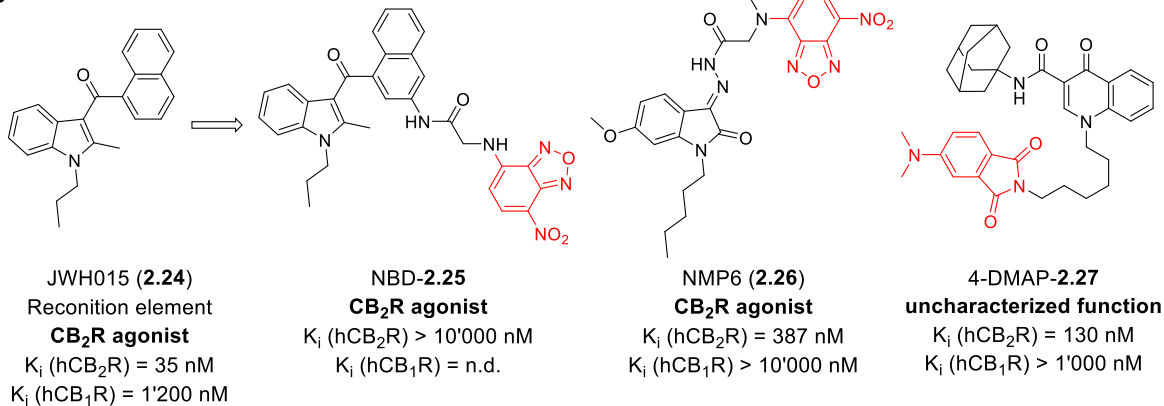
reporter tag in a two-step procedure called photoaffinity-based protein profiling (pAfBPP). The CB<sub>2</sub>R inverse agonist **2.23** has been exploited for CB<sub>2</sub>R visualization in both overexpressing and primary cells using flow cytometry for target engagement evaluation of unlabeled CB<sub>2</sub>R ligands. This compound has great potential for monitoring of endogenous receptor expression and engagement in human cells. However, the applications of covalent tools are limited due to the irreversible binding, which is not appropriate for many *in vitro* assays, such as kinetic studies and can lead to unfavorable *in vivo* off-target interactions due to unspecific reactivity.

### 2.1.3.3. Fluorescent Probes

The need for CB<sub>2</sub>R-selective fluoroprobes with reversible binding modes and improved physicochemical properties has prompted the synthesis and evaluation of structurally diverse compounds. Initial efforts used *in silico* tools to design 7-nitrobenzofurazan (NBD)-labeled derivatives based on JWH015 (**2.24**), a highly potent CB<sub>2</sub>R agonist (Figure 2.8).<sup>[150]</sup> Introduction of the linker-NBD construct, however, resulted in a significant loss in CB<sub>2</sub>R affinity (NBD-**2.25**). Modifications at the 3-position of the indole core for identifying less lipophilic linkers led to the discovery of the *N*-alkyl isatin acylhydrazone compound series.<sup>[151]</sup> A fluorescent version of this scaffold containing a NBD moiety generated the NMP6 probe (**2.26**) which retained the good affinity and selectivity values from its parent compound (Figure 2.8).<sup>[152]</sup> Confocal imaging and flow cytometry studies using ligand **2.26** showed specific CB<sub>2</sub>R binding on primary CD4<sup>+</sup> T cells and B lymphocytes, which was blocked by preincubation with a CB<sub>2</sub>R agonist (GW842166X, for ligand structure *see* **SI-1**, Supplementary figure S-1, Section 5.2.1.). Motivated by these results, the *N*-alkyl isatin acylhydrazone scaffold was further explored for attachment of the more relevant far-red fluorophore BODIPY 630/650. However, these attempts led to complete loss in affinity.<sup>[153]</sup>

Besides PET tracers, the oxoquinoline core also served as precursor for fluorescent ligands (*see* [<sup>11</sup>C]-**2.15** tracer, Figure 2.6.). A recent study evaluated different alkyl linker lengths at the *N*-1 position of the oxoquinoline scaffold for the attachment of green-emitting fluorophores, including NBD, 4-dimethylaminophthalimide (4-DMAP) and fluorescein.<sup>[154]</sup> However, as for the scaffold of **2.26**, only one labeled derivative demonstrated CB<sub>2</sub>R binding, the 4-DMAP-labeled **2.27** (Figure 2.8.). Compound **2.27** displayed 130 nM affinity for CB<sub>2</sub>R, being applied for flow cytometry imaging in both hCB<sub>2</sub>R over- and endogenously-expressing cells and for confocal microscopy in overexpressing cells.

### Synthetic cannabinoids



### Classical cannabinoids

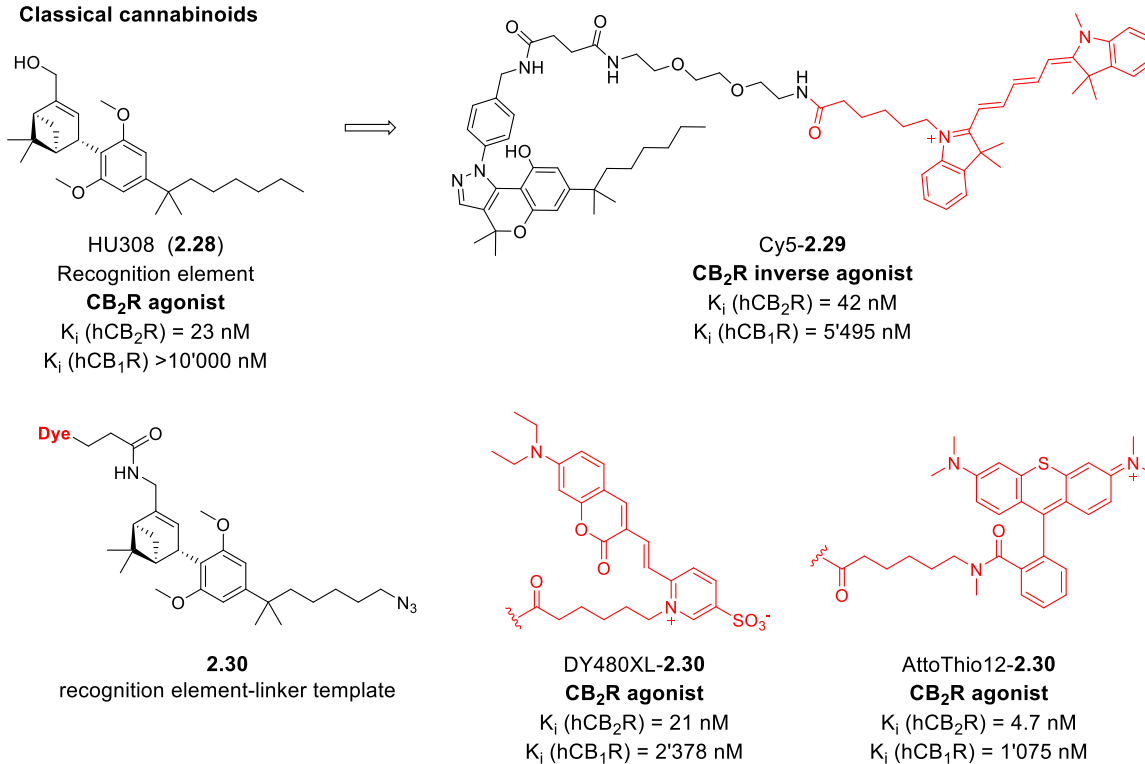


**Figure 2.8. Structures of recognition elements and CB<sub>2</sub>R-selective fluorescent probes.**<sup>[150, 152, 154-155]</sup> These probes are classified as synthetic and classical cannabinoids. Their functional efficacy at the CB<sub>2</sub>R and literature reported binding affinities towards CB<sub>2</sub>R and CB<sub>1</sub>R are given below each structure. Fluorophore structures are highlighted in red.

However, probe **2.27** suffered from unspecific binding in these experiments.<sup>[154]</sup>

Fluorescent probes bearing classical phytocannabinoid-derived compounds as recognition elements are currently under evaluation. The VERNALL GROUP from the University of Otago reported a Cy5-labeled CB<sub>2</sub>R inverse agonist (**2.29**, Figure 2.8.) which displayed 42 nM affinity toward the CB<sub>2</sub>R and 131-fold selectivity over the CB<sub>1</sub>R.<sup>[155b]</sup> Treatment of HEK-cells overexpressing hCB<sub>2</sub>R with Cy5-

labeled **2.29** for wide-field fluorescence microscopy analysis showed good selectivity and low unspecific binding. However, additional attempts to replace the Cy5 dye with other fluorophores, such as TAMRA and BODIPY were inactive on the hCB<sub>2</sub>R, underscoring that dye selection and placement at the pharmacophore strongly influenced probe's pharmacology.

The most selective and well-validated derivatives up to date were developed by the CARREIRA GROUP from the ETH Zürich. Linker studies at the HU308 scaffold (**2.28**, Figure 2.8.), a potent CB<sub>2</sub>R agonist, led to double-functionalized CB<sub>2</sub>R-selective ligands decorated with an electrophile moiety and a polyethylene glycol (PEG) linker (template **2.30**, Figure 2.8.).<sup>[156]</sup> Several reporter units were attached to the recognition element-linker template, including biotin, photoswitchable azobenzene and the NBD, DY480-XL, AttoThio12, and Alexa488 and 647 dyes.<sup>[155a]</sup> The agonist **2.30** labeled with AttoThio12 and DY480-XL fluorophores (Figure 2.8.) were the most active with K<sub>i</sub> values of 4.7 nM and 21 nM, respectively. These compounds were applied for flow cytometry, confocal microscopy, and time-resolved fluorescence resonance energy transfer (TR-FRET) assay in both over- and endogenous expressing cells with good CB<sub>2</sub>R specificity. Likewise the biotinylated and photoswitchable analogs were highly potent, but evaluation of their *in vitro* performance has not been performed yet.

The BAI GROUP from the Vanderbilt University developed the first successful NIR-probes targeting the CB<sub>2</sub>R by taking advantage of a different template: the biarylpyrazole mbc94 (**2.31**, Figure 2.9.).<sup>[157]</sup> This compound is a derivative of the CB<sub>2</sub>R inverse agonist **2.20** (Figure 2.7.) and was successful in retaining high receptor subtype selectivity and CB<sub>2</sub>R affinity despite linker and fluorophore conjugation. In the following years, the same group reported several NIR-**2.31** derivatives labeled with IRDye800CW,<sup>[158]</sup> NIR760<sup>[159]</sup>, IR700DX<sup>[160]</sup> and zwitterionic ZW760<sup>[161]</sup> fluorophores (Figure 2.9.). In addition, the quinolone NIR760-Q (**2.32**)<sup>[162]</sup> and the pyrazolopyrimidine NIR760-XLP6(**2.33**)<sup>[163]</sup> both containing the NIR-dye NIR760 were also synthesized by the same research group (Figure 2.9.). These compounds were applied for CB<sub>2</sub>R imaging in tumor cells and also for *in vivo* imaging but displayed high nonspecific binding. Among these derivatives, pyrazolopyrimidine **2.33** had the best selectivity profiles in the tested cellular settings.<sup>[163]</sup> The therapeutic properties of the photosensitizer IR700DX-**2.31** were also explored for the treatment of CB<sub>2</sub>R-positive tumors both *in vitro* and *in vivo*.<sup>[160, 164]</sup> Despite the promising results, no further studies exploiting these probes have been reported so far.

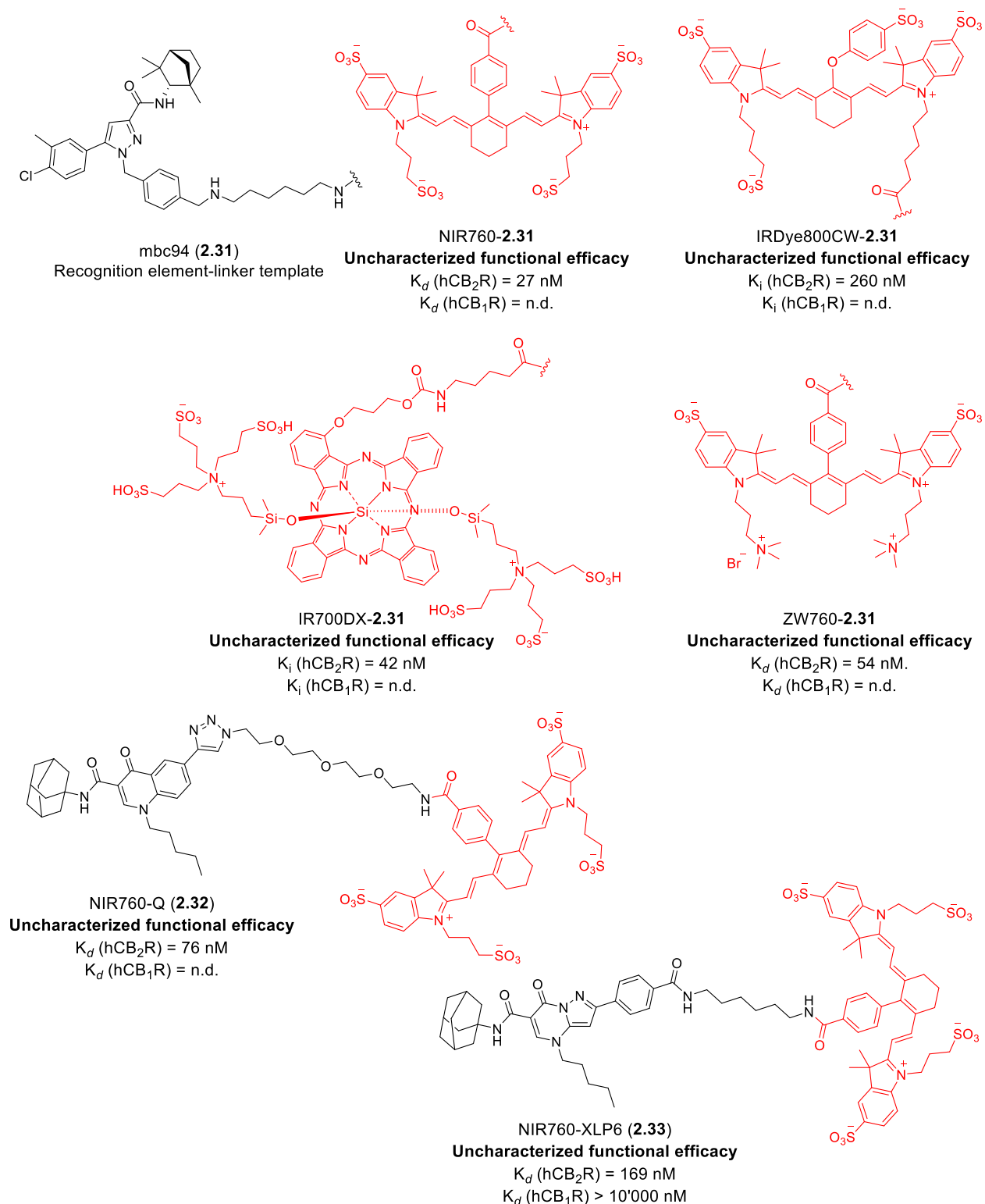


**Figure 2.9. Structures of CB<sub>2</sub>R-selective NIR-probes.**<sup>[158-163]</sup> These probes are based on synthetic cannabinoid scaffolds and have no described functional characterization. The literature reported equilibrium dissociation constant ( $K_d$ ) towards CB<sub>2</sub>R and CB<sub>1</sub>R are given below each structure. NIR-fluorophore structures are highlighted in red.

#### 2.1.3.4. Biotinylated Probes

Indirect generation of fluorescence by bioaffinity probes has also been applied for tracing the CB<sub>2</sub>R. These compounds exploit the high affinity of biotin for avidin conjugates to obtain dye conjugation via a two-step labeling procedure.<sup>[165]</sup> A biotinylated version of the HU308 ligand **2.28** (**2.34**, Figure 2.10.) was conjugated with streptavidin-Alexa488 for the visualization of CB<sub>2</sub>R in rat microglial cells using confocal microscopy.<sup>[166]</sup>

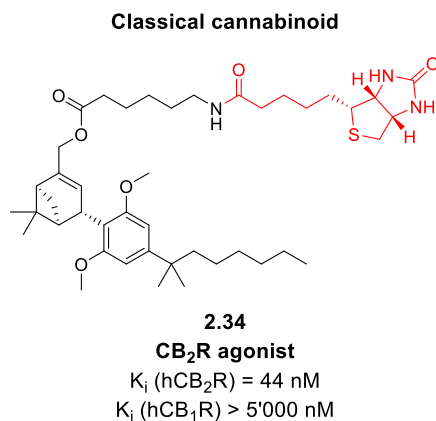


**Figure 2.10. Structure of CB<sub>2</sub>R-selective biotinylated probe 2.34.**<sup>[166]</sup> The probe's functional efficacy and literature reported binding affinities towards CB<sub>2</sub>R and CB<sub>1</sub>R are given below the structure. The biotin reporter is highlighted in red.

#### 2.1.3.5. Current Status and Major Limitations of the Reported Probes targeting the CB<sub>2</sub>R

Despite the elegant investigations described in this section, no reversible high affinity fluorescently labeled ligand with favorable photophysical and pharmacological properties is currently available. Major obstacles encountered in the development of such a set of highly versatile agents is a lack of understanding of modular agonist probe design based on receptor-ligand interactions. The binding affinity of such “one-probe-one-dye” conjugates strongly depends on the nature of the attached fluorescent label, and consequently, they are likely unsuitable for multiple imaging applications. Furthermore, the highly lipophilic nature of classical cannabinoids derived CB<sub>2</sub>R ligands, which often serve as starting points for probe generation, when combined with highly lipophilic dyes, synergistically leads to high levels of nonspecific membrane binding and insufficient overall properties for reliable general imaging applications.<sup>[167]</sup>

A further hurdle in the CB<sub>2</sub>R research field is the poor functional characterization of many CB<sub>2</sub>R fluorescent ligands reported. Determination on how the fluorescent tool activates the receptor is of fundamental importance since a combination of agonist and inverse agonist derived probes allows for targeting active and inactive states of respective receptor populations and the analysis of trafficking aspects. Current CB<sub>2</sub>R fluorescently labeled compounds with reported function and *in vitro* applications are restricted to both irreversible (**2.23**, Figure 2.7.)<sup>[149]</sup> and reversible (Cy5-**2.29**, Figure 2.8.)<sup>[155b]</sup> inverse agonists, addressing only the inactive state of the receptor. Conversely, approved drugs targeting the CB<sub>2</sub>R act as agonists. Therefore, the availability of reversible CB<sub>2</sub>R-agonist ligands with direct fluorophore attachment would allow exploration of the clinically more relevant activated state of CB<sub>2</sub>R and represent an important breakthrough and contribution to the existing CB<sub>2</sub>R probe toolset. The first CB<sub>2</sub>R fluorescent agonists with a reversible binding mode were recently reported exploiting the phytocannabinoid-derived HU308 (**2.28**) as recognition element (analog **2.30**, Figure 2.8.)<sup>[155a]</sup> However, as outlined above, ligand **2.28** displays a highly lipophilic structure, which may limit biological its applications.

As discussed previously (*see* Section 1.3.), the generation of high-quality chemical probes involves broad and in-depth validation using complementary biochemical and cell-based techniques. Additional evaluation of several parameters, such as chemical stability, water solubility – in particular important to avoid compound aggregation – membrane permeability, potency and selectivity are essential for the targeted performance of such probes.<sup>[24b, 70]</sup> Moreover, extensive pharmacological characterization of these tools across species is crucial for the clinical development of drugs targeting the CB<sub>2</sub>R. Ideally, these labeled compounds should have applicability for rodent and human CB<sub>2</sub>R at the same time to allow for a clear and well validated translational path from preclinical pharmacological *in vitro* and animal data to the human situation. Currently, there are no accepted biomarkers monitoring CB<sub>2</sub>R functionality which display these characteristics to enable both the interrogation of signaling aspects of this receptor subtype with confidence as well as an unambiguous interspecies cross-validation of (pre)clinical dataset.

## 2.1.4. Motivation for the Synthesis of a CB<sub>2</sub>R-Selective Fluorescent Ligand and Specific Aims

The successful development of new drugs targeting the CB<sub>2</sub>R strongly relies on the determination of the downstream signaling events driving their agonistic effect.<sup>[19]</sup> However, the lack of specific and reliable molecular imaging tools to study CB<sub>2</sub>R pharmacology currently hampers the exploration of its therapeutic potential.<sup>[62a, 154, 168]</sup> The acquisition and validation of such a data set requires the synergistic combination of diverse microscopic and imaging modalities. As each technique has its intrinsic readout that correlates to specific fluorophores, the knowledge of CB<sub>2</sub>R signaling cascades associated with pathology will likely be built upon structurally and functionally diverse CB<sub>2</sub>R modulators. Therefore, molecular imaging probes that can be tunable for multiple applications and have defined functional activity – particularly agonists – are urgently needed.

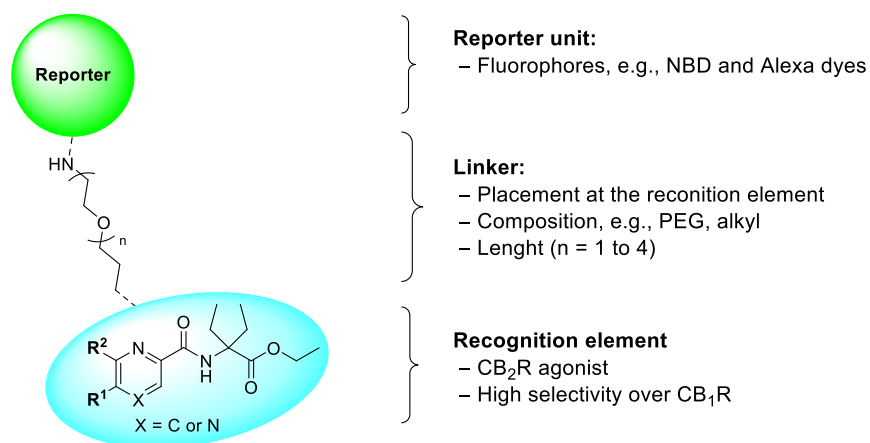


**Figure 2.11.** Components considered for the development of a CB<sub>2</sub>R-specific fluorescent probe: the appropriate recognition element, linker length and attachment site, and a suitable reporter unit, i.e., fluorophore.

The aim of this project was to develop a robust CB<sub>2</sub>R-selective probe template where binding affinity and selectivity would be largely independent of the reporter unit attachment (Figure 2.11.). Following a linear design (*see* Figure 1.3.A, Section 1.3.), a modular synthesis strategy was adopted for fluorescent ligand assembling. Paramount for the generation of such a derivative is the selection and optimization of its structural components – recognition element (pharmacophore), linker, and fluorescent dye. The recognition element should tolerate further chemical functionalization while preserving its affinity, functional efficacy, and selectivity towards the target. Furthermore, the linker attachment point at the pharmacophore, length, and composition are crucial aspects for fine-tuning the overall physicochemical properties of the probe. To avoid detrimental interactions of bulky and charged

fluorophores with the receptor,<sup>[169]</sup> the linker would ideally allow for placing of the fluorescent label outside the receptor in the extracellular space, reaching outside the binding pocket of the receptor. These considerations were combined with an *in silico* structure-based docking approach to guide synthesis efforts.

The novel fluorescent compounds should be applicable within a range of diverse imaging modalities while retaining the same recognition element. Therefore, a consistent interaction, i.e. activation cascades, binding dynamics, and expression profiles, with the CB<sub>2</sub>R was measured and validated across complementary techniques.

## 2.2. Results

### 2.2.1. Recognition Element Selection and Fluorescent Probe Design

In order to capitalize on agonist drug precursors with optimal affinity, lipophilicity, and drug-likeness, the 2,5,6-trisubstituted pyrazine RO6839251 (**2.35**)<sup>[170]</sup> and pyridine RO6852763 (**2.36**)<sup>[171]</sup> which are derived from a CB<sub>2</sub>R agonist drug discovery program<sup>[141, 170-171]</sup> were selected as starting points for probe design (Figure 2.12.A, *see* Table 2.1. for full pharmacological profile). Conceptually this reduces the risk of unspecific lipophilic interactions arising from phytocannabinoid-like derived ligands.

Physicochemical properties have direct influence on the efficacy, solubility, permeability, and metabolism of not only drug candidates, but also chemical probes.<sup>[172]</sup> For the identification of appropriate recognition elements for the development of a CB<sub>2</sub>R-selective probe, parameters such as atomic logP (AlogP)<sup>[173]</sup> and polar surface area (PSA)<sup>[174]</sup> were considered. The AlogP is an estimation of the lipophilicity of a compound (logP) which is based on the incremental contribution of each atom to the logP. In combination with PSA values, the AlogP can be used as a first predictor of cellular permeability – which then needs to be confirmed with experimental assays, such as the parallel artificial membrane permeability assay (PAMPA).<sup>[175]</sup>



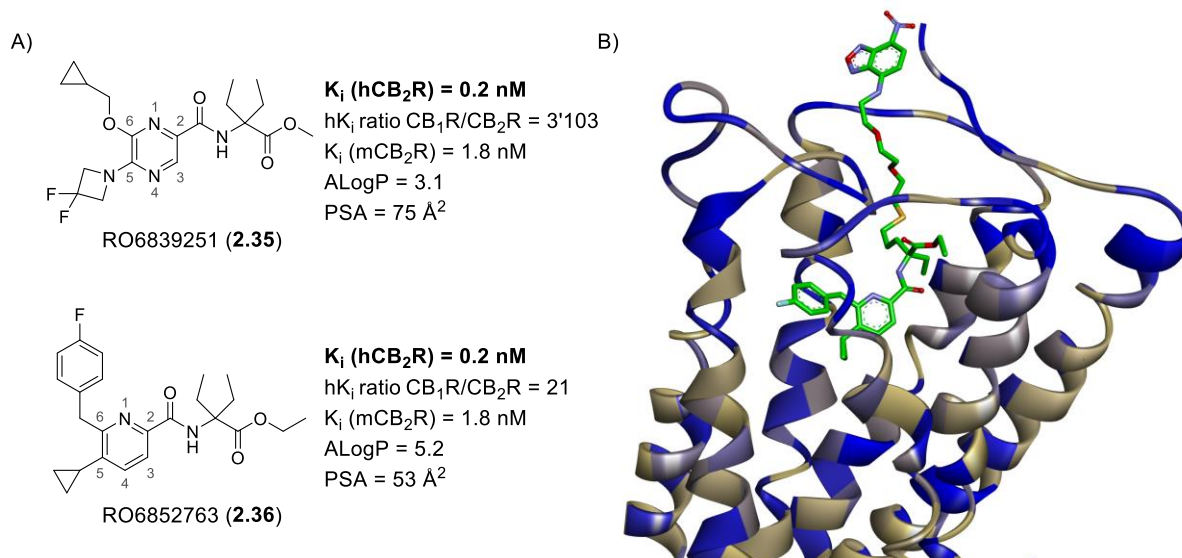


**Figure 2.12. Selected recognition element scaffolds and *in silico* studies used for probe design.** A) Drug discovery derived agonists **2.35** and **2.36**, used as starting points for the development of CB<sub>2</sub>R-selective fluorescent ligands; B) NBD-labeled **2.106** docked into the recently published co-crystal structure of active state CB<sub>2</sub>R in complex with agonist AM12033 (PDB 6KPF, for ligand structure *see* SI-2, Supplementary figure S-1, Section 5.2.1.);<sup>[81]</sup> Polar and hydrophobic amino acid residues are highlighted with blue and light brown colors, respectively; *In silico* studies were conducted by DR. WOLFGANG GUBA at Hoffmann La-Roche.

**Table 2.1. *In vitro* pharmacology profiles of recognition elements 2.35 and 2.36.**

Entry	Ligand	Structure	$K_i$ [nM]			hK <sub>i</sub> ratio CB <sub>1</sub> R/CB <sub>2</sub> R	cAMP EC <sub>50</sub> <sup>[a]</sup> [nM] (%eff.)			MW [g/mol]	PSA <sup>[b]</sup> [Å <sup>2</sup> ]	LE <sup>[c]</sup>	AlogP <sup>[d]</sup>	logD <sup>[e]</sup>
			hCB <sub>2</sub> R	hCB <sub>1</sub> R	mCB <sub>2</sub> R		hCB <sub>2</sub> R	hCB <sub>1</sub> R	mCB <sub>2</sub> R					
1	<b>2.35</b>		0.2	621	1.8	3103	1.2 (101)	297 (83)	2.2 (97)	412.4	75	0.3	3.1	3.7
2	<b>2.36</b>		0.2	5.4	1.8	27	0.7 (102)	4.4 (99)	1.9 (99)	412.5	53	0.3	5.2	n.d.

n.d. – not determined. <sup>[a]</sup> Functional potency (cAMP assay), percentage efficacy (%eff.) given in parenthesis; <sup>[b]</sup> Surface sum of all polar atoms in the molecule; <sup>[c]</sup> Ligand efficiency (LE), i.e., ratio between affinity and molecular size;<sup>[176]</sup> <sup>[d]</sup> Calculated partition coefficient values (AlogP) based on the contribution of each atom to the logP;<sup>[173]</sup> <sup>[e]</sup> Distribution coefficient values measured in a mixture of 1-octanol and water. Reference ligands data described in the Pharmacological Assessment, Section 5.2.10. Radioligand binding assays performed by ELISABETH ZIRWES and cAMP functional assays performed by ANJA OSTERWALD at Hoffmann La-Roche.

The calculated physicochemical properties of the ligands **2.35** and **2.36** are superior to classical cannabinoids with regard to AlogP and PSA, i.e., standard agonist HU308 (**2.28**, Figure 2.8., Section 2.1.3.) has an AlogP of 6.7 and a PSA of 27.4 Å<sup>2</sup> whereas the utilized derivatives **2.35** and **2.36** have a favorable AlogP values of 3.1 and 5.2, and PSA of 75 and 53 Å<sup>2</sup>, respectively (Figure 2.12.A and Table

2.1.). Both molecules possess subnanomolar affinities for the human (h) CB<sub>2</sub>R and similar good binding affinity (K<sub>i</sub>) for mouse (m) CB<sub>2</sub>R with K<sub>i</sub> values of 2 nM.<sup>[170-171]</sup> Pyrazine **2.35** and pyridine **2.36** also exhibit good binding selectivity over hCB<sub>1</sub>R, which is very important for the visualization of CB<sub>2</sub>R in the central nervous system, where CB<sub>1</sub>R is highly expressed.

Fluorescent analogs of **2.35** and **2.36** were designed with the support of molecular modeling studies conducted at Hoffmann La-Roche by DR. WOLFGANG GUBA using the X-ray structure of the active state of CB<sub>2</sub>R in complex with the agonist AM12033 (Figure 2.12.B; see Figure 2.1., Section 2.1.1. for the crystal structure, PDB 6KPF; for ligand structure see **SI-2**, Supplementary figure S-1, Section 5.2.1.).<sup>[81]</sup> Parent agonists **2.35** and **2.36** possess three potential exit vectors that have been investigated for the elaboration of an extensive structure activity relationship (SAR) study – the positions 5 and 6 of the heteroaryl group, and the geminal diethyl group (Figure 2.12.A),<sup>[170-171]</sup> thereby providing a basis for linker placement at different positions. Candidate molecules were docked into the CB<sub>2</sub>R binding cavity and prioritized on the likelihood of the linker trajectory to reach the extracellular space. This analysis suggested two different linker attachment sites preferentially: one at position 6 of the heteroaryl ring and the other at the geminal diethyl group (Figure 2.13.).

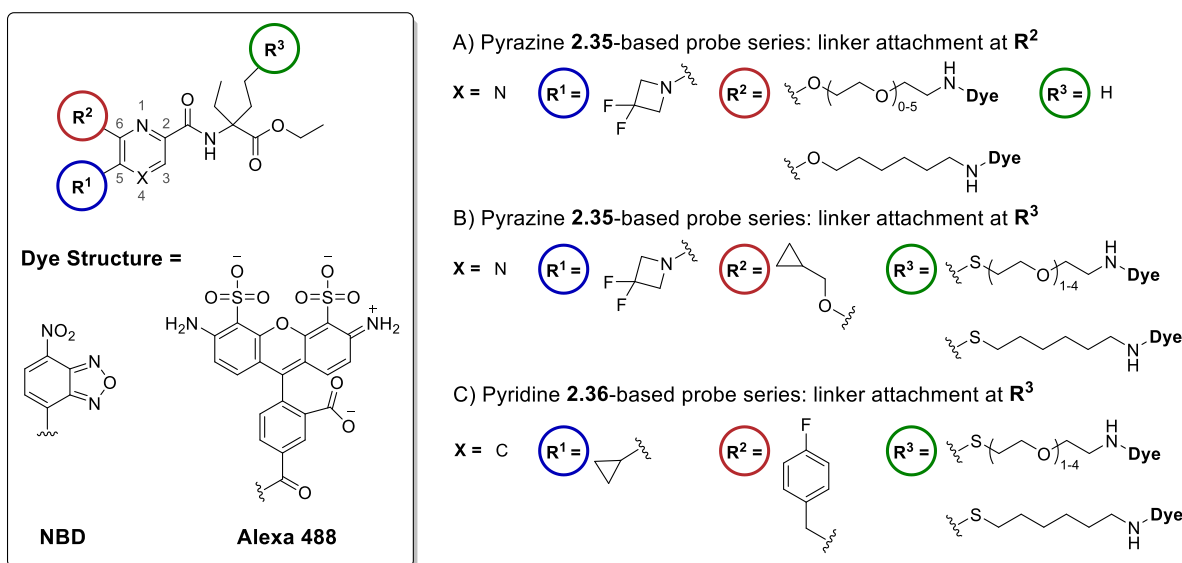


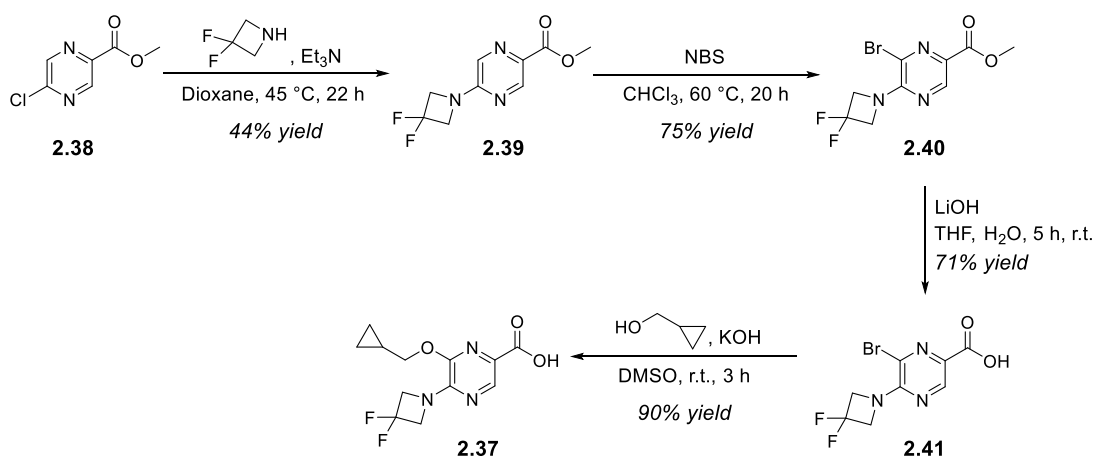
**Figure 2.13. Modular design of CB<sub>2</sub>R fluorescent probes and linker attachment strategies.** Structure of recognition element-linker template designed with the guidance of molecular docking for conjugation with fluorophores, such as NBD and Alexa 488. The docking analysis suggested positions A) **R<sup>2</sup>** and B) **R<sup>3</sup>** of the pyrazine **2.35** scaffold, or C) **R<sup>3</sup>** of the pyridine **2.36** scaffold as preferred for linker attachment.

Furthermore, *in silico* docking studies indicated that a linker length ranging from one to four polyethylene glycol (PEG) units would be sufficient to reach out to the extracellular space. For a

systematic investigation of the optimal linker, probes containing different linker lengths ranging from one to four ethylene glycol units were planned. PEG was chosen as an appropriate linker template to address issues of solubility and lipophilicity characteristics for CB<sub>2</sub>R-targeted ligands. However, considering the highly lipophilic nature of the CB<sub>2</sub>R binding cavity, a less polar alkyl linker was additionally selected in order to confirm the absence of detrimental effects by the pre-organized and highly hydrated PEG chain along the inner surface of the receptor.<sup>[177]</sup> For evaluation of binding affinity and physicochemical aspects, such as water solubility and chemical stability, the small, inexpensive, and non-charged 7-nitrobenzofurazan (NBD) dye would be initially conjugated to the probe template. The best ligand-linker systems identified *in vitro* would then be employed for the introduction of more relevant fluorophores for biological test settings, e.g., Alexa 488 (Figure 2.13).

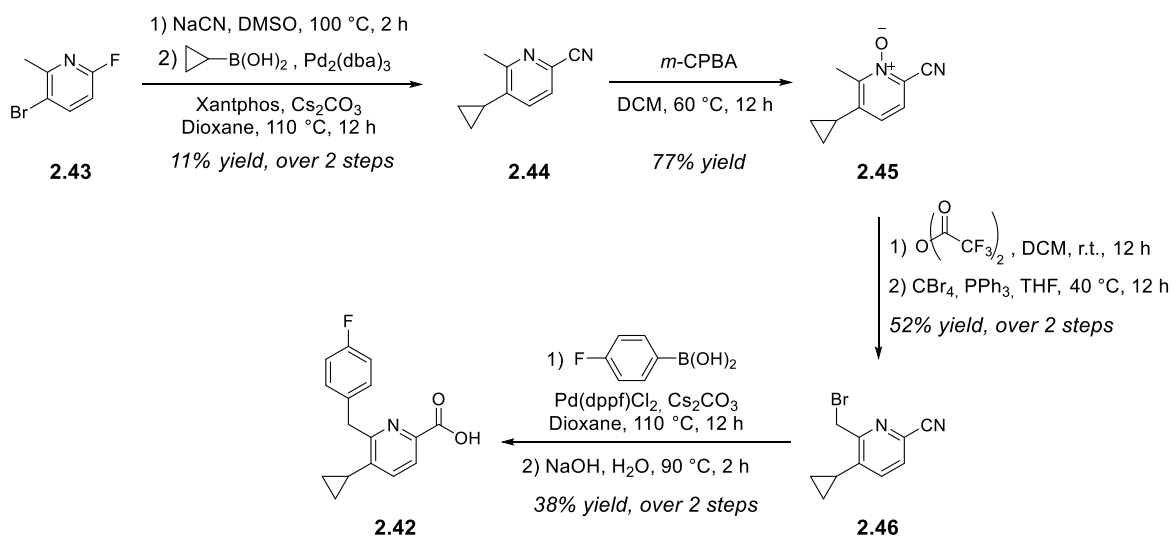
### 2.2.2. Synthesis of the Recognition Element Scaffolds

The synthesis of pyrazine carboxylic acid precursor (**2.37**) has been described by our collaboration partners<sup>[170]</sup> (Scheme 2.1). This route commenced with the treatment of commercially available 5-chloro-pyrazine **2.38** with 3,3-difluoroazetidene and a base to afford derivative **2.39** in a moderate 44% yield. Bromination of the 6-position of intermediate **2.39** using *N*-bromosuccinimide (NBS) and subsequent basic hydrolysis yielded the carboxylic acid **2.41** in a good 71% yield. Compound **2.41** was converted in a *O*-alkylation reaction with cyclopropyl-methanol under basic conditions to the desired pyrazine probe precursor **2.37** in 90% yield.



Scheme 2.1. Synthesis of pyrazine carboxylic acid building block **2.37**.

Picolinic acid **2.42** can be prepared in seven synthetic steps, according to literature procedures.<sup>[171]</sup> This approach started with the introduction of a nitrile group at the 2-position of pyridine **2.43** (Scheme 2.2.). The cyclopropyl ring was subsequently installed to the 5-position of the pyridine scaffold using Suzuki conditions to afford intermediate **2.44** in low 11% yield, over these two synthetic steps. Treatment of compound **2.44** with *m*-chloroperoxybenzoic acid (*m*-CPBA) afforded *N*-oxide **2.45** which underwent rearrangement upon trifluoroacetic anhydride treatment. Bromination at the 6-position of the pyridine scaffold enabled a second Suzuki coupling to introduce the *para*-fluorophenyl substitution in moderate yield. The final hydrolysis of the nitrile group afforded the desired acid building block **2.42**, leading to an overall 2% yield.



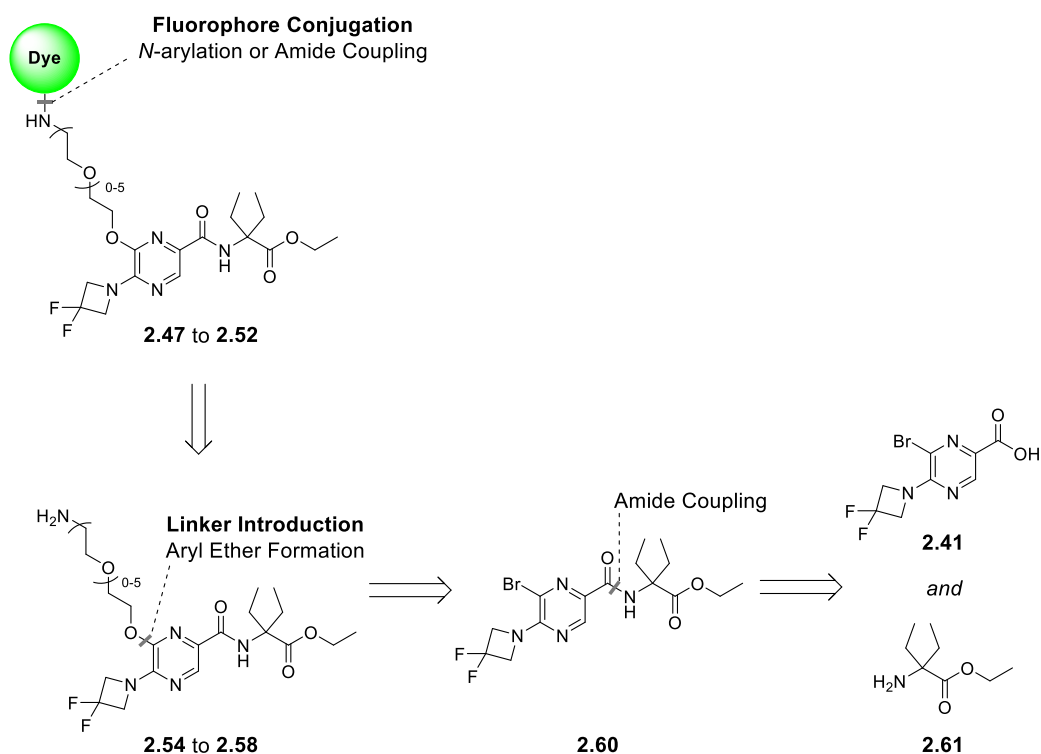
Scheme 2.2. Synthesis of picolinic acid building block **2.42**.<sup>[171]</sup>

The carboxylic acid building blocks **2.37**, **2.41**, and **2.42** were exploited as pharmacophores for fluorescent ligand assembling following the design strategies discussed in Figure 2.13. (Section 2.1.2.)

### 2.2.3. First Approach Towards $\text{CB}_2\text{R}$ -Selective Fluorescent Ligands: Probing the $\text{R}^2$ -Position of the Pyrazine Recognition Element as Linker Attachment Point

The initial strategy towards fluorescently labeled analogs containing the 2,5,6-trisubstituted heteroaryl core as recognition element explored the 6-position of the pyrazine **2.35** scaffold for linker attachment

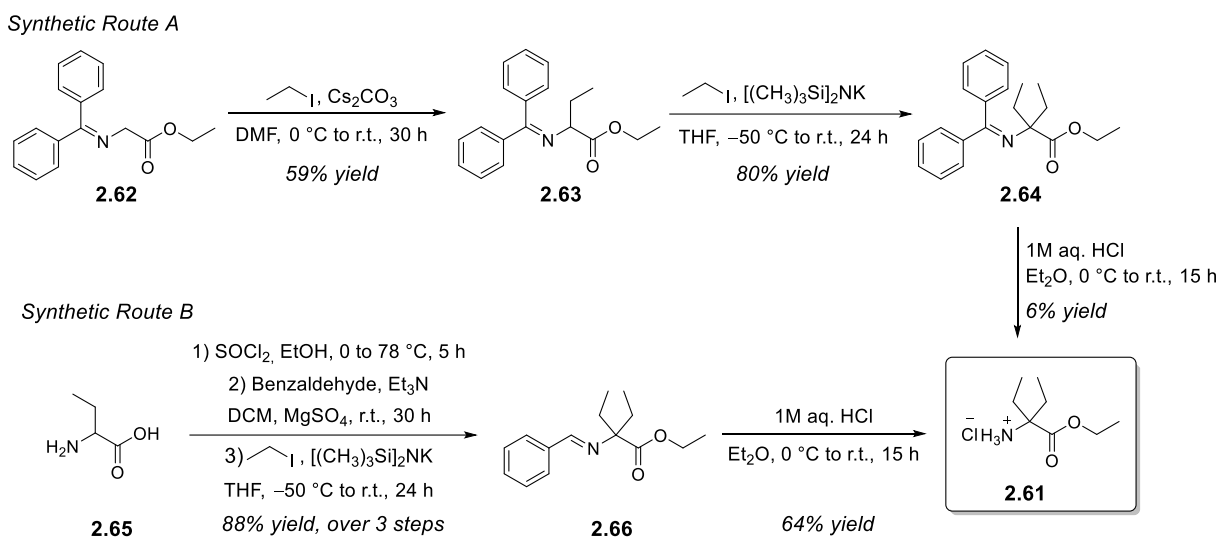
point (Figure 2.13.A, Section 2.2.1.). The concept behind the synthesis of this series was based on a modular approach with linker introduction and fluorophore conjugation as final steps (Scheme 2.3.). Such an approach would allow for a systematic evaluation of the linker length and composition as well as dye variation at the advanced probe template **2.60**. This intermediate could be prepared from an amide coupling reaction of carboxylic acid **2.41** (Scheme 2.1., Section 2.2.2.) with amino ester **2.61**.



**Scheme 2.3. Synthesis strategy for pyrazine probe series 2.47 to 2.53: Linker introduction at the 6-position of the pyrazine heteroaryl core.**

The preparation of amino ester **2.61** as a chloride salt has been already described by using a two-step synthetic route starting from diphenylmethylene protected glycine **2.62** (Scheme 2.4.).<sup>[178]</sup> However, attempts on performing the  $\alpha,\alpha$ -diethylation reaction of glycine **2.62** in *one-pot* to intermediate **2.64** were unsuccessful, even with increased amounts of base potassium bis(trimethylsilyl)amide – from 2.2 up to 6 equivalents. Full conversion to the desired compound was not observed at any attempted condition, instead, a mixture of starting material **2.62** with mono- (**2.63**) and diethylated (**2.64**) intermediates were obtained. The separation of these precursors also turned out to be challenging due to the nearly identical retention factors ( $R_f$ ) values under a variety of solvent systems. This procedure led to extremely low amounts of isolated product (3% overall yield).

To improve the outcome of this reaction, the dialkylation step was divided into two separated reactions as shown in Scheme 2.4. (Synthetic route A). First, deprotonation of the  $\alpha$ -carbon of glycine **2.62** using 3 equivalents of cesium carbonate, followed by alkylation using iodoethane gave monoethylated compound **2.63** in good 59% yield. The second  $\alpha$ -alkylation of the carbonyl group was performed using 1.5 equivalents of potassium bis(trimethylsilyl)amide and gave diethyl intermediate **2.64** in very good 80% yield. However, after acidic deprotection of the diphenylmethylene protective group, amino ester **2.61** could be isolated in 6% yield.

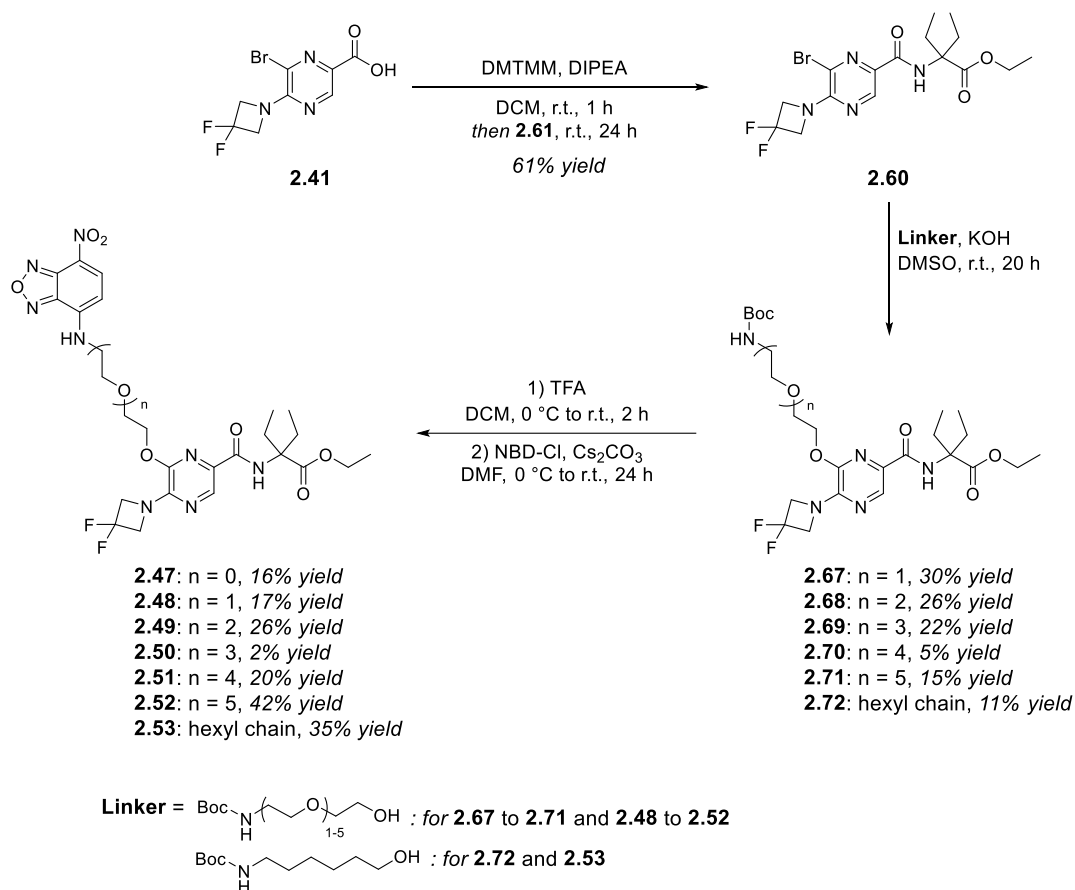


**Scheme 2.4.** Synthesis of amino ester intermediate **2.61** via the two investigated synthetic routes.

To circumvent the issues related to the Synthetic route A, the approach for the  $\alpha,\alpha$ -dialkylation of amino esters reported by LIU and collaborators<sup>[179]</sup> was adapted for the preparation of building block **2.61** (Scheme 2.4., Synthetic route B). Starting from aminobutyric acid **2.65**, classical Fischer esterification conditions, followed by protection of the primary amine using benzaldehyde led to the formation of an amino ester intermediate. Subsequent  $\alpha$ -alkylation of the carbonyl group using the same conditions as for diphenylmethylene **2.64** afforded diethyl ester **2.66**. Benzylidene deprotection under acidic conditions afforded the chloride salt form of amino ester **2.61** in 64% yield, without the need for chromatographic purification. The use of diphenylmethylene or benzylidene protective groups was crucial for the  $\alpha,\alpha$ -dialkylation of the amino acid building blocks since it prevented untoward *N*-alkylations.

The amide coupling of carboxylic acid **2.41** with amino ester **2.61** was carried out using 4-(4,6-dimethoxy-1,3,5-triazin-2-yl)-4-methylmorpholin-4-ium chloride (DMTMM) as coupling reagent to

afford probe template **2.60** in 61% yield (Scheme 2.5.). Subsequent screening of the linker length and composition was performed using PEG chains ranging from zero to five ethylene glycol units and an alkyl chain (Scheme 2.5.). Introduction of *N*-Boc protected linkers was achieved using potassium hydroxide in dimethyl sulfoxide. The consecutive deprotection of the Boc group under acidic conditions allowed for the final *N*-alkylation labeling step to yield NBD-pyrazine derivatives **2.47** to **2.53**. The synthesis of compound **2.47** bearing a methylene linker was accomplished with a slight modification of the main procedure, by introducing the NBD dye to the linker before conjugation to probe template **2.60**.

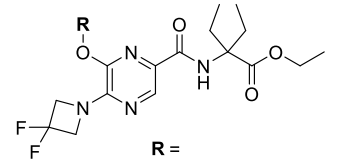
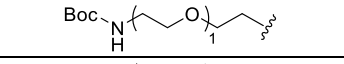
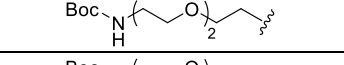
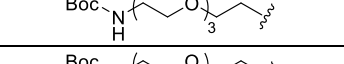
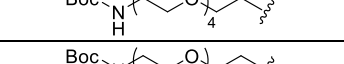
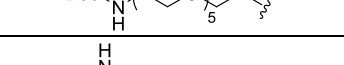
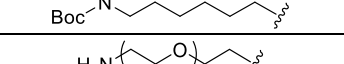
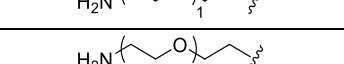
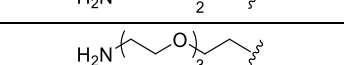
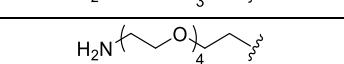
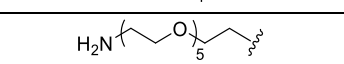
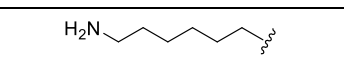
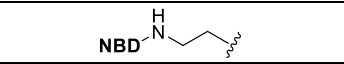
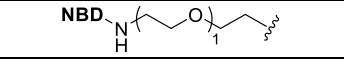
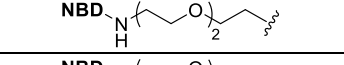
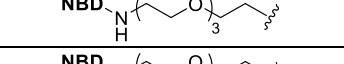
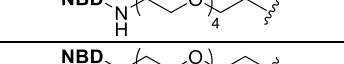
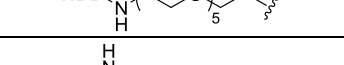
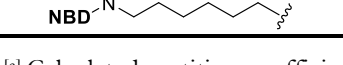
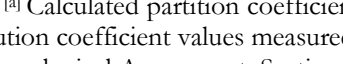


**Scheme 2.5. Synthesis of pyrazine-based NBD-labeled probes 2.47 to 2.53.**

The low yields obtained for compounds **2.67** to **2.72** can be mainly attributed to the observed chemical instability of the formed aryl ether intermediates under these conditions. At the 6-position of the pyrazine core, PEG linkers underwent hydrolytic cleavage, particularly upon heating (40 °C), limiting the alternative synthetic approaches that could be applied.

The fluorescently labeled NBD-ligands and selected pyrazine-linker intermediates were submitted to *in vitro* evaluation of their binding affinity towards the CB<sub>2</sub>R and selectivity over the CB<sub>1</sub>R subtype (Table 2.2.).

**Table 2.2. Linker studies at the 6-position of the heteroaryl core of pyrazine 2.35 and selected unlabeled intermediates.**

Entry	Ligand		K <sub>i</sub> hCB <sub>2</sub> R [nM]	K <sub>i</sub> hCB <sub>1</sub> R [nM]	hK <sub>i</sub> ratio CB <sub>1</sub> R/CB <sub>2</sub> R	MW [g/mol]	AlogP <sup>[a]</sup>	logD <sup>[b]</sup>
1	2.67		>10 <sup>0</sup> 000	>10 <sup>0</sup> 000	--	559.6	3.2	n.d.
2	2.68		>10 <sup>0</sup> 000	>10 <sup>0</sup> 000	--	603.7	3.1	3.5
3	2.69		>10 <sup>0</sup> 000	>10 <sup>0</sup> 000	--	647.7	3.0	4.0
4	2.70		>10 <sup>0</sup> 000	>10 <sup>0</sup> 000	--	691.8	2.8	3.9
5	2.71		>10 <sup>0</sup> 000	>10 <sup>0</sup> 000	--	735.8	2.7	3.7
6	2.72		958	4'470	5	571.7	4.9	n.d.
7	2.54		>10 <sup>0</sup> 000	>10 <sup>0</sup> 000	--	459.5	1.6	1.1
8	2.55		>10 <sup>0</sup> 000	>10 <sup>0</sup> 000	--	503.5	1.5	0.7
9	2.56		>10 <sup>0</sup> 000	>10 <sup>0</sup> 000	--	547.6	1.4	0.5
10	2.57		>10 <sup>0</sup> 000	>10 <sup>0</sup> 000	--	591.7	n.d.	n.d.
11	2.58		>10 <sup>0</sup> 000	>10 <sup>0</sup> 000	--	635.7	1.1	-0.04
12	2.59		1'213	1'762	2	471.5	3.3	1.5
13	2.47		3'164	3'219	1	578.5	3.5	n.d.
14	2.48		>10 <sup>0</sup> 000	2'624	<0.3	622.6	3.4	3.0
15	2.49		>10 <sup>0</sup> 000	>10 <sup>0</sup> 000	--	666.6	3.3	3.3
16	2.50		>10 <sup>0</sup> 000	>10 <sup>0</sup> 000	--	710.7	n.d.	n.d.
17	2.51		>10 <sup>0</sup> 000	>10 <sup>0</sup> 000	--	754.7	3.0	3.1
18	2.52		>10 <sup>0</sup> 000	>10 <sup>0</sup> 000	--	798.8	2.9	3.1
19	2.53		1'658	>10 <sup>0</sup> 000	>6	634.6	5.1	n.d.

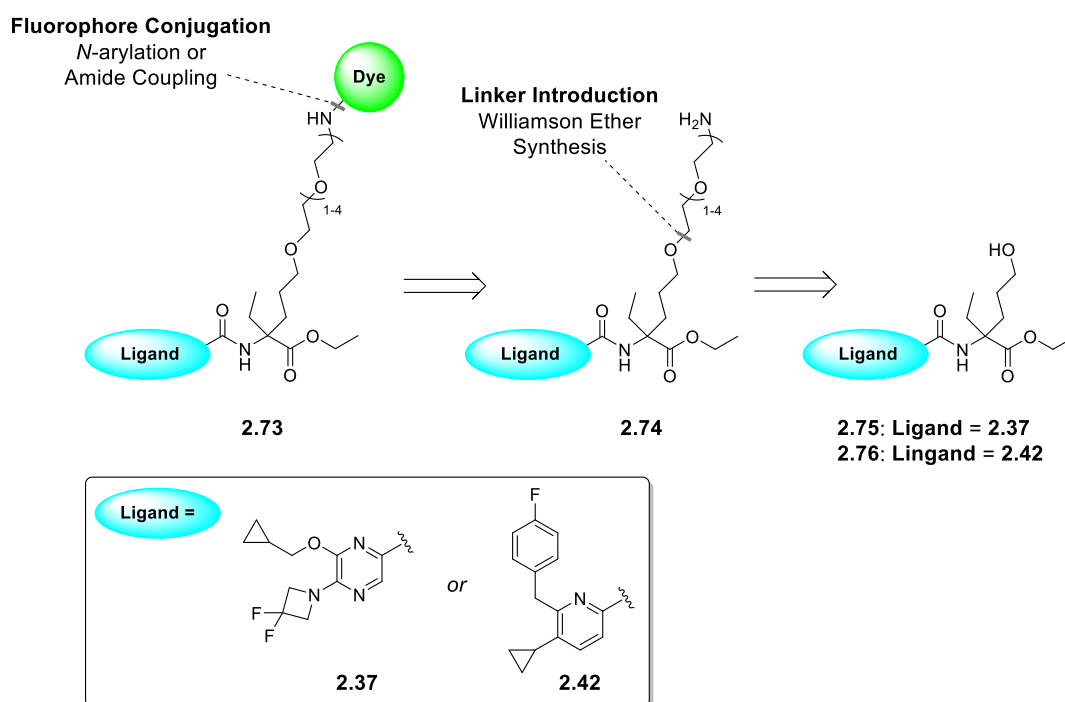
n.d. – not determined. <sup>[a]</sup> Calculated partition coefficient values (AlogP) based on the contribution of each atom to the logP;<sup>[173]</sup> <sup>[b]</sup> Distribution coefficient values measured in a mixture of 1-octanol and water. Reference ligands data described in the Pharmacological Assessment, Section 5.2.10. Radioligand binding assays performed by ELISABETH ZIRWES at Hoffmann La-Roche.



The radioligand binding assays were performed by ELISABETH ZIRWES at Hoffmann La-Roche using membrane preparations of Chinese Hamster Ovary (CHO) cells overexpressing either human CB<sub>2</sub>R or CB<sub>1</sub>R. None of the conjugated derivatives, however, exhibited the appropriate affinity for hCB<sub>2</sub>R. In addition, these molecules displayed insufficient stability in buffered aqueous media with linker hydrolytic cleavage observed over time.<sup>[180]</sup>

#### 2.2.4. Second Approach Towards CB<sub>2</sub>R-Selective Fluorescent Ligands: Probing the R<sup>3</sup>-Position with an Ether Functionality for Linker Attachment

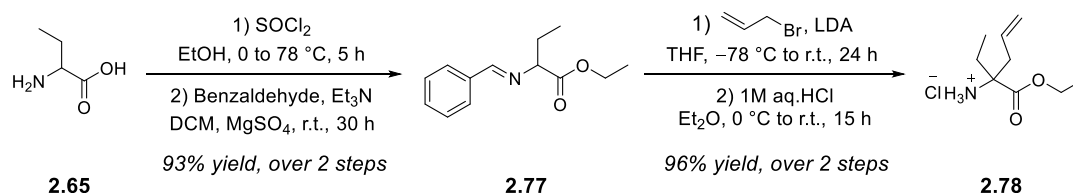
Due to the lack of affinity, selectivity, and chemical stability of the first approach, the geminal diethyl moiety (R<sup>3</sup>-exit vector, Figure 2.13.B and C, Section 2.2.1.) was investigated for the development of recognition elements **2.35** and **2.36** fluorescent analogs.



Scheme 2.6. Synthesis strategy for linker introduction through an ether linkage at the geminal diethyl portion of recognition elements **2.35** and **2.36**.

To allow for a straightforward introduction of different linkers, a modifiable ligation handle was required at this position. Several probe templates were docked by DR. WOLFGANG GUBA at Hoffmann La-Roche into the binding pocket of the hCB<sub>1</sub>R crystal structure in complex with antagonist AM6538 (for ligand structure *see* **SI-4**, Supplementary figure S-1, Section 5.2.1.),<sup>[181]</sup> which was the only cannabinoid receptor crystal structure reported by the beginning of this project. According to the *in silico* analysis, preferred linker attachment groups would not participate in hydrogen bonding. Thus, proton donating groups should be avoided at the linker portion. In addition, the configuration of the chiral center generated at the  $\alpha$ -carbon of this probe template was deemed not influential for *in vitro* potencies. In order to address these criteria, derivatives containing an ether linkage were initially pursued (Scheme 2.6).

Key building blocks for this synthetic pathway were alcohols **2.75** and **2.76**. The synthesis of these compounds was achieved through a hydroboration-oxidation stepwise reaction sequence of an alkene precursor. Similar as for the preparation of amino ester **2.6**, alkene **2.78** was obtained using an adapted procedure from the literature<sup>[179]</sup> (Scheme 2.7). The base required for  $\alpha$ -carbon deprotonation had, however, to be exchanged from potassium bis(trimethylsilyl)amide to lithium diisopropyl amide (LDA) for a better outcome (up to 98% yield). Using this protocol, alkene **2.78** was obtained in 4 synthetic steps from aminobutyric acid **2.65** without the need for chromatographic purification.



**Scheme 2.7. Synthesis of amino ester intermediate 2.78.**

The acid precursors **2.37** and **2.42** were conjugated to amino ester **2.78** using amide coupling conditions (Table 2.3.). Due to the low reactivity of both carboxylic acids and the tertiary amine, the coupling reagent used for this conversion had to be optimized. Using diisopropylethylamine (DIPEA) as a base in dichloromethane at room temperature, the uronium coupling reagents, i.e., 1-[bis(dimethylamino)methylene]-1H-1,2,3-triazolo[4,5-b]pyridinium 3-oxid hexafluorophosphate (HATU), *N,N,N',N'*-tetramethyl-O-(1H-benzotriazol-1-yl)uronium hexafluoro-phosphate (HBTU), and 2-(1H-benzotriazole-1-yl)-1,1,3,3-tetramethylammonium tetrafluoroborate (TBTU) (Table 2.3., entries 1 to 3) as well as benzotriazole-1-yl-oxy-tris-pyrrolidino-phosphonium hexafluorophosphate (PyBop, Table 2.3., entry 4), bis(2-oxo-3-oxazolidinyl)phosphinic chloride (BOP-Cl, Table 2.3., entry

5), and DMTMM (Table 2.3., entry 6) were tested for their efficiency in generating amides **2.79** and **2.80**.

The best outcomes were obtained when BOP-Cl was employed for the coupling of picolinic acid **2.42** with amine **2.78** (Table 2.3., entry 5) and DMTMM for the amide formation between pyridine carboxylic acid **2.37** and amine **2.78** (Table 2.3., entry 6). Importantly, these conditions were further exploited for subsequent amide coupling reactions involving the carboxylic acids **2.37** and **2.42**. Applying a hydroboration-oxidation reaction sequence,<sup>[182]</sup> treatment of allyl amides **2.79** and **2.80** with 9-borabicyclo[3.3.1]nonane (9-BBN) afforded the desired alcohols **2.75** and **2.76** in good yields (Scheme 2.8.).

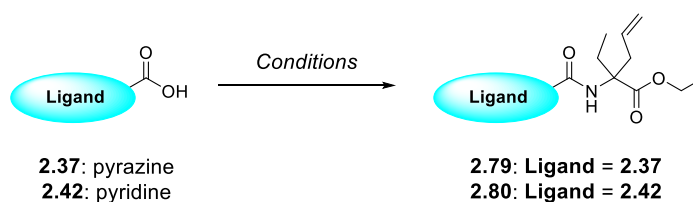
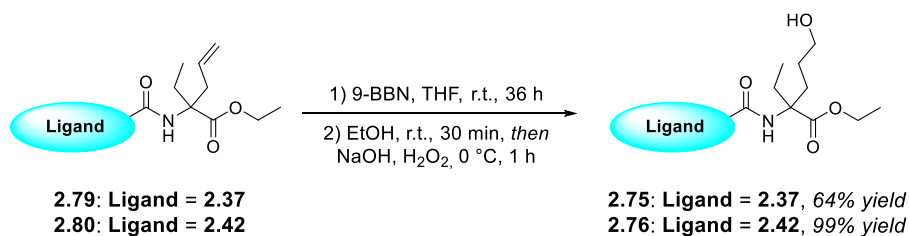


**Table 2.3. Coupling agents tested for the synthesis of amides 2.79 and 2.80.**

Entry	Coupling Agent	Result (Pyrazine 2.79)	Result (Pyridine 2.80)
1	HATU	No conversion	No conversion
2	HBTU	No conversion	No conversion
3	TBTU	32%	No conversion
4	PyBOP	41%	24%
5	BOP-Cl	No conversion	54%
6	DMTMM	72%	12%

Reaction conditions: carboxylic acid **2.37** or **2.42** (1.0 equiv.), amino ester **2.78** (1.0 equiv.), coupling agent (1.1 equiv.), DIPEA (5.0 equiv.), DCM (2 mL), room temperature, 24 h. For ligand structures *see* scheme 2.6.



**Scheme 2.8. Hydroboration-oxidation stepwise reaction of pyrazine 2.79 and pyridine 2.80.**

The following etherification step to generate probe precursor **2.74** (Scheme 2.6.) was particularly challenging. Both pyrazine and pyridine alcohols **2.75** and **2.76** (1.0 equiv.) were submitted to aliphatic ether formation conditions with tosyl- and triflate-activated PEG alcohols containing either *N*-Boc protected amine or a terminal azide for dye conjugation (1.5 equiv.). (*See* Supplementary table S-1,

Section 5.2.2. for more detailed information on the tested conditions.) For these attempts, different bases such as sodium hydride (7 to 12 equiv.), potassium *tert*-butoxide (7 equiv.) and lithium bases (LDA, LiHMDS, and *n*BuLi, 1.2 equiv.) were screened under varied temperatures ranging from –78 °C to room temperature for lithium bases and up to 70 °C heating for inorganic bases and in distinct solvents systems, such as tetrahydrofuran and dimethylformamide. However, none of these test settings led to *N*-Boc protected **2.74**. In particular, no conversion of starting material was observed when reactions were carried out at lower temperatures, and starting material degradation occurred with temperature increase. Moreover, the reaction duration (8 to 48 h) and the addition of more equivalents of base did not lead to an improved outcome. Therefore, an alternative approach for linker attachment was subsequently pursued.

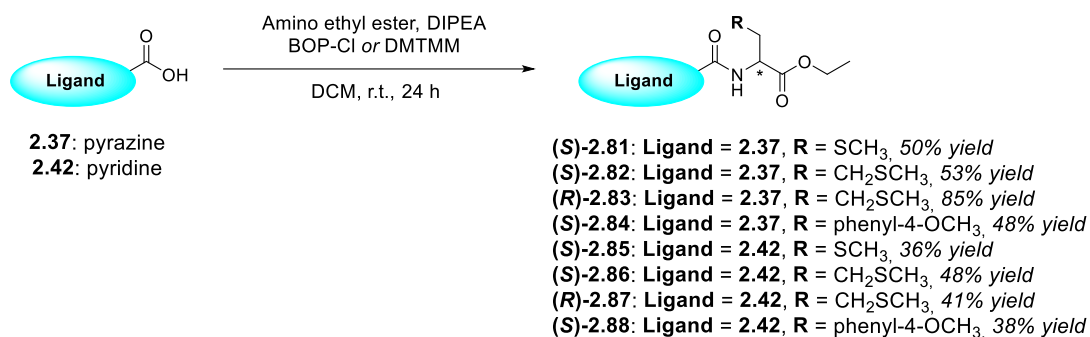
### **2.2.5. Small SAR of Unlabeled Ligands: Exploring Alternative Functionalities for Linker Attachment at the R<sup>3</sup>-Position**

The challenges encountered at the aliphatic ether formation step highlighted the poor suitability of this strategy for linker placement at the germinal diethyl portion of ligands **2.35** and **2.36** (Scheme 2.6., Section 2.2.4.). Therefore, a more general and reliable ligation handle was required for approaching this probe series. A prospective structure activity relationship (SAR) study was conducted to explore the tolerance of putative new conjugation sites at the pharmacophore. This analysis was also suitable for probing the relevance of the second ethyl substitution at the  $\alpha$ -carbon as well as the preferred enantiomeric configuration of the scaffold. To this end, unlabeled derivatives of **2.35** and **2.36** coupled to natural and non-proteinogenic, i.e., unnaturally encoded, amino esters were synthesized.

#### **2.2.5.1. Design and Synthesis of SAR Ligands**

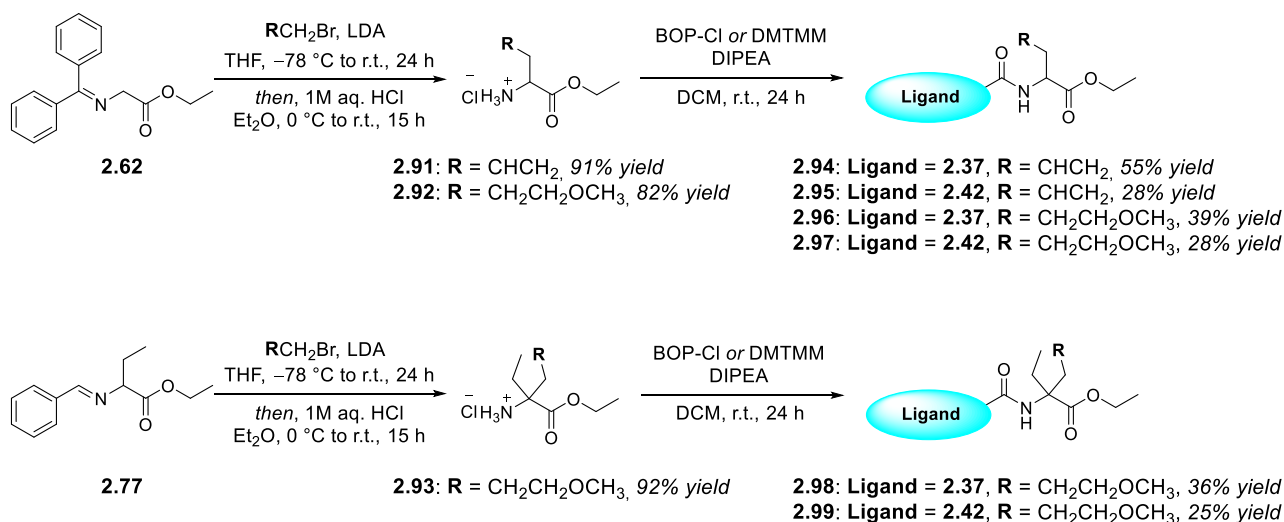
Natural amino acids, including cysteine, methionine, and tyrosine were selected for SAR investigations since their side chains provided potential thiol and phenol handles for linker conjugation. The respective thio- and aryl ether conjugates are accessible through a variety of mild reaction conditions,

which was crucial to avoid recognition element degradation upon linker installation. Both ether groups also had the advantage of not being hydrogen bond donors. Therefore, to suppress proton donating effects of the respective side chains, all amino acids were used as methyl ether conjugates (Scheme 2.9.). In addition, (*S*)- and (*R*)-enantiomers of methionine were evaluated for the influence of the ligand's chirality to CB<sub>2</sub>R binding. Amino ester derivatives of the selected natural amino acids were generated and conjugated to carboxylic acids pyrazine **2.37** and pyridine **2.42** using the previously established amide coupling conditions to afford the CB<sub>2</sub>R unlabeled ligands **2.81** to **2.88** (Scheme 2.9.).



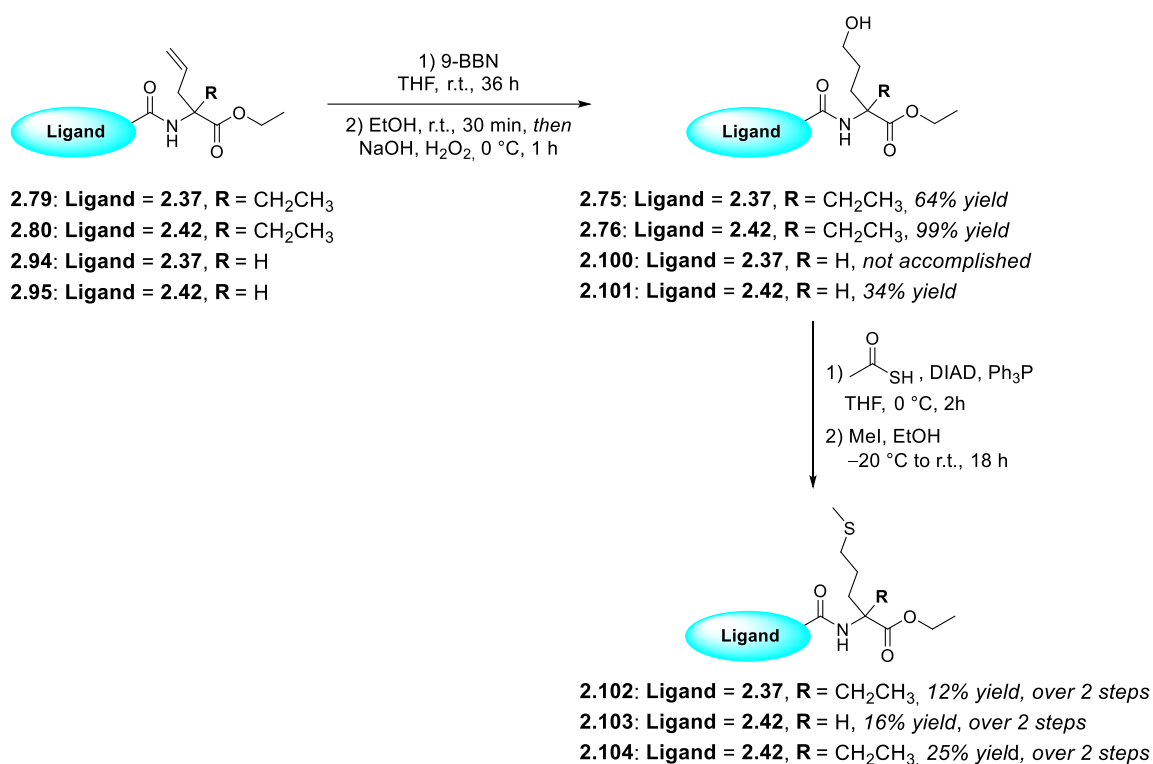
**Scheme 2.9. Synthesis of SAR ligands 2.81 to 2.88 based on natural amino acids.** Amino ethyl ester derivatives of: (*S*)-cysteine (**2.89**, R = SCH<sub>3</sub>), (*S*)-methionine (R = CH<sub>2</sub>SCH<sub>3</sub>), (*R*)-methionine (R = CH<sub>2</sub>SCH<sub>3</sub>), and (*S*)-tyrosine (**2.90**, R = phenyl-4-OCH<sub>3</sub>) were applied. For ligand structures *see* scheme 2.6., Section 2.2.4.

Non-proteinogenic amino esters bearing 3-methoxypropane and methyl propyl sulfide side chains were synthesized for comparing the influence of a thioether with an ether linkage to the binding affinity towards the CB<sub>2</sub>R (*see* **2.96**, **2.97** and **2.103**, Schemes 2.10. and 2.11.).



**Scheme 2.10. Synthesis of non-proteinogenic amino ester building blocks utilized for the preparation of SAR ligands 2.94 to 2.99.**

Furthermore, derivatives which encompass an ethyl substitution at the quaternary carbon were additionally prepared to evaluate the relevance of this moiety to the binding affinity (*see* **2.98**, **2.99**, **2.102** and **2.104**, Schemes 2.10. and 2.11.). For the synthesis of these ligands, diphenylmethylene protected glycine **2.62** and benzylidene protected **2.77** served as starting points (Scheme 2.10.). Introduction of the unnatural side chains was achieved using LDA as a base and either bromo-3-methoxypropane or allyl bromide as alkylating reagents. Subsequent acidic deprotection of the amine group led to the corresponding amino esters, which were coupled to acid building blocks **2.37** and **2.42** to yield the remaining SAR compounds **2.94** to **2.99** (Scheme 2.10.).



**Scheme 2.11.** Synthesis of non-proteinogenic amino ester building blocks utilized for the preparation of SAR ligands **2.101** to **2.104**.

Methyl sulfide amino esters were obtained in 3 steps from the allyl ligands **2.79**, **2.80**, and **2.95** (Scheme 2.11.). First, treatment of allyl derivatives with 9-BBN, followed by a base afforded primary alcohols **2.75**, **2.76** and **2.101** in moderate to good yields. Standard Mitsunobu conditions with thioacetic acid were applied to convert the alcohol functionality into a carbonylthio substituent, which could be cleaved *in situ* to the respective thiol upon basic treatment. Addition of iodomethane to the reaction mixture enabled the formation of the SAR ligands **2.102** to **2.104**. Several attempts were made for the synthesis of pyrazine monosubstituted **2.100** as congener of pyridine **2.101**, however, the alcohol

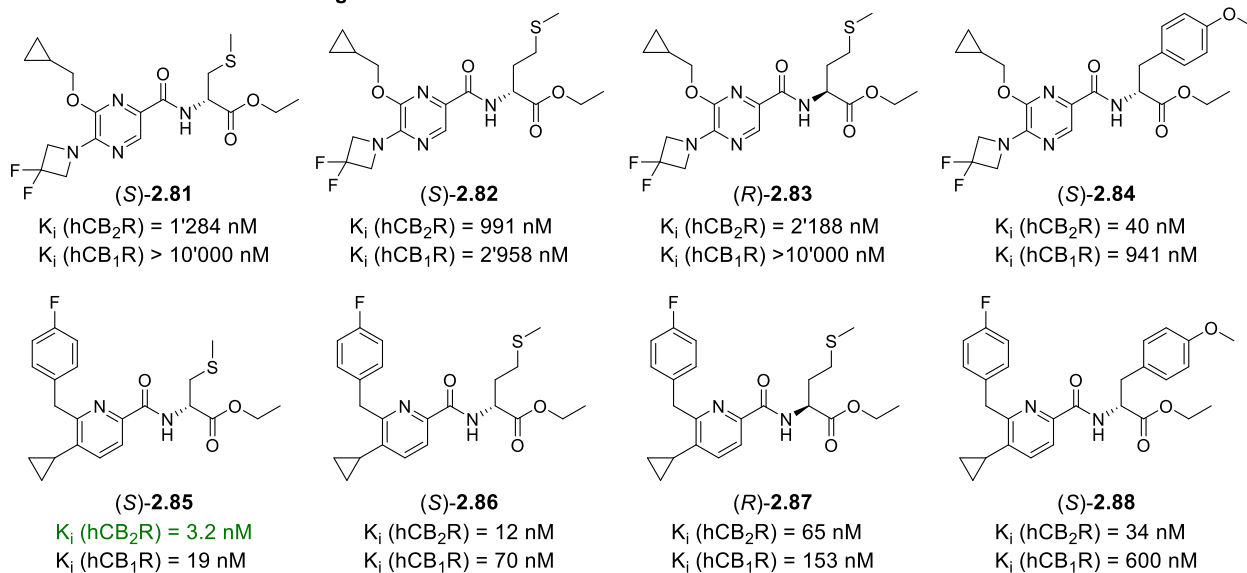
product was not formed at the hydroboration-oxidation step – instead, a complex mixture of unidentified side products was obtained. Of note, the use of other thiocarboxylic acids for the Mitsunobu protocol, such as thiobenzoic acid, led to the formation of highly lipophilic byproducts which required tedious purification and resulted in lower isolated yields than of intermediates **2.102** to **2.104**.

### 2.2.5.2. *In vitro* Pharmacology of SAR Ligands

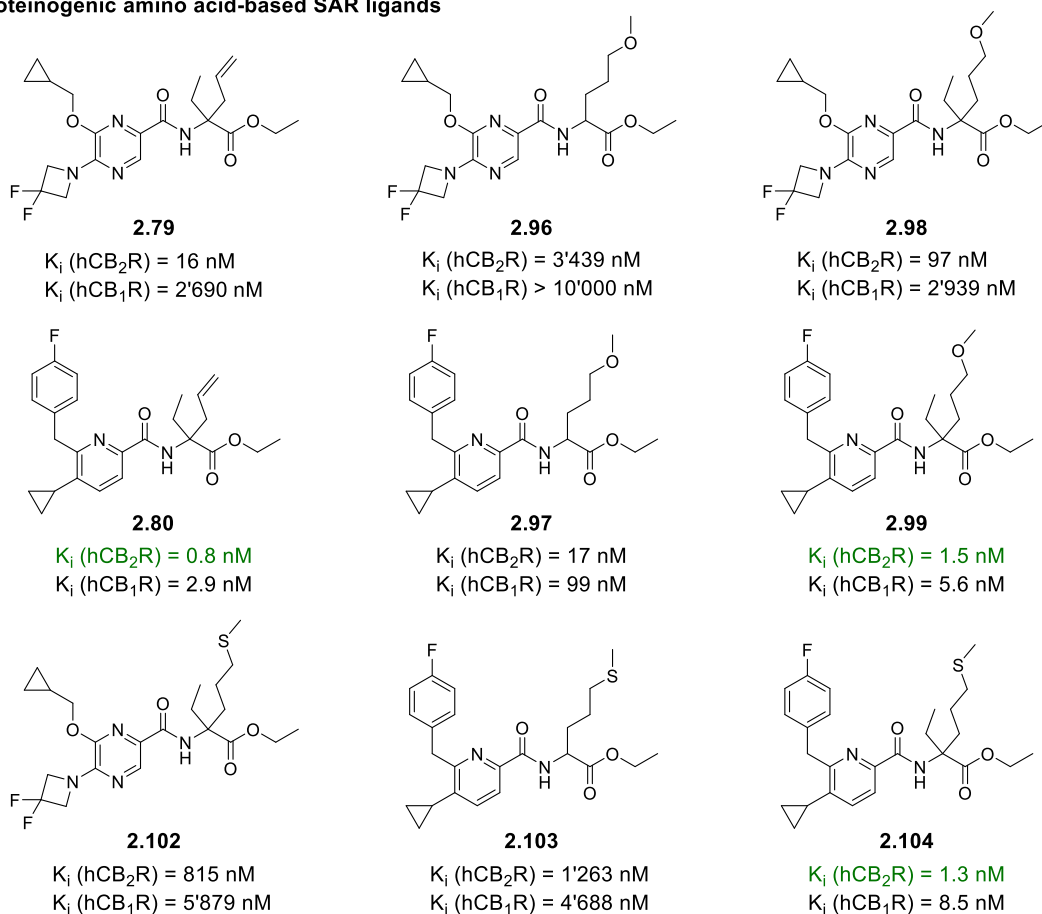
Compounds **2.79** to **2.88**, **2.94** to **2.99**, and **2.101** to **2.104** were subsequently evaluated in radioligand binding assays using membrane preparations of CHO cells overexpressing either human CB<sub>2</sub>R or CB<sub>1</sub>R which were performed by ELISABETH ZIRWES at Hoffmann La-Roche. The physicochemical parameters, i.e., PSA, AlogP, logD, aqueous solubility, and PAMPA of selected ligands were determined at Hoffmann La-Roche (Scheme 2.12 and Table 2.4.).

These studies indicated significant differences between the recognition element cores and provided valuable information about the tolerability of substitutions at the amino ester portion (Scheme 2.12 and Table 2.4.). Despite their structural similarity, pyridine **2.36** SAR analogs exhibited surprisingly higher affinity for CB<sub>2</sub>R compared to their corresponding pyrazine **2.35** derived congeners. The influence of the ethyl substitution motive at the  $\alpha$ -carbon position on ligand binding was confirmed as seen by the considerable loss in binding affinities of, e.g., methoxide ligand pairs  $\alpha$ - monosubstituted **2.97** vs.  $\alpha,\alpha$ -disubstituted **2.99** (cf. hCB<sub>2</sub>R K<sub>i</sub> of 17 nM vs. 1.5 nM, Table 2.4., entries 13 and 14) and methyl sulfide ligand pairs  $\alpha$ - monosubstituted **2.103** vs.  $\alpha,\alpha$ -disubstituted **2.104** (cf. hCB<sub>2</sub>R K<sub>i</sub> of 1263 nM vs. 1.3 nM, Table 2.4., entries 16 and 17). Initial investigations bearing enantiomeric pure (*S*)- and (*R*)-methionine derivatives anticipated a preference of the hCB<sub>2</sub>R towards (*S*)-configured derivatives up to fivefold (e.g., (*S*)-**2.86** vs. (*R*)-**2.87** cf. hCB<sub>2</sub>R K<sub>i</sub> of 12 nM vs. 65 nM, Table 2.4., entries 8 and 9). Introduction of allyl and anisyl side chains at the pyridine core were well tolerated by the receptor, e.g., allyl-**2.80** and anisyl-**2.88** (cf. hCB<sub>2</sub>R K<sub>i</sub> of 0.8 nM and 34 nM, Table 2.4., entries 2 and 10), indicating the feasibility for linker conjugation through thiol-ene *click*-reaction, metathesis, or Mitsunobu reactions.  $\alpha,\alpha$ -Disubstituted thioether **2.104** demonstrated equal potency to hCB<sub>2</sub>R and selectivity over hCB<sub>1</sub>R as the ether analog **2.99** (cf. **2.104**: hCB<sub>2</sub>R K<sub>i</sub> of 1.3 nM, hK<sub>i</sub> ratio CB<sub>1</sub>R/CB<sub>2</sub>R: 7 vs. **2.99**: 1.5 nM, hK<sub>i</sub> ratio CB<sub>1</sub>R/CB<sub>2</sub>R: 4, Table 2.4., entries 17 and 14).

### Natural amino acid-based SAR ligands



### Non-proteinogenic amino acid-based SAR ligands



**Scheme 2.12.** SAR ligands based on both natural and non-proteinogenic amino acids for evaluation of the new putative linker conjugation sites within recognition elements 2.35 and 2.36. Compounds with binding affinities towards the human CB<sub>2</sub>R lower than 10 nM are highlighted in green. Radioligand binding assays performed by ELISABETH ZIRWES at Hoffmann La-Roche.



**Table 2.4. SAR studies around the recognition elements pyrazine 2.35 and pyridine 2.36 as well as evaluation of selected physicochemical properties: Exploration of linker elongation options at the  $\alpha$ -position of the amino acid residue.**

Entry	Ligand	K <sub>i</sub> hCB <sub>2</sub> R [nM]	K <sub>i</sub> hCB <sub>1</sub> R [nM]	hK <sub>i</sub> ratio CB <sub>1</sub> R/CB <sub>2</sub> R	MW [g/mol]	PSA <sup>[a]</sup> [Å <sup>2</sup> ]	AlogP <sup>[b]</sup>	logD <sup>[c]</sup>	Kinetic solubility <sup>[d]</sup> [µg/mL]	PAMPA P <sub>eff</sub> <sup>[e]</sup> [10 <sup>-6</sup> cm/s] %Acceptor/%Membrane/%Donor <sup>[f]</sup>
1	<b>2.79</b>	16	2'690	169	438.5	75	3.5	n.d.	<0.6	2.21 2 / 69 / 28
2	<b>2.80</b>	0.8	2.9	3	424.5	53	3.5	n.d.	3.1	n.d.
3	<b>2.81</b>	1'284	>10'000	>8	430.5	76	2.3	3.6	n.d.	n.d.
4	<b>2.82</b>	991	2'958	3	444.5	77	2.4	3.6	n.d.	n.d.
5	<b>2.83</b>	2'188	>10'000	>5	444.5	77	2.4	3.6	n.d.	5.84 5 / 77 / 18
6	<b>2.84</b>	40	941	24	490.5	86	3.6	n.d.	<0.1	n.d.
7	<b>2.85</b>	3.2	19	6	416.5	54	4.1	n.d.	<0.1	n.d.
8	<b>2.86</b>	12	70	6	430.5	55	4.2	n.d.	<0.1	1.12 2 / 67 / 31
9	<b>2.87</b>	65	153	2	430.5	55	4.2	n.d.	n.d.	0 0 / 57 / 43
10	<b>2.88</b>	34	600	18	476.5	64	5.4	n.d.	1.6	n.d.
11	<b>2.96</b>	3'439	>10'000	>3	442.5	87	2.2	3.4	n.d.	4.27 9 / 39 / 52
12	<b>2.98</b>	97	2'939	30	470.5	85	3.1	3.3	4.1	0.58 1 / 55 / 44
13	<b>2.97</b>	17	99	6	428.5	65	4.0	3.3	0.6	0.66 1 / 75 / 24
14	<b>2.99</b>	1.5	5.6	4	456.6	63	4.9	n.d.	<0.1	n.d.
15	<b>2.102</b>	815	5'879	7	486.6	76	3.8	n.d.	n.d.	4.16 4 / 74 / 22
16	<b>2.103</b>	1'263	4'688	4	444.6	56	4.8	n.d.	1.4	0 0 / 61 / 40
17	<b>2.104</b>	1.3	8.5	7	472.6	54	5.6	n.d.	2.9	n.d.

n.d. – not determined. <sup>[a]</sup> Surface sum of all polar atoms in the molecule; <sup>[b]</sup> Calculated partition coefficient values (AlogP) based on the contribution of each atom to the logP;<sup>[173]</sup> <sup>[c]</sup> Distribution coefficient values in a water and 1-octanol mixture; <sup>[d]</sup> Solubility of the compound when diluted into aqueous environment from DMSO stock solution; <sup>[e]</sup> Parallel artificial membrane permeability assay (PAMPA) used to determine membrane permeation coefficient values (P<sub>eff</sub>);<sup>[175]</sup> <sup>[f]</sup> Percentage of compound found in acceptor, membrane and donor. Reference ligands data described in the Pharmacological Assessment, Section 5.2.10. Radioligand binding assays performed by ELISABETH ZIRWES at Hoffmann La-Roche. Kinetic solubility and PAMPA assays executed at Hoffmann La-Roche.

To assess the suitability of these compounds as recognition element precursors for probe development, the characterization of their physicochemical properties was carried out (Table 2.4). Special emphasis was put on lipophilicity and membrane permeation since these parameters are relevant for achieving sufficient exposures at the CB<sub>2</sub>R while counterbalancing the highly lipophilic and/or charged nature

of several fluorophores, such as Alexa- and Rhodamine-based dyes. The linker-dye construct has a significant impact on the molecular weight (MW) of the structure, thus pharmacophores with lower masses ( $MW < 500$  g/mol) were preferred. The ability to cross biological membranes is directly correlated with parameters such as the calculated polar surface area (PSA).<sup>[174]</sup> Particularly, a PSA value less than or equal to  $140 \text{ \AA}^2$  is an indicator of compound permeation through cellular membranes.<sup>[183]</sup> The SAR ligands correspond well to these criteria. While the molecular weight does not exceed 491 g/mol (cf. tyrosine derivative **2.84**, Table 2.4., entry 6), all molecules display PSA algorithms below  $140 \text{ \AA}^2$  (Table 2.4.). The passive membrane permeability of the SAR ligands was evaluated using the parallel artificial membrane permeability assay (PAMPA) model which was conducted at Hoffmann La-Roche. This method determines the permeation coefficient ( $P_{\text{eff}}$ ) of substances from a donor compartment, through a lipid-infused artificial membrane into an acceptor compartment, proving the concentration of the compound in all tested compartments – donor, membrane, and acceptor.<sup>[175]</sup> A permeation coefficient  $P_{\text{eff}}$  above  $0.5 \times 10^{-6}$  cm/s indicates passive membrane permeation, i.e., well partition of the molecule into the membrane to successfully reach the acceptor compartment. Here, methoxide pyrazine **2.96** exhibited the highest permeation coefficient and reached acceptor fractions of 9 % (Table 2.4., entry 11).

The lipophilicity contributes to the solubility, membrane permeability, and potency of ligands, having a strong impact on their selectivity profile.<sup>[184]</sup> It is experimentally measured as partition coefficients ( $\log P$ ) or as distribution coefficients ( $\log D$ ) of the ligand between water and an immiscible organic solvent, e.g., 1-octanol.<sup>[185]</sup> Whereas  $\log P$  is related solely with the non-ionizable portion of substrate in solution,  $\log D$  encompasses both ionized and non-ionized forms of the compound in the solvent phases and is measured at physiological pH. The lipophilicity of a compound should be adjusted to enable both good aqueous solubility and membrane permeability ( $2 < \log P < 3$ ).<sup>[186]</sup> All tested analogs displayed  $\log D$  values in the range of 3.3 to 3.6 (Table 2.4.) This result demonstrated the feasibility of these ligands to accommodate polar PEG-based linkers while maintaining favorable  $\log D$  values. In practice, calculated  $\log P$  values, such as  $\text{AlogP}$ ,<sup>[173]</sup> often replace measured lipophilicity when analyzing a set of novel ligands. Overall, pyrazine-based derivatives displayed best predicted lipophilicity as the pyridine series. Their  $\text{AlogP}$  spans from 2.3 for pyrazine cysteinylate **2.81** up to 5.6 for pyridine methyl sulfide **2.104** (Table 2.4., entries 3 and 17). The kinetic solubility assay provides the concentration of compound required for its precipitation in aqueous buffer and was conducted at Hoffmann La-Roche.<sup>[187]</sup> To resemble the conditions in *in vitro* binding assays, this measurement is performed by adding increased amounts of a solution of the compound in dimethyl sulfoxide into an aqueous buffer

until precipitation occurs. The SAR analogs with the best kinetic solubility concentrations are the allyl pyridine **2.80**, methoxide pyrazine **2.98**, and methyl sulfide pyridine **2.104** with values of 3.1, 4.1, and 2.9  $\mu\text{g/mL}$ , respectively (Table 2.4., entries 2, 12, and 17).

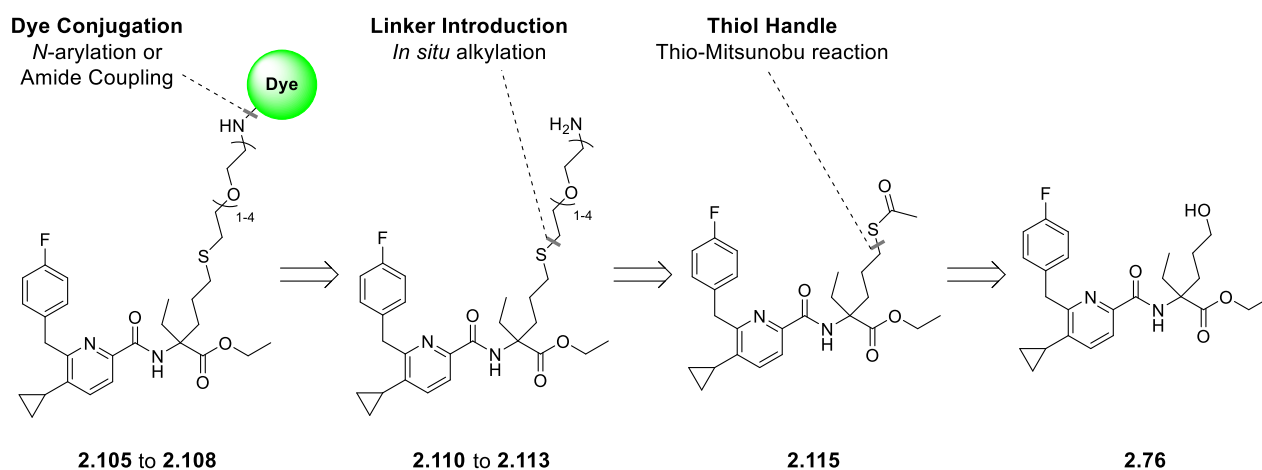
A careful evaluation of the *in vitro* pharmacology generated from SAR compounds (Scheme 2.12. and Table 2.4.), in combination with the molecular docking observations of linker composition, guided template selection for subsequent probe development. This analysis indicated that (i) modifications at the  $\alpha$ -carbon of the amino ester moiety of the recognition element construct were well tolerated by the hCB<sub>2</sub>R, demonstrating that this position could provide a good exit vector for linker placement towards the extracellular portion of the receptor, (ii) the pyridine scaffold provided better binding affinity profile as the pyrazine ligand series, thus it was selected for further investigations, (iii) the ethyl group substitution at the  $\alpha$ -carbon of the amino ester moiety was crucial for the SAR ligands to attain single digit nanomolar affinity at hCB<sub>2</sub>R (cf. 972-fold increase in hCB<sub>2</sub>R affinity for the  $\alpha,\alpha$ -disubstituted pyridine **2.104** over its monosubstituted congener **2.103**, Table 2.4., entries 16 and 17), (iv) a slight preference (fivefold) of the hCB<sub>2</sub>R for (*S*)-configured ligands was observed as seen by the (*S*)- and (*R*)-methionine congeners **2.86** and **2.87**, yet both compounds displayed affinities at the nanomolar range for the hCB<sub>2</sub>R, (v) the methyl sulfide construct **2.104** demonstrated equivalent binding and physicochemical properties as the methoxide analog **2.99**.

Taking these observations into account, linker elongation with a thioether while preserving the diethyl substitution motive at the  $\alpha$ -carbon position (ligand **2.104**) was preferred as the best template for further probe development.

### **2.2.6. Third Approach Towards CB<sub>2</sub>R-Selective Fluorescent Ligands: Probing the R<sup>3</sup>-Position with a Thioether Functionality for Linker Attachment**

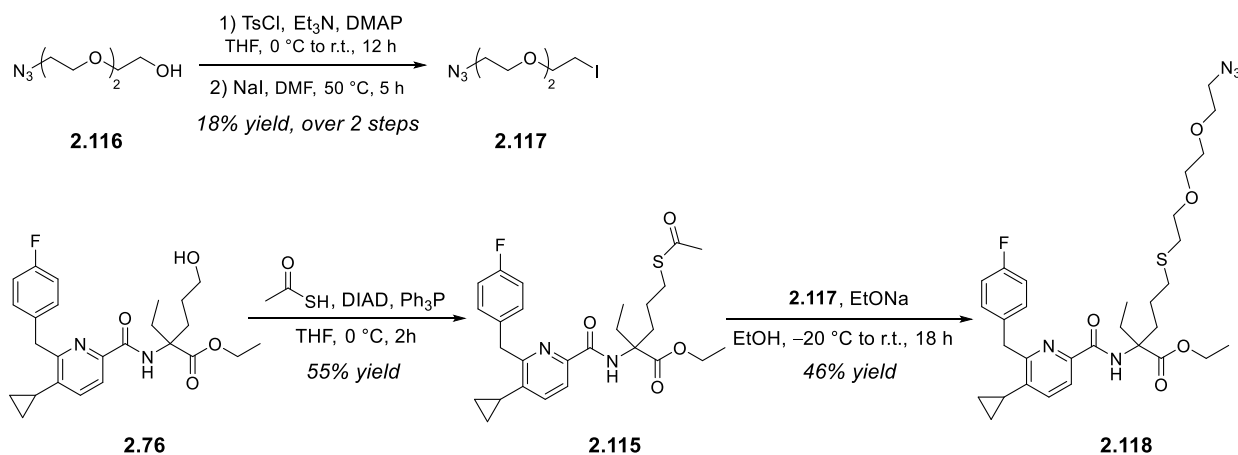
The preparation of racemic pyridine-based fluorescent ligands with a thioether handle for linker installation was developed upon the synthetic route of unlabeled congener **2.104** (Scheme 2.13.). Using this route, a thio-Mitsunobu reaction was employed to convert pyridine alcohol **2.76** into acetylthio intermediate **2.115**. This key intermediate could be cleaved under basic conditions to the

corresponding thiol and alkylated *in situ* with the desired linker chains to give recognition element-PEG-ylated linker constructs **2.110** to **2.113**. Treatment of amine probe precursors with NBD chloride could be performed to access racemic NBD-labeled congeners **2.105** to **2.108**.



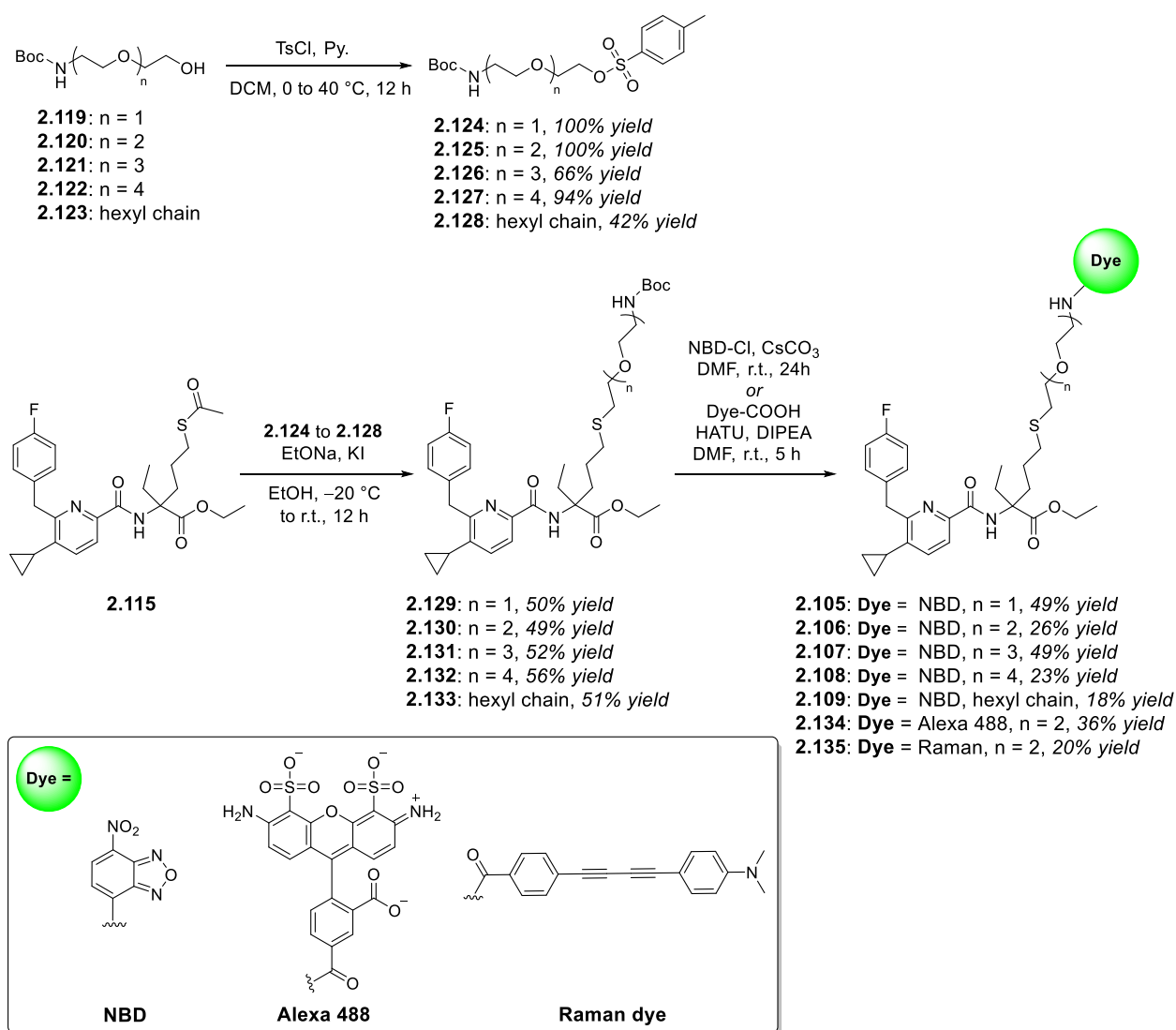
**Scheme 2.13.** Synthesis strategy for pyridine probe series **2.105** to **2.108**: Linker introduction through a thioether linkage at the geminal diethyl portion of the amino ester residue.

Initially, this route was tested applying iodinated azido-PEG2 linker **2.117** as a replacement for iodomethane, required for the preparation of SAR ligand **2.104** (see Scheme 2.11., Section 2.2.5.). Linker **2.117** was obtained in 2 steps from azido-PEG2 **2.116** with an overall low 18% yield and was subsequently subjected to identical conditions as for the synthesis of methyl sulfide **2.104** (Scheme 2.14.). Interestingly, azido-probe precursor **2.118** could be isolated in 25% yield from alcohol **2.76**, which is comparable to those previously obtained with iodomethane as an alkylating reagent. These results demonstrated the feasibility of this synthesis route for linker conjugation.



**Scheme 2.14.** Synthesis of probe precursor **2.118** using the protocol previously utilized for SAR ligand **2.104**.

A systematic investigation of the optimal linker length was next carried out based on racemic intermediate **2.115**. To this end, a modified procedure for linker installation was adopted to enable a straightforward synthesis of NDB-labeled **2.105** to **2.109** (Scheme 2.15). Alternatively to the iodination step used to prepare compound **2.118** bearing an azido-linker, compound **2.115** was directly treated with tosyl-PEG linkers **2.124** to **2.127** or tosyl-alkyl linker **2.128** to provide *N*-Boc protected **2.129** to **2.133**. For this conversion, catalytic amounts of potassium iodide (0.3 equiv.) were added in a Finkelstein type reaction conditions. Consecutive deprotection of the Boc group using trifluoroacetic acid and NBD conjugation allowed for assembling this probe series.



Scheme 2.15. Synthesis of pyridine-based racemic probe series labeled with NBD (**2.105** to **2.109**), Alexa 488 (**2.134**), and Raman dye (**2.135**).

Applying this procedure, NBD-labeled compounds containing different linker lengths ranging from one to four ethylene glycol units (**2.105** to **2.108**) and alkyl chain (**2.109**) were synthesized. Moreover, to validate the robustness of linker placement at the R<sup>3</sup>-position of the probe template and the chosen length, the bulkier and charged reporters Alexa 488 dye (**2.134**) and Raman dye (**2.135**) were coupled to racemic precursor **2.115** using HATU (Scheme 2.15.).

### 2.2.6.1. *In vitro* Pharmacology of Racemic Pyridine-based Probes

To verify the feasibility of this design approach with regard to CB<sub>2</sub>R affinity, the synthesized unlabeled intermediates and fluorescent ligands were submitted to *in vitro* profiling. These assays were performed by ELISABETH ZIRWES and ANJA OSTERWALD at Hoffmann La-Roche using membrane preparations of CHO cells overexpressing both human and mouse CB<sub>2</sub>R or human CB<sub>1</sub>R. The *in vitro* results were used to guide synthesis efforts and select the most suitable linker length for generating high-quality probes targeting the CB<sub>2</sub>R (Table 2.5.).

Racemic azido-derivative **2.118** displayed remarkable 60 nM affinity for the human CB<sub>2</sub>R and eightfold selectivity over the hCB<sub>1</sub>R (Table 2.5., entry 1). In addition, unlabeled **2.118** maintained low nanomolar affinity also towards mouse CB<sub>2</sub>R (c.f. mCB<sub>2</sub>R K<sub>i</sub> of 52 nM). In functional cAMP assays this intermediate was a potent agonist of the CB<sub>2</sub>R while retaining the high selectivity over hCB<sub>1</sub>R (c.f. hCB<sub>2</sub>R EC<sub>50</sub> of 1.9 nM and mCB<sub>2</sub>R EC<sub>50</sub> of 5.4 nM, hEC<sub>50</sub> ratio CB<sub>1</sub>R/CB<sub>2</sub>R > 10'000 nM). The performance of analog **2.118** in binding assays confirmed that linker elongation at the R<sup>3</sup>-position of the pyridine scaffold was well tolerated by the CB<sub>2</sub>R.

Subsequent evaluation of the linker length influence on binding affinity, selectivity, and potency revealed NBD construct with two ethylene glycol linker units **2.106** as the most favorable with regard to CB<sub>2</sub>R affinity (Table 2.5., entry 13). In particular, this NBD-derivative displayed potent agonistic effect at the human CB<sub>2</sub>R exhibiting 4.7 nM functional affinity in the cAMP assay towards hCB<sub>2</sub>R and 128-fold functional selectivity over the hCB<sub>1</sub>R at the (Table 2.5., entry 13). Despite the high PSA values of racemic NBD-congeners PEG3-**2.107**, PEG4-**2.108**, and alkyl-**2.109** (>140 Å, Table 2.5., entries 14, 15, and 16),<sup>[174]</sup> these compounds were presumably able to permeate biological membranes as demonstrated by the PAMPA assay<sup>[175]</sup> (cf. 0.65, 0.70, and 0.50 x10<sup>-6</sup> cm/s, respectively).

**Table 2.5. Linker studies on pyridine 2.36: Elongation vector at the  $\alpha$ -position of the amino acid residue.**

Entry	Probe ( $\pm$ )-		$K_i$ [nM]			$hK_i$ ratio CB <sub>1</sub> R/ CB <sub>2</sub> R	cAMP EC <sub>50</sub> <sup>[a]</sup> [nM] (%eff.)			MW [g/ mol]	PSA <sup>[b]</sup> [Å <sup>2</sup> ]	AlogP <sup>[c]</sup>	logD <sup>[d]</sup>	Kin. sol. <sup>[e]</sup> [μg/ mL]	PAMPA P <sub>eff</sub> <sup>[f]</sup> [10 <sup>-6</sup> cm/s]	
			hCB <sub>2</sub> R	hCB <sub>1</sub> R	mCB <sub>2</sub> R		hCB <sub>2</sub> R	hCB <sub>1</sub> R	mCB <sub>2</sub> R						%Acc./ %Memb./ %Donor <sup>[g]</sup>	
1	<b>2.118</b>		60	464	52	8	1.9 (93)	>10 <sup>0</sup> 000	5.4 (93)	615.8	116	6.1	n.d.	<0.1	n.d.	
2	<b>2.129</b>		112	1'297	389	12	3.2 (87)	>10 <sup>0</sup> 000	15 (90)	645.8	94	6.2	n.d.	<0.3	n.d.	
3	<b>2.130</b>		164	1'141	213	7	36 (93)	>10 <sup>0</sup> 000	131 (81)	689.9	102	6.1	n.d.	<0.1	0 0 / 79 / 21	
4	<b>2.131</b>		138	589	117	4	10 (91)	>10 <sup>0</sup> 000	21 (87)	733.9	111	6.0	n.d.	<0.2	n.d.	
5	<b>2.132</b>		140	731	93	5	13 (91)	>10 <sup>0</sup> 000	31 (84)	778.0	120	5.9	n.d.	<0.2	n.d.	
6	<b>2.133</b>		140	1'385	367	10	7.7 (85)	>10 <sup>0</sup> 000	78 (78)	657.9	86	7.9	n.d.	<0.1	n.d.	
7	<b>2.110</b>		60	200	10	3	8.2 (93)	0.6 (52)	13 (92)	545.7	84	4.6	2.7	98	0.29 1 / 48 / 51	
8	<b>2.111</b>		38	433	9.8	11	28 (92)	822 (96)	45 (93)	589.8	93	4.5	2.6	210	0 0 / 64 / 36	
9	<b>2.112</b>		18	724	2.8	41	9.9 (93)	146 (72)	14 (93)	633.8	101	4.4	2.7	168	0.28 1 / 41 / 58	
10	<b>2.113</b>		2.6	164	n.d.	63	n.d.	n.d.	n.d.	677.9	110	4.3	n.d.	>723	n.d.	
11	<b>2.114</b>		2.7	204	n.d.	75	n.d.	n.d.	n.d.	557.8	76	6.3	n.d.	0.3	n.d.	
12	<b>2.105</b>		22	418	59	19	171 (121)	2'059 (152)	181 (118)	708.8	151	6.4	n.d.	2	n.d.	
13	<b>2.106</b>		22	383	73	17	4.7 (100)	600 (126)	102 (123)	752.9	160	6.3	2.8	9	n.d.	
14	<b>2.107</b>		27	460	85	17	9.2 (100)	789 (96)	74 (113)	796.9	169	6.1	n.d.	14	0.65 2 / 38 / 61	
15	<b>2.108</b>		38	617	118	16	20 (102)	1'121 (110)	192 (117)	841.0	177	6.0	n.d.	6.1	0.70 2 / 45 / 53	
16	<b>2.109</b>		55	1'072	144	19	9.9 (100)	928 (122)	142 (122)	720.9	143	8.1	n.d.	14	0.50 2 / 12 / 87	
17	<b>2.134</b>		3.6	206	n.d.	57	12 (95)	>10 <sup>0</sup> 000	39 (77)	1'106.2	251	5.3	n.d.	n.d.	0 0 / 99 / 1	
18	<b>2.135</b>		40	713	n.d.	18	0.6 (95)	790 (74)	199 (88)	861.1	99	n.d.	n.d.	n.d.	0 0 / 9 / 91	

A – Alexa, n.d. – not determined. <sup>[a]</sup> Functional potency (cAMP assay), percentage efficacy (%eff.) given in parenthesis; <sup>[b]</sup> Surface sum of all polar atoms in the molecule; <sup>[c]</sup> Calculated partition coefficient values (AlogP) based on the contribution of each atom to the logP; <sup>[173]</sup> <sup>[d]</sup> Distribution coefficient values in a water and 1-octanol mixture; <sup>[e]</sup> Kinetic Solubility (Kin. sol.) of the compound when diluted into aqueous environment from DMSO stock solution; <sup>[f]</sup> Parallel artificial membrane permeability assay (PAMPA) used to determine membrane permeation coefficient values (P<sub>eff</sub>); <sup>[175]</sup> <sup>[g]</sup> Percentage of compound found in acceptor (Acc.), membrane (Memb.), and donor. Reference ligands data described in the Pharmacological Assessment, Section 5.2.10. Radioligand binding assays performed by ELISABETH ZIRWES and cAMP functional assays performed by ANJA OSTERWALD at Hoffmann La-Roche. Kinetic solubility and PAMPA assays were conducted at Hoffmann La-Roche.

To analyze the PEG2 linker length robustness towards different reporter units, bulkier and charged fluorophores Alexa 488 (**2.134**) and Raman dye (**2.135**) were investigated (Table 2.5., entries 17 and

18). As for NBD-labeled **2.106**, analogs **2.134** and **2.135** also exhibited agonist activity at hCB<sub>2</sub>R with low nanomolar binding to the target GPCR in both affinity and functional cAMP assays (cf. **2.134**: hCB<sub>2</sub>R K<sub>i</sub> of 3.6 nM and EC<sub>50</sub> of 12 nM and **2.139**: hCB<sub>2</sub>R K<sub>i</sub> of 40 nM and EC<sub>50</sub> of 0.6 nM). Consequently, further synthetic efforts towards enantiomerically pure probe scaffolds were conducted using PEG2 linker lengths.

### 2.2.7. Synthesis of Enantiomeric Pure Fluorescent CB<sub>2</sub>R-Probes

The linker attachment at one arm of the geminal diethyl moiety generated a quaternary chiral center at the  $\alpha$ -carbon of the amino ester residue. To understand the influence of the absolute configuration on compound affinity and activity, enantiomer pairs of *N*-Boc protected probe precursor **2.130** and NBD-labeled **2.106** were investigated.

#### 2.2.7.1. Determination of the Absolute Configuration

Suitable chiral resolution strategies for achieving an enantiomeric pure probe series were investigated in collaboration with KENNETH ATZ, BENJAMIN BERNNECKE, and ANDRE ALKER. Chiral separation of the racemic mixtures **2.130** and **2.106** through high-pressure liquid chromatography (HPLC) and supercritical fluid chromatography (SFC) – testing various combinations of chiral columns and solvent systems – was largely unsuccessful. Due to the high polarity of the PEG component and the flexibility of both scaffolds, enantiomeric separation of ( $\pm$ )-**2.130** and ( $\pm$ )-**2.106** was deemed unfeasible. In addition, these features would likely interfere with the determination of the absolute configuration of the corresponding enantiomer pairs via crystallography. Therefore, allyl amino ester building block **2.78** was chosen for further optical resolution efforts and determination of the absolute configuration of advanced intermediates. The rationale behind this decision was the facile preparation of ( $\pm$ )-**2.78** in gram scale which would not interfere with the overall yield of the synthetic route. Furthermore, envisioning future applications of this probe design, modifications at the stage of amino ester **2.78** would allow for a modular synthesis approach to enantiomeric pure derivatives – where the recognition element, amino ester-PEG2 linker, and fluorophore could be independently prepared.



Optical resolution of the racemic mixture **2.78** turned out to be extremely challenging. Using diastereomeric salt formation methods,<sup>[188]</sup> various chiral salts were screened, including camphor sulfonic acid, mandelic acid, lactic acid, dibenzoyl tartaric acid as well as tartaric acid, using different solvent and temperature systems (*see* Supplementary table S-2, Section 5.2.2. for more detailed information on the tested conditions). Salt pair (2*S*, 3*S*)- and (2*R*, 3*R*)-dibenzoyl tartaric acid in isopropanol gave the best separation results, however they were not satisfactory, leading to maximal 30% enantiomeric excess (*ee*) after several recrystallization rounds.

Enzyme-mediated kinetic resolution<sup>[189]</sup> attempts using four different commercially available enzymes, i.e., esterase from porcine liver (PLE), Alcalase® 2.4 L, Lipase Novozyme® 435, and Acylase I from porcine kidney, did not lead to conclusive results as, in all of the cases, amino ester **2.78** could not be extracted from the reaction mixture. Furthermore, kinetic resolution via amide coupling was tackled. This methodology relied on the principle that certain chiral amino acids, such as tosyl-(*S*)-proline<sup>[190]</sup> and (*R*)-*O*-acetylmandelic acid,<sup>[191]</sup> tend to form preferentially amides with one enantiomer of the racemic amine. Such a reactivity would lead to the isolation of the unreacted amine partner from the reaction mixture using either common column chromatography or precipitation techniques.

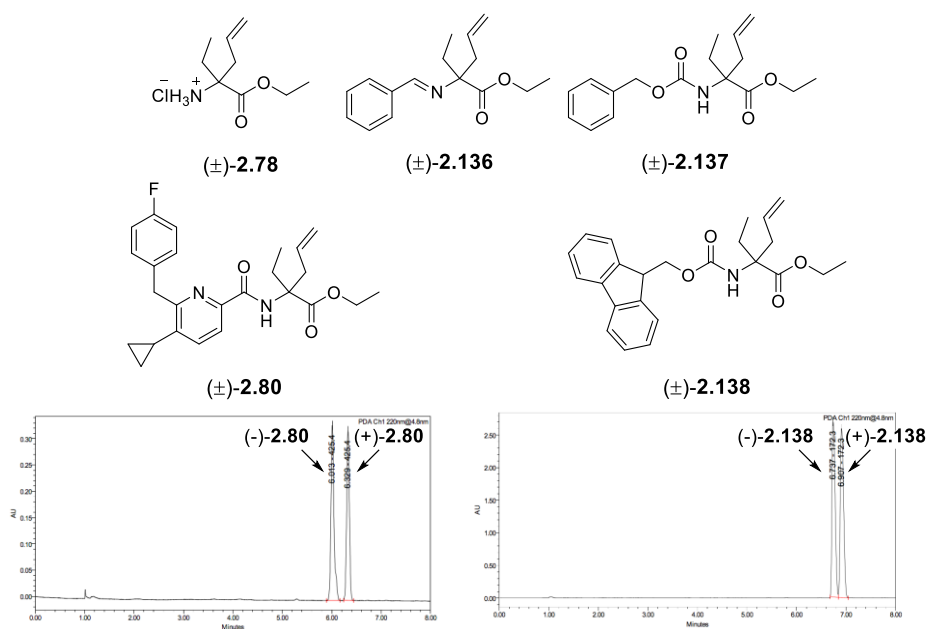


**Figure 2.14. Chiral HPLC and SFC separation attempts for racemic amino ester **2.78** and different analogs.** Enantiomeric separation of amino ester **2.78**, benzylidene protected-**2.136**, and Cbz protected-**2.137** was not accomplished due to high polarity and lack of UV-signal of these derivatives. Separation of the components of racemates **2.80** and **2.138** was possible using both techniques as shown by the chiral HPLC chromatograms below their structure. The chiral separation experiments were conducted by KENNETH ATZ at Hoffmann La-Roche, conditions are described in the Experimental Procedures, Section 5.1.

Nevertheless, the amide coupling of these chiral compounds with amine **2.78** resulted in a racemic salt with no enantioselectivity.

Both chiral HPLC and SFC were also applied for the enantiomeric separation of ( $\pm$ )-**2.78** and selected derivatives, including pyridine **2.80**, as well as benzylidene (**2.136**), Cbz (**2.137**) and Fmoc (**2.138**) protected analogs (Figure 2.14.). Using these methodologies, pyridine **2.80** and Fmoc-protected **2.138** could be separated into their enantiomeric pure constituents which were subjected to crystallization experiments. The use of chiral salts, such as dibenzoyl tartaric acid, did not induced crystal formation of enantiomer pairs **2.80** and **2.138**. To circumvent this issue, the amine group of (-)-**2.138** was modified for introducing different groups which could lead to the formation of a crystalline product, e.g., tosyl-(*S*)-proline, tosyl, and (*R*)-*O*-acetylmandelic acid. This attempt led to the assignment of compound (-)-**2.138** as the (*R*)-enantiomer as shown by the X-ray structure of its tosyl-(*S*)-proline congener **2.139** (Figure 2.15.).

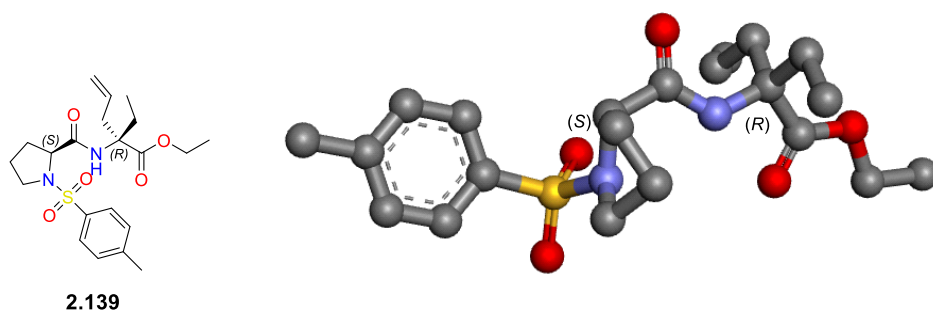
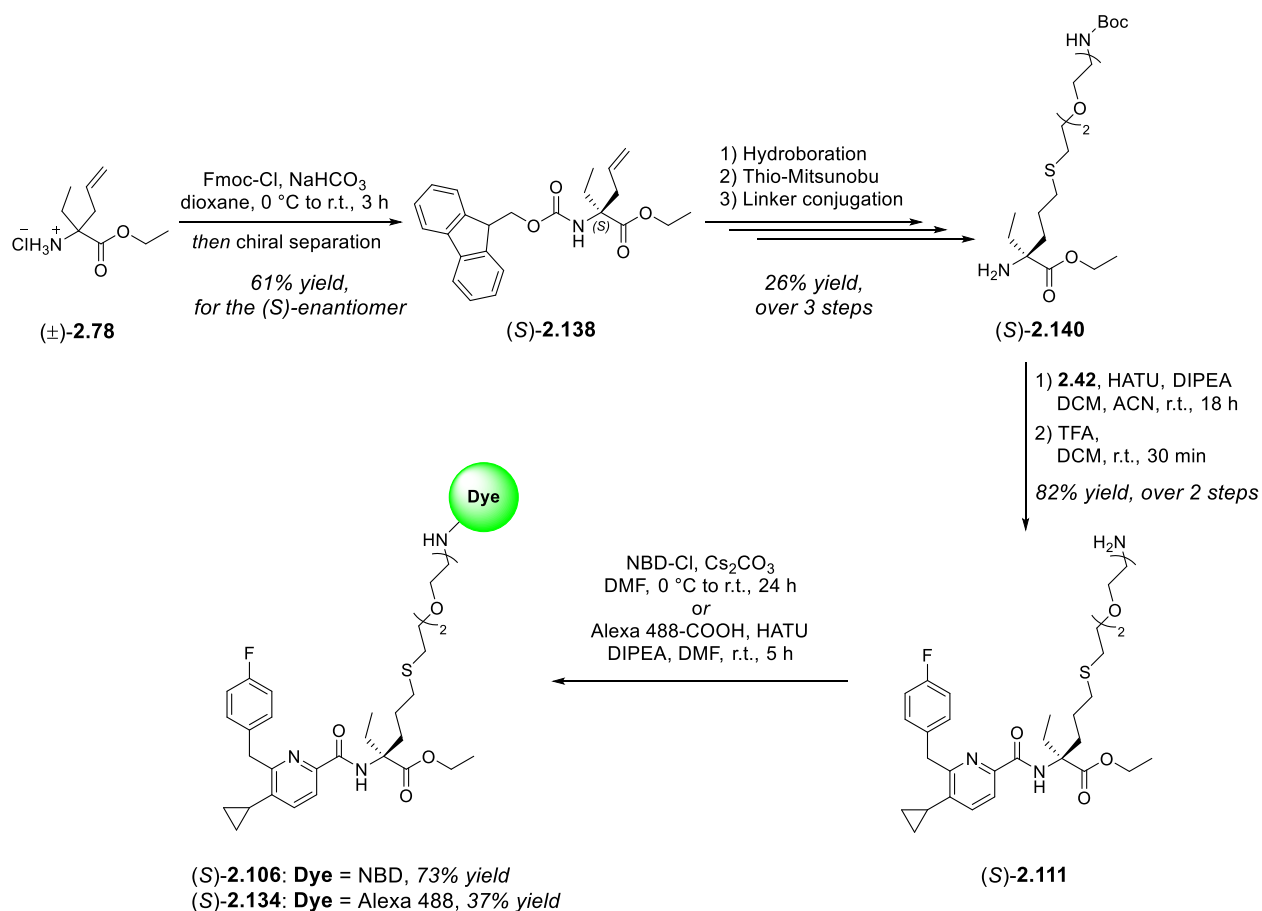


**Figure 2.15.** X-ray structure of tosyl-(*S*)-proline (*R*)-**2.139** derivative used to assign the absolute configuration of this probe series. The synthesis of compound **2.139** was performed by BENJAMIN BRENNER at FMP; X-ray measurement performed by ANDRE ALKER at Hoffmann La-Roche.

### 2.2.7.2. Synthesis and *in vitro* Binding Evaluation of Enantiomeric Pure CB<sub>2</sub>R-Ligands

Using Fmoc as a protective group for building block **2.78** was also well-suited to the modular concept pursued for the synthesis of this probe series. Based on this building block, a synthesis route for enantiomeric pure congeners was developed (Scheme 2.16.). In collaboration with BENJAMIN

BRENNECKE, this route was exploited for generating both (*S*)- and (*R*)-configured fluorescent analogs labeled with both NBD (**2.106**) and Alexa 488 (**2.134**). In brief, hydroboration-oxidation stepwise reaction sequence of enantiomeric pure Fmoc-protected **2.138**, followed by thio-Mitsunobu reaction, enabled the concomitant introduction of the desired PEG2 linker chain and its amine deprotection under basic conditions, providing amino ester-linker construct **2.140**. Subsequent amide coupling of **2.140** with picolinic acid **2.42** using HATU and consecutive removal of the Boc protecting group led to the final assembly step of the respective fluorescent probes (*R*) and (*S*)-NBD (**2.106**) and Alexa 488 (**2.134**).



**Scheme 2.16. Synthesis approach to enantiomeric pure CB<sub>2</sub>R-selective fluorescently labeled probes (S)-2.106 and (S)-2.134.** This synthesis route was also applied for (*R*)-configured **2.106** and **2.134**, leading to similar yields. Intermediate **2.111** was prepared using identical conditions as for the racemic probe series described in Scheme 2.11., Section 2.2.5. and Scheme 2.15., Section 2.2.6. For fluorophore structures *see* Figure 2.13., Section 2.2.1. The synthesis of (*S*) and (*R*)-configured intermediate **2.111** and (*R*)-**2.134** was performed by BENJAMIN BRENNECKE.

Enantiomer pairs of probe precursor **2.111**, NBD-labeled **2.106**, and Alexa 488-labeled **2.134** were subjected to *in vitro* binding and functional characterization at human and mouse CB<sub>2</sub>R and human CB<sub>1</sub>R (Table 2.6.). These assays were carried out by ELISABETH ZIRWES and ANJA OSTERWALD at

Hoffmann La-Roche. A comparison of the enantiomer pair of precursor **2.111** binding data indicated that there was sufficient space around the quaternary carbon junction within the binding cavity for accommodating both stereoisomers (cf. (*S*)-**2.111** hCB<sub>2</sub>R K<sub>i</sub> of 2.7 nM vs. (*R*)-**111** hCB<sub>2</sub>R K<sub>i</sub> of 4.6 nM, Table 2.6., entries 2 and 3). A similar observation was made for fully labeled Alexa 488 probe pair **2.134** (cf. (*S*)-**2.134** hCB<sub>2</sub>R K<sub>i</sub> of 44 nM vs. (*R*)-**2.134** hCB<sub>2</sub>R K<sub>i</sub> of 62 nM, Table 2.6., entries 7 to 9), where only 1.4-fold enantio-discrimination with regard to hCB<sub>2</sub>R binding affinity favoring the (*S*)-enantiomer was observed. The discrepancies between the biological data obtained from racemic Alexa 488-**2.134** and its enantiomeric pure congeners might derive from batch-to-batch intrinsic differences from *in vitro* assays as well as the purity and stability of purchased Alexa 488 carboxylic acid. Remarkably, for NBD-labeled probe pair **2.106** the enantio-discrimination favoring the (*S*)-enantiomer was more evident (18-fold, cf. (*S*)-**2.106** hCB<sub>2</sub>R K<sub>i</sub> of 9.1 nM vs. (*R*)-**2.106** hCB<sub>2</sub>R K<sub>i</sub> of 159 nM, Table 2.6., entries 4–6). Likewise, binding of both NBD- (*S*)-**2.106** and Alexa 488- (*S*)-**2.134** labeled (*S*)-enantiomers to mouse CB<sub>2</sub>R was also more pronounced with a 19- and 4-fold difference, respectively (cf. (*S*)-**2.106**: mCB<sub>2</sub>R K<sub>i</sub> of 33 nM vs. (*R*)-**2.106** mCB<sub>2</sub>R K<sub>i</sub> of 622 nM; and (*S*)-**2.134**: hCB<sub>2</sub>R K<sub>i</sub> of 28 nM vs. (*R*)-**2.134** hCB<sub>2</sub>R K<sub>i</sub> of 104 nM, Table 2.6., entries 4–9).

**Table 2.6. Key characteristics of recognition element pyridine 2.36, labeling precursor 2.111 and fluorescent probes 2.106 and 2.134.**

Entry	Ligand	Dye	K <sub>i</sub> [ <sup>a</sup> ] [nM]				hK <sub>i</sub> ratio CB <sub>1</sub> R/ CB <sub>2</sub> R	cAMP EC <sub>50</sub> [ <sup>b</sup> ] [nM] (%eff.)			hEC <sub>50</sub> ratio CB <sub>1</sub> R/ CB <sub>2</sub> R
			hCB <sub>2</sub> R	hCB <sub>1</sub> R	mCB <sub>2</sub> R	mCB <sub>1</sub> R		hCB <sub>2</sub> R	hCB <sub>1</sub> R	mCB <sub>2</sub> R	
1	<b>2.36</b>	n.a.	0.2	5.4	1.8	8.5	27	0.7 (102)	4.4 (99)	1.9 (99)	6.3
2	( <i>S</i> )- <b>2.111</b>	n.a. (NH <sub>2</sub> )	2.7	64	2.6	229	23	0.5 (91)	57 (84)	3.2 (91)	114
3	( <i>R</i> )- <b>2.111</b>	n.a. (NH <sub>2</sub> )	4.6	180	13	163	39	11 (81)	>10 <sup>000</sup>	424 (61)	>909
4	(±)- <b>2.106</b>	NBD	22	383	73	n.d.	17	4.7 (100)	600 (126)	102 (123)	128
5	( <i>S</i> )- <b>2.106</b>	NBD	9.1	617	33	691	68	2.2 (72)	>10 <sup>000</sup>	21 (95)	>4 <sup>545</sup>
6	( <i>R</i> )- <b>2.106</b>	NBD	159	4 <sup>925</sup>	622	n.d.	31	17 (84)	>10 <sup>000</sup>	1 <sup>093</sup> (69)	>588
7	(±)- <b>2.134</b>	Alexa488	3.6	206	n.d.	n.d.	57	12 (95)	>10 <sup>000</sup>	39 (77)	847
8	( <i>S</i> )- <b>2.134</b>	Alexa488	44	321	28	>10 <sup>000</sup>	7	1.3 (100)	86 (109)	n.d.	64
9	( <i>R</i> )- <b>2.134</b>	Alexa488	62	1 <sup>114</sup>	104	n.d.	18	12 (101)	343 (104)	14 (109)	28

n.a. – not applicable, n.d. – not determined. [<sup>a</sup>] mCB<sub>1</sub>R data generated using mouse brain membranes; [<sup>b</sup>] Functional potency (EC<sub>50</sub>), percentage efficacy (%eff.) given in parenthesis. Reference ligands data described in the Pharmacological Assessment, Section 5.2.10. Radioligand binding assays performed by ELISABETH ZIRWES and cAMP functional assays performed by ANJA OSTERWALD at Hoffmann La-Roche.

### 2.2.7.3. Development of a CB<sub>2</sub>R-Fluorescent Probe Toolbox

The promising binding data obtained for the (*S*)-configured fluorescent ligands NBD-**2.106** and Alexa 488-**2.134** (Table 2.6., Section 2.2.7.) motivated the synthesis of additional probes exploiting (*S*)-amine **2.111** as a template (Figure 2.16.). The strategy applied previously for the preparation of Alexa 488-labeled **2.134** (Scheme 2.16., Section 2.2.7.) was utilized by BENJAMIN BRENNECKE, DR. YELENA MOSTINSKI, MARIE WEISE, and LEONARD MACH for introducing diverse fluorescent labels tailored toward subsequent biological investigations, such as AttoThio12 (**2.141**), Silicon-Rhodamine (SiR, **2.142**), cyanine 5.5 (Cy5.5, **2.143**), and biotin (**2.144**) (Figure 2.16.).

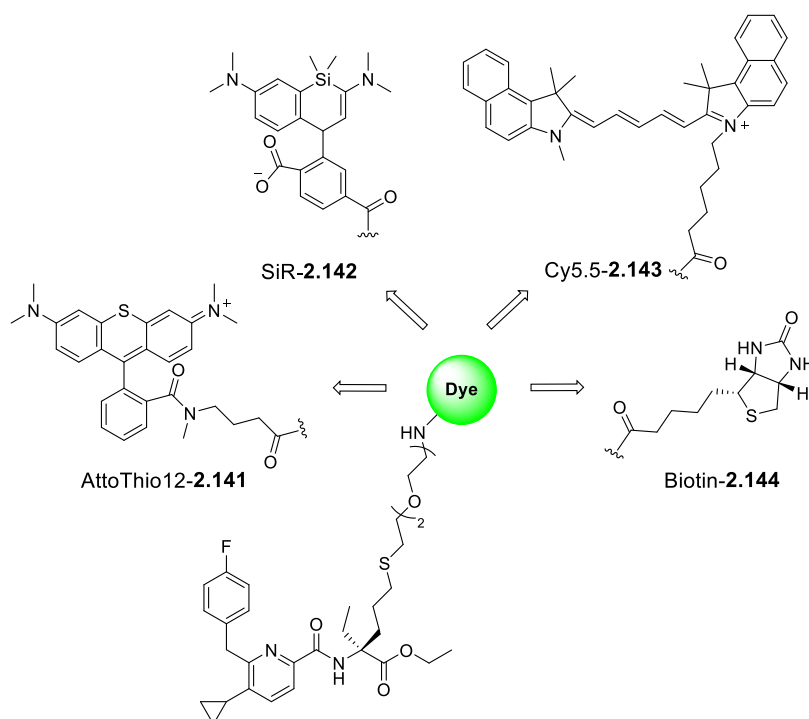


**Figure 2.16.** Structure of the conjugated fluorophores for the generation of the probes AttoThio12-**2.141**, SiR-**2.142**, Cy5.5-**2.143**, and biotinylated-**2.144** from probe precursor (*S*)-**2.111**. These probes were synthesized by BENJAMIN BRENNECKE (SiR-**2.142** and Cy5.5-**2.143**), DR. YELENA MOSTINSKI (AttoThio12-**2.141** and SiR-**2.142**), MARIE WEISE (Biotin-**2.144**), and LEONARD MACH ((*S*)-**2.111** re-synthesis).

The fluorescently labeled derivatives (*S*)-**2.141** to (*S*)-**2.144** were subjected to in depth molecular pharmacology profiling which were conducted by ELISABETH ZIRWES and ANJA OSTERWALD at Hoffmann La-Roche using membrane preparations of CHO cells overexpressing either human and mouse CB<sub>2</sub>R or human CB<sub>1</sub>R (Table 2.7.). In all cases the high potency, selectivity, and agonistic function of the probe were preserved despite linker introduction and demonstrated to be largely independent of nature, size, and functionality of the attached fluorophore. These CB<sub>2</sub>R-selective

fluorescent ligands were also capable of preserving interspecies affinity and selectivity for both mouse and human CB<sub>2</sub>R. For example, AttoThio12 analog **2.141** (hCB<sub>2</sub>R K<sub>i</sub> of 3.2 nM and mCB<sub>2</sub>R K<sub>i</sub> of 4.6 nM vs. hCB<sub>1</sub>R K<sub>i</sub> of 63 nM and mCB<sub>1</sub>R K<sub>i</sub> of 1721 nM, Table 2.7., entry 3) exhibited single digit nanomolar binding affinities on human and mouse CB<sub>2</sub>R, while retaining very good selectivity over the CB<sub>1</sub>R (hK<sub>i</sub> ratio CB<sub>1</sub>R/CB<sub>2</sub>R: 20 and mK<sub>i</sub> ratio CB<sub>1</sub>R/CB<sub>2</sub>R: 374, Table 2.7., entry 3). NBD-labeled (*S*)-**2.106** displayed the highest binding selectivity versus hCB<sub>1</sub>R (hK<sub>i</sub> ratio CB<sub>1</sub>R/CB<sub>2</sub>R: 68, Table 2.7., entry 1) which translated into functional selectivity in forskolin-stimulated cAMP release assays alongside with low nanomolar potency and full agonistic effects at CB<sub>2</sub>R. In particular, NBD derivative (*S*)-**2.106** outperformed with regard to functional selectivity versus hCB<sub>1</sub>R (hEC<sub>50</sub> ratio CB<sub>1</sub>R/CB<sub>2</sub>R for (*S*)-**2.106**: >4'545, Table 2.7., entry 1).

**Table 2.7. Key characteristics of (*S*)-configured fluorescent probes 2.106, 2.134, and 2.141 to 2.144.**

Entry	Probe	Dye	K <sub>i</sub> <sup>[a]</sup> [nM]				hK <sub>i</sub> ratio CB <sub>1</sub> R/ CB <sub>2</sub> R	cAMP EC <sub>50</sub> <sup>[b]</sup> [nM] (%eff.)			hEC <sub>50</sub> ratio CB <sub>1</sub> R/ CB <sub>2</sub> R	Abs (max)/ Ems (max) [nm]	AlogP <sup>[f]</sup>
			hCB <sub>2</sub> R	hCB <sub>1</sub> R	mCB <sub>2</sub> R	mCB <sub>1</sub> R		hCB <sub>2</sub> R	hCB <sub>1</sub> R	mCB <sub>2</sub> R			
1	( <i>S</i> )- <b>2.106</b>	NBD	9.1	617	33	691	68	6.3	>10'000	21 (95)	>4'545	474/550 <sup>[c]</sup>	6.3
2	( <i>S</i> )- <b>2.134</b>	Alexa488	44	321	28	>10'000	7	5.3	86 (109)	n.d.	64	494/526 <sup>[c]</sup>	5.3
3	( <i>S</i> )- <b>2.141</b>	AttoThio12	3.2	63	4.6	1721	20	9.0	n.d.	n.d.	n.d.	582/610 <sup>[c]</sup>	9.0
4	( <i>S</i> )- <b>2.142</b>	SiR	62	114	117	1'892	2	10.6	>10'000	66 (93)	>149	652/674 <sup>[d]</sup>	10.6
5	( <i>S</i> )- <b>2.143</b>	Cy5.5	14	108	50	n.d.	8	13.7	726 (118)	512 (119)	5	690/730 <sup>[c]</sup>	13.7
6	( <i>S</i> )- <b>2.144</b>	Biotin	3.0	62	3.2	n.d.	21	n.d.	>10'000	7.8 (85)	5'587	n.a.	n.d.

n.d. – not determined. <sup>[a]</sup> mCB<sub>1</sub>R data generated using mouse brain membranes; <sup>[b]</sup> Functional potency (EC<sub>50</sub>), percentage efficacy (%eff.) given in parenthesis; <sup>[c]</sup> Fluorescence excitation and emission maxima measured in aqueous solution (DPBS, Dulbecco's phosphate buffered saline); <sup>[d]</sup> Values derived from literature;<sup>[192]</sup> <sup>[e]</sup> Fluorescence excitation and emission maxima measured in DMSO; <sup>[f]</sup> Calculated partition coefficient values (AlogP) based on the contribution of each atom to the logP.<sup>[173]</sup> Reference ligands data described in the Pharmacological Assessment, Section 5.2.10. Radioligand binding assays performed by ELISABETH ZIRWES, cAMP functional assays performed by ANJA OSTERWALD, and absorption-emission spectra generated by SYLWIA HUBER at Hoffmann La-Roche.

Probe optimization and dye selection were supported by evaluation of the absorption and emission spectra of the CB<sub>2</sub>R ligands in buffer media, as well as in different organic solvents (Table 2.7., *see* Pharmacological Assessment, Section 5.2.10. for further details). This characterization provided important information for developing suitable test settings at the subsequent biological studies (Section 2.2.8.). These measurements were performed by SYLWIA HUBER at Hoffmann La-Roche and excluded the possibility of these compounds to form aggregates under the applied test settings.

Depending on the attached fluorescent label a broad lipophilicity range of AlogP values<sup>[173]</sup> from 6.3 for NBD-labeled agonist **2.106** up to 13.7 for Cy5.5 analog **2.143** was covered, influencing the overall physicochemical properties and cellular permeability of the ligands. This was further confirmed by measuring effective permeation coefficients of pyridine **2.36** linker dye adducts in the PAMPA assay.<sup>[175]</sup> Here all NBD-labeled probes were able to passively permeate through membranes (**2.107**:  $P_{\text{eff}} 0.7 \text{ cm/s} \cdot 10^{-6}$ , **2.108**:  $P_{\text{eff}} 0.7 \text{ cm/s} \cdot 10^{-6}$ , and **2.109**:  $P_{\text{eff}} 0.5 \text{ cm/s} \cdot 10^{-6}$ ; Table 2.5., entries 14 to 16, Section 2.2.6.), thereby suggesting that more lipophilic SiR- and Cy5.5-bearing structures **2.142** and **2.143**, respectively, are likely to be cell permeable as well.<sup>[192]</sup> Conversely, negatively charged Alexa-labeled **2.134** (AlogP = 5.3, Table 2.7., entry 2) was not capable of passive membrane permeation according to the PAMPA assay ((*S*)-**2.134**:  $P_{\text{eff}} 0.0 \text{ cm/s} \cdot 10^{-6}$ , *see* Experimental Procedures, Sections 5.2.9. and 5.2.10. for additional information). This feature enables investigation of extracellular membranes, but also intracellular compartments, by simple tuning the probe's physicochemical properties through fluorophore selection. Importantly, essentially similar CB<sub>2</sub>R affinity and selectivity were retained independent of the selected conjugated signal agent.

To identify potential off-targets of these labeled ligands, Alexa 488-labeled **2.134** was screened against the Cerep panel<sup>[193]</sup> which constitutes of a customized panel of 50 representative receptors and enzymes (Supplementary table S-3, data generated by Eurofins Cerep, Section 5.2.2.). In this assay, ligand **2.134** exhibited a very clean selectivity profile showing only a weak interaction with Adenosine A3 receptor, which was considered not relevant due to the high test concentration of 10  $\mu\text{M}$ .

### **2.2.8. Applications of Fluorescent Probes labeled with NBD, Alexa 488, and SiR for Detection and Visualization of the CB<sub>2</sub>R**

The applicability of this set of highly potent, selective and well-characterized CB<sub>2</sub>R fluorescent probes was further explored through broad comparative validation studies in an array of more complex chemical biology investigations. To this end, cross-validation experiments were elaborated in collaboration with three different laboratories, which are specialists in CB<sub>2</sub>R pharmacology. At first, these derivatives were subjected to flow cytometry studies using endogenously CB<sub>2</sub>R-expressing cell

lines, work which was performed by DR. CLAUDIA KORN, under the supervision of DR. CHRISTOPH ULMER and DR. UWE GREYER at HOFFMANN-LA ROCHE in Basel. The group of DR. DMITRY VEPRINTSEV in Nottingham, in particular DR. DAVID SYKES, was interested in developing kinetic binding studies at hCB<sub>2</sub>R applying time-resolved fluorescence resonance energy transfer (TR-FRET) with these fluoroprobes. Furthermore, SiR-labeled **2.142** was exploited for confocal time-lapse imaging in CB<sub>2</sub>R-overexpressing cells by DR. SERGIO ODDI and DR. MAURO MACARRONE at the University of Teramo.

In this section, proof-of-concept studies to verify the applicability and robustness of the fluorescent probe toolbox developed in this thesis across different cellular and molecular biology techniques, imaging modalities, and cell lines are presented. Moreover, interesting new findings regarding CB<sub>2</sub>R activation and expression which were unraveled by these ligands are discussed. A summary of the most relevant data generated in these collaborative efforts is given in the three following sections – flow cytometry, TR-FRET, and confocal time-resolved microscopy.

### 2.2.8.1. Flow Cytometry Enabled Visualization and Detection of CB<sub>2</sub>R in Living Cells

The specificity of these fluorescent analogs for human and mouse CB<sub>2</sub>R was evaluated by DR. CLAUDIA KORN at Hoffmann La-Roche using the flow cytometry technique in a fluorescence-activated cell sorting (FACS) instrument (Figure 2.17.). For this experiment, CHO cells overexpressing either hCB<sub>2</sub>R, mCB<sub>2</sub>R or hCB<sub>1</sub>R as well as wild-type (WT)-CHO cells were incubated with different concentrations of Alexa 488-labeled (*S*)-**2.134** (Figure 2.17.A). In comparison to its binding at the control WT cells or overexpressing hCB<sub>1</sub>R cells, fluorescent probe **2.134** was highly specific for CHO cells overexpressing both hCB<sub>2</sub>R and mCB<sub>2</sub>R. Moreover, Alexa 488-labeled **2.134** displayed excellent sensitivity profile down to low concentrations of 5 nM. In particular, significant concentration-dependent increase in mean fluorescence intensity was measured for concentrations up to 10 μM for both human and mouse CB<sub>2</sub>R.

Competition binding studies of fluorescently labeled (*S*)-**2.134** were performed to further confirm ligand specificity and exclude unspecific binding (Figure 2.17.B). The known unlabeled CB<sub>2</sub>R ligands, agonist JWH133 (**2.145**)<sup>[194]</sup> and inverse agonist RO6851228 (**2.146**)<sup>[195]</sup> (for structures *see* Supplementary figure S-1, Section 5.2.1.) were selected as blockers for this analysis. After pre-incubation of WT-CHO or hCB<sub>2</sub>R-CHO cells with ligands **2.145** and **2.146**, Alexa 488-**2.134** could



efficiently displace CB<sub>2</sub>R-agonist **2.145** at a broad concentration range. Moreover, the inverse agonist **2.146** was also displaced by 0.37 μM Alexa 488-**2.134**. The FACS assay illustrated the high degree of target specificity of fluoroprobe **2.134** in a cellular setting.

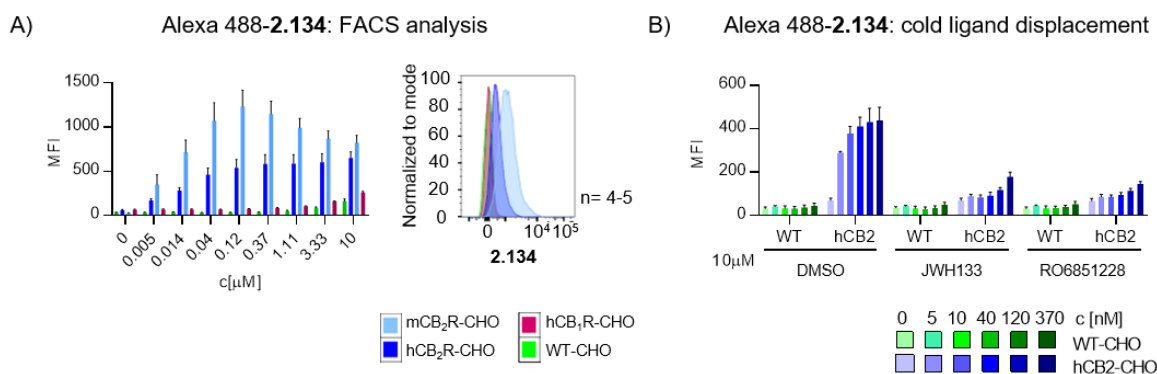


**Figure 2.17. Alexa 488 probe (S)-**2.134** enabled visualization and detection of human and mouse CB<sub>2</sub>R in flow Cytometry analysis.** A) FACS analysis of the mean fluorescent intensity (MFI) of WT, hCB<sub>2</sub>R, mCB<sub>2</sub>R and hCB<sub>1</sub>R overexpressing CHO cells incubated with different concentration of **2.134**. FACS plots show representative histograms of cells incubated with 0.37 μM ligand, and B) FACS analysis of the mean fluorescence intensity (MFI) of WT and hCB<sub>2</sub>R-CHO cells pretreated with JWH133 (**2.145**) or RO6851228 (**2.146**) (10 μM) and stained with different concentrations of **2.134**. For blocker structures see Supplementary figure S-1, Section 5.2.1). Experiments conducted by DR. CLAUDIA KORN at Hoffmann La-Roche.

### 2.2.8.2. Generation of Equilibrium and Kinetic Binding Parameters at hCB<sub>2</sub>R Using a Fluorescent-based TR-FRET Assay

Understanding ligand-binding kinetics has become an important aspect of drug discovery, as the kinetic parameters residence time (RT) and association rate constant ( $k_{on}$ ) are crucial for *in vivo* efficacy.<sup>[196]</sup> Particularly, as a considerable number of clinically approved drugs targeting GPCRs display non-equilibrium binding modes.<sup>[197]</sup> Currently, CB<sub>2</sub>R kinetic binding data is predominantly generated by radioligand binding assays which are based on tritiated CB<sub>2</sub>R ligands, precluding it from standard high throughput screening.<sup>[198]</sup> Alternatively, these data can be accessed exploiting Time-resolved fluorescence resonance energy transfer (TR-FRET) technology, thereby circumventing the need for radiometric facilities and handling radioactive material.<sup>[199]</sup>

A TR-FRET assay for measuring equilibrium binding constants has been reported applying SNAP-CB<sub>2</sub>R HEK-293T cells covalently linked to terbium (TR-FRET donor).<sup>[200]</sup> However, the determination of tracer and unlabeled ligand binding kinetics remains largely uncharted. Therefore, the CB<sub>2</sub>R-specific probes were explored by the group of DR. DMITRY VEPRINTSEV at The University

of Nottingham as tracers for TR-FRET applications. The binding affinities of CB<sub>2</sub>R specific unlabeled ligands, inverse agonist/antagonist SR144528 (**2.20**)<sup>[194, 201]</sup> and agonist HU308 (**2.28**),<sup>[194, 202]</sup> and were determined using NBD-**2.106** and Alexa 488-**2.134** congeners (Figure 2.18).

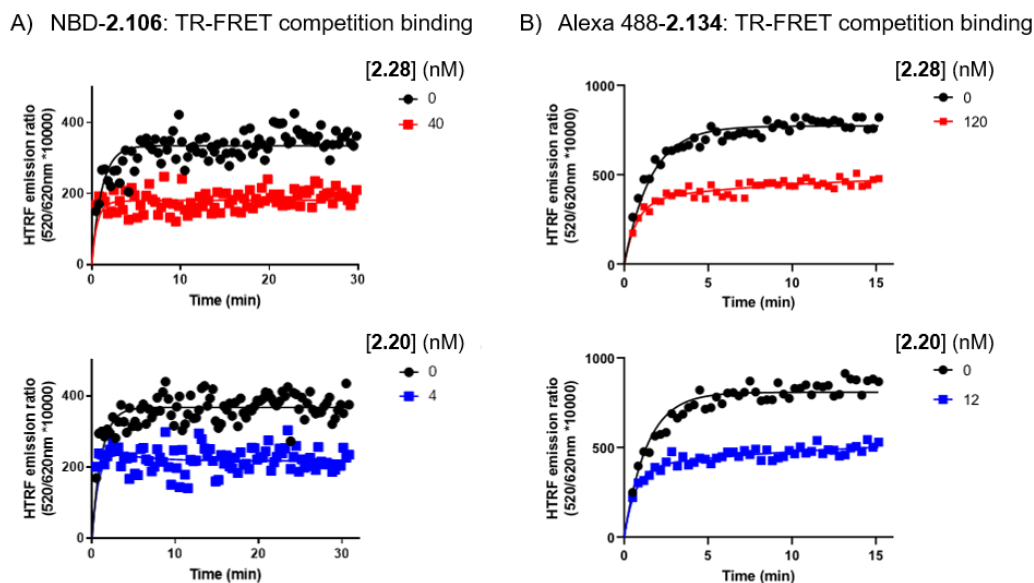


**Figure 2.18. TR-FRET competition association binding kinetics at hCB<sub>2</sub>R using NBD-2.106 and Alexa 488-2.134 as tracers.** A) NBD-2.106 and B) Alexa 488-2.134 competition association binding curves in the absence (black curves) or presence of HU308 (**2.28**, red curves, *upper panels*) and SR144528 (**2.20**, blue curves, *lower panels*) at a fixed concentration of ligand and tracer. Each dot represents a new time point in the measured association of a tracer. For ligand structures *see* Supplementary figure S-1, Section 5.2.1. Experiments performed by DR. DAVID SYKES at the University of Nottingham.

**Table 2.8. Kinetic and equilibrium affinity binding parameters for CB<sub>2</sub>R-selective ligands SR144528 (**2.20**) and HU308 (**2.28**) determined using fluorescent tracers NBD-2.106 and Alexa 488-2.134.**

Ligand	Structure	TR-FRET kinetic and equilibrium parameters	NBD ( $\pm$ )-2.106	Alexa 488 ( $\pm$ )-2.134
SR144528 ( <b>2.20</b> )  K <sub>i</sub> (nM) <sup>[a]</sup> : 0.6 <sup>[201]</sup> /13 <sup>[194]</sup> (radioligand assay)		$k_{on}$ (M <sup>-1</sup> min <sup>-1</sup> )	2.2 x10 <sup>8</sup>	6.9 x10 <sup>7</sup>
		$k_{off}$ (min <sup>-1</sup> )	0.30	0.17
		RT (min)	3.3	5.9
		Kinetic K <sub>d</sub> (nM)	1.5 <sup>[b]</sup>	2.6 <sup>[c]</sup>
		K <sub>i</sub> (nM)	1.8	5.1
HU308 ( <b>2.28</b> )  K <sub>i</sub> (nM) <sup>[a]</sup> : 23 <sup>[202]</sup> /36 <sup>[194]</sup> (radioligand assay)		$k_{on}$ (M <sup>-1</sup> min <sup>-1</sup> )	2.9 x10 <sup>7</sup>	7.7 x10 <sup>6</sup>
		$k_{off}$ (min <sup>-1</sup> )	0.35	0.20
		RT (min)	2.9	5.0
		Kinetic K <sub>d</sub> (nM)	16 <sup>[b]</sup>	28 <sup>[c]</sup>
		K <sub>i</sub> (nM)	12	61

<sup>[a]</sup> Literature data determined through radioligand binding assay provided  $k_{off}$  values for **2.20**: 0.12 min<sup>-1</sup> and for **2.28**: 0.25 min<sup>-1</sup>.<sup>[198]</sup> All values are represented by mean of <sup>[b]</sup> n = 3, <sup>[c]</sup> n = 5 experiments. Experiments performed by Dr. DAVID SYKES at the University of Nottingham.

The association and dissociation rates obtained for ligands SR144528 (**2.20**) and HU308 (**2.28**) were applied to calculate the equilibrium and kinetic parameters  $K_d$ ,  $k_{on}$ , and  $k_{off}$  (Table 2.8.). Both NBD-**2.106** and Alexa 488-**2.134** compounds were capable of generating CB<sub>2</sub>R equilibrium and kinetic binding constants. For the two CB<sub>2</sub>R modulators, the TR-FRET data with kinetic parameters and equilibrium affinity values were in excellent agreement with those previously obtained from radioligand binding assays.<sup>[194, 201-202]</sup> These results illustrated the potential for implementing this TR-FRET methodology for important applications, including the study of CB<sub>2</sub>R ligand residence time and the development of high-throughput screening assays.

### 2.2.8.3. Visualization of the CB<sub>2</sub>R with SiR-Probe **2.142**: Tracing Internalization Events by Live Cell Confocal Imaging

One primary advantage of cell permeable agonist probes is their ability to accumulate inside cells upon internalization and to track receptor recycling events. For imaging diagnosis, such a behavior provides amplified signal read-out, improved image contrast, and enhanced detection sensitivity.<sup>[55]</sup> In addition, fluorescent compounds with such properties have applicability for tracing receptor internalization and trafficking dynamics. As discussed in Section 2.2.8.3., SiR-labeled **2.142** was likely a cell permeable probe based on its physicochemical profile (Table 2.7., Section 2.2.7.3.). Therefore, this derivative was selected to specifically visualize hCB<sub>2</sub>R in living cells by confocal time-lapse imaging (Figure 2.19.). This investigation was conducted by DR. SERGIO ODDI at the University of Teramo.

In accordance with the results obtained for the NBD-labeled analogues in the PAMPA assay (Table 2.5., Section 2.2.6.), SiR-**2.142** was confirmed as a membrane-permeable ligand, being able to successively enter hCB<sub>2</sub>R-overexpressing cells and to reach internal membranes (Figure 2.19.A and 2.19.B). Treatment of hCB<sub>2</sub>R-overexpressing CHO cells with ligand **2.142** resulted in a time- and concentration dependent labeling of hCB<sub>2</sub>R at cell membranes, without the need for an intermediate washing step. In contrast to the long pre-incubation times (>30 min) often required by literature reported CB<sub>2</sub>R fluorescent probes for live cell imaging experiments,<sup>[152, 154, 155b, 159, 163]</sup> which contribute to unspecific staining, ligand **2.142** displayed an instantaneous labeling effect.

During the time-course of staining, the formation of small endosome-like vesicles (Figure 2.19.B, *white triangles*) within the cytosol was observed. These structures may indicate the presence of an agonist-

stimulated internalization process of the CB<sub>2</sub>R, which occurs concomitantly to passive diffusion of the probe.

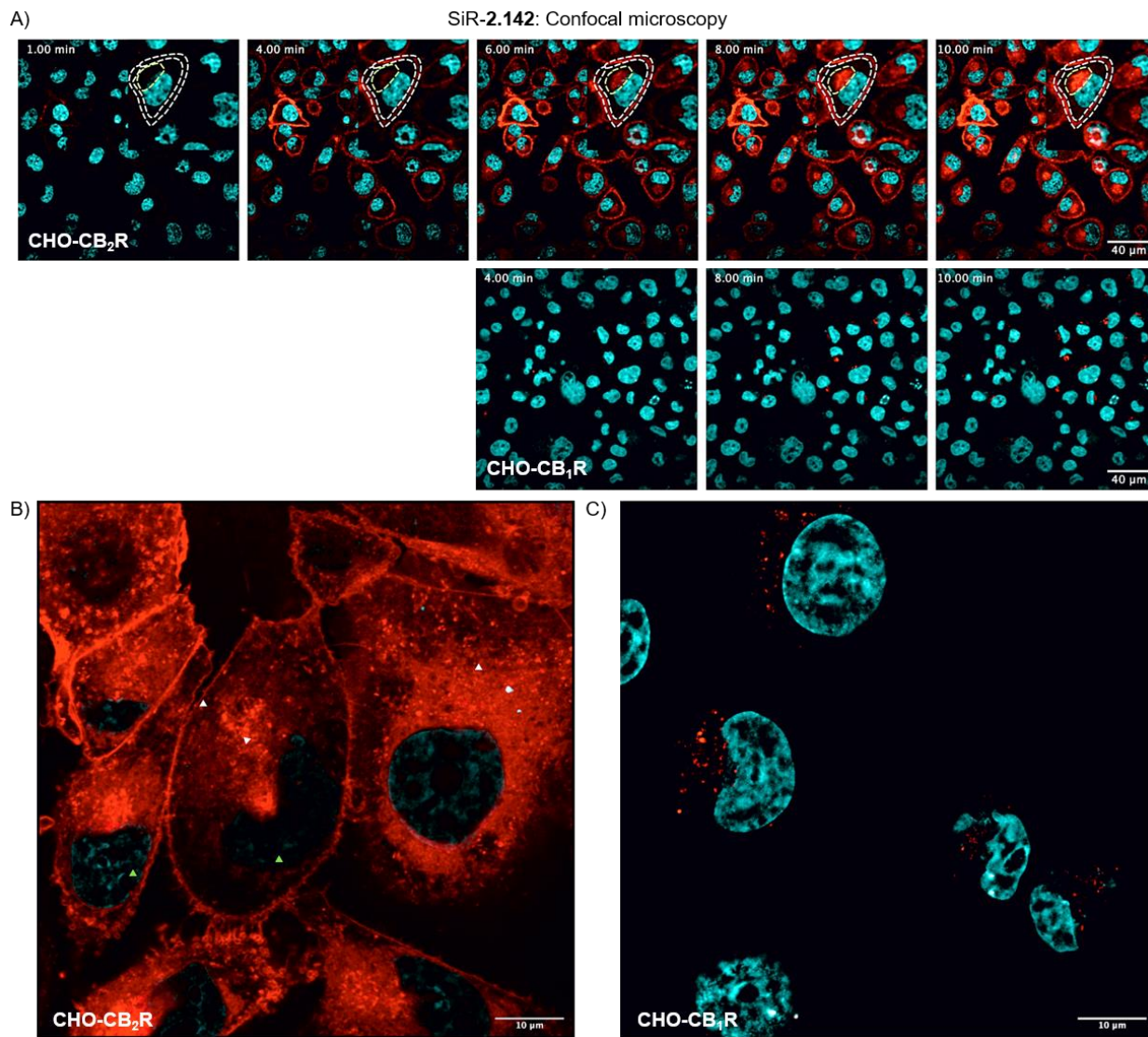


**Figure 2.19. Confocal Fluorescence Microscopy in live CHO cells using SiR probe-2.142 allowed for tracing CB<sub>2</sub>R internalization events.** A) Time-lapse confocal microscopy frames for hCB<sub>2</sub>R (*upper panels*) and hCB<sub>1</sub>R (*lower panels*). CHO cells co-stained with **2.142** (red) and Hoechst 33342 (cyan, nucleus counter stain) at 1, 4, 6, 8 and 10 min; Plasma and internal membranes are highlighted with white and yellow dashes, respectively. B, C) Airyscan high-resolution imaging of hCB<sub>1</sub>R- and hCB<sub>2</sub>R-overexpressing CHO cells incubated either for 10 min with 0.4 μM **2.142** (red) and counterstained with Hoechst 33342 (cyan), where B) hCB<sub>2</sub>R-CHO cells and C) control hCB<sub>1</sub>R-CHO cells. Experiments performed by DR. SERGIO ODDI at the University of Teramo.

Since SiR analog-**2.142** was practically non-fluorescent in the test settings, the bright labeling of cellular membranes was achieved even in the continued presence of the probe in the culture medium,<sup>[192, 203]</sup> thus permitting experimental imaging studies over prolonged time (Figure 2.19.A, *lower panels*, and

2.19.C). Of note, compound **2.142** did not produce membrane labeling in control hCB<sub>1</sub>R-overexpressing CHO cells, under the tested conditions (Figure 2.19.A, *lower panels*, and 2.19.C). Thus, highlighting the high CB<sub>2</sub>R-specificity and remarkably low extent of unspecific binding of this fluorescent ligand.

### 2.3. Conclusion and Outlook

As a part of these thesis, a set of highly potent fluorescent probes targeting the CB<sub>2</sub>R were designed, synthesized, and cross-validated in different experimental settings conducted in three collaborating laboratories.

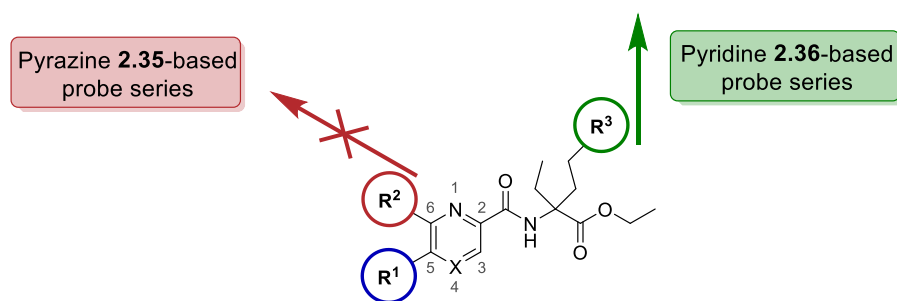
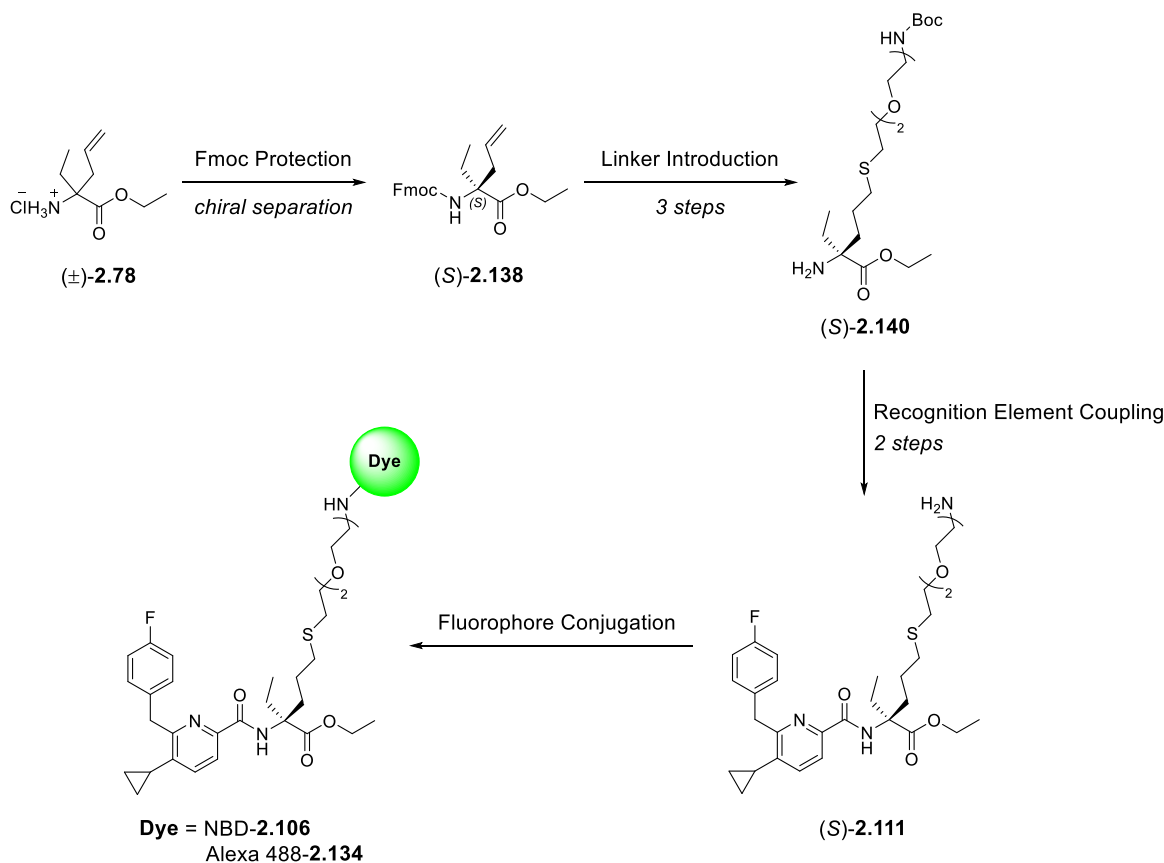


**Figure 2.20. Linker attachment sites investigated for the development of a CB<sub>2</sub>R-selective fluorescent agonist from recognition elements 2.35 and 2.36.** For pyrazine **2.35**, R<sup>1</sup> corresponds to 3,3-difluoroazetidide and X to a nitrogen atom. For pyridine **2.36**, R<sup>1</sup> corresponds to cyclopropyl ring and X to a carbon atom.

Assisted by molecular modeling studies, preclinical CB<sub>2</sub>R agonist drugs **2.35** and **2.36** were investigated as probe templates, which possessed two possible linker attachment sites: one at position 6 of the heteroaryl ring (R<sup>2</sup>) and the other at the geminal diethyl group (R<sup>3</sup>) (Figure 2.20). Since linker elongation at R<sup>2</sup>-position of pyrazine **2.35** resulted in hCB<sub>2</sub>R-inactive compounds, the synthesis of fluorescent ligands which were elongated at R<sup>3</sup>-position of the pharmacophores **2.35** and **2.36** was pursued. The tolerance of new conjugation sites for linker introduction within pyrazine **2.35** and pyridine **2.36** was explored through a small SAR analysis. These studies indicated that linker elongation of the pyridine **2.36** scaffold with a thioether at the diethyl substitution motive at the  $\alpha$ -carbon position, was the most successful strategy for retaining high CB<sub>2</sub>R affinity. Based on this scaffold, racemic probes were synthesized with a thioether handle for conjugation with different linker lengths ranging

from one to four ethylene glycol units, and an alkyl linker. Evaluation of these constructs revealed NBD analog ( $\pm$ )-**2.106** with PEG2 linker units as the most favorable template to advance optimization efforts.



**Scheme 2.17.** General modular approach for the synthesis of enantiomeric pure probe template (*S*)-**2.111**, which allowed for the generation of the CB<sub>2</sub>R-selective fluorescent probes **2.106** and **2.134**.

The influence of the absolute configuration of probe template **2.111** on the affinity and activity of this compound series was investigated (Scheme 2.17.). The Fmoc-protective group enabled, not only chiral separation of amino ester ( $\pm$ )-**2.138** using HPLC, but also the elucidation of its absolute configuration using X-ray. From this building block, a modular synthesis approach was developed for the preparation of enantiomer pairs of precursor **2.111** labeled with NBD (**2.106**) and Alexa 488 (**2.134**) dyes (Scheme 2.17.). Improved pharmacological profile was obtained with (*S*)-configured derivatives, thus amine (*S*)-**2.111** was further explored by BENJAMIN BRENNECKE, DR. YELENA MOSTINSKY, LEONARD MACH, and MARIE WEISE for the attachment of a variety of fluorophores with different physicochemical and photophysical properties tailored for diverse applications. Despite large structural modifications with regard to linker elongation and dye attachment, the high potency,

selectivity and agonistic properties of recognition element **2.36** were mostly preserved in all synthesized probes. These tools show unprecedented highly consistent interspecies affinity and efficacy for both human and mouse CB<sub>2</sub>R in the low nanomolar range.

The fluorescently labeled ligands were extensively validated using complementary *in vitro* experiments which demonstrated the versatility and robustness of probe platform (*S*)-**2.111** to generate a toolbox of fluorescently-labeled CB<sub>2</sub>R-agonists. In flow cytometry experiments performed by DR. CLAUDIA KORN, Alexa 488-derivative **2.134** allowed to specific detect CB<sub>2</sub>R in overexpressing cells and demonstrated target specificity by competition against CB<sub>2</sub>R reference ligands. The analogs NBD-**2.106** and Alexa 488-**2.134** were applied by DR. DAVID SYKES in a fluorescence-based TR-FRET assay for the generation of CB<sub>2</sub>R kinetic and equilibrium binding data, which were in excellent agreement with previous values obtained using radiometric ligand-binding assays. Finally, DR. SERGIO ODDI exploited SiR-**2.142** to reliably image and monitor CB<sub>2</sub>R distribution in real-time live cell imaging by confocal microscopy on overexpressing hCB<sub>2</sub>R-CHO cells. Thereby, for the first time visualization of CB<sub>2</sub>R trafficking and internalization in living cells was achieved.

Future applications involving the Raman-**2.135** and biotin-**2.144** probes, which were not to date explored, hold potential in interesting fields of research, such as in Raman spectroscopy and pulldown assays to identify relevant receptor-ligand interactions at the binding pocket. In particular, compound **2.135** could be utilized for generating the first Raman imaging of CB<sub>2</sub>R. Moreover, the recent elucidation of the human CB<sub>2</sub>R crystal structure in both antagonist- (ligand: AM10257, PDB 5ZTY)<sup>[204]</sup> and agonist-bound (ligand: AM12033, PDB 6KPF; *see* Figure 3.1., Section 2.1.1.)<sup>[81]</sup> states enable a deeper understanding of receptor-ligand interactions which could aid to new structure-based design strategies of probes with improved pharmacology.

Altogether, the probe platform described in this chapter have the potential to provide tools that would enable to: (i) overcome the large interspecies differences encountered between rodent and human CB<sub>2</sub>R, (ii) have high specificity and low nanomolar affinity for CB<sub>2</sub>R with full agonist efficacy, and (iii) perform complementary biologically and pharmacologically experiments used to detect CB<sub>2</sub>R and study its function. Ultimate, these compounds have diverse applications as surrogate markers, e.g., for target engagement studies of the CB<sub>2</sub>R, identification of mechanisms of action, and deepen the knowledge on CB<sub>2</sub>R expression profiles.



### 3. Development of a Cyclen-based Clickable Platform for Pancreatic Cancer Imaging

#### 3.1. Introduction

##### 3.1.1. Pancreatic Cancer – Current Status and Challenges

Pancreatic cancer is the fourth most killing cancer worldwide and has the lowest survival rate among human cancers with an overall 5-year survival rate of approximately 8%.<sup>[205]</sup> Despite the various tumors types identified in the pancreas, the vast majority of pancreatic tumors (up to 90%) are represented by a specific subtype named pancreatic ductal adenocarcinoma (PDAC).<sup>[206]</sup> The only curative treatment option for this cancer type to date is complete tumor surgical resection in combination with chemotherapy.<sup>[207]</sup>

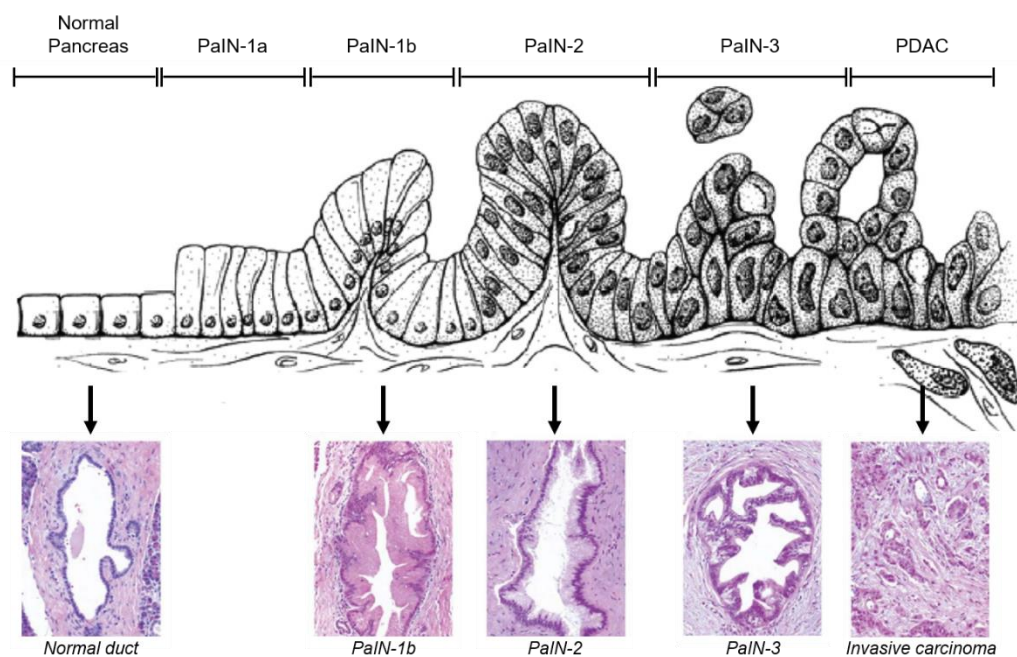


**Figure 3.1. Progression model for pancreatic cancer.** PanINs represent progressive stages of neoplastic growth, each step in the progression from normal epithelium to low-grade PanIN on to highgrade PanIN is distinguished by histological features. Modified after J. YU *et al.*<sup>[208]</sup> and R. H. HRUBAN *et al.*<sup>[209]</sup>



Pancreatic cancer originates from precursor lesions, being pancreatic intraneoplasia (PanIN) the most common.<sup>[210]</sup> In particular, PanIN develops into invasive carcinoma through a multistep carcinogenic process, from clinically benign PanIN-1 to carcinoma *in situ* PanIN-3 (Figure 3.1.). The pancreas is located behind the stomach and surrounded by other organs, including the spleen, liver, and small intestine, which makes pancreatic tumors rarely palpable. In addition, most symptoms of PDAC do not appear until the tumor has grown large enough to interfere with its own or other organ functions (invasive carcinoma, Figure 3.1.). The situation is further aggravated by the lack of appropriate diagnostic tools, which leads to definitive disease confirmation at locally advanced and unresectable cancer stages.<sup>[211]</sup> The median size of PDAC at the time of diagnosis is circa 3 cm – these statistics have not changed in the past three decades in spite of advances in imaging technologies, and in clinical procedures.<sup>[212]</sup> Resection of tumors while they are small, well-defined, and localized results in higher chances of complete tumor clearance. Therefore, the early detection of PDAC, before cancer metastasizes, is critical to improving survival rates.<sup>[213]</sup>

Due to its deep anatomical location, non-invasive imaging of the pancreas is extremely challenging. Imaging methodologies to diagnose PDAC are primarily based on endoscopy (invasive), computed tomography, MRI and ultrasonography, and have very low success rates at tracing early-stage tumors.<sup>[214]</sup> Detection and surgical removal of PanIN-3 is related to an increase in patient survival,<sup>[215]</sup> albeit distinguishing between tumorous and healthy tissue using current imaging techniques is often not possible, and may lead to incomplete tumor resection or even removal of healthy tissue.<sup>[216]</sup> In current practice, tumor identification is mainly subjective and relies heavily on the physician's experience, leading to a significant variability in surgical outcomes.<sup>[217]</sup> Moreover, both the benign pancreatitis and malignant PDAC have abundant stroma, which is difficult to distinguish using conventional non-targeted-based imaging techniques.

At present, carbohydrate antigen 19-9 (CA 19-9) is the only FDA approved biomarker for pancreatic cancer prognosis and following disease evolution, and is tested through radioimmunoassay.<sup>[218]</sup> Nevertheless, CA 19-9 is frequently associated with false positives as it lacks to differentiate between nonmalignant pancreatic diseases and cancer, as well as it fails to detect early-stage malignancies.<sup>[219]</sup> To improve conventional imaging outcomes, molecular imaging has the potential to precisely detect and characterize PanINs, as well as to provide real-time surgical guidance. It is known that patients life-time doubles after microscopically radical tumor resection (of at least 1 mm),<sup>[220]</sup> yet the only fluorophores so far approved by the FDA for peripheral tumor resection are non-specific, such as

methylene blue (3.1), fluorescein (3.2), and indocyanine green (ICG, 3.3) (Figure 3.2).<sup>[221]</sup> Since none of these agents provide any kind of directed, specific targeting of tumor cells, critical structures, including ureters and nerves, cannot be preserved during surgery. Hence, molecular imaging tools that allow not only early detection, but also intraoperative visualization of PDAC are urgently needed.

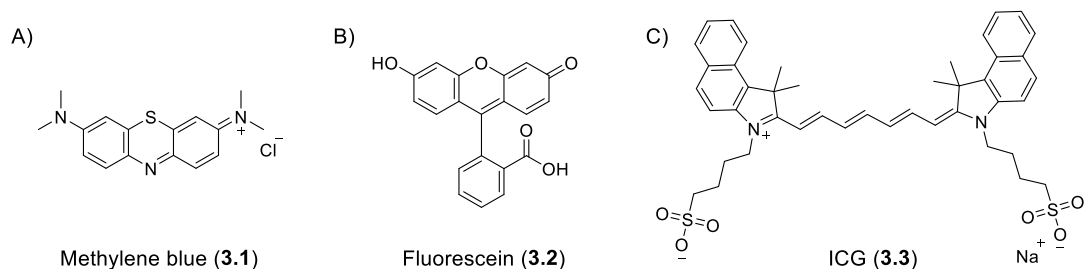


**Figure 3.2. Structures of the non-selective fluorophores approved for clinical applications.** A) Methylene blue (3.1), B) Fluorescein (3.2), and C) Indocyanine green (ICG, 3.3).

### 3.1.2. Plectin-1 as a Biomarker for Pancreatic Cancer

Cancer biomarkers are often used in oncology to differentiate between benign and malignant cells and characterize tumor types, holding the promise for the early detection of cancers. In particular, the ideal PDAC biomarker should be expressed in measurable concentrations at the early onset of the disease with high sensitivity and specificity.<sup>[222]</sup> Genetic alterations, such as mutations in the KRAS oncogene or p53, DPC4, and BRCA2 tumor suppressor genes generate an imbalance in key signaling pathways.<sup>[223]</sup> This process leads to the overexpression of specific biomarkers, which can be explored as targets for tumor-specific molecular agents. In stark contrast to the lack of effective contrast agents available, the cellular composition of PDAC provides a plethora of relevant targets for molecular imaging. Those targets include mesothelin,<sup>[224]</sup> plectin-1,<sup>[225]</sup> urokinase plasminogen activator,<sup>[226]</sup> insulin-like growth factor I receptor,<sup>[227]</sup> mucin 1,<sup>[228]</sup> vascular endothelial growth factor receptor 2 (VEGFR2),<sup>[229]</sup> and zinc transporter 4.<sup>[230]</sup> Among these, plectin-1 is a scaffolding cytoskeletal protein that undergoes aberrant mislocalization to the cell surface of PanIN-3 lesions and PDAC.<sup>[225, 231]</sup> The absent expression of plectin-1 in the healthy pancreas, liver and peritoneum,<sup>[232]</sup> makes it an exceptionally specific and sensitive target for the early detection of PDAC.

The generation of an appropriate recognition element with optimized affinity, selectivity and physicochemical properties follows identification of the biomarker. For imaging probe development, the ideal recognition element encompasses connectivity handles for the attachment of linker and reporter unit entities. Besides small molecules, as utilized in the previous section of this thesis, peptides, aptamers and antibodies can also serve as a targeting moiety.<sup>[55]</sup> Particularly, peptides offer the advantage of non-immunogenicity and are amenable to chemical modification. In addition, peptide libraries allow for systematic hit identification and optimization in a faster process than for small molecules. Such libraries can be synthesized chemically – which enables introduction of non-natural amino acids and scaffold alterations – or biologically via phage, yeast or bacteria.<sup>[233]</sup> Phage display, the major methodology to screen for peptides, exploits *Escherichia coli* to express peptide libraries which were encoded in a specific plasmid.<sup>[234]</sup> Through a phage-display study, KELLY and collaborators<sup>[225]</sup> have identified a plectin-targeting peptide NH<sub>2</sub>-KTLLPTP-COOH (PTP, **3.4**, Figure 3.3.A) which distinguished malignant pancreatic disease from chronic pancreatitis and healthy pancreas *in vivo*. In this study, the non-targeting and not selective peptide sequence NH<sub>2</sub>-SNLHPSD-COOH was also characterized (**3.5**, Figure 3.3.B). Successful preclinical trials applying the PET tracer In<sup>111</sup>-labelled tetrameric-**3.4** in PDAC mouse model<sup>[232]</sup> advanced this tracer for phase 0/ early phase I clinical trials, terminated in 2016.<sup>[235]</sup>

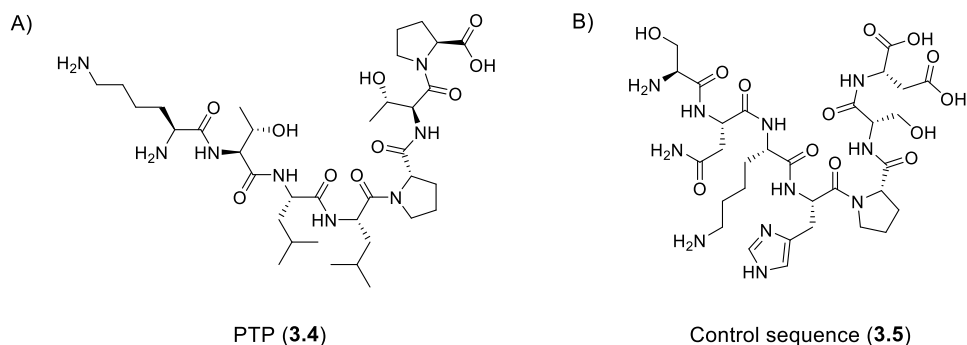


**Figure 3.3. Structures of plectin-1 targeting peptides identified by KELLY *et al.*<sup>[225]</sup>** A) Plectin-1 targeting peptide (PTP, **3.4**) and B) control peptide sequence (**3.5**).

### 3.1.3. Molecular Imaging Probes for Pancreatic Cancer Imaging

Cancer-targeted probes developed for diverse imaging modalities have been applied in both preclinical and clinical settings. For PDAC treatment, these tools have the potential to bridge the gap between diagnostic and intra-operative imaging and to monitor treatment response. Different classes of recognition elements were explored for the design of imaging tools for PDAC, including small molecules, peptides, aptamers, antibodies, and engineered protein fragments.<sup>[236]</sup> Most of these tools aim the specific binding to upregulated targets during the progress of the disease.

As discussed in Section 1.2., sufficient functional and structural information for a thorough diagnosis will likely derive from the synergistic combination of techniques, rather than using a single modality.<sup>[69]</sup> Targeted fluorescent probes are efficient tools for precise and real-time intra-operative guidance, whereas PET tracers allow for disease detection with high tissue penetration, and the very good soft-tissue contrast of MRI enables diagnosis confirmation and following surgery outcomes. In recent years, this concept has become very attractive for the design of integrated diagnostic and intra-operative tools. This section provides recent advances of molecular imaging strategies for PDAC, with an emphasis on clinical tests, dual-imaging and intra-operative applications.

The use of disease-specific ligands can significantly improve PET diagnosis, when compared to the unspecific [<sup>18</sup>F]FDG (**3.6**, Figure 3.4.). This was confirmed in humans using the <sup>18</sup>F-labeled cystine knot peptide **3.7** containing a 36 amino acid sequence peptide structured with a tertiary fold targeting integrin  $\alpha v\beta 6$ <sup>[237]</sup> (Figure 3.4.). In preclinical settings, PET tracers targeting not only integrin classes, such as  $\alpha v\beta 3$ <sup>[238]</sup> and  $\alpha v\beta 6$ ,<sup>[239]</sup> but also the tumor growth and metastasis promoters plectin-1,<sup>[232]</sup> tissue factor transmembrane glycoprotein,<sup>[240]</sup> activated leukocyte cell adhesion molecule,<sup>[241]</sup> and transferrin receptor<sup>[242]</sup> are currently being explored. Moreover, a dual PET and NIR tracer based on the monoclonal antibody mAB 5B1 which specifically binds to the clinically accepted CA 19-9 biomarker has been developed, showing promising results in identifying metastases foci in mice.<sup>[243]</sup> Nevertheless, several limitations, such as lack of specificity in detecting PDAC over other pancreatic abnormalities, short-half life, and high accumulation in the kidneys and liver still hamper the advance of these tracers into the human situation.

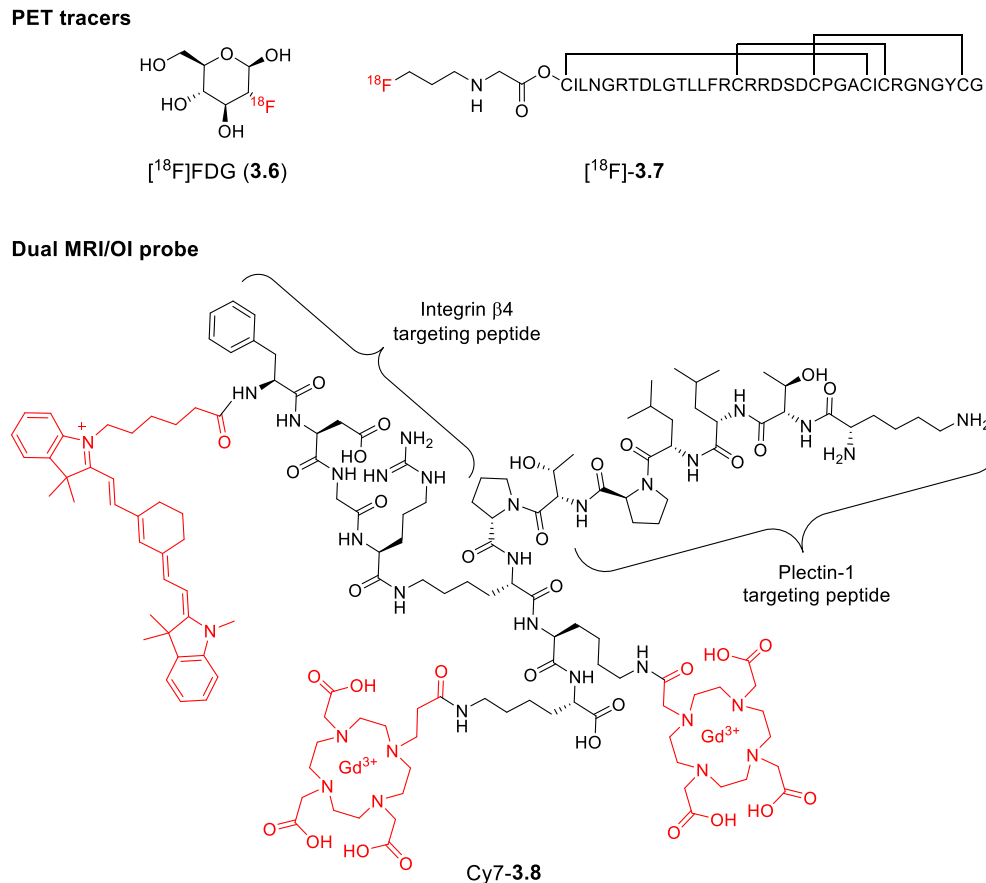


**Figure 3.4. Structures of PDAC-selective molecular imaging probes.**<sup>[237, 244]</sup> The reporter unit is highlighted in red.

Targeted microbubbles were applied to study the tumor vasculature of PDAC using contrast-enhanced ultrasound. These contrast agents were synthesized to specifically recognize and validate angiogenesis targets in mouse models, including VEGFR2, integrin, endoglin, and thymocyte antigen 1 (Thy1).<sup>[245]</sup> In particular, first-in-human clinical evaluation of VEGFR2-targeted microbubbles for the detection of breast and ovarian cancer have demonstrated the feasibility of this emerging technique.<sup>[13b, 246]</sup> MRI imaging nanoparticles based on quantum dots coated with single-chain anti-EGFR antibody to target the endothelial growth factor receptor (EGFR) have shown good specificity for PDAC both *in vivo* and *ex vivo* preclinical studies.<sup>[247]</sup> In addition, dual MRI and NIR molecular imaging agents targeting mucin-1 and plectin-1 were reported. These compounds contain a superparamagnetic iron oxide nanoparticle core labeled with Cy5.5<sup>[225, 248]</sup> or Cy7<sup>[249]</sup> fluorophores to allow for the visualization of PDAC in mouse. In general, the major drawback of nano-based imaging systems to image the pancreas is the eventual unsuccessful delivery to the site of interest due to PDAC dense stroma and hypoxic microenvironment.<sup>[250]</sup>

Currently, two PDAC-specific optical imaging (OI) agents are under clinical phase 1 evaluation for intraoperative guidance. These compounds share design similarities being both SGM-101<sup>[251]</sup> and cetuximab-IRDye800<sup>[252]</sup> NIR dye-antibody conjugates. In particular, cetuximab-IRDye800 probe targets EGFR and is additionally being tested in photoacoustic (PA) imaging settings. These trials have shown successful PDAC imaging but accompanied with interfering auto-fluorescence of the surrounding background, including tissues and blood. Importantly, these structures were capable of penetrating PDAC tumors, in converse to the hypothesis that the tumor density would restrict targeted imaging and therapy. Furthermore, the integrin  $\alpha v \beta 6$  has also been investigated for the synthesis of fluorescent imaging probes. Amide coupling of the 36-mer peptide cystine knot with a NIR dye (Atto740) led to the formation Atto740-**3.7**, which detected PDAC in mice both by fluorescent and photoacoustic techniques.<sup>[253]</sup> Another integrin  $\alpha v \beta 6$ -targeting theranostic and OI agent was synthesized using streptavidin-biotin as a core for the attachment of multiple NH<sub>2</sub>-HYK-COOH peptide sequences, composed of 22 amino acids, and a NIR dye (IRDye700DX).<sup>[254]</sup> First preclinical investigations in mice demonstrated the feasibility of this compound for PDAC treatment upon light irradiation and tumor surgical removal. More recently, WANG and collaborators<sup>[244]</sup> synthesized a dual MRI and NIR derivative targeting both plectin-1 and integrin  $\beta 4$  (Cy7-**3.8**) and demonstrated its potential applications in PDAC diagnosis using MRI, followed by UV-guided tumor resection (Figure 3.4).

All of these studies are currently in early clinical development and as such, their impact and contribution to revert PDAC prognosis are yet to be determined. Essential for a successful contrast agent is the high sensitivity and selectivity for cancerous over healthy tissue. In particular, dual-imaging probes that combine fluorophores with MRI signal agents, such as gadolinium(III) chelates, enable the use of a single molecule to non-invasively diagnose PDAC and guide surgical efforts. Dual fluorescent imaging tools are also very promising since different modalities, such as OI, photoacoustic imaging, and Raman spectroscopy utilize NIR dyes as a source of readout to provide complementary image information on depth, sensitivity, and resolution. These probes have also therapeutic applications, being used as theranostics to reduce or completely suppress cancer growth by light irradiation of the tumor region, after compound administration.

At present, the most advanced imaging agents encompass high molecular weight recognition elements, e.g., antibodies, nanobodies, long peptide sequences of over 20 amino acids, and often require a nanocarrier for improving administration and distribution of the compound *in vivo*. The recent work

of WANG and co-workers<sup>[244]</sup> has demonstrated that small molecule ligands are also successful in reaching out the tumor tissue and providing high-quality images for both cancer detection and resection (Cy7-**3.8**, Figure 3.4.), therefore paving the way for the development of small molecule PDAC-specific fluorescent ligands. However, the synthesis of multivalent and dual-imaging small molecule-based contrast agents is still extremely challenging and lacks modularity.<sup>[255]</sup>

### 3.1.4. Exploring the DOTA Scaffold for Multivalent Probe Design

Major advances in the medical diagnosis field have been achieved through the use of molecular cages that have the ability to complex, e.g., radionuclides and paramagnetic metals, for the development of imaging probes.<sup>[256]</sup> Molecular cages allow the reporter unit to provide a decent *in vivo* readout, while avoiding the inherent toxicity of such metals. In particular, macrocyclic polyamines, also known as complexones, belong to the most frequently employed cages for the design of imaging tools<sup>[257]</sup> (Figure 3.5).

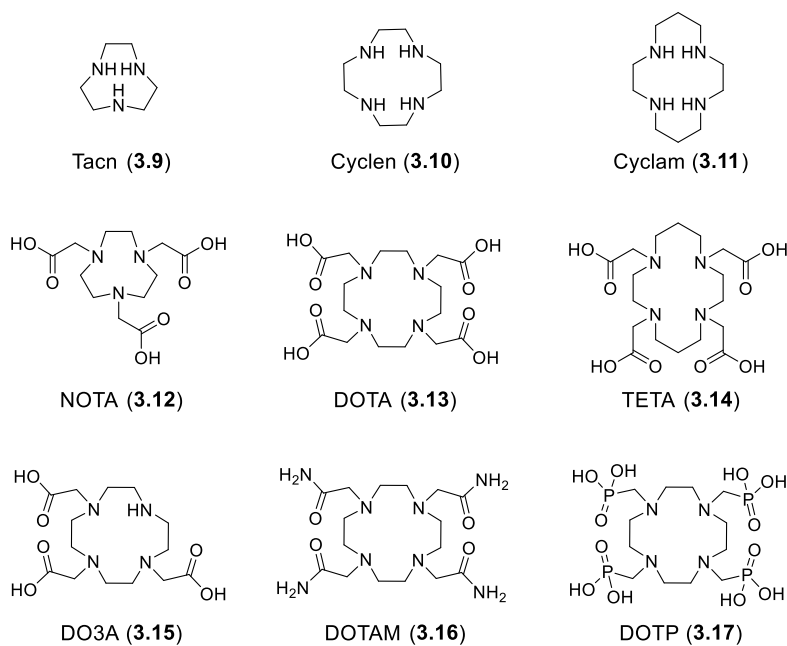


Figure 3.5. Structures of most common macrocyclic polyamines used in the medical field.

Among these, the cyclen (**3.10**)-based 1,4,7,10-tetraazacyclododecane-1,4,7,10-tetraacetic acid (DOTA, **3.13**) and its derivatives, such as 1,4,7,10-tetrakis(carbamoylmethyl)-1,4,7,10-tetraazacyclododecane (DOTAM, **3.16**) and 1,4,7,10-tetraazacyclododecane-1,4,7,10-tetra(methylene phosphonic acid) (DOTP, **3.17**), have found increasing applications in the clinics (Figure 3.5).<sup>[258]</sup> The presence of four nitrogen atoms, together with four carbonyl functionalities, generate an eightfold valency which can tightly bind to metal ions with high chemical stability and water solubility. Due to these attributes, cyclen-based gadolinium(III) chelates have become the gold standard of contrast agents for MRI.<sup>[34]</sup> However, these tools are not disease-specific and depend on the contrast of different tissue densities for a clear diagnosis. This methodology requires a large amount of contrast agent administration, which generally poses a risk of toxicity.<sup>[34]</sup> In recent years, this problem is being circumvented by the synthesis of targeted cyclen complexes by conjugating a recognition element prior to metal chelation.<sup>[258-259]</sup> Such a probe can be used *in vivo* for a multitude of imaging modalities, including MRI, PET, SPECT, luminescence imaging, and dual-imaging purposes, as exemplified by the dual NIR and OI analog reported for PDAC imaging<sup>[244]</sup> (Cy7-**3.8**, Figure 3.4., Section 3.1.3.).

As discussed in Section 1.3., multivalency, i.e., the combination of multiple recognition elements through covalent linkage to a template, is a useful strategy to enhance target avidity and *in vivo* retention times at the site of interest (*see* Figure 1.4.A, Section 1.3.). These features are particularly relevant for a contrast agent to reach out to the pancreas, and eventually provide high-quality images. The cyclen core (**3.10**) encodes remarkable topological information as it allows for functionalization with up to four acetic acid arms. This approach leads to a multivalent architecture, which can be either symmetrical, possessing fourfold decoration<sup>[260]</sup> (Figure 3.6.), or unsymmetrical, with tailored multiple components<sup>[261]</sup> (Figure 3.7.).

A series of symmetrical DOTA agents targeting the cancer biomarker integrin  $\alpha_v\beta_3$  were synthesized containing one and/or up to three cyclic-RGDfk peptide (cRGD) targeting moieties.<sup>[260a]</sup> The attachment of cRGD peptides at the DOTA core was achieved via subsequent amide coupling reactions. However, this strategy was not successful in providing a fourfold cRGD functionalized DOTA analog, leading to very low isolated amounts of product which were not sufficient for *in vitro* evaluation. To overcome the associated synthetic issues, the preparation of a fully cRGD functionalized derivative was tackled exploring the DOTP scaffold (**3.18**, Figure 3.6., *see* Figure 3.5. for DOTP-**3.17** structure).<sup>[262]</sup> The multivalent compounds were evaluated in competition binding <sup>125</sup>I-echistatin assays, demonstrating that their potency improved proportionally with the addition of



cRGD recognition elements.<sup>[260a]</sup> In particular, the tetra-decorated **3.18** displayed remarkable 0.1 nM potency towards integrin  $\alpha_v\beta_3$ , a 3800- and 130-fold increase in potency when compared to mono- and tri-substituted DOTA derivatives, respectively.<sup>[262]</sup>

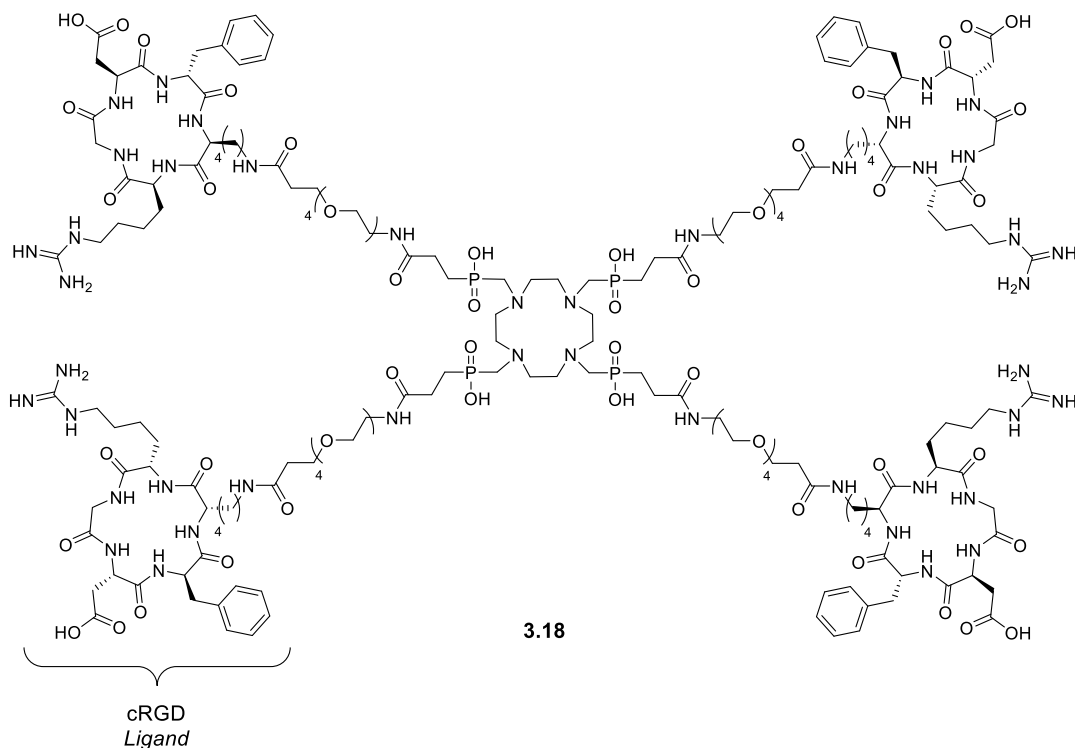


**Figure 3.6.** Symmetrically derivatized cyclen **3.18**, containing four cRGD peptides connected by PEG linkers to a DOTP center.<sup>[262]</sup>

Alternative to the amide formation strategy, the synthesis of DOTP-based derivatives containing four symmetrical substitutions has been recently described using both Copper (CuAAC)<sup>[263]</sup> and strain-promoted (SPAAC)<sup>[264]</sup> azide-alkyne cycloaddition.<sup>[260b]</sup> These synthetic strategies were applied for the preparation of prostate cancer-specific theranostic conjugates which showed promising results *in vivo*, leading to low nanomolar affinities and good tumor uptake.<sup>[260b]</sup>

The synthesis of more challenging heteromultifunctional DOTA compounds has been described by different research groups.<sup>[261, 265]</sup> The assembly of such constructs was predominantly accomplished using amide coupling reactions to introduce the linker, recognition element, and either a fluorescent dye – for an imaging probe – or a drug – for a drug-carrier. For example, HU and co-workers developed a multifunctionalized DOTAM template applied to image and treat osteoarthritis (**3.19**, Figure 3.7.).<sup>[261]</sup> The template **3.19** combined three peptide sequences targeting type II collagen (*N*-acetylated-WYRGRL-COOH) as ligands and a free amine which was exploited for conjugating either

the NIR dye Cy5.5 or Pepstatin A, a cathepsin D inhibitor against cartilage degradation. In *ex vivo* experiments, compound Pepstatin A-**3.19** demonstrated good inhibitory profile which was maintained up to 48 h.<sup>[261a]</sup>

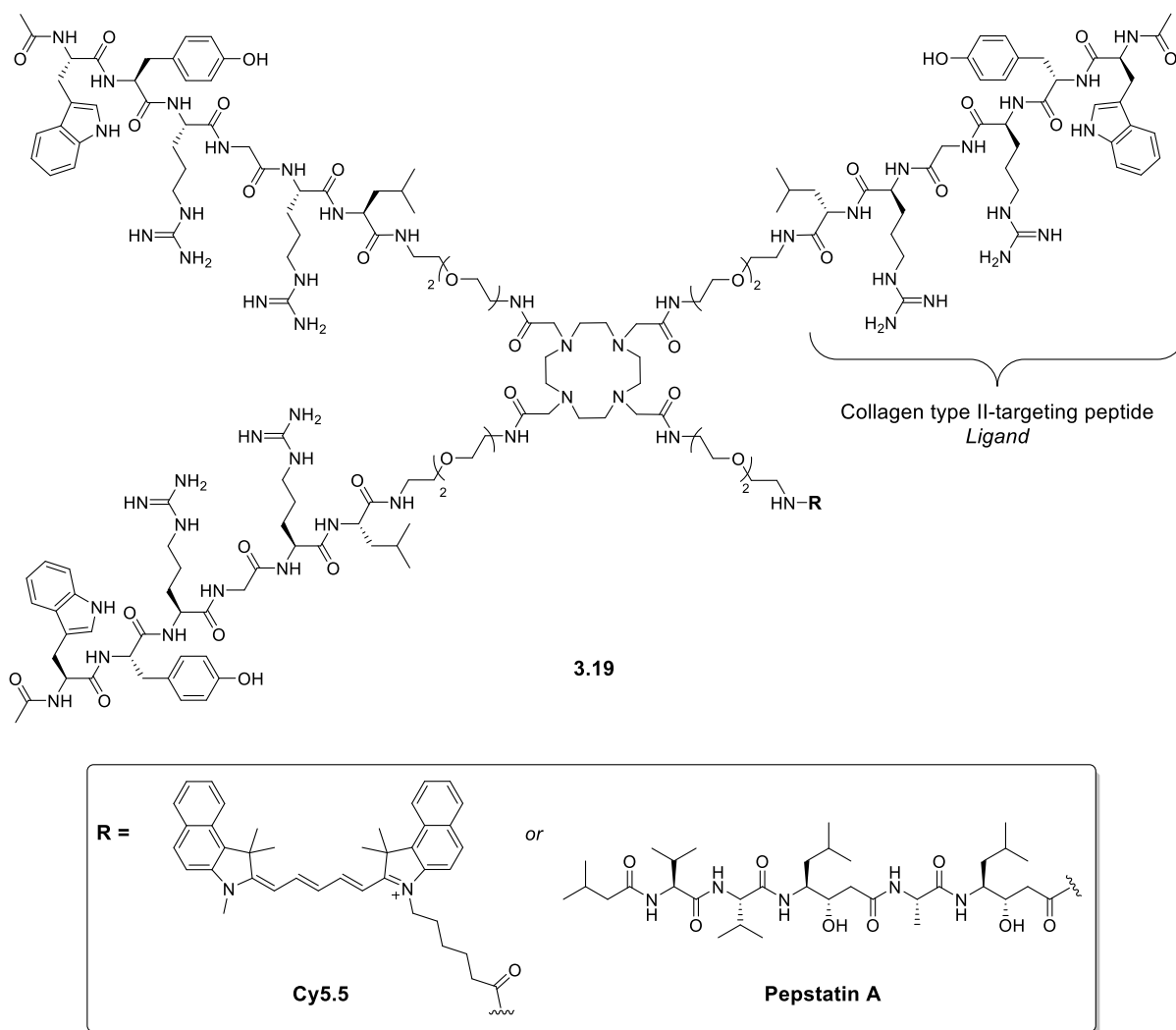


**Figure 3.7.** Unsymmetrically derivatized cyclen **3.19**, containing three collagen II-targeting peptide sequences and either the NIR dye Cy5.5 or the drug Pepstatin A.<sup>[261a]</sup>

This versatility in functionalization makes cyclen a general template for the modular synthesis of molecular imaging tools. Despite the numerous possible applications in medicine, the preparation of fully decorated DOTA compounds in heterogeneous fashion is challenging and often tedious.<sup>[266]</sup> In consequence, the assembly of hetero-multifunctional DOTA applying biorthogonal reactions remains largely uncharted. Current synthetic procedures are based on “protection-deprotection” steps, difficult

chromatographic purifications and low isolated yields, hampering further clinical development of these structures.

### 3.1.5. Motivation for the Synthesis of Multivalent Cyclen-based Fluorescent Ligands and Specific Aims

To overcome the aforementioned issues regarding the synthesis of hetero-multifunctional DOTA derivatives, the project described in this chapter aimed to develop a *clickable* imaging probe precursor using the DOTAM (3.16) as core. For the preparation of such a template, a three to one design was planned to allow for the incorporation of two distinct entities into the DOTAM scaffold – the recognition element and a reporter unit (Figure 3.8).

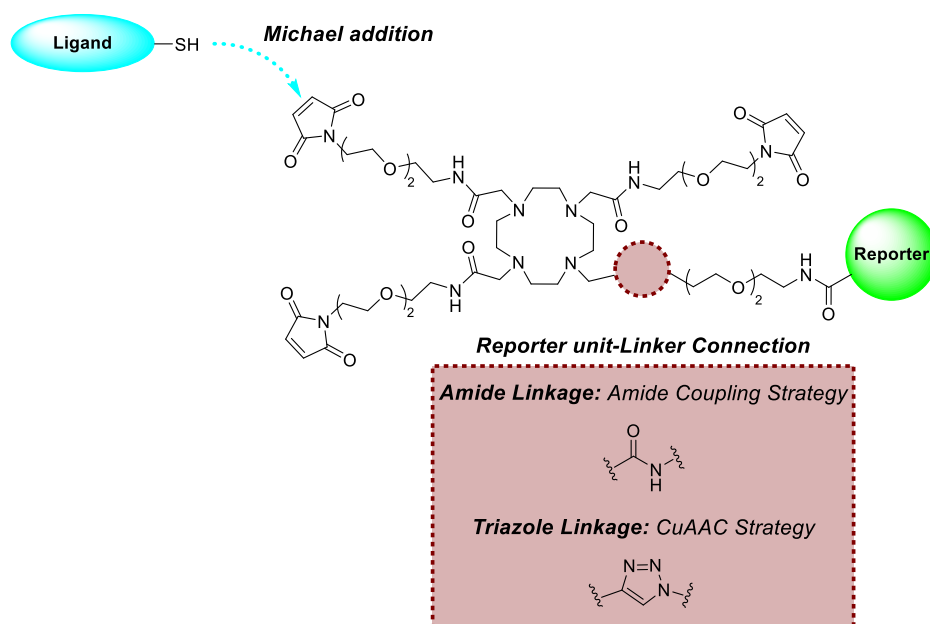


**Figure 3.8. DOTAM-based *clickable* probe template and reporter unit attachment linkages considered for the preparation of multivalent fluorescent ligands.** While terminal maleimides would enable introduction of three ligands to the DOTAM template, the reporter unit, i.e., fluorophore could be attached using either amide or triazole linkages.

Maleimide groups were chosen as multivalent handles for the attachment of the recognition element moieties due to its broad applicability for Michael-type addition coupling with cysteines and reactive

thiols.<sup>[267]</sup> These functionalities should be easily introduced at the targeting ligand structure. The fourth arm of the DOTAM core would allow for the orthogonal labeling of the signal agent through either amide or triazole linkages (Figure 3.8). As such, synthesis strategies based on amide coupling or CuAAC were investigated for probe assembling. Fluorescent dyes were selected as reporter unit for the *in vitro* validation of the DOTAM-based template using confocal microscopy techniques. To enhance compound solubility and add flexibility to the attached arms the linker would be composed by polyethylene glycol (PEG) chains containing two ethylene glycol units. Linker length optimization could be necessary depending on the target of choice and experimental test settings.

Ultimately, this new clickable precursor was utilized for the *one-pot* synthesis of heterogeneously tetrafunctionalized DOTA ligands applying subsequent biorthogonal conjugations in a modular and straightforward fashion.

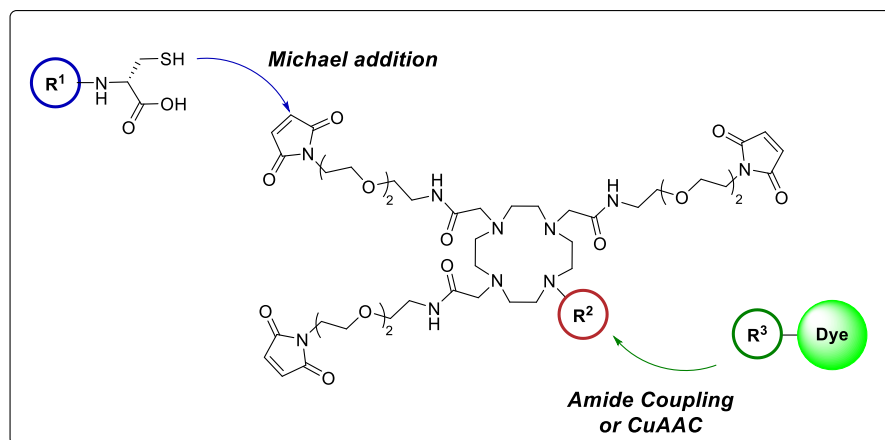
## 3.2. Results

### 3.2.1. Design of a Tetrasubstituted Cyclen-based Fluorescent Probe

The synthesis of a multivalent imaging agent to visualize early stages of PDAC was envisioned to explore the applicability and robustness of the clickable cyclen-based template. To this end, plectin-1 targeting PTP-ligand (**3.4**, Figure 3.3.A, Section 3.1.2.) was selected as recognition element. The non-targeting and, thus, not selective control peptide sequence (**3.5**, Figure 3.3.B, Section 3.1.2.) and a protected cysteine (**3.20**, **R<sup>1</sup>**, Figure 3.9.) were exploited for the synthesis of negative labeled controls. To both PTP-**3.4** and control-**3.5** peptide sequences an additional cysteine amino acid (Cys) was included in their C-terminus to enable their conjugation to the terminal maleimide groups at the probe template (**R<sup>1</sup>**, Figure 3.9.).

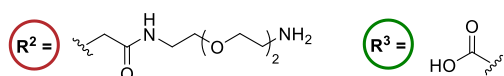
The cell permeable cyanine (Cy) Cy3 and Cy5.5 dyes were chosen as fluorescent reporter units due to their complementary photophysical properties and broad applicability in both *in vitro* and *in vivo* assays (Figure 3.9.). These fluorophores can be modifiable to bear various functionalities, including carboxylic acid, alkyne, and azide, which were investigated for their attachment to the probe template.

Therefore, the synthesis of cyclen building blocks encompassing three maleimides and either a terminal amine (Figure 3.9.A), azide (Figure 3.9.B), or alkyne groups (Figure 3.9.C) was planned.

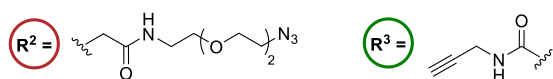


$R^1 =$   $\text{NH}_2\text{-KTLTPP-PEG}_2$  (**3.4**),  $\text{NH}_2\text{-SNLHPSD-PEG}_2$  (**3.5**) or *N*-acetyl cysteine methyl ester (**3.20**)

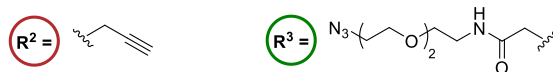
A) Amide Coupling Strategy for dye conjugation



B) CuAAC Strategy for dye conjugation: DOTAM-azide



C) CuAAC Strategy for dye conjugation: DOTAM-alkyne



Dye Structure =

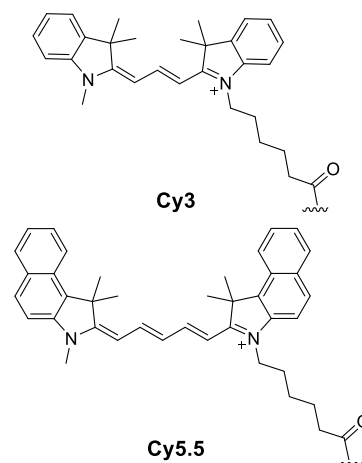


**Figure 3.9. Modular design of a cyclen-based precursor for the synthesis of multivalent fluorescent probes.**

Fluorophore labeling to probe template can be performed with A) amide coupling of the DOTAM-PEG2-amine to the carboxylic acid group of the dye, B) CuAAC reaction of the DOTAM-PEG2-azide to terminal alkyl functionality of the dye, or C) CuAAC reaction of the DOTAM-alkyne to the dye-PEG2-azide construct.

Depending on the *N*-substitution of the maleimide group, such constructs might undergo retro-Michael addition with other cysteine-containing cellular components.<sup>[268]</sup> To prevent this possible side-reaction, the succinimidyl thioether ring should be hydrolyzed before any biological application (Figure 3.10.A). This additional step could not only increase the stability and aqueous solubility of the fluorescent ligand, but also enhance the flexibility of its targeting arms.

The relevance of multivalence to image PDAC would be verified with mono-derivatized controls (Figure 3.10.B). These compounds would be synthesized encompassing a 1:1 recognition element and fluorophore ratio.

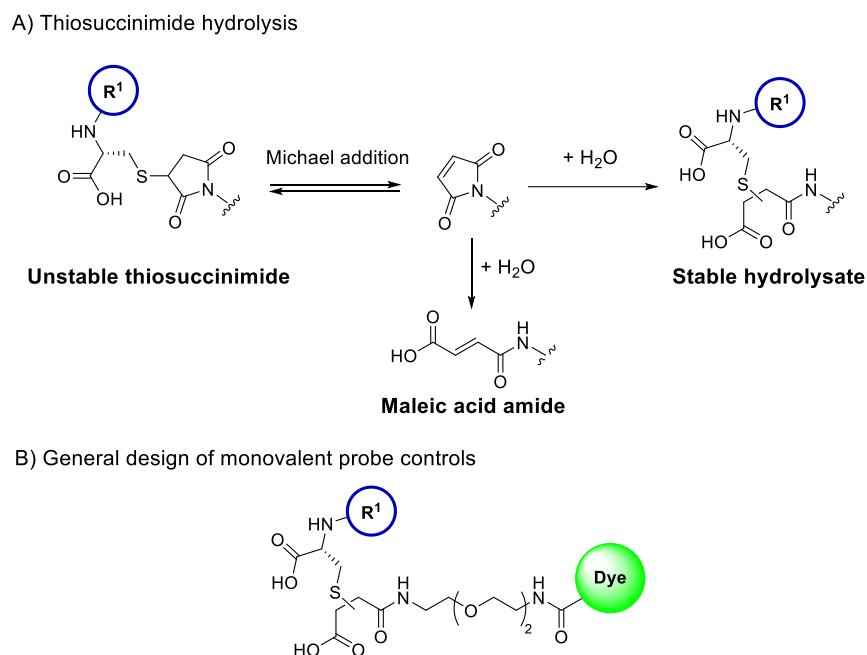


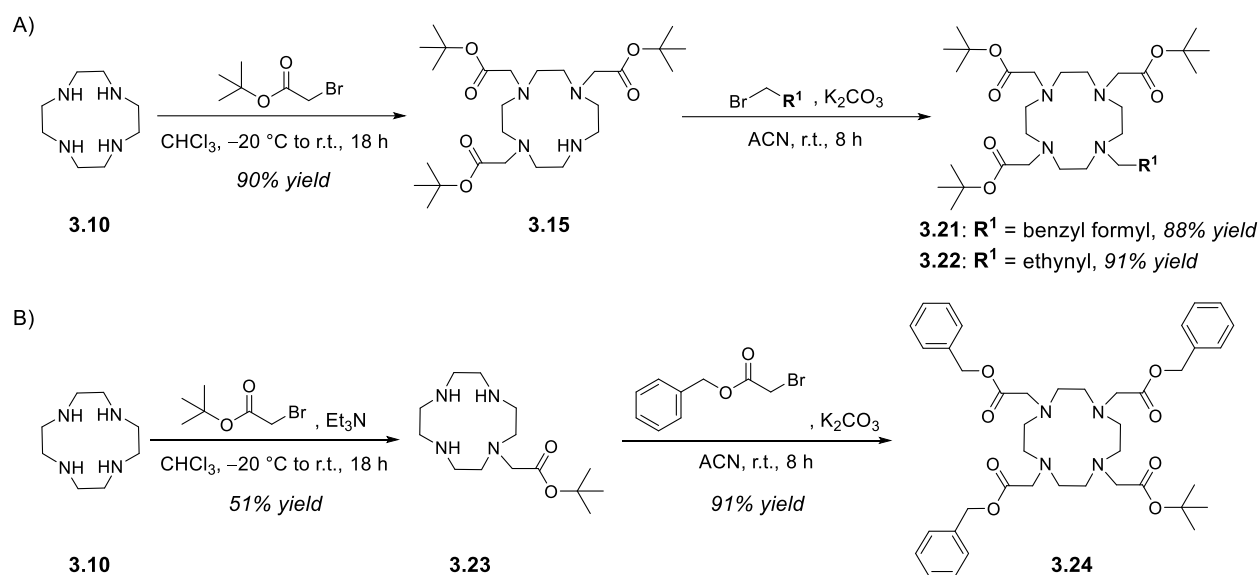
**Figure 3.10. Stabilization of thiol-maleimide adducts for biological systems and monovalent probe design.** Thiosuccinimide hydrolysis can be either achieved through mild ultrasonication or alkaline treatment.<sup>[268a]</sup> For  $R^1$  ligands and dye structures *see* Figure 3.9.

### 3.2.2. Preparation of Fourfold *N*-Functionalized Cyclen Building Blocks and Linker Synthesis

There are various synthesis routes which can be exploited to provide a bifunctional cyclen (**3.10**) scaffold.<sup>[261a, 266b, 269]</sup> In general, these routes exploit orthogonal protective groups, such as Fmoc, Boc and Cbz groups, to enable differentiation of one secondary amine of the cyclen ring over the remaining three. These groups are stable under common organic reaction conditions, yet are capable of sequential and selective removal. Thus, this strategy enables the use of amide coupling, reductive amination, and *N*-alkylation for the installation of the desired components for imaging probe

assembling. In this project, *tert*-butyl and benzyl were selected as protective groups for the conjugation of  $\alpha$ -halogenated carboxylic acids into the cyclen core using two different synthetic strategies.

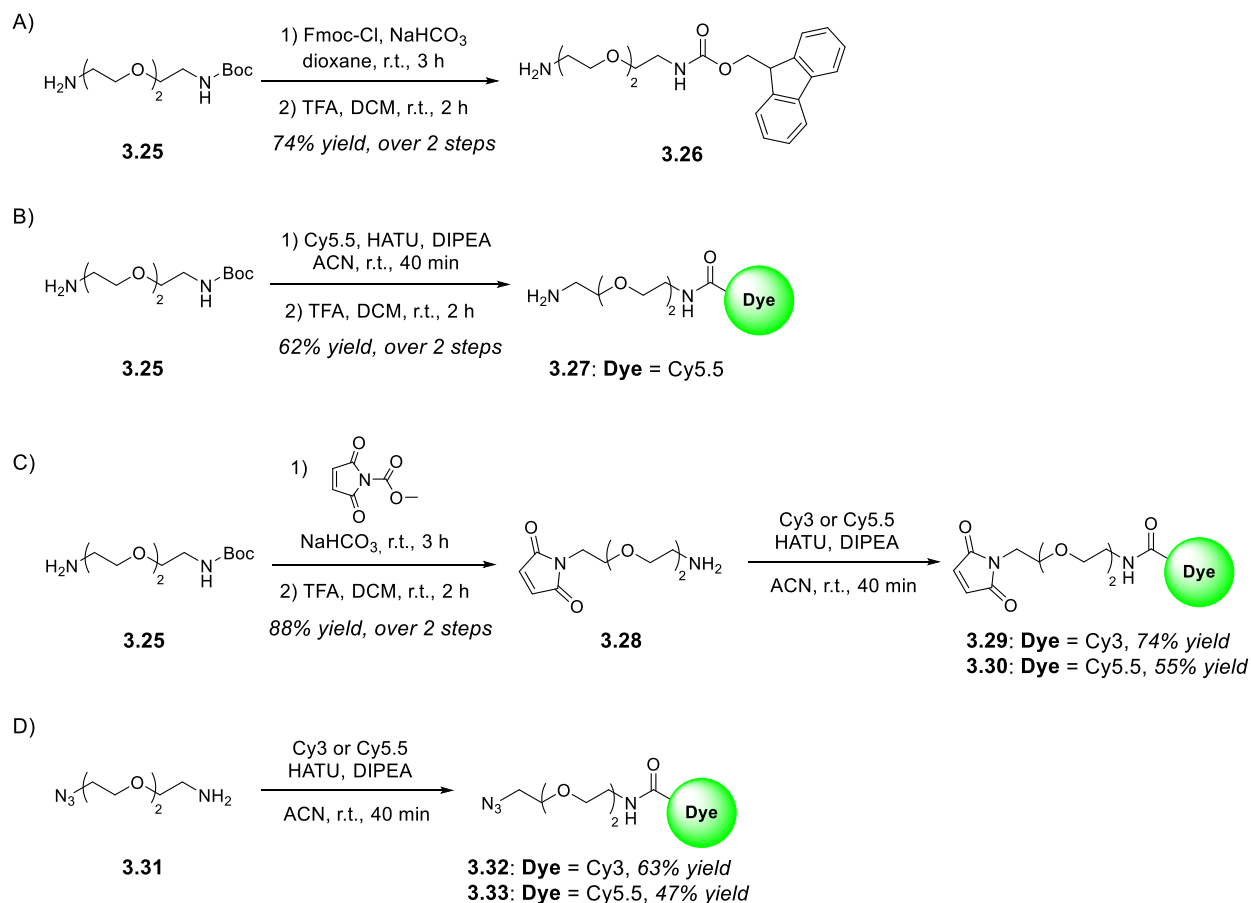
The first route started with a triple *N*-alkylation reaction on the cyclen scaffold (**3.10**) using *tert*-butyl bromoacetate to afford DO3A intermediate **3.15** in excellent 90% yield (Scheme 3.1.A). Subsequent *N*-alkylation applying either benzyl bromoacetate or propargyl bromide provided key building blocks **3.21** and **3.22**. Alternatively, the *N*-monoalkylation of cyclen **3.10** using *tert*-butyl bromoacetate provided intermediate **3.23** in moderate yield after reversed-phase medium pressure liquid chromatography (MPLC) chromatography (Scheme 3.1.B). Treatment with benzyl bromoacetate under basic conditions afforded tetra-substituted cyclen **3.24** in 90% yield. These building blocks (**3.21**, **3.22** and **3.24**) were further explored for the introduction of linker functionalities via amide coupling.



**Scheme 3.1. Synthesis of fourfold *N*-functionalized cyclen.** Synthesis route A) through DO3A intermediate **3.15** formation and B) through *N*-monoalkylated intermediate **3.23** formation.

The different linkers required for DOTA functionalization were synthesized either from the commercially available *N*-Boc protected PEG2-amine **3.25** or azido-PEG2-amine **3.31** (Scheme 3.2.). Standard Fmoc protection using Fmoc chloride and sodium bicarbonate in dioxane afforded Fmoc-linker **3.26** in a moderate 43% yield (Scheme 3.2.A). The preparation of Cy5.5-labeled PEG2 linker (**3.27**) was achieved through amide coupling using HATU (Scheme 3.2.B). Maleimide-functionalized linker **3.28** was obtained from the reaction with activated maleimide *N*-methyl carbamate<sup>[270]</sup> under aqueous basic conditions in a very good 88% yield (Scheme 3.2.C). After these reactions, subsequent

deprotection of the Boc group with trifluoroacetic acid provided the amine functionality in quantitative yields.



**Scheme 3.2. Synthesis of PEG2 linker building blocks from *N*-Boc protected PEG2 amine (3.25) and azido-PEG2 (3.31) linkers.** A) Fmoc-protection of 3.25, B) Cy5.5-labeling of 3.25, C) Introduction of the maleimide functionality at 3.25, followed by Cy3 or Cy5.5 conjugation, and D) Cy3 or Cy5.5-labeling of 3.31. For fluorophore structures *see* Figure 3.9., Section 3.2.1.

These linkers were employed for both the synthesis of novel DOTAM probe precursors, as described in the following sections, or further conjugated with the Cy3 and Cy5.5 fluorophores to investigate the fluorescent labeling strategies planned (Scheme 3.2.C and 3.2.D., for design approaches *see* Figure 3.9., Section 3.2.1.). Using standard amide coupling conditions, the maleimide-linker derivative 3.28 was conjugated to the carboxylic acid functionality of both cyanine 3 and cyanine 5.5 dyes in moderate to good yields (Scheme 3.2.C). The same conditions were also applied to azido-PEG2 3.25 to afford labeled azides 3.32 and 3.33 (Scheme 3.2.D).



### 3.2.3. Synthesis of Fluorescently Labeled Monovalent Control Probes

Before the development of the more complex *N*-functionalized cyclen tetrapodal templates, syntheses of monovalent congeners were carried out (Figure 3.10.B, Section 3.2.1.). These probes served as fluorescent controls for the biological validation of the DOTAM-based constructs (Figure 3.9., Section 3.2.1.). They can be applied in the assay design for optimization of the test settings as well as during the assay to compare the cellular uptake and imaging quality of mono- vs. tri-targeting peptides. Since these tools are devoid of the cyclen core, the influence of this macrocycle on the overall physicochemical properties of the probes can be additionally evaluated.

For the preparation of these control tools, a Michael-type addition reaction of ligand cysteinates to the maleimide moiety of cyanine-labeled PEG2 linkers (**3.29** and **3.30**, see Scheme 3.2.C, Section 3.2.2.) was planned. To avoid the unwanted hydrolysis of the maleimide group to maleic acid amide which prevents thiol conjugation under biological conditions<sup>[271]</sup> (Figure 3.10.A, Section 3.2.1.), this reaction step was evaluated in a set of different solvent systems (Table 3.1.). These investigations were conducted using cysteinyl PTP-**3.4** and Cy5.5-labeled **3.30** as model reagents.

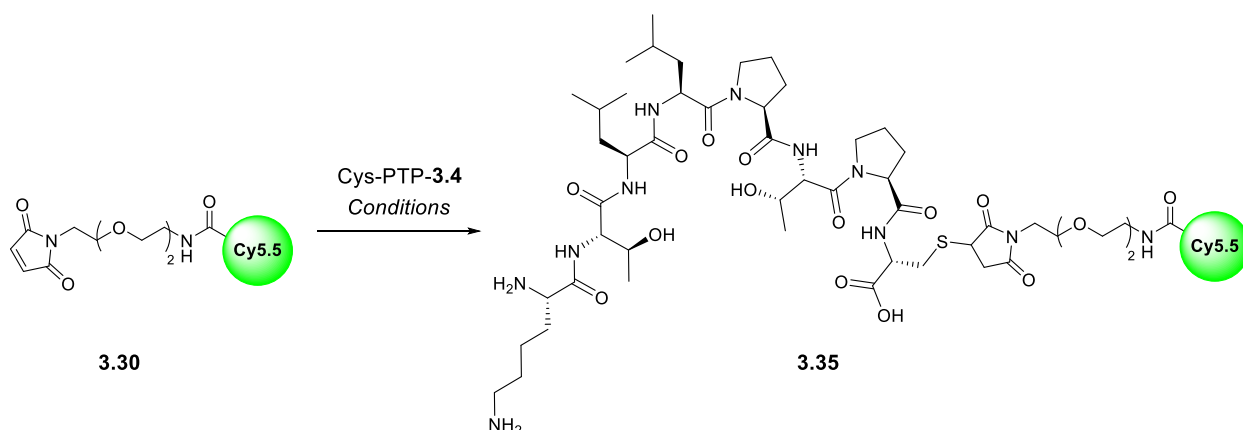
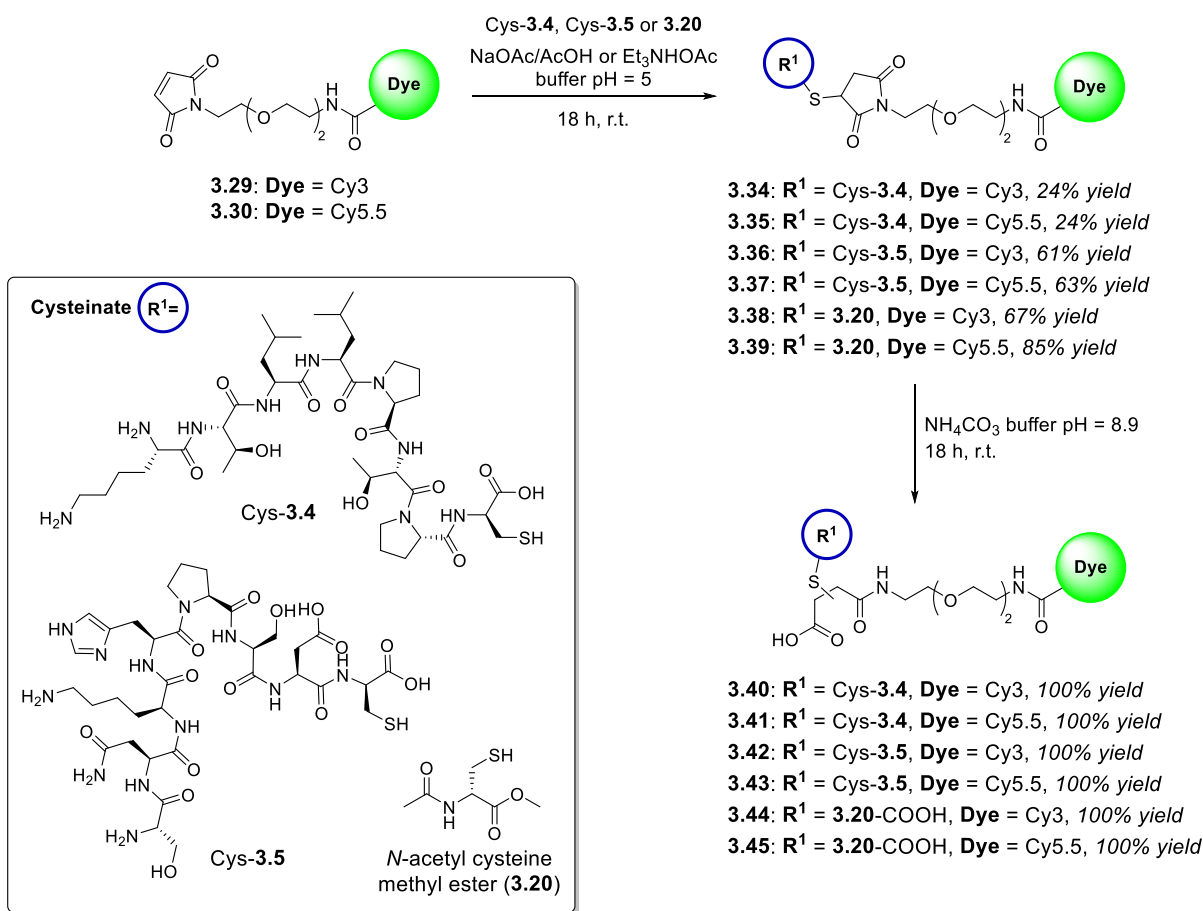


**Table 3.1.** Solvent systems tested for the Michael-type addition reaction between Cy5.5-labeled maleimide-PEG2 **3.30** and cyteinate PTP-**3.4**.

Entry	Solvent	Time	Result
1	ACN	n.a.	No conversion; suspension of <b>3.30</b> observed
2	ACN:DMF (1:1, <i>v/v</i> )	6 d	<b>3.35</b>
3	PBS buffer pH = 7.4	8 h	maleic acid amide formation
4	Sodium acetate-acetic acid buffer pH = 5	18 h	<b>3.35</b>
5	Triethylammonium acetate buffer pH = 5	18 h	<b>3.35</b>

n.a. – not applicable. Reaction conditions: Cy5.5-labeled PEG2 **3.30** (1.0 equiv.), Cys-PTP-**3.4** (1.5 equiv.), solvent (3 mL), room temperature.

Organic solvents, including dimethylformamide and acetonitrile were initially tested (Table 3.1., entries 1 and 2). Although product **3.35** formation was observed in a mixture of dimethylformamide and acetonitrile (1:1, *v/v*), this reaction was extremely slow, requiring up to six days for complete conversion to the desired thiosuccinimide **3.35** (Table 3.1., entry 2). Since the formation of maleic acid amide occurs faster at higher pH (> 7.4), two acetate-based buffer systems at pH = 5 and phosphate buffered saline (PBS) buffer at pH = 7.4 were additionally screened (Table 3.1., entries 3 to 5). Under physiological conditions (pH = 7.4), hydrolysis of maleimide **3.30** to its maleic acid amide congener occurred before the thiol-maleimide bond formation to product **3.35** could take place (Table 3.1., entry 3). However, at pH = 5, applying both acetate buffers, the reaction resulted in complete conversion to the desired product **3.35**, without maleic amide formation (Table 3.1., entries 4 and 5).



**Scheme 3.3. Synthesis of monovalent controls 3.40 to 3.45.** Either acetic acid-sodium acetate or triethylammonium acetate buffer systems at pH = 5 were applied for the thiol-maleimide Michael addition; Ammonium carbonate buffer at pH = 8.9 was applied for the hydrolysis of succinimide rings.

Using these conditions (volatile triethylammonium acetate buffer at pH = 5, Table 3.1., entry 5), the cysteinate ligands PTP (**3.4**), control peptide (**3.5**), and protected cysteine (**3.20**) were converted to the thiosuccinimide cyanine labeled intermediates **3.34** to **3.39** (Scheme 3.3). As discussed in Section 3.2.1., thiosuccinimide hydrolysis leads to stable succinamic acid thioether bioconjugates which cannot undergo retro-Michael addition<sup>[268]</sup> (Figure 3.10.A, Section 3.2.1.). Therefore, the labeled succinimide derivatives **3.34** to **3.39** were subsequently hydrolyzed upon alkaline treatment with volatile ammonium carbonate buffer (pH = 8.9) to the stable derivatives **3.40** to **3.45** (Scheme 3.3.).

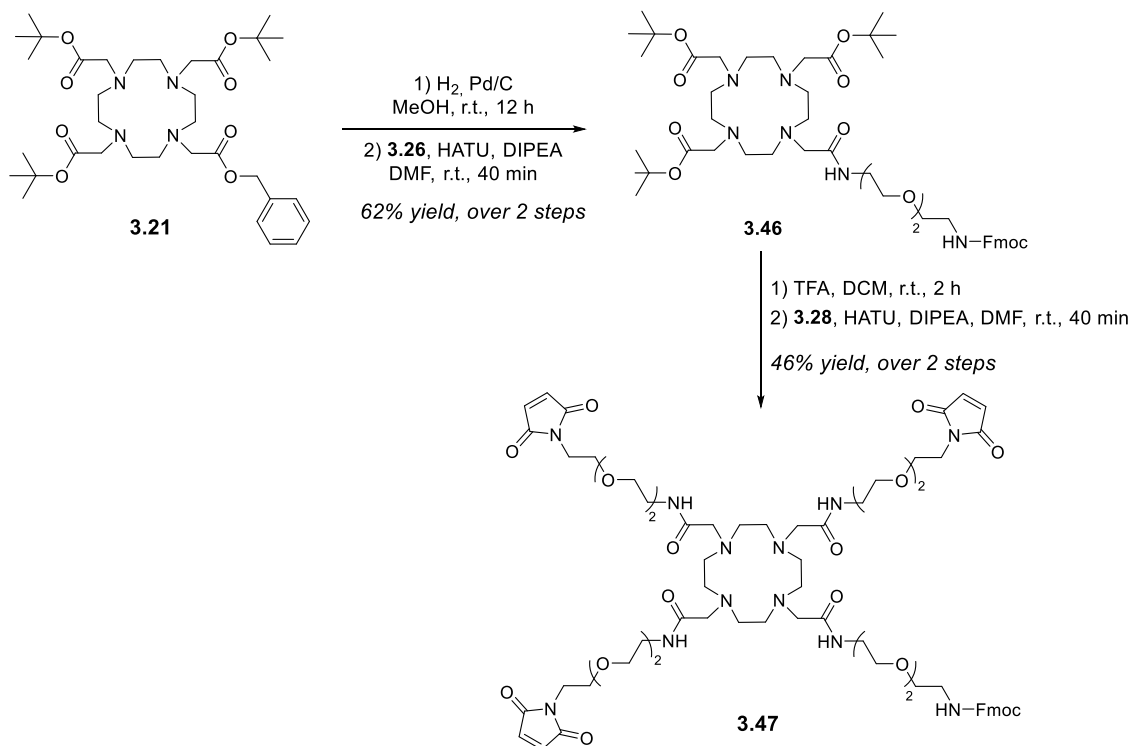
For the non-peptidic **3.44** and **3.45**, the methyl ester portion of their structures was further hydrolyzed to carboxylic acid under the reaction conditions (Scheme 3.3.). However, this additional conversion was not expected to interfere in the biological performance of compounds **3.44** and **3.45** as non-targeting controls. The use of volatile buffers was crucial to regulate the reactions' pH, while simplifying their work up to a single lyophilization step. This methodology avoided the need for dialysis or desalting columns to remove the excess of salt prevent from non-volatile buffers.

#### **3.2.4. First Approach Towards Cyclen-based Multivalent Ligands: Probing the R<sup>2</sup>-Substitution with an Amine for Fluorophore Attachment**

The preparation of functionalized DOTAM derivatives using fully protected cyclen intermediates **3.22** and **3.24** is well-known and has been described by several authors.<sup>[261a, 266, 269]</sup> Using these strategies, multiple entities can be conjugated to the probe scaffold through amide coupling reactions, usually with HATU as coupling reagent. Taking advantage of these established conditions, the first approach towards a DOTAM-based multivalent ligand template explored an amide bond formation for fluorophore introduction (Figure 3.9.A, Section 3.2.1.). With the DOTAM scaffolds **3.22** and **3.24** and the set of PEG2 amine linkers **3.25** to **3.28** in hand, many possible amide coupling strategies could lead to the desired probe template.

According to previously described conditions by HU and collaborators,<sup>[261a]</sup> heterovalent decorated DOTAM could be obtained through the Fmoc protected intermediate **3.47** (Scheme 3.4.). Using this methodology, benzyl deprotection of cyclen **3.21** followed by HATU-mediated coupling with *N*-Fmoc protected PEG2 **3.26** afforded amide derivative **3.46**. Subsequent acidic treatment of Fmoc

intermediate **3.46** allowed for deprotection of the *tert*-butyl moieties to afford free carboxylic acid functionalities, which were activated with HATU for coupling with maleimide PEG2 linker **3.28** (Scheme 3.4). Notably, this is the first report of cyclen functionalization with maleimide groups.



**Scheme 3.4.** Synthesis of the fourfold functionalized fmoc protected DOTAM **3.47**.

The following Fmoc deprotection of **3.47** with diethylamine or piperidine (Table 3.2., entries 1 and 2) led to multiple side-products, including Michael addition of the secondary amine of these bases to the methylene portions of **3.47**, without generating perceptible amounts of the desired macrocyclic free amine **3.48**. Moreover, the reactivity of the maleimide group also hampers the addition of ethanethiol, usually employed as a scavenger to trap the released dibenzofulvene.<sup>[272]</sup> Consequently, a number of alternatives to a conventional Fmoc deprotection were examined. Conditions exploring tertiary amines, such as diisopropylamine (Table 3.2., entry 3) and 1,8-diazabicyclo[5.4.0]undec-7-ene (DBU, Table 3.2., entries 4 and 5) did provide the desired amine from **3.48**, but the slow conversion to product led to the undesired hydrolysis of the maleimide to maleic amide over time.

As such, the use of tetra-*N*-butylammonium fluoride (TBAF) in the presence of isopropanol, instead of the thiol as fulvene scavenger was next investigated (Table 3.2., entry 6).<sup>[273]</sup> This method (2 equiv. TBAF, 10 equiv. *i*PrOH, DMF, 0 °C, 15 min) proved to be well suited to deprotect Fmoc in this

context under mild conditions. Nevertheless, the isolation of intermediate free amine **3.48** was highly challenging. Column chromatography using either normal- or reversed-phase was not successful in separating TBAF and dibenzofulvene from the reaction mixture. A desalting column, followed by washes with water led to complete removal of the fulvene byproduct, but only partially TBAF. Finally, several extraction rounds with chloroform was the best method to obtain pure **3.48** in 60% yield.

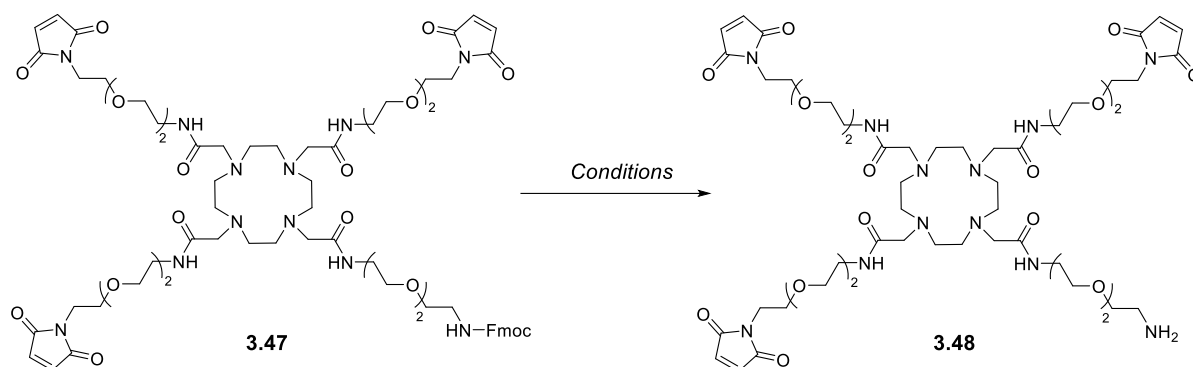


**Table 3.2. Conditions tested for the Fmoc-deprotection of intermediate 3.47.**

Entry	Base	Solvent	Time (min)	Result
1	10% Diethylamine	DMF	30	Complex mixture <sup>[b]</sup>
2	5% Piperidine	DMF	30	Complex mixture <sup>[b]</sup>
3	5% DIPEA	ACN	60	<b>3.48</b> + maleic acid amide side-product <sup>[c]</sup>
4	3% DBU	ACN	15	<b>3.48</b> + maleic acid amide side-product <sup>[c]</sup>
5	3% DBU	DMF	15	<b>3.48</b> + maleic acid amide side-product
6	TBAF, <i>i</i> PrOH <sup>[a]</sup>	DMF	15	<b>3.48</b> , 60% yield

All test reactions were conducted at 0 °C. <sup>[a]</sup> TBAF (2 equiv.) and *i*PrOH (10 equiv.); <sup>[b]</sup> Both Michael addition reaction of secondary amine moieties of these bases to Fmoc-**3.47** and hydrolysis of these side-products to maleic acid amide congeners observed via liquid chromatography–mass spectrometry (LC-MS); <sup>[c]</sup> Observed via LC-MS.

The subsequent amide coupling step for the installation of cyanine fluorophores to free amine **3.48** was, however, not accomplished (Table 3.3.). Activation of the carboxylic acid functionality from Cy3 and Cy5.5 dyes with several coupling reagents, including HATU, *N,N,N',N'*-tetramethyl-*O*-(*N*-succinimidyl)uronium hexafluorophosphate (HSTU), 1,1'-carbonyldiimidazole (CDI), DMTMM, and propanephosphonic acid anhydride (T3P) in the presence of DIPEA, followed by the subsequent treatment with free amine **3.48** led to no observable conversion to the desired labeled product (Table 3.3., entries 1 to 5). Up to 1 hour activation time of the acid portion before the addition of amine **3.48** did not improve the reaction outcomes.

In a similar manner, a pre-activation step using either *N*-hydroxysuccinimide (NHS), perfluorophenol (PFP), or fluoro-dipyrrolidinocarbenium hexafluorophosphate (BTFFH) to produce the congeners

NHS-ester, PFP-ester, or acid fluoride BTFFH-ester of the cyanine dyes was not sufficient to induce amide bond formation (Table 3.3., entries 6 to 8). To preclude the possible sterically hindrance from the pre-organized PEG chains, these reactions were executed in alternative solvent systems, such as acetonitrile, ethyl acetate, dichloromethane, and water using HATU (Table 3.3., entries 9 to 12). Yet, in all cases, starting materials could be recovered from the reaction mixture.

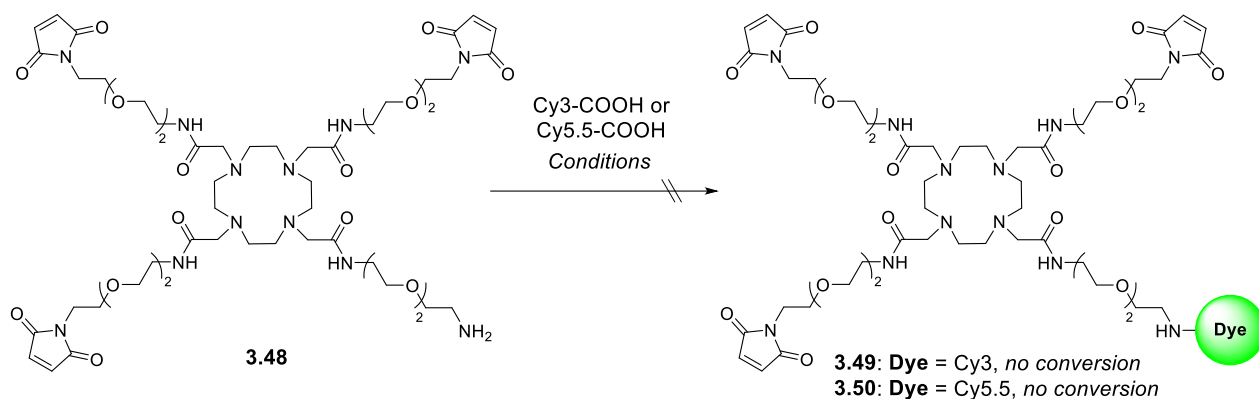
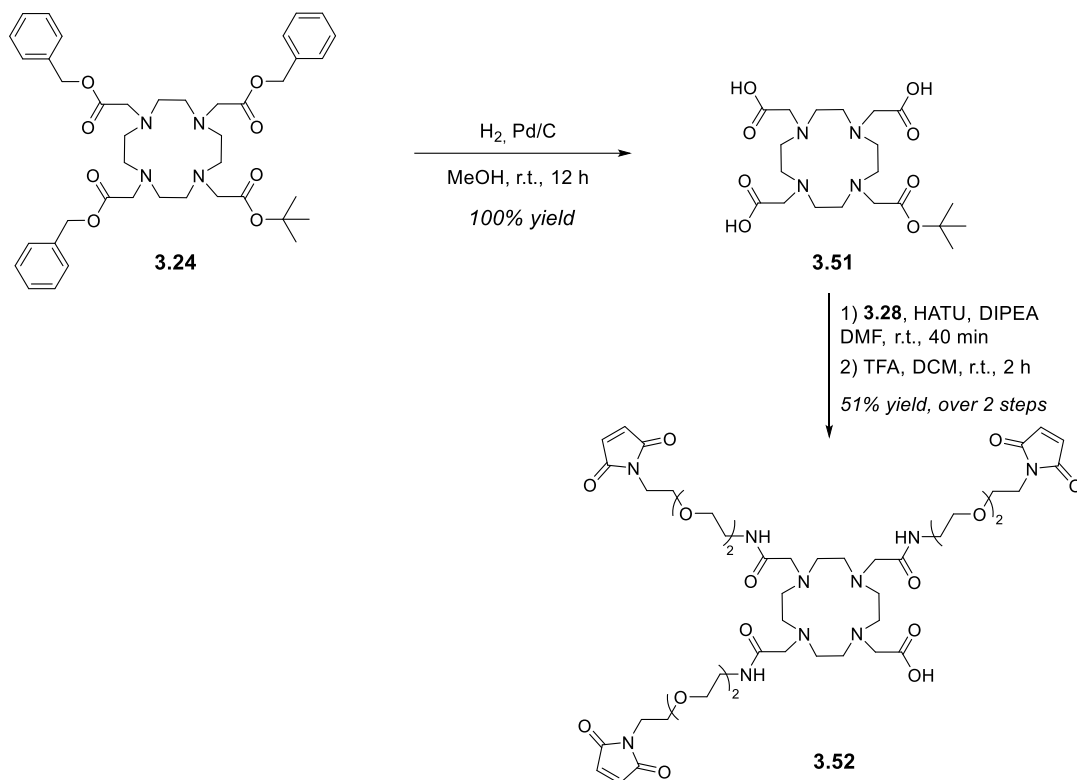


**Table 3.3. Amide coupling conditions for conjugating a cyanine dye at the free amine functionality of 3.48.**

Entry	Coupling Agent	Carboxylic acid	Solvent	Result
1	HATU	Cy3 or Cy5.5	DMF	No conversion
2	HSTU	Cy3 or Cy5.5	DMF	No conversion
3	CDI	Cy3 or Cy5.5	DMF	No conversion
4	DMTMM	Cy3 or Cy5.5	DMF	No conversion
5	T3P	Cy3 or Cy5.5	DMF	No conversion
6	n.a.	NHS-Cy5.5	DMF	No conversion
7	n.a.	PFP-Cy5.5	DMF	No conversion
8	n.a.	BTFFH-Cy5.5	DMF	No conversion
9	HATU	Cy3 or Cy5.5	ACN	No conversion
10	HATU	Cy3 or Cy5.5	EtOAc	No conversion
11	HATU	Cy3 or Cy5.5	DCM	No conversion
12	HATU	Cy3 or Cy5.5	Water	No conversion

n.a. – not applicable. Reaction conditions: amine **3.48** (1.0 equiv.), cyanine carboxylic acid (Cy3-COOH or Cy5.5-COOH, 1.0 equiv.), coupling agent (1.1 equiv.), DIPEA (5.0 equiv.), solvent (1 mL). Anhydrous solvents were used for all tested conditions, except for HSTU (entry 2).

To evaluate the reactivity of this coupling, an inversion of amide and carboxylic acid functionalities from the DOTAM scaffold and linker was investigated (Scheme 3.5.). Since the hydrogenation reaction conditions required for the removal of the benzyl group of **3.21** are not orthogonal to the maleimide functionalities, an adapted approach using the tri-substituted cyclen benzyl **3.24** was carried out.



Scheme 3.5. Synthesis of carboxylic acid **3.52** from DOTA-building block **3.24**.

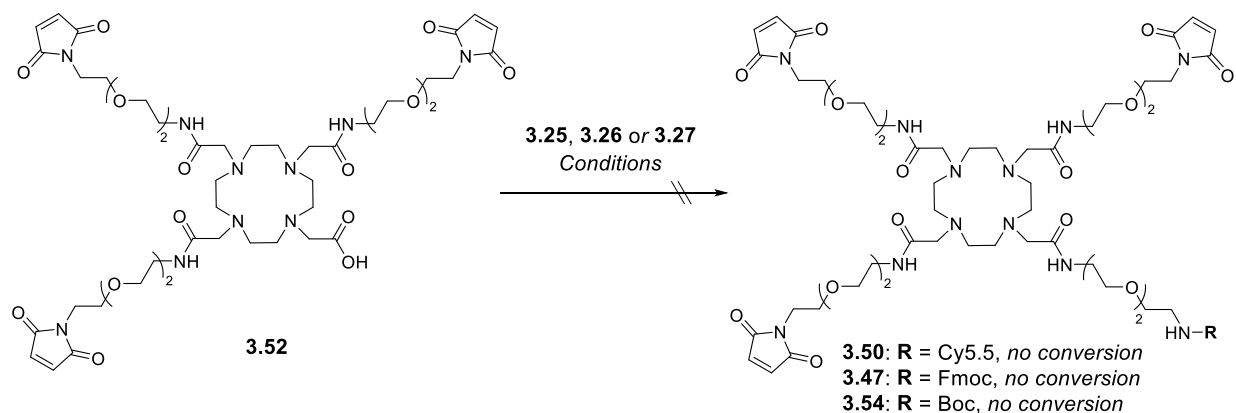
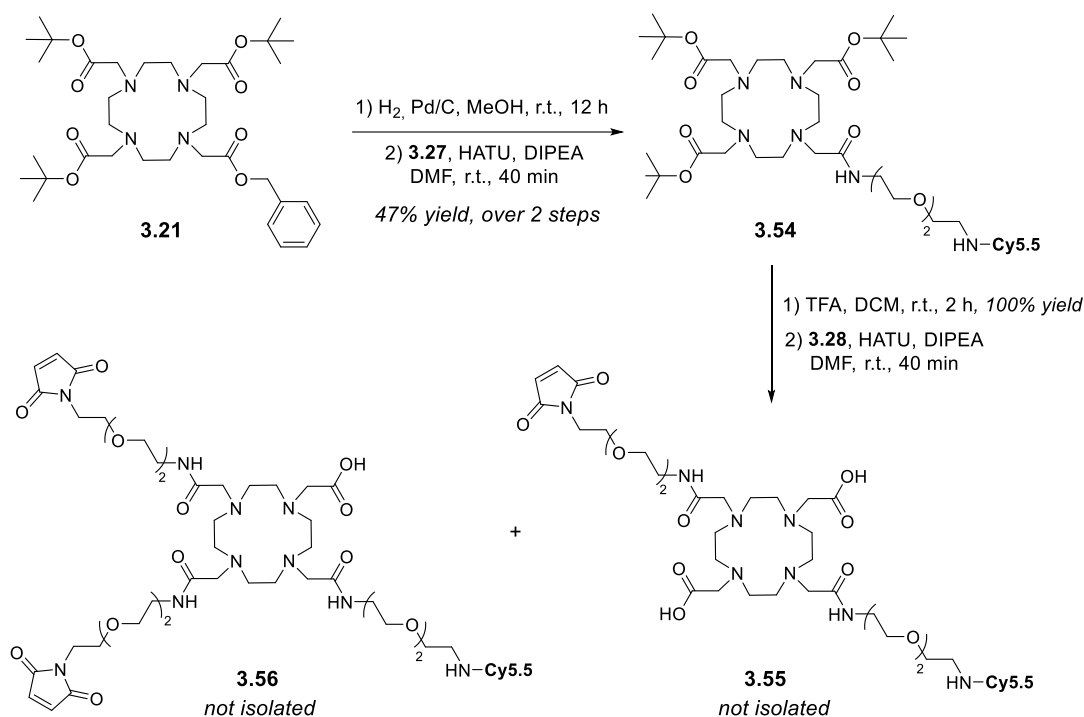


Table 3.4. Amide coupling conditions attempted for installing the fourth PEG2 linker unit at carboxylic acid intermediate **3.52**.

Entry	PEG2 amine	Coupling Agent	Base	Solvent	Result
1	Cy5.5- <b>3.27</b>	HATU	DIPEA	ACN	No conversion
2	Cy5.5- <b>3.27</b>	BOP-Cl	DIPEA	ACN	No conversion
3	Cy5.5- <b>3.27</b>	T3P	Triethylamine	ACN	No conversion
4	<i>N</i> -Boc- <b>3.25</b>	HATU	DIPEA	DMF	No conversion
5	<i>N</i> -Fmoc- <b>3.26</b>	HATU	DIPEA	DMF	No conversion

Reaction conditions: carboxylic acid **3.52** (1.0 equiv.), PEG2-amine **3.25**, **3.26**, or **3.27** (1.0 equiv.), coupling agent (1.1 equiv.), base (8.0 equiv.), solvent (1 mL). Anhydrous solvents were applied for all tested conditions.

Applying similar conditions as for the preparation of intermediate **3.47** (Scheme 3.4.), carboxylic acid **3.52** was obtained in moderate 51% yield as confirmed by <sup>1</sup>H-NMR and HR-MS analysis. However, the subsequent labeling procedure employing either HATU, BOP-Cl, or T3P for conjugation of intermediate **3.52** to Cy5.5-PEG2 linker **3.27** was unsuccessful (Table 3.4., entries 1 to 3). The installation of the smaller *N*-Boc (**3.25**) and *N*-Fmoc protected linkers (**3.26**) to acid **3.52** using HATU led to similar results (Table 3.4., entries 4 to 5). These attempts demonstrated the lack of feasibility of coupling the fluorophore-linker construct to cyclen template **3.52** by amide formation.



**Scheme 3.6.** Attempted synthesis of Cy5.5 labeling of building block **3.21** prior to the installation of maleimide-PEG2 linker **3.28**. Compounds **3.56** and **3.57** were obtained as a complex mixture which could not be separated under the tested HPLC conditions.

To overcome this problem, introduction of the cyanine fluorophore at earlier steps in the synthesis route, prior to maleimide-linker **3.28** conjugation to the probe template, was pursued (Scheme 3.6.). To this end, the conditions established for the preparation of Fmoc-protected **3.47** and carboxylic acid **3.52** were explored for the generation of Cy5.5-labeled **3.55**. Removal of the *tert*-butyl protective groups of **3.55** using trifluoroacetic acid exposed the carboxylic acids which were further treated with HATU (3.3 equiv.) and maleimide PEG linker **3.28** (3.3 equiv.). This amide coupling reaction, however, resulted only in the di- (**3.56**) and tri- (**3.57**) functionalized cyclen. Despite the addition of excess equivalents of coupling reagent and amine linker, conversion to the desired tri-substituted template

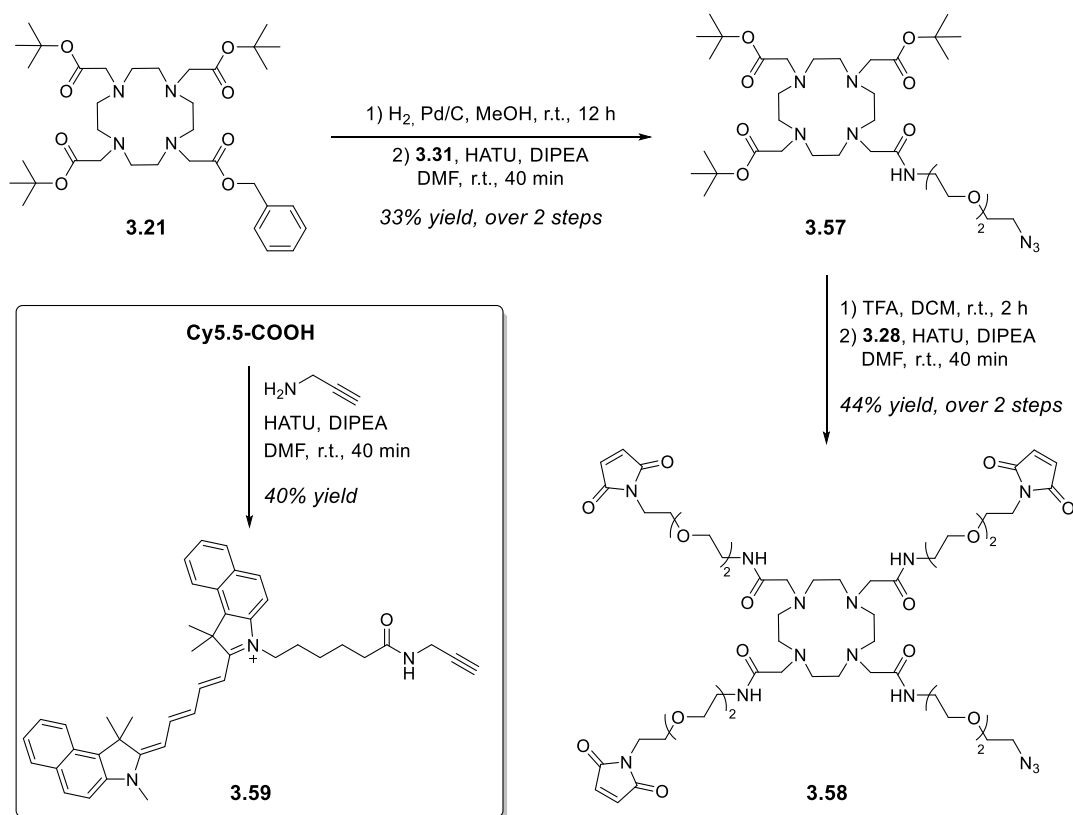


was not observed. Moreover, isolation of **3.56** and **3.57** was not achieved via HPLC due to the similar retention times of both intermediates in the screened conditions.

Probe assembling via subsequent amide coupling reactions was deemed unfeasible for the synthesis of the envisioned tetrasubstituted heterogeneous DOTA conjugates (Figure 3.9., Section 3.2.1.). Therefore, a new synthesis strategy based on CuAAC *click* chemistry for fluorophore conjugation was pursued.

### 3.2.5. Second Approach Towards Cyclen-based Multivalent Ligands: Probing the R<sup>2</sup>-Substitution with an Azide for Fluorophore Attachment

Since amide bond formation was not a reliable method for fluorophore labeling of the DOTAM template, a triazole connectivity was next investigated.



Scheme 3.7. Synthesis of the CuAAC partners azido-DOTAM **3.58** and alkyne-dye **3.59**.

The installation of an azide handle at the cyclen core would enable CuAAC reaction with a cyanine dye containing an alkyne functionality (Figure 3.9.B, Section 3.2.1.). Key building blocks for this synthesis pathway are the azido-DOTAM precursor **3.58** and Cy5.5 analog **3.59** (Scheme 3.7.). Starting from derivative **3.21**, azide-PEG2 linker **3.31** was installed in 4 steps using the synthetic conditions previously employed for the preparation of other analogs, e.g., Fmoc-protected **3.47** (see Scheme 3.4., Section 3.2.4.). The CuAAC reaction partner **3.59** was obtained in moderate yield from the HATU coupling of Cy5.5 carboxylic acid and propargyl amine.

There are several studies which describe the use of CuAAC to form stable conjugates within macrocyclic polyamines.<sup>[260b, 265a, 274]</sup> In the search for suitable conditions for the copper-catalyzed cycloaddition between azide **3.58** and alkyne **3.59**, the most common CuAAC literature procedures applied for triazole formation at DOTA and DOTA-like structures were evaluated (Table 3.5.). Despite the use of diverse copper catalysts both in catalytic and stoichiometric amounts, none of the conditions tested led to the formation of triazole **3.60**.

CuAAC is known to perform best at neutral and alkaline solvents ( $6 > \text{pH} > 8$ ), in particular at pH closer to 8.<sup>[275]</sup> At higher pH values, the cycloaddition proceeds at a faster rate, but hydrolysis of the maleimide to maleic amide is of greater concern. Therefore, the influence of the solvent and pH for conversion were also analyzed (Table 3.5., entries 1 to 4, 7 to 9, and 11 to 13), yet with no favorable result. In addition, tris(benzyltriazolylmethyl)amine (TBTA) was included to stabilize the Cu(I) oxidation state in solution while increasing the reaction rates<sup>[276]</sup> (Table 3.5., entries 4 to 6). However, in this case, no conversion to product **3.60** was observed.

Besides copper sulfate, different copper sources were investigated in order to promote the CuAAC reaction between azide **3.58** and alkyne **3.59**. As such, conditions exploiting Cu(II), Cu(I) and metallic copper catalysts were attempted, including copper iodide (Table 3.5, entries 7 to 10), tetrakis-(acetonitrile)copper(I) hexafluorophosphate ( $[\text{Cu}(\text{CH}_3\text{CN})_4]\text{PF}_6$ , Table 3.5, entries 11 to 14), copper powder (Table 3.5, entries 16 and 17), copper wire (Table 3.5, entry 18), and copper on carbon (Table 3.5, entry 19). None of these copper sources, however, led to successful outcomes. Moreover, all test reactions were maintained at room temperature since heating to 50 °C resulted in the degradation of DOTAM starting material **3.58**. The lack of stability of this reagent upon exposure to mild temperatures might be triggered by the copper ions since otherwise, these molecules showed to tolerate up to 75 °C heating overnight.

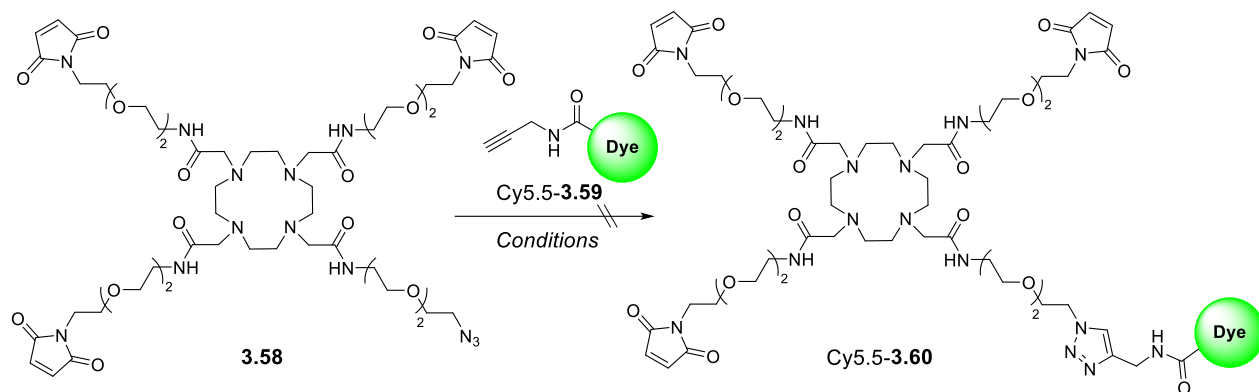


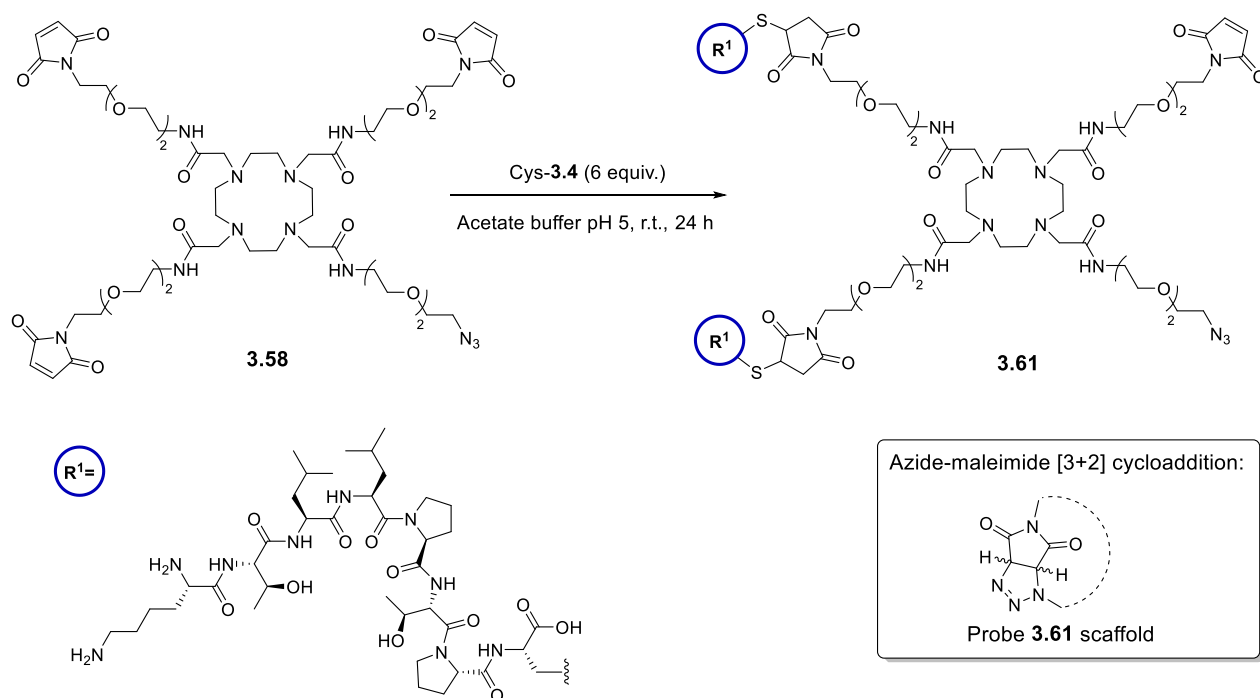
**Table 3.5. CuAAC reaction conditions attempted for the formation of triazole 3.60.**

Entry	Copper Source	Reducing Agent	Solvent	Result <sup>[a]</sup>
1	CuSO <sub>4</sub>	Sodium ascorbate	Acetate buffer pH = 5	No conversion
2	CuSO <sub>4</sub>	Sodium ascorbate	PBS buffer pH = 7	No conversion
3	CuSO <sub>4</sub>	Sodium ascorbate	PBS buffer pH = 7:ACN (3:1)	No conversion
4	CuSO <sub>4</sub>	Sodium ascorbate	PBS buffer pH = 7:ACN (3:1), TBTA	No conversion
5	CuSO <sub>4</sub>	Sodium ascorbate	DMF, TBTA	No conversion
6	CuSO <sub>4</sub>	Sodium ascorbate	DMSO: <i>tert</i> -BuOH, TBTA	No conversion
7	CuI	Sodium ascorbate	Acetate buffer pH = 5	No conversion
8	CuI	Sodium ascorbate	PBS buffer pH = 7	No conversion
9	CuI	Sodium ascorbate	PBS buffer pH = 7:ACN (3:1)	No conversion
10	CuI	Sodium ascorbate	DMF	No conversion
11	[Cu(CH <sub>3</sub> CN) <sub>4</sub> ]PF <sub>6</sub>	Sodium ascorbate	Acetate buffer pH = 5	No conversion
12	[Cu(CH <sub>3</sub> CN) <sub>4</sub> ]PF <sub>6</sub>	Sodium ascorbate	PBS buffer pH = 7	No conversion
13	[Cu(CH <sub>3</sub> CN) <sub>4</sub> ]PF <sub>6</sub>	Sodium ascorbate	PBS buffer pH = 7:ACN (3:1)	No conversion
14	[Cu(CH <sub>3</sub> CN) <sub>4</sub> ]PF <sub>6</sub>	Sodium ascorbate	DMF	No conversion
15	CuCl <sub>2</sub>	Ascorbic acid	Water	No conversion
16	CuSO <sub>4</sub> /Cu powder <sup>[b]</sup>	None	<i>n</i> PrOH:water (3:1)	No conversion
17	Cu powder <sup>[b]</sup>	None	<i>n</i> PrOH:water (3:1)	No conversion
18	Cu wire <sup>[b]</sup>	None	<i>n</i> PrOH:water (3:1)	No conversion
19	3% Cu <sup>0</sup> on carbon <sup>[b]</sup>	None	<i>n</i> PrOH:water (3:1)	No conversion

Reaction conditions: DOTAM-azide **3.58** (1.2 equiv.), Cyanine alkyne **3.59** (1 equiv.), copper catalyst (0.1 to 5 equiv. screened), reducing agent (4-to 10-fold equiv. excess in relation to copper catalyst). All test reactions were conducted at room temperature and stirred overnight. <sup>[a]</sup> No condition led to product formation, and starting material could be recovered in all test settings, <sup>[b]</sup> 50 to 100 equiv. screened.

The unreacted maleimide groups of **3.58** were deemed to deactivate the copper catalyst under the tested conditions (Table 3.5.), thus, a second stepwise sequence with thiol-maleimide conjugation, followed by CuAAC was analyzed (Scheme 3.8.). In spite of the large excess of cysteinyl-**3.4** (up to 6 equivalents), full conversion to the desired tripeptide was not achieved. The intramolecular [3+2] dipolar cycloaddition between azide and maleimide groups<sup>[277]</sup> could be a reason for the failure in obtaining both Cy5.5-**3.60** and difunctionalized **3.61** products (Scheme 3.8.). An evidence of this side-

reaction could be observed by  $^1\text{H}$  and  $^{13}\text{C}$ -NMR analysis, where polymerization of intermediate **3.58** was detected over time.



**Scheme 3.8.** Attempted synthesis of tripeptide conjugation at DOTAM-3.58 scaffold and presumed intramolecular side-reaction at the dipeptide 3.61 scaffold.

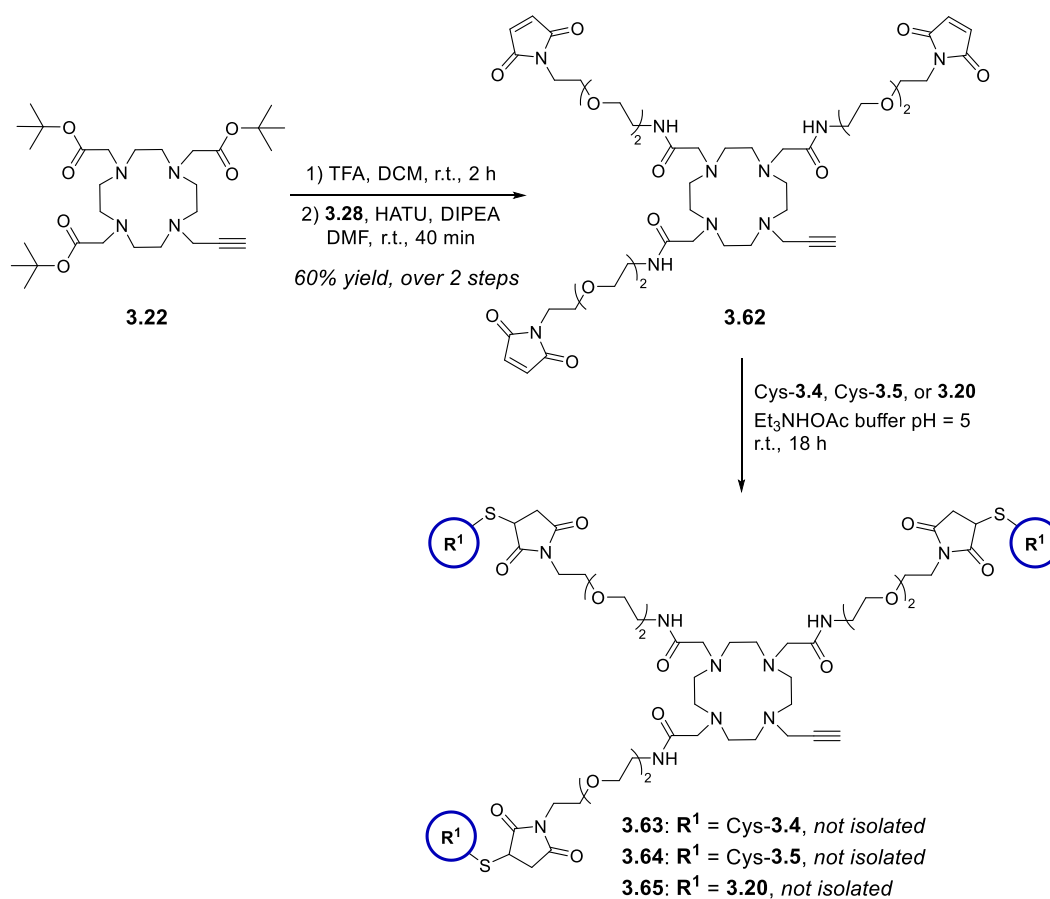
Due to the untoward outcomes related with azide probe precursor **3.58**, fluorophore labeling attempts exploring the CuAAC strategy required a new *clickable* functionality to replace the azide group, while retaining the orthogonality to maleimides. To this end, a terminal alkyne was selected as a suitable ligation handle for the subsequent investigations.

### 3.2.6. Third Approach Towards Cyclen-based Multivalent Ligands: Probing the $\text{R}^2$ -Substitution with an Alkyne for Fluorophore Attachment

To verify the feasibility of the *click* approach for fluorescent dye conjugation, while preventing possible intramolecular side-reactions (*see* Scheme 3.8., Section 3.2.5.), the reactive functionalities of cyanine dye and DOTAM coupling partners were exchanged (Figure 3.9.C, Section 3.2.1.). In contrast to the

previous attempt (Figure 3.9.B, Section 3.2.1.), this synthesis route was based on cyanine labeled azides **3.32** or **3.33** and DOTAM-alkyne **3.62** as key building blocks.

The fourfold bifunctionalized DOTAM **3.62** was prepared in four steps from the unsubstituted cyclen **3.10** (Scheme 3.9). The preparation of DOTAM **3.62** was more straightforward than of azide congener **3.58** (**3.62**: 50% yield from **3.22**, Scheme 3.9. vs. **3.58**: 13% yield from **3.21**, Scheme 3.7., Section 3.2.5.). Subsequent treatment of alkyne **3.62** with recognition element Cys-**3.4**, or non-targeting controls Cys-**3.5** and protected cysteine **3.20** (for structures *see* Scheme 3.3., Section 3.2.3.) at pH = 5 generated the multivalent alkyne derivatives **3.63** to **3.65** (Scheme 3.9.). The use of 4.5 equivalents of cysteinylate (**3.4**, **3.5**, or **3.20**) and at least 18 hours of stirring at room temperature was crucial for obtaining a clean conversion of **3.62** into the desired tri-substituted products, without residual mono- and di-valent intermediates. As discussed in Section 3.2.3., the volatile triethylammonium carbonate buffer pH = 5 was exploited for Michael addition procedures because of its facile removal from the reaction mixtures by a simple lyophilization process.



Scheme 3.9. Synthesis of multivalent DOTAM-alkyne intermediates **3.63** to **3.65**.

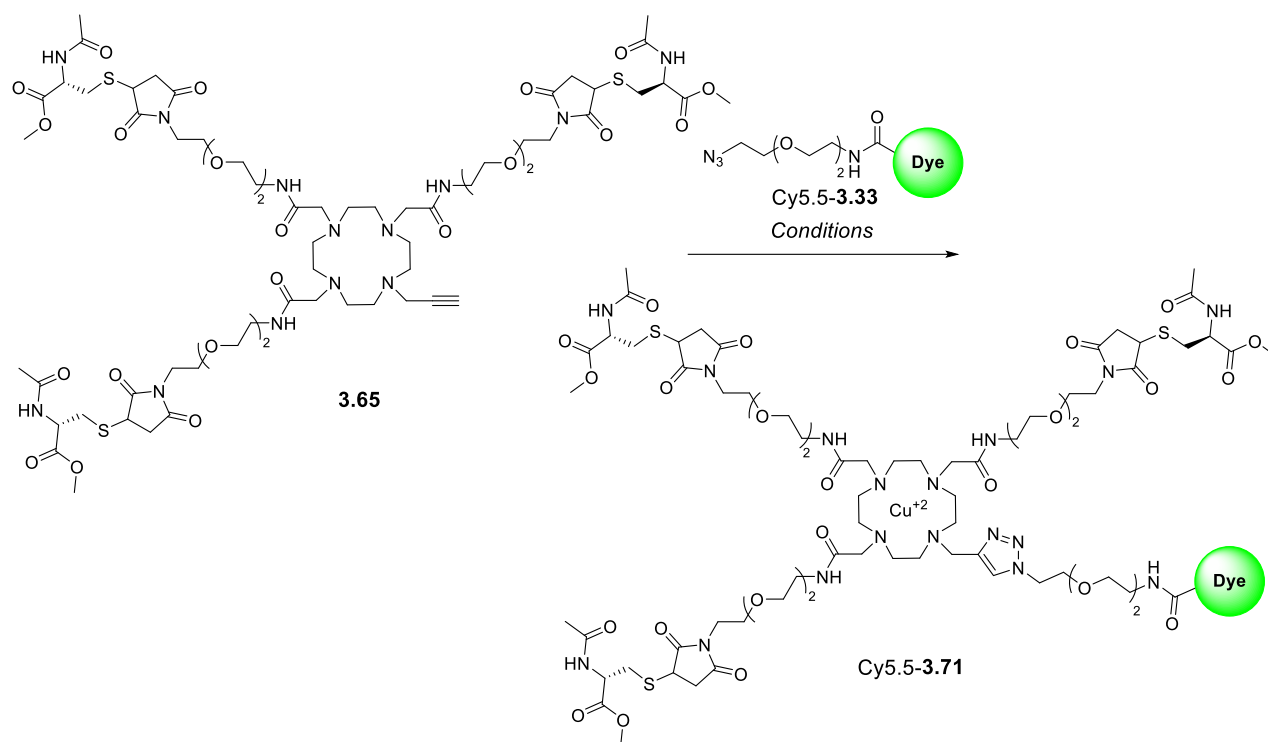


**Table 3.6. CuAAC reaction conditions tested for the formation of triazole 3.71.**

Entry	Copper Source	Reducing Agent	Solvent	Result
1	CuSO <sub>4</sub>	Sodium ascorbate	Acetate buffer pH = 5	No conversion
2	CuSO <sub>4</sub>	Sodium ascorbate	PBS buffer pH = 7	No conversion
3	CuSO <sub>4</sub>	Sodium ascorbate	PBS buffer pH = 7:ACN (3:1)	No conversion
4	CuSO <sub>4</sub>	Sodium ascorbate	PBS buffer pH = 7:ACN (3:1), TBTA	No conversion
5	CuSO <sub>4</sub>	Sodium ascorbate	DMF, TBAT as additive	No conversion
6	CuSO <sub>4</sub>	Sodium ascorbate	DMSO: <i>tert</i> -BuOH, TBTA	No conversion
7	CuI	Sodium ascorbate	Acetate buffer pH = 5	No conversion
8	CuI	Sodium ascorbate	PBS buffer pH = 7	No conversion
9	CuI	Sodium ascorbate	PBS buffer pH = 7:ACN (3:1)	No conversion
10	CuI	Sodium ascorbate	DMF	No conversion
11	[Cu(CH <sub>3</sub> CN) <sub>4</sub> ]PF <sub>6</sub>	Sodium ascorbate	Acetate buffer pH = 5	No conversion
12	[Cu(CH <sub>3</sub> CN) <sub>4</sub> ]PF <sub>6</sub>	Sodium ascorbate	PBS buffer pH = 7	No conversion
13	[Cu(CH <sub>3</sub> CN) <sub>4</sub> ]PF <sub>6</sub>	Sodium ascorbate	PBS buffer pH = 7:ACN (3:1)	No conversion
14	[Cu(CH <sub>3</sub> CN) <sub>4</sub> ]PF <sub>6</sub>	Sodium ascorbate	DMF	No conversion
15	CuCl <sub>2</sub>	Ascorbic acid	Water	No conversion
16	CuSO <sub>4</sub> /Cu powder	None	<i>n</i> PrOH:water (3:1)	<b>3.71</b> , quantitative <sup>[a]</sup>
17	Cu powder	None	<i>n</i> PrOH:water (3:1)	<b>3.71</b> , trace amounts <sup>[a]</sup>
18	Cu wire	None	<i>n</i> PrOH:water (3:1)	<b>3.71</b> , trace amounts <sup>[a]</sup>
19	3% Cu <sup>0</sup> on carbon	None	<i>n</i> PrOH:water (3:1)	<b>3.71</b> , trace amounts <sup>[a]</sup>

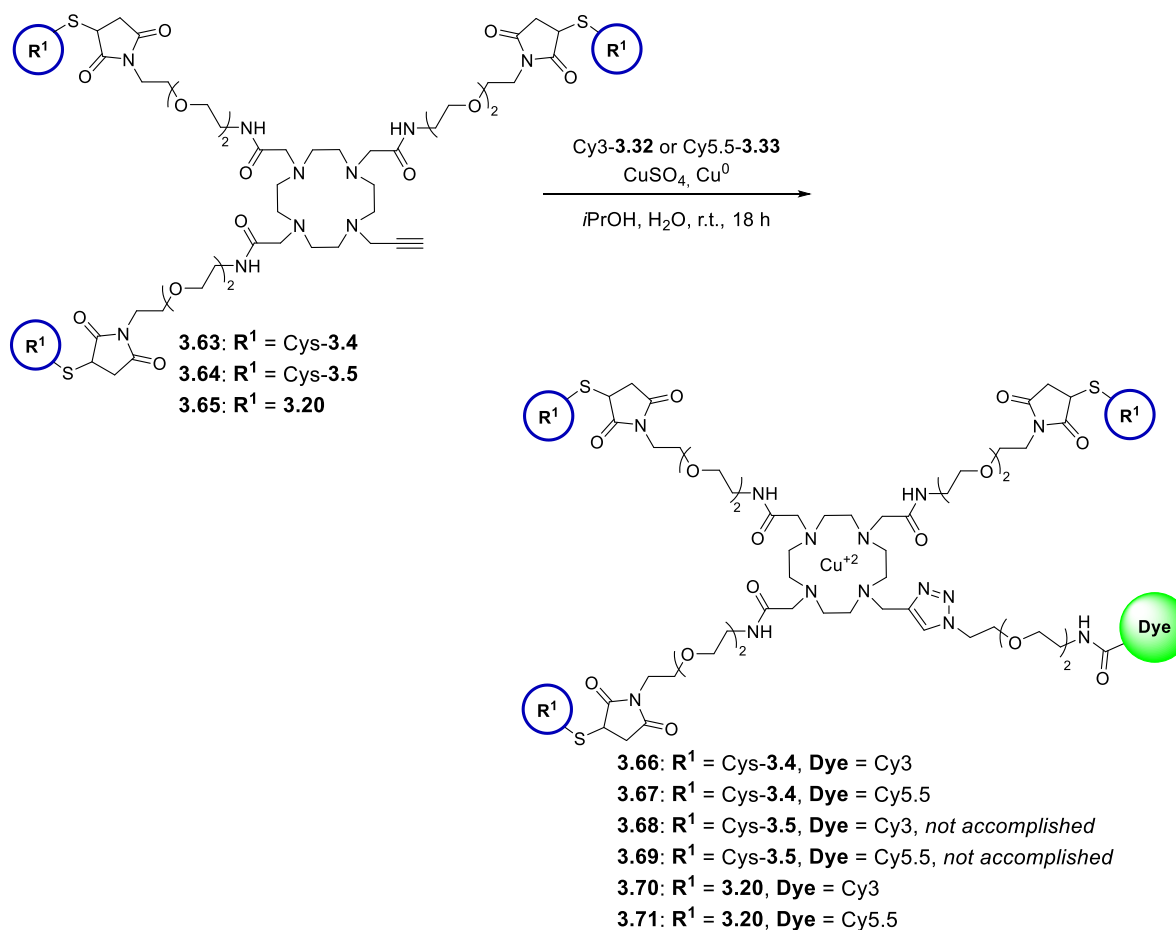
Reaction conditions: DOTAM-alkyne **3.65** (1 equiv.), cyanine azide **3.33** (1.2 equiv.), copper catalyst (0.1 to 5 equiv.), reducing agent (4- to 10-fold equiv. excess in relation to copper catalyst). All test reactions were conducted at room temperature and stirred overnight. <sup>[a]</sup> Conversion determined by LC-MS.

At pH = 5 the thiosuccinimide rings remained stable in the course of the reaction and lyophilization work up. As such, these intermediates were pure enough to be applied as crudes to the following copper-mediated cycloaddition attempts. The non-peptidic and smaller DOTAM-alkyne **3.65** was explored as a model compound for initial CuAAC attempts. Applying the fluorescent azide linker **3.33** as reaction partners for triazole formation, a set of copper catalysts and solvent systems were investigated (Table 3.6.). Interestingly, the outcome of these test reactions was highly dependent on the copper source and reducing agent of choice. Conditions applying copper(II) salts in combination with sodium ascorbate or ascorbic acid (4 equiv. fold-excess) are the most widely used method to generate the copper(I) catalyst *in situ*.<sup>[278]</sup> However, this approach was unsuitable for the conjugation of DOTA-alkyne **3.65** with azide Cy5.5-**3.33** (Table 3.6., entries 1 to 15), leading to the recovery of starting materials.

Alternatively, the generation of the copper(I) active species in solution can be achieved by a comproportionation reaction of a copper(II) source, e.g., copper sulfate, and copper(0).<sup>[279]</sup> A system that requires higher reaction times and catalyst loadings for completion than the more common copper(II)/sodium ascorbate conditions. Notably, the expected cyclization occurred under metallic copper catalysis (Table 3.6., entry 16). In particular, combination of 0.1 M aqueous solution of CuSO<sub>4</sub> (3.5 equiv.) with an excess of copper powder (50 equiv.) in isopropanol and water provided quantitative conversion of model compound **3.65** to Cy5.5-labeled multivalent analog **3.71**. The inclusion of copper sulfate showed to be essential for the outcome of this step as copper(0) sources alone, including copper powder, wire, and copper on palladium (Table 3.6., entries 17 to 19) resulted in only trace amounts of triazole product.

The combination of copper powder and copper sulfate was further exploited for preparing the cyanine labeled derivatives **3.66** to **3.70** (Scheme 3.10.). Under the tested conditions, the control peptide-targeting intermediates **3.68** and **3.69** were not formed, with the only outcome being degradation of starting material **3.64** upon copper sulfate treatment (ca. 5 hours). The presence of histidine at the control peptide sequence (**3.5**, *see* Figure 3.3., Section 3.1.2.), which has strong metal chelating properties, may provoke copper deactivation.<sup>[280]</sup> To understand this failed attempt, the cycloaddition between tri-histidine conjugate **3.64** with both azide linkers was analyzed using matrix-assisted laser desorption/ionization (MALDI).<sup>[281]</sup> The mass analysis of the crude mixture over time suggested that alkyne **3.64** indeed deactivated the copper catalyst by taking up to 4 copper ions in its scaffold before

degradation. Hence, further synthetic efforts were carried out on PTP (**3.66** and **3.67**) and cysteine (**3.70** and **3.71**) triazole conjugates.



**Scheme 3.10.** CuAAC reaction for the generation of fluorescent copper complexes **3.66** to **3.71**. Intermediates **3.66**, **3.67**, **3.70**, and **3.71** were used as crudes for the subsequent reaction steps.

Possibly due to the activation mechanism of metallic copper, together with the inherent copper complexation by the cyclen core and peptides, a catalytic CuAAC reaction was not accomplished. In line with this, the corresponding thiosuccinimidyl triazoles **3.66**, **3.67**, **3.70**, and **3.71** were furnished as copper-complexes (Scheme 3.10). Each triazole (**3.66**, **3.67**, **3.70**, and **3.71**) was bound to one copper ion as indicated by both MALDI and liquid chromatography–mass spectrometry (LC-MS) analysis.

Copper chelates may lead to not only in cellular toxicity, but also preclude complexation of more relevant imaging metals by the cyclen core, e.g., gadolinium(III) and gallium(III). Similarly as for CuAAC attempts, the smaller cysteine conjugates **3.70** and **3.71** were applied as a model for screening



of copper demetalation methodologies. Classical precipitation conditions using sodium sulfite (10 to 50 equiv. screened) failed in providing copper free congeners of **3.70** and **3.71**. Under physiological conditions reduction of copper(II) to copper(I) may result in the decomplexation of this metal.<sup>[282]</sup> Thus, a reductive medium was generated by treating target compounds with an excess in equivalent amounts of sodium ascorbate (120 equiv.) in PBS buffer pH = 7.4. However, unwanted retro-Michael addition occurred before copper demetalation. The tendency of DOTA to undergo transmetalation was next explored using gadolinium, iron, zinc, calcium, and sodium ions as its chloride salt form.<sup>[283]</sup> For these experiments, the chloride salts of the tested metals were given in large excess (1200 equiv.) to the copper chelates **3.70** and **3.71** at controlled pH, from acidic 2.5 to physiological 7.4 up to basic 12. However, these conditions were not suitable for copper removal at a preparative scale. Only iron chloride at physiological pH provided at very low rates a metal exchange.

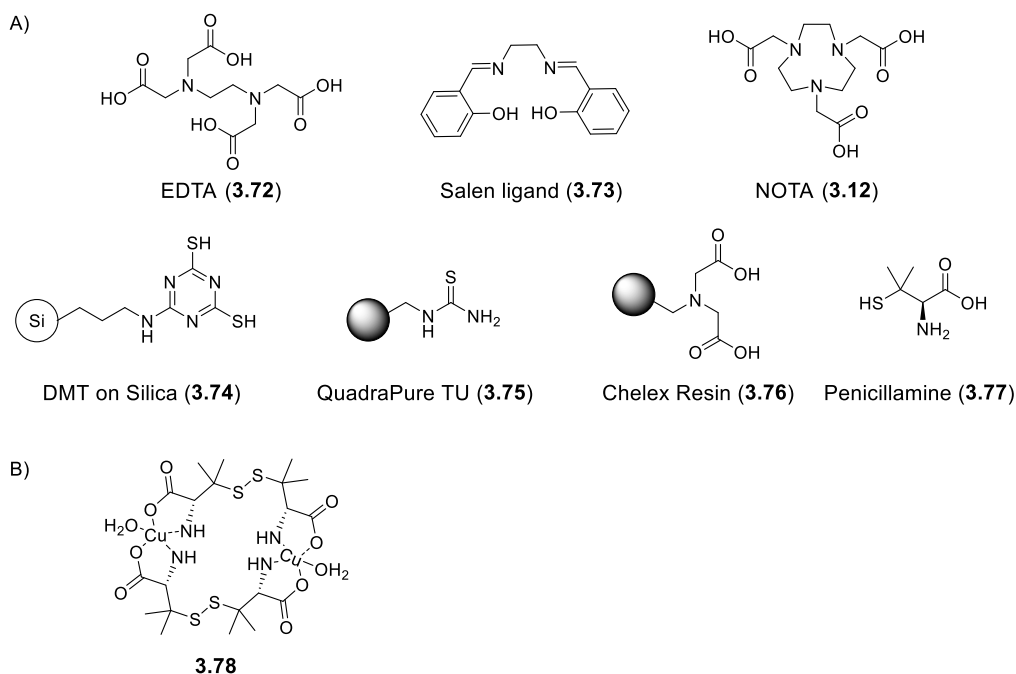


**Figure 3.11. Chelating agents screened for copper demetalation of *N*-acetyl cysteine thiosuccinimides **3.70** and **3.71**.** A) Structures of the chelating agents utilized in for copper demetalation attempts and B) Structure of the penicillamine (**3.77**) complex with copper as published by J. A. THICH *et al.*<sup>[284]</sup> (CCDC deposit number: 1133444).

Protonation of the macrocyclic core at a highly acidic media (pH = 2-3) is a known method to induce demetalation of cyclen derivatives.<sup>[285]</sup> The subsequent treatment of such acidic solution with a strong copper scavenger could capture metal ions from solution and avoid their re-complexation. To investigate this hypothesis, the chelating ligands ethylenediaminetetraacetic acid (EDTA, **3.72**),<sup>[286]</sup> Salen (**3.73**),<sup>[287]</sup> 1,4,7-triazacyclononane-1,4,7-triacetic acid (NOTA, **3.12**)<sup>[260b]</sup>, and penicillamine

(**3.77**),<sup>[288]</sup> as well as the polymer-bound metal scavengers dimercaptotriazine (DMT, **3.74**),<sup>[289]</sup> thiourea QuadraPure TU (**3.75**),<sup>[290]</sup> and iminodiacetic acid Chelex resin (**3.76**)<sup>[274g]</sup> were screened for their copper chelating capacity (Figure 3.11.A).

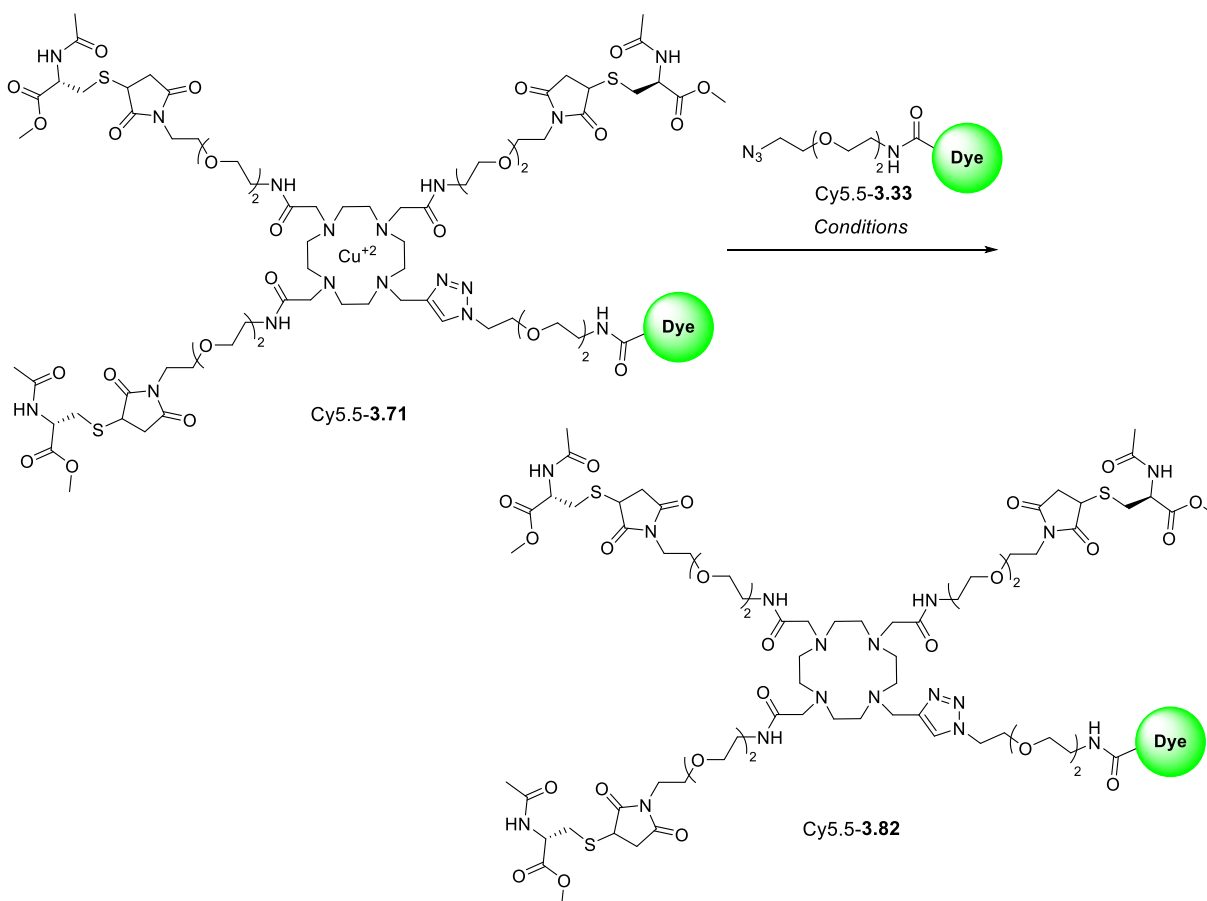


**Table 3.7. Conditions tested for copper demetalation of *N*-acetyl cysteine thiosuccinimide **3.71**.**

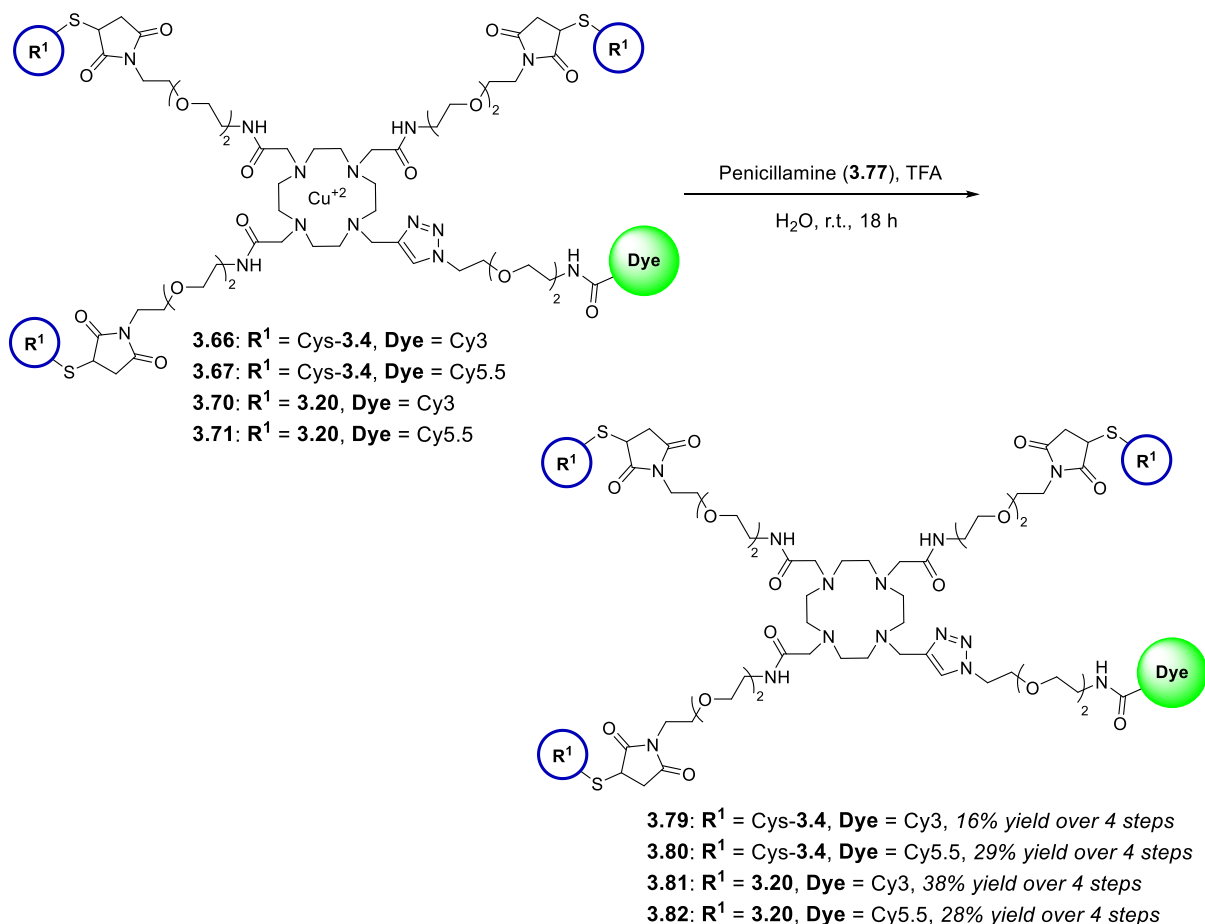
Entry	Chelating agent (CA) <sup>[a]</sup>	Equiv. amounts of CA	Temperature	pH	Result
1	EDTA, <b>3.72</b>	302	r.t.	12	No conversion
2	Salen ligand, <b>3.73</b>	302	r.t.	2.5	No conversion
3	NOTA, <b>3.12</b>	302	50 °C	2.5	60% conversion <sup>[c]</sup> , 25-30% isolated yields
4	DMT on Silica, <b>3.74</b> <sup>[b]</sup>	60	r.t.	2.5	70% conversion <sup>[c]</sup> , 0% isolated yield
5	QuadraPure TU, <b>3.75</b> <sup>[b]</sup>	60	r.t.	2.5	No conversion, degradation of <b>3.71</b>
6	Chelex resin, <b>3.76</b> <sup>[b]</sup>	24 mg resin/mg reactant	r.t.	2.5	No conversion
7	Penicillamine, <b>3.77</b>	604	r.t.	2.5	Full conversion to <b>3.82</b> <sup>[c]</sup> , 28% isolated yield <sup>[d]</sup>

Test reactions performed in 5 mg scale. Excess equivalent amounts of chelating agent were added to the reaction mixture after the adjustment of the solution pH with either TFA or sodium hydroxide. Reaction control performed via LC-MS analysis. All test reactions were stopped after 18 h stirring. <sup>[a]</sup> for structures *see* Figure 3.11.A, <sup>[b]</sup> equivalent amounts calculated as specified by the supplier; <sup>[c]</sup> Determined by LC-MS; <sup>[d]</sup> From HPLC chromatography.

The following copper removal attempts using chelating agents **3.12** and **3.72** to **3.77** were conducted using the trivalent DOTAM-cysteine labelled with Cy5.5 (**3.71**) as model reagent (Table 3.7.). At first, test derivative **3.71** was stirred at room temperature in a trifluoroacetic acid aqueous solution at pH = 2.2 until their copper free congeners could be mainly detected by LC-MS analysis (30 min). After this time, the selected chelating agents were added to these solutions in excess equivalent amounts and evaluated according to their copper complexation performance.

Experiments involving EDTA (**3.72**) were conducted exceptionally at basic pH = 12, where its copper coordination capacity reaches a maximum<sup>[291]</sup> (Table 3.7., entry 1). However, classical chelating metal ligands, such as EDTA (**3.72**) and Salen (**3.73**), were not suitable for this experiment, leading to no conversion to the desired copper free derivatives (Table 3.7., entries 1 and 2). Despite the cyclic amine NOTA (**3.12**) displayed promising copper scavenging properties with 60% conversion upon heating to 50 °C (Table 3.7., entry 3), these conditions might be unfavourable and too harsh for the more complex tri-peptides **3.66** and **3.67**. Therefore, the use of silica and polymer bound chelating agents (**3.74** to **3.76**) was next evaluated (Table 3.7., entries 4 to 6). These reagents have the advantage of facile removal of reaction mixtures via filtration, however in all cases model compound **3.71** associated likewise to the resin. Attempts on isolating the copper free analogs from the resins were either ineffective or resulted in their degradation.

Penicillamine (**3.77**) is a common drug used to treat heavy metal poisonings, in particular Wilson's disease, i.e., copper accumulation.<sup>[292]</sup> Due to the stable copper complexes formed, this ligand was additionally selected for this experiment (Table 3.7., entry 7). The coordination of copper by penicillamine **3.77** is shown in Figure 3.11.B (**3.78**) and requires two molecules of **3.77** to coordinate one metal ion.<sup>[284]</sup> Therefore, the double of equivalents was applied for the screening of this compound in comparison to other molecular cages which coordinate copper in a 1:1 model, i.e., Salen (**3.72**), EDTA (**3.73**), and NOTA (**3.12**). Remarkably, complete removal of the copper ions was achieved in aqueous trifluoroacetic acid solution, followed by addition of **3.77**. The large excess of chelating agent **3.77** was stringently necessary for improved outcomes, yet it could be recovered by filtration before the subsequent purification step. The HPLC column of the crude filtrate led to the desired product (copper free-**3.71**) in moderate 28% yield, over 4 reaction steps (Table 3.7., entry 7). A strategy which was then applied for the synthesis of the more biologically relevant cyanine labeled tri-peptides **3.79** and **3.80** (Scheme 3.11).



**Scheme 3.11.** Copper demetalation of using penicillamine 3.77 to afford DOTAM-based multivalent probes 3.79 to 3.82.

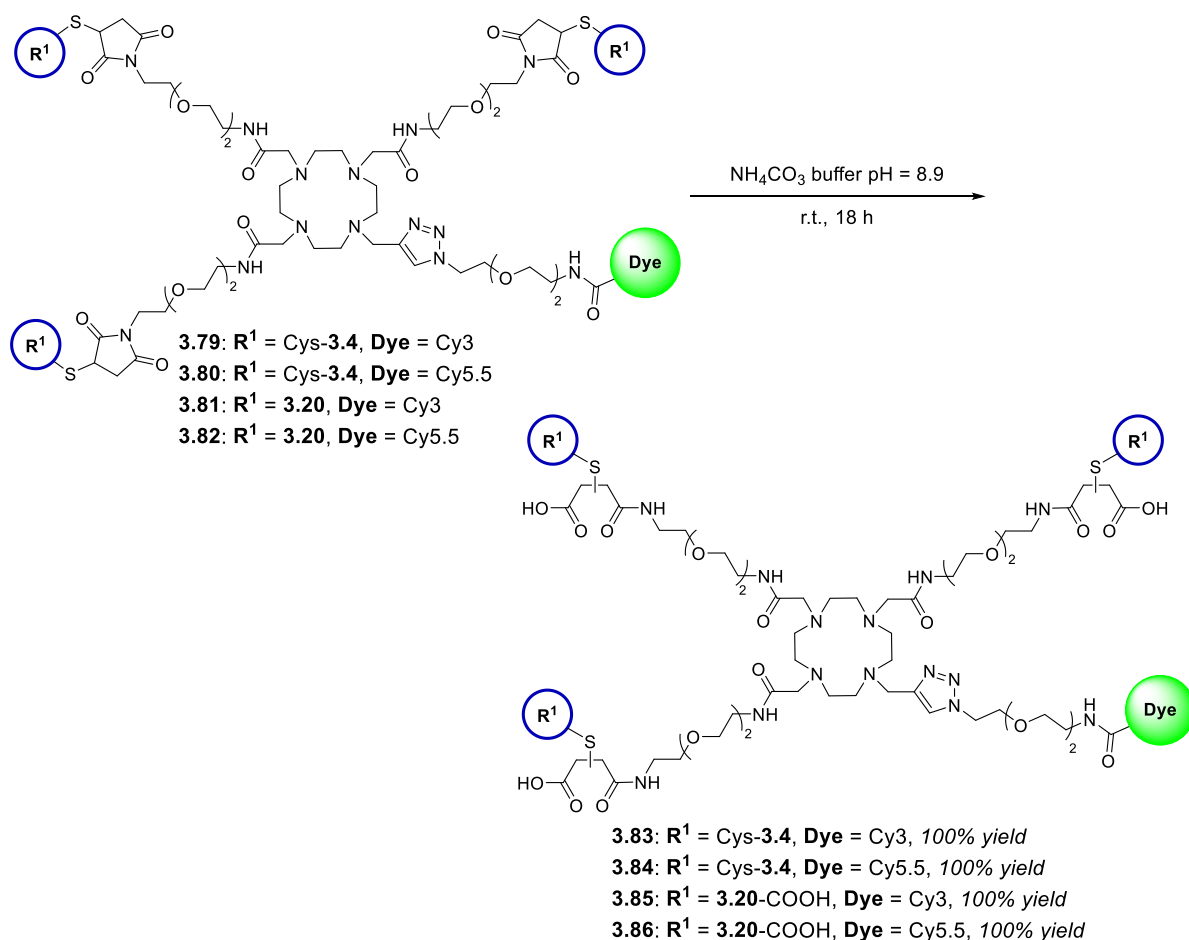
To detect remaining copper at the final derivatives **3.79** to **3.82** and, thereby, determine the efficacy of the applied copper removal strategy, the inductively coupled plasma mass spectrometry (ICP-MS) technique was used (Table 3.8.). The ICP-MS represents a highly sensitive analytical method to determine traces of metal in organic samples, including copper.<sup>[293]</sup> These measurements were performed in collaboration with SEBASTIAN FASSBENDER and ANDREAS SCHULTZ at the Bundesanstalt für Materialforschung und –prüfung (BAM). The copper levels of compounds **3.79** to **3.82** were in the ppm range of detection and were applied to calculate the efficacy of this reaction step (Table 3.8). In comparison to blank control samples, the detected copper levels demonstrated the high reliability of the tested conditions (penicillamine at pH = 2.2) to remove copper from cyclen derivatives **3.79** to **3.82** in nearly quantitative yields (Table 3.8., *see* Experimental Procedures, Section 5.3.7. for further details).

**Table 3.8. Determination of copper concentration levels in final probes 3.79 to 3.82, determined by ICP-MS, and calculated efficacy of copper removal.**

Entry	Probe	Copper levels (mol %)	Copper removal efficacy (%)
1	3.79	0.02	99.98
2	3.80	0.10	99.90
3	3.81	0.07	99.93
4	3.82	0.02	99.98

Analysis performed in 1 mg/mL sample. ICP-MS analysis performed at the BAM with the assistance of SEBASTIAN FASSBENDER and ANDREAS SCHULTZ.

With the copper free congeners **3.79** to **3.82** in hand, final hydrolysis of the thiosuccinimide rings was performed (Scheme 3.12.). Applying the same conditions as for monovalent controls **3.40** to **3.45** afforded complete conversion to the fluoroprobes **3.83** to **3.86**.



**Scheme 3.12. Hydrolysis of the thiosuccinimide rings to provide the DOTAM-based multivalent probes 3.83 to 3.86.**

Considering the concept of orthogonal *click* reactions, each step should occur in any order to furnish the same product.<sup>[294]</sup> Nevertheless, such orthogonal behavior could not be demonstrated in this study, e.g., DOTAM azide-**3.58** and Cy5.5 alkyne-**3.59** (Section 3.2.5.) vs. DOTAM alkyne-**3.62** and Cy5.5 azide-**3.33**. Furthermore, any modification at the successful stepwise sequence towards final probes **3.83** to **3.86** – i.e., from template **3.62**: thiol-maleimide Michael addition, CuAAC, and thiosuccinimide hydrolysis – was unattainable and largely ineffective. By starting the synthesis pathway with the best CuAAC conditions (CuSO<sub>4</sub>, Cu powder, *i*PrOH, water, r.t., 18 h, Scheme 3.11.) at unlabeled cyclen-based template **3.62**, no triazole formation could be observed. Likewise, employing the alkaline hydrolysis step before fluorophore conjugation resulted in no appreciable conversion. Altogether, these observations emphasize the assumption that maleimide groups might display a coordinative effect at copper ions under the tested protocol. Hence, the probe assembling should strictly follow the abovementioned sequence order.

### **3.2.7. Applications of Multivalent Fluorescent Ligands labeled with Cy3 and Cy5.5 for Pancreatic Cancer Detection by Plectin-1 Visualization**

With this set of fluorescent ligands, confocal imaging studies were elaborated in collaboration with DR. SILKE RADETZKI at the screening unit facility of the FMP to validate the specificity of PTP-targeted fluorescent ligands towards PDAC. To this end, the human pancreatic cancer cell lines Panc-1 and MiaPaCa-2 were investigated for initial imaging assays due to their known expression of the plectin-1 protein-target.<sup>[249, 295]</sup>

These cancer cell lines were incubated with different concentrations of the multivalent cyclen-based probes Cy3-**3.83** and Cy5.5-**3.84** (Figures 3.12. and 3.13.). For these experiments, the non-targeting cyclen-based controls Cy3-**3.85** and Cy5.5-**3.86** were utilized as unspecific negative controls. In comparison to the non-targeting control Cy3-**3.85**, PTP-targeted derivative **3.83** exhibited 2.7-fold mean increase in fluorescence at the two PDAC cells (Figure 3.12.A and B). This selectivity profile was observed for both cell lines in a concentration-dependent manner. In particular, a significant increase in mean fluorescence intensity was measured at 10  $\mu$ M targeted compound **3.83** (Figure

3.12.C and D, *left panels*). Importantly, at the same concentration control cysteinate **3.85** did not produce bright cellular labeling as its targeted congener **3.83** (Figure 3.12.C and D, *right panels*). A similar trend was observed for multivalent Cy5.5 analog **3.84**, where the mean fluorescence intensity rose with increasing concentrations of fluoroprobe (Figure 3.13.A and B). In both cell lines, PDAC-targeted Cy5.5-**3.84** displayed a mean 1.8-fold increase in fluorescence than its non-targeting analog Cy5.5-**3.86**, further illustrating the selectivity of the probe scaffold towards PDAC (Figure 3.13.C and D).

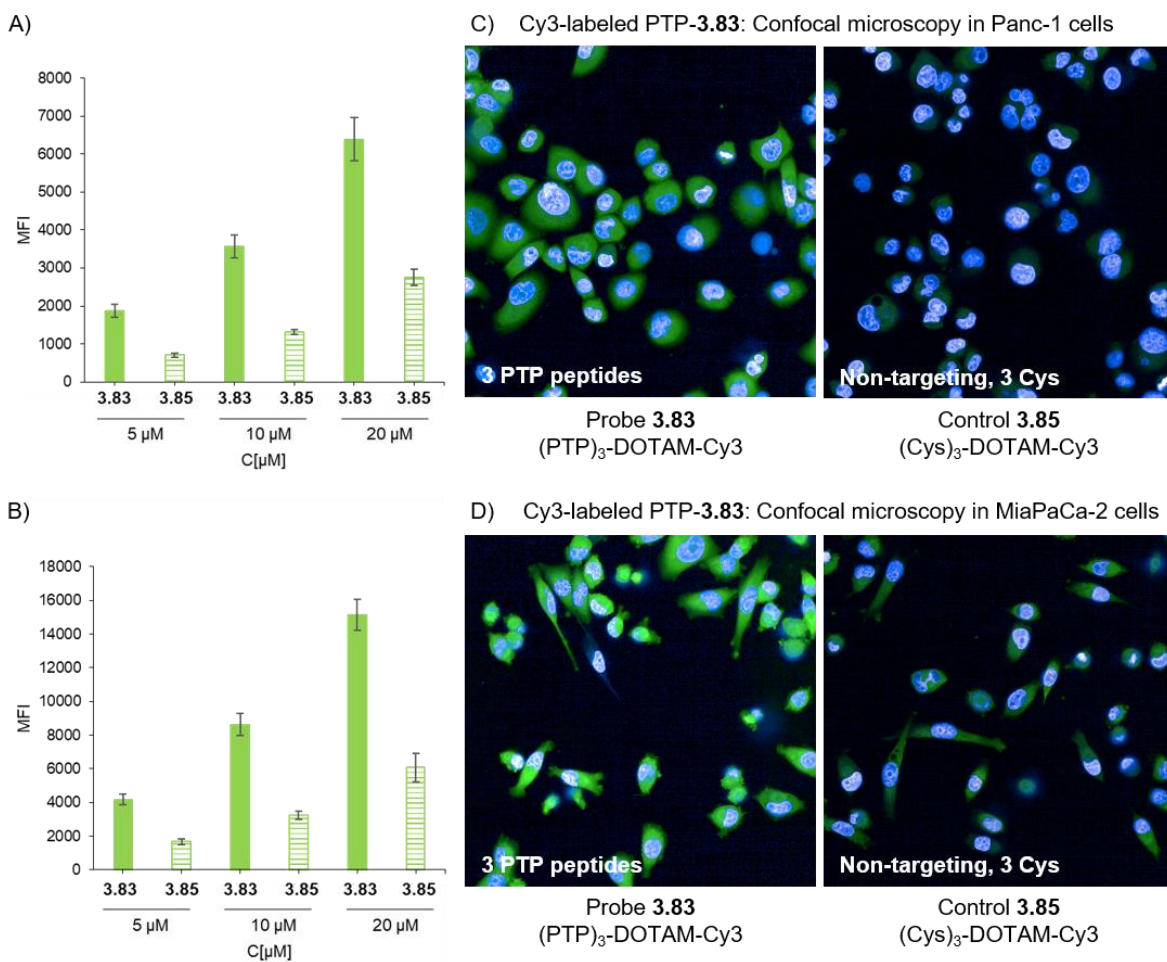


**Figure 3.12. Multivalent Cy3-labeled probe 3.83 enabled PDAC visualization in confocal fluorescence microscopy analysis.** A, B) Analysis of the mean fluorescence intensity (MFI) of Panc-1 and MiaPaCa-2 cells, respectively, incubated with different concentrations of either multivalent PTP **3.83** or non-targeting control **3.85**, where A) Panc-1 cells and B) MiaPaCa-2 cells. C, D) Confocal microscopy images of Panc-1 and MiaPaCa-2 cells, respectively, incubated for 4 h with either 10 μM PTP-targeted **3.83** (green, *left panel*) or 10 μM non-targeting control Cys-**3.85** (green, *right panel*) and counterstained with Hoechst 33342 (cyan, nucleus counter stain), where C) Panc-1 cells and D) MiaPaCa-2 cells. Experiments performed by DR. SILKE RADETZKI.

Since PDAC cells are reported to express plectin-1 at both cellular membrane and cytosol,<sup>[232]</sup> staining of this protein-target would ideally require a membrane permeable probe. As illustrated in Figures 3.11. and 3.12. (C and D, *left panel*), both fluorescent ligands Cy3-**3.83** and Cy5.5-**3.84** were confirmed to enter the tested Panc-1 and MiaPaCa-2 cell lines, reaching the cytosol. Under the applied test settings, however, the Cy3-labeled ligands generated an overall more intense and brighter fluorescence staining than the Cy5.5 analogs (cf., e.g., MFI of **3.83** at 20  $\mu\text{M}$  = 15'133, Figure 3.12.B vs. MFI of **3.84** at 20  $\mu\text{M}$  = 4'406, Figure 3.13.B). Therefore, subsequent *in vitro* investigations to evaluate the influence of multivalency for binding were carried out using Cy3-analog **3.83**.

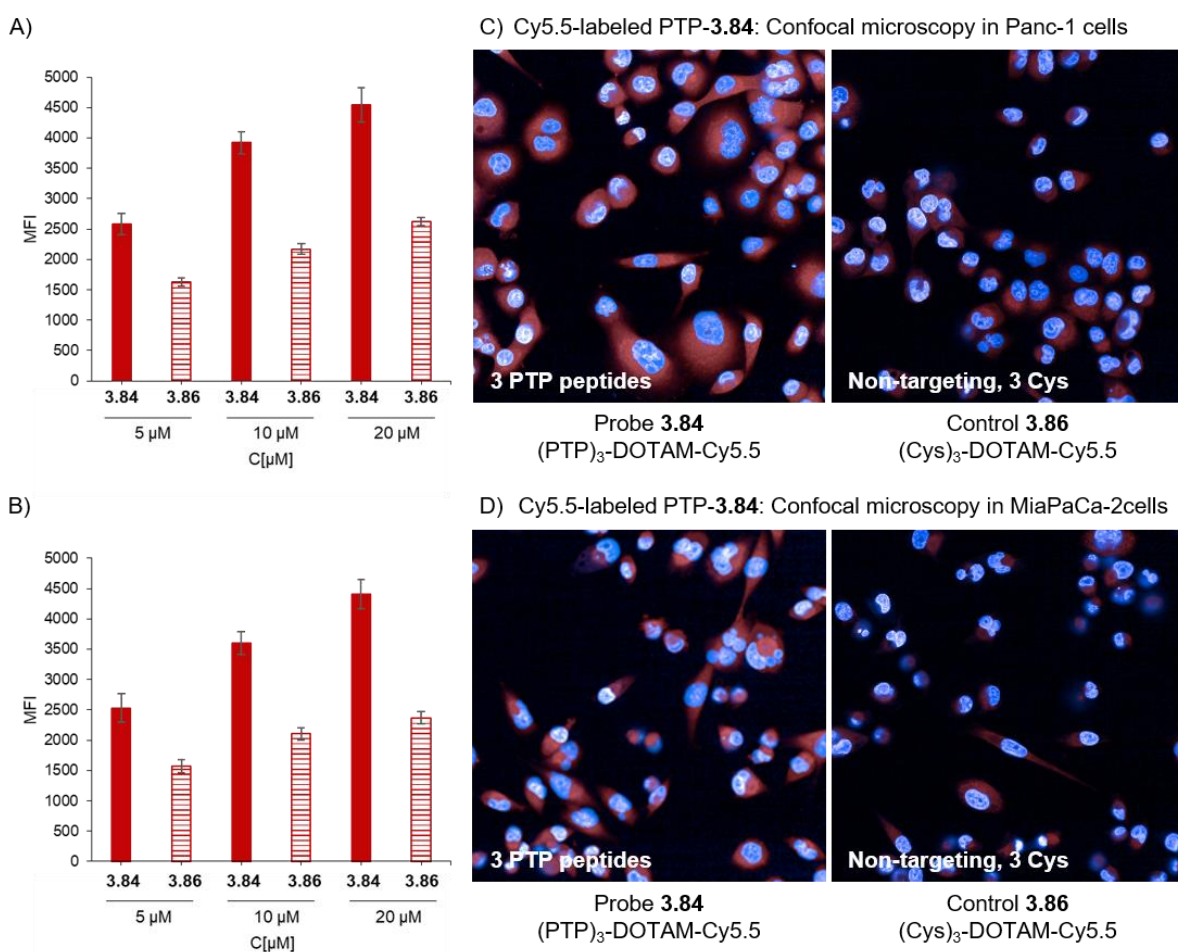


**Figure 3.13. Multivalent Cy5.5-labeled probe 3.84 enabled PDAC visualization in confocal fluorescence microscopy analysis.** A, B) Analysis of the mean fluorescence intensity (MFI) of Panc-1 and MiaPaCa-2 cells, respectively, incubated with different concentrations of either multivalent **3.84** or control **3.86**, where A) Panc-1 cells and B) MiaPaCa-2 cells. C, D) Confocal microscopy images of Panc-1 and MiaPaCa-2 cells, respectively, incubated for 4 h with either 10  $\mu\text{M}$  PTP-targeted **3.84** (red, *left panel*) or 10  $\mu\text{M}$  non-targeting control Cys-**3.86** (red, *right panel*) and counterstained with Hoechst 33342 (cyan, nucleus counter stain), where C) Panc-1 cells and D) MiaPaCa-2 cells. Experiments performed by DR. SILKE RADETZKI.



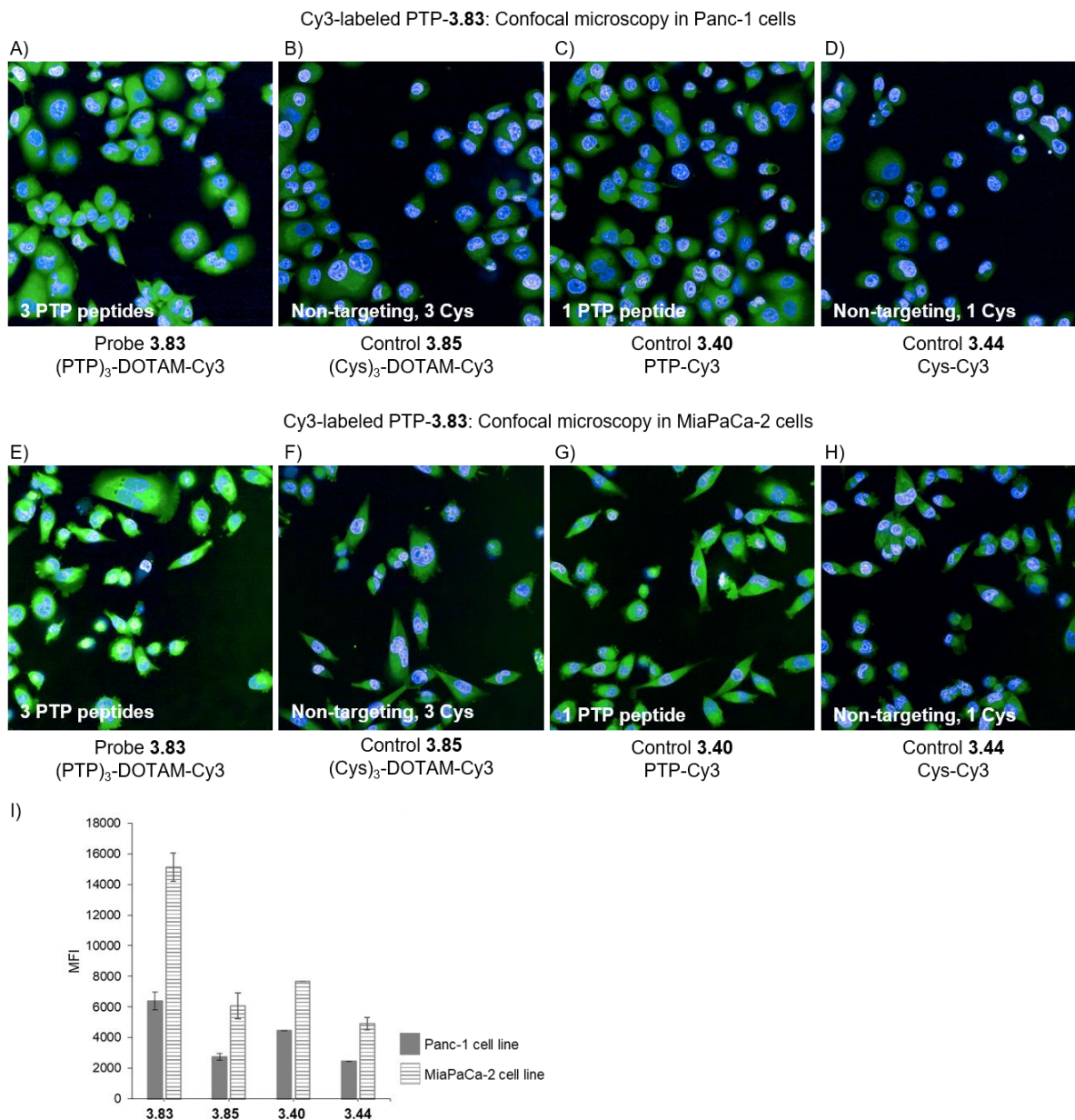


**Figure 3.14. Confocal fluorescence microscopy images of PDAC cell lines incubated with Cy3-labeled PTP probe 3.83 in comparison to non-targeting multivalent and monovalent controls.** A to H) Confocal microscopy images of Panc-1 cells (A to D) and MiaPaCa-2 cells (E to H) incubated for 4 h with 20  $\mu$ M either multivalent PTP-targeted **3.83** (green, A and E), multivalent non-targeting control Cys-**3.85** (green, B and F), monovalent PTP-targeted control **3.40** (green, C and G), or monovalent non-targeting control Cys-**3.44** (green, D and H) and counterstained with Hoechst 33342 (cyan, nucleus counter stain). I) Analysis of the mean fluorescence intensity (MFI) of Panc-1 and MiaPaCa-2 cells treated with 20  $\mu$ M either multivalent **3.83** or controls **3.85**, **3.40**, and **3.44**. Experiments performed by DR. SILKE RADETZKI.

The overall PDAC-targeting affinity of trisubstituted PTP DOTAM-**3.83** was compared to the non-targeting tricysteinate-**3.85** as well as to its monovalent analogs PTP-**3.40** and Cys-**3.44** (Figure 3.14.). For this experiment, Panc-1 and MiaPaCa-2 cells were incubated with 20  $\mu$ M fluorescent ligand for 4 h, then washed with PBS buffer to remove the nonbinding fraction of the respective fluorescent

compound. The following confocal fluorescence microscopy analysis indicated that both PTP-targeted ligands **3.83** (three targeting PTP peptides) and **3.40** (one targeting PTP peptide) were capable of penetrating the cell membrane and producing stable labeling of the cytosol (Figure 3.14A, C, E, and G). Quantification of probe accumulation by integration of fluorescence intensities in the cells revealed an increased content of targeted ligands over their non-targeting controls (Figure 3.14.I). The monovalent derivative **3.40** (one targeting PTP peptide) displayed 1.6 and 1.8-fold mean increase on Panc-1 and MiaPaCa-2 cells, respectively over the non-targeting analog **3.44**. Whereas, at the same concentration, multivalent targeting analog **3.83** (three targeting PTP peptides) showed a mean 2.5-fold increase over the non-targeting trisubstituted control **3.85**, a 1.8-fold over the monocysteinate-**3.44**, and a twofold increase over **3.40** (one targeting PTP peptide). These findings were observed in the two tested cell lines, demonstrating the superior specificity of multivalent **3.83** to PDAC cells compared to its controls.

In the course of the staining process, the fluorophores and controls demonstrated to be chemically stable and did not exhibit the tendency to form aggregates in physiological buffer conditions. To further confirm these observations, the stability of the fluorescent analogs in physiological conditions as well as their absorption emission spectra has to be evaluated in subsequent studies. To further confirm plectin-1 specific binding, blocking studies exploiting monoclonal anti-plectin-1 antibodies labeled with complementary fluorescent readouts to compounds **3.83** and **3.84** (Alexa 647-label for Cy3-**3.83** blocking assay and fluorescein-label for Cy5.5-**3.84** blocking assay) are planned.

After confirmation of the selectivity of probes **3.83** and **3.84** towards PDAC, several biological test settings were conceived to validate their applicability and robustness using different cell lines and tissue samples, both derived from healthy and PDAC models, as well as complementary optical imaging modalities. These studies will be additionally conducted in two laboratories which are interested in pancreatic cancer detection. The fluorescent ligand set will be subjected to in depth pharmacological characterization carried out in the group of HAIYU HU in Beijing, in particular QINGHUA WANG, and the group of HANA ALGÜL in Munich. These investigations will provide the staining efficacy of PTP-targeted **3.83** and **3.84** towards plectin-1 in primary cells and tumorous tissue as well as their photophysical properties, which will guide further imaging efforts. Moreover, staining of PDAC in tissue samples derived from both preclinical PDAC murine model and clinical patients will be pursued.

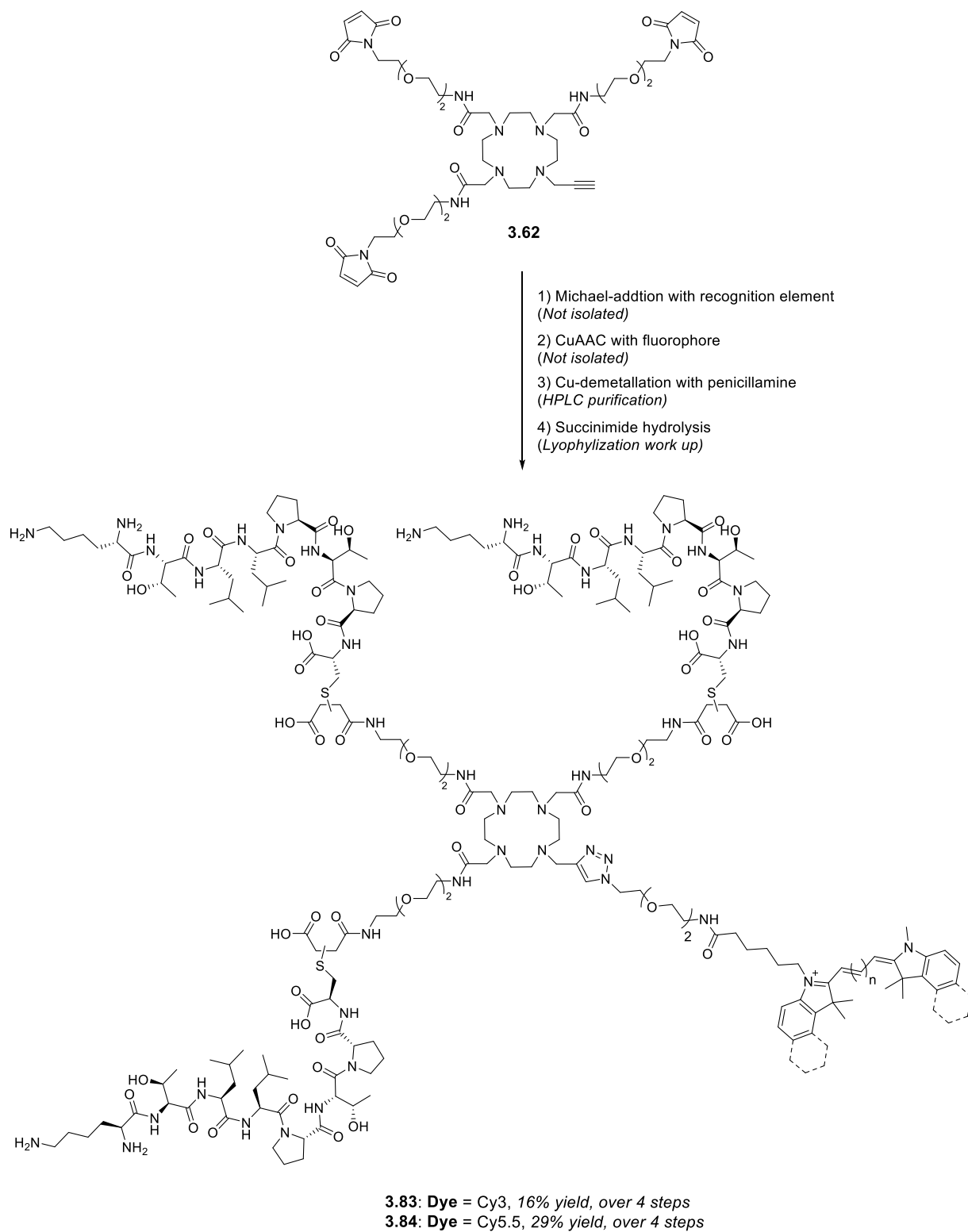
### 3.3. Conclusion and Outlook

The synthesis of multivalent small-molecule based contrast agents is highly challenging and often involves difficult chromatographic purifications and low isolated yields. In stark contrast to the current situation, a *clickable* probe template may enable the preparation of a number of imaging tools in a parallel fashion rather than by sequential synthesis. Such a parallel approach can significantly reduce the number of precursors and intermediates required for the synthesis of different imaging agents based on the same vector. Inspired by these concepts, the third chapter of this thesis described a multivalent platform for probe assembling via subsequent *click* reactions which was applied for the preparation of imaging agents for PDAC detection.

The selection of the macrocyclic amine cyclen as core for probe design was twofold. First, due to the broad applicability of cyclen-derived molecular cages, such as DOTA, among imaging modalities, including MRI, PET, SPECT, and dual-imaging. Second, the high versatility of this scaffold which allow for numerous strategies for linker installation at one, two, three, or all of its nitrogen atoms. In particular, the fourfold *N*-functionalization of cyclen was explored to introduce a 3 to 1 decoration pattern, allowing to differentiate one nitrogen exit vector over the remaining three. Suitable ligation handles were evaluated according to their orthogonality for conjugation of the recognition element and reporter unit.

Maleimide was selected for the coupling with three thiol containing targeting moieties, investigations for the *N*-derivatization of the fourth arm was carried out. This position was tested for fluorescent dye attachment with three different functionalities: amine, azide, and alkyne. Using this approach, probe assembling was attempted via consecutive Michael-type addition reaction, followed by either amide coupling or CuAAC. Installation of PEG2-maleimide linkers led to the respective bifunctionalized cyclen precursors encompassing either free amine (**3.48**), terminal azide (**3.58**), or terminal alkyne (**3.62**) groups. These building blocks were subjected to a number of stepwise sequence pathways and optimization rounds. Nevertheless, alkyne **3.62** was the only template to afford tri-substituted derivatives labeled with two cyanine dyes, Cy3 and Cy5.5.

From precursor **3.62**, these compounds have a stringent synthesis route which can be performed in *one-pot*: thiol-maleimide conjugation, followed by CuAAC (Scheme 3.13.). Removal of the copper ions from the reaction mixture was successful upon treatment with penicillamine. The final hydrolysis of



**Scheme 3.13.** General strategy for the synthesis of PTP-targeted congeners Cy3-3.83 and Cy5.5-3.84 from *clickable* probe platform 3.62.

succinimide groups afforded PTP-targeted Cy3-**3.83** and Cy5.5-**3.84** as well as cysteinate controls Cy3-**3.85** and Cy5.5-**3.86**. These reaction conditions were also applied for the synthesis of monovalent controls composed by one single targeting peptide or control moiety connected to both fluorophores.

With this set of ligands, biological studies were performed applying the targeted *clickable* platform **3.62** and follow up investigations are planned. The non-peptidic mono- (**3.44** and **3.45**) and cyclen-based controls (**3.85** and **3.86**) served as unspecific negative controls in the course of the evaluation process. Confocal microscopy imaging in two PDAC cell lines have illustrated the high specificity of the PTP-targeted analogs **3.83** and **3.84** in comparison to their respective controls. Importantly, the cyclen scaffolds demonstrated to be stable under the applied test settings and the tendency of forming aggregates in physiological buffer was not observed during the time course of staining.

Subsequent distribution of this toolset to collaboration partners at the HU group in Beijing and the ALGÜL group in Munich will provide in depth characterization of photophysical properties of the probes, provide their *in vitro* staining efficacy towards the plectin-1 protein, and PDAC imaging in tissue samples. This analysis is fundamental not only for a full profiling, but also for identifying possible limitations of the probe scaffold – such as unspecific binding or the need for labeling with other fluorescent dyes which provide complementary information to the already synthesized Cy3 and Cy5.5.

Future applications of PTP-targeted analogs **3.83** and **3.84** involve theranostics, photodynamic therapy and dual-imaging modalities. For example, replacement of the cyanine dye moiety with a photosensitizer, such as porphyrin or IRDye800 may help to circumvent the inherent unspecific accumulation of these fluorophores *in vivo*. Targeted therapies could benefit of alkyne template **3.62** for the attachment of anti-cancer drugs. Furthermore, the cyclen core allows for dual-OI and MRI or PET tracers to be explored by the complexation with, e.g., gadolinium(III) or <sup>68</sup>Ga. Upon conjugation with more relevant NIR dyes, including IRDye800 and ICG, dual-imaging ligands are valuable tools for the diagnosis and intra-operative visualization of PDAC. With the modular approach developed in this thesis, the probe platform **3.62** becomes readily accessible for the tailored synthesis of multivalent imaging derivatives that are not restricted to a certain target of choice and the imaging modality.

## 4. Conclusion

Targeted fluorescent ligands have found diverse applications in the biomedical field, contributing to the visualization of protein-targets and the characterization of pathologies in living systems. Challenges in the assembly of an efficient probe are unique to the specific imaging experiments foreseen and may arise from several structural aspects necessary for installation of the reporter group. Those include the selection of a suitable design strategy and optimization of each component of the probe, i.e., ligand, linker, and reporter unit. This thesis investigated distinct probe design concepts to develop two novel fluorescently labeled platforms with high specificity for relevant pharmacological targets, the CB<sub>2</sub>R (Chapter 2.) and plectin-1 protein (Chapter 3.).

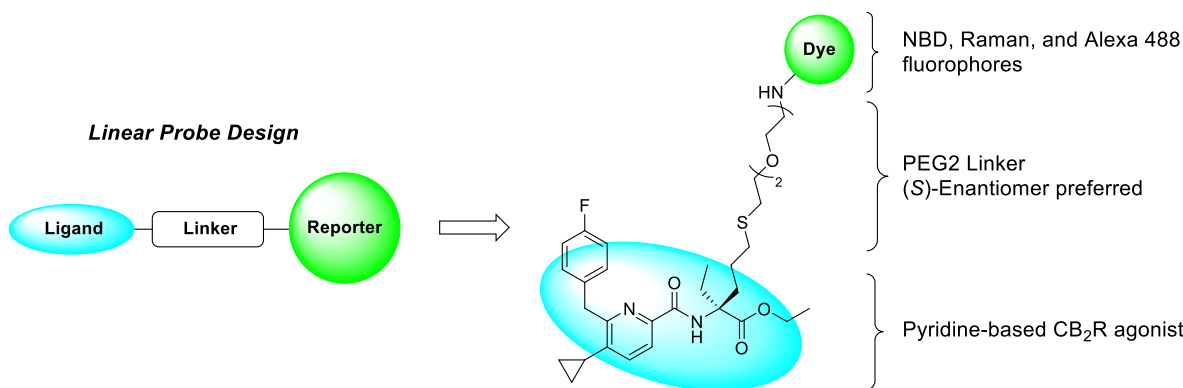


**Figure 4.1.** The linear design strategy was selected for generating a CB<sub>2</sub>R-selective fluorescent probe platform in Chapter 2.

The important, but still not fully elucidated, role of the CB<sub>2</sub>R in several inflammatory disorders as well as the lack of appropriate imaging tools to access its pharmacology demanded the need to develop versatile fluorescent ligands. A linear design strategy was employed to generate such imaging probes in the first part of this thesis (Figure 4.1.). Careful selection of a pharmacophore agonist as well as extensive evaluation of suitable linker placement and length allowed me to obtain a free amine precursor applied for labeling procedures. The synthesized fluorescent ligands displayed excellent affinity and selectivity values towards human and mouse CB<sub>2</sub>R, while retaining the agonistic effects of the selected recognition element. Moreover, their *in vitro* profiles were highly independent of the attached fluorophore structure and properties, highlighting the robustness of the developed probe template. These derivatives were cross-validated in a broad range of optical imaging techniques, as

illustrated by the FACS, TR-FRET, and confocal microscopy investigations conducted in three different laboratories. Currently, the probe set is being applied to study CB<sub>2</sub>R expression and function in native systems.

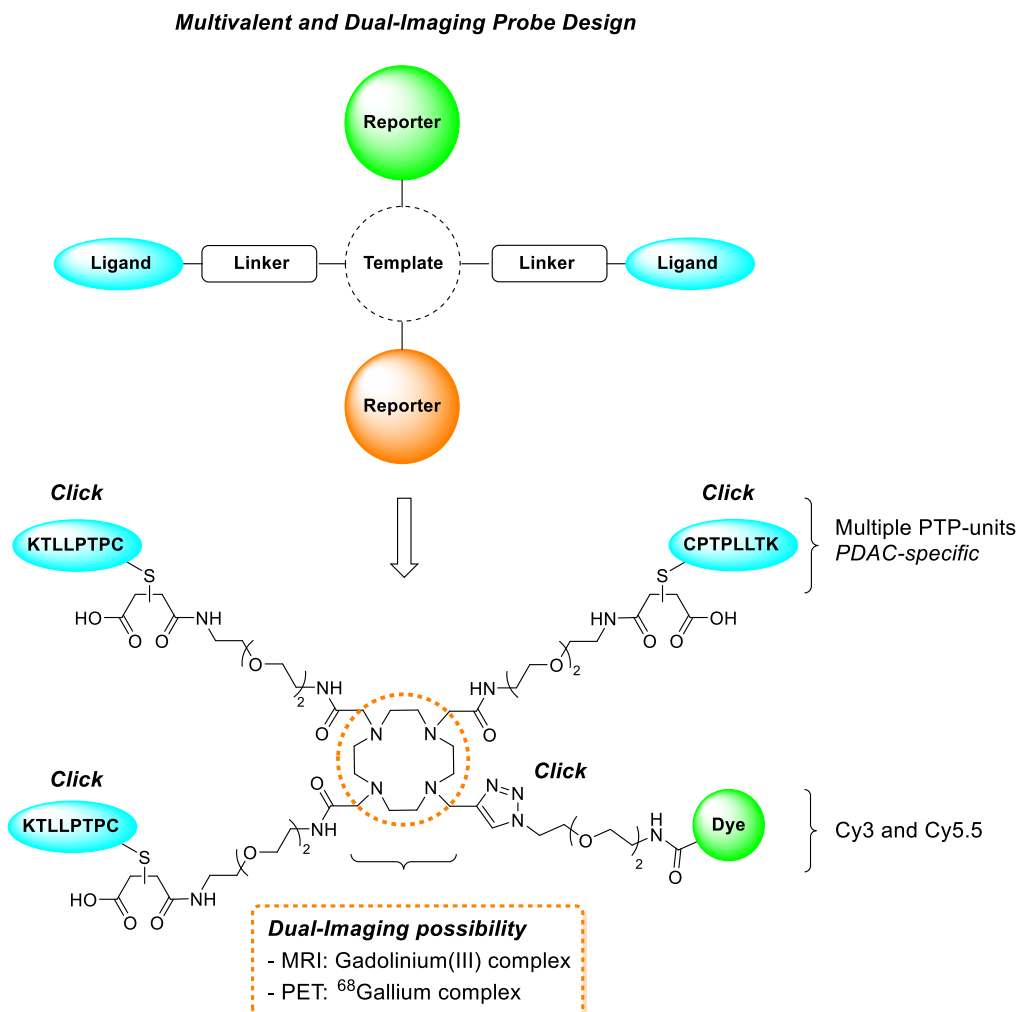


**Figure 4.2.** A cyclen-based multivalent probe template exploiting both the multivalent and the dual-imaging design strategies was developed for PDAC imaging in Chapter 3. The metal chelating properties of the DOTA core enables dual-imaging possibilities with both MRI and PET imaging modalities.

The second part of this thesis explored the cyclen core as a template for the synthesis of multivalent contrast agents, i.e., contain multiple targeting moieties (Figure 4.2.). The multivalent and the dual-imaging design strategies were combined to develop a fully *clickable* probe platform. This key precursor enabled the *one-pot* assembly of heterogeneously tetrafunctionalized cyclen-based fluorescent ligands in aqueous buffers. Furthermore, a new methodology to efficiently remove copper ions from the cyclen scaffold after CuAAC reaction (up to 99% efficiency) was identified. Such a synthetic route

could address major bottlenecks encountered for the unsymmetrically derivatization of cyclen, including long reaction sequences based on subsequent amide coupling procedures, followed by complex chromatographic purifications, which overall have led to low yields. Upon installation of three plectin-1 targeting peptides and a cyanine fluorophore (Cy3 or Cy5.5), these probes were utilized to precisely image plectin-1 in pancreatic cancer cell lines using confocal microscopy. These experiments demonstrated the superior selectivity and binding avidity of the tri-substituted ligands towards plectin-1 when compared to monovalent and unspecific controls.

The work performed in this thesis was successfully employed for interrogating several aspects of medicinal chemistry research and illustrated how well-characterized fluorescent probes support early stages of the drug development process. In particular, both CB<sub>2</sub>R and plectin-1 imaging platforms provided means to confidently detect the investigated protein targets *in vitro* and to visualize their downstream cellular events. In the CB<sub>2</sub>R case study, the synthesized labeled derivatives also enabled assessment of ligand-binding kinetics with the possibility of implementing optical-based HTS assays and aided in preclinical and translational test settings.

While attending to certain limitations in the probe development field, these toolset of fluorescent derivatives will enable to investigate specific unsolved questions regarding their protein-targets, highlighting remaining challenges. For the CB<sub>2</sub>R, exploring Raman spectroscopy to assess how the CB<sub>2</sub>R-selective labeled agonists bind to the target will be crucial for generating novel compound classes with improved binding to CB<sub>2</sub>R. In addition, the CB<sub>2</sub>R-targeted fluoroprobes hold promising applications in more advanced drug development stages, such as determining dose selection of in humans. The plectin-1 targeted probes still require follow up studies in healthy control cells and PDAC tissues. Afterwards, these cyclen-based derivatives have potential applications as dual-imaging tools when in complex form with gadolinium(III) or <sup>68</sup>Gallium. Such tools have important clinical applications to both evaluate the response of patients to PDAC treatment and guide intra-operative cancer resection. Moreover, the straightforward conditions established to assemble multivalent ligands from a novel cyclen-based template may guide and will facilitate the synthesis of analogs in diverse research fields.

Altogether, the design strategies exploited for the synthesis of both probe platforms presented in this thesis as well as the validation approaches used to characterize their pharmacology may serve as a general road map for the development and applicability of related fluorescent ligands.



## 5. Experimental Procedures

### 5.1. General Synthetic Information

Reactions with air or moisture-sensitive substances were, if not otherwise indicated, carried out under an inert atmosphere of argon or nitrogen with the help of the Schlenk technique. All other chemicals were purchased from commercial suppliers and used as received unless otherwise specified. Peptide sequences were purchased from Peptides and elephants. Control peptide (NH<sub>2</sub>-SNLHPSDC-COOH) was used as received from the supplier. Plectin-1 targeting peptide (PTP) was purchased in its protected crude form (Boc-NH-K(Boc)T(*tert*-Bu)LLPT(*tert*-Bu)PC(Trt)-COOH); PTP deprotection was performed following a conventional acidic deprotection protocol and purified by reversed-phase HPLC as specified in the corresponding subsection.

Reaction progress was monitored by thin layer chromatography on aluminum backed silica gel plates (silica gel 60 F 254 from E. Merck), visualizing with UV light ( $\lambda = 254$  nm). For reactants with high molecular weight ( $> 2'000$  g/mol), MALDI was additionally used to monitor reaction progress. MALDI measurements were performed on a Bruker Microflex MALDI-TOF LT/SH using 2,5-dihydroxyacetophenone (2,5-DHAP) matrix and dried droplet sample preparation. 2,5-DHAP matrix was prepared according to supplier specifications.

Chromatographic separations were carried out using Biotage Isolera One apparatus with RediSep®Rf columns from Teledyne Isco. High performance liquid chromatography (HPLC) separations were carried out using Waters LC150-System with a Macherey-Nagel VP 250/21 Nucleodur 100-7 C18Ec column, eluted with a gradient system of 10:90 to 90:10 acetonitrile:water with 0.1% TFA as acidic modifier at a 30 mL/min flow. Chiral separation was performed on Waters equipment using a 250 x 50 mm Reprosil Chiral NR column, eluted under isocratic mode with 90:10 heptane:(ethyl acetate with 0.01 mol ammonium acetate) at a 35ml/min flow.

The analytical data was obtained with the help of the following equipment.

<sup>1</sup>H and <sup>13</sup>C NMR spectra were recorded at either Bruker AV 300 (295K, 300 MHz, 75 MHz) or Bruker AV 600 (300K, 600 MHz, 151 MHz) spectrometers in CDCl<sub>3</sub> or DMSO-*d*<sub>6</sub> as solvents. Spin

multiplicities were described as singlet (s), duplet (d), triplet (t), quartet (q), and multiplet (m). Coupling constants ( $J$ ) were recorded in Hz. All  $^{13}\text{C}$  NMR-spectra were recorded with  $^1\text{H}$ -broad-band decoupling. All chemical shifts for experiments performed in  $\text{CDCl}_3$  are reported in ppm ( $\delta$ ) relative to tetramethylsilane ( $\delta = 0.00$  ppm) and were calibrated with respect to their deuterated solvents ( $\delta = ^1\text{H}$ : 7.26 ppm,  $^{13}\text{C}$ : 77.16 ppm). For experiments performed in  $\text{DMSO-}d_6$  the deuterated  $\text{DMSO-}d_6$  solvent signal was used as the reference with 2.50 ppm ( $\delta = ^1\text{H}$ : 2.50 ppm,  $^{13}\text{C}$ : 39.52 ppm). NMR data were analyzed with MestReNova software.

Mass and UV spectra were obtained with two different spectrometers using the same column. LC-MS (method 1): Agilent Technologies 6220 Accurate Mass TOF LC/MS linked to Agilent Technologies HPLC 1200 Series instrument using a Thermo Accuore RP-MS 2.6  $\mu\text{m}$ , 30 x 2.1 mm column at 25 °C (Eluent A = water with 0.1% TFA; Eluent B = acetonitrile with 0.1% TFA), at a flow of 0.8 mL/min with the following gradient: 0.0 min to 0.2 min, 95% A; 1.1 min, 1% A; 2.5 min, stop time; 1.3 min, post time; UV-detection: 220 nm, 254 nm, 300 nm. LC-MS (method 2): Agilent Technologies 6120 Quadrupole LC/MS instrument linked to Agilent Technologies HPLC 1290 Infinity using a Thermo Accuore RP-MS 2.6  $\mu\text{m}$ , 30 x 2.1 mm column at 25 °C (Eluent A = water with 0.1% TFA; Eluent B = acetonitrile with 0.1% TFA), at a flow of 0.8 mL/min with the following gradient: 0.0 min to 0.2 min, 95% A; 1.1 min, 1% A; 2.5 min, stop time; 1.3 min, post time; UV-detection: 220 nm, 254 nm, 300 nm. Alternatively, LC-high-resolution MS spectra were recorded with an Agilent LC system consisting of an Agilent 1290 high-pressure system, a CTC PAL autosampler, and an Agilent 6520 QTOF. The separation was achieved on a Zorbax Eclipse Plus C18 1.7  $\mu\text{m}$ , 2.1 mm x 50 mm column at 55 °C (Eluent A = water with 0.01% formic acid; Eluent B = acetonitrile with 0.01% formic acid) at a flow of 1 mL/min with the following gradient: 0.0 min, 5% B; 0.3 min, 5% B; 4.5 min, 99% B; 5 min, 99% B.

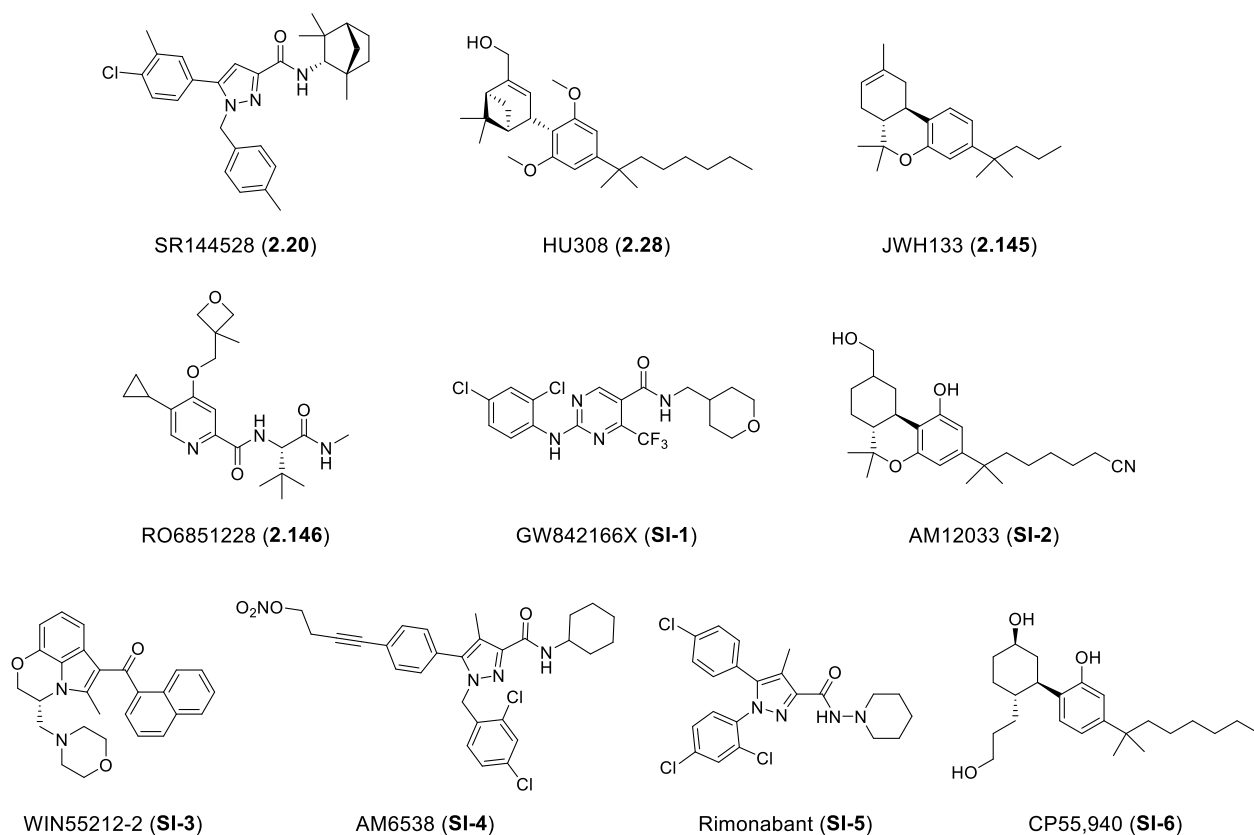
ICP-MS analysis was performed on a Thermo Element 2 (double-focusing sector-field ICP-MS) instrument equipped with nickel cones. A glass concentric nebulizer (200  $\mu\text{L}/\text{min}$ ) operated in self-aspirating mode and a glass cyclonic spray chamber (20 mL) were used for sample introduction. The analysis was conducted using 16 L/min cool gas flow, 1.05 L/min auxiliary gas flow, 1.171 to 1.190 L/min sample gas flow, and a plasma power of 1250 W. Copper isotopes  $^{63}\text{Cu}$  and  $^{65}\text{Cu}$  were detected at low ( $R = 300$ ) and medium ( $R = 4000$ ) resolution using an integration time of 10 ms. For each sample, three runs (with three passes each) per resolution were performed. Between each new sample, the sample tube was washed with 1% ( $v/v$ ) nitric acid for 60 s, followed by a sample take-up time of

90 s. For these experiments, the nitric acid (Geyer Chemsolute p.a., 65.0%) was distilled by sub-boiling (twice) at the BAM. The copper ICP multi-element standard solution IV containing 1000 mg/L copper in 6.5% suprapure nitric acid (Merc) was used for calibration.

Compound names are derived from Chemdraw and are not necessarily identical with the IUPAC nomenclature.

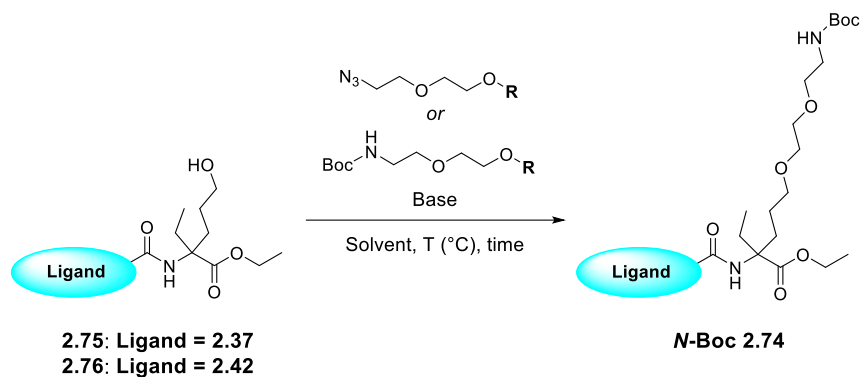
## 5.2. To “Tracing the Cannabinoid Type 2 Receptor with a Fluorescent Probe Toolbox”

### 5.2.1. Supplementary Figure



**Supplementary figure S-1. Structures of reference ligands.** SR144528 (**2.20**), CB<sub>2</sub>R agonist, reference ligand for TR-FRET assay. HU-308, CB<sub>2</sub>R agonist, reference ligand for TR-FRET assay (**2.28**). JWH133 (**2.145**), CB<sub>2</sub>R agonist, reference ligand for FACS, binding and cAMP assays. RO6851228 (**2.146**), CB<sub>2</sub>R agonist, reference ligand for FACS assay. GW842166X (**SI-1**), CB<sub>2</sub>R agonist, used for blocking experiments of NMP6-probe **2.26**.<sup>[152]</sup> AM12033, (**SI-2**) non-selective agonist, used for crystallization of the CB<sub>2</sub>R.<sup>[181]</sup> WIN55212-2 (**SI-3**), non-selective, reference ligand for binding and cAMP assays. AM6538 (**SI-4**), CB<sub>2</sub>R antagonist, used for crystallization of the CB<sub>2</sub>R.<sup>[181]</sup> Rimonabant (**SI-5**), CB<sub>1</sub>R agonist, reference ligand for binding and cAMP assays. CP55,940 (**SI-6**), non-selective agonist, reference ligand for binding and cAMP assays.

## 5.2.2. Supplementary Tables



R = tosyl or triflate group

**Supplementary table S-1. Reaction conditions tested for the synthesis of N-Boc protected 2.74.**

Entry	Base	Base equiv.	Solvent	T (°C)	time	Result	
						N-Boc pyrazine-2.74	N-Boc pyridine-2.74
1	NaH	7.0	THF	0 to 66 °C	5 h	SM degradation	SM degradation
2	NaH	7.0	DMF	0 to 50 °C	5 h	SM degradation	SM degradation
3	NaH	12.0	THF	0 °C to r.t.	24 h	No conversion	No conversion
4	KOtBU	7.0	THF	0 to 66 °C.	5 h	SM degradation	SM degradation
5	KOtBU	7.0	DMF	0 to 50 °C.	5 h	SM degradation	SM degradation
6	NaH, Bu <sub>4</sub> BnBr	7.0	DMF	0 °C to r.t.	3 d	No conversion	No conversion
7	KOtBu, Bu <sub>4</sub> BnBr	7.0	DMF	0 °C to r.t.	3 d	No conversion	No conversion
8	LDA	1.2	THF	-78 °C to r.t.	3 d	No conversion	No conversion
9	LiHMDS	1.2	THF	-78 °C to r.t.	3 d	No conversion	No conversion
10	nBuLi	1.2	THF	-78 °C to r.t.	3 d	No conversion	No conversion

T – temperature, R = tosyl or triflate leaving groups. Reaction conditions: **2.75** or **2.76** (1.0 equiv.), N-Boc PEG2 or azido-PEG2 linker (1.5 equiv.).

Supplementary table S-2. Reaction conditions tested for the crystallization of amino ester ( $\pm$ )-2.78 using diastereomeric salt formation strategies.

Entry	Chiral salt	Equiv. of chiral salt	Solvent	Volume ( $\mu$ L)	Result
1			methanol	70	No crystal formation
2			isopropanol	200	No crystal formation
3	(R)-Tartaric acid	0.5	ethyl acetate	100	No crystal formation
4			chloroform	110	No crystal formation
5			tetrahydrofuran	90	No crystal formation
6			methanol	70	No crystal formation
7			isopropanol	200	No crystal formation
8	(S)-Tartaric acid	0.5	ethyl acetate	100	No crystal formation
9			chloroform	110	No crystal formation
10			tetrahydrofuran	90	No crystal formation
11			methanol	70	No crystal formation
12			isopropanol	200	No crystal formation
13	(S)-Camphor Sulfonic acid	1.0	ethyl acetate	350	No crystal formation
14			chloroform	290	No crystal formation
15			tetrahydrofuran	170	No crystal formation
16			methanol	70	No crystal formation
17			isopropanol	200	No crystal formation
18	(R)-Camphor Sulfonic acid	1.0	ethyl acetate	350	No crystal formation
19			chloroform	290	No crystal formation
20			tetrahydrofuran	130	No crystal formation
21			methanol	70	No crystal formation
22			isopropanol	200	No crystal formation
23	(S)-Mandelic acid	1.0	ethyl acetate	160	No crystal formation
24			chloroform	270	No crystal formation
25			tetrahydrofuran	90	No crystal formation
26			methanol	70	No crystal formation
27			isopropanol	200	No crystal formation
28	(R)-Mandelic acid	1.0	ethyl acetate	160	No crystal formation
29			chloroform	270	No crystal formation
30			tetrahydrofuran	90	No crystal formation
31			methanol	70	No crystal formation
32			isopropanol	200	No crystal formation
33	(S)-Lactic acid	1.0	ethyl acetate	100	No crystal formation
34			chloroform	110	No crystal formation
35			tetrahydrofuran	90	No crystal formation
36			methanol	70	No crystal formation
37			isopropanol	200	53% yield, 31% <i>ee</i>
38	(S)-Dibenzoyl tartaric acid	0.5	ethyl acetate	100	No crystal formation
39			chloroform	110	15% yield, <i>ee</i> not calculated
40			tetrahydrofuran	110	No crystal formation
41			methanol	70	No crystal formation
42			isopropanol	200	28% yield, 30% <i>ee</i>
43	(R)-Dibenzoyl tartaric acid	0.5	ethyl acetate	100	No crystal formation
44			chloroform	110	No crystal formation
45			tetrahydrofuran	110	No crystal formation

Reaction conditions: Amino ester ( $\pm$ )-2.78 (20 mg, 0.17 mmol) and the corresponding chiral salt were dissolved in the minimum amount of solvent necessary for their complete dilution (described for each example at the volume column). The solution was shaken at 50 °C for 2 h with 700 rpm, cooled to room temperature and stored at 4 °C for 18 h. Tubes containing crystals were centrifuged at 4 °C for 25 min (120 rcf), and the crystals were washed with ice cold solvent. This procedure was repeated twice.

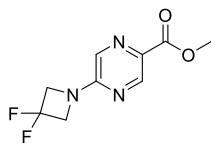
**Supplementary table S-3. *In vitro* pharmacology data of Alexa 488-2.134 for a representative set of common off-targets.**

Assay name	Readout	Value (% inhibition)
MAO-A (h)	Enzymatic activity	1
5-HT transporter (h) (antagonist radioligand)	Specific binding	-8
5-HT1A (h) (agonist radioligand)	Specific binding	1
5-HT2A (h) (agonist radioligand)	Specific binding	5
5-HT2B (h) (agonist radioligand)	Specific binding	2
5-HT3 (h) (antagonist radioligand)	Specific binding	6
A1 (h) (agonist radioligand)	Specific binding	2
A3 (h) (agonist radioligand)	Specific binding	77
Abl kinase (h)	Enzymatic activity	13
ACE (h)	Enzymatic activity	-22
acetylcholinesterase (h)	Enzymatic activity	-5
alpha 1A (h) (antagonist radioligand)	Specific binding	0
alpha 2A (h) (antagonist radioligand)	Specific binding	5
AR(h) (agonist radioligand)	Specific binding	1
AT1 (h) (antagonist radioligand)	Specific binding	0
beta 1 (h) (agonist radioligand)	Specific binding	9
beta 2 (h) (antagonist radioligand)	Specific binding	7
BZD (central) (agonist radioligand)	Specific binding	-1
Ca2+ channel (L, diltiazem site) (benzothiazepines) (antagonist radioligand)	Specific binding	6
CB1 (h) (agonist radioligand)	Specific binding	41
CCK1 (CCKA) (h) (agonist radioligand)	Specific binding	23
CDK2 (h) (cycA)	Enzymatic activity	5
Cl- channel (GABA-gated) (antagonist radioligand)	Specific binding	30
COX2(h)	Enzymatic activity	-5
D1 (h) (antagonist radioligand)	Specific binding	10
D2S (h) (agonist radioligand)	Specific binding	-11
Estrogen ER alpha (h) (agonist radioligand)	Specific binding	0
FP (h) (agonist radioligand)	Specific binding	14
glycine (strychnine-insensitive) (antagonist radioligand)	Specific binding	8
GR (h) (agonist radioligand)	Specific binding	33
GSK3alpha (h)	Enzymatic activity	-13
GSK3beta (h)	Enzymatic activity	-10
H1 (h) (antagonist radioligand)	Specific binding	2
H2 (h) (antagonist radioligand)	Specific binding	15
H3 (h) (agonist radioligand)	Specific binding	-1
HIV-1 protease	Enzymatic activity	47
ZAP70 kinase (h)	Specific binding	35
M1 (h) (antagonist radioligand)	Specific binding	-5
M2 (h) (antagonist radioligand)	Specific binding	8
MMP-9 (h)	Enzymatic activity	21
mu (MOP) (h) (agonist radioligand)	Specific binding	0
N muscle-type (h) (antagonist radioligand)	Specific binding	14
N neuronal alpha 4beta 2 (h) (agonist radioligand)	Specific binding	-7
norepinephrine transporter (h) (antagonist radioligand)	Specific binding	9
PCP (antagonist radioligand)	Specific binding	4
PDE3B (h)	Enzymatic activity	15
PDE4D2 (h)	Enzymatic activity	32
PPARgamma (h) (agonist radioligand)	Specific binding	29
xanthine oxidase/ superoxide O2- scavenging	Enzymatic activity	-6
ZAP70 kinase (h)	Enzymatic activity	39

Representative off target testing.<sup>[193]</sup> Data shown is the mean percentage of inhibition for binding assays and the mean percentage of inhibition for enzyme and cell-based assays at a test concentration of 10  $\mu$ M (n=2). Data were generated at Eurofins Cerep (France).

### 5.2.3. Synthesis of Pyrazine Carboxylic Acid 2.37

#### *5-(3,3-Difluoro-azetidin-1-yl)-pyrazine-2-carboxylic acid methyl ester (2.39)*

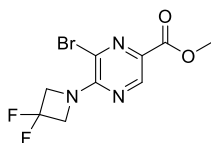


5-Chloro-pyrazine-2-carboxylic acid methyl ester **2.38** (100 mg, 0.58 mmol) was dissolved in 1,4-dioxane (1 mL). To this solution was added 3,3-difluoroazetidine hydrochloride (91 mg, 0.70 mmol), and triethylamine (0.2 mL, 1.51 mmol). The mixture was stirred 22 h at 45 °C, and then cooled to room temperature. Brine (1 mL) was added to the stirring mixture, and the mixture was extracted with ethyl acetate (3x). The organic phases were combined and washed successively with 10% sodium bicarbonate solution (5 mL) and brine (5 mL), dried over MgSO<sub>4</sub>, filtered, and concentrated under reduced pressure. The crude was purified by column chromatography (Silica gel, 4 g, cHex:EtOAc, 30 to 50% EtOAc) to yield a 59 mg (44%) of **2.39** as a white solid.

<sup>1</sup>H NMR (300 MHz, CDCl<sub>3</sub>) δ ppm 8.83 (s, 1H), 7.87 (s, 1H), 4.54 (t, *J* = 11.7 Hz, 4H), 3.96 (s, 3H).

The analytical data are in accordance with those reported in the literature.<sup>[170]</sup>

#### *6-Bromo-5-(3,3-difluoro-azetidin-1-yl)-pyrazine-2-carboxylic acid methyl ester (2.40)*

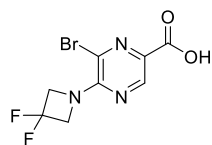


To a solution of **2.39** (59 mg, 0.25 mmol) in chloroform (1 mL) was added *N*-bromosuccinimide (89 mg, 0.52 mmol). The reaction mixture was stirred at 60 °C for 20 h. After cooling to room temperature, water (2 mL) was added to quench, and the organic phase was separated and washed successively with water (3 mL) and brine (3 mL), dried over MgSO<sub>4</sub>, filtered, and concentrated under reduced pressure. The crude material was purified by column chromatography (Silica gel, 4 g, cHex:EtOAc, 50% EtOAc) to give the desired product **2.40** (57.9 mg, 75%) as a light yellow solid.

<sup>1</sup>H NMR (600 MHz, DMSO-*d*<sub>6</sub>) δ ppm 8.71 (s, 1H), 4.79 (t, *J* = 12.5 Hz, 4H), 3.85 (s, 3H).

The analytical data are in accordance with those reported in the literature.<sup>[170]</sup>

**6-Bromo-5-(3,3-difluoro-azetidin-1-yl)-pyrazine-2-carboxylic acid (2.41)**

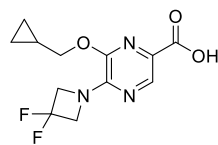


To a solution of **2.40** (4.6 g, 14.9 mmol) in tetrahydrofuran (18 mL) and water (9 mL) was added lithium hydroxide (467 mg, 19.5 mmol) at room temperature, and stirred at this temperature for 20 h. Afterwards, the solvent was concentrated under reduced pressure, and the aqueous phase acidified with hydrochloric acid aq. sol. (1 M, pH 2-3). The solid was separated, triturated with toluene (3 mL) and dried in vacuo to give the title compound **2.41** (3.1 g, 71%) as a white solid.

<sup>1</sup>H NMR (300 MHz, DMSO-*d*<sub>6</sub>) δ ppm 8.69 (s, 1H), 4.76 (t, *J* = 12.5 Hz, 4H).

The analytical data are in accordance with those reported in the literature.<sup>[170]</sup>

**6-Cyclopropylmethoxy-5-(3,3-Difluoro-azetidin-1-yl)-pyrazine-2-carboxylic acid (2.37)**



To a solution of cyclopropanemethanol (0.55 mL, 6.79 mmol) in anhydrous dimethyl sulfoxide (9 mL) was added potassium hydroxide (0.66 g, 11.8 mmol) at room temperature. To the mixture was added a solution of **2.41** (1.0 g, 3.40 mmol) in dimethyl sulfoxide (1 mL). The reaction mixture was stirred at room temperature for 3 h. Afterwards, water (3 mL) was added, and the aqueous mixture was acidified with hydrochloric acid aq. sol. (1 M, pH 3-4). The solid was filtered, triturated with toluene (3 mL) and dried in vacuo to give compound **2.37** (873 mg, 90%) as a white solid.

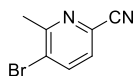
<sup>1</sup>H NMR (600 MHz, DMSO-*d*<sub>6</sub>) δ 12.72 (s, 1H), 8.30 (s, 1H), 4.64 (t, *J* = 12.4 Hz, 4H), 4.15 (d, *J* = 7.2 Hz, 2H), 1.31 – 1.22 (m, 1H), 0.60 – 0.53 (m, 2H), 0.41 – 0.34 (m, 2H).

The analytical data are in accordance with those reported in the literature.<sup>[170]</sup>



#### 5.2.4. Synthesis of Picolinic Acid **2.42**

##### *5-Bromo-6-methylpicolinonitrile (SI-7)*

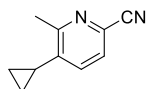


To a stirring solution of 3-bromo-6-fluoro-2-methyl-pyridine **2.43** (30 g, 158 mmol) in dimethyl sulfoxide (40 mL) sodium cyanide (31 g, 633 mmol) was added at room temperature. The reaction mixture was heated to 100 °C and stirred for 2 h. After cooling to room temperature, the reaction was quenched with the addition of water (40 mL) and the mixture extracted with diethyl ether (3x). The combined organic phases were dried over MgSO<sub>4</sub>, and concentrated under reduced pressure to obtain a crude oil. Purification by column chromatography (Silica gel, 80 g, cHex:EtOAc, 25% EtOAc) gave the title compound **SI-7** as a colorless oil (5.3 g, 17%).

<sup>1</sup>H NMR (300 MHz, CDCl<sub>3</sub>) δ ppm 7.95 (d, *J* = 8.1 Hz, 1H), 7.40 (d, *J* = 8.1 Hz, 1H), 2.71 (s, 3H).

The analytical data are in accordance with those reported in the literature.<sup>[171]</sup>

##### *5-Cyclopropyl-6-methylpicolinonitrile (2.44)*

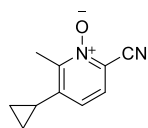


Compound **SI-7** (371 mg, 1.88 mmol), cyclopropylboronic acid (258 mg, 3.01 mmol), tris(dibenzylideneacetone)dipalladium(0) (Pd<sub>2</sub>(dba)<sub>3</sub>, 138 mg, 150 μmol), Xantphos (113 mg, 196 μmol) and cesium carbonate (735 mg, 2.26 mmol) were suspended in 1,4-dioxane (10 mL) and purged with argon. The mixture was stirred at 110 °C for 12 h, cooled to room temperature, filtered, and concentrated under reduced pressure. Purification by column chromatography (Silica gel, 25 g, cHex:EtOAc, 5 to 20% EtOAc) afforded the title compound **2.44** in 64% yield (1.9 g) as a light orange solid.

<sup>1</sup>H NMR (300 MHz, CDCl<sub>3</sub>) δ ppm 7.45 (d, *J* = 7.9 Hz, 1H), 7.29 (d, *J* = 7.9 Hz, 1H), 2.68 (s, 3H), 2.00 – 1.88 (m, 1H), 1.15 – 1.05 (m, 2H), 0.77 – 0.64 (m, 2H).

The analytical data are in accordance with those reported in the literature.<sup>[171]</sup>

### ***6-Cyano-3-cyclopropyl-2-methylpyridine 1-oxide (2.45)***

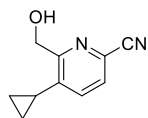


To a solution of compound **2.44** (1.9 g, 11.9 mmol) in dichloromethane (20 mL) 3-chloroperbenzoic acid (4.8 g, 27.6 mmol) was added. The reaction mixture was stirred for 12 h at 60 °C. Afterwards, the mixture was cooled to room temperature, filtered, and concentrated under reduced pressure. Subsequent purification by column chromatography (Silica gel, 40 g, cHex:EtOAc, 35% EtOAc) afforded *N*-oxide **2.45** (1.6 g, 77%) as a yellow solid.

**<sup>1</sup>H NMR** (300 MHz, CDCl<sub>3</sub>) δ ppm 7.44 (d, *J* = 8.3 Hz, 1H), 6.90 (d, *J* = 8.3 Hz, 1H), 2.65 (s, 3H), 2.03 – 1.88 (m, 1H), 1.21 – 1.08 (m, 2H), 0.79 – 0.71 (m, 2H).

The analytical data are in accordance with those reported in the literature.<sup>[171]</sup>

### ***5-Cyclopropyl-6-(hydroxymethyl)picolinonitrile (SI-8)***

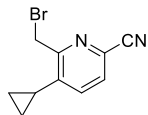


To a stirring solution of *N*-oxide **2.45** (1.6 g, 9.18 mmol) in dichloromethane (20 mL) 2,2,2-trifluoroacetic anhydride (6.5 mL, 45.9 mmol) was added. The reaction mixture was stirred at room temperature for 8 h, poured onto water (40 mL) and extracted with dichloromethane (3x). The combined organic layers were dried over MgSO<sub>4</sub>, filtered, and concentrated under reduced pressure. The crude residue was purified by column chromatography (Silica gel, 25 g, cHex:EtOAc, 15% EtOAc) to give the title compound **SI-8** in 95% yield (1.5 g) as a yellow oil.

**<sup>1</sup>H NMR** (300 MHz, CDCl<sub>3</sub>) δ ppm 7.56 (dd, *J* = 8.0, 0.9 Hz, 1H), 7.37 (dd, *J* = 7.9, 0.8 Hz, 1H), 4.93 (s, 2H), 4.12 (bs, 1H), 1.80 (tt, *J* = 8.4, 5.3 Hz, 1H), 1.19 – 1.09 (m, 2H), 0.78 – 0.70 (m, 2H).

The analytical data are in accordance with those reported in the literature.<sup>[171]</sup>

### **6-(Bromomethyl)-5-cyclopropylpicolinonitrile (2.46)**

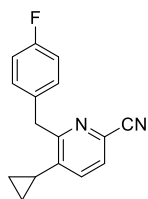


Intermediate **SI-8** (1.5 g, 8.61 mmol) was dissolved in tetrahydrofuran (20 mL). Tetrabromomethane (5.7 g, 17.2 mmol) and triphenylphosphine (2.2 g, 17.2 mmol) were added. The reaction mixture was stirred for 12 h at room temperature and concentrated under reduced pressure. n-Heptane (30 mL) and EtOAc (20 mL) were added to the crude residue and the suspension was stirred for 15 min at room temperature. The resulting precipitate composed by triphenylphosphine was filtered off. The filtrate was poured onto water (30 mL) and extracted with ethyl acetate (3x). The combined organic layers were dried over MgSO<sub>4</sub>, filtered, and concentrated under reduced pressure. The crude material was purified by column chromatography (Silica gel, 25 g, cHex:EtOAc, 10% EtOAc) to give the title compound **2.46** in 55% yield (1.1 g) as a light orange solid.

<sup>1</sup>H NMR (300 MHz, CDCl<sub>3</sub>) δ ppm 7.89 (d, *J* = 8.1 Hz, 1H), 7.60 (d, *J* = 8.1 Hz, 1H), 4.88 (s, 2H), 2.25 – 2.14 (m, 1H), 1.20 – 1.09 (m, 2H), 0.93 – 0.82 (m, 2H).

The analytical data are in accordance with those reported in the literature.<sup>[171]</sup>

### **5-Cyclopropyl-6-(4-fluorobenzyl)picolinonitrile (SI-9)**

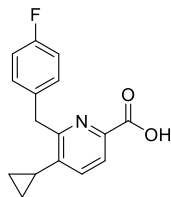


Compound **2.46** (650 mg, 2.74 mmol) was dissolved in 1,4-dioxane (20 mL). To the stirring solution cesium carbonate (1.3 g, 4.11 mmol), [1,1'-bis(diphenylphosphino)ferrocene]dichloropalladium(II) (Pd(dppf)Cl<sub>2</sub>, 380 mg, 466 μmol) and 4-fluorophenylboronic acid (671 mg, 4.80 mmol) were added and the mixture was purged with argon. The reaction mixture was heated to 110 °C for 12 h. After cooling to room temperature, the crude mixture was filtered, poured onto water (10 mL) and extracted with ethyl acetate (3x). The combined organic layers were dried over MgSO<sub>4</sub>, and concentrate under reduced pressure. The crude material was purified by column chromatography (Silica gel, 4 g, cHex:EtOAc, 5% EtOAc) to give the title compound **SI-9** in 47% yield (465 mg) as a colorless oil.

**<sup>1</sup>H NMR** (300 MHz, CDCl<sub>3</sub>) δ ppm 7.50 (d, *J* = 7.9 Hz, 1H), 7.33 (dd, *J* = 8.0, 0.7 Hz, 1H), 7.21 – 7.13 (m, 2H), 7.01 – 6.91 (m, 2H), 4.34 (s, 2H), 1.94 – 1.83 (m, 1H), 1.07 – 0.98 (m, 2H), 0.71 – 0.61 (m, 2H).

The analytical data are in accordance with those reported in the literature.<sup>[171]</sup>

### ***5-Cyclopropyl-6-(4-fluorobenzyl)picolinic acid (2.42)***



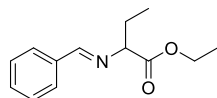
Intermediate **SI-9** (300 mg, 1.19 mmol) was dissolved in water (10 mL) and methanol (3 mL). Sodium hydroxide (190 mg, 4.76 mmol) was added, and the reaction mixture was heated to 80 °C upon stirring for 24 h. After this time, the reaction mixture was poured onto hydrochloric acid aq. sol. (0.5 M, 25 mL) and extracted with ethyl acetate (3x). The combined organic layers were dried over MgSO<sub>4</sub> and concentrated under reduced pressure. The crude material was diluted in a mixture of acetonitrile and water (1:1) and purified by reversed-phase preparative HPLC (C-18, Water:ACN with 0.1% TFA, 10 to 90% ACN) to give the title compound **2.42** (257 mg, 80%) as a white solid after lyophilization.

**<sup>1</sup>H NMR** (600 MHz, DMSO-*d*<sub>6</sub>) δ ppm 7.82 (d, *J* = 8.0 Hz, 1H), 7.47 (d, *J* = 8.0 Hz, 1H), 7.29 – 7.22 (m, 2H), 7.12 – 7.06 (m, 2H), 4.34 (s, 2H), 2.01 (ddt, *J* = 10.7, 7.4, 3.7 Hz, 1H), 1.00 – 0.90 (m, 2H), 0.70 – 0.62 (m, 2H).

The analytical data are in accordance with those reported in the literature.<sup>[171]</sup>

## 5.2.5. Synthesis of Amino Ester Building Blocks

### *Ethyl 2-(benzylideneamino)butanoate (2.77)*



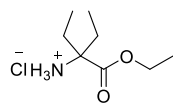
Thionyl chloride (3.5 mL, 47.9 mmol) was added dropwise to a solution of amino butyric acid **2.65** (3.8 g, 36.9 mmol) in ethanol (40 mL), over a period of 5 min at 0 °C. The reaction mixture was stirred at 0 °C for 1 additional hour. Afterwards, the resulting solution was refluxed (78 °C) for 4 h. The reaction mixture was cooled to room temperature and concentrated under reduced pressure to yield ethyl 2-aminobutanoate as a colorless oil (4.8 g, quant.), used without further purification for the next step.

Ethyl 2-aminobutanoate (4.8 g, 36.9 mmol) and dried magnesium sulfate (4.4 g, 36.9 mmol) were stirred in anhydrous dichloromethane (30 mL) at room temperature for 20 min. After which time, benzaldehyde (3.8 mL, 36.9 mmol) and triethylamine (9.5 mL, 68.2 mmol) were added sequentially and dropwise. The resulting mixture was stirred for 30 h at the same temperature then filtered and concentrated. The residue was dissolved in diethyl ether (8 mL) and water (8 mL) and the separated aqueous layer was extracted with ether. The combined ether solutions were washed with brine (8 mL), dried over MgSO<sub>4</sub>, filtered and concentrated under reduced pressure to give the desired imine **2.77** as a clear oil (7.5 g, 93%).

<sup>1</sup>H NMR (600 MHz, CDCl<sub>3</sub>) δ ppm 8.28 (s, 1H), 7.80 – 7.76 (m, 2H), 7.44 – 7.39 (m, 3H), 4.25 – 4.17 (m, 2H), 3.87 (dd, *J* = 8.2, 5.5 Hz, 1H), 2.09 – 2.00 (m, 1H), 1.94 – 1.88 (m, 1H), 1.27 (t, *J* = 7.1 Hz, 3H), 0.92 (t, *J* = 7.4 Hz, 3H).

The analytical data are in accordance with those reported in the literature.<sup>[296]</sup>

***Ethyl 2-amino-2-ethylbutanoate hydrochloride (2.61)***



Potassium bis(trimethylsilyl)amide (820 mg, 4.11 mmol) in tetrahydrofuran (12 mL) was added dropwise to a solution of **2.77** (600 mg, 2.74 mmol) in tetrahydrofuran (4 mL) and cooled to  $-50\text{ }^{\circ}\text{C}$ . After 1 h, iodoethane (0.3 mL, 3.56 mmol) was added at the same temperature. The cooling bath was removed, and the mixture was stirred at room temperature for additional 20 h. Afterwards, the reaction mixture was concentrated under reduced pressure, to remove most of the solvent. The residue was then partitioned between dichloromethane (10 mL) and water (10 mL). The organic layer was separated, and the aqueous phase was extracted with dichloromethane (4x). The combined organic extracts were washed with brine (5 mL), dried over  $\text{MgSO}_4$ , filtered and concentrated under reduced pressure to yield ethyl 2-(benzylideneamino)-2-ethylbutanoate **2.66** (643 mg, 95%) as a dark yellow oil, used without further purification for the subsequent deprotection.

To a solution of **2.66** (643 mg, 2.60 mmol) in diethyl ether (12 mL) hydrochloric acid aq. sol. (1 M, 10.3 mL) was added dropwise at  $0\text{ }^{\circ}\text{C}$ . After the addition, the reaction mixture was allowed to warm to room temperature and stirred for additional 15 h. The ether layer was then separated, and the water phase was extracted with dichloromethane (2x). The organic extracts were extracted with hydrochloric acid aq. sol. (1 M, 2x). The aqueous layers were combined to give **2.61** (328 mg, 64%) as light yellow solid after lyophilization.

**$^1\text{H NMR}$**  (300 MHz,  $\text{DMSO}-d_6$ )  $\delta$  ppm 8.51 (s, 3H), 4.19 (q,  $J = 6.9\text{ Hz}$ , 2H), 1.80 (q,  $J = 7.3\text{ Hz}$ , 4H), 1.19 (t,  $J = 6.9\text{ Hz}$ , 3H), 0.84 (t,  $J = 7.4\text{ Hz}$ , 6H).

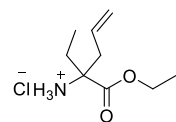
**$^{13}\text{C NMR}$**  (75 MHz,  $\text{DMSO}-d_6$ )  $\delta$  ppm 171.0, 64.1, 62.6, 28.9, 14.4, 8.1.

**HR-MS** (ESI)  $m/z$   $[\text{M}+\text{H}]^+$  calcd. for  $\text{C}_8\text{H}_{17}\text{NO}_2$ : 160.1332, found 160.1333.

### **General procedure for the synthesis of racemic $\alpha,\alpha$ -disubstituted $\alpha$ -amino esters**

To a solution of lithium diisopropylamine (LDA, 1.5 equiv.) in tetrahydrofuran (4 mL) at  $-78\text{ }^{\circ}\text{C}$  was added **2.77** (1.0 equiv.) in tetrahydrofuran (4 mL), followed by the dropwise addition of allyl bromide or 1-bromo-3-methoxypropane (1.5 equiv.). The mixture was stirred at room temperature for 24 h, and then concentrated under reduced pressure. The residue was then partitioned between ethyl acetate (15 mL) and water (15 mL). The organic layer was separated, and the aqueous phase was extracted with ethyl acetate (4x). The combined organic extracts were washed with brine, dried over  $\text{MgSO}_4$ , filtered and concentrated under reduced pressure. The crude residue was dissolved in diethyl ether (15 mL) and treated with hydrochloric acid aq. sol. (1 M, 3.5 equiv.) at  $0\text{ }^{\circ}\text{C}$ . The reaction mixture was allowed to warm to room temperature, and stirred for additional 15 h. The ether layer was separated, and the water phase washed with dichloromethane (2x). The combined dichloromethane phases were extracted with hydrochloric acid aq. sol. (0.2 M, 2x). The aqueous layers were combined and lyophilized to yield the corresponding amino ester hydrochloric salt, without the need of further purification steps.

#### ***Ethyl 2-amino-2-ethylpent-4-enoate (2.78)***



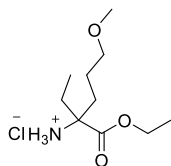
Following the general procedure above, **2.78** was obtained in 96% yield as a light yellow oil, over 2 steps (1.1 g) starting from allyl bromide (0.73 mL, 8.41 mmol).

**$^1\text{H}$  NMR** (300 MHz,  $\text{CDCl}_3$ )  $\delta$  ppm 5.74 – 5.60 (m, 1H), 5.21 – 5.05 (m, 2H), 4.15 (q,  $J = 7.1$  Hz, 2H), 2.53 (dd,  $J = 13.5, 6.4$  Hz, 1H), 2.21 (dd,  $J = 13.5, 8.4$  Hz, 1H), 1.84 – 1.66 (m, 3H), 1.60 – 1.48 (m, 1H), 1.25 (t,  $J = 7.1$  Hz, 3H), 0.83 (t,  $J = 7.5$  Hz, 3H).

**$^{13}\text{C}$  NMR** (75 MHz,  $\text{CDCl}_3$ )  $\delta$  ppm 176.8, 132.9, 119.5, 119.4, 61.0, 44.0, 32.9, 14.4, 8.3.

**HR-MS** (ESI)  $m/z$   $[\text{M}+\text{H}]^+$  calcd. for  $\text{C}_9\text{H}_{17}\text{NO}_2$ : 173.1366, found 173.1374.

***Ethyl 2-amino-2-ethyl-5-methoxypentanoate (2.93)***



Following the general procedure above, **2.93** was obtained in 92% yield as a colorless oil, over 2 steps (158 mg) starting from 1-bromo-3-methoxypropane (0.15 mL, 1.40 mmol).

**<sup>1</sup>H NMR** (600 MHz, CDCl<sub>3</sub>) δ ppm 8.86 (bs, 2H), 4.30 – 4.26 (m, 2H), 3.44 – 3.29 (m, 2H), 3.29 (s, 3H), 2.15 – 1.95 (m, 5H), 1.65 – 1.58 (m, 1H), 1.32 (t, *J* = 7.1 Hz, 3H), 1.09 (t, *J* = 7.5 Hz, 3H).

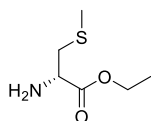
**<sup>13</sup>C NMR** (151 MHz, CDCl<sub>3</sub>) δ ppm 170.2, 72.0, 64.9, 62.6, 58.5, 33.3, 30.0, 24.1, 14.3, 8.5.

**HR-MS** (ESI) *m/z* [M+H]<sup>+</sup> calcd. for C<sub>10</sub>H<sub>21</sub>NO<sub>3</sub>: 204.1595, found 204.1588.

***General ethyl esterification procedure for natural amino acids***

Thionyl chloride (2.0 equiv.) was added dropwise to a solution of amino acid (1.0 equiv.) in ethanol (2 mL) at 0 °C. The reaction mixture was stirred at 0 °C for additional 1 h. Afterwards, the resulting solution was refluxed (78 °C) for 4 h. The reaction mixture was cooled to room temperature, while stirring for 20 h. The reaction mixture was concentrated under reduced pressure. The obtained hydrochloric salts were used without further purification for the next step.

***Ethyl S-methyl-L-cysteinate (2.89)***



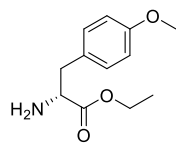
Following the general procedure above, **2.89** was obtained in quantitative yield (68 mg) as a white solid starting from *S*-Methyl-*L*-Cysteine (50 mg, 0.37 mmol).

**<sup>1</sup>H NMR** (300 MHz, CDCl<sub>3</sub>) δ ppm 8.90 (bs, 2H), 4.51 – 4.20 (m, 3H), 3.26 (s, 2H), 2.22 (s, 3H), 1.33 (s, 3H).

The analytical data are in accordance with those reported in the literature.<sup>[297]</sup>



***Ethyl L-2-amino-3-(4-methoxyphenyl)propanoate (2.90)***



Following the general procedure above, **2.90** was obtained in quantitative yield (94 mg) as a white solid starting from *O*-Methyl-*L*-Tyrosine (72 mg, 0.37 mmol).

**<sup>1</sup>H NMR** (300 MHz, DMSO-*d*<sub>6</sub>) δ ppm 8.76 (bs, 2H), 7.16 (d, *J* = 8.3 Hz, 2H), 6.88 (d, *J* = 8.4 Hz, 2H), 4.16 – 4.05 (m, 3H), 3.73 (s, 3H), 3.24 – 2.96 (m, 2H), 1.11 (t, *J* = 7.1, 3H).

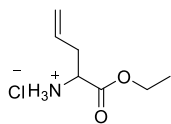
The analytical data are in accordance with those reported in the literature.<sup>[298]</sup>

***General procedure for the synthesis of racemic α-monosubstituted α-amino esters***

To a solution of lithium diisopropylamine (1.05 equiv.) in anhydrous tetrahydrofuran (3 mL) cooled to –78 °C was added *N*-(diphenylmethylene)glycine ethyl ester **2.62** (1.0 equiv.). The reaction mixture was stirred for 1 h at this temperature. Afterwards, allyl bromide or 1-bromo-3-methoxypropane (1.05 equiv.) was slowly added. The mixture was stirred at –78 °C for additional 1 h, and at room temperature for additional 22 h. The reaction was concentrated under reduced pressure, and the remained residue partitioned between ethyl acetate (12 mL) and water (12 mL). The organic layer was separated, and the aqueous phase was extracted with ethyl acetate (4x). The combined organic extracts were washed with brine (5 mL), dried over MgSO<sub>4</sub>, filtered and concentrated under reduced pressure.

The crude diphenylmethylene ester analog was dissolved in diethyl ether (3 mL) and treated with hydrochloric acid aq. sol. (1 M, 3.5 equiv.) at 0 °C. The reaction mixture was allowed to warm to room temperature, and stirred for additional 15 h. The ether layer was separated, and the water phase was extracted with dichloromethane (2x). The dichloromethane extracts were extracted with hydrochloric acid aq. sol. (0.2 M, 2x). The aqueous layers were combined and lyophilized to yield the corresponding amino ester hydrochloric salt, without the need of further purification.

***Ethyl 2-aminopent-4-enoate (2.91)***



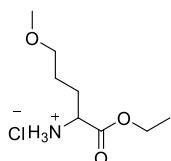
Following the general procedure above, **2.91** was obtained in 91% yield as a light yellow oil, over 2 steps (277 mg) starting from allyl bromide (0.17 mL, 1.96 mmol).

**<sup>1</sup>H NMR** (600 MHz, CDCl<sub>3</sub>) δ ppm 8.68 (bs, 2H), 5.88 – 5.81 (m, 1H), 5.29 (d, *J* = 16.8 Hz, 1H), 5.22 (d, *J* = 9.7 Hz, 1H), 4.31 – 4.15 (m, 3H), 2.86 – 2.79 (m, 2H), 1.27 (t, *J* = 6.6 Hz, 3H).

**<sup>13</sup>C NMR** (151 MHz, CDCl<sub>3</sub>) δ ppm 168.7, 130.3, 121.3, 62.6, 52.9, 34.5, 14.1.

**HR-MS** (ESI) *m/z* [M+H]<sup>+</sup> calcd. for C<sub>7</sub>H<sub>13</sub>NO<sub>2</sub>: 144.1019, found 144.1020.

***Ethyl 2-amino-5-methoxypentanoate (2.92)***



Following the general procedure above, **2.92** was obtained in 82% yield as a colorless oil, over 2 steps (106 mg) starting from 1-bromo-3-methoxypropane (0.09 mL, 0.79 mmol).

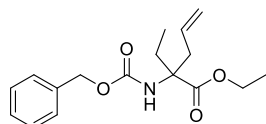
**<sup>1</sup>H NMR** (600 MHz, CDCl<sub>3</sub>) δ ppm 8.65 (bs, 2H), 4.22 (d, *J* = 54.0 Hz, 3H), 3.44 (bs, 2H), 3.33 (s, 3H), 2.17 (bs, 2H), 1.80 (bs, 2H), 1.30 (s, 3H).

**<sup>13</sup>C NMR** (151 MHz, CDCl<sub>3</sub>) δ ppm 169.4, 71.9, 62.8, 58.8, 53.2, 27.8, 25.4, 14.3.

**HR-MS** (ESI) *m/z* [M+H]<sup>+</sup> calcd. for C<sub>8</sub>H<sub>17</sub>NO<sub>3</sub>: 176.1281, found 176.1281.

## Synthesis of chiral amino ester building blocks

### *Ethyl 2-(((benzyloxy)carbonyl)amino)-2-ethylpent-4-enoate (2.137)*



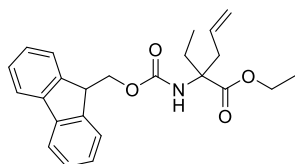
Ethyl 2-amino-2-ethylpent-4-enoate hydrochloride **2.78** (100 mg, 0.48 mmol) and benzyl chloroformate (0.5 mL, 3.38 mmol) were stirred in water (1.5 mL) at 0 °C. Subsequently sodium bicarbonate (0.41 g, 4.89 mmol) dissolved in water (3.5 mL) was dropwise added to the reaction mixture. The reaction was stirred for additional 30 min at 0 °C and then 36 h at room temperature. After this time, ethyl acetate (15 mL) was added to quench the reaction. The aqueous layer was extracted with ethyl acetate (3x). The combined organic layers were dried over MgSO<sub>4</sub>, filtered and concentrated under reduced pressure. The crude product was purified by column chromatography (Silica gel, 25 g, cHex:EtOAc, 10 to 50% EtOAc) to give (±)-**2.137** (116 mg, 79%) as a colorless oil.

<sup>1</sup>H NMR (CDCl<sub>3</sub>, 300 MHz) δ ppm 7.31 – 7.27 (m, 2H), 7.25 – 7.16 (m, 2H), 5.77 – 5.66 (m, 1H), 5.61 – 5.42 (m, 1H), 5.10 – 4.89 (m, 4H), 4.13 (q, *J* = 7.1 Hz, 2H), 3.00 (dd, *J* = 14.1, 7.3 Hz, 1H), 2.42 (ddt, *J* = 14.0, 7.4, 1.1 Hz, 1H), 2.26 (dq, *J* = 14.7, 7.5 Hz, 1H), 1.81 – 1.65 (m, 1H), 1.19 (t, *J* = 7.1 Hz, 3H), 0.69 (t, *J* = 7.4 Hz, 3H).

<sup>13</sup>C NMR (CDCl<sub>3</sub>, 75 MHz) δ ppm 173.2, 154.2, 136.8, 132.5, 128.6, 128.1, 128.0, 118.9, 66.3, 64.5, 61.9, 39.7, 28.4, 14.4, 8.4.

HR-MS (ESI) *m/z* [M+H]<sup>+</sup> calcd. for C<sub>17</sub>H<sub>25</sub>NO<sub>4</sub> [M+H]<sup>+</sup> 306.1629, found 306.1701.

**Ethyl 2-((((9H-fluoren-9-yl)methoxy)carbonyl)amino)-2-ethylpent-4-enoate (2.138)**



Ethyl 2-amino-2-ethylpent-4-enoate hydrochloride **2.78** (700 mg, 4.09 mmol) was dissolved in sodium carbonate aq. sol. (1 M, 20 mL) and cooled to 0 °C. 9H-Fluoren-9-ylmethyl chloroformate (Fmoc-Cl, 1.1 g, 4.09 mmol) in 1,4-dioxane (20 mL) was added at 0 °C. The reaction mixture was stirred for 3 h at room temperature, poured onto water (30 mL) and extracted with ethyl acetate (3x 50 mL). The combined organic layers were dried over MgSO<sub>4</sub> and concentrated under reduced pressure. The crude material was purified by column chromatography (Silica gel, 80 g, cHex:EtOAc, 10 to 50% EtOAc) to give (±)-**2.138** (1.1 g, 70%) as a colorless oil.

**<sup>1</sup>H NMR** (300 MHz, CDCl<sub>3</sub>) δ ppm 7.77 (dt, *J* = 7.5, 0.9 Hz, 2 H), 7.61 (d, *J* = 7.4 Hz, 2 H), 7.41 (td, *J* = 7.5, 1.4 Hz, 2 H), 7.32 (td, *J* = 7.5, 1.2 Hz, 2 H), 5.85 (s, 1 H), 5.52 – 5.70 (m, 1 H), 5.12 – 5.01 (m, 2 H), 4.47 – 4.17 (m, 5 H), 3.12 (dd, *J* = 14.0, 7.2 Hz, 1 H), 2.52 (dd, *J* = 14.0, 7.5 Hz, 1 H), 2.37 (dq, *J* = 14.6, 7.4 Hz, 1 H), 1.82 (dq, *J* = 14.6, 7.3 Hz, 1 H), 1.31 (t, *J* = 7.1 Hz, 3 H), 0.79 (t, *J* = 7.4 Hz, 3 H).

**<sup>13</sup>C NMR** (75 MHz, CDCl<sub>3</sub>) δ ppm 173.4, 154.1, 144.1, 144.0, 141.4, 132.5, 127.8, 127.8, 127.2, 125.2, 125.2, 120.1, 119.0, 77.2, 66.3, 64.5, 62.0, 47.4, 39.7, 28.4, 14.4, 8.4.

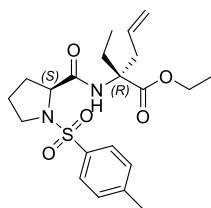
**HR-MS** (ESI) *m/z* [M+H]<sup>+</sup> calcd. for C<sub>24</sub>H<sub>27</sub>NO<sub>4</sub>: 394.1941, found 394.2016.

The chiral separation of **2.138** was performed by KENNETH ATZ at Hoffmann La-Roche, Basel.

The racemic mixture was separated into the two enantiomers by reversed-phase chiral HPLC (Nucleosil-Si, 40 g, nHep:EtOAc, 0 to 100% EtOAc).

[α]<sub>D</sub><sup>20</sup> = –3.16° for (*S*)-**2.138** and [α]<sub>D</sub><sup>20</sup> = +4.63° for (*R*)-**2.138** (*c* = 1.0, MeOH).

***Ethyl (S)-2-ethyl-2-((R)-1-tosylpyrrolidine-2-carboxamido)pent-4-enoate (2.139)***



This synthesis procedure was performed by BENJAMIN BRENNER at FMP, Berlin.

To a stirring solution of (R)-**2.138** (199 mg, 0.51 mmol) in dichloromethane (10 mL) at room temperature piperidine (250  $\mu$ L, 2.53 mmol) was added. After 4 h stirring, the reaction mixture was concentrated under reduced pressure to give the corresponding free amine as colorless oil, which was used crude for the next reaction.

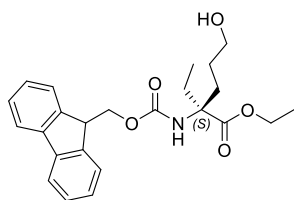
*N*-Toluenesulfonyl-(*S*)-proline (53 mg, 0.20 mmol) was dissolved in acetonitrile (5 mL). *N,N*-diisopropylethylamine (70  $\mu$ L, 0.40 mmol) and HATU (76 mg, 0.20 mmol) were subsequently added, and the solution was stirred for 10 min at room temperature. The crude amine (ethyl (R)-2-amino-2-ethylpent-4-enoate, 34 mg, 0.20 mmol) was then added and the reaction was stirred at room temperature for 12 h. The solvents were evaporated under reduced pressure and the crude material was purified by column chromatography (Silica gel, 4 g, cHex:EtOAc 20 to 30% EtOAc) to provide 42 mg of **2.139** (50%) as colorless oil.

**<sup>1</sup>H NMR** (300 MHz, CDCl<sub>3</sub>)  $\delta$  ppm 7.79 – 7.69 (m, 2 H), 7.65 (s, 1 H), 7.38 – 7.27 (m, 2 H), 5.83 – 5.64 (m, 1 H), 5.13 – 5.08 (m, 1 H), 5.08 – 5.02 (m, 1 H), 4.22 (qd,  $J = 7.1, 1.6$  Hz, 2 H), 4.07 – 4.02 (m, 1 H), 3.59 – 3.49 (m, 1 H), 3.23 – 3.13 (m, 1 H), 3.15 – 3.05 (m, 1 H), 2.50 (dd,  $J = 13.9, 8.2$  Hz, 1 H), 2.43 (s, 3 H), 2.42 – 2.31 (m, 1 H), 2.13 – 2.05 (m, 1 H), 1.91 (dt,  $J = 14.1, 7.3$  Hz, 1 H), 1.86 – 1.54 (m, 3 H, 3-H), 1.28 (t,  $J = 7.1$  Hz, 3 H), 0.76 (t,  $J = 7.4$  Hz, 3 H).

**<sup>13</sup>C NMR** (75 MHz, CDCl<sub>3</sub>)  $\delta$  ppm 172.9, 170.3, 144.3, 133.3, 132.6, 130.0, 128.0, 118.9, 64.8, 62.9, 61.8, 49.8, 39.5, 30.4, 27.7, 24.6, 21.7, 14.4, 8.4.

**HR-MS** (ESI)  $m/z$  [M+H]<sup>+</sup> calcd. for C<sub>21</sub>H<sub>31</sub>N<sub>2</sub>O<sub>5</sub>S: 423.1948, found: 423.1950.

**Ethyl 2-((((9H-fluoren-9-yl)methoxy)carbonyl)amino)-2-ethyl-5-hydroxypentanoate (SI-10)**



(*S*)-**2.138** (484 mg, 1.23 mmol) was dissolved in tetrahydrofuran (20 mL) and 9-Borabicyclo[3.3.1]nonane (9-BBN, 0.5 M in THF, 6 mL, 3 mmol) was added. The reaction was stirred for 20 h at room temperature, then sodium hydroxide aq. sol. (2 M, 5.5 mL, 11.1 mmol) and hydrogen peroxide aq. sol. (35%, 4.3 mL, 44.3 mmol) were added and the reaction was stirred for further 45 min. Water (10 mL) was added and the mixture was extracted with ethyl acetate (2x). The combined organic layers were washed with brine (1x), dried over MgSO<sub>4</sub>, filtered, and concentrated under reduced pressure. Purification of the crude by column chromatography (Silica gel, 40 g, cHex:EtOAc, 10 to 50% EtOAc) yielded **SI-10** (379 mg, 75% yield) as colorless oil.

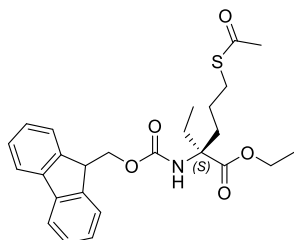
**<sup>1</sup>H NMR** (600 MHz, DMSO-*d*<sub>6</sub>) δ ppm 7.89 (d, *J* = 7.6 Hz, 2 H), 7.71 (br d, *J* = 7.4 Hz, 2 H), 7.45 – 7.37 (m, 3 H), 7.35 – 7.29 (m, 2 H), 4.26 (br d, *J* = 7.2 Hz, 2 H), 4.23 – 4.17 (m, 1 H), 4.05 (q, *J* = 7.0 Hz, 2 H), 3.34 (br t, *J* = 6.0 Hz, 5 H), 1.77 – 1.70 (m, 1 H), 1.88 – 1.66 (m, 3 H), 1.29 – 1.21 (m, 1 H), 1.30 – 1.20 (m, 1 H), 1.12 (t, *J* = 7.1 Hz, 3 H), 0.71 (br t, *J* = 7.4 Hz, 3 H).

**<sup>13</sup>C NMR** (151 MHz, DMSO-*d*<sub>6</sub>) δ ppm 173.0, 154.4, 143.8, 140.7, 127.6, 127.0, 125.2, 120.1, 65.2, 60.8, 60.2, 46.7, 29.4, 26.5, 26.0, 14.8, 7.5.

**HR-MS** (ESI) *m/z* [M+H]<sup>+</sup> calcd. for C<sub>24</sub>H<sub>29</sub>NO<sub>5</sub>: 412.2046, found 412.2119.

The procedure above was applied for the synthesis of (*R*)-**SI-10**, which was performed by BENJAMIN BRENNECKE at FMP, Berlin.

**Ethyl 2-((((9H-fluoren-9-yl)methoxy)carbonyl)amino)-5-(acetylthio)-2-ethylpentanoate (SI-11)**



Triphenylphosphine (546 mg, 2.08 mmol) was dissolved in tetrahydrofuran (6 mL), the solution was cooled to 0° C and diisopropyl azodicarboxylate (409  $\mu$ L, 2.08 mmol) was added dropwise. After 10 min the Mitsunobu betaine formed as a precipitate and (S)-SI-10 (428 mg, 1.04 mmol) and thioacetic acid (149  $\mu$ L, 2.08 mmol) dissolved in tetrahydrofuran (6 mL) were added. The mixture was stirred for 45 min at 0 °C, then the cooling was removed and the reaction was stirred for 1 additional hour. The solvent was evaporated under reduced pressure and the residue was purified by column chromatography (Silica gel, 40 g, cHex:EtOAc, 0 to 20% EtOAc) to obtain the title product (S)-SI-11 (380 mg, 78% yield) as colorless oil.

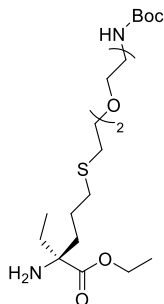
**<sup>1</sup>H NMR** (600 MHz, CDCl<sub>3</sub>)  $\delta$  ppm 7.77 (d,  $J$  = 7.5 Hz, 2H), 7.60 (d,  $J$  = 7.5 Hz, 2H), 7.42 – 7.38 (m, 2H), 7.34 – 7.30 (m, 2H), 5.83 (s, 1H), 4.43 – 4.34 (m, 2H), 4.24 (dq,  $J$  = 19.1, 6.3 Hz, 3H), 2.85 – 2.76 (m, 2H), 2.42 – 2.31 (m, 2H), 2.28 (s, 3H), 1.79 – 1.73 (m, 1H), 1.33 – 1.25 (m, 5H), 0.74 (t,  $J$  = 7.4 Hz, 3H).

**<sup>13</sup>C NMR** (151 MHz, CDCl<sub>3</sub>)  $\delta$  ppm 195.7, 173.7, 168.8, 154.0, 144.1, 141.5, 127.8, 127.2, 125.2, 120.1, 72.5, 66.3, 64.5, 62.1, 47.5, 34.6, 30.7, 29.0, 28.7, 27.1, 25.1, 24.6, 21.7, 14.4, 8.4.

**HR-MS** (ESI)  $m/z$  [M+H]<sup>+</sup> calcd. for C<sub>26</sub>H<sub>31</sub>NO<sub>5</sub>S: 470.1923, found 470.1996.

The procedure above was applied for the synthesis of (R)-SI-11, which was performed by BENJAMIN BRENNECKE at FMP, Berlin.

***Ethyl 18-amino-18-ethyl-2,2-dimethyl-4-oxo-3,8,11-trioxa-14-thia-5-azanonadecan-19-oate***  
**(2.140)**



The synthesis of both enantiomers of **2.140** was performed by BENJAMIN BRENNECKE at FMP, Berlin.

(*S*)-**SI-11** (100 mg, 0.21 mmol) and PEG2 linker 2,2-dimethyl-4-oxo-3,8,11-trioxa-5-azatriodecan-13-yl 4-methylbenzenesulfonate **2.125** (155 mg, 0.38 mmol) were dissolved in absolute ethanol (8 mL) and the solution was deoxygenated by a stream of argon. After, the reaction mixture was cooled to  $-25\text{ }^{\circ}\text{C}$  and potassium iodide (11 mg, 64  $\mu\text{mol}$ ) and sodium ethanolate (44 mg, 0.64 mmol) were added. The solution was slowly allowed to warm up to room temperature and stirred for 2 h at the same temperature. Water (8 mL) was added and the aqueous phase was extracted with ethyl acetate (3x). The combined organic layers were dried over  $\text{MgSO}_4$ , filtered, and concentrated under reduced pressure. The crude material was purified by column chromatography (Silica gel, 10 g, DCM:MeOH, 3 to 5% MeOH,  $\text{KMnO}_4$  stain) to yield the title product (*S*)-**2.140** (41 mg, 44%) as colorless oil.

**$^1\text{H NMR}$**  (600 MHz,  $\text{DMSO}-d_6$ )  $\delta$  ppm 6.74 (m, 1 H), 4.09 (q,  $J = 7.1$ , 2 H), 3.55 – 3.45 (m, 6 H), 3.37 (t,  $J = 6.1$  Hz, 2 H), 3.07 – 3.03 (m, 2 H), 2.62 – 2.61 (m, 2 H), 2.49 – 2.44 (m, 2 H), 1.71 – 1.41 (m, 5 H), 1.37 (s, 9 H), 1.35 - 1.22 (m, 1 H), 1.18 (t,  $J = 7.1$  Hz, 3 H), 0.77 (t,  $J = 7.5$  Hz, 3 H).

**$^{13}\text{C NMR}$**  (151 MHz,  $\text{DMSO}-d_6$ )  $\delta$  ppm 175.8, 155.6, 77.6, 70.2, 69.5, 69.1, 60.7, 60.2, 39.8, 38.2, 32.3, 31.7, 30.4, 28.2, 23.8, 14.2, 8.1.

**HR-MS** (ESI)  $m/z$   $[\text{M}+\text{H}]^+$  calcd. for  $\text{C}_{20}\text{H}_{41}\text{N}_2\text{O}_6\text{S}$ : 437.2680, found: 437.2690.

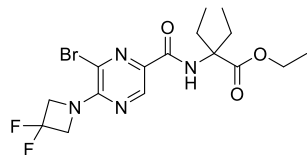
$[\alpha]_d^{20} = -1.08^{\circ}$  ( $c = 1.0$ , MeOH).

The same procedure was applied for the synthesis of (*R*)-**2.140**,  $[\alpha]_d^{20} = +1.90^{\circ}$  ( $c = 1.0$ , MeOH).



### 5.2.6. Synthesis of Pyrazine-based NBD-Labeled Probes

#### *Ethyl 2-(6-bromo-5-(3,3-difluoroazetidin-1-yl)pyrazine-2-carboxamido)-2-ethylbutanoate (2.60)*

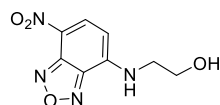


To a solution of 6-Bromo-5-(3,3-difluoro-azetidin-1-yl)-pyrazine-2-carboxylic acid **2.41** (300 mg, 1.02 mmol) in dichloromethane (10 mL) at room temperature were added *N,N*-diisopropylethylamine (0.82 mL, 4.76 mmol) and DMTMM (207.5 mg, 0.75 mmol). The mixture was stirred for 1 h at room temperature before ethyl 2-amino-2-ethylbutanoate hydrochloride **2.61** (133.1 mg, 0.68 mmol) in dichloromethane (2 mL) was added. The mixture was stirred at room temperature for 40 h. Afterwards, the reaction was diluted with dichloromethane (8 mL) and washed with hydrochloric acid aq. sol. (0.2 M, 3x) and brine (1x). The organic layer was dried over  $\text{MgSO}_4$ , and concentrated under reduced pressure. Purification by column chromatography (Silica gel, 25 g, cHex:EtOAc, 25% EtOAc) afforded 272 mg (61%) of compound **2.60** as a white solid.

$^1\text{H NMR}$  (300 MHz,  $\text{CDCl}_3$ )  $\delta$  ppm 8.78 (s, 1H), 8.29 (s, 1H), 4.70 (t,  $J = 12.0$  Hz, 4H), 4.29 (q,  $J = 7.1$  Hz, 2H), 2.55 (dq,  $J = 14.8, 7.5$  Hz, 2H), 1.90 (dq,  $J = 14.5, 7.4$  Hz, 2H), 1.32 (t,  $J = 7.1$  Hz, 3H), 0.77 (t,  $J = 7.4$  Hz, 6H).

The analytical data are in accordance with those reported in the literature.<sup>[170]</sup>

#### *2-((7-Nitrobenzo[*c*][1,2,5]oxadiazol-4-yl)amino)ethan-1-ol (SI-12)*

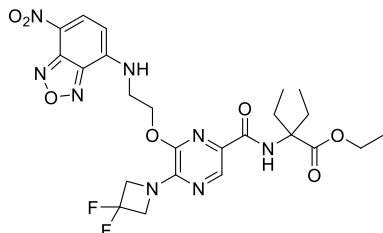


To a solution of ethanolamine (36  $\mu\text{L}$ , 0.60 mmol) and cesium carbonate (353 mg, 1.00 mmol) in dimethylformamide (5 mL) at room temperature 7-chloro-4-nitrobenzofurazan (NBD-Cl, 100 mg, 0.50 mmol) was added. The reaction mixture was stirred at room temperature for 20 h, and concentrated under reduced pressure. The residue was diluted in a mixture of acetonitrile and water (1:1) and purified by reversed-phase preparative HPLC (C-18, Water:ACN with 0.1% TFA, 30 to 90% ACN). The fractions containing the product were combined and lyophilized to afford 60 mg (54%) of compound **SI-12** as an orange solid.

**<sup>1</sup>H NMR** (300 MHz, DMSO-*d*<sub>6</sub>) δ ppm 9.44 (s, 1H), 8.50 (d, *J* = 8.9 Hz, 1H), 6.45 (d, *J* = 9.0 Hz, 1H), 4.95 (t, *J* = 5.0 Hz, 1H), 3.69 (q, *J* = 5.5 Hz, 2H), 3.55 (bs, 2H).

The analytical data are in accordance with those reported in the literature.<sup>[299]</sup>

***Ethyl 2-(5-(3,3-difluoroazetidin-1-yl)-6-(2-((7-nitrobenzo[*c*][1,2,5]oxadiazol-4-yl)amino) ethoxy)pyrazine-2-carboxamido)-2-ethylbutanoate (2.47)***



To a solution of **SI-12** (31 mg, 0.14 mmol) in dimethyl sulfoxide (1 mL) was added potassium hydroxide (8 mg, 0.14 mmol) at room temperature. After 30 min, a solution of **2.60** (50 mg, 0.12 mmol) in dimethyl sulfoxide (1 mL) was added to the mixture. The reaction was stirred at room temperature for additional 20 h, and quenched with water (3 mL). The reaction mixture was concentrated under reduced pressure, taken up in a mixture of acetonitrile and water (1:1) and purified by reversed-phase preparative HPLC (C-18, Water:ACN with 0.1% TFA, 30 to 90% ACN). The fractions containing product were combined and lyophilized to yield compound **2.47** as an orange solid in 29% yield (20 mg).

**<sup>1</sup>H NMR** (300 MHz, DMSO-*d*<sub>6</sub>) δ ppm 9.58 (t, *J* = 5.8 Hz, 1H), 8.53 (d, *J* = 8.8 Hz, 1H), 8.24 (s, 1H), 8.13 (s, 1H), 6.57 (d, *J* = 8.9 Hz, 1H), 4.73 – 4.54 (m, 6H), 4.19 (q, *J* = 7.1 Hz, 2H), 4.00 (bs, 2H), 2.32 (dq, *J* = 14.6, 7.2 Hz, 2H), 1.80 (dq, *J* = 14.5, 7.3 Hz, 2H), 1.21 (t, *J* = 7.0 Hz, 3H), 0.65 (t, *J* = 7.4 Hz, 6H).

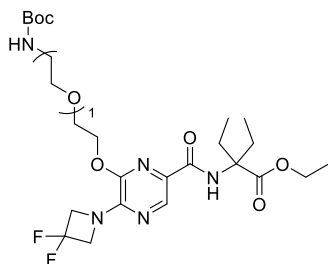
**<sup>13</sup>C NMR** (75 MHz, DMSO-*d*<sub>6</sub>) δ ppm 173.1, 161.7, 158.6, 158.1, 147.7, 147.4, 145.0, 137.9, 133.5, 130.5, 117.2, 99.6, 76.6, 64.6, 62.8, 61.4, 42.3, 27.4, 14.1, 8.2.

**HR-MS** (ESI) *m/z* [M+H]<sup>+</sup> calcd. for C<sub>24</sub>H<sub>28</sub>F<sub>2</sub>N<sub>8</sub>O<sub>7</sub>: 579.2122, found 579.2132.

### **General procedure for PEG linker attachment on pyrazine probe precursor 2.60**

To a solution of *N*-Boc PEG1-5 or hydroxyhexyl linker (1.2 equiv.) in dimethyl sulfoxide (2.5 mL) was added potassium hydroxide (2.0 equiv.) at room temperature. After 30 min, a solution of **2.60** (1.0 equiv.) in dimethyl sulfoxide (1 mL) was added to the mixture. The reaction was stirred at room temperature for additional 20 h, after which time water (3 mL) was added. The reaction mixture was concentrated under reduced pressure and purified by column chromatography (Silica gel, 4 g, cHex:EtOAc, 20 to 50% EtOAc).

### ***Ethyl 2-(6-(2-(2-((tert-butoxycarbonyl)amino)ethoxy)ethoxy)-5-(3,3-difluoroazetidin-1-yl)pyrazine-2-carboxamido)-2-ethylbutanoate (2.67)***



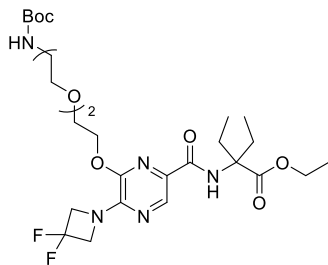
Following the general procedure above, **2.67** was obtained in 30% yield (39 mg) as a light yellow solid starting from linker *tert*-butyl (2-(2-hydroxyethoxy)ethyl)carbamate (58 mg, 0.28 mmol).

**<sup>1</sup>H NMR** (300 MHz, DMSO-*d*<sub>6</sub>) δ ppm 8.24 (s, 1H), 8.22 (s, 1H), 6.78 (bs, 1H), 4.62 (t, *J* = 12.5 Hz, 4H), 4.46 (dd, *J* = 5.8, 3.4 Hz, 2H), 4.22 (q, *J* = 7.1 Hz, 2H), 3.89 – 3.74 (m, 2H), 3.48 (t, *J* = 5.9 Hz, 2H), 3.09 (q, *J* = 5.8 Hz, 2H), 2.34 (dq, *J* = 14.8, 7.4 Hz, 2H), 1.83 (dq, *J* = 14.4, 7.3 Hz, 2H), 1.35 (s, 9H), 1.22 (t, *J* = 7.1 Hz, 3H), 0.70 (t, *J* = 7.4 Hz, 6H).

**<sup>13</sup>C NMR** (75 MHz, DMSO-*d*<sub>6</sub>) δ ppm 173.1, 161.8, 156.6, 148.8, 147.5, 133.3, 130.7, 117.1, 77.6, 69.1, 67.9, 65.5, 64.6, 62.8, 61.5, 28.2, 27.4, 26.4, 14.1, 8.2.

**HR-MS** (ESI) *m/z* [M+Na]<sup>+</sup> calcd. for C<sub>25</sub>H<sub>39</sub>F<sub>2</sub>N<sub>5</sub>O<sub>7</sub>: 582.2710, found 582.2723.

***Ethyl 2-(5-(3,3-difluoroazetidin-1-yl)-6-((2,2-dimethyl-4-oxo-3,8,11-trioxa-5-azatridecan-13-yl)oxy)pyrazine-2-carboxamido)-2-ethylbutanoate (2.68)***



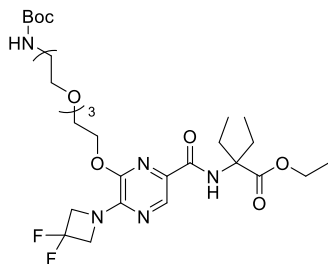
Following the general procedure above, **2.68** was obtained in 26% yield (36 mg) as a light yellow solid starting from linker *tert*-butyl (2-(2-(2-hydroxyethoxy)ethoxy)ethyl)carbamate (70 mg, 0.28 mmol).

**<sup>1</sup>H NMR** (300 MHz, DMSO-*d*<sub>6</sub>) δ ppm 8.24 (s, 1H), 8.22 (s, 1H), 6.73 (bs, 1H), 4.62 (t, *J* = 12.5 Hz, 4H), 4.52 – 4.41 (m, 2H), 4.22 (q, *J* = 7.1 Hz, 2H), 3.89 – 3.78 (m, 2H), 3.60 (dd, *J* = 6.1, 3.4 Hz, 2H), 3.52 (dd, *J* = 6.0, 3.4 Hz, 2H), 3.39 – 3.37 (m, 2H), 3.05 (q, *J* = 6.0 Hz, 2H), 2.34 (dq, *J* = 14.9, 7.5 Hz, 2H), 1.83 (dq, *J* = 14.4, 7.2 Hz, 2H), 1.34 (s, 9H), 1.22 (t, *J* = 7.1 Hz, 3H), 0.70 (t, *J* = 7.4 Hz, 6H).

**<sup>13</sup>C NMR** (75 MHz, DMSO-*d*<sub>6</sub>) δ ppm 173.1, 161.8, 155.6, 147.5, 133.3, 130.7, 77.6, 76.6, 69.7, 69.5, 69.2, 65.3, 64.6, 62.9, 61.5, 28.2, 27.4, 14.1, 8.2.

**HR-MS** (ESI) *m/z* [M+Na]<sup>+</sup> calcd. for C<sub>27</sub>H<sub>43</sub>F<sub>2</sub>N<sub>5</sub>O<sub>8</sub>: 626.2972, found 626.2985.

***Ethyl 2-(5-(3,3-difluoroazetidin-1-yl)-6-((2,2-dimethyl-4-oxo-3,8,11,14-tetraoxa-5-azahexadecan-16-yl)oxy)pyrazine-2-carboxamido)-2-ethylbutanoate (2.69)***



Following the general procedure above, **2.69** was obtained in 22% yield (49 mg) as a light yellow solid starting from linker *tert*-butyl (2-(2-(2-(2-hydroxyethoxy)ethoxy)ethoxy)ethyl) carbamate (121 mg, 0.41 mmol).

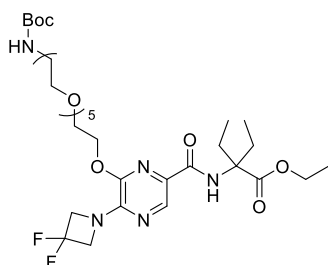
**<sup>1</sup>H NMR** (300 MHz, DMSO-*d*<sub>6</sub>) δ ppm 8.24 (s, 1H), 8.22 (s, 1H), 6.74 (bs, 1H), 4.62 (t, *J* = 12.6 Hz, 4H), 4.51 – 4.45 (m, 2H), 4.22 (q, *J* = 7.0 Hz, 2H), 3.86 – 3.78 (m, 2H), 3.64 – 3.44 (m, 9H), 3.36 (d, *J*

= 6.1 Hz, 2H), 3.04 (q,  $J = 6.0$  Hz, 2H), 2.34 (dq,  $J = 14.9, 7.5$  Hz, 2H), 1.83 (dq,  $J = 14.4, 7.1$  Hz, 2H), 1.35 (s, 9H), 1.22 (t,  $J = 7.1$  Hz, 4H), 0.70 (t,  $J = 7.3$  Hz, 7H).

$^{13}\text{C NMR}$  (75 MHz, DMSO- $d_6$ )  $\delta$  ppm 173.1, 161.8, 155.6, 147.5, 133.3, 130.7, 77.6, 76.5, 69.8, 69.7, 69.4, 69.2, 68.1, 65.3, 64.6, 61.4, 28.2, 27.4, 14.1, 8.2.

**HR-MS** (ESI)  $m/z$   $[\text{M}+\text{Na}]^+$  calcd. for  $\text{C}_{29}\text{H}_{47}\text{F}_2\text{N}_5\text{O}_9$ : 670.3234, found 670.3252.

***Ethyl 2-(5-(3,3-difluoroazetidin-1-yl)-6-((2,2-dimethyl-4-oxo-3,8,11,14,17,20-hexaoxa-5-azadocosan-22-yl)oxy)pyrazine-2-carboxamido)-2-ethylbutanoate (2.71)***



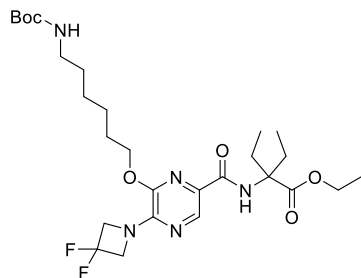
Following the general procedure above, **2.71** was obtained in 15% yield (51 mg) as a light yellow solid starting from linker *tert*-butyl (17-hydroxy-3,6,9,12,15-pentaoxaheptadecyl) carbamate (210 mg, 0.55 mmol).

$^1\text{H NMR}$  (300 MHz, DMSO- $d_6$ )  $\delta$  ppm 8.24 (s, 1H), 8.22 (s, 1H), 6.74 (bs, 1H), 4.62 (t,  $J = 12.5$  Hz, 4H), 4.48 (dd,  $J = 5.8, 3.6$  Hz, 2H), 4.22 (q,  $J = 7.1$  Hz, 2H), 3.83 (dd,  $J = 5.7, 3.6$  Hz, 2H), 3.64 – 3.43 (m, 17H), 3.40 – 3.30 (m, 3H), 3.04 (q,  $J = 6.0$  Hz, 2H), 2.34 (dq,  $J = 14.9, 7.5$  Hz, 2H), 1.83 (dq,  $J = 14.4, 7.3$  Hz, 2H), 1.36 (s, 9H), 1.22 (t,  $J = 7.1$  Hz, 3H), 0.70 (t,  $J = 7.4$  Hz, 6H).

$^{13}\text{C NMR}$  (75 MHz, DMSO- $d_6$ )  $\delta$  ppm 173.1, 161.8, 155.6, 147.8, 147.5, 133.3, 130.7, 78.0, 69.8, 69.8, 69.8, 69.5, 69.1, 68.1, 65.3, 64.6, 62.8, 61.4, 28.2, 27.4, 14.1, 8.2.

**HR-MS** (ESI)  $m/z$   $[\text{M}+\text{Na}]^+$  calcd. for  $\text{C}_{33}\text{H}_{55}\text{F}_2\text{N}_5\text{O}_{11}$ : 758.3758, found 758.3768.

***Ethyl 2-(6-(((tert-butoxycarbonyl)amino)hexyl)oxy)-5-(3,3-difluoroazetidin-1-yl)pyrazine-2-carboxamido)-2-ethylbutanoate (2.72)***



Following the general procedure above, **2.72** was obtained in 11% yield (14 mg) as light yellow solid starting from linker *tert*-butyl (6-hydroxyhexyl)carbamate (100 mg, 0.23 mmol).

**<sup>1</sup>H NMR** (300 MHz, CDCl<sub>3</sub>) δ ppm 8.43 (s, 1H), 8.40 (s, 1H), 4.58 (t, *J* = 12.1 Hz, 4H), 4.41 (t, *J* = 6.3 Hz, 2H), 4.28 (q, *J* = 7.1 Hz, 2H), 3.13 (q, *J* = 6.5 Hz, 2H), 2.62 (dq, *J* = 14.8, 7.4 Hz, 2H), 1.93 – 1.80 (m, 4H), 1.66 (bs, 1H), 1.56 – 1.38 (m, 16H), 1.32 (t, *J* = 7.1 Hz, 3H), 0.76 (t, *J* = 7.4 Hz, 6H).

**<sup>13</sup>C NMR** (75 MHz, CDCl<sub>3</sub>) δ ppm 174.3, 162.8, 156.1, 147.8, 147.1, 147.0, 134.1, 131.7, 120.1, 116.5, 112.9, 79.2, 66.7, 66.4, 63.7, 63.4, 63.0, 61.8, 40.6, 30.2, 28.8, 28.6, 28.5, 26.6, 26.1, 14.4, 8.8.

**HR-MS** (ESI) *m/z* [M+H]<sup>+</sup> calcd. for C<sub>27</sub>H<sub>43</sub>F<sub>2</sub>N<sub>5</sub>O<sub>6</sub>: 594.3074, found 594.3091.

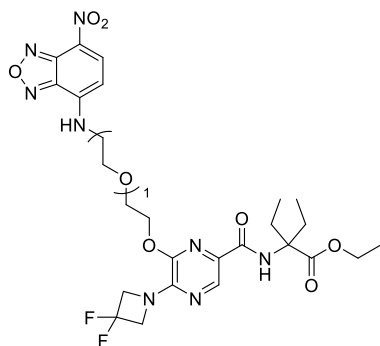
**General Boc-deprotection and NBD-labeling procedure**

Trifluoroacetic acid (0.25 mL) was added dropwise to a stirring solution of the corresponding *N*-Boc-protected compound **2.67** to **2.72** (1.0 equiv.) in dichloromethane (2.25 mL) at 0 °C. The reaction mixture was stirred at room temperature for 2 h. Afterwards, the mixture was concentrated under reduced pressure, and the residue re-suspended in ethyl acetate (5 mL). The solvent was removed under reduced pressure. This process was repeated 3 times to remove trifluoroacetic acid traces. The removal of the *tert*-butyloxycarbonyl group was quantitative as observed by TLC (50% EtOAc in *c*Hex). Free amine intermediates **2.54** to **2.59** were obtained as the corresponding trifluoroacetic acid salts, without the need of further purification steps.

To a solution of amine intermediates **2.54** to **2.59** (1.0 equiv.) and cesium carbonate (5.0 equiv.) in dimethylformamide (2 mL) at room temperature 7-chloro-4-nitrobenzofurazan (NBD-Cl, 1.0 equiv.) was added. The reaction was stirred at room temperature for 24 h. The reaction mixture was concentrated under reduced pressure, and the obtained residue was diluted in a mixture of acetonitrile and water (1:1) and purified by reversed-phase preparative HPLC (C-18, Water:ACN with 0.1% TFA,

30 to 90% ACN). The fractions containing product were combined and lyophilized to yield the desired product.

***Ethyl 2-(5-(3,3-difluoroazetidin-1-yl)-6-(2-(2-((7-nitrobenzo[c][1,2,5]oxadiazol-4-yl)amino)ethoxy)ethoxy)pyrazine-2-carboxamido)-2-ethylbutanoate (2.48)***



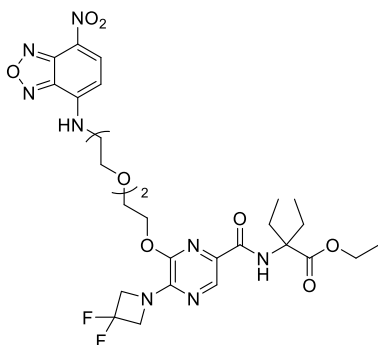
Following the general procedure above, **2.48** was obtained in 17% yield (2 mg) as a dark yellow solid starting from **2.67** (27 mg, 0.05 mmol).

**<sup>1</sup>H NMR** (600 MHz, DMSO-*d*<sub>6</sub>) δ ppm 9.44 (s, 1H), 8.41 (d, *J* = 8.9 Hz, 1H), 8.17 (d, *J* = 2.3 Hz, 2H), 6.46 (d, *J* = 9.0 Hz, 1H), 4.55 – 4.41 (m, 6H), 4.21 (q, *J* = 7.1 Hz, 2H), 3.90 – 3.85 (m, 2H), 3.82 (t, *J* = 5.2 Hz, 2H), 2.34 (dq, *J* = 14.8, 7.4 Hz, 2H), 1.83 (dq, *J* = 14.5, 7.3 Hz, 2H), 1.22 (t, *J* = 7.1 Hz, 3H), 0.70 (t, *J* = 7.4 Hz, 6H).

**<sup>13</sup>C NMR** (151 MHz, DMSO-*d*<sub>6</sub>) δ ppm 173.1, 161.7, 147.4, 147.3, 137.6, 133.2, 130.5, 116.9, 99.4, 65.3, 64.6, 62.6, 61.4, 43.5, 27.4, 14.0, 8.2.

**HR-MS** (ESI) *m/z* [M+H]<sup>+</sup> calcd. for C<sub>26</sub>H<sub>32</sub>F<sub>2</sub>N<sub>8</sub>O<sub>8</sub>: 623.2384, found 623.2395.

*Ethyl 2-(5-(3,3-difluoroazetidin-1-yl)-6-(2-(2-(2-((7-nitrobenzo[c][1,2,5]oxadiazol-4-yl)amino)ethoxy)ethoxy)ethoxy)pyrazine-2-carboxamido)-2-ethylbutanoate (2.49)*



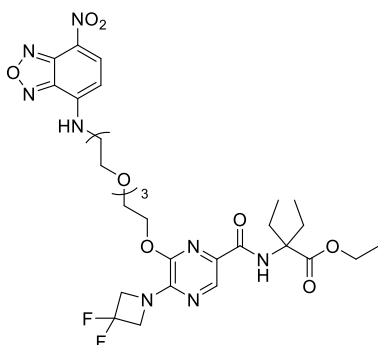
Following the general procedure above, **2.49** was obtained in 26% yield (4 mg) as a dark yellow solid starting from **2.68** (29 mg, 0.05 mmol).

**<sup>1</sup>H NMR** (600 MHz, DMSO-*d*<sub>6</sub>) δ ppm 9.41 (s, 1H), 8.54 – 8.42 (m, 1H), 8.25 – 8.16 (m, 2H), 6.46 (d, *J* = 8.9 Hz, 1H), 4.57 (t, *J* = 12.4 Hz, 4H), 4.46 – 4.41 (m, 2H), 4.22 (q, *J* = 7.1 Hz, 2H), 3.84 – 3.79 (m, 2H), 3.73 (t, *J* = 5.4 Hz, 2H), 3.68 – 3.59 (m, 6H), 2.34 (dt, *J* = 14.9, 7.4 Hz, 2H), 1.84 (dq, *J* = 14.5, 7.3 Hz, 2H), 1.22 (t, *J* = 7.1 Hz, 3H), 0.71 (t, *J* = 7.4 Hz, 6H).

**<sup>13</sup>C NMR** (151 MHz, DMSO-*d*<sub>6</sub>) δ ppm 173.1, 161.7, 147.6, 147.3, 137.8, 133.2, 130.7, 117.1, 99.4, 69.9, 69.6, 68.1, 67.9, 64.6, 62.7, 61.4, 43.3, 27.4, 14.1, 8.2.

**HR-MS** (ESI) *m/z* [M+H]<sup>+</sup> calcd. for C<sub>28</sub>H<sub>36</sub>F<sub>2</sub>N<sub>8</sub>O<sub>9</sub>: 668.2675, found 668.2688.

*Ethyl 2-(5-(3,3-difluoroazetidin-1-yl)-6-(2-(2-(2-(2-((7-nitrobenzo[c][1,2,5]oxadiazol-4-yl)amino)ethoxy)ethoxy)ethoxy)ethoxy)pyrazine-2-carboxamido)-2-ethylbutanoate (2.50)*



Following the general procedure above, **2.50** was obtained in 2% yield (1 mg) as a dark yellow solid starting from **2.69** (39 mg, 0.06 mmol).

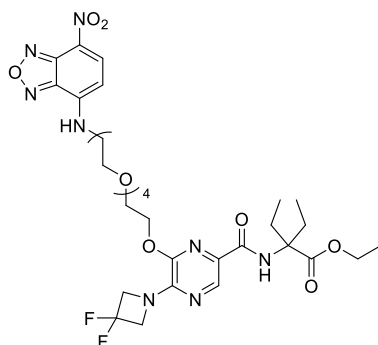


**<sup>1</sup>H NMR** (600 MHz, DMSO-*d*<sub>6</sub>) δ ppm 9.41 (s, 1H), 8.54 – 8.45 (m, 1H), 8.20 (d, *J* = 14.6 Hz, 1H), 6.46 (d, *J* = 9.0 Hz, 1H), 4.58 (t, *J* = 12.4 Hz, 4H), 4.47 – 4.42 (m, 2H), 4.21 (q, *J* = 7.1 Hz, 2H), 3.81 – 3.76 (m, 2H), 3.70 (t, *J* = 5.3 Hz, 2H), 3.64 (s, 2H), 3.57 – 3.53 (m, 4H), 3.53 – 3.48 (m, 5H), 2.33 (dt, *J* = 14.9, 7.4 Hz, 2H), 1.83 (dq, *J* = 14.5, 7.3 Hz, 2H), 1.22 (t, *J* = 7.1 Hz, 3H), 0.69 (t, *J* = 7.4 Hz, 6H).

**<sup>13</sup>C NMR** (151 MHz, DMSO-*d*<sub>6</sub>) δ ppm 173.1, 161.8, 147.7, 147.4, 137.8, 133.2, 130.7, 118.9, 117.1, 115.3, 99.5, 69.8, 69.8, 69.7, 69.7, 68.1, 65.3, 64.6, 62.8, 61.4, 27.4, 14.1, 8.2.

**HR-MS** (ESI) *m/z* [M+H]<sup>+</sup> calcd. for C<sub>30</sub>H<sub>40</sub>F<sub>2</sub>N<sub>8</sub>O<sub>10</sub>: 711.2908, found 711.2919.

***Ethyl 2-(5-(3,3-difluoroazetidin-1-yl)-6-((14-((7-nitrobenzo[*c*][1,2,5]oxadiazol-4-yl)amino)-3,6,9,12-tetraoxatetradecyl)oxy)pyrazine-2-carboxamido)-2-ethylbutanoate (2.51)***



Following the “General procedure for PEG linker attachment on pyrazine probe precursor **2.60**” described on page 160, ethyl 2-(5-(3,3-difluoroazetidin-1-yl)-6-((2,2-dimethyl-4-oxo-3,8,11,14,17-pentaoxa-5-azanonadecan-19-yl)oxy)pyrazine-2-carboxamido)-2-ethylbutanoate (**2.70**) was obtained in 5% yield (17 mg) as a light yellow solid starting from linker *tert*-butyl (14-hydroxy-3,6,9,12-tetraoxatetradecyl)carbamate (186 mg, 0.55 mmol).

**<sup>1</sup>H NMR** (300 MHz, DMSO-*d*<sub>6</sub>) δ ppm 8.24 (s, 1H), 8.22 (s, 1H), 6.74 (bs, 1H), 4.62 (t, *J* = 12.6 Hz, 4H), 4.52 – 4.44 (m, 2H), 4.22 (q, *J* = 7.1 Hz, 2H), 3.82 (dd, *J* = 5.8, 3.6 Hz, 2H), 3.64 – 3.43 (m, 12H), 3.36 (d, *J* = 6.2 Hz, 2H), 3.04 (q, *J* = 6.1 Hz, 2H), 2.34 (dq, *J* = 15.3, 8.0, 7.5 Hz, 2H), 1.83 (dq, *J* = 14.5, 7.2 Hz, 2H), 1.36 (s, 9H), 1.22 (t, *J* = 7.0 Hz, 3H), 0.70 (t, *J* = 7.4 Hz, 6H).

**HR-MS** (ESI) *m/z* [M+Na]<sup>+</sup> calcd. for C<sub>31</sub>H<sub>51</sub>F<sub>2</sub>N<sub>5</sub>O<sub>10</sub>: 714.3496, found 714.3509.

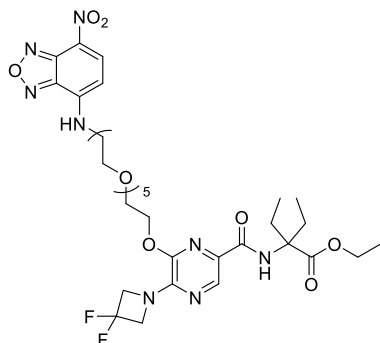
Boc-protected **2.70** (12 mg, 0.02 mmol) was applied as starting material following the general procedure described above to give NBD-labeled **2.51** 20% yield (3 mg) as a dark yellow solid.

**<sup>1</sup>H NMR** (600 MHz, DMSO-*d*<sub>6</sub>) δ ppm 9.44 (s, 1H), 8.50 (d, *J* = 8.9 Hz, 1H), 8.21 (d, *J* = 15.3 Hz, 2H), 6.47 (d, *J* = 9.0 Hz, 1H), 4.60 (t, *J* = 12.4 Hz, 4H), 4.48 – 4.44 (m, 2H), 4.22 (q, *J* = 7.1 Hz, 2H), 3.82 – 3.79 (m, 2H), 3.71 (t, *J* = 5.3 Hz, 2H), 3.65 (s, 2H), 3.58 (dd, *J* = 5.9, 3.5 Hz, 2H), 3.55 (dd, *J* = 5.9, 3.4 Hz, 2H), 3.52 – 3.48 (m, 5H), 2.34 (dq, *J* = 14.8, 7.5 Hz, 2H), 1.84 (dq, *J* = 14.5, 7.4 Hz, 2H), 1.22 (t, *J* = 7.1 Hz, 3H), 0.70 (t, *J* = 7.4 Hz, 6H).

**<sup>13</sup>C NMR** (151 MHz, DMSO-*d*<sub>6</sub>) δ ppm 173.1, 161.8, 147.7, 147.4, 137.8, 133.2, 130.7, 117.1, 99.5, 69.8, 68.8, 69.7, 69.7, 68.1, 68.0, 65.3, 64.6, 62.8, 61.4, 43.4, 27.4, 14.1, 8.2.

**HR-MS** (ESI) *m/z* [M+Na]<sup>+</sup> calcd. for C<sub>32</sub>H<sub>44</sub>F<sub>2</sub>N<sub>8</sub>O<sub>11</sub>: 777.2990, found 777.3020.

***Ethyl 2-(5-(3,3-difluoroazetidin-1-yl)-6-((17-((7-nitrobenzo[*c*][1,2,5]oxadiazol-4-yl)amino)-3,6,9,12,15-pentaoxaheptadecyl)oxy)pyrazine-2-carboxamido)-2-ethylbutanoate (2.52)***



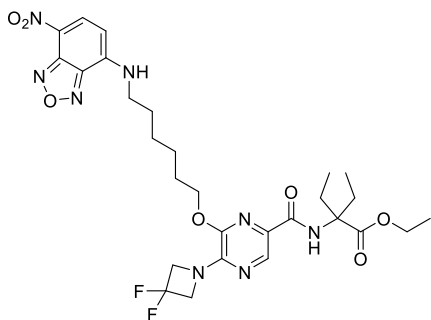
Following the general procedure above, **2.52** was obtained in 42% yield (20 mg) as a dark yellow solid starting from **2.71** (46 mg, 0.06 mmol).

**<sup>1</sup>H NMR** (600 MHz, DMSO-*d*<sub>6</sub>) δ ppm 9.44 (s, 1H), 8.50 (d, *J* = 8.9 Hz, 1H), 8.22 (d, *J* = 15.0 Hz, 1H), 6.48 (d, *J* = 8.9 Hz, 1H), 4.61 (t, *J* = 12.4 Hz, 4H), 4.49 – 4.45 (m, 2H), 4.22 (q, *J* = 7.1 Hz, 2H), 3.86 – 3.80 (m, 2H), 3.74 – 3.41 (m, 20H), 2.34 (dq, *J* = 14.9, 7.5 Hz, 2H), 1.84 (dq, *J* = 14.5, 7.3 Hz, 2H), 1.22 (t, *J* = 7.1 Hz, 3H), 0.70 (t, *J* = 7.4 Hz, 6H).

**<sup>13</sup>C NMR** (151 MHz, DMSO-*d*<sub>6</sub>) δ ppm 173.1, 161.8, 158.4, 158.2, 147.7, 147.4, 137.8, 133.2, 130.7, 118.9, 117.1, 99.5, 69.8, 69.8, 69.8, 69.7, 68.1, 68.0, 65.3, 64.6, 62.8, 61.4, 43.4, 27.4, 14.1, 8.2.

**HR-MS** (ESI) *m/z* [M+Na]<sup>+</sup> calcd. for C<sub>34</sub>H<sub>48</sub>F<sub>2</sub>N<sub>8</sub>O<sub>12</sub>: 821.3252, found 821.3260.

***Ethyl 2-(5-(3,3-difluoroazetidin-1-yl)-6-((6-((7-nitrobenzo[c][1,2,5]oxadiazol-4-yl)amino)hexyl)oxy)-pyrazine-2-carboxamido)-2-ethylbutanoate (2.53)***



Following the general procedure above, **2.53** was obtained in 35% yield (4 mg) as a dark yellow solid starting from **2.72** (10 mg, 0.02 mmol).

**<sup>1</sup>H NMR** (300 MHz, DMSO-*d*<sub>6</sub>) δ ppm 9.54 (t, *J* = 5.8 Hz, 1H), 8.50 (d, *J* = 8.9 Hz, 1H), 8.22 (d, *J* = 5.6 Hz, 1H), 6.41 (d, *J* = 9.0 Hz, 1H), 4.60 (t, *J* = 12.5 Hz, 4H), 4.37 (t, *J* = 6.4 Hz, 2H), 4.20 (q, *J* = 7.1 Hz, 2H), 3.48 (q, *J* = 7.0 Hz, 2H), 2.36 (dq, *J* = 14.7, 7.4 Hz, 2H), 1.81 (dq, *J* = 14.1, 7.2 Hz, 4H), 1.75 – 1.70 (m, 2H), 1.51 – 1.44 (m, 4H), 1.21 (t, *J* = 7.1 Hz, 3H), 0.68 (t, *J* = 7.4 Hz, 6H).

**<sup>13</sup>C NMR** (75 MHz, DMSO-*d*<sub>6</sub>) δ ppm 173.1, 161.8, 147.6, 145.2, 144.4, 144.1, 137.9, 132.9, 130.7, 121.5, 99.0, 66.2, 64.7, 62.8, 61.4, 43.3, 27.9, 27.5, 26.1, 25.3, 14.0, 8.2.

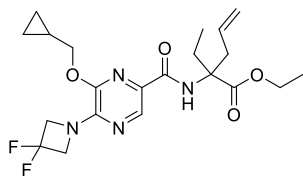
**HR-MS** (ESI) *m/z* [M+H]<sup>+</sup> calcd. for C<sub>28</sub>H<sub>36</sub>F<sub>2</sub>N<sub>8</sub>O<sub>7</sub>: 635.2748, found 635.2759.

## 5.2.7. Synthesis of SAR Compounds

### ***General peptide coupling procedure***

To 1.0 equiv. of 6-(cyclopropylmethoxy)-5-(3,3-difluoroazetidin-1-yl)pyrazine-2-carboxylic acid (**2.37**) or 5-cyclopropyl-6-(4-fluorobenzyl)picolinic acid (**2.42**) in dichloromethane (2 mL) at room temperature were added *N,N*-diisopropylethylamine (5.0 equiv.) and 4-(4,6-Dimethoxy-1,3,5-triazin-2-yl)-4-methylmorpholinium chloride (DMTMM) or Bis(2-oxo-3-oxazolidinyl)phosphinic chloride (BOP-Cl) (1.1 equiv.). The mixture was stirred at room temperature for 1 h before the desired amino ester (1.0 equiv.) in dichloromethane (1 mL) was added. The mixture was stirred at room temperature for 24 h, diluted with dichloromethane (5 mL) and washed with hydrochloric acid aq. sol. (0.2 M, 3x) and brine (1x). The organic layer was dried over MgSO<sub>4</sub> and concentrated under reduced pressure. Purification was performed either by reversed-phase preparative HPLC or MPLC methodologies as described for each example. For reversed-phase preparative HPLC purifications, the crude residues were dissolved in acetonitrile and water (1:1) mixture. Fractions containing the product were combined and either lyophilized (HPLC) or concentrated under reduced pressure (MPLC) to yield the desired non-labeled compound.

### ***Ethyl 2-(6-(cyclopropylmethoxy)-5-(3,3-difluoroazetidin-1-yl)pyrazine-2-carboxamido)-2-ethylpent-4-enoate (2.79)***



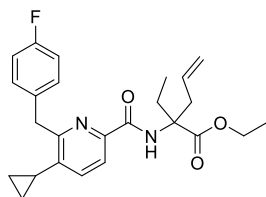
Following the general procedure above, **2.79** was obtained in 72% yield (166 mg) as a light yellow oil starting from pyrazine carboxylic acid **2.37** (150 mg, 0.53 mmol) and ethyl 2-aminopent-4-enoate **2.78** (91 mg, 0.53 mmol). Purification was performed by column chromatography (Silica gel, 4 g, cHex:EtOAc, 30% EtOAc).

**<sup>1</sup>H NMR** (300 MHz, CDCl<sub>3</sub>) δ ppm 8.42 (s, 1H), 8.31 (s, 1H), 5.68 – 5.54 (m, 1H), 5.08 – 4.98 (m, 2H), 4.61 (t, *J* = 12.1 Hz, 4H), 4.25 (t, *J* = 7.3 Hz, 4H), 3.34 (dd, *J* = 13.9, 7.0 Hz, 1H), 2.67 – 2.54 (m, 2H), 1.97 – 1.85 (m, 1H), 1.36 – 1.22 (m, 4H), 0.77 (t, *J* = 7.4 Hz, 3H), 0.69 – 0.62 (m, 2H), 0.43 – 0.37 (m, 2H).

<sup>13</sup>C NMR (75 MHz, CDCl<sub>3</sub>) δ ppm 173.6, 162.0, 147.8, 147.2, 134.2, 132.8, 131.4, 118.7, 116.5, 71.4, 65.4, 63.4 (t, <sup>3</sup>J<sub>CF</sub> = 27.7 Hz), 61.8, 39.7, 28.4, 14.5, 9.9, 8.6, 3.6.

HR-MS (ESI) *m/z* [M+H]<sup>+</sup> calcd. for C<sub>21</sub>H<sub>28</sub>F<sub>2</sub>N<sub>4</sub>O<sub>4</sub>: 439.2112, found 439.2184.

***Ethyl 2-(5-cyclopropyl-6-(4-fluorobenzyl)picolinamido)-2-ethylpent-4-enoate (2.80)***



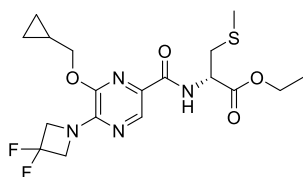
Following the general procedure above, **2.80** was obtained in 56% yield (239 mg) as a light yellow oil starting from picolinic acid **2.42** (300 mg, 1.01 mmol) and ethyl 2-aminopent-4-enoate **2.78** (173 mg, 1.01 mmol). Purification was performed by column chromatography (Silica gel, 4 g, cHex:EtOAc, 10% EtOAc).

<sup>1</sup>H NMR (300 MHz, CDCl<sub>3</sub>) δ ppm 8.95 (s, 1H), 7.92 (d, *J* = 7.9 Hz, 1H), 7.40 (d, *J* = 8.0 Hz, 1H), 7.31 – 7.20 (m, 2H), 6.97 (t, *J* = 8.6 Hz, 2H), 5.72 – 5.58 (m, 1H), 5.16 – 4.96 (m, 2H), 4.43 – 4.22 (m, 4H), 3.30 (dd, *J* = 14.0, 6.9 Hz, 1H), 2.69 – 2.49 (m, 2H), 2.00 – 1.88 (m, 2H), 1.33 (t, *J* = 7.1 Hz, 3H), 1.05 – 0.96 (m, 2H), 0.81 (t, *J* = 7.4 Hz, 3H), 0.83 – 0.65 (m, 2H).

<sup>13</sup>C NMR (75 MHz, CDCl<sub>3</sub>) δ ppm 173.3, 1643.6, 163.2, 160.0, 158.5, 146.9, 139.9, 134.8, 134.8, 134.8, 132.8, 130.6, 130.5, 119.8, 118.6, 115.3, 115.1, 65.0, 61.8, 40.8, 39.4, 28.3, 14.4, 12.8, 8.5, 7.9.

HR-MS (ESI) *m/z* [M+Na]<sup>+</sup> calcd. for C<sub>25</sub>H<sub>29</sub>FN<sub>2</sub>O<sub>3</sub>: 447.2055, found 447.2083.

***Ethyl N-(6-(cyclopropylmethoxy)-5-(3,3-difluoroazetid-1-yl)pyrazine-2-carbonyl)-(S)-methyl-(L)-cysteinate (2.81)***



Following the general procedure above, **2.81** was obtained in 50% yield (39 mg) as a colorless oil starting from pyrazine carboxylic acid **2.37** (51 mg, 0.18 mmol) and ethyl (*S*)-methyl-(*L*)-cysteinate

**2.89** (30 mg, 0.18 mmol). Purification was performed by column chromatography (Silica gel, 4 g, cHex:EtOAc, 30% EtOAc).

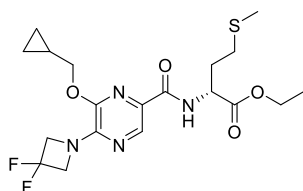
**<sup>1</sup>H NMR** (300 MHz, CDCl<sub>3</sub>) δ ppm 8.41 (s, 1H), 8.13 (d, *J* = 7.9 Hz, 1H), 7.95 (s, 1H), 4.95 (dt, *J* = 7.9, 5.1 Hz, 1H), 4.65 (t, *J* = 12.0 Hz, 4H), 4.36 – 4.14 (m, 4H), 3.17 – 2.97 (m, 2H), 2.12 (s, 3H), 1.31 (t, *J* = 7.1 Hz, 3H), 0.76 – 0.60 (m, 2H), 0.46 – 0.32 (m, 2H).

**<sup>13</sup>C NMR** (75 MHz, CDCl<sub>3</sub>) δ ppm 170.9, 164.2, 148.0, 147.1, 147.1, 147.0, 134.6, 129.9, 119.8, 116.2, 71.9, 63.6 (t, <sup>3</sup>*J*<sub>CF</sub> = 27.8 Hz), 62.1, 51.9, 36.3, 16.4, 14.2, 9.8, 3.6, 3.6.

**HR-MS** (ESI) *m/z* [M+H]<sup>+</sup> calcd. for C<sub>18</sub>H<sub>24</sub>F<sub>2</sub>N<sub>4</sub>O<sub>4</sub>S: 431.1559, found 431.1568.

[α]<sub>d</sub><sup>20</sup> = -0.03° (*c* = 1.0, CHCl<sub>3</sub>).

***Ethyl (6-(cyclopropylmethoxy)-5-(3,3-difluoroazetidin-1-yl)pyrazine-2-carbonyl)-(L)-methioninate (2.82)***



Following the general procedure above, **2.82** was obtained in 53% yield (80 mg) as a colorless oil starting from pyrazine carboxylic acid **2.37** (97 mg, 0.34 mmol) and ethyl (*L*)-methioninate (60 mg, 0.34 mmol). Purification was performed by column chromatography (Silica gel, 4 g, cHex:EtOAc, 30% EtOAc).

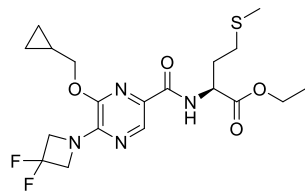
**<sup>1</sup>H NMR** (300 MHz, CDCl<sub>3</sub>) δ ppm 10.63 (s, 1H), 8.40 (s, 1H), 8.13 (d, *J* = 8.1 Hz, 1H), 4.86 (td, *J* = 7.4, 5.0 Hz, 1H), 4.69 (t, *J* = 12.0 Hz, 4H), 4.32 – 4.15 (m, 4H), 2.57 (t, *J* = 6.9 Hz, 2H), 2.36 – 2.12 (m, 2H), 2.10 (s, 3H), 1.31 (t, *J* = 7.1 Hz, 3H), 0.75 – 0.62 (m, 2H), 0.39 (dt, *J* = 6.3, 4.7 Hz, 2H).

**<sup>13</sup>C NMR** (75 MHz, CDCl<sub>3</sub>) δ ppm 171.8, 164.4, 159.3, 158.8, 148.0, 146.8, 146.7, 146.7, 134.1, 129.7, 116.1, 133.2, 112.5, 72.1, 63.8 (t, <sup>3</sup>*J*<sub>CF</sub> = 27.8 Hz), 62.0, 51.9, 31.7, 30.1, 15.6, 14.2, 9.7, 3.6, 3.5.

**HR-MS** (ESI) *m/z* [M+H]<sup>+</sup> calcd. for C<sub>19</sub>H<sub>26</sub>F<sub>2</sub>N<sub>4</sub>O<sub>4</sub>S: 445.1716, found 445.1736.

[α]<sub>d</sub><sup>20</sup> = +0.04° (*c* = 1.0, CHCl<sub>3</sub>).

***Ethyl (6-(cyclopropylmethoxy)-5-(3,3-difluoroazetidin-1-yl)pyrazine-2-carbonyl)-(D)-methioninate (2.83)***



Following the general procedure above, **2.83** was obtained in 85% yield (27 mg) as a colorless oil starting from pyrazine carboxylic acid **2.37** (21 mg, 0.07 mmol) and ethyl (*D*)-methioninate (13 mg, 0.07 mmol). Purification was performed by column chromatography (Silica gel, 4 g, cHex:EtOAc, 30% EtOAc).

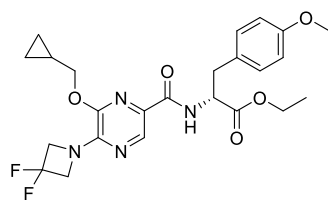
**<sup>1</sup>H NMR** (300 MHz, CDCl<sub>3</sub>) δ ppm 8.43 (s, 1H), 7.99 (d, *J* = 8.1 Hz, 1H), 4.85 (td, *J* = 7.5, 5.0 Hz, 1H), 4.64 (t, *J* = 12.1 Hz, 4H), 4.30 – 4.16 (m, 4H), 2.64 – 2.52 (m, 2H), 2.33 – 2.22 (m, 1H), 2.17 – 2.06 (m, 1H), 2.10 (s, 3H), 1.33 – 1.26 (m, 4H), 0.751 – 0.64 (m, 2H), 0.41 – 0.36 (m, 2H).

**<sup>13</sup>C NMR** (75 MHz, CDCl<sub>3</sub>) δ ppm 172.0, 164.2, 147.9, 147.2, 134.9, 130.3, 120.0, 116.4, 112.8, 71.7, 63.5 (t, <sup>3</sup>*J*<sub>CF</sub> = 27.8 Hz), 61.9, 51.7, 32.1, 30.2, 15.7, 14.3, 9.8, 3.6, 3.6.

**HR-MS** (ESI) *m/z* [M+H]<sup>+</sup> calcd. for C<sub>19</sub>H<sub>26</sub>F<sub>2</sub>N<sub>4</sub>O<sub>4</sub>S: 445.1716, found 445.1689.

[α]<sub>D</sub><sup>20</sup> = -0.09° (*c* = 1.0, CHCl<sub>3</sub>).

***Ethyl (L)-2-(6-(cyclopropylmethoxy)-5-(3,3-difluoroazetidin-1-yl)pyrazine-2-carboxamido)-3-(4-methoxyphenyl)propanoate (2.84)***



Following the general procedure above, **2.84** was obtained in 48% yield (47 mg) as a colorless oil starting from pyrazine carboxylic acid **2.37** (57 mg, 0.20 mmol) and ethyl (*L*)-2-amino-3-(4-methoxyphenyl)propanoate **2.90** (45 mg, 0.20 mmol). Purification was performed by column chromatography (Silica gel, 4 g, cHex:EtOAc, 30% EtOAc).

**<sup>1</sup>H NMR** (300 MHz, CDCl<sub>3</sub>) δ ppm 9.44 (s, 1 H), 8.39 (s, 1H), 7.77 (d, *J* = 8.1 Hz, 1H), 7.05 (d, *J* = 8.5 Hz, 2H), 6.79 (d, *J* = 8.5 Hz, 2H), 4.96 (dt, *J* = 8.2, 5.6 Hz, 1H), 4.67 (t, *J* = 12.0 Hz, 4H), 4.21 (q,

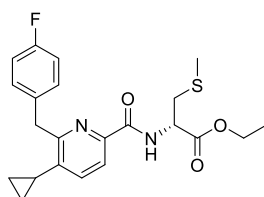
$J = 7.1$  Hz, 2H), 4.06 (qd,  $J = 11.2, 7.3$  Hz, 2H), 3.77 (s, 3H), 3.27 – 3.06 (m, 2H), 1.27 (t,  $J = 7.1$  Hz, 3H), 1.22 – 1.14 (m, 1H), 0.72 – 0.60 (m, 2H), 0.40 – 0.29 (m, 2H).

$^{13}\text{C NMR}$  (75 MHz,  $\text{CDCl}_3$ )  $\delta$  ppm 171.5, 164.1, 158.9, 147.9, 146.9, 146.8, 134.1, 130.5, 129.7, 127.6, 116.1, 114.1, 112.5, 72.0, 63.8 (t,  $^3J_{\text{CF}} = 27.8$  Hz), 61.9, 55.3, 53.2, 37.1, 14.3, 9.7, 3.6, 3.5.

**HR-MS** (ESI)  $m/z$   $[\text{M}+\text{H}]^+$  calcd. for  $\text{C}_{24}\text{H}_{28}\text{F}_2\text{N}_4\text{O}_5$ : 491.2101, found 491.2107.

$[\alpha]_D^{20} = +0.49^\circ$  ( $c = 1.0$ ,  $\text{CHCl}_3$ ).

***Ethyl N-(5-cyclopropyl-6-(4-fluorobenzyl)picolinoyl)-(S)-methyl-(L)-cysteinate (2.85)***



Following the general procedure above, **2.85** was obtained in 36% yield (27 mg) as a colorless oil starting from picolinic acid **2.42** (49 mg, 0.18 mmol) and ethyl (*S*)-methyl-(*L*)-cysteinate **2.89** (30 mg, 0.18 mmol). Purification was performed by column chromatography (Silica gel, 4 g,  $\text{cHex:EtOAc}$ , 10%  $\text{EtOAc}$ ).

$^1\text{H NMR}$  (300 MHz,  $\text{CDCl}_3$ )  $\delta$  ppm 8.70 (d,  $J = 8.2$  Hz, 1H), 7.94 (d,  $J = 7.9$  Hz, 1H), 7.39 (d,  $J = 8.0$  Hz, 1H), 7.22 (dd,  $J = 8.4, 5.4$  Hz, 2H), 6.97 (t,  $J = 8.6$  Hz, 2H), 4.97 (dt,  $J = 8.3, 5.4$  Hz, 1H), 4.36 (s, 2H), 4.26 (q,  $J = 7.1$  Hz, 2H), 3.05 (dd,  $J = 5.3, 2.6$  Hz, 2H), 2.11 (s, 3H), 1.96 – 1.86 (m, 1H), 1.31 (t,  $J = 7.1$  Hz, 3H), 1.09 – 0.91 (m, 2H), 0.67 (t,  $J = 5.2$  Hz, 2H).

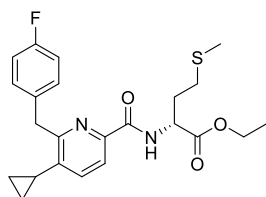
$^{13}\text{C NMR}$  (75 MHz,  $\text{CDCl}_3$ )  $\delta$  ppm 170.7, 164.2, 163.0, 159.8, 158.5, 145.7, 140.3, 134.5, 134.4, 130.4, 130.3, 120.2, 115.2, 114.9, 61.7, 51.9, 40.6, 36.5, 16.2, 14.1, 12.6, 7.8.

**HR-MS** (ESI)  $m/z$   $[\text{M}+\text{Na}]^+$  calcd. for  $\text{C}_{22}\text{H}_{25}\text{FN}_2\text{O}_3\text{S}$ : 439.14621, found 439.1478.

$[\alpha]_D^{20} = -0.04^\circ$  ( $c = 1.0$ ,  $\text{CHCl}_3$ ).



***Ethyl (5-cyclopropyl-6-(4-fluorobenzyl)picolinoyl)-(L)-methioninate (2.86)***



Following the general procedure above, **2.86** was obtained in 48% yield (70 mg) as a colorless oil starting from picolinic acid **2.42** (92 mg, 0.34 mmol) and ethyl (*L*)-methioninate (60 mg, 0.34 mmol). Purification was performed by column chromatography (Silica gel, 4 g, cHex:EtOAc, 10% EtOAc).

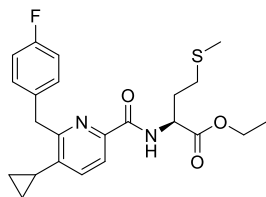
**<sup>1</sup>H NMR** (300 MHz, CDCl<sub>3</sub>) δ ppm 8.56 (d, *J* = 8.4 Hz, 1H), 7.94 (d, *J* = 7.9 Hz, 1H), 7.40 (d, *J* = 8.0 Hz, 1H), 7.21 (dd, *J* = 8.4, 5.4 Hz, 2H), 6.98 (t, *J* = 8.7 Hz, 2H), 4.86 (td, *J* = 7.9, 5.0 Hz, 1H), 4.36 (s, 2H), 4.24 (q, *J* = 7.1 Hz, 2H), 2.55 (t, *J* = 7.6 Hz, 2H), 2.35 – 2.20 (m, 1H), 2.09 (s, 4H), 1.95 – 1.86 (m, 1H), 1.30 (t, *J* = 7.1 Hz, 3H), 1.08 – 0.89 (m, 2H), 0.78 – 0.56 (m, 2H).

**<sup>13</sup>C NMR** (75 MHz, CDCl<sub>3</sub>) δ ppm 171.8, 164.5, 163.2, 159.9, 158.5, 145.8, 140.6, 134.6, 134.5, 130.5, 130.4, 120.4, 115.4, 115.1, 61.7, 51.6, 40.7, 32.2, 30.1, 15.5, 14.2, 12.7, 8.0, 8.0.

**HR-MS** (ESI) *m/z* [M+Na]<sup>+</sup> calcd. for C<sub>23</sub>H<sub>27</sub>FN<sub>2</sub>O<sub>3</sub>S: 453.1619, found 453.1619.

[α]<sub>D</sub><sup>20</sup> = +0.04° (*c* = 1.0, CHCl<sub>3</sub>).

***Ethyl (5-cyclopropyl-6-(4-fluorobenzyl)picolinoyl)-(D)-methioninate (2.87)***



Following the general procedure above, **2.87** was obtained in 41% yield (12 mg) as a colorless oil starting from picolinic acid **2.42** (20 mg, 0.07 mmol) and ethyl (*D*)-methioninate (13 mg, 0.07 mmol). Purification was performed by column chromatography (Silica gel, 4 g, cHex:EtOAc, 10% EtOAc).

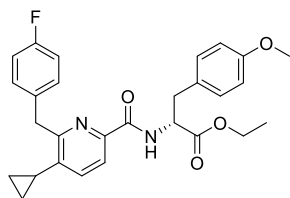
**<sup>1</sup>H NMR** (300 MHz, CDCl<sub>3</sub>) δ ppm 8.52 (d, *J* = 8.5 Hz, 1H), 7.94 (d, *J* = 7.9 Hz, 1H), 7.39 (d, *J* = 8.0 Hz, 1H), 7.25 – 7.15 (m, 2H), 7.03 – 6.93 (m, 2H), 4.86 (td, *J* = 7.9, 5.0 Hz, 1H), 4.36 (s, 2H), 4.24 (q, *J* = 7.1 Hz, 2H), 2.54 (t, *J* = 8.0 Hz, 2H), 2.32 – 2.20 (m, 1H), 2.14 – 2.02 (m, 1H), 2.09 (s, 4H), 1.94 – 1.85 (m, 1H), 1.30 (t, *J* = 7.1 Hz, 3H), 1.03 – 0.97 (m, 2H), 0.69 – 0.64 (m, 2H).

<sup>13</sup>C NMR (75 MHz, CDCl<sub>3</sub>) δ ppm 171.9, 164.5, 163.2, 160.0, 158.5, 145.9, 140.6, 134.7, 130.6, 130.5, 120.5, 115.4, 115.2, 61.7, 51.7, 40.8, 32.3, 30.2, 15.6, 14.3, 12.8, 8.0, 8.0.

HR-MS (ESI)  $m/z$  [M+Na]<sup>+</sup> calcd. for C<sub>23</sub>H<sub>27</sub>FN<sub>2</sub>O<sub>3</sub>S: 445.1619, found 453.1594.

[α]<sub>d</sub><sup>20</sup> = -0.06° (c = 1.0, CHCl<sub>3</sub>).

***Ethyl (L)-2-(5-cyclopropyl-6-(4-fluorobenzyl)picolinamido)-3-(4-methoxyphenyl) propanoate (2.88)***



Following the general procedure above, **2.88** was obtained in 38% yield (37 mg) as a colorless oil starting from picolinic acid **2.42** (54 mg, 0.20 mmol) and ethyl (*L*)-2-amino-3-(4-methoxyphenyl)propanoate **2.90** (45 mg, 0.20 mmol). Purification was performed by column chromatography (Silica gel, 4 g, cHex:EtOAc, 10% EtOAc).

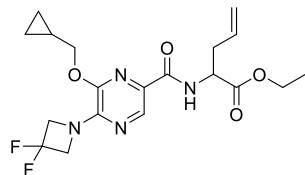
<sup>1</sup>H NMR (300 MHz, CDCl<sub>3</sub>) δ ppm 8.58 (d, *J* = 8.2 Hz, 1H), 7.94 (d, *J* = 8.0 Hz, 1H), 7.41 (d, *J* = 7.9 Hz, 1H), 7.20 – 7.12 (m, 2H), 7.11 – 7.04 (m, 2H), 7.01 – 6.91 (m, 2H), 6.88 – 6.71 (m, 2H), 4.97 (dt, *J* = 8.3, 6.0 Hz, 1H), 4.33 (d, *J* = 5.0 Hz, 2H), 4.21 (q, *J* = 7.1 Hz, 2H), 3.76 (s, 3H), 3.33 – 3.03 (m, 2H), 2.02 – 1.81 (m, 1H), 1.27 (t, *J* = 7.1 Hz, 3H), 1.10 – 0.95 (m, 2H), 0.68 (d, *J* = 3.8 Hz, 2H).

<sup>13</sup>C NMR (75 MHz, CDCl<sub>3</sub>) δ ppm 171.3, 164.7, 163.2, 160.0, 158.8, 158.6, 145.4, 140.9, 134.8, 134.4, 130.5, 130.4, 127.9, 120.6, 115.4, 115.1, 114.0, 61.7, 55.3, 53.7, 40.7, 37.3, 14.3, 12.8, 8.1, 8.1.

HR-MS (ESI)  $m/z$  [M+H]<sup>+</sup> calcd. for C<sub>28</sub>H<sub>29</sub>FN<sub>2</sub>O<sub>4</sub>: 477.2184, found 477.2188.

[α]<sub>d</sub><sup>20</sup> = +0.54° (c = 1.0, CHCl<sub>3</sub>).

***Ethyl 2-(6-(cyclopropylmethoxy)-5-(3,3-difluoroazetidin-1-yl)pyrazine-2-carboxamido)pent-4-enoate (2.94)***



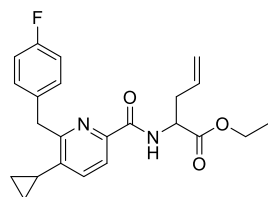
Following the general procedure above, **2.94** was obtained in 55% yield (157 mg) as a light yellow oil starting from pyrazine carboxylic acid **2.37** (200 mg, 0.70 mmol) and ethyl 2-aminopent-4-enoate **2.91** (126 mg, 0.70 mmol). Purification was performed by column chromatography (Silica gel, 4 g, cHex:EtOAc, 30% EtOAc).

**<sup>1</sup>H NMR** (300 MHz, CDCl<sub>3</sub>) δ ppm 8.43 (s, 1H), 7.77 (d, *J* = 7.9 Hz, 1H), 5.82 – 5.68 (m, 1H), 5.18 – 5.11 (m, 2H), 4.82 – 4.75 (m, 1H), 4.61 (t, *J* = 12.1 Hz, 4H), 4.28 – 4.15 (m, 4H), 2.71 – 2.58 (m, 2H), 1.29 (t, *J* = 7.1 Hz, 4H), 0.69 – 0.63 (m, 2H), 0.39 – 0.34 (m, 2H).

**<sup>13</sup>C NMR** (75 MHz, CDCl<sub>3</sub>) δ ppm 171.9, 163.7, 147.8, 147.2, 134.9, 132.6, 130.6, 119.2, 116.5, 71.5, 63.4 (t, <sup>3</sup>*J*<sub>CF</sub> = 27.8 Hz), 61.6, 51.4, 36.9, 14.4, 9.9, 3.6, 3.5.

**HR-MS** (ESI) *m/z* [M+H]<sup>+</sup> calcd. for C<sub>19</sub>H<sub>24</sub>F<sub>2</sub>N<sub>4</sub>O<sub>4</sub>: 411.1838, found 411.1832.

***Ethyl 2-(5-cyclopropyl-6-(4-fluorobenzyl)picolinamido)pent-4-enoate (2.95)***



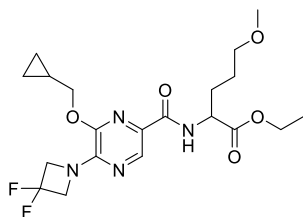
Following the general procedure above, **2.95** was obtained in 28% yield (83 mg) as a light yellow oil starting from picolinic acid **2.42** (200 mg, 0.74 mmol) and ethyl 2-aminopent-4-enoate **2.91** (133 mg, 0.74 mmol). Purification was performed by column chromatography (Silica gel, 4 g, cHex:EtOAc, 10% EtOAc).

**<sup>1</sup>H NMR** (300 MHz, CDCl<sub>3</sub>) δ ppm 8.46 (d, *J* = 8.3 Hz, 1H), 7.93 (d, *J* = 8.0 Hz, 1H), 7.38 (d, *J* = 8.0 Hz, 1H), 7.24 – 7.15 (m, 2H), 7.03 – 6.91 (m, 2H), 5.78 – 5.67 (m, 1H), 5.16 – 5.09 (m, 2H), 4.84 – 4.78 (m, 1H), 4.34 (d, *J* = 3.1 Hz, 2H), 4.30 – 4.17 (m, 2H), 2.75 – 2.54 (m, 2H), 1.95 – 1.86 (m, 1H), 1.29 (t, *J* = 7.1 Hz, 3H), 1.03 – 0.96 (m, 2H), 0.69 – 0.63 (m, 2H).

<sup>13</sup>C NMR (75 MHz, CDCl<sub>3</sub>) δ ppm 171.5, 164.3, 163.2, 160.0, 158.5, 146.0, 140.4, 134.7, 132.6, 130.6, 130.5, 120.4, 119.2, 115.4, 115.1, 61.5, 51.8, 40.8, 36.9, 14.4, 12.8, 8.0, 7.9.

HR-MS (ESI)  $m/z$  [M+Na]<sup>+</sup> calcd. for C<sub>23</sub>H<sub>25</sub>FN<sub>2</sub>O<sub>3</sub>: 419.1741, found 419.1736.

***Ethyl 2-(6-(cyclopropylmethoxy)-5-(3,3-difluoroazetidin-1-yl)pyrazine-2-carboxamido)-5-methoxy-pentanoate (2.96)***



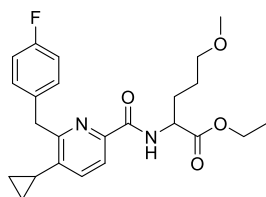
Following the general procedure above, **2.96** was obtained in 39% yield (48 mg) as a colorless oil starting from pyrazine carboxylic acid **2.37** (80 mg, 0.28 mmol) and ethyl 2-amino-5-methoxypentanoate **2.92** (50 mg, 0.28 mmol). Purification was performed by reversed-phase preparative HPLC (C-18, Water:ACN with 0.1% TFA, 30 to 90% ACN).

<sup>1</sup>H NMR (600 MHz, CDCl<sub>3</sub>) δ ppm 8.43 (s, 1H), 7.77 (d, *J* = 8.3 Hz, 1H), 4.77 – 4.74 (m, 1H), 4.61 (t, *J* = 12.0 Hz, 4H), 4.24 – 4.14 (m, 4H), 3.39 (t, *J* = 6.3 Hz, 2H), 3.29 (s, 3H), 2.05 – 2.00 (m, 1H), 1.92 – 1.80 (m, 1H), 1.73 – 1.56 (m, 2H), 1.31 – 1.23 (m, 4H), 0.71 – 0.61 (m, 2H), 0.38 (t, *J* = 5.1 Hz, 2H).

<sup>13</sup>C NMR (151 MHz, CDCl<sub>3</sub>) δ ppm 172.5, 163.9, 147.8, 147.3, 147.2, 147.2, 134.9, 130.6, 118.3, 116.5, 114.7, 72.0, 71.6, 63.4 (t, <sup>3</sup>*J*<sub>CF</sub> = 27.8 Hz), 61.6, 58.6, 51.9, 29.7, 25.6, 14.3, 9.8, 3.5, 3.5.

HR-MS (ESI)  $m/z$  [M+H]<sup>+</sup> calcd. for C<sub>20</sub>H<sub>28</sub>F<sub>2</sub>N<sub>4</sub>O<sub>5</sub>: 443.2101, found 443.2105.

***Ethyl 2-(5-cyclopropyl-6-(4-fluorobenzyl)picolinamido)-5-methoxypentanoate (2.97)***



Following the general procedure above, **2.97** was obtained in 23% yield (27 mg) as a colorless oil starting from picolinic acid **2.42** (76 mg, 0.28 mmol) and ethyl 2-amino-5-methoxypentanoate **2.92**

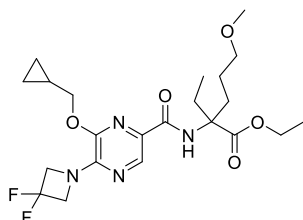
(50 mg, 0.28 mmol). Purification was performed by reversed-phase preparative HPLC (C-18, Water:ACN with 0.1% TFA, 30 to 90% ACN).

**<sup>1</sup>H NMR** (300 MHz, CDCl<sub>3</sub>) δ ppm 8.44 (d, *J* = 8.4 Hz, 1H), 7.94 (d, *J* = 7.9 Hz, 1H), 7.38 (d, *J* = 7.9 Hz, 1H), 7.23 – 7.14 (m, 2H), 7.03 – 6.93 (m, 2H), 4.78 – 4.71 (m, 1H), 4.35 (s, 2H), 4.22 (q, *J* = 7.1 Hz, 2H), 3.39 (t, *J* = 6.2 Hz, 2H), 3.31 (s, 3H), 2.09 – 1.97 (m, 1H), 1.94 – 1.79 (m, 2H), 1.69 – 1.59 (m, 2H), 1.29 (t, *J* = 7.1 Hz, 3H), 1.02 – 0.96 (m, 2H), 0.69 – 0.63 (m, 2H).

**<sup>13</sup>C NMR** (75 MHz, CDCl<sub>3</sub>) δ ppm 172.3, 164.5, 162.5, 160.8, 158.5, 146.1, 140.4, 134.6, 130.5, 120.5, 115.4, 115.2, 72.1, 61.5, 58.7, 52.2, 40.8, 29.6, 25.7, 14.4, 12.8, 8.0, 8.0.

**HR-MS** (ESI) *m/z* [M+H]<sup>+</sup> calcd. for C<sub>24</sub>H<sub>29</sub>FN<sub>2</sub>O<sub>4</sub>: 429.2184, found 429.2190.

***Ethyl 2-(6-(cyclopropylmethoxy)-5-(3,3-difluoroazetidin-1-yl)pyrazine-2-carboxamido)-2-ethyl-5-methoxypentanoate (2.98)***



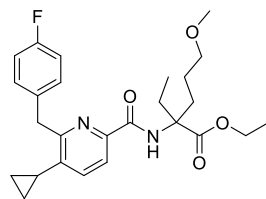
Following the general procedure above, **2.98** was obtained in 60% yield (121 mg) as a colorless oil starting from pyrazine carboxylic acid **2.37** (123 mg, 0.43 mmol) and ethyl 2-amino-2-ethyl-5-methoxypentanoate **2.93** (88 mg, 0.43 mmol). Purification was performed by reversed-phase preparative HPLC (C-18, Water:ACN with 0.1% TFA, 30 to 90% ACN).

**<sup>1</sup>H NMR** (300 MHz, CDCl<sub>3</sub>) δ ppm 8.40 (s, 1H), 4.61 (t, *J* = 12.1 Hz, 4H), 4.34 – 4.19 (m, 4H), 3.37 – 3.26 (m, 2H), 2.68 – 2.54 (m, 2H), 1.98 – 1.81 (m, 2H), 1.58 – 1.48 (m, 1H), 1.37 – 1.25 (m, 5H), 0.75 (t, *J* = 7.4 Hz, 3H), 0.67 – 0.63 (m, 2H), 0.43 – 0.38 (m, 2H).

**<sup>13</sup>C NMR** (75 MHz, CDCl<sub>3</sub>) δ ppm 174.1, 162.9, 147.8, 147.2, 134.2, 131.6, 116.6, 72.6, 71.4, 63.4 (t, <sup>3</sup>*J*<sub>CF</sub> = 27.8 Hz), 61.9, 58.6, 32.1, 28.7, 24.9, 14.4, 10.0, 8.7, 3.6.

**HR-MS** (ESI) *m/z* [M+H]<sup>+</sup> calcd. for C<sub>22</sub>H<sub>32</sub>F<sub>2</sub>N<sub>4</sub>O<sub>5</sub>: 471.2414, found 471.2417.

***Ethyl 2-(5-cyclopropyl-6-(4-fluorobenzyl)picolinamido)-2-ethyl-5-methoxypentanoate (2.99)***



Following the general procedure above, **2.99** was obtained in 25% yield (50 mg) as a colorless oil starting from picolinic acid **2.42** (117 mg, 0.43 mmol) and ethyl 2-amino-2-ethyl-5-methoxypentanoate **2.93** (88 mg, 0.43 mmol). Purification was performed by reversed-phase preparative HPLC (C-18, Water:ACN with 0.1% TFA, 30 to 90% ACN).

**<sup>1</sup>H NMR** (600 MHz, CDCl<sub>3</sub>) δ ppm 9.00 (s, 1H), 7.90 (d, *J* = 7.9 Hz, 1H), 7.38 (d, *J* = 7.9 Hz, 1H), 7.27 – 7.24 (m, 2H), 6.96 (t, *J* = 8.7 Hz, 2H), 4.36 (s, 2H), 4.32 – 4.25 (m, 2H), 3.35 – 3.27 (m, 2H), 3.26 (d, *J* = 1.1 Hz, 3H), 2.60 – 2.50 (m, 2H), 2.00 – 1.86 (m, 3H), 1.59 – 1.48 (m, 1H), 1.41 – 1.34 (m, 1H), 1.32 (t, *J* = 7.1 Hz, 3H), 1.02 – 0.96 (m, 2H), 0.77 (t, *J* = 7.4 Hz, 3H), 0.67 – 0.64 (m, 2H).

**<sup>13</sup>C NMR** (151 MHz, CDCl<sub>3</sub>) δ ppm 173.8, 163.4, 162.4, 160.8, 158.5, 147.0, 139.9, 134.8, 134.8, 130.6, 130.5, 119.8, 115.3, 115.2, 72.6, 65.1, 61.8, 58.5, 40.8, 31.9, 28.6, 24.7, 14.4, 12.8, 8.6, 7.9.

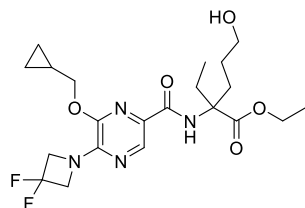
**HR-MS** (ESI) *m/z* [M+Na]<sup>+</sup> calcd. for C<sub>26</sub>H<sub>33</sub>FN<sub>2</sub>O<sub>4</sub>: 479.2317, found 479.2318.

***Synthesis of the aliphatic ether series: PEG elongation through a thioether linkage***

***General Hydroboration-oxidation procedure***

To a solution of the corresponding alkene (1.0 equiv.) in tetrahydrofuran (2 mL) at room temperature and nitrogen atmosphere were added 9-Borabicyclo[3.3.1]nonane (9-BBN, 0.5 M in THF, 1.5 equiv.). The mixture was stirred at room temperature for 36 h, after which time the excess of 9-BBN was quenched with ethanol (3.5 equiv.). The mixture was stirred at room temperature for 30 min, followed by the concurrent dropwise addition of sodium hydroxide aq. sol. (2 M, 4 mL/mmol) and hydrogen peroxide aq. sol. (30%, 4 mL/mmol) at 0 °C. After complete addition, stirring was continued at the same temperature for additional 1 h. The solution was extracted with diethyl ether (3x), dried over Mg<sub>2</sub>SO<sub>4</sub>, filtered, and concentrated under reduced pressure. Subsequent purification by column chromatography (Silica gel, 4 g or 15 g, cHex:EtOAc, 0 to 50% EtOAc) was performed to yield the desired product.

***Ethyl 2-(6-(cyclopropylmethoxy)-5-(3,3-difluoroazetidin-1-yl)pyrazine-2-carboxamido)-2-ethyl-5-hydroxypentanoate (2.75)***



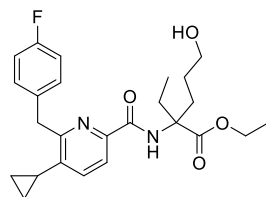
Following the general procedure above, **2.75** was obtained in 64% yield (79 mg) as a colorless oil starting from alkene **2.79** (117 mg, 0.27 mmol).

**<sup>1</sup>H NMR** (600 MHz, CDCl<sub>3</sub>) δ ppm 8.43 – 8.37 (m, 2H), 4.61 (td, *J* = 12.1, 3.3 Hz, 4H), 4.35 – 4.22 (m, 5H), 3.62 – 3.53 (m, 1H), 2.76 – 2.55 (m, 2H), 2.22 – 1.91 (m, 2H), 1.86 (dp, *J* = 14.5, 7.4 Hz, 1H), 1.76 – 1.67 (m, 1H), 1.56 – 1.45 (m, 1H), 1.35 – 1.25 (m, 4H), 0.75 (t, *J* = 7.4 Hz, 3H), 0.68 – 0.63 (m, 2H), 0.43 – 0.39 (m, 2H).

**<sup>13</sup>C NMR** (151 MHz, CDCl<sub>3</sub>) δ ppm 173.7, 163.1, 147.8, 147.3, 134.3, 131.2, 116.5, 71.5, 67.9, 65.4, 65.1, 63.6, 63.4, 63.2, 62.2, 31.3, 28.8, 23.7, 14.3, 9.9, 8.6, 3.6, 3.6.

**HR-MS** (ESI) *m/z* [M+H]<sup>+</sup> calcd. for C<sub>21</sub>H<sub>30</sub>F<sub>2</sub>N<sub>4</sub>O<sub>5</sub>: 457.2218, found 457.2295.

***Ethyl 2-(5-cyclopropyl-6-(4-fluorobenzyl)picolinamido)-2-ethyl-5-hydroxypentanoate (2.76)***



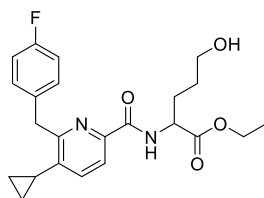
Following the general procedure above, **2.76** was obtained in 99% yield (246 mg) as a colorless oil starting from alkene **2.80** (239 mg, 0.56 mmol).

**<sup>1</sup>H NMR** (600 MHz, CDCl<sub>3</sub>) δ ppm 9.02 (s, 1H), 7.89 (d, *J* = 8.0 Hz, 1H), 7.27 – 7.24 (m, 3H), 6.99 – 6.94 (m, 2H), 4.41 (s, 2H), 4.36 (s, 2H), 4.33 – 4.27 (m, 2H), 3.62 – 3.55 (m, 1H), 2.65 – 2.60 (m, 1H), 2.56 – 2.52 (m, 1H), 2.05 – 1.95 (m, 1H), 1.95 – 1.85 (m, 2H), 1.55 – 1.49 (m, 1H), 1.43 – 1.35 (m, 1H), 1.33 (td, *J* = 7.1, 1.8 Hz, 3H), 1.02 – 0.98 (m, 2H), 0.77 (td, *J* = 7.4, 2.6 Hz, 3H), 0.67 – 0.65 (m, 2H).

**<sup>13</sup>C NMR** (151 MHz, CDCl<sub>3</sub>) δ ppm 173.8, 163.6, 160.9, 158.6, 146.9, 140.0, 134.8, 130.5, 130.5, 119.9, 115.3, 115.2, 65.1, 62.8, 61.9, 40.8, 31.5, 28.9, 27.8, 14.4, 14.4, 12.9, 8.6, 7.9.

**HR-MS** (ESI)  $m/z$   $[M+H]^+$  calcd. for  $C_{23}H_{31}FN_2O_4$ : 443.2301, found 443.2337.

***Ethyl 2-(5-cyclopropyl-6-(4-fluorobenzyl)picolinamido)-5-hydroxypentanoate (2.101)***



Following the general procedure above, **2.101** was obtained in 34% yield (29 mg) as a colorless oil starting from alkene **2.95** (83 mg, 0.21 mmol).

**$^1H$  NMR** (300 MHz,  $CDCl_3$ )  $\delta$  ppm 8.52 (d,  $J = 8.3$  Hz, 1H), 7.93 (d,  $J = 7.9$  Hz, 1H), 7.38 (d,  $J = 8.0$  Hz, 1H), 7.24 – 7.14 (m, 2H), 7.04 – 6.90 (m, 2H), 4.79 (td,  $J = 7.9, 5.2$  Hz, 1H), 4.35 (s, 2H), 4.23 (q,  $J = 7.1$  Hz, 2H), 3.69 (t,  $J = 6.2$  Hz, 2H), 2.12 – 1.98 (m, 2H), 1.95 – 1.82 (m, 3H), 1.70 – 1.57 (m, 2H), 1.29 (t,  $J = 7.1$  Hz, 3H), 1.04 – 0.95 (m, 2H), 0.71 – 0.61 (m, 2H).

**$^{13}C$  NMR** (75 MHz,  $CDCl_3$ )  $\delta$  ppm 172.3, 164.6, 163.2, 160.0, 158.5, 145.9, 140.5, 134.7, 130.6, 130.5, 120.5, 115.4, 115.1, 62.3, 61.6, 52.0, 40.8, 29.7, 28.4, 14.3, 12.8, 8.0, 8.0.

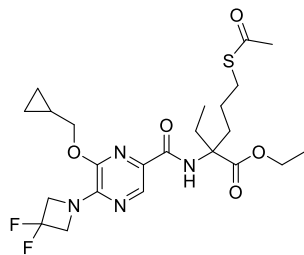
**HR-MS** (ESI)  $m/z$   $[M+H]^+$  calcd. for  $C_{23}H_{27}FN_2O_4$ : 415.2028, found 415.2018.

**General thio-Mitsunobu procedure**

Diisopropyl azodicarboxylate (DIAD, 2.0 equiv.) in anhydrous tetrahydrofuran (0.2 mL) was added dropwise to a stirred solution of triphenylphosphine (2.0 equiv.) in anhydrous tetrahydrofuran (1 mL) at 0 °C under nitrogen atmosphere. The mixture was stirred at this temperature for 30 min, until formation of a white precipitate of Mitsunobu betaine, and a solution of thioacetic acid (2.0 equiv.) and the corresponding alcohol (2.0 equiv.) in anhydrous tetrahydrofuran (1 mL) was added slowly. The reaction was stirred at 0 °C for 1 h and then allowed to reach room temperature, and stirred for additional 1 h. The reaction mixture was concentrated under reduced pressure, and the residue taken up into a mixture of diethyl ether and cyclohexane (1:1) and triturated at 0 °C. The resulting white solid was filtered off and washed with diethyl ether and cyclohexane (1:1) mixture. The filtrate was evaporated under reduced pressure, and the residue purified by column chromatography (Silica gel, 4 g, cHex:EtOAc, 5 to 15% EtOAc).



***Ethyl 5-(acetylthio)-2-(6-(cyclopropylmethoxy)-5-(3,3-difluoroazetidin-1-yl)pyrazine-2-carboxamido)-2-ethylpentanoate (SI-13)***



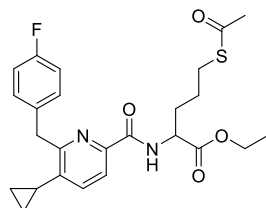
Following the general procedure above, **SI-13** was obtained in 32% yield (13 mg) as a light yellow oil starting from compound **2.75** (36 mg, 0.08 mmol).

**<sup>1</sup>H NMR** (600 MHz, CDCl<sub>3</sub>) δ ppm 8.42 (s, 1H), 8.40 (s, 1H), 4.63 (t, *J* = 12.0 Hz, 4H), 4.32 – 4.24 (m, 4H), 2.87 – 2.77 (m, 2H), 2.71 – 2.56 (m, 2H), 2.28 (s, 3H), 1.96 – 1.82 (m, 2H), 1.61 – 1.50 (m, 1H), 1.36 – 1.24 (m, 5H), 0.75 (t, *J* = 7.4 Hz, 3H), 0.70 – 0.63 (m, 2H), 0.43 – 0.40 (m, 2H).

**<sup>13</sup>C NMR** (151 MHz, CDCl<sub>3</sub>) δ ppm 195.9, 173.9, 163.2, 147.8, 147.1, 134.1, 131.1, 116.5, 71.6, 65.5, 63.5, 62.1, 34.6, 30.7, 29.0, 28.7, 24.8, 14.4, 10.0, 8.6, 3.6.

**HR-MS** (ESI) *m/z* [M+Na]<sup>+</sup> calcd. for C<sub>23</sub>H<sub>32</sub>F<sub>2</sub>N<sub>4</sub>O<sub>5</sub>S: 537.1954, found 537.1966.

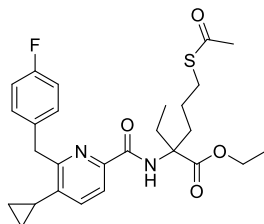
***Ethyl 5-(acetylthio)-2-(5-cyclopropyl-6-(4-fluorobenzyl)picolinamido)pentanoate (SI-14)***



Following the general procedure above, **SI-14** synthesized starting from compound **2.101** (29 mg, 0.07 mmol). After filtration work-up, intermediate **SI-14** was obtained, along with diisopropyl azodicarboxylate by-products, and used crude for further reaction steps.

**HR-MS** (ESI) *m/z* [M+H]<sup>+</sup> calcd. for C<sub>25</sub>H<sub>29</sub>FN<sub>2</sub>O<sub>4</sub>S: 474.1936, found 474.1936.

***Ethyl 5-(acetylthio)-2-(5-cyclopropyl-6-(4-fluorobenzyl)picolinamido)-2-ethylpentanoate***  
**(2.115)**



Following the general procedure above, **2.115** was obtained in 55% yield (24 mg) as a light yellow oil starting from compound **2.76** (39 mg, 0.09 mmol).

**<sup>1</sup>H NMR** (300 MHz, CDCl<sub>3</sub>) δ ppm 8.99 (s, 1H), 7.90 (d, *J* = 7.9 Hz, 1H), 7.38 (d, *J* = 8.0 Hz, 1H), 7.30 – 7.19 (m, 3H), 7.02 – 6.91 (m, 2H), 4.39 – 4.23 (m, 4H), 2.88 – 2.76 (m, 2H), 2.69 – 2.45 (m, 2H), 2.28 (s, 3H), 2.01 – 1.81 (m, 3H), 1.64 – 1.49 (m, 1H), 1.43 – 1.23 (m, 5H), 1.04 – 0.95 (m, 2H), 0.76 (t, *J* = 7.4 Hz, 3H), 0.70 – 0.62 (m, 2H).

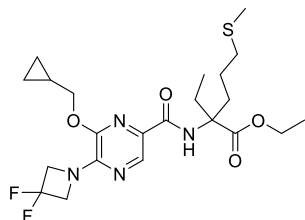
**<sup>13</sup>C NMR** (75 MHz, CDCl<sub>3</sub>) δ ppm 195.8, 173.6, 163.5, 160.0, 158.5, 146.8, 140.0, 134.8, 134.8, 130.6, 130.5, 119.8, 115.4, 115.1, 65.0, 61.9, 40.8, 34.4, 30.7, 29.1, 28.6, 24.7, 24.7, 14.4, 12.8, 8.5, 7.9, 7.9.

**HR-MS** (ESI) *m/z* [M+Na]<sup>+</sup> calcd. for C<sub>27</sub>H<sub>33</sub>FN<sub>2</sub>O<sub>4</sub>S: 523.2037, found 523.2058.

**General acetylthio cleavage procedure using iodomethane**

Thioether derivative (1.0 equiv.) and iodomethane (1.0 equiv.) were added to oxygen-free absolute ethanol (2 mL) under nitrogen atmosphere. The suspension was cooled to –20 °C, sodium ethoxide (2.2 equiv.) was added, and the mixture was allowed to warm up slowly to room temperature. The resulting pale yellow solution was stirred for 20 h. The reaction mixture was concentrated, and the resulting residue was dissolved in an acetonitrile and water (1:1) solution and purified by reversed-phase preparative HPLC (C-18, Water:ACN with 0.1% TFA, 30 to 90% ACN). The fractions containing product were combined and lyophilized to yield the desired compound.

***Ethyl 2-(6-(cyclopropylmethoxy)-5-(3,3-difluoroazetidin-1-yl)pyrazine-2-carboxamido)-2-ethyl-5-(methylthio)pentanoate (2.102)***



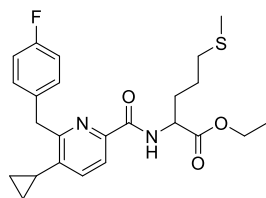
Following the general procedure above, **2.102** was obtained in 38% yield (3 mg) as a light yellow oil starting from compound **SI-13** (8 mg, 0.02 mmol).

**<sup>1</sup>H NMR** (600 MHz, CDCl<sub>3</sub>) δ ppm 8.41 (s, 1H), 8.39 (s, 1H), 4.64 (t, *J* = 12.0 Hz, 4H), 4.31 – 4.25 (m, 4H), 2.71 – 2.58 (m, 2H), 2.51 – 2.38 (m, 2H), 2.07 – 1.94 (m, 4H), 1.90 – 1.84 (m, 1H), 1.63 – 1.56 (m, 1H), 1.36 – 1.24 (m, 5H), 0.75 (t, *J* = 7.4 Hz, 3H), 0.71 – 0.64 (m, 2H), 0.45 – 0.39 (m, 2H).

**<sup>13</sup>C NMR** (151 MHz, CDCl<sub>3</sub>) δ ppm 174.0, 162.9, 147.8, 147.0, 133.9, 131.4, 116.5, 71.6, 65.5, 63.5, 62.0, 34.7, 34.1, 28.8, 24.4, 15.6, 14.5, 10.0, 8.6, 3.6.

**HR-MS** (ESI) *m/z* [M+H]<sup>+</sup> calcd. for C<sub>22</sub>H<sub>32</sub>F<sub>2</sub>N<sub>4</sub>O<sub>4</sub>S: 487.2146, found 487.2231.

***Ethyl 2-(5-cyclopropyl-6-(4-fluorobenzyl)picolinamido)-5-(methylthio)pentanoate (2.103)***



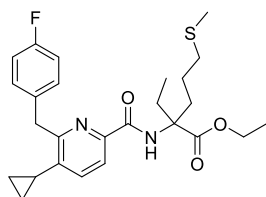
Following the general procedure above, **2.103** was obtained in 16% yield (4 mg) as a light yellow oil, over 2 steps starting from crude compound **SI-14**.

**<sup>1</sup>H NMR** (600 MHz, DMSO-*d*<sub>6</sub>) δ ppm 8.58 (d, *J* = 8.1 Hz, 1H), 7.78 (d, *J* = 8.0 Hz, 1H), 7.52 (d, *J* = 8.0 Hz, 1H), 7.38 – 7.29 (m, 2H), 7.11 (tt, *J* = 9.8, 3.0 Hz, 2H), 4.51 – 4.47 (m, 1H), 4.41 – 4.34 (m, 2H), 4.19 – 4.09 (m, 2H), 2.53 – 2.51 (m, 1H), 2.48 – 2.44 (m, 1H), 2.10 – 2.03 (m, 1H), 2.00 – 1.84 (m, 5H), 1.57 – 1.52 (m, 2H), 1.20 (t, *J* = 7.1 Hz, 3H), 1.03 – 0.95 (m, 2H), 0.70 – 0.68 (m, 2H).

**<sup>13</sup>C NMR** (151 MHz, DMSO-*d*<sub>6</sub>) δ ppm 171.6, 163.7, 161.6, 160.0, 158.1, 146.5, 140.4, 135.0, 134.1, 130.7, 130.6, 120.0, 115.0, 114.8, 60.7, 52.0, 32.5, 30.0, 24.7, 14.4, 14.0, 12.1, 8.3, 8.2.

**HR-MS** (ESI) *m/z* [M+Na]<sup>+</sup> calcd. for C<sub>24</sub>H<sub>29</sub>FN<sub>2</sub>O<sub>3</sub>S: 467.1775, found 467.1746.

***Ethyl 2-(5-cyclopropyl-6-(4-fluorobenzyl)picolinamido)-2-ethyl-5-(methylthio)pentanoate***  
**(2.104)**



Following the general procedure above, **2.104** was obtained in 46% yield (9 mg) as a light yellow oil starting from compound **2.115** (20 mg, 0.04 mmol).

**<sup>1</sup>H NMR** (300 MHz, CDCl<sub>3</sub>) δ ppm 9.06 (s, 1H), 7.91 (d, *J* = 8.0 Hz, 1H), 7.40 (d, *J* = 8.0 Hz, 1H), 7.31 – 7.21 (m, 2H), 7.04 – 6.91 (m, 2H), 4.38 (s, 2H), 4.29 (q, *J* = 7.1 Hz, 2H), 2.67 – 2.36 (m, 4H), 2.09 – 1.83 (m, 6H), 1.67 – 1.52 (m, 1H), 1.42 – 1.31 (m, 4H), 1.03 – 0.97 (m, 2H), 0.77 (t, *J* = 7.4 Hz, 3H), 0.71 – 0.64 (m, 2H).

**<sup>13</sup>C NMR** (75 MHz, CDCl<sub>3</sub>) δ ppm 173.8, 163.3, 160.0, 158.5, 146.7, 140.2, 135.0, 134.7, 130.6, 130.5, 120.0, 115.4, 115.1, 65.2, 61.9, 40.7, 34.4, 34.1, 28.6, 24.2, 15.5, 14.5, 12.8, 8.6, 8.0.

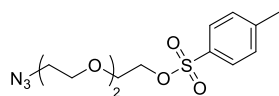
**HR-MS** (ESI) *m/z* [M+H]<sup>+</sup> calcd. for C<sub>26</sub>H<sub>33</sub>FN<sub>2</sub>O<sub>3</sub>S: 473.2296, found 473.2283.

### 5.2.8. Synthesis of Racemic NBD-Labeled Probes

#### ***General procedure for linker tosylation***

*N*-Boc PEG2–5, azido PEG2, or *N*-Boc hydroxyhexyl (1.0 equiv.) was dissolved in dichloromethane (1.5 mL) and treated with *p*-toluenesulfonyl chloride (3.0 equiv.) and pyridine (5.0 equiv.) at 0 °C. The reaction was allowed to warm to room temperature, and then stirred at 40 °C for 12h. The mixture was diluted with dichloromethane, and washed with hydrochloric acid aq. sol. (0.2 M, 5 mL), water (5 mL), and brine (5 mL), dried over MgSO<sub>4</sub>, and concentrated under reduced pressure. The crude product was purified by column chromatography (Silica gel, 4 g, cHex:EtOAc, 15 to 30% EtOAc), giving a colorless oil.

### **2-(2-(2-Azidoethoxy)ethoxy)ethyl 4-methylbenzenesulfonate (SI-15)**

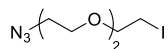


Following the general procedure above, **SI-15** was obtained in 83% yield (80 mg) as a colorless oil starting from 2-(2-(2-azidoethoxy)ethoxy)ethan-1-ol **2.116** (50 mg, 0.29 mmol). This example was synthesized with replacement of the base pyridine by triethylamine (5.0 equiv.) and addition of catalytic amounts of N,N-dimethylaminopyridine (DMAP, 0.1 equiv.).

**<sup>1</sup>H NMR** (300 MHz, CDCl<sub>3</sub>) δ ppm 7.79 (d, *J* = 8.2 Hz, 2H), 7.33 (d, *J* = 8.1 Hz, 2H), 4.19 – 4.12 (m, 2H), 3.72 – 3.59 (m, 8H), 3.22 – 3.05 (m, 1H), 3.35 (t, *J* = 5.1 Hz, 2H), 1.13 (t, *J* = 7.2 Hz, 2H).

The analytical data are in accordance with those reported in the literature.<sup>[300]</sup>

### **1-Azido-2-(2-(2-iodoethoxy)ethoxy)ethane (2.117)**

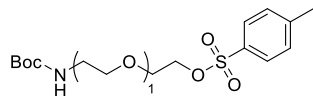


Tosylate **SI-15** (80 mg, 0.24 mmol) and sodium iodide (109 mg, 0.72 mmol) were dissolved in dimethylformamide (2 mL). The mixture was stirred at 50 °C for 5 h under nitrogen atmosphere. The solvent was evaporated under reduced pressure, and the residue dissolved in ethyl acetate (5 mL). The organic solution was washed with water (3 mL), and the aqueous phase, extracted with ethyl acetate (3x). The combined organic extracts were washed with brine (5 mL), dried over MgSO<sub>4</sub>, and evaporated under reduced pressure. Purification by column chromatography (Silica gel, 4 g, cHex:EtOAc, 15% EtOAc) afforded linker **2.117** as colorless oil in 22% yield (15 mg).

**<sup>1</sup>H NMR** (300 MHz, CDCl<sub>3</sub>) δ ppm 3.77 (t, *J* = 6.8 Hz, 2H), 3.73 – 3.65 (m, 6H), 3.40 (t, *J* = 5.1 Hz, 2H), 3.27 (t, *J* = 6.8 Hz, 2H).

The analytical data are in accordance with those reported in the literature.<sup>[301]</sup>

### **2-(2-((tert-Butoxycarbonyl)amino)ethoxy)ethyl 4-methylbenzenesulfonate (2.124)**

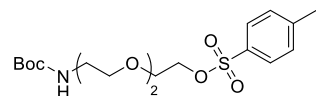


Following the general procedure above, **2.124** was obtained in quantitative yield (86 mg) as a colorless oil starting from linker *tert*-butyl (2-(2-hydroxyethoxy)ethyl)carbamate **2.119** (50 mg, 0.24 mmol).

**<sup>1</sup>H NMR** (300 MHz, CDCl<sub>3</sub>) δ ppm 7.81 (d, *J* = 8.2 Hz, 2H), 7.35 (d, *J* = 8.1 Hz, 2H), 4.80 (s, 1H), 4.16 (dd, *J* = 5.7, 3.6 Hz, 2H), 3.63 (dd, *J* = 5.5, 3.8 Hz, 2H), 3.44 (t, *J* = 5.1 Hz, 2H), 3.24 (q, *J* = 5.2 Hz, 2H), 2.45 (s, 3H), 1.45 (s, 9H).

The analytical data are in accordance with those reported in the literature.<sup>[302]</sup>

***2,2-Dimethyl-4-oxo-3,8,11-trioxa-5-azatridecan-13-yl 4-methylbenzenesulfonate (2.125)***

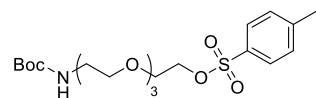


Following the general procedure above, **2.125** was obtained in quantitative yield (114 mg) as a colorless oil starting from linker *tert*-butyl (2-(2-(2-hydroxyethoxy)ethoxy)ethyl)carbamate **2.120** (60 mg, 0.24 mmol).

**<sup>1</sup>H NMR** (300 MHz, CDCl<sub>3</sub>) δ ppm 7.79 (d, *J* = 8.1 Hz, 2H), 7.34 (d, *J* = 8.0 Hz, 2H), 4.93 (bs, 1H), 4.16 (t, *J* = 4.8 Hz, 2H), 3.68 (t, *J* = 4.8 Hz, 2H), 3.60 – 3.45 (m, 6H), 3.34 – 3.22 (m, 2H), 2.44 (s, 3H), 1.43 (s, 9H).

The analytical data are in accordance with those reported in the literature.<sup>[303]</sup>

***2,2-Dimethyl-4-oxo-3,8,11,14-tetraoxa-5-azahexadecan-16-yl 4-methylbenzenesulfonate (2.126)***

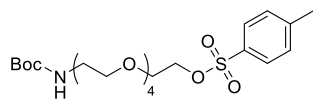


Following the general procedure above, **2.126** was obtained in 66% yield (71 mg) as a colorless oil starting from linker *tert*-butyl (2-(2-(2-(2-hydroxyethoxy)ethoxy)ethoxy)ethyl)carbamate **2.121** (70 mg, 0.24 mmol).

**<sup>1</sup>H NMR** (300 MHz, CDCl<sub>3</sub>) δ ppm 7.79 (d, *J* = 8.2 Hz, 2H), 7.34 (d, *J* = 8.1 Hz, 2H), 5.00 (bs, 1H), 4.20 – 4.11 (m, 2H), 3.73 – 3.65 (m, 2H), 3.59 (s, 8H), 3.54 – 3.49 (m, 2H), 3.34 – 3.25 (m, 2H), 2.44 (s, 3H), 1.43 (s, 9H).

The analytical data are in accordance with those reported in the literature.<sup>[304]</sup>

**2,2-Dimethyl-4-oxo-3,8,11,14,17-pentaoxa-5-azanonadecan-19-yl 4-methylbenzenesulfonate (2.127)**

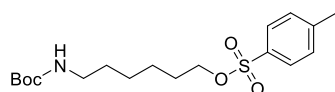


Following the general procedure above, **2.127** was obtained in 94% yield (111 mg) as a colorless oil starting from linker *tert*-butyl (14-hydroxy-3,6,9,12-tetraoxatetradecyl)carbamate **2.122** (81 mg, 0.24 mmol).

**<sup>1</sup>H NMR** (300 MHz, CDCl<sub>3</sub>) δ ppm 7.78 (d, *J* = 8.0 Hz, 2H), 7.33 (d, *J* = 7.9 Hz, 2H), 5.01 (bs, 1H), 4.18 – 4.09 (m, 2H), 3.70 – 3.64 (m, 2H), 3.64 – 3.55 (m, 12H), 3.54 – 3.48 (m, 2H), 3.28 (t, *J* = 5.0 Hz, 2H), 2.43 (s, 3H), 1.42 (s, 9H).

The analytical data are in accordance with those reported in the literature.<sup>[305]</sup>

**6-((*Tert*-butoxycarbonyl)amino)hexyl 4-methylbenzenesulfonate (2.128)**



Following the general procedure above, **2.128** was obtained in 42% yield (38 mg) as a colorless oil starting from linker *tert*-butyl (6-hydroxyhexyl)carbamate **2.123** (52 mg, 0.24 mmol).

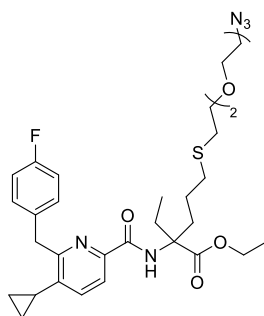
**<sup>1</sup>H NMR** (300 MHz, CDCl<sub>3</sub>) δ ppm 7.78 (d, *J* = 8.2 Hz, 2H), 7.34 (d, *J* = 8.1 Hz, 2H), 4.49 (s, 1H), 4.00 (t, *J* = 6.4 Hz, 2H), 3.12 – 2.98 (m, 2H), 2.44 (s, 3H), 1.69 – 1.56 (m, 2H), 1.43 (s, 11H), 1.35 – 1.21 (m, 4H).

The analytical data are in accordance with those reported in the literature.<sup>[306]</sup>

### **General procedure for linker attachment at pyridine ( $\pm$ )-2.115 scaffold**

Thioderivative ( $\pm$ )-2.115 (1.0 equiv.) and the corresponding tosyl linker **2.124** to **2.128** or iodinated linker **2.117** (1.8 equiv.) were added to absolute ethanol previously degassed (2 mL) under nitrogen atmosphere. The suspension was cooled to  $-20$  °C, sodium ethoxide (3.0 equiv.) was added along with catalytic amounts of potassium iodide (0.3 equiv.), and the mixture was allowed to warm up slowly to room temperature. The resulting solution was stirred for 20 h. The reaction mixture was concentrated under reduced pressure. The resulting residue was dissolved in acetonitrile and water (1:1) and purified by reversed-phase preparative HPLC (C-18, Water:ACN with 0.1% TFA, 30 to 90% ACN).

### ***Ethyl 5-((2-(2-(2-azidoethoxy)ethoxy)ethyl)thio)-2-(5-cyclopropyl-6-(4-fluorobenzyl)picolinamido)-2-ethylpentanoate* ( $\pm$ )-2.118**



Following the general procedure above, ( $\pm$ )-2.118 was obtained in 46% yield (7 mg) as a pale yellow solid starting from linker 1-azido-2-(2-(2-iodoethoxy)ethoxy)ethane **2.117** (10 mg, 0.04 mmol). This example was synthesized without addition of potassium iodide.

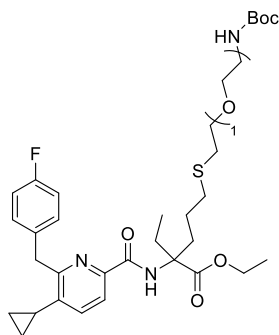
**$^1\text{H NMR}$**  (600 MHz, DMSO- $d_6$ )  $\delta$  ppm 8.71 (s, 1H), 7.76 (d,  $J$  = 8.0 Hz, 1H), 7.53 (d,  $J$  = 8.0 Hz, 1H), 7.36 – 7.30 (m, 2H), 7.14 – 7.06 (m, 2H), 4.36 (s, 2H), 4.22 (q,  $J$  = 7.1 Hz, 2H), 3.58 – 3.55 (m, 2H), 3.52 – 3.42 (m, 6H), 3.38 – 3.34 (m, 2H), 2.54 (t,  $J$  = 6.8 Hz, 2H), 2.50 – 2.44 (m, 2H), 2.40 – 2.26 (m, 2H), 2.10 – 2.06 (m, 1H), 1.92 – 1.88 (m, 1H), 1.87 – 1.80 (m, 1H), 1.41 – 1.35 (m, 1H), 1.30 – 1.21 (m, 4H), 1.01 – 0.98 (m, 2H), 0.71 – 0.66 (m, 5H).

**$^{13}\text{C NMR}$**  (151 MHz, DMSO- $d_6$ )  $\delta$  ppm 173.8, 162.3, 161.6, 160.0, 158.0, 145.8, 140.2, 135.0, 134.4, 130.7, 119.3, 115.0, 114.9, 70.2, 69.6, 69.4, 69.2, 63.6, 61.34, 50.0, 33.4, 31.3, 30.4, 27.6, 23.9, 14.0, 12.1, 8.1, 8.0.

**HR-MS** (ESI)  $m/z$   $[\text{M}+\text{Na}]^+$  calcd. for  $\text{C}_{31}\text{H}_{42}\text{FN}_5\text{O}_5\text{S}$ : 638.2783, found 638.2801.



***Ethyl 15-(5-cyclopropyl-6-(4-fluorobenzyl)picolinamido)-15-ethyl-2,2-dimethyl-4-oxo-3,8-dioxa-11-thia-5-azahexadecan-16-oate ((±)-2.129)***



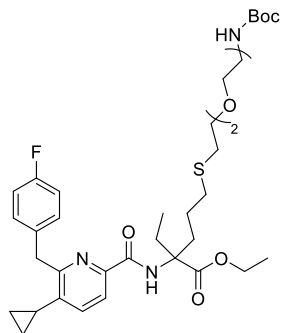
Following the general procedure above, (±)-**2.129** was obtained in 50% yield (16 mg) as a pale yellow solid starting from linker 2-(2-((*tert*-butoxycarbonyl)amino)ethoxy)ethyl 4-methylbenzenesulfonate **2.124** (32 mg, 0.09 mmol).

**<sup>1</sup>H NMR** (300 MHz, CDCl<sub>3</sub>) δ ppm 9.02 (s, 1H), 7.89 (d, *J* = 7.9 Hz, 1H), 7.39 (d, *J* = 8.0 Hz, 1H), 7.30 – 7.21 (m, 2H), 6.97 (t, *J* = 8.6 Hz, 2H), 4.95 (bs, 1H), 4.46 – 4.19 (m, 4H), 3.56 – 3.43 (m, 4H), 3.29 – 3.24 (m, 2H), 2.67 – 2.47 (m, 6H), 2.06 – 1.82 (m, 4H), 1.64 – 1.56 (m, 1H), 1.43 (s, 9H), 1.33 (t, *J* = 7.1 Hz, 3H), 1.05 – 0.94 (m, 2H), 0.76 (t, *J* = 7.4 Hz, 3H), 0.79 – 0.64 (m, 2H).

**<sup>13</sup>C NMR** (75 MHz, CDCl<sub>3</sub>) δ ppm 173.7, 163.5, 163.2, 160.0, 158.5, 156.1, 146.8, 140.1, 134.8, 130.6, 130.5, 119.8, 115.4, 115.1, 79.4, 70.7, 70.0, 65.1, 61.9, 40.8, 40.5, 34.5, 32.5, 31.6, 28.6, 28.6, 24.8, 14.5, 12.8, 8.6, 7.9.

**HR-MS** (ESI) *m/z* [M+Na]<sup>+</sup> calcd. for C<sub>34</sub>H<sub>48</sub>FN<sub>3</sub>O<sub>6</sub>S: 668.3140, found 668.3154.

***Ethyl 18-(5-cyclopropyl-6-(4-fluorobenzyl)picolinamido)-18-ethyl-2,2-dimethyl-4-oxo-3,8,11-trioxa-14-thia-5-azanonadecan-19-oate ((±)-2.130)***



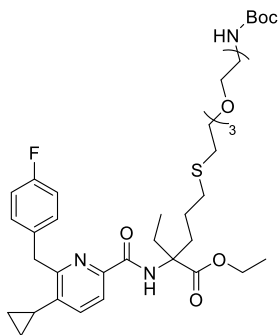
Following the general procedure above, (±)-**2.130** was obtained in 49% yield (13 mg) as a pale yellow solid starting from linker 2,2-dimethyl-4-oxo-3,8,11-trioxa-5-azatridecan-13-yl 4-methylbenzenesulfonate **2.125** (29 mg, 0.07 mmol).

**<sup>1</sup>H NMR** (300 MHz, CDCl<sub>3</sub>) δ ppm 9.01 (s, 1H), 7.89 (d, *J* = 7.9 Hz, 1H), 7.38 (d, *J* = 8.0 Hz, 1H), 7.30 – 7.20 (m, 2H), 7.03 – 6.92 (m, 2H), 5.02 (bs, 1H), 4.40 – 4.23 (m, 4H), 3.62 – 3.45 (m, 8H), 3.34 – 3.30 (m, 2H), 2.68 – 2.44 (m, 6H), 2.05 – 1.82 (m, 3H), 1.64 – 1.55 (m, 1H), 1.43 (s, 9H), 1.35 – 1.18 (m, 4H), 1.03 – 0.97 (m, 2H), 0.76 (t, *J* = 7.4 Hz, 3H), 0.72 – 0.62 (m, 2H).

**<sup>13</sup>C NMR** (75 MHz, CDCl<sub>3</sub>) δ ppm 173.7, 163.5, 163.2, 158.5, 156.1, 146.8, 140.0, 134.8, 130.6, 130.5, 119.8, 115.4, 115.1, 79.3, 71.0, 70.4, 70.3, 65.1, 61.9, 40.9, 40.4, 34.5, 32.5, 31.5, 28.6, 24.9, 14.5, 12.9, 8.6, 7.9.

**HR-MS** (ESI) *m/z* [M+Na]<sup>+</sup> calcd. for C<sub>36</sub>H<sub>52</sub>FN<sub>3</sub>O<sub>7</sub>S: 712.3402, found 712.3346.

***Ethyl 21-(5-cyclopropyl-6-(4-fluorobenzyl)picolinamido)-21-ethyl-2,2-dimethyl-4-oxo-3,8,11,14-tetra-oxa-17-thia-5-azadocosan-22-oate ((±)-2.131)***



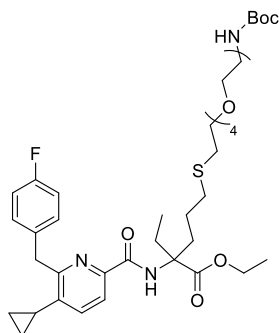
Following the general procedure above, (±)-**2.131** was obtained in 52% yield (19 mg) as a pale yellow solid starting from linker 2,2-dimethyl-4-oxo-3,8,11,14-tetraoxa-5-azahexadecan-16-yl 4-methylbenzenesulfonate **2.126** (40 mg, 0.09 mmol).

**<sup>1</sup>H NMR** (300 MHz, CDCl<sub>3</sub>) δ ppm 9.01 (s, 1H), 7.89 (d, *J* = 7.9 Hz, 1H), 7.38 (d, *J* = 8.0 Hz, 1H), 7.30 – 7.21 (m, 2H), 6.97 (t, *J* = 8.6 Hz, 2H), 5.03 (bs, 1H), 4.43 – 4.21 (m, 4H), 3.66 – 3.68 (m, 12H), 3.33 – 3.27 (m, 2H), 2.69 – 2.44 (m, 6H), 2.08 – 1.76 (m, 4H), 1.64 – 1.55 (m, 1H), 1.43 (s, 9H), 1.33 (t, *J* = 7.1 Hz, 3H), 1.03 – 0.96 (m, 2H), 0.76 (t, *J* = 7.4 Hz, 3H), 0.78 – 0.64 (m, 2H).

**<sup>13</sup>C NMR** (75 MHz, CDCl<sub>3</sub>) δ ppm 173.7, 163.5, 163.2, 160.0, 158.5, 156.1, 146.8, 134.8, 130.6, 130.5, 119.8, 115.4, 115.1, 79.3, 71.0, 70.7, 70.4, 70.4, 65.1, 61.9, 40.8, 34.5, 32.5, 31.5, 28.6, 24.9, 14.5, 12.8, 8.6, 7.9.

**HR-MS** (ESI) *m/z* [M+Na]<sup>+</sup> calcd. for C<sub>38</sub>H<sub>56</sub>FN<sub>3</sub>O<sub>8</sub>S: 756.3664, found 756.3682.

***Ethyl 24-(5-cyclopropyl-6-(4-fluorobenzyl)picolinamido)-24-ethyl-2,2-dimethyl-4-oxo-3,8,11,14,17-pentaoxa-20-thia-5-azapentacosan-25-oate ((±)-2.132)***



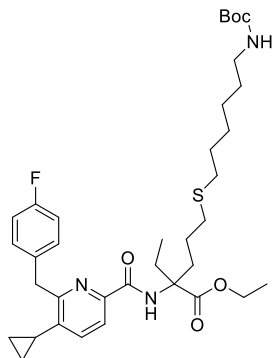
Following the general procedure above, (±)-**2.132** was obtained in 56% yield (22 mg) as a pale yellow solid starting from linker 2,2-dimethyl-4-oxo-3,8,11,14,17-pentaoxa-5-azanonadecan-19-yl 4-methylbenzenesulfonate **2.127** (44 mg, 0.09 mmol).

**<sup>1</sup>H NMR** (300 MHz, CDCl<sub>3</sub>) δ ppm 9.01 (s, 1H), 7.89 (d, *J* = 7.9 Hz, 1H), 7.38(d, *J* = 8.0 Hz, 1H), 7.29 – 7.21 (m, 2H), 6.97 (t, *J* = 8.6 Hz, 2H), 5.04 (bs, 1H), 4.39 – 4.24 (m, 4H), 3.68 – 3.47 (m, 16H), 3.35 – 3.30 (m, 2H), 2.69 – 2.42 (m, 6H), 2.08 – 1.80 (m, 4H), 1.65 – 1.51 (m, 1H), 1.43 (s, 9H), 1.33 (t, *J* = 7.1 Hz, 3H), 1.04 – 0.95 (m, 2H), 0.76 (t, *J* = 7.4 Hz, 3H), 0.78 – 0.64 (m, 2H).

**<sup>13</sup>C NMR** (75 MHz, CDCl<sub>3</sub>) δ ppm 173.7, 163.4, 160.0, 158.5, 156.1, 146.8, 140.1, 134.9, 130.6, 130.5, 119.9, 115.4, 115.1, 79.3, 70.7, 70.7, 70.7, 70.4, 70.3, 65.1, 61.9, 40.8, 40.5, 34.5, 32.5, 31.5, 28.6, 24.8, 14.5, 12.8, 8.6, 7.9.

**HR-MS** (ESI) *m/z* [M+Na]<sup>+</sup> calcd. For C<sub>40</sub>H<sub>60</sub>FN<sub>3</sub>O<sub>9</sub>S: 801.3958, found 801.3977.

***Ethyl 5-((6-((tert-butoxycarbonyl)amino)hexyl)thio)-2-(5-cyclopropyl-6-(4-fluorobenzyl) picolinamido)-2-ethylpentanoate ((±)-2.133)***



Following the general procedure above, (±)-**2.133** was obtained in 51% yield (17 mg) as a pale yellow solid starting from linker 6-((*tert*-butoxycarbonyl)amino)hexyl 4-methylbenzenesulfonate **2.128** (33 mg, 0.09 mmol).

**<sup>1</sup>H NMR** (300 MHz, CDCl<sub>3</sub>) δ ppm 9.02 (s, 1H), 7.89 (d, *J* = 7.9 Hz, 1H), 7.38 (d, *J* = 8.0 Hz, 1H), 7.32 – 7.19 (m, 2H), 6.96 (t, *J* = 8.6 Hz, 2H), 4.53 (s, 1H), 4.38 – 4.24 (m, 4H), 3.11 – 3.04 (m, 2H), 2.67 – 2.37 (m, 6H), 2.07 – 1.84 (m, 3H), 1.60 – 1.24 (m, 22H), 1.06 – 0.94 (m, 2H), 0.76 (t, *J* = 7.4 Hz, 3H), 0.79 – 0.63 (m, 2H).

**<sup>13</sup>C NMR** (75 MHz, CDCl<sub>3</sub>) δ ppm 173.8, 163.5, 160.0, 158.3, 156.1, 146.8, 140.0, 134.8, 130.6, 130.5, 119.8, 115.4, 115.1, 79.2, 65.1, 61.9, 40.8, 34.6, 32.1, 32.0, 30.1, 29.6, 28.6, 28.6, 26.5, 24.7, 14.4, 12.8, 8.6, 7.9, 7.9.

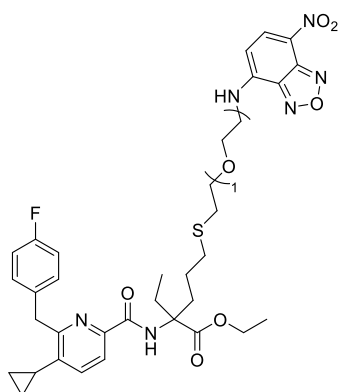
**HR-MS** (ESI) *m/z* [M+Na]<sup>+</sup> calcd. for C<sub>36</sub>H<sub>52</sub>FN<sub>3</sub>O<sub>5</sub>S: 680.3504, found 680.3516.

### **General Boc-deprotection and NBD-labeling procedure**

Trifluoroacetic acid (0.3 mL) was added dropwise to a stirring solution of the corresponding *N*-Boc-protected compound ( $\pm$ )-**2.129** to ( $\pm$ )-**2.133** (1.0 equiv.) in dichloromethane (2.3 mL) at 0 °C. The reaction mixture was stirred at room temperature for 2 h. Afterwards, the mixture was concentrated under reduced pressure, and the residue re-suspended in ethyl acetate (5 mL). The solvent was removed under reduced pressure. This process was repeated 3 times to remove trifluoroacetic acid traces. The removal of the *tert*-butyloxycarbonyl group was quantitative as observed by TLC (50% EtOAc in *c*Hex). The free amines ( $\pm$ )-**2.110** to ( $\pm$ )-**2.114** were obtained as the corresponding trifluoroacetic acid salts, without the need of further purification.

To a solution of ( $\pm$ )-**2.110** to ( $\pm$ )-**2.114** (1.0 equiv.) and cesium carbonate (5.0 equiv.) in dimethylformamide (2 mL) at room temperature 7-chloro-4-nitrobenzofurazan (NBD-Cl, 1.0 equiv.) was added. The reaction was stirred at room temperature for 24 h. The reaction mixture was concentrated under reduced pressure, and the obtained residue was diluted in a mixture of acetonitrile and water (1:1) and purified by reversed-phase preparative HPLC (C-18, Water:ACN with 0.1% TFA, 30 to 90% ACN). The fractions containing the product were combined and lyophilized to yield the desired product.

### ***Ethyl 2-(5-cyclopropyl-6-(4-fluorobenzyl)picolinamido)-2-ethyl-5-((2-(2-((7-nitrobenzo[*c*]-[1,2,5]oxa-diazol-4-yl)amino)ethoxy)ethyl)thio)pentanoate* (( $\pm$ )-**2.105**)**



Following the general procedure above, ( $\pm$ )-**2.105** was obtained in 49% yield (5 mg) as a dark yellow solid starting from compound ( $\pm$ )-**2.129** (10 mg, 0.02 mmol).

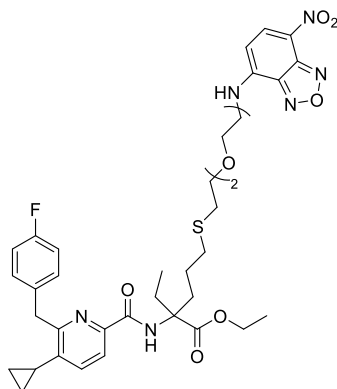
**<sup>1</sup>H NMR** (*cryo* 600 MHz, DMSO-*d*<sub>6</sub>)  $\delta$  ppm 9.41 (s, 1H), 8.69 (s, 1H), 8.50 (d, *J* = 8.9 Hz, 1H), 7.74 (d, *J* = 8.0 Hz, 1H), 7.51 (d, *J* = 8.1 Hz, 1H), 7.34 – 7.29 (m, 2H), 7.11 – 7.06 (m, 2H), 6.44 (d, *J* = 9.0

Hz, 1H), 4.34 (s, 2H), 4.20 (q,  $J = 7.1$  Hz, 2H), 3.70 – 3.63 (m, 4H), 3.51 (t,  $J = 6.7$  Hz, 2H), 2.54 (t,  $J = 6.7$  Hz, 2H), 2.46 – 2.41 (m, 2H), 2.34 – 2.24 (m, 2H), 2.09 – 2.05 (m, 1H), 1.88 – 1.75 (m, 2H), 1.38 – 1.32 (m, 2H), 1.20 (t,  $J = 7.1$  Hz, 4H), 1.10 – 0.96 (m, 2H), 0.70 – 0.64 (m, 4H).

$^{13}\text{C NMR}$  (*cryo* 151 MHz, DMSO- $d_6$ )  $\delta$  ppm 172.8, 162.3, 161.6, 160.0, 158.2, 158.0, 146.1, 145.3, 144.4, 144.1, 140.3, 137.8, 135.0, 134.4, 130.7, 120.9, 119.3, 114.9, 99.5, 70.2, 67.6, 63.6, 61.4, 43.3, 33.4, 31.3, 30.5, 26.6, 23.9, 14.4, 12.1, 8.2, 8.1, 8.0.

**HR-MS** (ESI)  $m/z$   $[\text{M}+\text{Na}]^+$  calcd. for  $\text{C}_{35}\text{H}_{41}\text{FN}_6\text{O}_7\text{S}$ : 731.2634, found 731.2646.

***Ethyl 2-(5-cyclopropyl-6-(4-fluorobenzyl)picolinamido)-2-ethyl-5-((2-(2-(2-((7-nitrobenzo-  
[c][1,2,5]-o-xadiazol-4-yl)amino)ethoxy)ethoxy)ethyl)thio)pentanoate ((±)-2.106)***



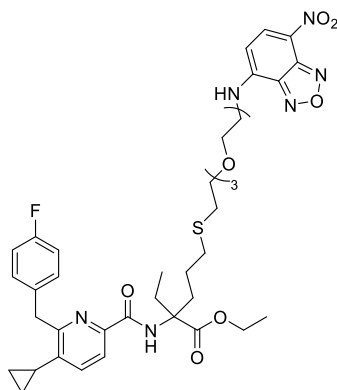
Following the general procedure above, (±)-**2.106** was obtained in 26% yield (3 mg) as a dark yellow solid starting from compound (±)-**2.130** (10 mg, 0.01 mmol).

$^1\text{H NMR}$  (*cryo* 600 MHz, DMSO- $d_6$ )  $\delta$  ppm 9.43 (s, 1H), 8.70 (s, 1H), 8.49 (d,  $J = 9.0$  Hz, 1H), 7.74 (d,  $J = 8.0$  Hz, 1H), 7.51 (d,  $J = 8.0$  Hz, 1H), 7.34 – 7.30 (m, 2H), 7.11 – 7.06 (m, 2H), 6.54 (d,  $J = 9.0$  Hz, 1H), 4.34 (s, 2H), 4.31 (q,  $J = 7.1$  Hz, 2H), 3.69 (t,  $J = 5.3$  Hz, 2H), 3.49 – 3.51 (m, 3H), 3.43 – 3.39 (m, 3H), 2.48 (t,  $J = 6.7$  Hz, 2H), 2.40 – 2.45 (m, 2H), 2.35 – 2.26 (m, 3H), 2.10 – 2.04 (m, 2H), 1.92 – 1.77 (m, 3H), 1.38 – 1.33 (m, 2H), 1.21 (t,  $J = 7.1$  Hz, 3H), 1.01 – 0.96 (m, 2H), 0.70 – 0.65 (m, 4H).

$^{13}\text{C NMR}$  (*cryo* 151 MHz, DMSO- $d_6$ )  $\delta$  ppm 172.8, 162.3, 161.6, 160.0, 158.0, 145.8, 145.3, 144.4, 144.1, 140.3, 137.8, 135.0, 134.4, 130.7, 130.6, 120.8, 119.3, 115.1, 114.9, 99.5, 70.2, 69.8, 69.4, 63.6, 61.4, 43.4, 33.4, 31.3, 30.4, 27.6, 23.9, 14.1, 12.1, 8.1, 8.0.

**HR-MS** (ESI)  $m/z$   $[\text{M}+\text{Na}]^+$  calcd. for  $\text{C}_{37}\text{H}_{45}\text{FN}_6\text{O}_8\text{S}$ : 775.2896, found 775.2911.

***Ethyl 16-(5-cyclopropyl-6-(4-fluorobenzyl)picolinamido)-16-ethyl-1-((7-nitrobenzo[c][1,2,5]-oxa-dia-zol-4-yl)amino)-3,6,9-trioxa-12-thiaheptadecan-17-oate ((±)-2.107)***



Following the general procedure above, (±)-**2.107** was obtained in 49% yield (3 mg) as a dark yellow solid starting from compound (±)-**2.131** (10 mg, 0.01 mmol).

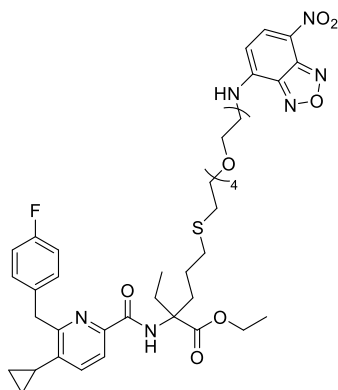
**<sup>1</sup>H NMR** (*cryo* 600 MHz, DMSO-*d*<sub>6</sub>) δ ppm 9.44 (s, 1H), 8.70 (s, 1H), 8.50 (d, *J* = 8.8 Hz, 1H), 7.75 (d, *J* = 8.0 Hz, 1H), 7.51 (d, *J* = 8.0 Hz, 1H), 7.34 – 7.30 (m, 2H), 7.12 – 7.06 (m, 2H), 6.47 (d, *J* = 9.0 Hz, 1H), 4.34 (s, 2H), 4.21 (q, *J* = 7.1 Hz, 2H), 3.70 (t, *J* = 5.3 Hz, 2H), 3.70 – 3.62 (m, 2H), 3.55 – 3.53 (m, 2H), 3.49 – 3.47 (m, 3H), 3.41 – 3.39 (m, 5H), 3.37 – 3.34 (m, 2H), 2.45 (td, *J* = 7.1, 3.0 Hz, 2H), 2.37 – 2.26 (m, 2H), 2.10 – 2.05 (m, 2H), 1.92 – 1.87 (m, 1H), 1.84 – 1.79 (m, 1H), 1.41 – 1.33 (m, 2H), 1.21 (t, *J* = 7.1 Hz, 3H), 1.01 – 0.97 (m, 2H), 0.70 – 0.65 (m, 4H).

**<sup>13</sup>C NMR** (*cryo* 151 MHz, DMSO-*d*<sub>6</sub>) δ ppm 172.8, 162.3, 161.6, 160.0, 158.0, 145.8, 145.3, 144.1, 140.3, 137.8, 135.0, 134.4, 130.7, 130.6, 120.8, 119.3, 115.1, 114.9, 99.5, 70.1, 69.8, 69.7, 69.4, 68.0, 63.6, 61.4, 43.4, 33.4, 31.3, 30.4, 27.6, 23.9, 14.1, 12.1, 8.1, 8.0.

**HR-MS** (ESI) *m/z* [M+Na]<sup>+</sup> calcd. for C<sub>39</sub>H<sub>49</sub>FN<sub>6</sub>O<sub>9</sub>S: 819.3158, found 819.3161.



**Ethyl 19-(5-cyclopropyl-6-(4-fluorobenzyl)picolinamido)-19-ethyl-1-((7-nitrobenzo[c][1,2,5]-oxa-diaz-ol-4-yl)amino)-3,6,9,12-tetraoxa-15-thiaicosan-20-oate ((±)-2.108)**



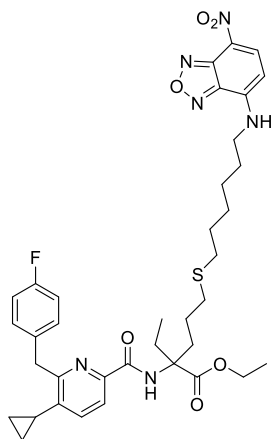
Following the general procedure above, (±)-**2.108** was obtained in 23% yield (3 mg) as a dark yellow solid starting from compound (±)-**2.132** (14 mg, 0.02 mmol).

**<sup>1</sup>H NMR** (*cryo* 600 MHz, DMSO-*d*<sub>6</sub>) δ ppm 9.45 (s, 1H), 8.71 (s, 1H), 8.50 (d, *J* = 9.0 Hz, 1H), 7.75 (d, *J* = 8.0 Hz, 1H), 7.52 (d, *J* = 7.9 Hz, 1H), 7.35 – 7.30 (m, 2H), 7.12 – 7.07 (m, 2H), 6.47 (d, *J* = 9.0 Hz, 1H), 4.34 (s, 2H), 4.21 (q, *J* = 7.1 Hz, 2H), 3.70 (t, *J* = 5.3 Hz, 1H), 3.56 – 3.54 (m, 2H), 3.50 – 3.48 (m, 2H), 3.46 – 3.40 (m, 16H), 3.38 – 3.36 (m, 2H), 2.47 – 2.44 (m, 1H), 2.37 – 2.27 (m, 2H), 2.10 – 2.06 (m, 1H), 1.93 – 1.97 (m, 1H), 1.85 – 1.79 (m, 1H), 1.41 – 1.33 (m, 1H), 1.22 (t, *J* = 7.1 Hz, 3H), 1.03 – 0.95 (m, 2H), 0.72 – 0.64 (m, 4H).

**<sup>13</sup>C NMR** (*cryo* 151 MHz, DMSO-*d*<sub>6</sub>) δ ppm 172.8, 162.3, 161.6, 160.0, 158.0, 145.8, 145.3, 144.4, 144.1, 140.3, 137.8, 135.0, 134.4, 130.7, 130.6, 120.8, 119.3, 115.0, 114.9, 99.5, 70.2, 69.8, 69.7, 69.7, 69.4, 68.0, 63.6, 61.4, 60.2, 43.4, 33.4, 31.3, 30.4, 27.6, 23.9, 14.1, 12.1, 8.2, 8.0.

**HR-MS** (ESI) *m/z* [M+Na]<sup>+</sup> calcd. for C<sub>41</sub>H<sub>53</sub>FN<sub>6</sub>O<sub>10</sub>S: 863.3420, found 863.3483.

***Ethyl 2-(5-cyclopropyl-6-(4-fluorobenzyl)picolinamido)-2-ethyl-5-((6-((7-nitrobenzo[c][1,2,5]oxa-diazol-4-yl)amino)hexyl)thio)pentanoate ((±)-2.109)***



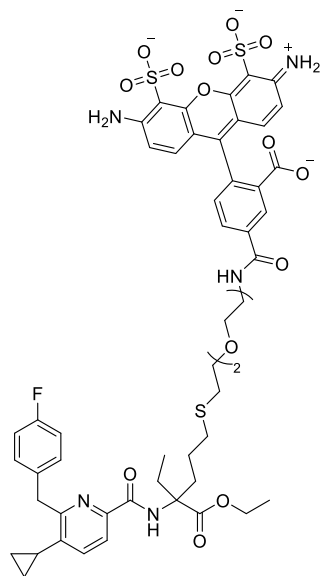
Following the general procedure above, (±)-**2.109** was obtained in 18% yield (2 mg) as a dark yellow solid starting from compound (±)-**2.133** (11 mg, 0.02 mmol).

**<sup>1</sup>H NMR** (*cryo* 600 MHz, DMSO-*d*<sub>6</sub>) δ ppm 9.52 (t, *J* = 5.7 Hz, 1H), 8.72 (s, 1H), 8.50 (d, *J* = 8.9 Hz, 1H), 7.75 (d, *J* = 8.0 Hz, 1H), 7.51 (d, *J* = 8.0 Hz, 1H), 7.35 – 7.31 (m, 2H), 7.11 – 7.06 (m, 2H), 6.38 (d, *J* = 9.0 Hz, 1H), 4.34 (d, *J* = 3.5 Hz, 2H), 4.21 (q, *J* = 7.1 Hz, 2H), 3.42 (q, *J* = 6.8, 6.3 Hz, 2H), 2.40 (t, *J* = 7.1 Hz, 2H), 2.37 – 2.27 (m, 4H), 2.10 – 2.06 (m, 1H), 1.93 – 1.78 (m, 3H), 1.59 – 1.64 (m, 2H), 1.44 – 1.20 (m, 11H), 1.02 – 0.96 (m, 2H), 0.70 – 0.65 (m, 4H).

**<sup>13</sup>C NMR** (*cryo* 151 MHz, DMSO-*d*<sub>6</sub>) δ ppm 172.8, 162.3, 161.6, 160.0, 158.0, 145.8, 145.2, 144.4, 144.1, 140.3, 138.0, 135.0, 134.4, 130.7, 130.6, 120.5, 119.3, 115.0, 114.9, 99.1, 63.6, 61.4, 43.3, 33.4, 30.8, 30.7, 28.9, 27.8, 27.7, 27.5, 25.9, 23.7, 14.1, 12.1, 8.2, 8.1.

**HR-MS** (ESI) *m/z* [M+Na]<sup>+</sup> calcd. for C<sub>37</sub>H<sub>45</sub>FN<sub>6</sub>O<sub>6</sub>S: 743.2998, found 743.3021.

***Ethyl (S)-1-(3,7-bis(dimethylamino)-5,5-dimethyl-3'-oxo-3'H,5H-spiro[dibenzo[b,e]siline-10,1'-iso-benzofuran]-6'-yl)-15-(5-cyclopropyl-6-(4-fluorobenzyl)picolinamido)-15-ethyl-1-oxo-5,8-dioxa-11-thia-2-azahexadecan-16-oate ((±)-2.134)***

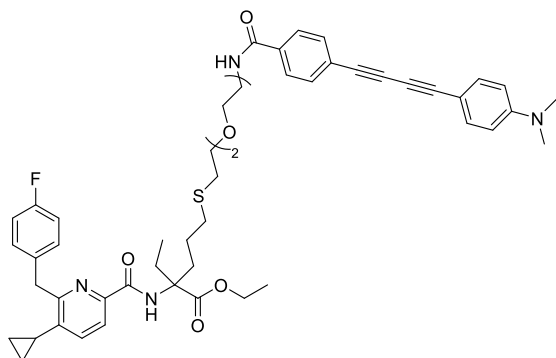


Alexa 488 carboxylic acid tris-triethylammonium salt (2.5 mg, 3.0  $\mu\text{mol}$ ) was dissolved in dimethylformamide (1 ml) and *N,N*-diisopropylethylamine (1  $\mu\text{l}$ , 6.0  $\mu\text{mol}$ ) was added. HATU (1.2 mg, 3.0  $\mu\text{mol}$ ) was added and the solution was stirred at room temperature for 10 min, then ( $\pm$ )-**2.111** (1.8 mg, 3.0  $\mu\text{mol}$ ) was added and stirring was continued for 5 h at room temperature. The mixture was concentrated under reduced pressure and then purified by reversed-phase preparative HPLC (C-18, Water:ACN with 0.1% TFA, 05 to 75% ACN) to yield Alexa 488 conjugate ( $\pm$ )-**2.134** (3.3 mg, 36%) as a purple powder after lyophilization.

Due to the low amount of compound, NMR spectra of probe **2.134** could not be recorded.

**HR-MS** (ESI)  $m/z$   $[\text{M}+\text{H}]^+$  calcd. for  $\text{C}_{52}\text{H}_{57}\text{FN}_5\text{O}_{15}\text{S}_3$ : 1106.2992, found: 1106.2977.

***Ethyl 15-(5-cyclopropyl-6-(4-fluorobenzyl)picolinamido)-1-(4-((4-(dimethylamino)phenyl)buta-1,3-diy-1-yl)phenyl)-15-ethyl-1-oxo-5,8-dioxo-11-thia-2-azahexadecan-16-oate ((±)-2.135)***



Raman emitter 4-((4-(dimethylamino)phenyl)buta-1,3-diy-1-yl)benzoic acid (1.1 mg, 3.8  $\mu\text{mol}$ ) was dissolved in dimethylformamide (400  $\mu\text{L}$ ) and *N,N*-diisopropylethylamine (1.8  $\mu\text{L}$ , 10.2  $\mu\text{mol}$ ) was added. HATU (1.5 mg, 3.8  $\mu\text{mol}$ ) was added and the solution was stirred at room temperature for 10 min, then ( $\pm$ )-**2.111** (1.5 mg, 2.5  $\mu\text{mol}$ ) was added and stirring was continued for 1 h at room temperature. The mixture was concentrated under reduced pressure and then purified by reversed-phase preparative HPLC (C-18, Water:ACN with 0.1% TFA, 25 to 90% ACN) to yield Raman emitter conjugate ( $\pm$ )-**2.135** (0.8 mg, 20%) as an orange powder after lyophilization.

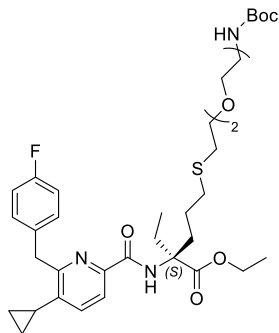
**$^1\text{H NMR}$**  (600 MHz,  $\text{DMSO-}d_6$ )  $\delta$  ppm  $\delta$  8.71 (s, 1H), 8.59 (t,  $J = 5.6$  Hz, 1H), 7.86 (d,  $J = 8.4$  Hz, 2H), 7.76 (d,  $J = 8.0$  Hz, 1H), 7.63 (d,  $J = 8.4$  Hz, 1H), 7.52 (d,  $J = 8.0$  Hz, 1H), 7.41 (d,  $J = 8.9$  Hz, 2H), 7.33 (dd,  $J = 8.6, 5.6$  Hz, 2H), 7.14 – 7.06 (m, 2H), 6.70 (d,  $J = 9.0$  Hz, 2H), 4.35 (s, 2H), 4.21 (q,  $J = 7.1$  Hz, 2H), 3.54 – 3.41 (m, 14H), 2.97 (s, 6H), 2.47 – 2.43 (m, 2H), 2.33 (ddd,  $J = 30.8, 13.8, 6.0$  Hz, 2H), 2.08 (ddd,  $J = 13.7, 8.4, 5.3$  Hz, 1H), 1.94 – 1.78 (m, 2H), 1.41 – 1.32 (m, 1H), 1.31 – 1.18 (m, 6H), 1.03 – 0.94 (m, 2H), 0.69 (dd,  $J = 4.5, 2.4$  Hz, 2H).

**$^{13}\text{C NMR}$**  (151 MHz,  $\text{DMSO-}d_6$ )  $\delta$  ppm 172.8, 165.3, 162.3, 161.6, 160.0, 158.0, 150.9, 145.8, 140.3, 135.0, 134.6, 134.4, 133.7, 132.0, 130.7, 130.6, 127.5, 123.8, 119.3, 114.9, 115.0, 111.8, 105.5, 85.2, 80.4, 76.4, 71.8, 70.1, 69.5, 69.4, 68.8, 67.0, 63.6, 61.4, 40.1, 39.9, 39.8, 39.7, 39.5, 39.4, 39.2, 39.1, 33.4, 31.3, 30.4, 27.6, 23.9, 14.1, 12.1, 8.2, 8.0.

**HR-MS** (ESI)  $m/z$   $[\text{M}+\text{H}]^+$  calcd. for  $\text{C}_{50}\text{H}_{57}\text{FN}_4\text{O}_6\text{S}$ : 861.4056, found: 861.4078.

## 5.2.9. Synthesis of Pyridine-based Enantiomeric Pure Probes

### *Ethyl (S)-18-(5-cyclopropyl-6-(4-fluorobenzyl)picolinamido)-18-ethyl-2,2-dimethyl-4-oxo-3,8,11-tri-oxa-14-thia-5-azanonadecan-19-oate ((S)-2.130)*



Picolinic acid **2.42** (50 mg, 184  $\mu\text{mol}$ ) was dissolved in a mixture of dichloromethane and acetonitrile (1 mL, 1:1, *v/v*). *N,N*-diisopropylethylamine (48  $\mu\text{L}$ , 276  $\mu\text{mol}$ ) and HATU (70 mg, 184  $\mu\text{mol}$ ) were added, and the reaction mixture was stirred at room temperature for 10 min. Afterwards, (*S*)-**2.140** (89 mg, 203  $\mu\text{mol}$ ) dissolved in a mixture of dichloromethane and acetonitrile (1 mL, 1:1, *v/v*) was added and the reaction was stirred at room temperature for 18 h. The solvents were evaporated under reduced pressure and the residue was purified by column chromatography (Silica gel, 4 g, cHex:EtOAc, 10 to 90% EtOAc) to yield (*S*)-**2.130** (105 mg, 82%) as a colorless oil.

**<sup>1</sup>H NMR** (600 MHz,  $\text{CDCl}_3$ )  $\delta$  ppm 9.00 (s, 1 H), 7.89 (d,  $J = 7.9$  Hz, 1 H), 7.39 (m, 1 H), 7.26 (m, 2 H), 6.97 (m, 2 H), 5.00 (bs, 1 H), 4.37 (s, 2 H), 4.33 – 4.23 (m, 2 H), 3.64 – 3.47 (m, 8 H), 3.36 – 3.23 (m, 2 H), 2.67 – 2.62 (m, 2 H), 2.62 – 2.44 (m, 4 H), 2.07 – 1.97 (m, 1 H), 1.95 – 1.83 (m, 2 H), 1.58 (m, 1 H), 1.43 (s, 9 H), 1.33 (t,  $J = 7.1$  Hz, 3 H), 1.32 (m, 1 H), 1.03 – 0.97 (m, 2 H), 0.76 (t,  $J = 7.4$  Hz, 3 H), 0.69 – 0.60 (m, 2 H).

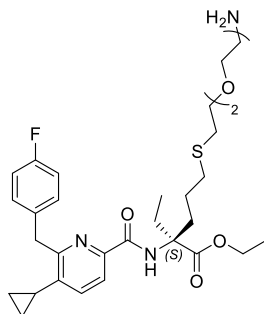
**<sup>13</sup>C NMR** (151 MHz,  $\text{CDCl}_3$ )  $\delta$  ppm 173.7, 163.5, 162.5, 160.9, 158.6, 146.9, 140.0, 134.8, 134.8, 130.6, 130.5, 119.8, 115.4, 115.2, 79.3, 71.0, 70.4, 65.1, 61.9, 40.9, 40.5, 34.6, 32.5, 31.5, 28.6, 28.6, 24.9, 14.5, 12.9, 8.6, 7.9, 7.9.

**HR-MS** (ESI)  $m/z$   $[\text{M}+\text{H}]^+$  calcd. for  $\text{C}_{36}\text{H}_{53}\text{FN}_3\text{O}_7\text{S}$ : 690.3583, found: 690.3586.

$[\alpha]_d^{20} = +6.34^\circ$  ( $c = 1.0$ ,  $\text{CHCl}_3$ ).

The same procedure was applied for the synthesis of (*R*)-**2.130**, which was performed by BENJAMIN BRENNECKE at FMP, Berlin;  $[\alpha]_d^{20} = -6.17^\circ$  ( $c = 1.0$ ,  $\text{CHCl}_3$ ).

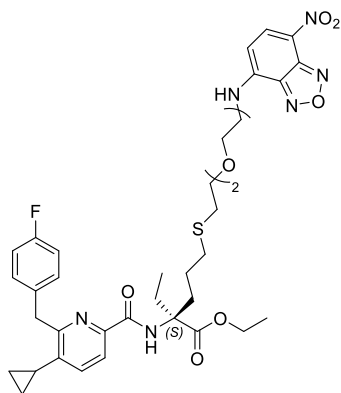
***Ethyl (S)-5-((2-(2-(2-aminoethoxy)ethoxy)ethyl)thio)-2-(5-cyclopropyl-6-(4-fluorobenzyl)picolinamido)-2-ethylpentanoate ((S)-2.111)***



Compound (S)-**2.130** (27 mg, 39  $\mu$ mol) was dissolved in dichloromethane (2 mL) and trifluoroacetic acid (2 mL) was added. The solution was stirred at room temperature for 30 min, then poured into potassium bicarbonate aq. sol. (2 M, 30 mL). The mixture was extracted with ethyl acetate (2x). The combined organic layers were washed with sodium hydroxide aq. sol. (1 M), dried over MgSO<sub>4</sub> and filtered. Evaporation of the solvent under reduced pressure yielded the free amine (S)-**2.111** (28 mg, 97%) as a colorless oil, which was used crude for the subsequent dye conjugation.

The same procedure was applied for the synthesis of (R)-**2.111**, which was performed by BENJAMIN BRENNER at FMP, Berlin.

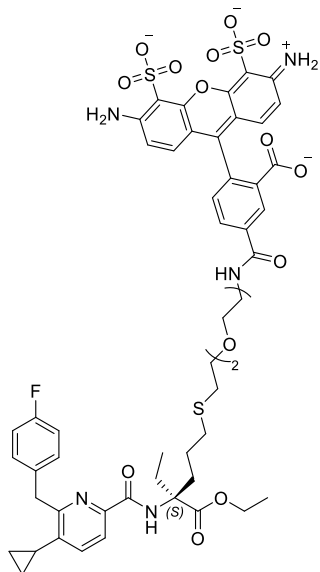
***Ethyl 2-(5-cyclopropyl-6-(4-fluorobenzyl)picolinamido)-2-ethyl-5-((2-(2-(2-((7-nitrobenzo-[1,2,5]-oxadiazol-4-yl)amino)ethoxy)ethoxy)ethyl)thio)pentanoate (NBD-2.106)***



Following the general NBD-labeling procedure described for racemic compound ( $\pm$ )-**2.106**, 2.8 mg of (S)-NBD conjugate **2.106** were obtained (73%) starting from amine (S)-**2.111** (3 mg, 5.1  $\mu$ mol) as a dark yellow solid.

Following the general NBD-labeling procedure described for racemic compound ( $\pm$ )-**2.106**, 4.5 mg of (R)-NBD conjugate **2.106** were obtained (54%) starting from amine (R)-**2.111** (6.2 mg, 11.0  $\mu$ mol).

**Ethyl (S)-1-(3,7-bis(dimethylamino)-5,5-dimethyl-3'-oxo-3'H,5H-spiro[dibenzo[b,e]siline-10, 1'-iso-benzofuran]-6'-yl)-15-(5-cyclopropyl-6-(4-fluorobenzyl)picolinamido)-15-ethyl-1-oxo-5,8-dioxo-11-thia-2-azahexadecan-16-oate** (Alexa 488-**2.134**)



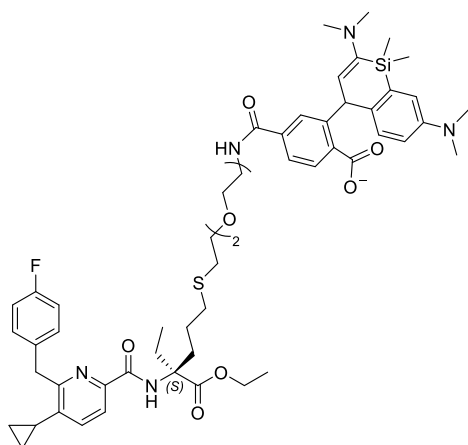
Following the Alexa 488-labeling procedure described for racemic compound ( $\pm$ )-**2.134**, 3.7 mg of (S)-Alexa 488 conjugate **2.134** were obtained (37%) starting from amine (S)-**2.111** (4.1 mg, 7.0  $\mu$ mol) as a purple powder.

NMR spectra of probe **2.134** could not be recorded due to the low amount of compound obtained.

**HR-MS** (ESI)  $m/z$  [M+H]<sup>+</sup> calcd. for C<sub>52</sub>H<sub>57</sub>FN<sub>5</sub>O<sub>15</sub>S<sub>3</sub>: 1106.2992, found: 1106.2986.

**PAMPA assay**: P<sub>eff</sub>: 0 cm/s\*10<sup>-6</sup>, Acceptor: 0%; Membrane: 99.2%; Donor: 0.7%.

***Ethyl (S)-1-(3,7-bis(dimethylamino)-5,5-dimethyl-3'-oxo-3'H,5H-spiro[dibenzo[b,e]siline-10, 1'-iso-benzofuran]-6'-yl)-15-(5-cyclopropyl-6-(4-fluorobenzyl)picolinamido)-15-ethyl-1-oxo-5,8-dioxa-11-thia-2-azahexadecan-16-oate*** (SiR-2.142)



The synthesis of this compound was performed by BENJAMIN BRENNECKE at FMP, Berlin.

Silicon Rhodamine carboxylic acid (5 mg, 10.6  $\mu\text{mol}$ ) was dissolved in acetonitrile (2 mL) and *N,N*-diisopropylethylamine (4  $\mu\text{L}$ , 21.2  $\mu\text{mol}$ ) and HATU (4 mg, 10.6  $\mu\text{mol}$ ) were added successively. The solution was stirred for 5 min, then (*S*)-**2.111** (7 mg, 11.7  $\mu\text{mol}$ ) was added and the reaction was stirred at room temperature for 24 h. The mixture was purified by reversed-phase preparative HPLC (C-18, Water:ACN with 0.1% TFA, 30 to 90% ACN) to yield 8 mg (73%) SiR-(*S*)-**2.142** as blue powder after lyophilization.

**$^1\text{H NMR}$**  (600 MHz,  $\text{CDCl}_3$ )  $\delta$  ppm 9.03 (s, 1 H), 8.02 (d,  $J = 8.0$  Hz, 1 H), 7.94 (dd,  $J = 8.0, 1.4$  Hz, 1 H), 7.86 (d,  $J = 8.0$  Hz, 1 H), 7.75 (d,  $J = 1.4$  Hz, 1 H), 7.37 (d,  $J = 8.0$  Hz, 1H), 7.35 (d,  $J = 2.7$  Hz, 2 H), 7.26 – 7.23 (m, 2 H), 7.10 (bs, 1 H), 7.00 – 6.94 (m, 4 H), 6.90 (m, 2 H), 4.36 (s, 2 H), 4.28 (m, 2 H), 3.65 – 3.51 (m, 10 H), 3.08 (s, 12 H), 2.56 (t,  $J = 6.7$  Hz, 2 H), 2.62 – 2.55 (m, 1 H), 2.52 – 2.40 (m, 3 H), 2.02 – 1.96 (m, 1 H), 1.95 – 1.83 (m, 2 H), 1.61 – 1.49 (m, 1 H), 1.32 (t,  $J = 7.1$  Hz, 3 H), 1.35 – 1.27 (m, 1 H), 1.01 (m, 2 H), 0.75 (t,  $J = 7.4$  Hz, 3 H), 0.70 (s, 3 H), 0.66 (m, 2 H), 0.62 (s, 3 H).

**$^{13}\text{C NMR}$**  (151 MHz,  $\text{CDCl}_3$ )  $\delta$  ppm 173.6, 169.1, 166.3, 163.7, 161.2, 161.0, 160.9, 158.7, 152.7, 147.5, 146.6, 140.3, 140.0, 139.0, 136.5, 134.8, 134.7, 130.6, 130.6, 129.9, 129.0, 127.9, 127.0, 124.4, 121.0, 119.8, 116.9, 115.4, 115.2, 69.6, 70.2, 70.3, 70.9, 65.1, 62.0, 42.8, 40.8, 40.3, 34.5, 32.5, 31.6, 28.7, 24.8, 14.4, 12.9, 8.5, 8.0, 8.0, 1.2, 0.1.

**HR-MS** (ESI)  $m/z$   $[\text{M}+\text{H}]^+$  calcd. for  $\text{C}_{58}\text{H}_{71}\text{FN}_5\text{O}_8\text{SSi}$ : 1044.4771, found: 1044.4814.

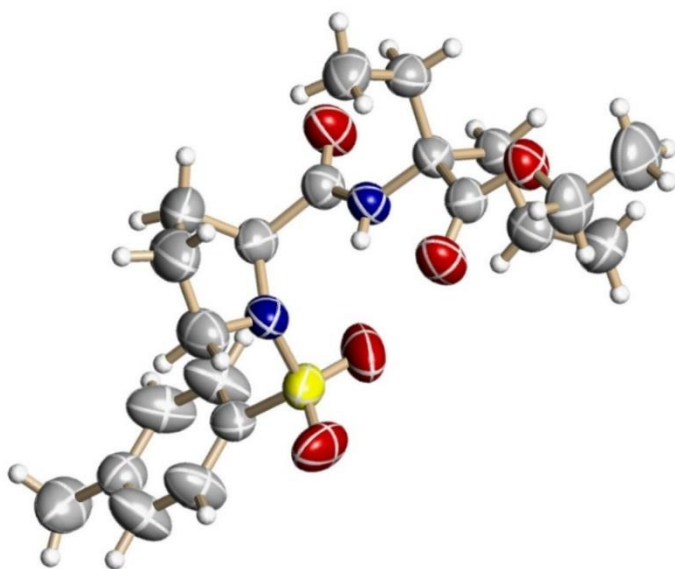


## 5.2.10. Pharmacological Assessment of CB<sub>2</sub>R-Agonist Probes and Fluorescence Imaging Experiments

### 5.2.10.1. X-Ray Crystal Structure of Proline Derivative 2.139

The following experiment were performed by ANDRE ALKER at Hoffmann La-Roche, Basel.

*Ethyl (S)-2-ethyl-2-((R)-1-tosylpyrrolidine-2-carboxamido)pent-4-enoate (2.139)*



Crystals were grown by vapor diffusion using chloroform. A suitable single crystal was mounted in a loop. Data were collected at room temperature on a Synergy-S diffractometer (Rigaku) with Cu-K-alpha-radiation (1.54184Å) and processed with the CrysAlis-package. Structure solution and refinement was performed using the ShelXTL software (Bruker AXS, Karlsruhe).

Formula: C<sub>21</sub>H<sub>31</sub>N<sub>2</sub>O<sub>5</sub>S

Unit Cell Parameters: a 11.8304 (10) Å, b 12.8390 (10) Å, c 15.0869 (10) Å, P2(1)2(1)2(1)

CCDC 1923120 contains the supplementary crystallographic data for this structure. These data can be obtained free of charge from The Cambridge Crystallographic Data Centre via [www.ccdc.cam.ac.uk/structures](http://www.ccdc.cam.ac.uk/structures).

### 5.2.10.2. Molecular Docking

The docking studies were conducted by DR. WOLFGANG GUBA at Hoffmann La-Roche, Basel.

The X-ray structure of active state CB<sub>2</sub>R in complex with agonist AM1203 (PDB 6KPF) was used as template to dock CB<sub>2</sub>R ligands.<sup>[81]</sup> The docking experiments were performed with the software GOLD (Chemical Computing Group) with default settings.<sup>[307]</sup> The best 10 docking poses for each compound were energy-minimized within the binding pocket using MOE (Molecular Operating environment ver. 2014.09, Chemical Computing Group, Montreal, Canada) and examined visually to select the most reasonable docking mode with respect to molecular interactions and internal conformational strain. Finally, the consistency of the selected poses was evaluated using the available structure-activity relationship information.

### 5.2.10.3. Absorption-Emission Spectra of Fluorescent Probes

The following experiments were conducted by SYLWIA HUBER at Hoffmann La-Roche, Basel.

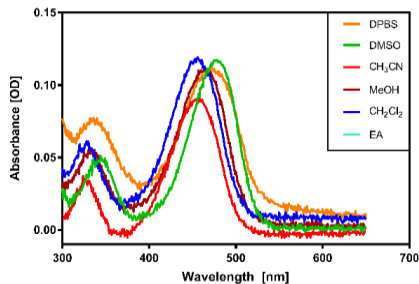
UV/Vis absorbance spectra of 50  $\mu$ M probes **2.106**, **2.134**, **2.141**, and **2.143** in various solvents (see below) were recorded in wavelength range of 250-750 nm to determine the wavelength with the maximal absorbance signal used later for excitation of the compound (1 cm path length, room temperature, scan step 1 nm; Thermo Evolution 600 UV/Vis spectrophotometer, Thermo Electron Scientific Instruments LLC, Madison, WI, USA). Due to the limited solubility of the probes in DPBS, the spectra in DPBS were measured in a cuvette with 10 cm path length at 5  $\mu$ M in presence of 0.1 % (*v/v*) dimethyl sulfoxide. Technical excitation and emission fluorescence spectra (uncorrected for chromatic aberrations) of the fluorescent probes were measured at 10  $\mu$ M compound concentration (20°C, integration time 1s scan step 2 nm, slits 2.4 mm and 2 mm in excitation and emission, respectively; ISS Inc. PC1 fluorometer, Champaign, IL, USA) in organic dimethyl sulfoxide, dichloromethane, acetonitrile, ethyl acetate and methanol, and aqueous solvent DPBS (Dulbecco's phosphate buffered saline). Exceptionally, the spectra in DPBS were measured at 1.0  $\mu$ M in the presence of 0.1 % (*v/v*) dimethyl sulfoxide and then scaled to expected fluorescence signal intensity at concentration of 10  $\mu$ M by multiplication of the signal intensity by factor of 10.

As expected, the observed fluorescence intensity increased with decreasing dielectric constant of the solvents: aqueous solution (PBS,  $\epsilon_{25} = 79.0$ ) < dimethyl sulfoxide ( $\epsilon_{20} = 47$ ) < acetonitrile ( $\epsilon_{20} = 36.64$ )  $\leq$  methanol ( $\epsilon_{25} = 32.6$ ) < dichloromethane ( $\epsilon_{20} = 9.08$ )  $\leq$  ethyl acetate ( $\epsilon_{25} = 6$ ).<sup>[308]</sup> Thus, the fluorescence intensity (quantum yield) of the fluorescence of probes **2.106**, **2.134**, **2.141**, and **2.143** is expected to increase when in close proximity of the cell membrane ( $\epsilon = 3$ ) or when bound to the hydrophobic binding site of CB<sub>2</sub>R. The relatively lower fluorescence intensity values observed for **2.106** (NBD-labeled) and **2.141** (AttoThio12-labeled) in methanol and ethyl acetate, respectively, may indicate on specific solvent effects, but overall the expected trend of increasing of fluorescence signal intensity with reduction of solvent polarity is observed. Overall, the fluorescence features of these probes enable their applications in e.g. tissue imaging for CB<sub>2</sub>R-specific disorders.

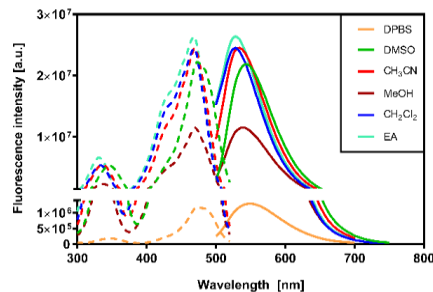
**Supplementary table S-4. Fluorescence excitation and emission wavelengths for fluoroprobes 2.106, 2.134, 2.141, and 2.143 with corresponding fluorescence intensities and Stokes' shifts recorded in distinct solvents.**

Probe	Fluorescence data	DPBS	DMSO	ACN	MeOH	DCM	EtOAc
(±)- <b>2.106</b> (NBD)	Excitation $\lambda$ [nm]	474	478	470	470	468	468
	Emission $\lambda$ [nm]	550	544	534	538	528	528
	Stokes shift [nm]	76	66	64	68	60	60
	Signal intensity *10 <sup>6</sup> [a.u.]	1.2	22.2	24.5	11.5	24.5	26.4
<i>(S)</i> - <b>2.134</b> (Alexa 488)	Excitation $\lambda$ [nm]	494	512	498	494	498	498
	Emission $\lambda$ [nm]	526	540	526	526	526	526
	Stokes shift [nm]	32	28	28	32	28	28
	Signal intensity *10 <sup>6</sup> [a.u.]	64.2	49.9	52.9	70.7	43.2	37.0
<i>(S)</i> - <b>2.141</b> (AttoThio12)	Excitation $\lambda$ [nm]	582	584	574	574	574	574
	Emission $\lambda$ [nm]	610	618	606	606	600	604
	Stokes shift [nm]	28	34	32	32	26	30
	Signal intensity *10 <sup>6</sup> [a.u.]	11.4	12.2	17.5	13.7	20.0	9.6
<i>(S)</i> - <b>2.143</b> (Cy5.5)	Excitation $\lambda$ [nm]	n.t.	690	690	690	690	690
	Emission $\lambda$ [nm]	n.t.	730	707	710	722	714
	Stokes shift [nm]	n.a.	40	17	20	32	24
	Signal intensity *10 <sup>6</sup> [a.u.]	n.t.	2.7	3.1	2.2	2.9	3.4

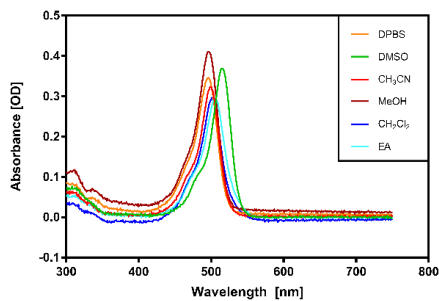
A) UV-Vis spectra of ( $\pm$ )-**2.106** (NBD)



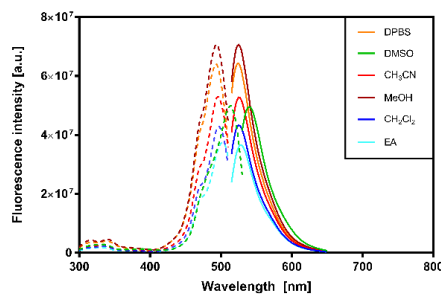
B) Fluorescence spectra of ( $\pm$ )-**2.106** (NBD)



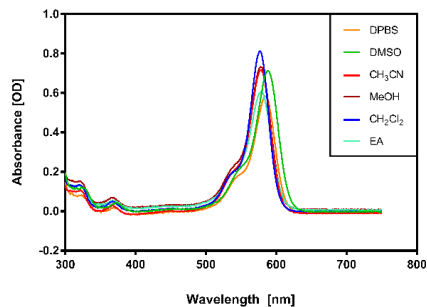
C) UV-Vis spectra of **2.134** (Alexa 488)



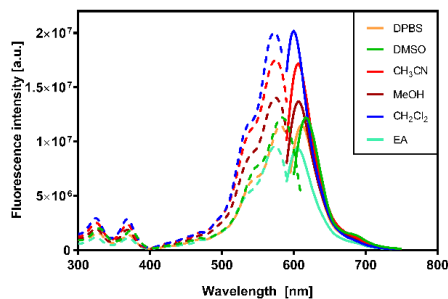
D) Fluorescence spectra of **2.134** (Alexa 488)



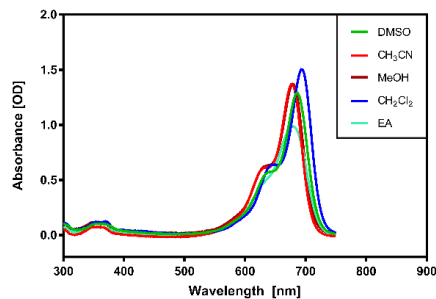
E) UV-Vis spectra of **2.141** (AttoThio12)



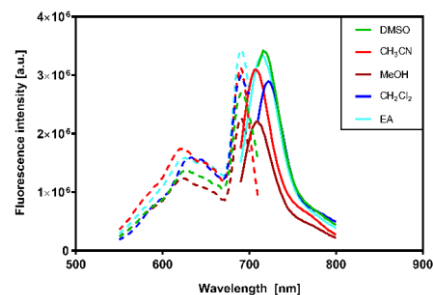
F) Fluorescence spectra of **2.141** (AttoThio12)



G) UV-Vis spectra of **2.143** (Cy5.5)



H) Fluorescence spectra of **2.143** (Cy5.5)



**Supplementary figure S-2. Solution spectra of compounds NBD-2.106 (A and B), Alexa 488-2.134 (C and D), AttoThio12-2.141 (E and F), and Cy5.5-2.143 (G and H).** A), C), E) and G) UV-Vis spectra (50  $\mu$ M probe for A, C and G; 10  $\mu$ M probe for E). B), D), F) and H) technical excitation and emission fluorescence spectra not corrected for chromatic aberrations (10  $\mu$ M probe) in indicated organic solvents and aqueous solution. Excitation and emission spectra are depicted with dashed or solid lines, respectively.

#### 5.2.10.4. *In vitro* Pharmacology and ADME Profile

The binding affinity ( $K_i$ ) of all compounds reported in this thesis were determined by ELISABETH ZIRWES and the cAMP functional assays ( $EC_{50}$ ) of these compounds were performed by ANJA OSTERWALD, both at Hoffmann La-Roche, Basel.

##### *Radioligand binding assay and cAMP assay*

Radioligand binding assays and forskolin-stimulated cAMP assays were performed as described by Soethoudt *et al.*<sup>[194]</sup> CHO-DUKX\_HOMSA\_CNR2\_Clone\_90\_CRE-Luc, CHO-DUKX\_HOMSA\_CNR1\_Clone\_20\_CRE-Luc, and CHO-K1\_MUSMU\_CNR2\_beta\_arrestin (DiscoverX #93-0472C2) cells were cultured and membranes for radioligand binding assays were prepared in analogy to Soethoudt *et al.*<sup>[194]</sup> Excluding the culturing step, mouse brain\_140603 membranes were prepared using the same protocol (protein concentration: 2290  $\mu\text{g}/\text{ml}$ ,  $K_D$ : 8.291 nM,  $B_{\text{max}}$ : 9.67 pmol/ mg protein).  $K_i$  measurements were performed using 0.3 nM 3H-CP55'940 (**SI-6**) radioligand for hCB<sub>1</sub>R, hCB<sub>2</sub>R and mCB<sub>2</sub>R and 1.5 nM 3H- **SI-6** radioligand for mCB<sub>1</sub>R. Reference compounds for binding and cAMP assays were selected in accordance to literature.<sup>[194]</sup> The corresponding mean  $K_i$  and  $EC_{50}$  values, as well as standard error of the mean (SEM), are stated below. Data are means from one or two independent experiments performed in triplicate.

hCB<sub>2</sub>R  $K_i$ : the mean  $K_i$  value of the positive control JWH133 (**2.145**) used for each run was 34.9 nM and standard error of the mean (SEM) for this standard compound was  $\pm 3.4$  nM (n=128).

hCB<sub>1</sub>R  $K_i$ : the mean  $K_i$  value of the positive control Rimonabant (**SI-5**) used for each run was 2.8 nM and standard error of the mean (SEM) for this standard compound was  $\pm 0.2$  nM (n=105).

mCB<sub>2</sub>R  $K_i$ : the mean  $K_i$  value of the positive control WIN55212-2 (**SI-3**) used for each run was 5.8 nM and standard error of the mean (SEM) for this standard compound was  $\pm 1.3$  nM (n=57).

hCB<sub>2</sub>R, mCB<sub>2</sub>R, and hCB<sub>1</sub>R cAMP  $EC_{50}$ : the mean  $EC_{50}$  value of the positive control CP55,940 (**SI-6**) used for each run were 0.08 nM, 0.05 nM and 0.11 nM, respectively, and standard error of the mean (SEM) for this standard compound was  $\pm 0.011$  nM (n=114),  $\pm 0.007$  nM (n=94), and  $\pm 0.013$  nM (n=95), respectively.

The chemical structures of reference compounds JWH133 (**2.145**, CB<sub>2</sub>R selective agonist), Rimonabant (**SI-5**, CB<sub>1</sub>R selective agonist), WIN55212-2 (**SI-3**, non-selective agonist) and CP55,940 (**SI-6**, non-selective agonist) are shown in Supplementary figure S-1, Section 5.2.1.

Lipophilicity (logD), kinetic solubility and PAMPA assays were prepared and carried out as described in literature.<sup>[194]</sup>

#### 5.2.10.5. Fluorescence Assays: FACS, TR-FRET, and Confocal Imaging

##### FACS Assay

The following experiments were performed by DR. CLAUDIA KORN at Hoffmann La-Roche, Basel.

##### General procedure for FACS in hCB<sub>2</sub>R-overexpressing CHO cells

For the validation of CB<sub>2</sub>R-selective fluoroprobes via FACS analysis, 50'000 WT-CHO (wildtype), or CHO cells overexpressing hCB<sub>2</sub>R, mCB<sub>2</sub>R, or hCB<sub>1</sub>R were incubated with different concentrations of CB<sub>2</sub>R-agonist probes (0.005 μM – 10 μM) in PBS/0.5% BSA/2 mM EDTA for 30 min at 4 °C. For cold ligand replacement experiments, 50'000 WT-CHO cells or CHO cells overexpressing hCB<sub>2</sub>R were pre-incubated with 10 μM JWH133 (**2.145**) or RO6851228 (**2.146**) (*see* Supplementary figure S-1, Section 5.2.1. for chemical structures) in PBS/0.5% BSA/2 mM EDTA at room temperature. After 30 min, different concentrations of probe Alexa 488-**2.134** were added to the cell suspensions (5 nM – 370 nM) and cells were incubated for another 30 min at 4 °C. In both experiments, after probe incubation, cells were washed 3 times with PBS/0.5% BSA/2 mM EDTA and re-suspended in PBS/0.5% BSA/2 mM EDTA containing 1:1000 AquaZombie (Biolegend 423102). After exclusion of dead cells, mean fluorescent intensity of viable cells was determined. Data are presented in mean ± SEM from a representative of 3-5 experiments.

## **TR-FRET Assay**

The following experiments were performed by DR. DAVID SYKES at The University of Nottingham, Nottingham.

### **General procedure for TR-FRET assay**

Cell culture: Cells were maintained under classical cell culture conditions in a humidified environment at 37 °C and 5% CO<sub>2</sub> in Dulbecco's modified Eagle's medium (DMEM) with 10% fetal bovine serum (FBS) containing blasticidin (5 µg/ml; Invitrogen) and Zeocin (20 µg/ml; Invitrogen). For inducible expression, SNAP-tagged hCB<sub>2</sub>R cDNAs, in pcDNA4/TO were introduced through transfection, using PEI into HEK293-TR cells (Invitrogen, which express Tet repressor protein to allow inducible expression). A mixed population stable line was selected by resistance to blasticidin (TR vector, 5 µg/ml) and Zeocin; (receptor plasmid, 20 µg/ml). For receptor-inducible expression, cells were seeded into t175 cm<sup>2</sup> flasks, grown to 70% confluence and DMEM containing 1 µg/ml tetracycline added. 24h later cells were labelled with SNAP-Lumi4-Tb (CisBio) and membranes prepared as described in detail below.

Terbium labeling of SNAP-tagged CB<sub>2</sub>R HEK293-TR cells: Cell culture medium was removed from the t175 cm<sup>2</sup> flasks containing confluent adherent CB<sub>2</sub>R HEK293-TR cells. Cells were washed once in PBS (GIBCO Carlsbad, CA) and once in Tag-lite labeling medium (LABMED, CisBio) to remove the excess cell culture media, then ten milliliter of LABMED containing 100 nM of SNAP-Lumi4-Tb was added to the flask and incubated for 1 h at 37 °C under 5% CO<sub>2</sub>. Cells were washed once in PBS (GIBCO Carlsbad, CA) to remove the excess of SNAP-Lumi4-Tb then detached using 5 ml of GIBCO enzyme-free Hank's-based cell dissociation buffer (GIBCO, Carlsbad, CA) and collected in a vial containing 5 ml of DMEM (Sigma-Aldrich) supplemented with 10% fetal calf serum. Cells were pelleted by centrifugation (5 min at 1500 rpm) and the pellets were frozen to -80 °C. To prepare membranes, homogenization steps were conducted at 4 °C (to avoid receptor degradation) as described by Herenbrink *et al.*<sup>[309]</sup>

Fluorescent ligand-binding assays: All fluorescent ligand binding experiments were conducted in white 384-well Optiplate plates, in assay binding buffer LABMED (Cisbio, Codolet, France) containing 5mM HEPES, 0.5% BSA, 0.02% pluronic acid pH 7.4, and 100 µM GppNHp. GppNHp prevents G protein binding to GPCRs and was included to remove the G protein-coupled population of receptors

that can result in two distinct populations of binding sites in membrane preparations, since the Motulsky-Mahan model is only appropriate for ligands competing at a single site. In all cases, nonspecific binding was determined by the presence of 1  $\mu$ M SR144528 (**2.20**). Data are presented in mean  $\pm$  SEM from a representative of 3-8 experiments.

Determination of fluorescent ligand binding kinetics and equilibrium affinity: To accurately determine association rate ( $k_{on}$ ) and dissociation rate ( $k_{off}$ ) values, the observed rate of association ( $k_{obs}$ ) was calculated using at least five different concentrations fluorescent ligand. The appropriate concentration of fluorescent ligand binding was incubated with human CB<sub>2</sub>R HEK293-TR cell membranes (4  $\mu$ g per well) in assay binding buffer (final assay volume, 40  $\mu$ L). The degree of fluorescent ligand bound to the receptor was assessed at multiple time points by HTRF detection to allow construction of association kinetic curves. The resulting data were globally fitted to the association kinetic model (Eq. 1, *see* signal detection and data analysis section below) to derive a single best-fit estimate for  $k_{on}$  and  $k_{off}$  as described under data analysis. Fluorescent probe  $K_d$  values were determined through saturation analysis. The appropriate concentration of fluorescent ligand binding was incubated with hCB<sub>2</sub>R HEK293-TR cell membranes (4  $\mu$ g per well) in assay binding buffer (final assay volume: 40  $\mu$ L) performed at equilibrium, by simultaneously fitting total and nonspecific (NSB) binding data (Eq. 2, *see* signal detection and data analysis section below) allowing the determination of fluorescent ligand binding affinity.

Determination of ligand binding kinetics: To determine the association and dissociation rates of CB<sub>2</sub>R specific ligands, we used a competition-association binding assay.<sup>[310]</sup> This approach involves the simultaneous addition of both fluorescent ligand and competitor to the receptor preparation so that at  $t = 0$  all receptors are unoccupied. To achieve this aim HEK293 cell membranes containing hCB<sub>2</sub>R (4  $\mu$ g per well) were added to wells containing 62.5 nM NBD-**2.106** or 150 nM Alexa 488-**2.134**, concentrations which avoid ligand depletion in the assay volume, and a fixed concentration of modulators SR144528 (**2.20**) or HU308 (**2.28**), designed to produce approximately 50% inhibition of probe binding, in a total assay volume of 40  $\mu$ L. The degree of fluorescent ligand bound to the receptor was assessed at multiple time points by HTRF detection. The kinetic parameters of fluorescent ligands NBD-**2.106** and Alexa 488-**2.134**, plus those of unlabeled compounds, were determined using a start time of  $\sim$ 30 s and an interval time of 20 s. Non-specific binding was determined as the amount of HTRF signal detected in the presence of **2.20** (1 $\mu$ M) and was subtracted from each time point, meaning that the signal at  $t = 0$  was always equal to zero. Each time point was conducted on the same



384-well plate incubated at room temperature with orbital mixing (1 sec of 100 RPM/cycle). Data were globally fitted using Eq. 3 (see below) to simultaneously calculate  $k_{on}$  and  $k_{off}$  of unlabelled compounds.

Competition binding: To determine the affinity of CB<sub>2</sub>R-specific ligands, a simple competition kinetic binding assay was used. This approach involved the simultaneous addition of both fluorescent ligand and competitor to the CB<sub>2</sub>R preparation. 62.5 nM NBD-**2.106** or 150 nM Alexa 488-**2.134**, concentrations which avoid ligand depletion in the assay volume, were added simultaneously with increasing concentrations of the unlabeled compound to CB<sub>2</sub>R cell membranes (4 µg per well) in 40 µL of assay buffer in a 384-well plate incubated at room temperature with orbital mixing. The degree of fluorescent ligand bound to the receptor was assessed at equilibrium by HTRF detection. Nonspecific binding was determined as the amount of HTRF signal detected in the presence of **2.20** (1 µM) and was subtracted from total binding, to calculate specific binding for construction of IC<sub>50</sub> curves. Data were fitted to Eq. 4 to calculate IC<sub>50</sub> estimates which were converted to K<sub>i</sub> values using the Cheng-Prusoff correction Eq. 5.

Signal detection and data analysis: Signal detection was performed on a Pherastar FSX (BMG Labtech, Offenburg, Germany). The terbium donor was always excited with eight laser flashes at a wavelength of 337 nm. TR-FRET signals were collected at 520 (acceptor) and 620 nm when using the green acceptor fluorescent ligands (±)-NBD-**2.106** and Alexa 488 (R)-**2.134**.

HTRF ratios were obtained by dividing the acceptor signal by the donor signal and multiplying this value by 10<sup>7</sup>000. All experiments were analyzed by non-regression using Prism 8.0 (GraphPad Software, San Diego, USA).

Fluorescent ligand association data were fitted as follows to a global fitting model using GraphPad Prism 8.0 to simultaneously calculate  $k_{on}$  and  $k_{off}$  using the following equation,

$$k_{ob} = [L]*k_{on} + k_{off} \quad (\text{Eq. 1})$$

$$Y = Y_{max}*(1-\exp(-1*k_{ob}*X))$$

Where,  $k_{ob}$  equals the observed rate of ligand association and  $k_{on}$  and  $k_{off}$  are the association and dissociation-rate constants respectively of the fluorescent ligand. In this globally fitted model of tracer binding, tracer concentrations [L] are fixed,  $k_{on}$  and  $k_{off}$  are shared parameters whilst  $k_{ob}$  is allowed to vary. Here, Y is the level of receptor-bound tracer, Y<sub>max</sub> is the level of tracer binding at equilibrium, X is in units of time (eg., min) and  $k_{ob}$  is the rate in which equilibrium is approached (eg., min<sup>-1</sup>).

Saturation binding data were analyzed by non-linear regression according to a one-site equation by globally fitting total and nonspecific binding (NSB). Individual estimates for the fluorescent ligand dissociation constant ( $K_d$ ) were calculated using the following equations where L is the fluorescent ligand concentration:

$$\text{Total Binding} = \text{Specific} + \text{NSB} = \frac{B_{\max} \cdot [L]}{K_d + [L]} + \text{slope}[L] + \text{background} \quad (\text{Eq. 2})$$

$$\text{NSB} = \text{Slope}[L] + \text{background}$$

Fitting the total and NSB data sets globally (simultaneously), sharing the value of slope, provides one best-fit value for both the  $K_d$  and the  $B_{\max}$ .

Association and dissociation rates for unlabeled compounds were calculated using the following equations first described by Motulsky and Mahan:<sup>[310]</sup>

$$K_A = k_1[L] + k_2 \quad (\text{Eq. 3})$$

$$K_B = k_3[I] + k_4$$

$$S = \sqrt{((K_A - K_B)^2 + 4 \cdot K_1 K_3 \cdot L \cdot I \cdot 10^{-18})}$$

$$K_F = 0.5(k_A + k_B + S)$$

$$K_S = 0.5(k_A + k_B - S)$$

$$Q = \frac{B_{\max} \cdot K_1 \cdot L \cdot 10^{-9}}{K_F - K_S}$$

$$Y = Q \left( \frac{K_4(K_F - K_S)}{K_F \cdot K_S} \right) + \frac{K_4 - K_F}{K_F} \exp(-K_F \cdot X) - \frac{K_4 \cdot K_S}{K_S} \exp(-K_S \cdot X)$$

Where: X = Time (min), Y = Specific binding (eg. HTRF units, HTRF ratio 520nm/620nm\*10,000),  $k_1 = k_{on}$  tracer ( $M^{-1}min^{-1}$ ),  $k_2 = k_{off}$  tracer ( $min^{-1}$ ), L = Concentration of tracer used (nM), I = Concentration unlabeled ligand (nM). Fixing the above parameters allows the following to be calculated:  $k_3 =$  Association-rate constant of unlabeled ligand ( $M^{-1}min^{-1}$ ),  $k_4 =$  Dissociation-rate constant of unlabeled ligand ( $min^{-1}$ ),  $B_{\max} =$  Maximal specific binding of the system at equilibrium binding (eg. HTRF units, HTRF ratio 520nm/620nm\*10,000).

Competition displacement binding data were fitted to sigmoidal (variable slope) curves using a “four-parameter logistic equation”:

$$Y = \text{Bottom} + (\text{Top}-\text{Bottom}) / (1 + 10^{(\log IC_{50} - X) \cdot \text{Hill coefficient}}) \quad (\text{Eq. 4})$$

IC<sub>50</sub> values obtained from the inhibition curves were converted to K<sub>i</sub> values using the method of Cheng and Prusoff:<sup>[311]</sup>

$$K_i = IC_{50}/(1+[fluorescent\ tracer\ concentration]/K_d) \quad (\text{Eq. 5})$$

### **Time-lapse confocal microscopy and Airyscan high-resolution imaging**

The following experiments were performed by DR. SERGIO ODDI at The University of Teramo, Teramo.

#### **General procedure for imaging acquisition**

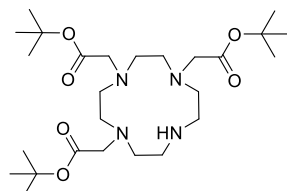
To minimize receptor internalization and, thus, to maximize the signal on the plasma membrane, confocal imaging experiments were performed at 22 °C. For real-time labelling studies, cells were plated onto 8-well chamber slides (Ibidi, Milan, Italy), at a density of 20'000 cells/well and cultured for 24 h. For a nuclear staining, the medium was replaced by 1 µg/mL Hoechst 33342 in RPMI (Sigma-Aldrich, Milan, Italy) and the cells were incubated for 10 min at 37 °C, then washed with PBS twice. A small volume of SiR-**2.142**, dissolved at 10 mM in DMSO, was mixed with the 20% (*w/v*) Pluronic F-127 stock solution in DMSO (Sigma-Aldrich) at a ratio of 1:1 immediately before use. Prior to imaging, the solution of **2.142** and Pluronic F-127 was diluted at 0.4 µM in HEPES-buffered RPMI and quickly added to the cells without any washing step. SiR-**2.142** was excited using a 640 nm laser line and the corresponding fluorescence emission was detected using a 655 nm long-pass filter, whereas Hoechst 33342 was excited with a dedicated 405 nm UV diode, and the corresponding fluorescence emission was detected using a 490/40 nm band-pass filter. Images within each experiment were collected by using identical laser-power, offset, and gain setting that was adjusted to minimize the level of auto-fluorescence under 640 nm. Live imaging was performed at 22 ± 2 °C by recording one frame every 15 sec for 10 min. At the end of recording session, living cells were imaged using the Airyscan mode. Each image was taken at the equatorial plan of the cells, using the ZEN Blue 2.3 software (Zeiss). Super-resolution image processing was performed using the Airyscan processing toolbox within the ZEN software package. The data were exported as TIFF files and analyzed using the Fiji software (National Institutes of Health; <https://imagej.net/Fiji>). A Gaussian kernel filter was applied to the images using a standard deviation of 0.8 pixels. All intensity profiles were background subtracted and normalized to the frame taken at the end of registration. For

presentation purposes, images were exported in Artstudio Pro version 2.0.13 (Lucky Clan, Lodz, Poland; <http://www.luckyclan.com>) for adjustments of brightness and contrast.

### 5.3. To “Development of a DOTA-based Clickable Platform for Pancreatic Cancer Imaging”

#### 5.3.1. Synthesis of DOTA Building Blocks

##### *Tri-tert-butyl 2,2',2''-(1,4,7,10-tetraazacyclododecane-1,4,7-triyl)triacetate (3.15)*

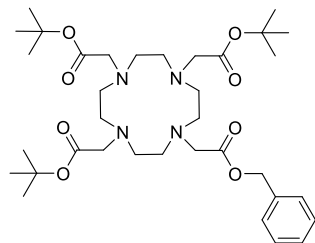


A suspension of cyclen **3.10** (1.0 g, 5.80 mmol) and sodium acetate (1.6 g, 19.0 mmol) in dimethylacetamide (12 mL) was stirred at  $-20\text{ }^{\circ}\text{C}$ . To this suspension, a solution of *tert*-butyl bromoacetate (2.8 mL, 19.1 mmol) in dimethylacetamide (4 mL) was added dropwise over a period of 30 min. The temperature was maintained at  $-20\text{ }^{\circ}\text{C}$  during the addition. After which, the reaction mixture was allowed to warm slowly to room temperature. After 20 hours of vigorous stirring, the reaction mixture was poured into water (60 mL), which gave a clear solution. Subsequent portion wise addition of potassium bicarbonate (3.0 g, 30.0 mmol) stimulated the precipitation of compound **3.15** to a white solid. The precipitate was collected by filtration and dissolved in chloroform (50 mL). The organic solution was washed with water (20 mL), dried over  $\text{MgSO}_4$ , filtered and concentrated under reduced pressure to about 15 mL. Addition of ethyl ether (50 mL) led to crystallization of compound **3.15** to a white fluffy solid (2.7 g, 90%).

$^1\text{H NMR}$  (300 MHz,  $\text{CDCl}_3$ )  $\delta$  ppm 3.37 (s, 4H), 3.29 (s, 2H), 3.10 (t,  $J = 4.7\text{ Hz}$ , 3H), 2.99 – 2.80 (m, 10H), 1.66 (s, 4H), 1.46 (s, 27H).

The analytical data are in accordance with those reported in the literature.<sup>[269]</sup>

***2,2',2''-(10-(2-Oxo-2-phenylethyl)-1,4,7,10-tetraazacyclododecane-1,4,7-triyl)triacetic acid***  
**(3.21)**

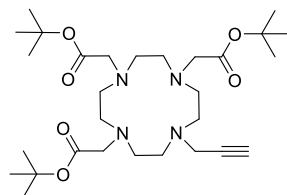


To a suspension of compound **3.15** (2.0 g, 3.88 mmol) in acetonitrile (20 mL), potassium carbonate (0.8 g, 5.82 mmol) and subsequently benzyl bromoacetate (0.7 mL, 4.66 mmol) were added. The reaction was vigorously stirred at room temperature for 15 h. The precipitated solids were removed by filtration, and the filtrate was concentrated under reduced pressure to give the crude product, which was purified by column chromatography (Silica gel, 15 g, DCM:MeOH, 0 to 10% MeOH) to afford *tert*-butyl analog **3.21** in 88% yield (2.3 g) as a light yellow oil.

**<sup>1</sup>H NMR** (300 MHz, CDCl<sub>3</sub>) δ ppm 7.32 – 7.27 (m, 1H), 7.26 – 7.20 (m, 3H), 5.08 (dd, *J* = 16.0, 3.2 Hz, 2H), 3.61 – 3.53 (m, 1H), 3.34 (s, 11H), 3.18 – 2.57 (m, 13H), 1.45 – 1.26 (m, 27H).

The analytical data are in accordance with those reported in the literature.<sup>[261a]</sup>

### ***Tri-carboxylic acid DOTAM alkyne (3.22)***

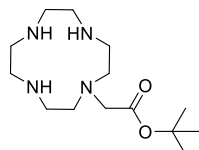


To a solution of **3.15** (1.6 g, 2.91 mmol) in acetonitrile (60 mL) was added potassium carbonate (1.0 g, 7.35 mmol) and the suspension was stirred for 20 min. The solution was placed in an ice-bath and propargyl bromide (0.35 mL, 2.92 mmol) was added dropwise. The ice-bath was removed, and the reaction was allowed to reach room temperature and stirred over night at room temperature. Inorganic solids were removed by filtration, and the filtrate was concentrated under reduced pressure to give the crude product. Purification by column chromatography (Silica gel, 4 g, DCM:MeOH, 5 to 15% MeOH) was performed to yield *t*-butyl protected **3.22** as a colorless solid (1.5 g, 91%).

**<sup>1</sup>H NMR** (300 MHz, CDCl<sub>3</sub>) δ ppm 3.92 (d, *J* = 41.7 Hz, 2H), 3.46 (d, *J* = 9.2 Hz, 2H), 3.39 – 3.25 (m, 3H), 3.24 – 2.98 (m, 8H), 2.94 – 2.21 (m, 9H), 2.17 – 2.11 (m, 1H), 1.50 – 1.40 (m, 27H), 1.24 (s, 2H).

The analytical data are in accordance with those reported in the literature.<sup>[274d]</sup>

### ***Tert-butyl 2-(1,4,7,10-tetraazacyclododecan-1-yl)acetate (3.23)***

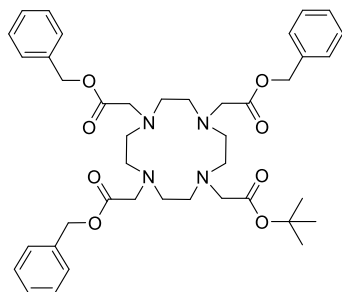


To a stirring solution of cyclen **3.10** (3.4 g, 20.0 mmol) in chloroform (40 mL) at 0 °C *tert*-butyl bromoacetate (1.5 mL, 10.0 mmol) in chloroform (10 mL) was slowly added (1 h). Stirring was continued for additional 3 hours, and the reaction mixture was concentrated under reduced pressure. Subsequently, the crude residue was purified by reversed-phase column chromatography (C-18, 30 g, Water:MeOH with 0.1% triethylamine, 25 to 90% MeOH) to yield the title compound **3.23** in 51% yield (2.9 g) as a white solid.

**<sup>1</sup>H NMR** (300 MHz, DMSO-*d*<sub>6</sub>) δ ppm 3.22 (s, 2H), 2.78 – 2.52 (m, 16H), 2.48 – 2.41 (m, 3H), 1.41 (s, 9H).

The analytical data are in accordance with those reported in the literature.<sup>[261a]</sup>

***Tribenzyl 2,2',2''-(10-(2-(tert-butoxy)-2-oxoethyl)-1,4,7,10-tetraazacyclododecane-1,4,7-triyl)-triaceta-te (3.24)***



A suspension of compound **3.23** (100 mg, 0.35 mmol) and potassium carbonate (134 mg, 0.97 mmol) in acetonitrile (7 mL) was purged with nitrogen. To this suspension, a solution of benzyl bromoacetate (0.2 mL, 1.40 mmol) in acetonitrile (3 mL) was added dropwise at room temperature. The reaction mixture was stirred at room temperature for 8 h. Afterwards, the crude mixture was filtered and concentrated under reduced pressure. The crude material was diluted with dichloromethane (10 mL), washed with water (3x), and brine (3x), dried over MgSO<sub>4</sub>, and concentrated under reduced pressure. The crude material was purified by column chromatography (Silica gel, 4 g, DCM:MeOH, 0 to 4% MeOH) to afford the title compound **3.24** in 91% yield as a colorless oil (232 mg).

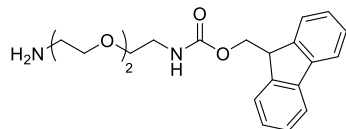
<sup>1</sup>H NMR (300 MHz, CDCl<sub>3</sub>) δ ppm δ 7.38 – 7.27 (m, 15H), 5.23 – 5.02 (m, 6H), 3.88 – 1.69 (m, 25H), 1.44 (s, 9H).

The analytical data are in accordance with those reported in the literature.<sup>[261a]</sup>



### 5.3.2. Synthesis of Linker Building Blocks

#### *(9H-Fluoren-9-yl)methyl (2-(2-(2-aminoethoxy)ethoxy)ethyl)carbamate (3.26)*



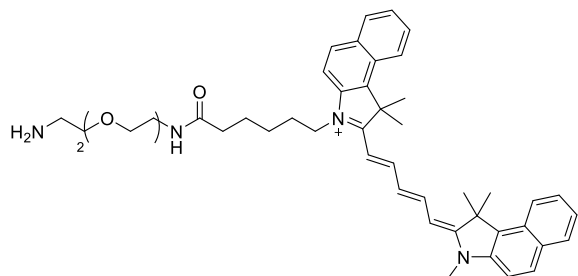
9-Fluorenylmethyl chloroformate (228 mg, 0.88 mmol) was added to a solution of *N*-Boc-1,2-bis(2-aminoethoxy)ethane **3.25** (200 mg, 0.80 mmol) dissolved in a mixture of 1,4-dioxane and sodium carbonate aq. sol. (15% *w/w*, 2.5 mL, 1:1, *v/v*), and the reaction mixture was stirred at room temperature. After 3 h, the reaction mixture was diluted with chloroform (5 mL), and washed with water (1x), hydrochloric acid aq. sol. (1M, 1x) and brine (1x). The organic layer was dried over MgSO<sub>4</sub>, filtered and evaporated under reduced pressure. The crude residue was purified by column chromatography (Silica gel, 15 g, DCM:MeOH, 3% MeOH) to afford *N*-Boc protected compound **3.26** in 74% yield (278 mg) as a colorless oil.

<sup>1</sup>H NMR (300 MHz, CDCl<sub>3</sub>) δ ppm 7.75 (d, *J* = 7.5 Hz, 2H), 7.60 (d, *J* = 7.4 Hz, 2H), 7.39 (td, *J* = 7.5, 1.2 Hz, 2H), 7.30 (td, *J* = 7.5, 1.3 Hz, 2H), 5.45 (s, 1H), 5.15 – 4.98 (m, 1H), 4.41 (d, *J* = 7.0 Hz, 2H), 4.22 (t, *J* = 7.0 Hz, 1H), 3.67 – 3.46 (m, 7H), 3.39 (q, *J* = 5.3 Hz, 2H), 3.30 (q, *J* = 5.2 Hz, 2H), 1.43 (s, 9H).

The analytical data are in accordance with those reported in the literature.<sup>[312]</sup>

Subsequently, *N*-Boc protected **3.26** (278 mg, 0.58 mmol) was dissolved in dichloromethane (3 mL) and trifluoroacetic acid (3 mL) was slowly added to the solution. The reaction mixture was stirred at room temperature for 2 h to complete conversion to product. Afterwards, the solvent was removed under reduced pressure, and co-evaporated with toluene (3x) to yield free amine **3.26** as a white solid (quant.). The residue was directly used as a trifluoroacetic acid salt for the next reaction step, without the need of further purification.

**3-(6-((2-(2-(2-Aminoethoxy)ethoxy)ethyl)amino)-6-oxohexyl)-1,1-dimethyl-2-((1E,3E,5E)-5-(1,1,3-tri-methyl-1,3-dihydro-2H-benzo[e]indol-2-ylidene)penta-1,3-dien-1-yl)-1H-benzo[e]indol-3-ium (3.27)**



Cyanine 5.5 carboxylic acid (20 mg, 0.03 mmol), HATU (13 mg, 0.03 mmol), and *N,N*-diisopropylethylamine (18  $\mu$ L, 0.10 mmol) were dissolved in dimethylformamide (2 mL) at room temperature under nitrogen atmosphere. After 10 min, *N*-Boc-1,2-bis(2-aminoethoxy)ethane **3.25** (8.5 mg, 0.03 mmol) in dimethylformamide (1 mL) was added to the reaction mixture and stirred for 30 min at room temperature. After completion, the reaction mixture was concentrated under reduced pressure, taken up in a mixture of acetonitrile and water (1:1) and purified by reversed-phase preparative HPLC (C-18, Water:ACN with 0.1% TFA, 30 to 95% ACN). The fractions containing product were combined and lyophilized to yield *tert*-butyl protected **3.27** in 62% yield (17 mg) as a blue powder.

<sup>1</sup>H NMR (600 MHz, DMSO-*d*<sub>6</sub>)  $\delta$  ppm 8.45 (t, *J* = 13.1 Hz, 2H), 8.25 (dd, *J* = 8.5, 3.2 Hz, 2H), 8.12 – 8.03 (m, 3H), 7.82 – 7.65 (m, 5H), 7.51 (t, *J* = 7.5 Hz, 2H), 6.73 (t, *J* = 5.7 Hz, 1H), 6.62 (t, *J* = 12.3 Hz, 1H), 6.34 (dd, *J* = 24.0, 13.8 Hz, 2H), 4.22 (t, *J* = 7.4 Hz, 2H), 3.73 (s, 3H), 3.34 (td, *J* = 6.1, 3.7 Hz, 7H), 3.15 (q, *J* = 5.9 Hz, 2H), 3.04 (q, *J* = 6.1 Hz, 2H), 2.07 (t, *J* = 7.3 Hz, 2H), 1.96 (d, *J* = 3.3 Hz, 13H), 1.78 – 1.71 (m, 2H), 1.56 (p, *J* = 7.3 Hz, 2H), 1.39 (dt, *J* = 11.8, 6.9 Hz, 2H), 1.34 (s, 9H).

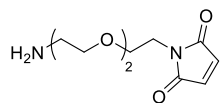
<sup>13</sup>C NMR (151 MHz, DMSO-*d*<sub>6</sub>)  $\delta$  ppm 174.3, 171.9, 157.5, 155.7, 155.6, 152.8, 140.4, 139.7, 133.1, 131.3, 130.3, 130.2, 129.9, 127.7, 127.6, 127.5, 125.5, 124.7, 122.1, 122.1, 111.6, 103.1, 102.8, 87.1, 84.6, 77.6, 69.5, 69.4, 69.1, 50.7, 39.9, 39.8, 39.7, 39.5, 39.4, 39.2, 39.1, 38.4, 35.0, 31.5, 28.2, 27.0, 26.8, 26.6, 25.7, 24.9.

HR-MS (ESI) *m/z* [M+2] calcd. for C<sub>51</sub>H<sub>66</sub>N<sub>4</sub>O<sub>5</sub>: 407.2511, found 407.2460.

Subsequently, *tert*-butyl protected **3.27** (17 mg, 0.02 mmol) was dissolved in dichloromethane (0.2 mL) and trifluoroacetic acid (0.2 mL) was slowly added to the solution. The reaction mixture was stirred at room temperature for 2 h to complete conversion to product. Afterwards, the solvent was removed under reduced pressure, and co-evaporated with toluene (3x) to yield free amine **3.27** as a blue solid

(quant.). The residue was directly used as a trifluoroacetic acid salt for the next reaction step, without the need of further purification.

***1-(2-(2-(2-Aminoethoxy)ethoxy)ethyl)-1H-pyrrole-2,5-dione (3.28)***



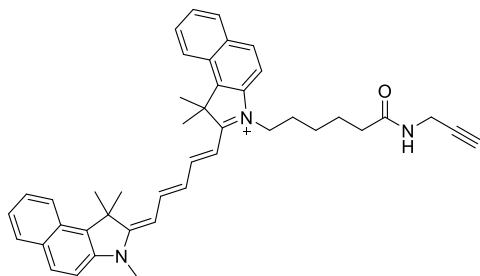
*N*-Boc-1,2-bis(2-aminoethoxy)ethane **3.25** (500 mg, 2.01 mmol) was dissolved in sodium bicarbonate sat. sol. and cooled to 0 °C. The activated maleimide (methyl 2,5-dioxo-2,5-dihydro-1H-pyrrole-1-carboxylate, 344 mg, 2.21 mmol) was added. The reaction mixture was stirred at 0 °C for 1 h, and then at room temperature for 45 min. The mixture was extracted with chloroform (3x) and the combined organic phases were dried over MgSO<sub>4</sub>, filtered over celite, and concentrated under reduced pressure. The crude residue was purified by column chromatography (Silica gel, 15 g, DCM:MeOH, 4% MeOH) to afford *N*-Boc protected compound **3.28** as a colorless oil in 80% yield (527 mg).

<sup>1</sup>H NMR (300 MHz, CDCl<sub>3</sub>) δ ppm 6.68 (s, 2H), 5.02 (s, 1H), 3.73 – 3.67 (m, 2H), 3.63 – 3.43 (m, 8H), 3.25 (t, *J* = 5.2 Hz, 2H), 1.40 (s, 9H).

The analytical data are in accordance with those reported in the literature.<sup>[313]</sup>

Subsequently, *tert*-butyl protected **3.28** (500 mg, 1.52 mmol) was dissolved in dichloromethane (5 mL) and trifluoroacetic acid (5 mL) was slowly added to the solution. The reaction mixture was stirred at room temperature for 2 h to complete conversion to product. Afterwards, the solvent was removed under reduced pressure, and co-evaporated with toluene (3x) to yield free amine **3.28** as a light yellow oil (quant.). The residue was directly used as a trifluoroacetic acid salt for the next reaction step, without the need of further purification.

**1,1-Dimethyl-3-(6-oxo-6-(prop-2-yn-1-ylamino)hexyl)-2-((1E,3E,5E)-5-(1,1,3-trimethyl-1,3-dihydro-2H-benzo[e]indol-2-ylidene)penta-1,3-dien-1-yl)-1H-benzo[e]indol-3-ium (3.59)**



Cyanine 5.5 carboxylic acid (20 mg, 0.03 mmol), HATU (13 mg, 0.03 mmol), and *N,N*-diisopropylethylamine (18  $\mu$ L, 0.10 mmol) were dissolved in dimethylformamide (2 mL) at room temperature under nitrogen atmosphere. After 10 min, propargyl amine (38 mg, 0.03 mmol) in dimethylformamide (1 mL) was added to the reaction mixture and stirred for 30 min at room temperature. After completion, the reaction mixture was concentrated under reduced pressure, taken up in a mixture of acetonitrile and water (1:1) and purified by reversed-phase preparative HPLC (C-18, Water:ACN with 0.1% TFA, 30 to 90% ACN). The fractions containing product were combined and lyophilized to yield the title compound **3.59** in 93% yield (20 mg) as a blue powder.

**<sup>1</sup>H NMR** (600 MHz, DMSO-*d*<sub>6</sub>)  $\delta$  ppm 8.46 (t, *J* = 13.2 Hz, 2H), 8.31 – 8.19 (m, 3H), 8.12 – 8.05 (m, 4H), 7.79 – 7.72 (m, 2H), 7.71 – 7.67 (m, 2H), 7.52 (t, *J* = 7.5 Hz, 2H), 6.64 (t, *J* = 12.2 Hz, 1H), 6.36 (dd, *J* = 22.3, 14.1 Hz, 2H), 4.26 – 4.21 (m, 2H), 3.85 – 3.81 (m, 2H), 3.75 (s, 2H), 3.06 (s, 1H), 2.09 (s, 3H), 1.97 (s, 12H), 1.76 (t, *J* = 7.9 Hz, 2H), 1.61 – 1.53 (m, 2H), 1.44 – 1.38 (m, 2H).

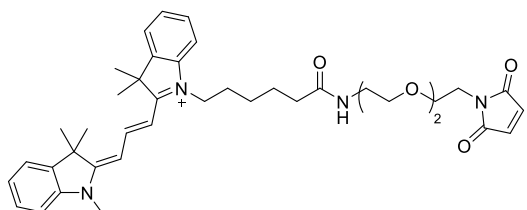
**<sup>13</sup>C NMR** (151 MHz, DMSO-*d*<sub>6</sub>)  $\delta$  ppm 174.3, 173.5, 171.6, 152.8, 140.4, 139.7, 133.1, 133.0, 131.3, 131.2, 130.3, 130.2, 129.9, 127.7, 127.6, 127.5, 125.5, 124.7, 122.1, 122.1, 111.6, 103.1, 102.8, 81.3, 72.8, 50.7, 43.4, 39.9, 39.8, 39.7, 39.5, 39.4, 39.2, 39.1, 34.8, 31.5, 30.7, 27.7, 26.9, 26.8, 26.6, 25.7, 24.7.

**HR-MS** (ESI)  $m/z$  [M+2] calcd. for C<sub>43</sub>H<sub>47</sub>N<sub>3</sub>O: 310.6854, found 310.6835.

### **General procedure for maleimide-PEG-dye constructs**

Cy3 or Cy5.5 carboxylic acid (1 equiv., 0.05 mmol), HATU (1 equiv.) and *N,N*-diisopropylethylamine (3 equiv.) were dissolved in ACN (4 mL). After 10 min, maleimide-PEG2 linker **3.28** (1 equiv.) dissolved in ACN (1 mL) was added to the reaction mixture and stirred at room temperature for 30 min. Afterwards, the reaction mixture was directly purified by reversed-phase preparative HPLC (C-18, Water:ACN with 0.1% TFA, 30 to 95% ACN). The fractions containing product were combined and lyophilized to yield the desired product.

### ***1-(6-((2-(2-(2-(2,5-Dioxo-2,5-dihydro-1H-pyrrol-1-yl)ethoxy)ethoxy)ethyl)amino)-6-oxohexyl)-3,3-dimethyl-2-((E)-3-((E)-1,3,3-trimethylindolin-2-ylidene)prop-1-en-1-yl)-3H-indol-1-ium (3.29)***



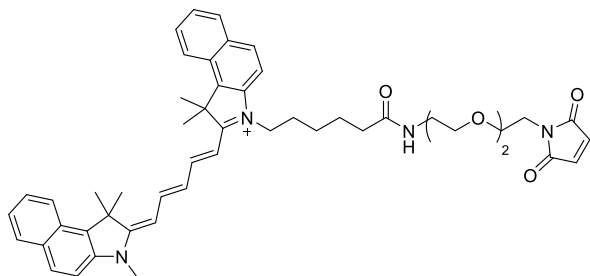
Following the general procedure described above, linker **3.29** was obtained in 74% yield (24 mg) starting from Cy3 carboxylic acid (23 mg, 0.05 mmol).

**<sup>1</sup>H NMR** (300 MHz, CDCl<sub>3</sub>) δ ppm 8.38 (t, *J* = 13.4 Hz, 1H), 7.45 – 7.33 (m, 5H), 7.28 (s, 1H), 7.23 (s, 1H), 7.18 – 7.06 (m, 2H), 6.90 (s, 1H), 6.71 (s, 1H), 6.65 – 6.46 (m, 2H), 4.06 (q, *J* = 7.8 Hz, 2H), 3.75 – 3.38 (m, 13H), 2.49 (t, *J* = 6.8 Hz, 1H), 2.29 (t, *J* = 7.3 Hz, 1H), 1.91 – 1.78 (m, 2H), 1.72 (s, 15H), 1.64 – 1.44 (m, 3H).

**<sup>13</sup>C NMR** (75 MHz, CDCl<sub>3</sub>) δ ppm 175.2, 174.9, 174.6, 174.1, 173.8, 170.9, 150.7, 142.8, 142.1, 140.7, 140.5, 134.5, 129.1, 125.7, 125.6, 125.5, 122.4, 122.3, 122.2, 122.1, 118.5, 114.6, 111.2, 111.0, 110.9, 104.5, 104.1, 103.8, 103.6, 70.3, 70.0, 69.9, 68.0, 49.2, 49.2, 49.2, 49.1, 44.6, 44.4, 39.2, 37.3, 36.1, 34.3, 31.7, 31.5, 28.3, 28.2, 28.1, 27.2, 26.4, 26.0, 25.4.

**HR-MS** (ESI) *m/z* [M]<sup>+</sup> calcd. for C<sub>40</sub>H<sub>51</sub>N<sub>4</sub>O<sub>5</sub>: 667.3854, found 667.3820.

**3-(6-((2-(2-(2-(2,5-Dioxo-2,5-dihydro-1H-pyrrol-1-yl)ethoxy)ethoxy)ethyl)amino)-6-oxohexyl)-1,1-dimethyl-2-((1E,3E,5E)-5-(1,1,3-trimethyl-1,3-dihydro-2H-benzo[e]indol-2-ylidene)penta-1,3-dien-1-yl)-1H-benzo[e]indol-3-ium (3.30)**



Following the general procedure described above, linker **3.30** was obtained in 55% yield (23 mg) starting from Cy5.5 carboxylic acid (30 mg, 0.07 mmol).

**<sup>1</sup>H NMR** (600 MHz, DMSO-*d*<sub>6</sub>)  $\delta$  ppm 8.46 (t, *J* = 13.1 Hz, 2H), 8.26 (dd, *J* = 8.8, 4.1 Hz, 2H), 8.13 – 8.03 (m, 4H), 7.79 – 7.72 (m, 2H), 7.69 (t, *J* = 7.7 Hz, 2H), 7.52 (t, *J* = 7.5 Hz, 2H), 7.00 (s, 2H), 6.63 (t, *J* = 12.3 Hz, 1H), 6.35 (dd, *J* = 25.4, 13.8 Hz, 2H), 4.23 (t, *J* = 7.5 Hz, 2H), 3.74 (s, 3H), 3.55 – 3.53 (m, 2H), 3.51 – 3.48 (m, 2H), 3.47 – 3.44 (m, 2H), 3.41 – 3.39 (m, 2H), 3.31 (t, *J* = 6.0 Hz, 2H), 3.16 – 3.12 (m, 2H), 2.07 (s, 3H), 1.97 (s, 12H), 1.79 – 1.72 (m, 2H), 1.60 – 1.54 (m, 2H), 1.42 – 1.36 (m, 2H).

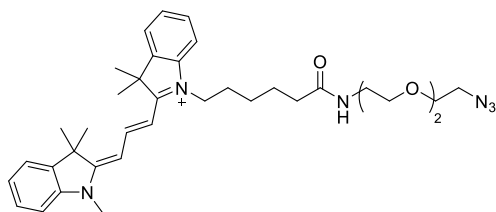
**<sup>13</sup>C NMR** (151 MHz, DMSO-*d*<sub>6</sub>)  $\delta$  ppm 174.3, 173.5, 171.9, 170.8, 164.2, 157.8, 152.8, 143.7, 140.4, 139.7, 134.5, 133.0, 133.0, 131.3, 131.2, 130.3, 130.2, 129.9, 127.7, 127.6, 127.5, 125.5, 124.7, 122.1, 122.1, 118.0, 111.6, 103.1, 102.8, 69.4, 69.3, 69.1, 66.9, 50.7, 43.4, 40.0, 39.8, 39.7, 39.5, 39.4, 39.2, 39.1, 38.4, 36.7, 35.0, 31.5, 27.0, 26.8, 26.6, 25.7, 24.9.

**HR-MS** (ESI) *m/z* [M]<sup>+</sup> calcd. for C<sub>50</sub>H<sub>57</sub>N<sub>4</sub>O<sub>5</sub>: 793.4323, found 793.4352.

### **General procedure for PEG azide-dye construct**

Cy3 or Cy5.5 carboxylic acid (1 equiv., 0.07 mmol), HATU (1 equiv.) and *N,N*-diisopropylethylamine (3 equiv.) were dissolved in ACN (4 mL). After 10 min, azido-PEG2 linker **3.31** (1.2 equiv.) dissolved in ACN (1 mL) was added to the reaction mixture and stirred at room temperature for 30 min. Afterwards, the reaction mixture was purified by reversed-phase preparative HPLC (C-18, Water:ACN with 0.1% TFA, 30 to 90% ACN). The fractions containing product were combined and lyophilized to yield the desired product.

### ***1-(6-((2-(2-(2-Azidoethoxy)ethoxy)ethyl)amino)-6-oxohexyl)-3,3-dimethyl-2-((E)-3-((E)-1,3,3-trimethylindolin-2-ylidene)prop-1-en-1-yl)-3H-indol-1-ium* (3.32)**



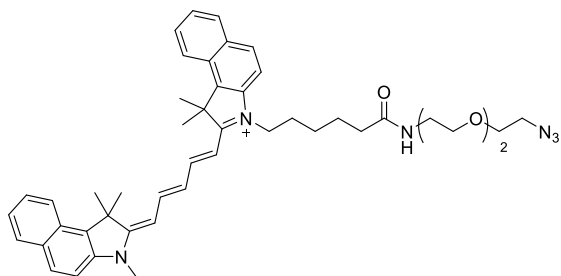
Following the general procedure described above, linker **3.32** was obtained in 63% yield (26 mg) starting from Cy3 carboxylic acid (30 mg, 0.07 mmol).

**<sup>1</sup>H NMR** (300 MHz, CDCl<sub>3</sub>) δ ppm 8.39 (t, *J* = 13.5 Hz, 1H), 7.46 – 7.32 (m, 4H), 7.30 – 7.27 (m, 1H), 7.25 – 7.23 (m, 1H), 7.13 (dd, *J* = 8.0, 4.0 Hz, 2H), 6.74 – 6.53 (m, 3H), 4.07 (t, *J* = 7.8 Hz, 2H), 3.71 – 3.60 (m, 8H), 3.59 – 3.53 (m, 2H), 3.49 – 3.36 (m, 4H), 3.22 (s, 4H), 2.28 (t, *J* = 7.3 Hz, 2H), 1.88 – 1.77 (m, 2H), 1.75 – 1.69 (m, 12H), 1.61 – 1.48 (m, 2H).

**<sup>13</sup>C NMR** (75 MHz, CDCl<sub>3</sub>) δ ppm 174.6, 174.1, 173.8, 142.8, 142.7, 140.6, 140.5, 129.1, 128.9, 125.6, 124.2, 122.2, 122.1, 111.2, 111.0, 104.2, 103.9, 101.2, 1000.0, 97.6, 83.4, 70.6, 70.4, 70.1, 69.9, 66.1, 62.1, 50.8, 50.6, 49.3, 49.1, 44.6, 39.2, 36.3, 34.7, 31.5, 28.2, 28.2, 27.2, 26.5, 25.4.

**HR-MS** (ESI) *m/z* [M]<sup>+</sup> calcd. for C<sub>36</sub>H<sub>50</sub>N<sub>6</sub>O<sub>3</sub>: 615.3970, found 615.3983.

**3-(6-((2-(2-(2-Azidoethoxy)ethoxy)ethyl)amino)-6-oxohexyl)-1,1-dimethyl-2-((1E,3E,5E)-5-(1,1,3-trimethyl-1,3-dihydro-2H-benzo[e]indol-2-ylidene)penta-1,3-dien-1-yl)-1H-benzo[e]indol-3-ium (3.33)**



Following the general procedure described above, linker **3.33** was obtained in 79% yield (43 mg) starting from Cy5.5 carboxylic acid (42 mg, 0.07 mmol).

**<sup>1</sup>H NMR** (600 MHz, DMSO-*d*<sub>6</sub>) δ ppm 8.46 (t, *J* = 13.1 Hz, 2H), 8.30 – 8.23 (m, 2H), 8.14 – 8.04 (m, 4H), 7.83 – 7.65 (m, 5H), 7.52 (t, *J* = 7.5 Hz, 2H), 6.63 (t, *J* = 12.2 Hz, 1H), 6.35 (dd, *J* = 23.7, 13.8 Hz, 2H), 4.23 (t, *J* = 7.5 Hz, 2H), 3.74 (s, 4H), 3.59 – 3.56 (m, 2H), 3.55 – 3.51 (m, 2H), 3.50 – 3.46 (m, 2H), 3.40 – 3.33 (m, 4H), 3.17 (q, *J* = 5.9 Hz, 2H), 2.08 (t, *J* = 7.3 Hz, 2H), 2.03 – 1.92 (m, 11H), 1.79 – 1.72 (m, 2H), 1.60 – 1.53 (m, 2H), 1.43 – 1.36 (m, 2H).

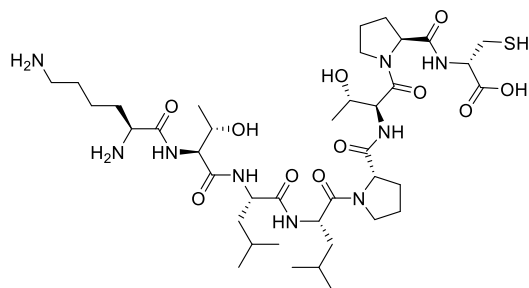
**<sup>13</sup>C NMR** (151 MHz, DMSO-*d*<sub>6</sub>) δ ppm 174.3, 173.5, 171.9, 158.0, 157.7, 152.8, 140.4, 139.7, 133.0, 133.0, 131.3, 131.2, 130.3, 130.2, 129.9, 127.7, 127.6, 127.5, 125.5, 124.7, 122.1, 122.1, 111.6, 103.1, 102.8, 69.6, 69.5, 69.2, 50.7, 50.0, 43.4, 38.4, 35.0, 31.5, 31.5, 29.4, 27.0, 26.8, 26.6, 25.7, 24.9.

**HR-MS** (ESI) *m/z* [M]<sup>+</sup> calcd. for C<sub>46</sub>H<sub>56</sub>N<sub>6</sub>O<sub>3</sub>: 740.4408, found 740.4338.



### 5.3.3. Plectin-1 Targeting Peptide Deprotection Procedure

#### *L-lysyl-L-threonyl-L-leucyl-L-leucyl-L-prolyl-L-threonyl-L-prolyl-L-cysteine* (Cys-3.4)



The crude PTP sequence **3.4** (200 mg, 0.14 mmol) was dissolved in a fresh prepared deprotection cocktail (10 mL, composed by trifluoroacetic acid (94%), water (2.5%), dithiothreitol (DTT, 2.5%) and triisopropyl silane (TIPS, 1%), purged with nitrogen and stirred at room temperature for 20 h. After full conversion to product, the crude mixture concentrated under reduced pressure and co-evaporated with toluene (2x). The crude powder was taken up in a mixture of acetonitrile and water (1:1) and purified by reversed-phase preparative HPLC (C-18, Water:ACN with 0.1% TFA, 10 to 60% ACN, 220 nm). The fractions containing product were combined and lyophilized to yield the title compound **3.4** as a white powder (77 mg, 64%).

**HR-MS** (ESI)  $m/z$   $[M+H]^+$ ,  $[M+2H]^{+2}$  calcd. for  $C_{39}H_{69}N_9O_{11}S$ :  $[M+H]^+$  872.4910, found 872.5027;  $[M+2H]^{+2}$  436.7491, found 436.7552.

### 5.3.4. Synthesis of Monovalent Control Probes

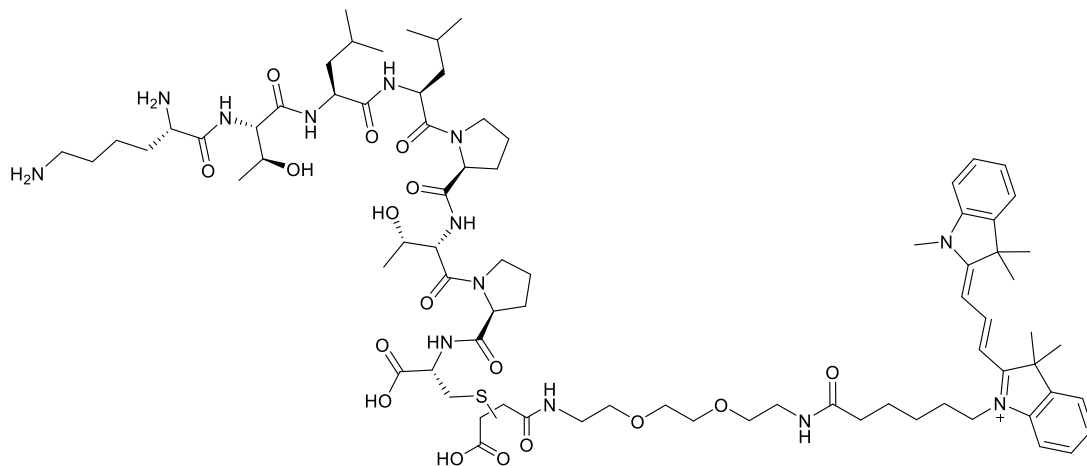
#### General procedure

A mixture of maleimide-linker-dye construct **3.29** or **3.30** (1.0 equiv.) and ligand (1.3 equiv.) was stirred in volatile triethylammonium acetate buffer pH=5.0 (1 mL) and acetonitrile (0.3 mL) at room temperature for 20 h. The completion of the reaction was monitored by LC-MS, where quantitative conversion to product was seen. Subsequently, the reaction mixture was filtered and directly purified by reversed-phase preparative HPLC (C-18, Water:ACN with 0.1% TFA, 15 to 75% ACN, 220 nm detection). The fractions containing product were lyophilized to give compounds **3.34** to **3.39**.

Afterward, intermediates **3.34** to **3.39** (1 equiv.) were stirred at room temperature in a mixture of volatile ammonium carbonate buffer pH 8.9 and water (1:1, *v/v*, 1.5 mL). Hydrolysis of succinimide

rings was observed after 12 h of stirring at room temperature. After completion, the reaction mixture was lyophilized to deliver quantitative yield of the desired products **3.40** to **3.45**.

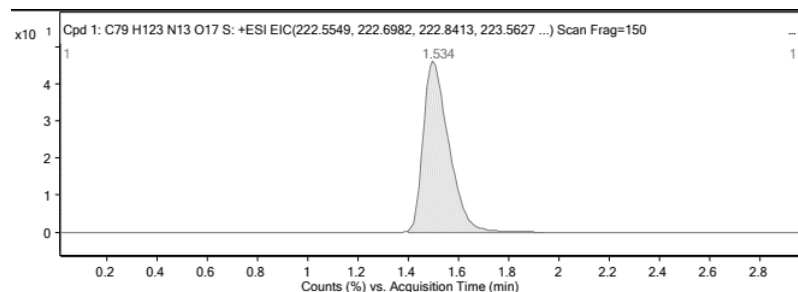
**1-((3S,6R)-1-((S)-1-(L-lysyl-L-allothroonyl-L-leucyl-L-leucyl-L-prolyl-L-threonyl)pyrrolidin-2-yl)-3,6-dicarboxy-1,8,19-trioxo-12,15-dioxo-5-thia-2,9,18-triazatetracosan-24-yl)-3,3-dimethyl-2-((E)-3-((E)-1,3,3-trimethylindolin-2-ylidene)prop-1-en-1-yl)-3H-indol-1-ium (3.40)**



Following the general procedure described above, compound **3.40** was obtained in 25% yield (3.5 mg) as a pink powder starting from maleimide-PEG2-Cy3 **3.29** (8.5 mg, 0.01 mmol) and Cys-PTP-**3.4** (KTLLPTPC, 4.3 mg, 0.006 mmol).

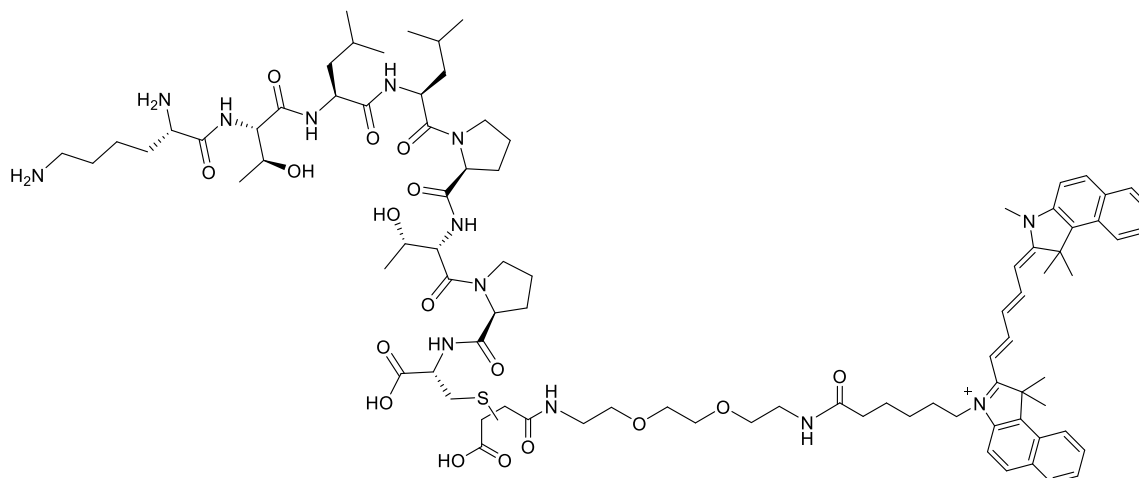
**3.34** (*succinimide precursor*): **HR-MS** (ESI)  $m/z$  [M+2] calcd. for C<sub>79</sub>H<sub>121</sub>N<sub>13</sub>O<sub>16</sub>S: 769.9382, found 769.9348.

**3.40**: **HR-MS** (ESI)  $m/z$  [M+2], [M+3H]<sup>+3</sup> calcd. for C<sub>79</sub>H<sub>123</sub>N<sub>13</sub>O<sub>17</sub>S: [M+2] 778.9435, found 778.9526; [M+3H]<sup>+3</sup> 520.3033, found 520.3062.



Supplementary figure S-3. HR-MS trace (+ ESI) of purified compound **3.40**.

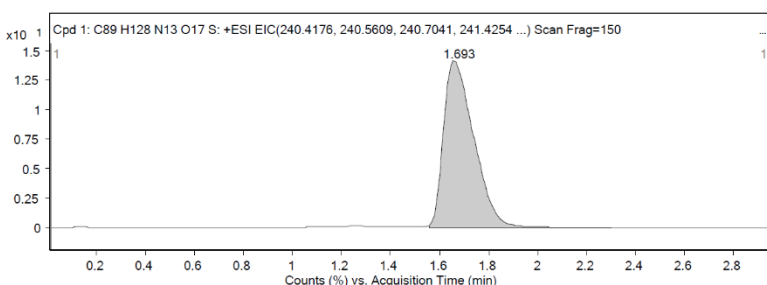
**3-((3*S*,6*R*)-1-((*S*)-1-(*L*-lysyl-*L*-allothreonyl-*L*-leucyl-*L*-leucyl-*L*-prolyl-*L*-threonyl)pyrrolidin-2-yl)-3,6-dicarb-oxy-1,8,19-trioxo-12,15-dioxa-5-thia-2,9,18-triazatetracosan-24-yl)-1,1-dimethyl-2-((1*E*,3*E*,5*E*)-5-(1,1,3-trimethyl-1,3-dihydro-2*H*-benzo[*e*]indol-2-ylidene)penta-1,3-dien-1-yl)-1*H*-benzo[*e*]indol-3-ium (3.41)**



Following the general procedure described above, compound **3.41** was obtained in 45% yield (3.0 mg) as a blue powder starting from maleimide-PEG2-Cy5.5 **3.30** (6.7 mg, 0.008 mmol) and Cys-PTP-**3.4** (KTLLPTPC, 9.5 mg, 0.011 mmol).

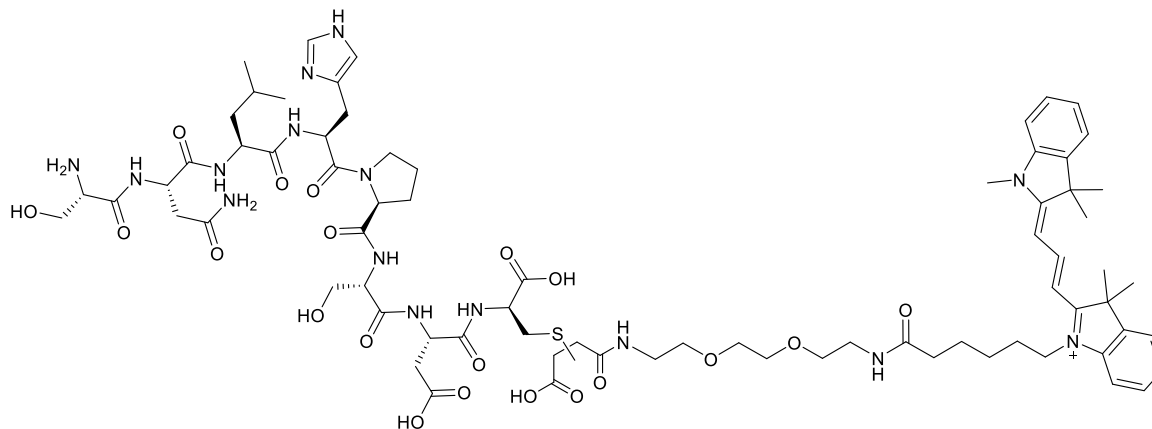
**3.35** (*succinimide precursor*): **HR-MS** (ESI)  $m/z$  [M+3] calcd. for C<sub>89</sub>H<sub>127</sub>N<sub>13</sub>O<sub>16</sub>S: 555.6420, found 555.6429.

**3.41**: **HR-MS** (ESI)  $m/z$  [M+3H]<sup>+3</sup>, [M+2H]<sup>+2</sup> calcd. for C<sub>89</sub>H<sub>128</sub>N<sub>13</sub>O<sub>17</sub>S: [M+3H]<sup>+3</sup> 561.9830, found 561.9851; [M+2H]<sup>+2</sup> 842.4709, 842.4733.



Supplementary figure S-4. HR-MS trace (+ ESI) of purified compound 3.41.

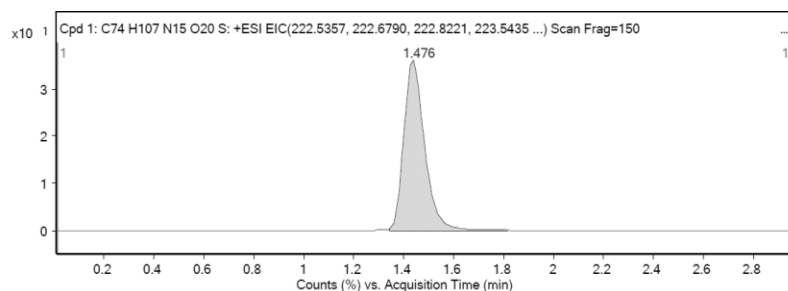
**1-((2*S*,5*S*)-2-((*S*)-2-((*S*)-1-(*L*-seryl-*L*-asparaginy-*L*-leucyl-*L*-histidyl)pyrrolidine-2-carboxamido)-3-hydroxypropanamido)-1,5,8-tricarboxy-3,10,21-trioxo-14,17-dioxa-7-thia-4,11,20-triazahexacosan-26-yl)-3,3-dimethyl-2-((*E*)-3-((*E*)-1,3,3-trimethylindolin-2-ylidene)prop-1-en-1-yl)-3*H*-indol-1-ium (3.42)**



Following the general procedure described above, compound **3.42** was obtained in 61% (6 mg) as a pink powder starting from maleimide-PEG2-Cy3 **3.29** (4.3 mg, 0.006 mmol) and Cys-control peptide **3.5** (SNLHPSDC, 8.5 mg, 0.01 mmol).

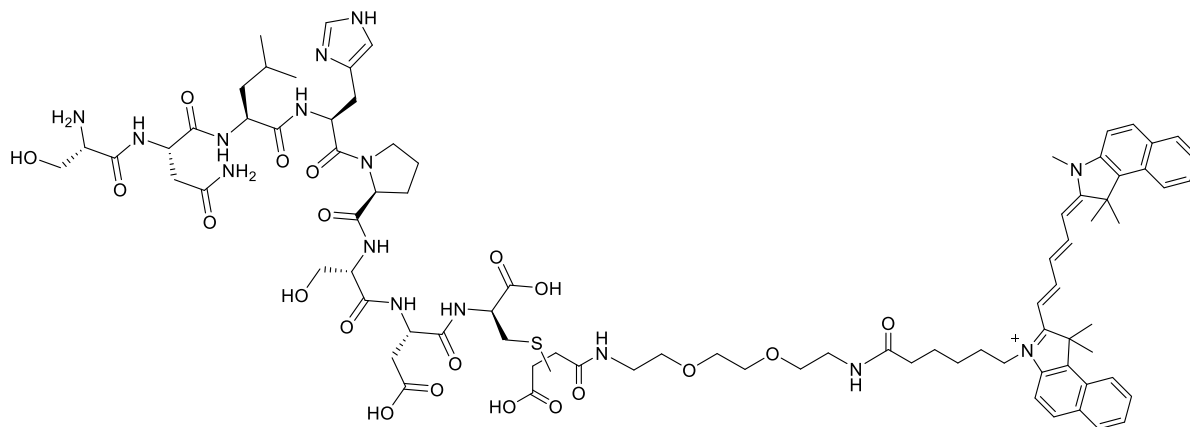
**3.36** (*succinimide precursor*): **HR-MS** (ESI)  $m/z$  [M+2] calcd. for C<sub>74</sub>H<sub>105</sub>N<sub>15</sub>O<sub>19</sub>S: 769.8710, found 769.8692.

**3.42**: **HR-MS** (ESI)  $m/z$  [M+3H]<sup>+3</sup>, [M+2] calcd. for C<sub>74</sub>H<sub>107</sub>N<sub>15</sub>O<sub>20</sub>S: [M+3H]<sup>+3</sup> 520.2585, found 520.2606; [M+2] 778.8763, found 778.8850.



Supplementary figure S-5. HR-MS trace (+ ESI) of purified compound **3.42**.

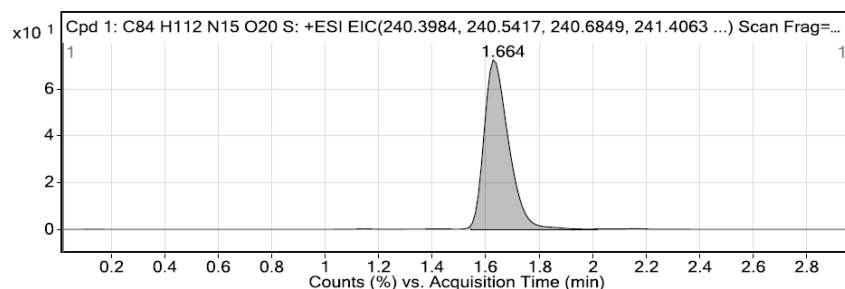
**3-((2*S*,5*S*)-2-((*S*)-2-((*S*)-1-(*L*-seryl-*L*-asparaginy-*L*-leucyl-*L*-histidyl)pyrrolidine-2-carboxamido)-3-hydroxypropanamido)-1,5,8-tricarboxy-3,10,21-trioxo-14,17-dioxa-7-thia-4,11,20-triazahexacosan-26-yl)-1,1-dimethyl-2-((1*E*,3*E*,5*E*)-5-(1,1,3-trimethyl-1,3-dihydro-2*H*-benzo[*e*]indol-2-ylidene)penta-1,3-dien-1-yl)-1*H*-benzo[*e*]indol-3-ium (3.43)**



Following the general procedure described above, compound **3.43** was obtained in 63% (7.2 mg) as a blue powder starting from maleimide-PEG2-Cy5.5 **3.30** (5.4 mg, 0.007 mmol) and Cys-control peptide **3.5** (SNLHPSDC, 7.8 mg, 0.009 mmol).

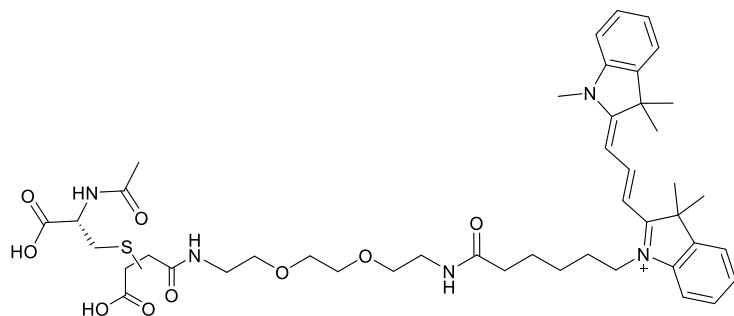
**3.37** (*succinimide precursor*): **HR-MS** (ESI)  $m/z$   $[M+3H]^{+3}$ ,  $[M+2]$  calcd. for  $C_{84}H_{111}N_{15}O_{19}S$ :  $[M+2]$  556.2707, found 556.2720;  $[M+2]$  833.3960, found 833.4021.

**3.43**: **HR-MS** (ESI)  $m/z$   $[M+3H]^{+3}$ ,  $[M+2H]^{+2}$  calcd. for  $C_{84}H_{112}N_{15}O_{20}S$ :  $[M+3H]^{+3}$  561.9382, found 561.9388;  $[M+2H]^{+2}$  842.4037, found 842.4045.



Supplementary figure S-6. HR-MS trace (+ ESI) of purified compound **3.43**.

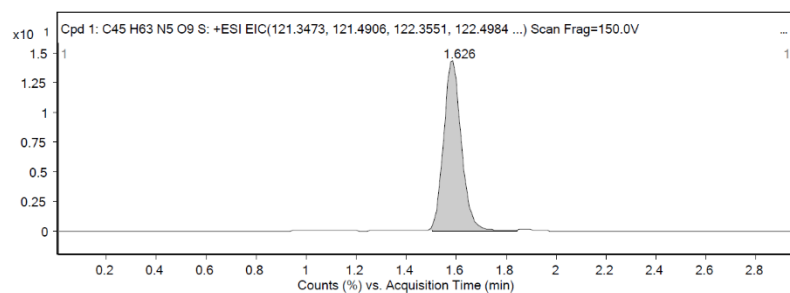
**1-((4*S*,7*R*)-4,7-Dicarboxy-2,9,20-trioxo-13,16-dioxa-6-thia-3,10,19-triazapentacosan-25-yl)-3,3-dimethyl-2-((*E*)-3-((*E*)-1,3,3-trimethylindolin-2-ylidene)prop-1-en-1-yl)-3*H*-indol-1-ium (3.44)**



Following the general procedure described above, compound **3.44** was obtained in 67% (3.6 mg) as a pink powder starting from maleimide-PEG2-Cy3 **3.29** (4.3 mg, 0.006 mmol) and methyl acetyl-*L*-cysteinate **3.20** (1.7 mg, 0.01 mmol).

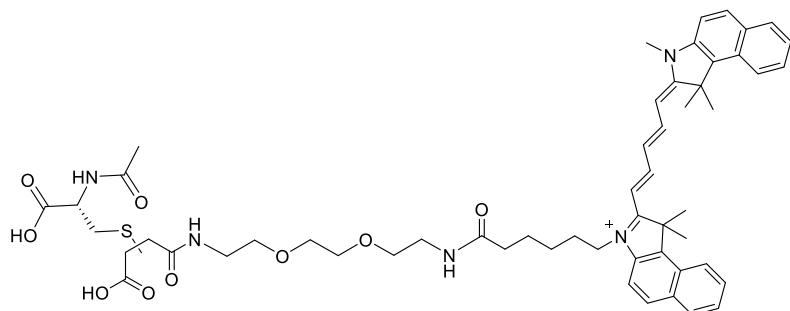
**3.38** (*succinimide precursor*): **HR-MS** (ESI)  $m/z$   $[M]^+$  calcd. for  $C_{46}H_{63}N_5O_8S$ : 845.4392, found 845.4321.

**3.44**: **HR-MS** (ESI)  $m/z$   $[M]^+$ ,  $[M+2]$  calcd. for  $C_{45}H_{63}N_5O_9S$ :  $[M]^+$  849.4341, found 849.4419;  $[M+2]$  424.7168, found 424.7238.



Supplementary figure S-7. HR-MS trace (+ ESI) of purified compound 3.44.

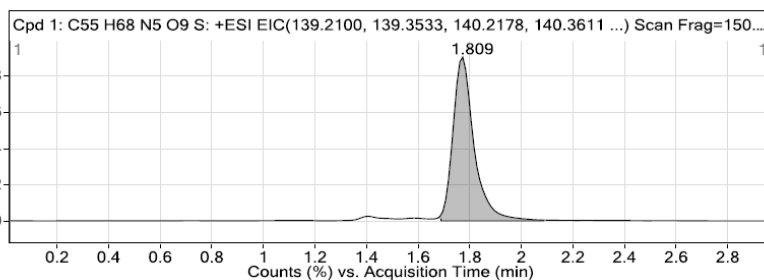
**3-((4*S*,7*R*)-4,7-Dicarboxy-2,9,20-trioxo-13,16-dioxa-6-thia-3,10,19-triazapentacosan-25-yl)-1,1-dimethyl-2-((1*E*,3*E*,5*E*)-5-(1,1,3-trimethyl-1,3-dihydro-2*H*-benzo[*e*]indol-2-ylidene)penta-1,3-dien-1-yl)-1*H*-benzo[*e*]indol-3-ium (3.45)**



Following the general procedure described above, compound **3.45** was obtained in 85% (5.5 mg) as a blue powder starting from maleimide-PEG2-Cy5.5 **3.30** (5.4 mg, 0.007 mmol) and methyl acetyl-*L*-cysteinate **3.20** (1.6 mg, 0.009 mmol).

**3.39** (*succinimide precursor*): **HR-MS** (ESI)  $m/z$   $[M]^+$  calcd. for  $C_{56}H_{69}N_5O_8S$ : 971.4861, found 971.4861.

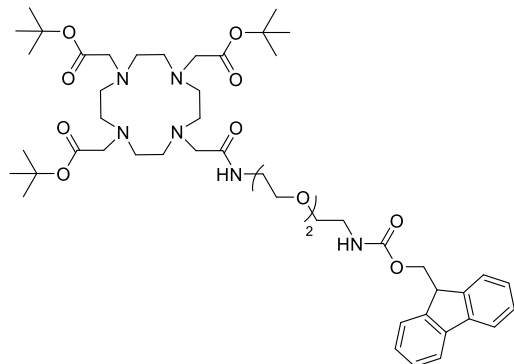
**3.45**: **HR-MS** (ESI)  $m/z$   $[M]^+$ ,  $[M+2H]^{+2}$  calcd. for  $C_{55}H_{68}N_5O_9S$ :  $[M]^+$  974.4732, found 974.4832;  $[M+2H]^{+2}$  488.2442, found 488.2438.



Supplementary figure S-8. HR-MS trace (+ ESI) of purified compound 3.45.

### 5.3.5. Synthesis of Tetravalent DOTAM Probe Precursors

*Tri-tert-butyl 2,2',2''-(10-(1-(9H-fluoren-9-yl)-3,14-dioxo-2,7,10-trioxa-4,13-diazapentadecan-15-yl)-1,4,7,10-tetraazacyclododecane-1,4,7-triyl)triacetate (3.46)*



Benzyl-protected intermediate **3.21** (1.2 g, 1.80 mmol) was hydrogenolyzed over 10 % palladium on activated carbon (180 mg) in methanol (100 mL) for 12 h at room temperature. The catalyst was removed by filtration, and the filtrate was concentrated under reduced pressure. The crude material was subsequently used for amide coupling with Fmoc-protected linker **3.26**.

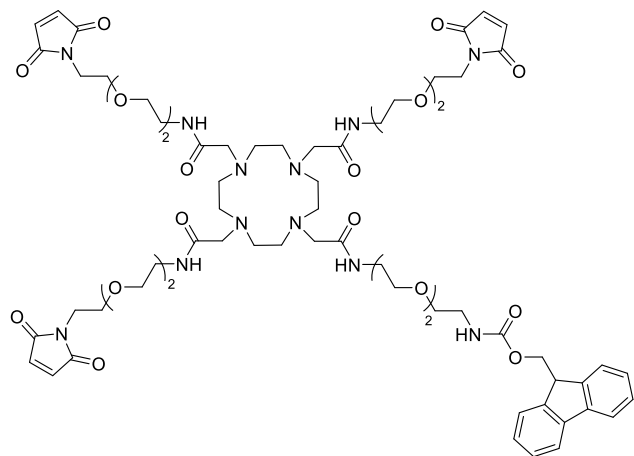
To a stirring solution of crude hydrogenolyzed material (572 mg, 1.0 mmol) in dimethylformamide (8 mL) at room temperature HATU (380 mg, 1.0 mmol) and *N,N*-diisopropylethylamine (0.7 mL, 4.0 mmol) were added. After 10 min, Fmoc-PEG2 linker **3.26** (407 mg, 1.0 mmol) dissolved in dimethylformamide (2 mL) was added to the stirring mixture. The reaction mixture was stirred for additional 30 min at room temperature. Subsequently, the solution was diluted with ethyl acetate (50 mL) and washed with water (2x). The organic layer was dried over  $\text{MgSO}_4$ , filtered, and concentrated under reduced pressure. The crude oil was purified by column chromatography (Silica gel, 15 g, DCM:MeOH, 0 to 10% MeOH) to afford Fmoc-protected compound **3.46** as a colorless oil in 62% yield (574 mg).

**$^1\text{H NMR}$**  (300 MHz,  $\text{CDCl}_3$ )  $\delta$  ppm 8.01 (s, 1H), 7.78 – 7.72 (m, 2H), 7.61 (d,  $J = 7.5$  Hz, 2H), 7.43 – 7.27 (m, 4H), 6.52 (s, 1H), 5.54 – 5.41 (m, 1H), 4.36 (d,  $J = 7.1$  Hz, 2H), 4.21 (t,  $J = 7.2$  Hz, 1H), 3.64 – 3.49 (m, 8H), 3.42 – 3.35 (m, 3H), 2.95 (s, 4H), 2.88 (d,  $J = 0.7$  Hz, 4H), 2.79 (s, 11H), 1.87 (s, 4H), 1.44 (d,  $J = 3.2$  Hz, 28H).

The analytical data are in accordance with those reported in the literature.<sup>[261a]</sup>



**(9H-Fluoren-9-yl)methyl (2-(2-(2-(2-(4,7,10-tris(2-((2-(2-(2-(2,5-dioxo-2,5-dihydro-1H-pyrrol-1-yl)ethoxy)ethoxy)ethyl)amino)-2-oxoethyl)-1,4,7,10-tetraazacyclododecan-1-yl)acetamido)ethoxy)ethoxy)ethyl)carbamate (3.47)**



*Tert*-butyl protected **3.46** (570 mg, 0.62 mmol) was dissolved in dichloromethane (8 mL) and trifluoroacetic acid (4 mL) was slowly added to the solution. The reaction mixture was stirred at room temperature for 16 h to complete conversion to product. Afterwards, the solvent was removed under reduced pressure, and co-evaporated with toluene (3x) to yield the free amine as a white solid (quant.). The residue was directly used for the next reaction step, without the need of further purification.

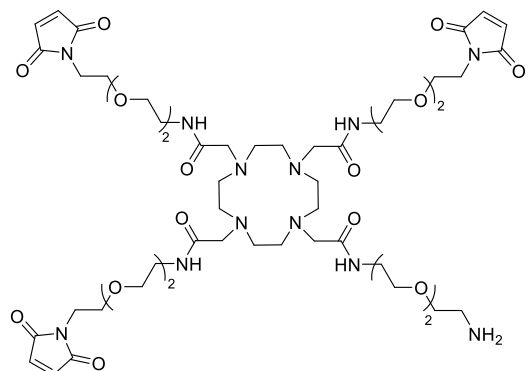
To a stirring solution of crude tricarboxylic acid (164 mg, 0.22 mmol) in dimethylformamide (4 mL) at room temperature HATU (246 mg, 0.65 mmol) and *N,N*-diisopropylethylamine (0.3 mL, 1.73 mmol) were added. After 10 min, maleimide-PEG2 linker **3.28** (148 mg, 0.65 mmol) dissolved in dimethylformamide (3 mL) was added to the stirring mixture. The reaction mixture was stirred for additional 30 min at room temperature. Subsequently, the solution was concentrated under reduced pressure, taken up in a mixture of acetonitrile and water (1:1) and purified by reversed-phase preparative HPLC (C-18, Water:ACN with 0.1% TFA, 30 to 90% ACN). The fractions containing product were lyophilized to afford Fmoc-protected **3.47** as a white powder in 46% yield (138 mg).

<sup>1</sup>H NMR (300 MHz, DMSO-*d*<sub>6</sub>) δ ppm 8.34 (s, 3H), 7.89 (d, *J* = 7.5 Hz, 3H), 7.68 (d, *J* = 7.5 Hz, 2H), 7.37 (dt, *J* = 27.3, 7.4 Hz, 5H), 7.02 (s, 5H), 4.53 – 3.86 (m, 14H), 3.72 – 2.70 (m, 62H).

<sup>13</sup>C NMR (75 MHz, DMSO-*d*<sub>6</sub>) δ ppm 170.9, 143.9, 140.8, 134.6, 127.6, 127.1, 125.1, 120.2, 69.5, 69.3, 69.1, 68.9, 67.0, 49.6, 36.8.

HR-MS (ESI) *m/z* [M+2]<sup>+</sup> calcd. for C<sub>67</sub>H<sub>94</sub>N<sub>12</sub>O<sub>20</sub>: 694.3426, found 694.3432.

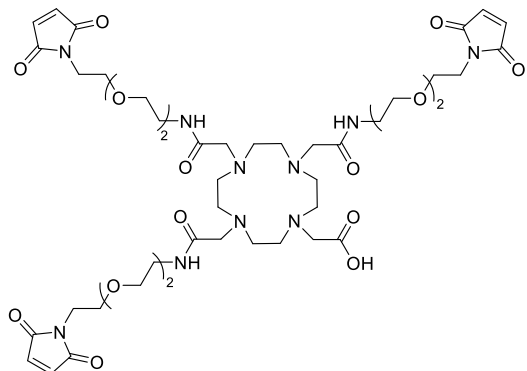
**2,2',2''-(10-(2-((2-(2-(2-Aminoethoxy)ethoxy)ethyl)amino)-2-oxoethyl)-1,4,7,10-tetraazacyclododecane-1,4,7-triyl)tris(N-(2-(2-(2-(2,5-dioxo-2,5-dihydro-1H-pyrrol-1-yl)ethoxy)ethoxy)ethyl)acetamide) (3.48)**



To a stirring solution of Fmoc-protected **3.47** (221 mg, 0.16 mmol) in dimethylformamide (7 mL) at room temperature and under nitrogen atmosphere, isopropanol (121  $\mu$ L, 1.58 mmol) in dimethylformamide (0.5 mL) was added, followed by tetrabutylammonium fluoride (TBAF, 320  $\mu$ L, 0.32 mmol) in dimethylformamide (0.5 mL). After 15 min stirring at room temperature, the reaction mixture was concentrated under reduced pressure and taken up in acidic water (8.0 mL water with 0.1% TFA). This aqueous solution was extracted with chloroform (10x), and the combined organic phase was extracted with water (1x). The combined aqueous phase was lyophilized to yield crude compound **3.48** as a red solid in 97% yield (180 mg, 0.16 mmol) without the need of further purification procedure.

**HR-MS** (ESI)  $m/z$  [M]<sup>+</sup> calcd. for C<sub>52</sub>H<sub>84</sub>N<sub>12</sub>O<sub>18</sub>: 1164.6027, found 1164.6036.

**2-(4,7,10-Tris(2-((2-(2-(2-(2,5-dioxo-2,5-dihydro-1H-pyrrol-1-yl)ethoxy)ethoxy)ethyl)amino)-2-oxoethyl)-1,4,7,10-tetraazacyclododecan-1-yl)acetic acid (3.52)**



Tri-benzyl protected intermediate **3.24** (215 mg, 0.29 mmol) was hydrogenolyzed over 10 % Palladium on Carbon (7.5 mg) in methanol (10 mL) for 12 h at room temperature. The catalyst was removed by filtration, and the filtrate was concentrated under reduced pressure. The crude tricarboxylic acid **3.51** was subsequently used for amide coupling with maleimide-PEG2 linker **3.28**.

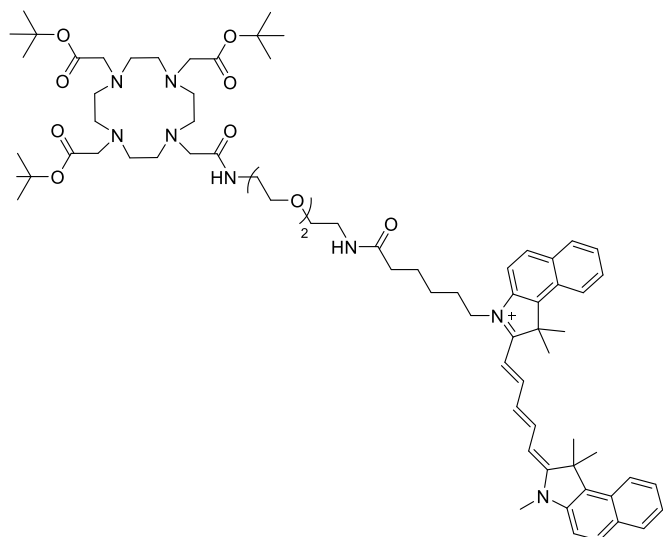
To a stirring solution of crude hydrogenolyzed **3.51** (100 mg, 0.22 mmol) in dimethylformamide (6 mL) at room temperature HATU (256 mg, 0.67 mmol) and *N,N*-diisopropylethylamine (0.5 mL, 2.6 mmol) were added. After 10 min, maleimide-PEG2 linker **3.28** (153 mg, 0.67 mmol) dissolved in dimethylformamide (2 mL) was added to the stirring mixture. The reaction mixture was stirred for additional 30 min at room temperature. Subsequently, the crude material was concentrated under reduced pressure, diluted in a mixture of acetonitrile and water (1:1) and purified by reversed-phase preparative HPLC (C-18, Water:ACN with 0.1% TFA, 5 to 75% ACN, 220 nm detection). The fractions containing product were lyophilized to give *tert*-butyl protected **3.52** as a pale yellow powder in 51% yield (120 mg).

**<sup>1</sup>H NMR** (300 MHz, CDCl<sub>3</sub>) δ ppm 6.76 – 6.70 (m, 6H), 3.71 (t, *J* = 5.4 Hz, 7H), 3.64 – 3.59 (m, 7H), 3.57 – 3.52 (m, 18H), 2.44 – 2.11 (m, 31H), 1.45 (s, 9H).

**HR-MS** (ESI) *m/z* [M+H]<sup>+</sup> calcd. for C<sub>50</sub>H<sub>78</sub>N<sub>10</sub>O<sub>17</sub>: 1091.5619, found 1091.5681.

The obtained *tert*-butyl protected analog of compound **3.52** (120 mg, 0.11 mmol) was subsequently dissolved in dichloromethane (3 mL) and trifluoroacetic acid (3 mL) was slowly added to the solution. The reaction mixture was stirred at room temperature for 2 h to complete conversion to the free carboxylic acid **3.52**. Afterwards, the solvent was removed under reduced pressure, and co-evaporated with toluene (3x) to yield **3.52** as a white solid (quant.). The residue was directly used for the next reaction step, without the need of further purification.

*Tri-tert-butyl 2,2',2''-(10-(18-(1,1-dimethyl-2-((1E,3E,5E)-5-(1,1,3-trimethyl-1,3-dihydro-2H-benzo[e]-indol-2-ylidene)penta-1,3-dien-1-yl)-1H-314-benzo[e]indol-3-yl)-2,13-dioxo-6,9-dioxo-3,12-diazaocta-decyl)-1,4,7,10-tetraazacyclododecane-1,4,7-triyl)triacetate (3.54)*



Benzyl-protected intermediate **3.21** (1.2 g, 1.8 mmol) was hydrogenolyzed over 10 % palladium on activated carbon (180 mg) in methanol (100 mL) for 12 h at room temperature. The catalyst was removed by filtration, and the filtrate was concentrated under reduced pressure.

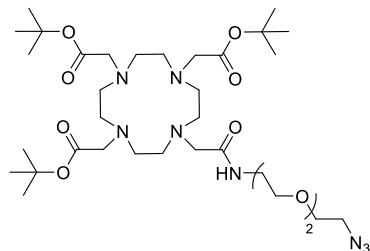
To a stirring solution of crude hydrogenolyzed material (20 mg, 0.03 mmol) in dimethylformamide (1 mL) at room temperature HATU (11 mg, 0.03 mmol) and *N,N*-diisopropylethylamine (41  $\mu$ L, 0.24 mmol) were added. After 10 min, Cy5.5-PEG2 linker **3.27** (21 mg, 0.03 mmol) dissolved in dimethylformamide (0.5 mL) was added to the stirring mixture. The reaction mixture was stirred for additional 30 min at room temperature. Subsequently, the reaction mixture was concentrated under reduced pressure, diluted in a mixture of acetonitrile and water (1:1) and purified by reversed-phase preparative HPLC (C-18, Water:ACN with 0.1% TFA, 30 to 90% ACN). The fractions containing product were lyophilized to afford compound tri-*tert*-butyl protected analog of **3.54** as a blue powder in 47% yield (20 mg).

**HR-MS** (ESI)  $m/z$   $[M+2]$ ,  $[M+3H]^{+3}$  calcd. for  $C_{74}H_{108}N_8O_{10}$ :  $[M+2]$  634.4089, found 634.4097;  $[M+3H]^{+3}$  423.9469, found 423.9440.

This compound (20 mg, 0.02 mmol) was subsequently dissolved in dichloromethane (1 mL) and trifluoroacetic acid (1 mL) was slowly added to the solution. The reaction mixture was stirred at room temperature for 2 h to complete conversion to tricarboxylic acid analog of title compound **3.54**. Afterwards, the solvent was removed under reduced pressure, and co-evaporated with toluene (3x) to

yield compound **3.54** as a white solid (quant.). The residue was directly used for the next reaction step, without the need of further purification.

***Tri-tert-butyl 2,2',2''-(10-(2-((2-(2-(2-azidoethoxy)ethoxy)ethyl)amino)-2-oxoethyl)-1,4,7,10-tetraaza-cyclododecane-1,4,7-triyl)triacetate (3.57)***



Benzyl-protected intermediate **3.21** (1.2 g, 1.8 mmol) was hydrogenolyzed over 10 % Palladium on Carbon (180 mg) in MeOH (100 mL) for 12 h at room temperature. The catalyst was removed by filtration, and the filtrate was concentrated under reduced pressure.

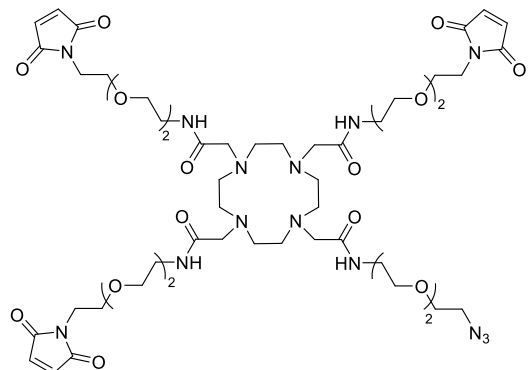
To a stirring solution of crude hydrogenolyzed material (300 mg, 0.52 mmol) in dimethylformamide (8 mL) at room temperature HATU (198 mg, 0.52 mmol) and *N,N*-diisopropylethylamine (0.4 mL, 2.1 mmol) were added. After 10 min, azido-PEG2 linker **3.31** (100 mg, 0.57 mmol) dissolved in dimethylformamide (2 mL) was added to the stirring mixture. The reaction mixture was stirred for additional 30 min at room temperature. Subsequently, the reaction mixture was diluted with ethyl acetate (50 mL) and stirred for additional 10 min. The crude solution was washed with water (2x), dried over MgSO<sub>4</sub>, filtered, and concentrated under reduced pressure. The crude material was purified by column chromatography (Silica gel, 4 g, DCM:MeOH, 0 to 10% MeOH) to afford compound **3.57** in 33% yield (125 mg).

**<sup>1</sup>H NMR** (300 MHz, CDCl<sub>3</sub>) δ ppm 8.00 (s, 1H), 3.71 – 3.48 (m, 8H), 3.43 – 3.32 (m, 4H), 3.01 – 2.70 (m, 16H), 2.49 – 2.03 (s, 8H), 1.49 – 1.37 (m, 27H).

**<sup>13</sup>C NMR** (75 MHz, CDCl<sub>3</sub>) δ ppm 172.7, 171.7, 162.7, 81.9, 81.9, 77.6, 77.2, 76.7, 70.5, 70.3, 70.1, 69.5, 56.0, 55.8, 55.7, 50.8, 39.2, 38.7, 36.6, 31.5, 28.1, 28.0, 28.0.

**HR-MS** (ESI)  $m/z$  [M+2]<sup>+</sup> calcd. for C<sub>34</sub>H<sub>64</sub>N<sub>8</sub>O<sub>9</sub>: 365.2471, found 365.2467.

**2,2',2''-(10-(2-((2-(2-(2-Azidoethoxy)ethoxy)ethyl)amino)-2-oxoethyl)-1,4,7,10-tetraazacyclododecane-1,4,7-triyl)tris(N-(2-(2-(2-(2,5-dioxo-2,5-dihydro-1H-pyrrol-1-yl)ethoxy)ethoxy)ethyl)acetamide) (3.58)**



*Tert*-butyl protected **3.57** (125 mg, 0.17 mmol) was dissolved in dichloromethane (2 mL) and trifluoroacetic acid (4 mL) was slowly added to the solution. The reaction mixture was stirred at room temperature for 2 h to complete conversion to product. Afterwards, the solvent was removed under reduced pressure, and co-evaporated with toluene (3x) to yield the free tricarboxylic acid intermediate as a white solid (quant.). The residue was directly used for the next reaction step, without the need of further purification.

To a stirring solution of crude tricarboxylic acid (120 mg, 0.22 mmol) in dimethylformamide (8 mL) at room temperature HATU (257 mg, 0.67 mmol) and *N,N*-diisopropylethylamine (0.19 mL, 1.10 mmol) were added. After 10 min, maleimide-PEG2 linker **3.28** (153 mg, 0.67 mmol) dissolved in dimethylformamide (2 mL) was added to the stirring mixture. The reaction mixture was stirred for additional 30 min at room temperature. Subsequently, the solution was concentrated under reduced pressure, diluted in a mixture of acetonitrile and water (1:1) and purified by reversed-phase preparative HPLC (C-18 column, Water:ACN with 0.1% TFA, 30 to 90% ACN). The fractions containing product were lyophilized to afford the title compound **3.58** as a white powder in 44% yield (115 mg).

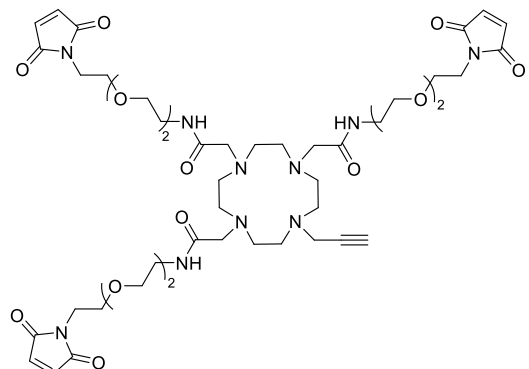
Polymerization of intermediate **3.58** was observed during the  $^1\text{H}$  and  $^{13}\text{C}$ -NMR analysis.

$^1\text{H}$  NMR (300 MHz,  $\text{DMSO-}d_6$ )  $\delta$  ppm 8.32 – 7.89 (m, 4H), 7.13 – 6.92 (m, 2H), 3.66 – 3.34 (m, 52H), 3.26 – 3.17 (m, 8H), 2.97 – 2.69 (m, 16H).

$^{13}\text{C}$  NMR (75 MHz,  $\text{DMSO-}d_6$ )  $\delta$  ppm 171.0, 163.4, 134.6, 118.9, 69.8, 69.7, 69.6, 69.3, 69.3, 69.1, 69.0, 68.8, 67.0, 40.4, 40.1, 39.8, 39.5, 39.2, 39.0, 38.7, 38.1, 37.8, 36.8, 30.3.

HR-MS (ESI)  $m/z$   $[\text{M}+3]^{+3}$  calcd. for  $\text{C}_{52}\text{H}_{82}\text{N}_{14}\text{O}_{18}$ : 398.2060, found 398.2044.

**2,2',2''-(10-(Prop-2-yn-1-yl)-1,4,7,10-tetraazacyclododecane-1,4,7-triyl)tris(N-(2-(2-(2-(2,5-dioxo-2,5-dihydro-1H-pyrrol-1-yl)ethoxy)ethoxy)ethyl)acetamide) (3.62)**



Alkyne-DOTA intermediate **3.22** (227 mg, 0.59 mmol), HATU (673 mg, 1.77 mmol) and *N,N*-diisopropylethylamine (0.5 mL, 2.95 mmol) were stirred in anhydrous dimethylformamide (6 mL) under nitrogen at room temperature. After 10 min, maleimide-PEG2 linker **3.28** (690 mg, 1.77 mmol) dissolved in dimethylformamide (4 mL) was added to the reaction mixture and stirred further for 30 min. After completion, the reaction mixture was concentrated under reduced pressure, diluted in a mixture of acetonitrile and water (1:1) and purified by reversed-phase preparative HPLC (C-18, Water:ACN with 0.1% TFA, 5 to 60% ACN, 220 nm detection) to afford probe template **3.62** as a colorless solid (358 mg, 60%) after lyophilization.

**<sup>1</sup>H NMR** (300 MHz, CDCl<sub>3</sub>) δ ppm 8.11 (d, *J* = 32.9 Hz, 3H), 6.74 (s, 6H), 3.92 – 3.66 (m, 15H), 3.66 – 3.47 (m, 26H), 3.47 – 3.20 (m, 19H), 2.50 (s, 1H).

**<sup>13</sup>C NMR** (75 MHz, CDCl<sub>3</sub>) δ ppm 171.0, 134.4, 78.1, 70.1 69.3. 68.0, 68.0, 51.7, 51.1, 43.5, 39.5, 39.4, 37.5, 37.4.

**HR-MS** (ESI) *m/z* [M+H]<sup>+</sup> calcd. for C<sub>47</sub>H<sub>70</sub>N<sub>10</sub>O<sub>15</sub>: 1015.5095, found 1015.5148.

### 5.3.6. Synthesis of DOTAM-based Probes

#### *General procedure*

A mixture of trimaleimide-PEG2 DOTAM alkyne **3.62** (1.0 equiv.) and terminal cysteine ligands **3.4**, **3.5**, or **3.20** (4.5 equiv.) was stirred in volatile buffer triethylammonium acetate pH = 5.0 (2 mL) at room temperature for 20 h. The completion of the reaction was monitored by LC-MS, where quantitative conversion to product was seen. Afterward, the reaction mixture was lyophilized to give crudes **3.63** to **3.65**, which were used without further chromatographic purification for the next reaction steps.

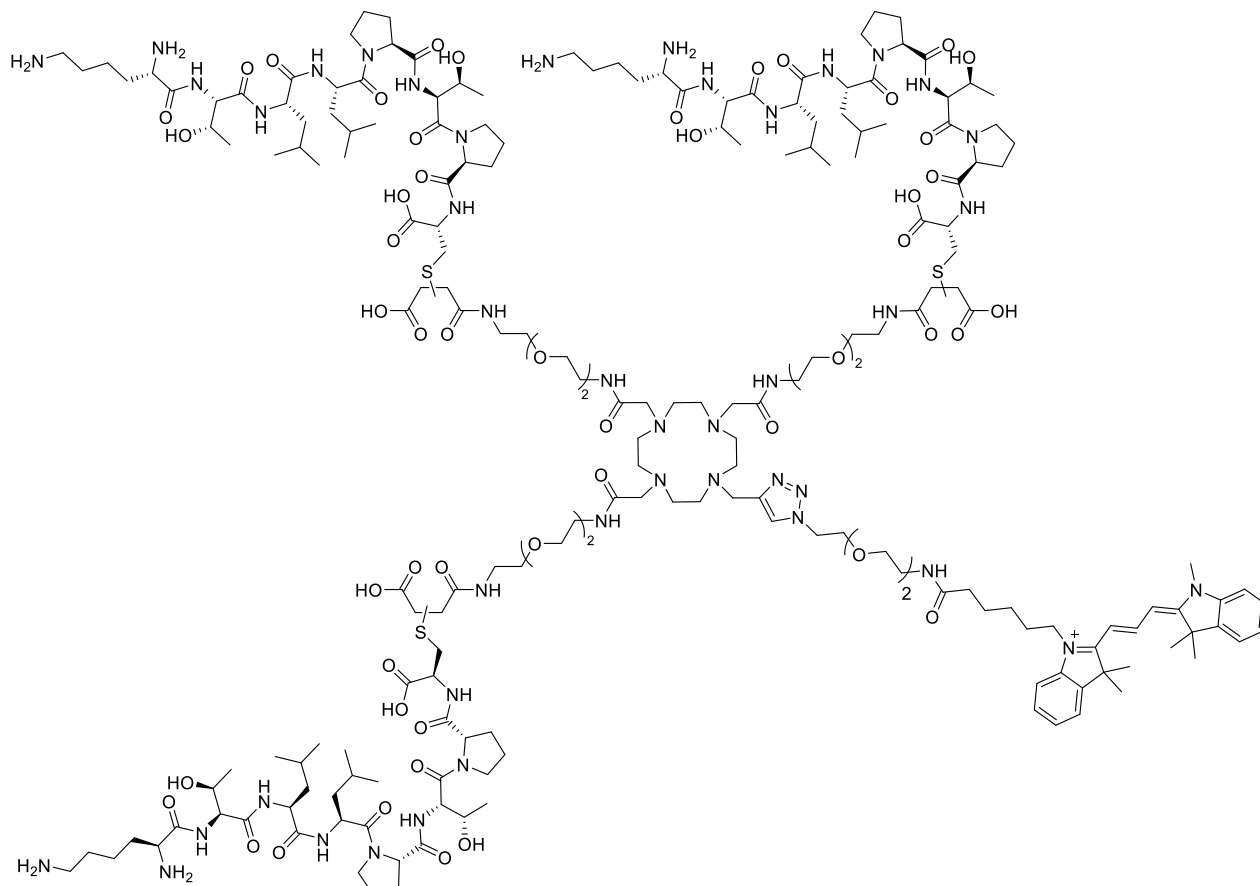
To a solution of alkyne **3.63** or **3.65** (1.0 equiv.), azido-PEG2-dye construct **3.32** or **3.33** (1.2 equiv.), and copper powder (125 equiv.) in a mixture of isopropanol and water (6 mL, 2:1, *v/v*) copper sulfate aq. sol. (0.1M, 3.5 equiv.) was added. The reaction was stirred at room temperature for 2 h until the DOTA core of **3.63** or **3.65** was saturated with copper. After which time, additional copper sulfate aq. sol. (0.1M, 3.5 equiv.) was added to the reaction mixture and it was allowed to stir at the same temperature for additional 16 h. After full conversion to product, the reaction mixture was filtered, and the filtrate was lyophilized to give crude intermediates **3.66**, **3.67**, **3.70**, or **3.71** as copper complexes. Of note, in all examples, product mass with one additional copper ion was observed in the LC-MS analysis, indicating copper complexation by the DOTAM core.

Subsequent copper demetalation was performed. To a stirring solution of crude copper complex **3.66**, **3.67**, **3.70**, or **3.71** labeled with either Cy3 or Cy5.5 (1 equiv.) in trifluoroacetic acid aq. sol. (pH = 2.2, 8 mL) at room temperature *D*-penicillamine **3.77** (260 equiv.) was added. The reaction mixture was stirred at room temperature for 18 h. The completion of the reaction was monitored by LC-MS, where product mass without copper was exclusively observed. Afterwards, the crude product was filtered and purified by reversed-phase preparative HPLC (C-18 Hydro Synergi, Water:ACN with 0.1% TFA, 25 to 60% ACN). The fractions containing product were collected and lyophilized to give copper free compounds **3.79** to **3.82**.

Copper free intermediates **3.79** to **3.82** labeled with either Cy3 or Cy5.5 (1 equiv.) were stirred at room temperature in a mixture of volatile ammonium carbonate buffer pH 8.9 and water (6 mL, 1:1, *v/v*). Hydrolysis of succinimide rings was observed after 18 h of stirring. After completion, the reaction mixture was lyophilized to afford the desired products **3.83** to **3.86** in quantitative yield.



**Tri-PTP-PEG2 DOTAM probe labeled with Cy3 (3.83)**

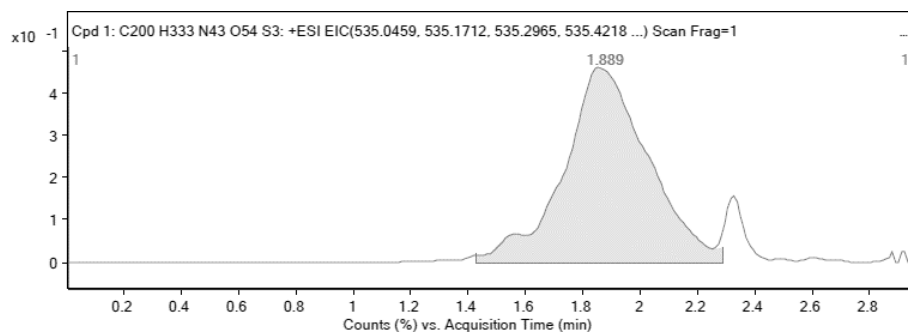


Following the general procedure described above, compound **3.83** was obtained in 15% yield as a pink powder starting from DOTAM-based platform **3.62** (5.0 mg, 4.93  $\mu\text{mol}$ ), Cys-PTP-**3.4** (KTLTPPC, 19.3 mg, 22.2  $\mu\text{mol}$ ), and Cy3-labeled azide linker **3.32** (3.6 mg, 5.92  $\mu\text{mol}$ ).

**3.63** (*alkyne precursor*): **HR-MS** (ESI)  $m/z$   $[\text{M}+2\text{H}]^{+2}$  calcd. for  $\text{C}_{164}\text{H}_{277}\text{N}_{37}\text{O}_{48}\text{S}_3$ : 1816.4873, found 1816.4922.

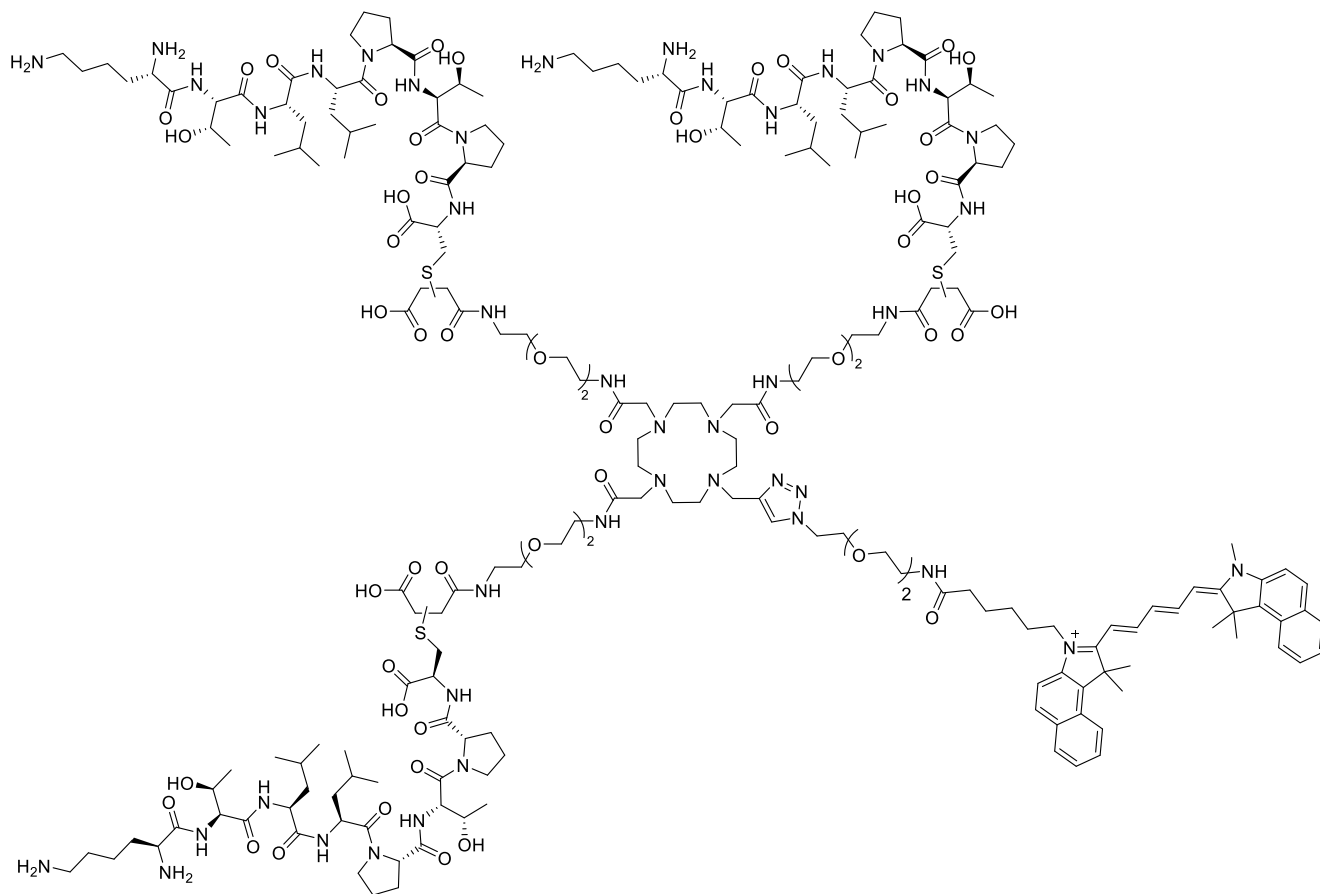
**3.79** (*succinimide precursor*): **HR-MS** (ESI)  $m/z$   $[\text{M}+7\text{H}]^{+7}$ ,  $[\text{M}+6]$  calcd. for  $\text{C}_{200}\text{H}_{327}\text{N}_{43}\text{O}_{51}\text{S}_3$ :  $[\text{M}+7\text{H}]^{+7}$  607.3431, found 607.3413;  $[\text{M}+6]$  708.2263, found 708.2238.

**3.83**: **HR-MS** (ESI)  $m/z$   $[\text{M}+7\text{H}]^{+7}$ ,  $[\text{M}+6]$ ,  $[\text{M}+5\text{H}]^{+5}$  calcd. for  $\text{C}_{200}\text{H}_{333}\text{N}_{43}\text{O}_{54}\text{S}_3$ :  $[\text{M}+7\text{H}]^{+7}$  614.9186, found 614.9184;  $[\text{M}+6]$  717.2316, found 717.2370;  $[\text{M}+5\text{H}]^{+5}$  860.8843, found 860.8849.



Supplementary figure S-9. HR-MS trace (+ ESI) of purified compound **3.83**.

***Tri-PTP-PEG2 DOTAM probe labeled with Cy5.5 (3.84)***

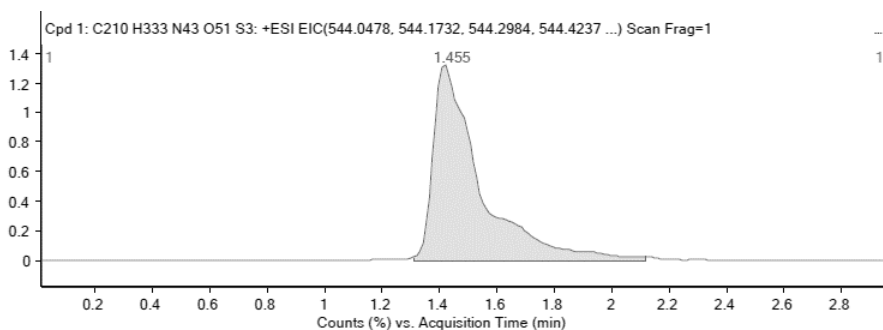


Following the general procedure described above, compound **3.84** was obtained in 29% yield as a blue powder starting from DOTAM-based platform **3.62** (5.0 mg, 4.93  $\mu\text{mol}$ ), Cys-PTP-**3.4** (KTLLPTPC, 19.3 mg, 22.2  $\mu\text{mol}$ ), and Cy5.5-labeled azide linker **3.33** (4.4 mg, 5.92  $\mu\text{mol}$ ).

**3.63** (*alkyne precursor*): **HR-MS** (ESI)  $m/z$   $[M+2H]^{+2}$  calcd. for  $\text{C}_{164}\text{H}_{277}\text{N}_{37}\text{O}_{48}\text{S}_3$ : 1816.4873, found 1816.4922.

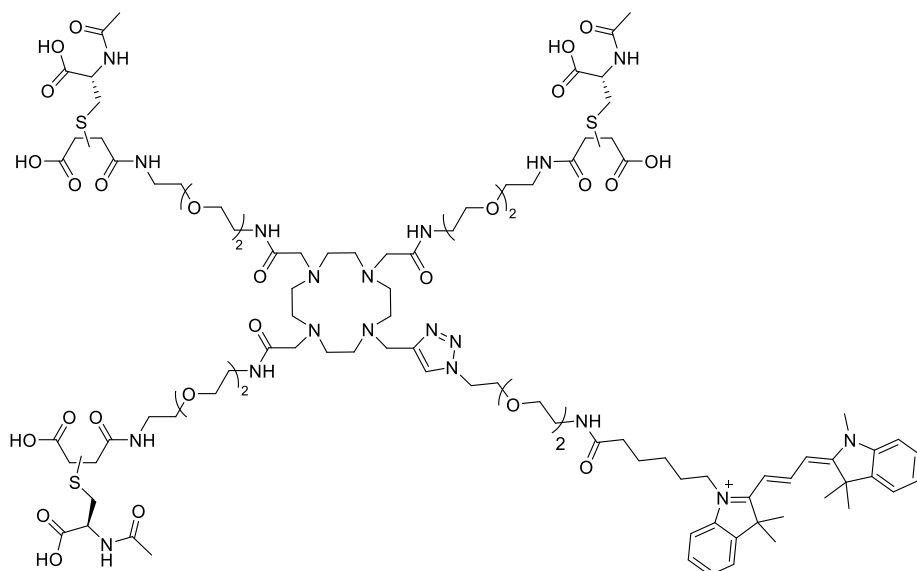
**3.80** (*succinimide precursor*): **HR-MS** (ESI)  $m/z$  [M+7], [M+6] calcd. for C<sub>210</sub>H<sub>333</sub>N<sub>43</sub>O<sub>51</sub>S<sub>3</sub>: [M+7] 625.0578, found 625.0612; [M+6] 728.9002, found 728.9016.

**3.84**: **HR-MS** (ESI)  $m/z$  [M+7H]<sup>+7</sup>, [M+6H]<sup>+6</sup>, [M+5H]<sup>+5</sup> calcd. for C<sub>210</sub>H<sub>339</sub>N<sub>45</sub>O<sub>54</sub>S<sub>3</sub>: [M+7H]<sup>+7</sup> 632.9253, found 632.9255; [M+6]<sup>+6</sup> 738.2450, found 738.2436; [M+5H]<sup>+5</sup> 886.0937, found 886.0947.



Supplementary figure S-10. HR-MS trace (+ ESI) of purified compound 3.84.

### *Tri-cysteine-PEG2 DOTAM probe labeled with Cy3 (3.85)*

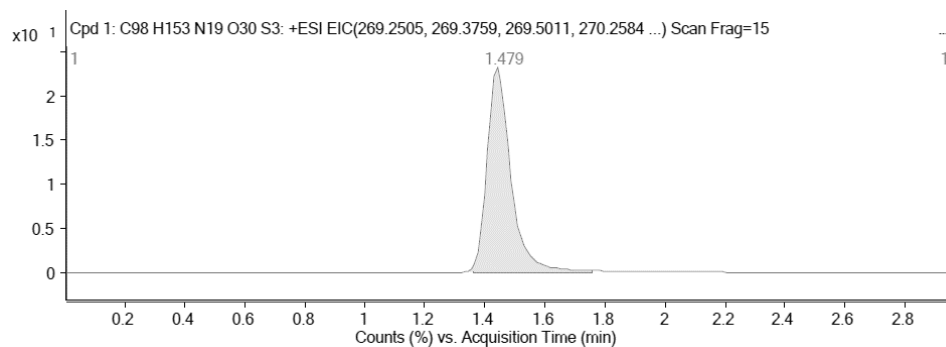


Following the general procedure described above, compound **3.85** was obtained in 38% yield as a pink powder starting from DOTAM-based platform **3.62** (10 mg, 9.85  $\mu$ mol), methyl acetyl-L-cysteinate **3.20** (7.9 mg, 44.3  $\mu$ mol), and Cy3-labeled azide linker **3.32** (7.3 mg, 11.8  $\mu$ mol).

**3.65** (*alkyne precursor*): **HR-MS** (ESI)  $m/z$  [M+2H]<sup>+2</sup>, [M+H]<sup>+</sup> calcd. for C<sub>65</sub>H<sub>103</sub>N<sub>13</sub>O<sub>24</sub>S<sub>3</sub>: [M+2H]<sup>+2</sup> 773.8273, found 773.8365; [M+H]<sup>+</sup> 1546.6474, found 1546.6578.

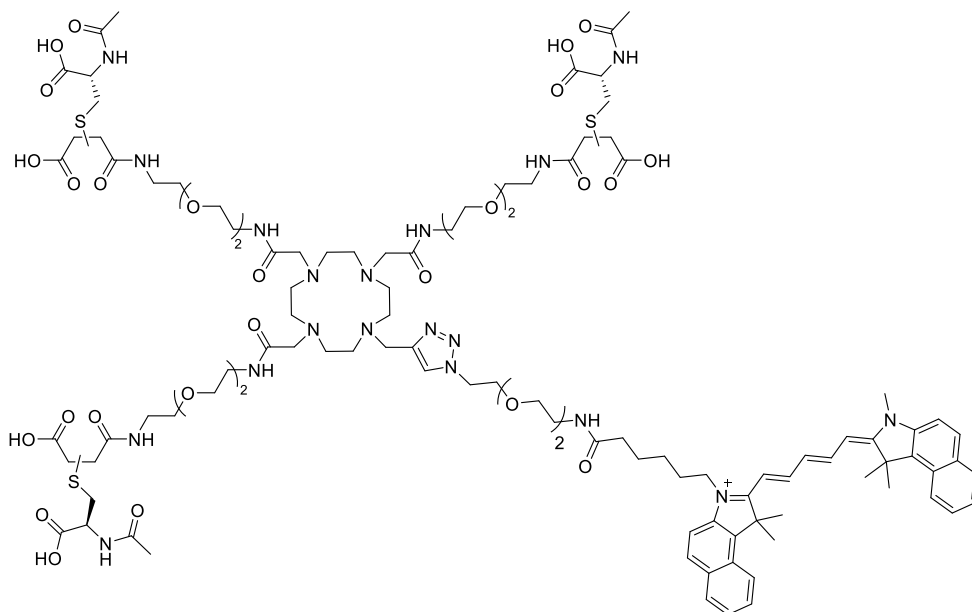
**3.81** (*succinimide precursor*): **HR-MS** (ESI)  $m/z$  [M+2], [M+3] calcd. for  $C_{101}H_{153}N_{19}O_{27}S_3$ : [M+2] 1080.5507, found: 1080.5182, [M+3] 720.7032, found: 720.6791.

**3.85**: **HR-MS** (ESI)  $m/z$  [M+3], [M+2] calcd. for  $C_{98}H_{153}N_{19}O_{30}S_3$ : [M+3] 724.3402, found 724.3520; [M+2] 1086.0091, 1086.0198.



Supplementary figure S-11. HR-MS trace (+ ESI) of purified compound 3.85.

**Tri-cysteine-PEG2 DOTAM probe labeled with Cy5.5 (3.86)**

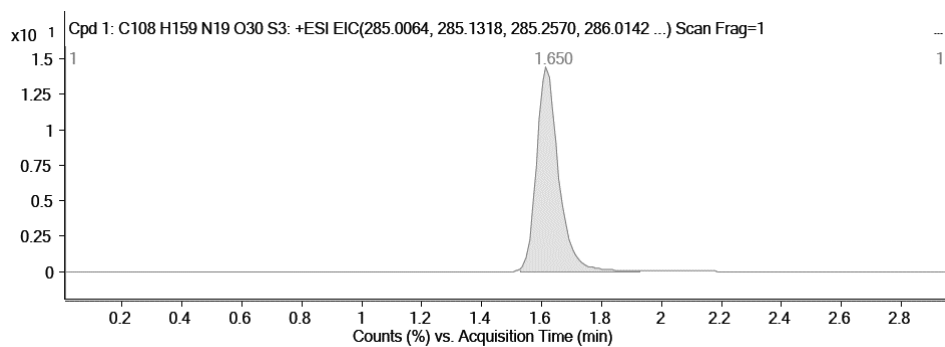


Following the general procedure described above, compound **3.86** was obtained in 38% yield as a blue powder starting from DOTAM-based platform **3.62** (10 mg, 9.85  $\mu$ mol), methyl acetyl-*L*-cysteinate **3.20** (7.9 mg, 44.3  $\mu$ mol), and Cy3-labeled azide linker **3.33** (8.7 mg, 11.8  $\mu$ mol).

**3.65** (*alkyne precursor*): **HR-MS** (ESI)  $m/z$  [M+2H]<sup>2+</sup>, [M+H]<sup>+</sup> calcd. for  $C_{65}H_{103}N_{13}O_{24}S_3$ : [M+2H]<sup>2+</sup> 773.8273, found 773.8365; [M+H]<sup>+</sup> 1546.6474, found 1546.6578.

**3.82: HR-MS** (ESI)  $m/z$   $[M+3H]^+3$ ,  $[M+2]$  calcd. for  $C_{111}H_{159}N_{19}O_{27}S_3$ :  $[M+3H]^+3$  763.0344, found: 763.0332,  $[M+2]$  1143.0402, 1143.0399.

**3.86: HR-MS** (ESI)  $m/z$   $[M+3]$ ,  $[M+3Na]^+3$  calcd. for  $C_{108}H_{159}N_{19}O_{30}S_3$ :  $[M+3]$  766.3559, found 766.3648;  $[M+3Na]^+3$  789.0113, 789.0124.



Supplementary figure S-12. HR-MS trace (+ ESI) of purified compound 3.86.

### 5.3.7. Determination of the Copper Content of final DOTAM probes by ICP-MS Analysis

The following experiments were performed by SEBASTIAN FASSBENDER and ANDREAS SCHULTZ at the Bundesanstalt für Materialforschung und –prüfung (BAM), Berlin.

#### *Sample preparation*

Stock solutions of the DOTA-fluoroprobe **3.79** to **3.82** were prepared by dissolving 1-2 mg of probe into 1 mL ultrapure water (MilliQ). An additional blank control with no sample was also prepared. The stock solutions and blank were acidified by adding 100  $\mu\text{L}$  concentrated sub-boiled nitric acid. For the preparation of the measuring solutions, 50  $\mu\text{L}$  of acidified stock solutions or blank were pipetted into a disposable pre-washed sample tube filled with around 45 mL of MilliQ. Additional 500  $\mu\text{L}$  concentrated sub-boiled nitric acid was added and the sample tube was filled up to 50 mL with MilliQ.

A blank solution containing 500  $\mu\text{L}$  concentrated sub-boiled nitric acid pipetted into a disposable pre-washed sample tube, which was then filled up to 50 mL with MilliQ, was additionally prepared (SBW1).

A standard spiked solution containing a concentration of 100  $\mu\text{g/L}$  copper was prepared by performing twice a 1:100 dilution of Merc ICP multi-element standard solution IV (999 mg/L Cu in 6.5% suprapur nitric acid) in 2% (*v/v*) nitric acid. Spiked calibration solutions of 1, 2, and 3  $\mu\text{g/L}$  copper were prepared by pipetting 50  $\mu\text{L}$  measuring sample solution and 500, 1000, 1500  $\mu\text{L}$  standard spiked solution (100  $\mu\text{g/L}$  Cu), respectively, and 500  $\mu\text{L}$  concentrated sub-boiled nitric acid into disposable pre-washed sample tubes, which were then filled up to 50 mL with MilliQ.

#### *Data evaluation*

Instrumental limits of detection (LOD) and quantitation (LOQ) were determined as 3x/10x the standard deviation of 7 measurements of blank measuring solution SBW1 conducted during the whole sequence.

No differences were found between measurement results obtained using low and medium resolution with the exception of the intensity of measuring solution **3.81**. This was found to be below LOQ for medium resolution. The signal stability was better for  $^{65}\text{Cu}$  at low resolution. In conclusion, a

significant contribution of interferences on Copper detection in low resolution could be precluded and the results of  $^{65}\text{Cu}$  at low resolution were used for calculating the final results and uncertainties.

The intensity of the blank measuring solution was found to be indistinguishable from the intensities of the blank stock solution. Therefore, no contribution of the sample preparation to copper concentrations in the measuring solutions containing probes was expected. Uncertainty estimation was done following the GUM guidelines<sup>[314]</sup> using the Kragten approach.<sup>[315]</sup>

**Supplementary table S-5. Copper concentrations in measuring probe samples determined by ICP-MS.**

Probe	Cu concentration in solid sample ( $\mu\text{g/g}$ )	Expanded uncertainty U ( $k=2, 95\%$ ) ( $\mu\text{g/g}$ )	Relative uncertainty (%)
3.79	228	15	6.5
3.80 (batch 01)	1068	43	4.0
3.80 (batch 02)	1392	35	2.5
3.81 (batch 01)	741	17	2.3
3.81 (batch 02)	762	70	9.2
3.82	209	15	7.0

### 5.3.8. Confocal Fluorescence Microscopy using Multivalent DOTAM-based Probes and Controls

The following experiments were performed by DR. SILKE RADETZKI at FMP, Berlin.

#### ***General procedure for confocal imaging in human pancreatic cell lines***

The human pancreatic cancer lines Panc-1 and MiaPaCa-2, which have amplified plectin-1 expression, were grown according to established protocols,<sup>[249, 295]</sup> using Dulbecco's modified Eagle's medium (DMEM, Gibco BRL, Gaithersburg, MD, USA) containing 4.5 g/L glucose, supplemented with 10% (*v/v*) fetal bovine serum (FBS, Gibco BRL), 100 U/mL penicillin-streptomycin (Gibco BRL). For Panc-1 cells, 2mM Glutamin was included in the culture medium. Cells were plated onto 384-well microplates (CellCarrier-384 ultra, PerkinElmer) at a density of 3'000 cells/well in 40µl medium/well and incubated for 20 h in a 5% carbon dioxide, humidified atmosphere at 37° C. Live cell nuclei staining was achieved with the addition of 1µM Hoechst 33342, followed by 1 h incubation at 37 °C. Cells were fixed with 4% paraformaldehyde in PBS buffer for 20 min, then washed three times with PBS buffer (70 µL/well). Cells were incubated with 50 µL/well probe (either PTP-labeled DOTA probes **3.83** and **3.84**, monovalent controls **3.40** to **3.45**, or non-targeting DOTA-labeled controls **3.85** and **3.86**) in PBS for 4 h at room temperature in the dark, then washed three times with PBS buffer (70 µL/well). Images were acquired using an Opera Phenix™ High Content Screening System microscope (PerkinElmer) with 40 times magnification. Confocal images were captured using Hoechst 33342, Cy3, and Cy5.5 fluorescence channels by recording nine frames per well. Images were processed with the Harmony software (v4.9), designed for High Content Screening Systems (PerkinElmer) using the mean fluorescence intensity in cytoplasmic cell region as readout parameter. Data are presented in mean fluorescence from a representative of 6 replicates per condition.



## 6. References

- [1] R. Hooke, *Micrographia: or some Physiological Descriptions of Minute Bodies made by Magnifying Glasses. With Observations and Inquiries thereupon.*, Dover Publications, New York, **2003**.
- [2] E. Abbe, *Arch. Mikroskop. Anat.* **1873**, *9*, 413-468.
- [3] R. Virchow, *Disease, life, and man: selected essays*, Stanford University Press, Stanford **1958**.
- [4] F. H. Kasten, in *Cell Structure and Function by Microspectrofluorometry* (Ed.: E. Kohen), Academic Press, **1989**, pp. 3-50.
- [5] A. Baeyer, *Ber. Dtsch. Chem. Ges.* **1871**, *4*, 555-558.
- [6] P. Ehrlich, *Arch. Mikrosk. Anat.* **1877**, *13*, 263-278.
- [7] K. Strebhardt, A. Ullrich, *Nat. Rev. Cancer* **2008**, *8*, 473-480.
- [8] W. G. Bradley, *Proc. Am. Philos. Soc.* **2008**, *152*, 349-361.
- [9] R. Weissleder, U. Mahmood, *Radiology* **2001**, *219*, 316-333.
- [10] a) D. Miladinova, *Nucl. Med. Mol. Imaging* **2019**, *53*, 313-319; b) O. Schillaci, N. Urbano, *Eur. J. Nucl. Med. Mol. Imaging* **2019**, *46*, 1222-1225; c) J. Tang, D. Salloum, B. Carney, C. Brand, S. Kossatz, A. Sadique, J. S. Lewis, W. A. Weber, H.-G. Wendel, T. Reiner, *Proc. Natl. Acad. Sci. U.S.A.* **2017**, *114*, E7441.
- [11] a) S. Robu, M. Schottelius, M. Eiber, T. Maurer, J. Gschwend, M. Schwaiger, H.-J. Wester, J. *Nucl. Med.* **2017**, *58*, 235-242; b) L. Wei, J. Petryk, C. Gaudet, M. Kamkar, W. Gan, Y. Duan, T. D. Ruddy, *J. Nucl. Cardiol.* **2019**, *26*, 1169-1178.
- [12] a) A. A. A. Ali, F.-T. Hsu, C.-L. Hsieh, C.-Y. Shiau, C.-H. Chiang, Z.-H. Wei, C.-Y. Chen, H.-S. Huang, *Sci. Rep.* **2016**, *6*, 36650; b) A. Lasocki, R. J. Hicks, *Cancer Imaging* **2019**, *19*, 57.
- [13] a) A. Ingels, I. Leguerney, P.-H. Cournède, J. Irani, S. Ferlicot, C. Sébrié, B. Benatsou, L. Jourdain, S. Pitre-Champagnat, J.-J. Patard, N. Lassau, *Sci. Rep.* **2020**, *10*, 7308; b) J. K. Willmann, L. Bonomo, A. C. Testa, P. Rinaldi, G. Rindi, K. S. Valluru, G. Petrone, M. Martini, A. M. Lutz, S. S. Gambhir, *J. Clin. Oncol.* **2017**, *35*, 2133-2140.
- [14] a) Y.-S. Chen, Y. Zhao, S. J. Yoon, S. S. Gambhir, S. Emelianov, *Nat. Nanotechnol.* **2019**, *14*, 465-472; b) Y. Liu, P. Bhattarai, Z. Dai, X. Chen, *Chem. Soc. Rev.* **2019**, *48*, 2053-2108; c) L. Xie, X. Pang, X. Yan, Q. Dai, H. Lin, J. Ye, Y. Cheng, Q. Zhao, X. Ma, X. Zhang, G. Liu, X. Chen, *ACS Nano* **2020**, *14*, 2880-2893.
- [15] a) X. Chen, D. Lee, S. Yu, G. Kim, S. Lee, Y. Cho, H. Jeong, K. T. Nam, J. Yoon, *Biomaterials* **2017**, *122*, 130-140; b) J. Huang, J. Li, Y. Lyu, Q. Miao, K. Pu, *Nat. Mater.* **2019**, *18*, 1133-1143; c) X. Yang, W. Liu, J. Tang, P. Li, H. Weng, Y. Ye, M. Xian, B. Tang, Y. Zhao, *Chem. Commun.* **2018**, *54*, 11387-11390.
- [16] a) J. Noonan, S. M. Asiala, G. Grassia, N. MacRitchie, K. Gracie, J. Carson, M. Moores, M. Girolami, A. C. Bradshaw, T. J. Guzik, G. R. Meehan, H. E. Scales, J. M. Brewer, I. B. McInnes, N. Sattar, K. Faulds, P. Garside, D. Graham, P. Maffia, *Theranostics* **2018**, *8*, 6195-6209; b) N. MacRitchie, G. Grassia, J. Noonan, P. Garside, D. Graham, P. Maffia, *Heart* **2018**, *104*, 460-467.
- [17] a) T. F. Massoud, S. S. Gambhir, *Genes Dev.* **2003**, *17*, 545-580; b) T. E. Peterson, H. C. Manning, *J. Nucl. Med. Technol.* **2009**, *37*, 151-161; c) J. Zhao, J. Chen, S. Ma, Q. Liu, L. Huang, X. Chen, K. Lou, W. Wang, *Acta Pharm. Sin. B* **2018**, *8*, 320-338; d) A. Walter, P. Paul-Gilloteaux, B. Plochberger, L. Sefc, P. Verkade, J. G. Mannheim, P. Slezak, A. Unterhuber, M. Marchetti-Deschmann, M. Ogris, K. Bühler, D. Fixler, S. H. Geyer, W. J. Weninger, M. Glösmann, S.

- Handschuh, T. Wanek, *Front. Phys.* **2020**, *8*; e) A. Chaichi, A. Prasad, M. R. Gartia, *Biosensors* **2018**, *8*.
- [18] J. R. Lindner, J. Link, *Circ. Cardiovasc. Imaging* **2018**, *11*, e005355-e005355.
- [19] G. M. Simon, M. J. Niphakis, B. F. Cravatt, *Nat. Chem. Biol.* **2013**, *9*, 200-205.
- [20] a) O. Gordon, C. A. Ruiz-Bedoya, A. A. Ordonez, E. W. Tucker, S. K. Jain, *mBio* **2019**, *10*, e00317-00319; b) H. A. Loomans-Kropp, A. Umar, *NPJ Precis. Oncol.* **2019**, *3*, 3; c) A. A. Ordonez, M. A. Sellmyer, G. Gowrishankar, C. A. Ruiz-Bedoya, E. W. Tucker, C. J. Palestro, D. A. Hammoud, S. K. Jain, *Sci. Transl. Med.* **2019**, *11*, eaax8251.
- [21] a) W. Chen, V. Dilsizian, *JACC Cardiovasc. Imaging* **2020**, *13*, 1348-1352; b) N. Nishio, N. S. van den Berg, S. van Keulen, B. A. Martin, S. Fakurnejad, N. Teraphongphom, S. U. Chirita, N. J. Oberhelman, G. Lu, C. E. Horton, M. J. Kaplan, V. Divi, A. D. Colevas, E. L. Rosenthal, *Nat. Comm.* **2019**, *10*, 5044.
- [22] a) M. A. Pysz, S. S. Gambhir, J. K. Willmann, *Clin. Radiol.* **2010**, *65*, 500-516; b) B. Qi, A. J. Crawford, N. E. Wojtynek, G. A. Talmon, M. A. Hollingsworth, Q. P. Ly, A. M. Mohs, *Theranostics* **2020**, *10*, 3413-3429; c) A. Teatini, E. Pelanis, D. L. Aghayan, R. P. Kumar, R. Palomar, Å. A. Fretland, B. Edwin, O. J. Elle, *Sci. Rep.* **2019**, *9*, 18687.
- [23] a) C. J. Gerry, S. L. Schreiber, *Nat. Rev. Drug Discov.* **2018**, *17*, 333-352; b) J. A. Frearson, I. T. Collie, *Drug Discov. Today* **2009**, *14*, 1150-1158.
- [24] a) H. Stark, *Expert Opin. Drug Discov.* **2020**, 1-3; b) J. Blagg, P. Workman, *Cancer Cell* **2017**, *32*, 9-25; c) R. M. Garbaccio, E. R. Parmee, *Cell Chem. Biol.* **2016**, *23*, 10-17; d) M. E. Bunnage, E. L. P. Chekler, L. H. Jones, *Nat. Chem. Biol.* **2013**, *9*, 195-199.
- [25] S. L. Pimlott, A. Sutherland, *Chem. Soc. Rev.* **2011**, *40*, 149-162.
- [26] S. M. Ametamey, M. Honer, P. A. Schubiger, *Chem. Rev.* **2008**, *108*, 1501-1516.
- [27] N. Bom, C. T. Lancée, G. van Zwieten, F. E. Kloster, J. O. S. Roelandt, *Circulation* **1973**, *48*, 1066-1074.
- [28] E. Brown, J. R. Lindner, *Curr. Cardiol. Rep.* **2019**, *21*, 30.
- [29] a) L. Abou-Elkacem, S. V. Bachawal, J. K. Willmann, *Eur. J. Radiol.* **2015**, *84*, 1685-1693; b) G. M. Lanza, S. A. Wickline, *Curr. Probl. Cardiol.* **2003**, *28*, 625-653.
- [30] a) P. C. Lauterbur, *Nature* **1973**, *242*, 190-191; b) F. F. Jöbsis, *Science* **1977**, *198*, 1264-1267.
- [31] V. P. B. Grover, J. M. Tognarelli, M. M. E. Crossey, I. J. Cox, S. D. Taylor-Robinson, M. J. W. McPhail, *J. Clin. Exp. Hepatol.* **2015**, *5*, 246-255.
- [32] Y. Xiao, R. Paudel, J. Liu, C. Ma, Z. Zhang, S. Zhou, *Int. J. Mol. Med.* **2016**, *38*, 1319-1326.
- [33] E. Boros, E. M. Gale, P. Caravan, *Dalton Trans.* **2015**, *44*, 4804-4818.
- [34] J. Wahsner, E. M. Gale, A. Rodríguez-Rodríguez, P. Caravan, *Chem. Rev.* **2019**, *119*, 957-1057.
- [35] S. Gioux, H. S. Choi, J. V. Frangioni, *Mol. Imaging* **2010**, *9*, 237-255.
- [36] S. Nioka, Y. Chen, *Transl. Med. UniSa* **2011**, *1*, 51-150.
- [37] J. Liu, C. Liu, W. He, *Curr. Org. Chem.* **2013**, *17*, 564-579.
- [38] O. T. Bruns, T. S. Bischof, D. K. Harris, D. Franke, Y. Shi, L. Riedemann, A. Bartelt, F. B. Jaworski, J. A. Carr, C. J. Rowlands, M. W. B. Wilson, O. Chen, H. Wei, G. W. Hwang, D. M. Montana, I. Coropceanu, O. B. Achorn, J. Kloepper, J. Heeren, P. T. C. So, D. Fukumura, K. F. Jensen, R. K. Jain, M. G. Bawendi, *Nat. Biomed. Eng.* **2017**, *1*, 0056.
- [39] U. Cho, D. P. Riordan, P. Ciepla, K. S. Kocherlakota, J. K. Chen, P. B. Harbury, *Nat. Chem. Biol.* **2018**, *14*, 15-21.
- [40] J. V. Frangioni, *Curr. Opin. Chem. Biol.* **2003**, *7*, 626-634.
- [41] C. A. Combs, H. Shroff, *Curr. Protoc. Neurosci.* **2017**, *79*, 2.1.1-2.1.25.
- [42] L. Schermelleh, A. Ferrand, T. Huser, C. Eggeling, M. Sauer, O. Biehlmaier, G. P. C. Drummen, *Nat. Cell Biol.* **2019**, *21*, 72-84.

- [43] E. Betzig, G. H. Patterson, R. Sougrat, O. W. Lindwasser, S. Olenych, J. S. Bonifacino, M. W. Davidson, J. Lippincott-Schwartz, H. F. Hess, *Science* **2006**, *313*, 1642-1645.
- [44] M. J. Rust, M. Bates, X. Zhuang, *Nat. Methods* **2006**, *3*, 793-795.
- [45] T. Müller, C. Schumann, A. Kraegeloh, *ChemPhysChem* **2012**, *13*, 1986-2000.
- [46] S. H. Han, *Neurospine* **2018**, *15*, 306-322.
- [47] V. Gujrati, A. Mishra, V. Ntziachristos, *Chem. Commun.* **2017**, *53*, 4653-4672.
- [48] C. V. Raman, K. S. Krishnan, *Nature* **1928**, *121*, 501-502.
- [49] H. J. Butler, L. Ashton, B. Bird, G. Cinque, K. Curtis, J. Dorney, K. Esmonde-White, N. J. Fullwood, B. Gardner, P. L. Martin-Hirsch, M. J. Walsh, M. R. McAinsh, N. Stone, F. L. Martin, *Nat. Protoc.* **2016**, *11*, 664-687.
- [50] Y. Zhang, H. Hong, W. Cai, *Curr. Pharm. Biotechnol.* **2010**, *11*, 654-661.
- [51] D. I. Ellis, D. P. Cowcher, L. Ashton, S. O'Hagan, R. Goodacre, *Analyst* **2013**, *138*, 3871-3884.
- [52] M. D. Schaeberle, V. F. Kalasinsky, J. L. Luke, E. N. Lewis, I. W. Levin, P. J. Treado, *Anal. Chem.* **1996**, *68*, 1829-1833.
- [53] T. Vankeirsbilck, A. Vercauteren, W. Baeyens, G. Van der Weken, F. Verpoort, G. Vergote, J. P. Remon, *TrAC, Trends Anal. Chem.* **2002**, *21*, 869-877.
- [54] a) S. Schlücker, *Chemphyschem* **2009**, *10*, 1344-1354; b) S. Wachsmann-Hogiu, T. Weeks, T. Huser, *Curr. Opin. Biotechnol.* **2009**, *20*, 63-73; c) R. R. Jones, D. C. Hooper, L. Zhang, D. Wolverson, V. K. Valev, *Nanoscale Res. Lett.* **2019**, *14*, 231.
- [55] F. Reynolds, K. A. Kelly, *Mol. Imaging* **2011**, *10*, 407-419.
- [56] a) S. S. Gambhir, *Nat. Rev. Cancer* **2002**, *2*, 683-693; b) R. Weissleder, *Science* **2006**, *312*, 1168-1171.
- [57] K. Chen, X. Chen, *Curr. Top. Med. Chem.* **2010**, *10*, 1227-1236.
- [58] S. Patel, K. Schmidt, J. Hesterman, J. Hoppin, *Mol. Imaging Biol.* **2017**, *19*, 348-356.
- [59] H. Kobayashi, M. R. Longmire, M. Ogawa, P. L. Choyke, *Chem. Soc. Rev.* **2011**, *40*, 4626-4648.
- [60] M. Garland, Joshua J. Yim, M. Bogoyo, *Cell Chemical Biology* **2016**, *23*, 122-136.
- [61] a) J. G. Baker, R. Middleton, L. Adams, L. T. May, S. J. Briddon, B. Kellam, S. J. Hill, *Br. J. Pharmacol.* **2010**, *159*, 772-786; b) S. Liu, D. S. Edwards, *Bioconjug. Chem.* **2001**, *12*, 7-34.
- [62] a) A. Cooper, S. Singh, S. Hook, J. D. A. Tyndall, A. J. Vernall, *Pharmacol. Rev.* **2017**, *69*, 316-353; b) E. Smith, I. Collins, *Future Med. Chem.* **2015**, *7*, 159-183.
- [63] F. Barbieri, A. Bajetto, A. Pattarozzi, M. Gatti, R. Würth, S. Thellung, A. Corsaro, V. Villa, M. Nizzari, T. Florio, *Int. J. Pept.* **2013**, *2013*, 926295.
- [64] C. Santini, J. Kuil, A. Bunschoten, S. Pool, E. de Blois, Y. Ridwan, J. Essers, M. R. Bernsen, F. W. van Leeuwen, M. de Jong, *J. Nucl. Med.* **2016**, *57*, 1289-1295.
- [65] a) K. C. Tjandra, P. Thordarson, *Bioconjug. Chem.* **2019**, *30*, 503-514; b) A. Louie, *Chem. Rev.* **2010**, *110*, 3146-3195; c) H. L. Handl, J. Vagner, H. Han, E. Mash, V. J. Hruby, R. J. Gillies, *Expert Opin. Ther. Targets* **2004**, *8*, 565-586.
- [66] a) X. Gao, L. Yang, J. A. Petros, F. F. Marshall, J. W. Simons, S. Nie, *Curr. Opin. Biotechnol.* **2005**, *16*, 63-72; b) M. Han, X. Gao, J. Z. Su, S. Nie, *Nat. Biotechnol.* **2001**, *19*, 631-635; c) Y. Ye, S. Bloch, S. Achilefu, *J. Am. Chem. Soc.* **2004**, *126*, 7740-7741.
- [67] A. L. Petersen, T. Binderup, R. I. Jølck, P. Rasmussen, J. R. Henriksen, A. K. Pfeifer, A. Kjær, T. L. Andresen, *J. Control. Release* **2012**, *160*, 254-263.
- [68] W. B. Edwards, B. Xu, W. Akers, P. P. Cheney, K. Liang, B. E. Rogers, C. J. Anderson, S. Achilefu, *Bioconjug. Chem.* **2008**, *19*, 192-200.
- [69] L. E. Jennings, N. J. Long, *Chem. Commun.* **2009**, 3511-3524.
- [70] P. Workman, I. Collins, *Chem. Biol.* **2010**, *17*, 561-577.
- [71] H. C. Kolb, M. G. Finn, K. B. Sharpless, *Angew. Chem. Int. Ed.* **2001**, *40*, 2004-2021.

- [72] R. Sridharan, J. Zuber, S. M. Connelly, E. Mathew, M. E. Dumont, *Biochim. Biophys. Acta* **2014**, *1838*, 15-33.
- [73] J. P. Overington, B. Al-Lazikani, A. L. Hopkins, *Nat. Rev. Drug Discov.* **2006**, *5*, 993-996.
- [74] K. Sriram, P. A. Insel, *Mol. Pharmacol.* **2018**, *93*, 251-258.
- [75] a) A. S. Hauser, M. M. Attwood, M. Rask-Andersen, H. B. Schiöth, D. E. Gloriam, *Nat. Rev. Drug Discov.* **2017**, *16*, 829-842; b) A. Jazayeri, S. P. Andrews, F. H. Marshall, *Chem. Rev.* **2017**, *117*, 21-37.
- [76] M. Congreve, C. de Graaf, N. A. Swain, C. G. Tate, *Cell* **2020**, *181*, 81-91.
- [77] S. Moro, F. Deflorian, G. Spalluto, G. Pastorin, B. Cacciari, S.-K. Kim, K. A. Jacobson, *Chem. Commun.* **2003**, 2949-2956.
- [78] a) H. B. Schiöth, R. Fredriksson, *Gen. Comp. Endocrinol.* **2005**, *142*, 94-101; b) G.-M. Hu, M. K. Secario, C.-M. Chen, *Database* **2019**, *2019*, baz073.
- [79] C. Southan, J. L. Sharman, H. E. Benson, E. Faccenda, A. J. Pawson, S. P. Alexander, O. P. Buneman, A. P. Davenport, J. C. McGrath, J. A. Peters, M. Spedding, W. A. Catterall, D. Fabbro, J. A. Davies, *Nucleic Acids Res.* **2016**, *44*, D1054-1068.
- [80] R. Fredriksson, M. C. Lagerström, L. G. Lundin, H. B. Schiöth, *Mol. Pharmacol.* **2003**, *63*, 1256-1272.
- [81] T. Hua, X. Li, L. Wu, C. Iliopoulos-Tsoutsouvas, Y. Wang, M. Wu, L. Shen, C. A. Johnston, S. P. Nikas, F. Song, X. Song, S. Yuan, Q. Sun, Y. Wu, S. Jiang, T. W. Grim, O. Benchama, E. L. Stahl, N. Zvonok, S. Zhao, L. M. Bohn, A. Makriyannis, Z. J. Liu, *Cell* **2020**, *180*, 655-665.
- [82] M. Bouvier, *Nat. Struct. Mol. Biol.* **2013**, *20*, 539-541.
- [83] D. M. Rosenbaum, S. G. Rasmussen, B. K. Kobilka, *Nature* **2009**, *459*, 356-363.
- [84] D. Hilger, M. Masureel, B. K. Kobilka, *Nat. Struct. Mol. Biol.* **2018**, *25*, 4-12.
- [85] Z. Rankovic, T. F. Brust, L. M. Bohn, *Bioorg. Med. Chem. Lett.* **2016**, *26*, 241-250.
- [86] D. Wacker, R. C. Stevens, B. L. Roth, *Cell* **2017**, *170*, 414-427.
- [87] L. A. Stoddart, L. E. Kilpatrick, S. J. Briddon, S. J. Hill, *Neuropharmacology* **2015**, *98*, 48-57.
- [88] R. Mechoulam, L. Hanus, *Chem. Phys. Lipids* **2000**, *108*, 1-13.
- [89] A. Makriyannis, *J. Med. Chem.* **2014**, *57*, 3891-3911.
- [90] Y. Gaoni, R. Mechoulam, *J. Am. Chem. Soc.* **1964**, *86*, 1646-1647.
- [91] J. M. McPartland, M. Duncan, V. Di Marzo, R. G. Pertwee, *Br. J. Pharmacol.* **2015**, *172*, 737-753.
- [92] L. A. Matsuda, S. J. Lolait, M. J. Brownstein, A. C. Young, T. I. Bonner, *Nature* **1990**, *346*, 561-564.
- [93] M. R. Elphick, M. Egertová, *Handb. Exp. Pharmacol.* **2005**, 283-297.
- [94] M. Pyszniak, J. Tabarkiewicz, J. J. Łuszczki, *Onco Targets Ther* **2016**, *9*, 4323-4336.
- [95] A. C. Howlett, F. Barth, T. I. Bonner, G. Cabral, P. Casellas, W. A. Devane, C. C. Felder, M. Herkenham, K. Mackie, B. R. Martin, R. Mechoulam, R. G. Pertwee, *Pharmacol. Rev.* **2002**, *54*, 161-202.
- [96] a) N. Stella, P. Schweitzer, D. Piomelli, *Nature* **1997**, *388*, 773-778; b) T. Bisogno, F. Howell, G. Williams, A. Minassi, M. G. Cascio, A. Ligresti, I. Matias, A. Schiano-Moriello, P. Paul, E. J. Williams, U. Gangadharan, C. Hobbs, V. Di Marzo, P. Doherty, *J. Cell Biol.* **2003**, *163*, 463-468.
- [97] J. L. Blankman, G. M. Simon, B. F. Cravatt, *Chem. Biol.* **2007**, *14*, 1347-1356.
- [98] X. H. Jin, T. Uyama, J. Wang, Y. Okamoto, T. Tonai, N. Ueda, *Biochim. Biophys. Acta* **2009**, *1791*, 32-38.
- [99] K. Tsuboi, Y. X. Sun, Y. Okamoto, N. Araki, T. Tonai, N. Ueda, *J. Biol. Chem.* **2005**, *280*, 11082-11092.
- [100] a) S. Munro, K. L. Thomas, M. Abu-Shaar, *Nature* **1993**, *365*, 61-65; b) W. A. Devane, F. A. Dysarz, M. R. Johnson, L. S. Melvin, A. C. Howlett, *Mol. Pharmacol.* **1988**, *34*, 605-613.

- [101] a) R. B. Laprairie, A. M. Bagher, E. M. Denovan-Wright, *Curr. Opin. Pharmacol.* **2017**, *32*, 32-43; b) M. Soethoudt, U. Grether, J. Fingerle, T. W. Grim, F. Fezza, L. de Petrocellis, C. Ullmer, B. Rothenhausler, C. Perret, N. van Gils, D. Finlay, C. MacDonald, A. Chicca, M. D. Gens, J. Stuart, H. de Vries, N. Mastrangelo, L. Xia, G. Alachouzos, M. P. Baggelaar, A. Martella, E. D. Mock, H. Deng, L. H. Heitman, M. Connor, V. Di Marzo, J. Gertsch, A. H. Lichtman, M. Maccarrone, P. Pacher, M. Glass, M. van der Stelt, *Nat. Commun.* **2017**, *8*, 13958-13972.
- [102] a) S. Mukherjee, M. Adams, K. Whiteaker, A. Daza, K. Kage, S. Cassar, M. Meyer, B. B. Yao, *Eur. J. Pharmacol.* **2004**, *505*, 1-9; b) M. S. Ibsen, M. Connor, M. Glass, *Cannabis Cannabinoid Res.* **2017**, *2*, 48-60.
- [103] M. Aghazadeh Tabrizi, P. G. Baraldi, P. A. Borea, K. Varani, *Chem. Rev.* **2016**, *116*, 519-560.
- [104] K. Mackie, *Handb. Exp. Pharmacol.* **2005**, 299-325.
- [105] a) C. Turcotte, M.-R. Blanchet, M. Laviolette, N. Flamand, *Cell. Mol. Life Sci.* **2016**, *73*, 4449-4470; b) S. Galiegue, S. Mary, J. Marchand, D. Dussossoy, D. Carriere, P. Carayon, M. Bouaboula, D. Shire, G. Le Fur, P. Casellas, *Eur. J. Biochem.* **1995**, *232*, 54-61.
- [106] F. A. Moreira, M. Grieb, B. Lutz, *Best. Pract. Res. Clin. Endocrinol. Metab.* **2009**, *23*, 133-144.
- [107] S. Mukhopadhyay, S. Das, E. A. Williams, D. Moore, J. D. Jones, D. S. Zahm, M. M. Ndengele, A. J. Lechner, A. C. Howlett, *J. Neuroimmunol.* **2006**, *181*, 82-92.
- [108] C. Turcotte, M. R. Blanchet, M. Laviolette, N. Flamand, *Cell. Mol. Life Sci.* **2016**, *73*, 4449-4470.
- [109] a) P. Pacher, R. Mechoulam, *Prog. Lipid Res.* **2011**, *50*, 193-211; b) J. Guindon, A. G. Hohmann, *Br. J. Pharmacol.* **2008**, *153*, 319-334.
- [110] a) R. P. Picone, D. A. Kendall, *Mol. Endocrinol.* **2015**, *29*, 801-813; b) A. M. Malfitano, S. Basu, K. Maresz, M. Bifulco, B. N. Dittel, *Semin. Immunol.* **2014**, *26*, 369-379; c) R. G. Pertwee, *Philos. Trans. R. Soc.* **2012**, *367*, 3353-3363.
- [111] a) G. A. Thakur, R. Tichkule, S. Bajaj, A. Makriyannis, *Expert Opin. Ther. Pat.* **2009**, *19*, 1647-1673; b) E. Pop, *Curr. Opin. Chem. Biol.* **1999**, *3*, 418-425.
- [112] P. Morales, L. Hernandez-Folgado, P. Goya, N. Jagerovic, *Expert Opin. Ther. Pat.* **2016**, *26*, 843-856.
- [113] a) M. E. Badowski, P. K. Yanful, *Ther. Clin. Risk. Manag.* **2018**, *14*, 643-651; b) M. B. May, A. E. Glode, *Cancer Manag. Res.* **2016**, *8*, 49-55; c) AbbVie. MARINOL (dronabinol) [drug label]. US Food and Drug Administration (revised on August 2017). Available online: [https://www.accessdata.fda.gov/drugsatfda\\_docs/label/2017/018651s029lbl.pdf](https://www.accessdata.fda.gov/drugsatfda_docs/label/2017/018651s029lbl.pdf) (accessed on 19 July 2020); d) J. V. Pergolizzi, Jr., R. Taylor, J. A. LeQuang, G. Zampogna, R. B. Raffa, *Cancer Chemother. Pharmacol.* **2017**, *79*, 467-477; e) Valeant Pharmaceuticals International. Cesamet (nabilone) [drug label]. US Food and Drug Administration (revised on May 2006). Available online: [https://www.accessdata.fda.gov/drugsatfda\\_docs/label/2006/018677s011lbl.pdf](https://www.accessdata.fda.gov/drugsatfda_docs/label/2006/018677s011lbl.pdf) (accessed on 19 July 2020).
- [114] a) T. Bisogno, L. Hanuš, L. De Petrocellis, S. Tchilibon, D. E. Ponde, I. Brandi, A. S. Moriello, J. B. Davis, R. Mechoulam, V. Di Marzo, *Br. J. Pharmacol.* **2001**, *134*, 845-852; b) R. B. Laprairie, A. M. Bagher, M. E. Kelly, E. M. Denovan-Wright, *Br. J. Pharmacol.* **2015**, *172*, 4790-4805.
- [115] Greenwich Biosciences. Epidiolex (cannabidiol) [drug label]. US Food and Drug Administration (revised on June 2018). Available online: [https://www.accessdata.fda.gov/drugsatfda\\_docs/label/2018/210365lbl.pdf](https://www.accessdata.fda.gov/drugsatfda_docs/label/2018/210365lbl.pdf) (accessed on 19 July 2020).
- [116] a) G. Podda, C. S. Constantinescu, *Expert Opin. Biol. Ther.* **2012**, *12*, 1517-1531; b) P. Robson, *Expert Opin. Drug Saf.* **2011**, *10*, 675-685.
- [117] a) V. Werth, C. V. Oddis, I. E. Lundberg, D. Fiorentino, C. Cornwall, N. Dgetluck, S. Constantine, B. White, *Ann. Rheum. Dis.* **2019**, *78*, 1228-1228; b) Corbus Pharmaceuticals. Lenabasum (JBT-101) [Corbus Pharmaceuticals pipeline]. Corbus Pharmaceuticals (revised on

- 2020). Available online: <https://www.corbuspharma.com/our-science/lenabasum> (accessed on 19 July 2020); c) M. Tepper, *Ultrapure tetrahydrocannabinol-11-oic acids*, **2017**, US9801849B2; d) Arena Pharmaceuticals. Olorinab (APD371) [Arena Pharmaceuticals Pipeline]. Arena Pharmaceuticals (revised on 2020). Available online: <https://www.arenapharm.com/pipeline/apd371/> (accessed on 19 July 2020); e) R. M. Jones, S. Han, L. Thoresen, J.-K. Jung, S. Strah-Pleyne, X. Zhu, Y. Xiong, D. Yue, *Cannabinoid receptor modulators*, **2014**, US8778950B2.
- [118] D. Riether, F. P. C. Binder, H. Doods, S. G. Müller, J. R. Nicholson, A. Sauer, *(Cyano-dimethyl)-isoxazoles and -[1,3,4]thiadiazoles*, **2018**, US10112934B2.
- [119] V. Di Marzo, *Nat. Rev. Drug Discov.* **2018**, *17*, 623-639.
- [120] a) Centrexion Therapeutics. CNTX-6016 [Centrexion Therapeutics Pipeline]. U.S. National Library of Medicine (revised on November 2019). Available online: <https://clinicaltrials.gov/ct2/show/NCT04154501> (accessed on 19 July 2020); b) Cmxtwenty. CMX-020 [Cmxtwenty Pipeline]. Australian New Zealand Clinical Trials Registry (revised on December 2018). Available online: <https://www.anzctr.org.au/Trial/Registration/TrialReview.aspx?id=371547&isReview=true> (accessed on 19 July 2020); c) Emerald Health Pharmaceuticals Inc. EHP-101 [Emerald Health Pharmaceuticals Pipeline]. U.S. National Library of Medicine (revised on October 2019). Available online: <https://clinicaltrials.gov/ct2/show/NCT03745001?term=Emerald+Health+Pharmaceuticals&rank=1> (accessed on 19 July 2020); d) NeuroTherapia, Inc. NTRX-07 [NeuroTherapia Pipeline]. U.S. National Library of Medicine (revised on May 2020). Available online: <https://clinicaltrials.gov/ct2/show/NCT04375436> (accessed on 19 July 2020); e) M. Naguib, P. Diaz, J. J. Xu, F. Astruc-Diaz, S. Craig, P. Vivas-Mejia, D. L. Brown, *Br. J. Pharmacol.* **2008**, *155*, 1104-1116.
- [121] A. Dhopeswarkar, K. Mackie, *Mol. Pharmacol.* **2014**, *86*, 430-437.
- [122] a) S. M. Paul, D. S. Mytelka, C. T. Dunwiddie, C. C. Persinger, B. H. Munos, S. R. Lindborg, A. L. Schacht, *Nat. Rev. Drug Discov.* **2010**, *9*, 203-214; b) A. A. Seyhan, *Transl. Med. Commun.* **2019**, *4*, 18.
- [123] a) P. M. Sexton, A. Christopoulos, *Cell* **2018**, *172*, 636-638; b) S. P. H. Alexander, D. A. Kendall, *British journal of pharmacology* **2007**, *152*, 602-623; c) L. Cristino, T. Bisogno, V. Di Marzo, *Nat. Rev. Neurol.* **2020**, *16*, 9-29.
- [124] B. K. Atwood, A. Straiker, K. Mackie, *Prog. Neuropsychopharmacol. Biol. Psychiatry* **2012**, *38*, 16-20.
- [125] P. Pacher, R. Mechoulam, *Prog. Lipid Res.* **2011**, *50*, 193-211.
- [126] a) D. S. Tyler, J. Vappiani, T. Caneque, E. Y. N. Lam, A. Ward, O. Gilan, Y. C. Chan, A. Hienzsch, A. Rutkowska, T. Werner, A. J. Wagner, D. Lugo, R. Gregory, C. Ramirez Molina, N. Garton, C. R. Wellaway, S. Jackson, L. MacPherson, M. Figueiredo, S. Stolzenburg, C. C. Bell, C. House, S. J. Dawson, E. D. Hawkins, G. Drewes, R. K. Prinjha, R. Rodriguez, P. Grandi, M. A. Dawson, *Science* **2017**, *356*, 1397-1401; b) G. M. Simon, M. J. Niphakis, B. F. Cravatt, *Nat. Chem. Biol.* **2013**, *9*, 200-205.
- [127] a) A. C. Schmöle, R. Lundt, B. Gennequin, H. Schrage, E. Beins, A. Krämer, T. Zimmer, A. Limmer, A. Zimmer, D. M. Otte, *PLoS One* **2015**, *10*, e0138986; b) S. C. Locatelli-Hoops, I. Gorshkova, K. Gawrisch, A. A. Yeliseev, *Biochim. Biophys. Acta Proteins Proteom.* **2013**, *1834*, 2045-2056; c) S. C. Locatelli-Hoops, I. Gorshkova, K. Gawrisch, A. A. Yeliseev, *FASEB J.* **2013**, *27*, 790.718-790.718.
- [128] N. L. Grimsey, C. E. Goodfellow, M. Dragunow, M. Glass, *Biochim. Biophys. Acta* **2011**, *1813*, 1554-1560.

- [129] a) Y. Gómez-Gálvez, C. Palomo-Garo, J. Fernández-Ruiz, C. García, *Prog. Neuropsychopharmacol. Biol. Psychiatry* **2016**, *64*, 200-208; b) E. Bakali, J. McDonald, R. A. Elliott, D. G. Lambert, D. G. Tincello, *Int. Urogynecol. J.* **2016**, *27*, 129-139.
- [130] a) C. Fede, G. Albertin, L. Petrelli, M. M. Sfriso, C. Biz, R. De Caro, C. Stecco, *Eur. J. Histochem.* **2016**, *60*, 2643; b) R. García-Cabrerizo, M. J. García-Fuster, *Neurosci. lett.* **2016**, *615*, 60-65.
- [131] a) H. Y. Zhang, H. Shen, C. J. Jordan, Q. R. Liu, E. L. Gardner, A. Bonci, Z. X. Xi, *Acta Pharmacol. Sin.* **2019**, *40*, 398-409; b) B. Cécyre, S. Thomas, M. Ptitto, C. Casanova, J.-F. Bouchard, *Naunyn-Schmiedeberg's Arch. Pharmacol.* **2014**, *387*, 175-184; c) Y. Marchalant, P. W. Brownjohn, A. Bonnet, T. Kleffmann, J. C. Ashton, *J. Histochem. Cytochem.* **2014**, *62*, 395-404; d) Y. Li, J. Kim, *Neuroscience* **2015**, *311*, 253-267.
- [132] F. Basagni, M. Rosini, M. Decker, *ChemMedChem* **2020**, *15*, 1-17.
- [133] F. Spinelli, L. Mu, S. M. Ametamey, *J. Labelled Compd. Radiopharm.* **2018**, *61*, 299-308.
- [134] A. R. Kherlopian, T. Song, Q. Duan, M. A. Neimark, M. J. Po, J. K. Gohagan, A. F. Laine, *BMC Syst. Biol.* **2008**, *2*, 74-92.
- [135] a) A. G. Horti, Y. Gao, H. T. Ravert, P. Finley, H. Valentine, D. F. Wong, C. J. Endres, A. V. Savonenko, R. F. Dannals, *Biorg. Med. Chem.* **2010**, *18*, 5202-5207; b) A. V. Savonenko, T. Melnikova, Y. Wang, H. Ravert, Y. Gao, J. Koppel, D. Lee, O. Pletnikova, E. Cho, N. Sayyida, A. Hiatt, J. Troncoso, P. Davies, R. F. Dannals, M. G. Pomper, A. G. Horti, *PLoS One* **2015**, *10*, e0129618.
- [136] G. Pottier, V. Gómez-Vallejo, D. Padro, R. Boisgard, F. Dollé, J. Llop, A. Winkeler, A. Martín, *J. Cereb. Blood. Flow. Metab.* **2017**, *37*, 1163-1178.
- [137] R.-P. Moldovan, R. Teodoro, Y. Gao, W. Deuther-Conrad, M. Kranz, Y. Wang, H. Kuwabara, M. Nakano, H. Valentine, S. Fischer, M. G. Pomper, D. F. Wong, R. F. Dannals, P. Brust, A. G. Horti, *J. Med. Chem.* **2016**, *59*, 7840-7855.
- [138] N. Evens, G. G. Muccioli, N. Houbrechts, D. M. Lambert, A. M. Verbruggen, K. Van Laere, G. M. Bormans, *Nucl. Med. Biol.* **2009**, *36*, 455-465.
- [139] a) R. Ahmad, A. Postnov, G. Bormans, J. Versijpt, M. Vandenbulcke, K. Van Laere, *Eur. J. Nucl. Med. Mol. Imaging* **2016**, *43*, 2219-2227; b) T. Hosoya, D. Fukumoto, T. Kakiuchi, S. Nishiyama, S. Yamamoto, H. Ohba, H. Tsukada, T. Ueki, K. Sato, Y. Ouchi, *J. Neuroinflammation* **2017**, *14*, 69; c) C. Vandeputte, C. Casteels, T. Struys, M. Koole, D. van Veghel, N. Evens, A. Gerits, T. Dresselaers, I. Lambrechts, U. Himmelreich, G. Bormans, K. Van Laere, *Eur. J. Nucl. Med. Mol. Imaging* **2012**, *39*, 1796-1806; d) H. D. Burns, K. Van Laere, S. Sanabria-Bohórquez, T. G. Hamill, G. Bormans, W.-s. Eng, R. Gibson, C. Ryan, B. Connolly, S. Patel, S. Krause, A. Vanko, A. Van Hecken, P. Dupont, I. De Lepeleire, P. Rothenberg, S. A. Stoch, J. Cote, W. K. Hagmann, J. P. Jewell, L. S. Lin, P. Liu, M. T. Goulet, K. Gottesdiener, J. A. Wagner, J. de Hoon, L. Mortelmans, T. M. Fong, R. J. Hargreaves, *Proc. Natl. Acad. Sci. U.S.A.* **2007**, *104*, 9800-9805.
- [140] a) C. Vandeputte, N. Evens, J. Toelen, C. M. Deroose, B. Bosier, A. Ibrahimi, A. Van der Perren, R. Gijssbers, P. Janssen, D. M. Lambert, A. Verbruggen, Z. Debyser, G. Bormans, V. Baekelandt, K. Van Laere, *J. Nucl. Med.* **2011**, *52*, 1102-1109; b) N. Evens, C. Vandeputte, G. G. Muccioli, D. M. Lambert, V. Baekelandt, A. M. Verbruggen, Z. Debyser, K. Van Laere, G. M. Bormans, *Biorg. Med. Chem.* **2011**, *19*, 4499-4505; c) M. Ahamed, D. van Veghel, C. Ullmer, K. Van Laere, A. Verbruggen, G. M. Bormans, *Front. Neurosci.* **2016**, *10*, 431; d) B. Attili, S. Celen, M. Ahamed, M. Koole, C. V. D. Haute, W. Vanduffel, G. Bormans, *Br. J. Pharmacol.* **2019**, *176*, 1481-1491; e) A. Haider, J. Kretz, L. Gobbi, H. Ahmed, K. Atz, M. Bürkler, C. Bartelmus, J. Fingerle, W. Guba, C. Ullmer, M. Honer, I. Knuesel, M. Weber, A. Brink, A. M. Herde, C. Keller, R. Schibli, L. Mu, U. Grether, S. M. Ametamey, *J. Med. Chem.* **2019**, *62*, 11165-11181.
- [141] R. Slavik, U. Grether, A. Müller Herde, L. Gobbi, J. Fingerle, C. Ullmer, S. D. Krämer, R. Schibli, L. Mu, S. M. Ametamey, *J. Med. Chem.* **2015**, *58*, 4266-4277.



- [142] D. Weichert, P. Gmeiner, *ACS Chem. Biol.* **2015**, *10*, 1376-1386.
- [143] P. P. Geurink, L. M. Prely, G. A. van der Marel, R. Bischoff, H. S. Overkleeft, *Top. Curr. Chem.* **2012**, *324*, 85-113.
- [144] a) R. P. Picone, A. D. Khanolkar, W. Xu, L. A. Ayotte, G. A. Thakur, D. P. Hurst, M. E. Abood, P. H. Reggio, D. J. Fournier, A. Makriyannis, *Mol. Pharmacol.* **2005**, *68*, 1623-1635; b) G. Ogawa, M. A. Tius, H. Zhou, S. P. Nikas, A. Halikhedkar, S. Mallipeddi, A. Makriyannis, *J. Med. Chem.* **2015**, *58*, 3104-3116.
- [145] a) Y. Pei, R. W. Mercier, J. K. Anday, G. A. Thakur, A. M. Zvonok, D. Hurst, P. H. Reggio, D. R. Janero, A. Makriyannis, *Chem. Biol.* **2008**, *15*, 1207-1219; b) D. W. Szymanski, M. Papanastasiou, K. Melchior, N. Zvonok, R. W. Mercier, D. R. Janero, G. A. Thakur, S. Cha, B. Wu, B. Karger, A. Makriyannis, *J. Proteome Res.* **2011**, *10*, 4789-4798.
- [146] a) J. Fichna, M. Bawa, G. A. Thakur, R. Tichkule, A. Makriyannis, D. M. McCafferty, K. A. Sharkey, M. Storr, *PLoS One* **2014**, *9*, e109115; b) C. M. Keenan, M. A. Storr, G. A. Thakur, J. T. Wood, J. Wager-Miller, A. Straiker, M. R. Eno, S. P. Nikas, M. Bashashati, H. Hu, K. Mackie, A. Makriyannis, K. A. Sharkey, *Br. J. Pharmacol.* **2015**, *172*, 2406-2418.
- [147] a) R. W. Mercier, Y. Pei, L. Pandarinathan, D. R. Janero, J. Zhang, A. Makriyannis, *Chem. Biol.* **2010**, *17*, 1132-1142; b) S. Mallipeddi, S. Kreimer, N. Zvonok, K. Vemuri, B. L. Karger, A. R. Ivanov, A. Makriyannis, *J. Proteome Res.* **2017**, *16*, 2419-2428.
- [148] D. D. Dixon, M. A. Tius, G. A. Thakur, H. Zhou, A. L. Bowman, V. G. Shukla, Y. Peng, A. Makriyannis, *Bioorg. Med. Chem. Lett.* **2012**, *22*, 5322-5325.
- [149] M. Soethoudt, S. C. Stolze, M. V. Westphal, L. van Stralen, A. Martella, E. J. van Rooden, W. Guba, Z. V. Varga, H. Deng, S. I. van Kasteren, U. Grether, A. P. IJzerman, P. Pacher, E. M. Carreira, H. S. Overkleeft, A. Ioan-Facsinay, L. H. Heitman, M. van der Stelt, *J. Am. Chem. Soc.* **2018**, *140*, 6067-6075.
- [150] A. S. Yates, S. W. Doughty, D. A. Kendall, B. Kellam, *Bioorg. Med. Chem. Lett.* **2005**, *15*, 3758-3762.
- [151] P. Diaz, J. Xu, F. Astruc-Diaz, H.-M. Pan, D. L. Brown, M. Naguib, *J. Med. Chem.* **2008**, *51*, 4932-4947.
- [152] R. R. Petrov, M. E. Ferrini, Z. Jaffar, C. M. Thompson, K. Roberts, P. Diaz, *Bioorg. Med. Chem. Lett.* **2011**, *21*, 5859-5862.
- [153] A. G. Cooper, C. MacDonald, M. Glass, S. Hook, J. D. A. Tyndall, A. J. Vernall, *Eur. J. Med. Chem.* **2018**, *145*, 770-789.
- [154] F. Spinelli, R. Giampietro, A. Stefanachi, C. Riganti, J. Kopecka, F. S. Abatematteo, F. Leonetti, N. A. Colabufo, G. F. Mangiatordi, O. Nicolotti, M. G. Perrone, J. Brea, M. I. Loza, V. Infantino, C. Abate, M. Contino, *Eur. J. Med. Chem.* **2020**, *188*, 112037.
- [155] a) R. C. Sarott, M. Westphal, P. Pfaff, C. Korn, D. A. Sykes, T. Gazzzi, B. Brennecke, K. Atz, M. Weise, Y. Mostinski, P. Hompluem, E. Koers, T. Miljus, N. J. Roth, H. Asmelash, M. C. Vong, J. Piovesan, W. Guba, A. Rufer, E. A. Kuszniir, S. Huber, C. Raposo, E. A. Zirwes, A. Osterwald, A. Pavlovic, S. Moes, J. Beck, I. Benito-Cuesta, T. Grande, S. Ruiz de Martin, A. A. Yeliseev, F. Drawnel, G. Widmer, D. Holzer, T. van der Wel, H. Mandhair, C.-Y. Yuan, W. Drobyski, Y. Saroz, N. L. Grimsey, M. Honer, J. Fingerle, K. Gawrisch, J. Romero, C. Hillard, Z. Varga, M. van der Stelt, P. Pacher, J. Gertsch, P. McCormick, C. Ullmer, S. Oddi, M. Maccarrone, D. Veprintsev, M. Nazaré, U. Grether, E. M. Carreira, *J. Am. Chem. Soc.* **2020**, *142*, 16953-16964; b) S. Singh, C. R. M. Oyagawa, C. Macdonald, N. L. Grimsey, M. Glass, A. J. Vernall, *ACS Med. Chem. Lett.* **2019**, *10*, 209-214.
- [156] M. V. Westphal, R. C. Sarott, E. A. Zirwes, A. Osterwald, W. Guba, C. Ullmer, U. Grether, E. M. Carreira, *Chem. Eur. J.* **2020**, *26*, 1380-1387.
- [157] M. Bai, M. Sexton, N. Stella, D. J. Bornhop, *Bioconj. Chem.* **2008**, *19*, 988-992.



- [158] M. Sexton, G. Woodruff, E. A. Horne, Y. H. Lin, G. G. Muccioli, M. Bai, E. Stern, D. J. Bornhop, N. Stella, *Chem. Biol.* **2011**, *18*, 563-568.
- [159] S. Zhang, P. Shao, M. Bai, *Bioconjug. Chem.* **2013**, *24*, 1907-1916.
- [160] S. Zhang, N. Jia, P. Shao, Q. Tong, X.-Q. Xie, M. Bai, *Chem. Biol.* **2014**, *21*, 338-344.
- [161] Z. Wu, P. Shao, S. Zhang, M. Bai, *J. Biomed. Opt.* **2014**, *19*, 36006.
- [162] Z. Wu, P. Shao, S. Zhang, X. Ling, M. Bai, *J. Biomed. Opt.* **2014**, *19*, 76016.
- [163] X. Ling, S. Zhang, P. Shao, W. Li, L. Yang, Y. Ding, C. Xu, N. Stella, M. Bai, *Biomaterials* **2015**, *57*, 169-178.
- [164] N. Jia, S. Zhang, P. Shao, C. Bagia, J. M. Janjic, Y. Ding, M. Bai, *Mol. Pharm.* **2014**, *11*, 1919-1929.
- [165] W. X. Ren, J. Han, S. Uhm, Y. J. Jang, C. Kang, J.-H. Kim, J. S. Kim, *Chem. Commun.* **2015**, *51*, 10403-10418.
- [166] L. Martin-Couce, M. Martin-Fontecha, O. Palomares, L. Mestre, A. Cordomi, M. Hernangomez, S. Palma, L. Pardo, C. Guaza, M. L. Lopez-Rodriguez, S. Ortega-Gutierrez, *Angew. Chem. Int. Ed. Engl.* **2012**, *51*, 6896-6899.
- [167] A. J. Vernall, S. J. Hill, B. Kellam, *Br. J. Pharmacol.* **2014**, *171*, 1073-1084.
- [168] a) B. Cecyre, S. Thomas, M. Ptito, C. Casanova, J. F. Bouchard, *Naunyn Schmiedebergs Arch Pharmacol* **2014**, *387*, 175-184; b) Y. Marchalant, P. W. Brownjohn, A. Bonnet, T. Kleffmann, J. C. Ashton, *J. Histochem. Cytochem.* **2014**, *62*, 395-404.
- [169] K. A. Jacobson, *Bioconjug. Chem.* **2009**, *20*, 1816-1835.
- [170] B. Dhurwasulu, U. Grether, M. Nettekoven, S. Roever, M. Rogers-Evans, T. Schulz-Gasch, *Novel pyrazine derivatives as CB2 receptor agonists*, **2014**, WO2014086807A1.
- [171] C. Bissantz, U. Grether, P. Hebeisen, A. Kimbara, Q. Liu, M. Nettekoven, M. Prunotto, S. Roever, M. Rogers-Evans, T. Schulz-Gasch, C. Ullmer, Z. Wang, W. Yang, *Pyridin-2-amides useful as CB2 agonists.*, **2012**, WO2012168350A1.
- [172] a) M. M. Hann, G. M. Keserü, *Nat. Rev. Drug Discov.* **2012**, *11*, 355-365; b) P. D. Leeson, B. Springthorpe, *Nat. Rev. Drug Discov.* **2007**, *6*, 881-890.
- [173] A. K. Ghose, G. M. Crippen, *J. Comput. Chem.* **1986**, *7*, 565-577.
- [174] P. Matsson, J. Kihlberg, *J. Med. Chem.* **2017**, *60*, 1662-1664.
- [175] M. Kansy, F. Senner, K. Gubernator, *J. Med. Chem.* **1998**, *41*, 1007-1010.
- [176] A. L. Hopkins, G. M. Keserü, P. D. Leeson, D. C. Rees, C. H. Reynolds, *Nat. Rev. Drug Discov.* **2014**, *13*, 105-121.
- [177] A. J. Vernall, S. J. Hill, B. Kellam, *Brit. J. Pharmacol.* **2014**, *171*, 1073-1084.
- [178] T. J. Commons, A. Fensome, G. D. Heffernan, C. C. Mccomas, R. P. Woodworth, M. B. Webb, M. A. Marella, E. G. Melenski, *Pyrrolidine and related derivatives useful as pr modulators*, **2008**, WO2008021339A2.
- [179] W. Liu, P. Ray, S. A. Benezra, *J. Chem. Soc., Perkin Trans. 1* **1995**, 553-559.
- [180] S. P. Mcmanus, R. M. Karaman, M. R. Sedaghat-Herati, T. G. Shannon, T. W. Hovatter, J. M. Harris, *J. Polym. Sci., Part A: Polym. Chem.* **1990**, *28*, 3337-3346.
- [181] T. Hua, K. Vemuri, M. Pu, L. Qu, G. W. Han, Y. Wu, S. Zhao, W. Shui, S. Li, A. Korde, R. B. Laprairie, E. L. Stahl, J. H. Ho, N. Zvonok, H. Zhou, I. Kufareva, B. Wu, Q. Zhao, M. A. Hanson, L. M. Bohn, A. Makriyannis, R. C. Stevens, Z. J. Liu, *Cell* **2016**, *167*, 750-762.e714.
- [182] T. den Hartog, B. Maciá, A. J. Minnaard, B. L. Feringa, *Adv. Synth. Catal.* **2010**, *352*, 999-1013.
- [183] D. F. Veber, S. R. Johnson, H. Y. Cheng, B. R. Smith, K. W. Ward, K. D. Kopple, *J. Med. Chem.* **2002**, *45*, 2615-2623.
- [184] a) P. D. Leeson, B. Springthorpe, *Nat. Rev. Drug Discov.* **2007**, *6*, 881-890; b) X. Liu, B. Testa, A. Fahr, *Pharm. Res.* **2011**, *28*, 962-977.
- [185] J. A. Arnott, S. L. Planey, *Expert Opin. Drug Discov.* **2012**, *7*, 863-875.

- [186] a) M. P. Gleeson, *J. Med. Chem.* **2008**, *51*, 817-834; b) M. J. Waring, *Expert Opin. Drug Discov.* **2010**, *5*, 235-248.
- [187] C. Saal, A. C. Peterleit, *Eur. J. Pharm. Sci.* **2012**, *47*, 589-595.
- [188] a) A. Collet, *Angew. Chem. Int. Ed.* **1998**, *37*, 3239-3241; b) S. Müller, M. C. Afraz, R. de Gelder, G. J. A. Ariaans, B. Kaptein, Q. B. Broxterman, A. Bruggink, *Eur. J. Org. Chem.* **2005**, *2005*, 1082-1096.
- [189] H. E. Schoemaker, D. Mink, M. G. Wubbolts, *Science* **2003**, *299*, 1694-1697.
- [190] D. A. Gruzdev, S. A. Vakarov, G. L. Levit, V. P. Krasnov, *Chem. Heterocycl. Comp.* **2014**, *49*, 1795-1807.
- [191] E. Suna, *Synthesis* **2003**, *2003*, 0251-0254.
- [192] G. Lukinavicius, K. Umezawa, N. Olivier, A. Honigmann, G. Yang, T. Plass, V. Mueller, L. Reymond, I. R. Correa, Jr., Z. G. Luo, C. Schultz, E. A. Lemke, P. Heppenstall, C. Eggeling, S. Manley, K. Johnsson, *Nat. Chem.* **2013**, *5*, 132-139.
- [193] S. Bendels, C. Bissantz, B. Fasching, G. Gerebtzoff, W. Guba, M. Kansy, J. Migeon, S. Mohr, J.-U. Peters, F. Tillier, R. Wyler, C. Lerner, C. Kramer, H. Richter, S. Roberts, *J. Pharmacol. Toxicol. Methods* **2019**, *99*, 106609.
- [194] M. Soethoudt, U. Grether, J. Fingerle, T. W. Grim, F. Fezza, L. de Petrocellis, C. Ullmer, B. Rothenhäusler, C. Perret, N. van Gils, D. Finlay, C. MacDonald, A. Chicca, M. D. Gens, J. Stuart, H. de Vries, N. Mastrangelo, L. Xia, G. Alachouzos, M. P. Baggelaar, A. Martella, E. D. Mock, H. Deng, L. H. Heitman, M. Connor, V. Di Marzo, J. Gertsch, A. H. Lichtman, M. Maccarrone, P. Pacher, M. Glass, M. van der Stelt, *Nat. Commun.* **2017**, *8*, 13958.
- [195] N. Ouali Alami, C. Schurr, F. Olde Heuvel, L. Tang, Q. Li, A. Tasdogan, A. Kimbara, M. Nettekoven, G. Ottaviani, C. Raposo, S. Röver, M. Rogers-Evans, B. Rothenhäusler, C. Ullmer, J. Fingerle, U. Grether, I. Knuesel, T. M. Boeckers, A. Ludolph, T. Wirth, F. Roselli, B. Baumann, *EMBO J.* **2018**, *37*, e98697.
- [196] W. van der Velden, L. H. Heitman, M. M. Rosenkilde, *ACS Pharmacol. Transl. Sci.* **2020**, *3*, 179-189.
- [197] D. A. Schuetz, W. E. A. de Witte, Y. C. Wong, B. Knasmueller, L. Richter, D. B. Kokh, S. K. Sadiq, R. Bosma, I. Nederpelt, L. H. Heitman, E. Segala, M. Amaral, D. Guo, D. Andres, V. Georgi, L. A. Stoddart, S. Hill, R. M. Cooke, C. De Graaf, R. Leurs, M. Frech, R. C. Wade, E. C. M. de Lange, A. P. IJzerman, A. Müller-Fahrnow, G. F. Ecker, *Drug Discov. Today* **2017**, *22*, 896-911.
- [198] A. Martella, H. Sijben, A. Rufer, J. Fingerle, U. Grether, C. Ullmer, T. Hartung, A. IJzerman, M. van der Stelt, L. Heitman, *Mol. Pharmacol.* **2017**, *92*, 389-400.
- [199] L. Chen, L. Jin, N. Zhou, *Expert Opin. Drug Discov.* **2012**, *7*, 791-806.
- [200] E. Martínez-Pinilla, O. Rabal, I. Reyes-Resina, M. Zamarbide, G. Navarro, J. A. Sánchez-Arias, I. de Miguel, J. L. Lanciego, J. Oyarzabal, R. Franco, *J. Pharmacol. Exp. Ther.* **2016**, *358*, 580-587.
- [201] M. Rinaldi-Carmona, F. Barth, J. Millan, J. M. Derocq, P. Casellas, C. Congy, D. Oustric, M. Sarran, M. Bouaboula, B. Calandra, M. Portier, D. Shire, J. C. Breliere, G. L. Le Fur, *J. Pharmacol. Exp. Ther.* **1998**, *284*, 644-650.
- [202] L. Hanuš, A. Breuer, S. Tchilibon, S. Shiloah, D. Goldenberg, M. Horowitz, R. G. Pertwee, R. A. Ross, R. Mechoulam, E. Fride, *PNAS* **1999**, *96*, 14228-14233.
- [203] L. Wang, M. S. Frei, A. Salim, K. Johnsson, *JACS* **2019**, *141*, 2770-2781.
- [204] X. Li, T. Hua, K. Vemuri, J.-H. Ho, Y. Wu, L. Wu, P. Popov, O. Benchama, N. Zvonok, K. a. Locke, L. Qu, G. W. Han, M. R. Iyer, R. Cinar, N. J. Coffey, J. Wang, M. Wu, V. Katritch, S. Zhao, G. Kunos, L. M. Bohn, A. Makriyannis, R. C. Stevens, Z.-J. Liu, *Cell* **2019**, *176*, 459-467.
- [205] C. Allemani, T. Matsuda, V. Di Carlo, R. Harewood, M. Matz, M. Niksic, A. Bonaventure, M. Valkov, C. J. Johnson, J. Esteve, O. J. Ogunbiyi, E. S. G. Azevedo, W. Q. Chen, S. Eser, G.

- Engholm, C. A. Stiller, A. Monnereau, R. R. Woods, O. Visser, G. H. Lim, J. Aitken, H. K. Weir, M. P. Coleman, *Lancet* **2018**, *391*, 1023-1075.
- [206] I. Grantzdorffer, S. Carl-McGrath, M. P. Ebert, C. Rocken, *Pancreas* **2008**, *36*, 329-336.
- [207] J. Kleeff, M. Korc, M. Apte, C. La Vecchia, C. D. Johnson, A. V. Biankin, R. E. Neale, M. Tempero, D. A. Tuveson, R. H. Hruban, J. P. Neoptolemos, *Nat. Rev. Dis. Primers* **2016**, *2*, 16022.
- [208] J. Yu, A. Li, S.-M. Hong, R. H. Hruban, M. Goggins, *Clin. Cancer Res.* **2012**, *18*, 981-992.
- [209] R. H. Hruban, M. Goggins, J. Parsons, S. E. Kern, *Clin. Cancer Res.* **2000**, *6*, 2969-2972.
- [210] T. C. Cornish, R. H. Hruban, *Surg. Pathol. Clin.* **2011**, *4*, 523-535.
- [211] O. Strobel, J. Neoptolemos, D. Jager, M. W. Buchler, *Nat. Rev. Clin. Oncol.* **2019**, *16*, 11-26.
- [212] P. Tummala, O. Junaidi, B. Agarwal, *J. Gastrointest. Oncol.* **2011**, *2*, 168-174.
- [213] S. P. Pereira, L. Oldfield, A. Ney, P. A. Hart, M. G. Keane, S. J. Pandol, D. Li, W. Greenhalf, C. Y. Jeon, E. J. Koay, C. V. Almario, C. Halloran, A. M. Lennon, E. Costello, *Lancet Gastroenterol. Hepatol.* **2020**, *in press*.
- [214] P. Moutinho-Ribeiro, G. Macedo, S. A. Melo, *Front. Endocrinol. (Lausanne)* **2019**, *9*, 779-779.
- [215] A. Jemal, R. Siegel, J. Xu, E. Ward, *CA Cancer J. Clin.* **2010**, *60*, 277-300.
- [216] a) R. P. Merkow, K. Y. Bilimoria, D. J. Bentrem, H. A. Pitt, D. P. Winchester, M. C. Posner, C. Y. Ko, T. M. Pawlik, *Ann. Surg. Oncol.* **2014**, *21*, 1067-1074; b) D. K. Chang, A. L. Johns, N. D. Merrett, A. J. Gill, E. K. Colvin, C. J. Scarlett, N. Q. Nguyen, R. W. Leong, P. H. Cosman, M. I. Kelly, R. L. Sutherland, S. M. Henshall, J. G. Kench, A. V. Biankin, *J. Clin. Oncol.* **2009**, *27*, 2855-2862; c) I. Esposito, J. Kleeff, F. Bergmann, C. Reiser, E. Herpel, H. Friess, P. Schirmacher, M. W. Buchler, *Ann. Surg. Oncol.* **2008**, *15*, 1651-1660.
- [217] A. L. Vahrmeijer, M. Hutteman, J. R. van der Vorst, C. J. van de Velde, J. V. Frangioni, *Nat. Rev. Clin. Oncol.* **2013**, *10*, 507-518.
- [218] T. Sugiura, K. Uesaka, H. Kanemoto, T. Mizuno, K. Sasaki, H. Furukawa, K. Matsunaga, A. Maeda, *J. Gastrointest. Surg.* **2012**, *16*, 977-985.
- [219] S. Bunger, T. Laubert, U. J. Roblick, J. K. Habermann, *J. Cancer Res. Clin. Oncol.* **2011**, *137*, 375-389.
- [220] a) A. M. Schlitter, I. Esposito, *Cancers (Basel)* **2010**, *2*, 2001-2010; b) G. Garcea, A. R. Dennison, C. J. Pattenden, C. P. Neal, C. D. Sutton, D. P. Berry, *JOP* **2008**, *9*, 99-132.
- [221] T. Nagaya, Y. A. Nakamura, P. L. Choyke, H. Kobayashi, *Front. Oncol.* **2017**, *7*, 314.
- [222] S. H. Loosen, U. P. Neumann, C. Trautwein, C. Roderburg, T. Luedde, *Tumor Biol.* **2017**, *39*, 1010428317692231.
- [223] S. Jones, X. Zhang, D. W. Parsons, J. C.-H. Lin, R. J. Leary, P. Angenendt, P. Mankoo, H. Carter, H. Kamiyama, A. Jimeno, S.-M. Hong, B. Fu, M.-T. Lin, E. S. Calhoun, M. Kamiyama, K. Walter, T. Nikolskaya, Y. Nikolsky, J. Hartigan, D. R. Smith, M. Hidalgo, S. D. Leach, A. P. Klein, E. M. Jaffee, M. Goggins, A. Maitra, C. Iacobuzio-Donahue, J. R. Eshleman, S. E. Kern, R. H. Hruban, R. Karchin, N. Papadopoulos, G. Parmigiani, B. Vogelstein, V. E. Velculescu, K. W. Kinzler, *Science* **2008**, *321*, 1801-1806.
- [224] P. Argani, C. Iacobuzio-Donahue, B. Ryu, C. Rosty, M. Goggins, R. E. Wilentz, S. R. Murugesan, S. D. Leach, E. Jaffee, C. J. Yeo, J. L. Cameron, S. E. Kern, R. H. Hruban, *Clin. Cancer Res.* **2001**, *7*, 3862-3868.
- [225] K. A. Kelly, N. Bardeesy, R. Anbazhagan, S. Gurumurthy, J. Berger, H. Alencar, R. A. Depinho, U. Mahmood, R. Weissleder, *PLoS Med.* **2008**, *5*, e85.
- [226] D. Cantero, H. Friess, J. Deflorin, A. Zimmermann, M. A. Bründler, E. Riesle, M. Korc, M. W. Büchler, *Br. J. Cancer* **1997**, *75*, 388-395.
- [227] J.-W. Xu, T.-X. Wang, L. You, L.-F. Zheng, H. Shu, T.-P. Zhang, Y.-P. Zhao, *PLoS One* **2014**, *9*, e92847.
- [228] N. Jonckheere, N. Skrypek, I. Van Seuning, *Cancers (Basel)* **2010**, *2*, 1794-1812.

- [229] M. Niedergethmann, R. Hildenbrand, B. Wostbrock, M. Hartel, J. W. Sturm, A. Richter, S. Post, *Pancreas* **2002**, *25*, 122-129.
- [230] C. Xu, M. B. Wallace, J. Yang, L. Jiang, Q. Zhai, Y. Zhang, C. Hong, Y. Chen, T. S. Frank, J. A. Stauffer, H. J. Asbun, M. Raimondo, T. A. Woodward, Z. Li, S. Guha, L. Zheng, M. Li, *Curr. Mol. Med.* **2014**, *14*, 309-315.
- [231] S. J. Shin, J. A. Smith, G. A. Reznicek, S. Pan, R. Chen, T. A. Brentnall, G. Wiche, K. A. Kelly, *Proc. Natl. Acad. Sci. U.S.A.* **2013**, *110*, 19414-19419.
- [232] D. Bausch, S. Thomas, M. Mino-Kenudson, C. C. Fernandez-del, T. W. Bauer, M. Williams, A. L. Warshaw, S. P. Thayer, K. A. Kelly, *Clin. Cancer Res.* **2011**, *17*, 302-309.
- [233] K. Bozovičar, T. Bratkovič, *Int. J. Mol. Sci.* **2020**, *21*, 215.
- [234] P. E. Saw, E.-W. Song, *Protein Cell* **2019**, *10*, 787-807.
- [235] US National Library of Medicine. ClinicalTrials.gov (revised on 2013). Available online: <https://clinicaltrials.gov/ct2/show/NCT01962909> (accessed on 25 July 2020).
- [236] L. Qian, Q. Li, K. Baryeh, W. Qiu, K. Li, J. Zhang, Q. Yu, D. Xu, W. Liu, R. E. Brand, X. Zhang, W. Chen, G. Liu, *Transl. Res.* **2019**, *213*, 67-89.
- [237] R. H. Kimura, L. Wang, B. Shen, L. Huo, W. Tummers, F. V. Filipp, H. H. Guo, T. Haywood, L. Abou-Elkacem, L. Baratto, F. Habte, R. Devulapally, T. H. Witney, Y. Cheng, S. Tikole, S. Chakraborti, J. Nix, C. A. Bonagura, N. Hatami, J. J. Mooney, T. Desai, S. Turner, R. S. Gaster, A. Otte, B. C. Visser, G. A. Poultsides, J. Norton, W. Park, M. Stolowitz, K. Lau, E. Yang, A. Natarajan, O. Ilovich, S. Srinivas, A. Srinivasan, R. Paulmurugan, J. Willmann, F. T. Chin, Z. Cheng, A. Iagaru, F. Li, S. S. Gambhir, *Nat. Commun.* **2019**, *10*, 4673.
- [238] W. Aung, Z. H. Jin, T. Furukawa, M. Claron, D. Boturnyn, C. Sogawa, A. B. Tsuji, H. Wakizaka, T. Fukumura, Y. Fujibayashi, P. Dumy, T. Saga, *Mol. Imaging* **2013**, *12*, 376-387.
- [239] B. J. Hackel, R. H. Kimura, Z. Miao, H. Liu, A. Sathirachinda, Z. Cheng, F. T. Chin, S. S. Gambhir, *J. Nucl. Med.* **2013**, *54*, 1101-1105.
- [240] H. Hong, Y. Zhang, T. R. Nayak, J. W. Engle, H. C. Wong, B. Liu, T. E. Barnhart, W. Cai, *J. Nucl. Med.* **2012**, *53*, 1748-1754.
- [241] K. E. McCabe, B. Liu, J. D. Marks, J. S. Tomlinson, H. Wu, A. M. Wu, *Mol. Imaging Biol.* **2012**, *14*, 336-347.
- [242] A. Sugyo, A. B. Tsuji, H. Sudo, K. Nagatsu, M. Koizumi, Y. Ukai, G. Kurosawa, M. R. Zhang, Y. Kurosawa, T. Saga, *Nucl. Med. Commun.* **2015**, *36*, 286-294.
- [243] J. L. Houghton, B. M. Zeglis, D. Abdel-Atti, R. Aggeler, R. Sawada, B. J. Agnew, W. W. Scholz, J. S. Lewis, *Proc. Natl. Acad. Sci. U. S. A.* **2015**, *112*, 15850-15855.
- [244] Q. Wang, H. Yan, Y. Jin, Z. Wang, W. Huang, J. Qiu, F. Kang, K. Wang, X. Zhao, J. Tian, *Biomaterials* **2018**, *183*, 173-184.
- [245] a) M. A. Pysz, S. B. Machtaler, E. S. Seeley, J. J. Lee, T. A. Brentnall, J. Rosenberg, F. Tranquart, J. K. Willmann, *Radiology* **2015**, *274*, 790-799; b) N. Deshpande, Y. Ren, K. Foygel, J. Rosenberg, J. K. Willmann, *Radiology* **2011**, *258*, 804-811; c) K. Foygel, H. Wang, S. Machtaler, A. M. Lutz, R. Chen, M. Pysz, A. W. Lowe, L. Tian, T. Carrigan, T. A. Brentnall, J. K. Willmann, *Gastroenterology* **2013**, *145*, 885-894.e883.
- [246] L. Abou-Elkacem, S. V. Bachawal, J. K. Willmann, *Eur. J. Radiol.* **2015**, *84*, 1685-1693.
- [247] L. Yang, H. Mao, Y. A. Wang, Z. Cao, X. Peng, X. Wang, H. Duan, C. Ni, Q. Yuan, G. Adams, M. Q. Smith, W. C. Wood, X. Gao, S. Nie, *Small* **2009**, *5*, 235-243.
- [248] a) Z. Medarova, W. Pham, Y. Kim, G. Dai, A. Moore, *Int. J. Cancer* **2006**, *118*, 2796-2802; b) A. Moore, Z. Medarova, A. Potthast, G. Dai, *Cancer Res.* **2004**, *64*, 1821-1827.
- [249] X. Chen, H. Zhou, X. Li, N. Duan, S. Hu, Y. Liu, Y. Yue, L. Song, Y. Zhang, D. Li, Z. Wang, *EBioMedicine* **2018**, *30*, 129-137.
- [250] P. P. Adiseshaiah, R. M. Crist, S. S. Hook, S. E. McNeil, *Nat. Rev. Clin. Oncol.* **2016**, *13*, 750-765.

- [251] C. E. S. Hoogstins, L. S. F. Boogerd, B. G. Sibinga Mulder, J. S. D. Mieog, R. J. Swijnenburg, C. J. H. van de Velde, A. Farina Sarasqueta, B. A. Bonsing, B. Framery, A. Pèlegri, M. Gutowski, F. Cailler, J. Burggraaf, A. L. Vahrmeijer, *Ann. Surg. Oncol.* **2018**, *25*, 3350-3357.
- [252] W. S. Tummers, S. E. Miller, N. T. Teraphongphom, A. Gomez, I. Steinberg, D. M. Huland, S. Hong, S.-R. Kothapalli, A. Hasan, R. Ertsey, B. A. Bonsing, A. L. Vahrmeijer, R.-J. Swijnenburg, T. A. Longacre, G. A. Fisher, S. S. Gambhir, G. A. Poultides, E. L. Rosenthal, *Ann. Surg. Oncol.* **2018**, *25*, 1880-1888.
- [253] C. Zhang, R. Kimura, L. Abou-Elkacem, J. Levi, L. Xu, S. S. Gambhir, *J. Nucl. Med.* **2016**, *57*, 1629-1634.
- [254] D. Gao, L. Gao, C. Zhang, H. Liu, B. Jia, Z. Zhu, F. Wang, Z. Liu, *Biomaterials* **2015**, *53*, 229-238.
- [255] a) S. Munneke, K. Kodar, G. F. Painter, Bridget L. Stocker, M. S. M. Timmer, *RSC Adv.* **2017**, *7*, 45260-45268; b) Y. Gai, G. Xiang, X. Ma, W. Hui, Q. Ouyang, L. Sun, J. Ding, J. Sheng, D. Zeng, *Bioconjugate Chem.* **2016**, *27*, 515-520; c) E. M. Peck, P. M. Battles, D. R. Rice, F. M. Roland, K. A. Norquest, B. D. Smith, *Bioconjugate Chem.* **2016**, *27*, 1400-1410; d) Y. Sun, X. Ma, K. Cheng, B. Wu, J. Duan, H. Chen, L. Bu, R. Zhang, X. Hu, Z. Deng, L. Xing, X. Hong, Z. Cheng, *Angew. Chem. Int. Ed.* **2015**, *54*, 5981-5984; e) H. Li, H. Zhou, S. Krieger, J. J. Parry, J. J. Whittenberg, A. V. Desai, B. E. Rogers, P. J. A. Kenis, D. E. Reichert, *Bioconjugate Chem.* **2014**, *25*, 761-772; f) L. Xu, J. S. Josan, J. Vagner, M. R. Caplan, V. J. Hruby, E. A. Mash, R. M. Lynch, D. L. Morse, R. J. Gillies, *Proc. Natl. Acad. Sci. U.S.A.* **2012**, *109*, 21295-21300; g) V. Humblet, P. Misra, K. R. Bhushan, K. Nasr, Y.-S. Ko, T. Tsukamoto, N. Pannier, J. V. Frangioni, W. Maison, *J. Med. Chem.* **2009**, *52*, 544-550.
- [256] R. E. Mewis, S. J. Archibald, *Coord. Chem. Rev.* **2010**, *254*, 1686-1712.
- [257] X. Yu, J. Zhang, *Macrocyclic Polyamines: Synthesis and Applications*, Wiley-VCH, Weinheim, **2018**.
- [258] G. J. Stasiuk, N. J. Long, *Chem. Commun.* **2013**, *49*, 2732-2746.
- [259] P. Lejault, K. Duskova, C. Bernhard, I. E. Valverde, A. Romieu, D. Monchaud, *Eur. J. Org. Chem.* **2019**, *2019*, 6146-6157.
- [260] a) X. Zhang, H. Liu, Z. Miao, R. Kimura, F. Fan, Z. Cheng, *Bioorg. Med. Chem. Lett.* **2011**, *21*, 3423-3426; b) A. Wurzer, A. Vágner, D. Horváth, F. Fellegi, H.-J. Wester, F. K. Kálmán, J. Notni, *Front. Chem.* **2018**, *6*, A107.
- [261] a) H.-Y. Hu, N.-H. Lim, D. Ding-Pfennigdorff, J. Saas, K. U. Wendt, O. Ritzeler, H. Nagase, O. Plettenburg, C. Schultz, M. Nazare, *Bioconjug. Chem.* **2015**, *26*, 383-388; b) H.-Y. Hu, N.-H. Lim, H.-P. Juretschke, D. Ding-Pfennigdorff, P. Florian, M. Kohlmann, A. Kandira, J. Peter von Kries, J. Saas, K. A. Rudolphi, K. U. Wendt, H. Nagase, O. Plettenburg, M. Nazare, C. Schultz, *Chem. Sci.* **2015**, *6*, 6256-6261.
- [262] J. Šimeček, P. Hermann, J. Havlíčková, E. Herdtweck, T. G. Kapp, N. Engelbogen, H. Kessler, H.-J. Wester, J. Notni, *Chem. Eur. J.* **2013**, *19*, 7748-7757.
- [263] P. Thirumurugan, D. Matosiuk, K. Jozwiak, *Chem. Rev.* **2013**, *113*, 4905-4979.
- [264] M. F. Debets, S. S. van Berkel, J. Dommerholt, A. T. Dirks, F. P. Rutjes, F. L. van Delft, *Acc. Chem. Res.* **2011**, *44*, 805-815.
- [265] a) K. Ferreira, H.-Y. Hu, V. Fetz, H. Prochnow, B. Rais, P. P. Müller, M. Brönstrup, *Angew. Chem. Int. Ed.* **2017**, *56*, 8272-8276; b) J. Singh, D. Lopes, D. Gomika Udugamasooriya, *Biopolymers* **2016**, *106*, 673-684.
- [266] a) N. Cakić, S. Gündüz, R. Rengarasu, G. Angelovski, *Tetrahedron Lett.* **2015**, *56*, 759-765; b) M. Suchý, R. H. E. Hudson, *Eur. J. Org. Chem.* **2008**, *2008*, 4847-4865.
- [267] C. E. Hoyle, C. N. Bowman, *Angew. Chem. Int. Ed.* **2010**, *49*, 1540-1573.

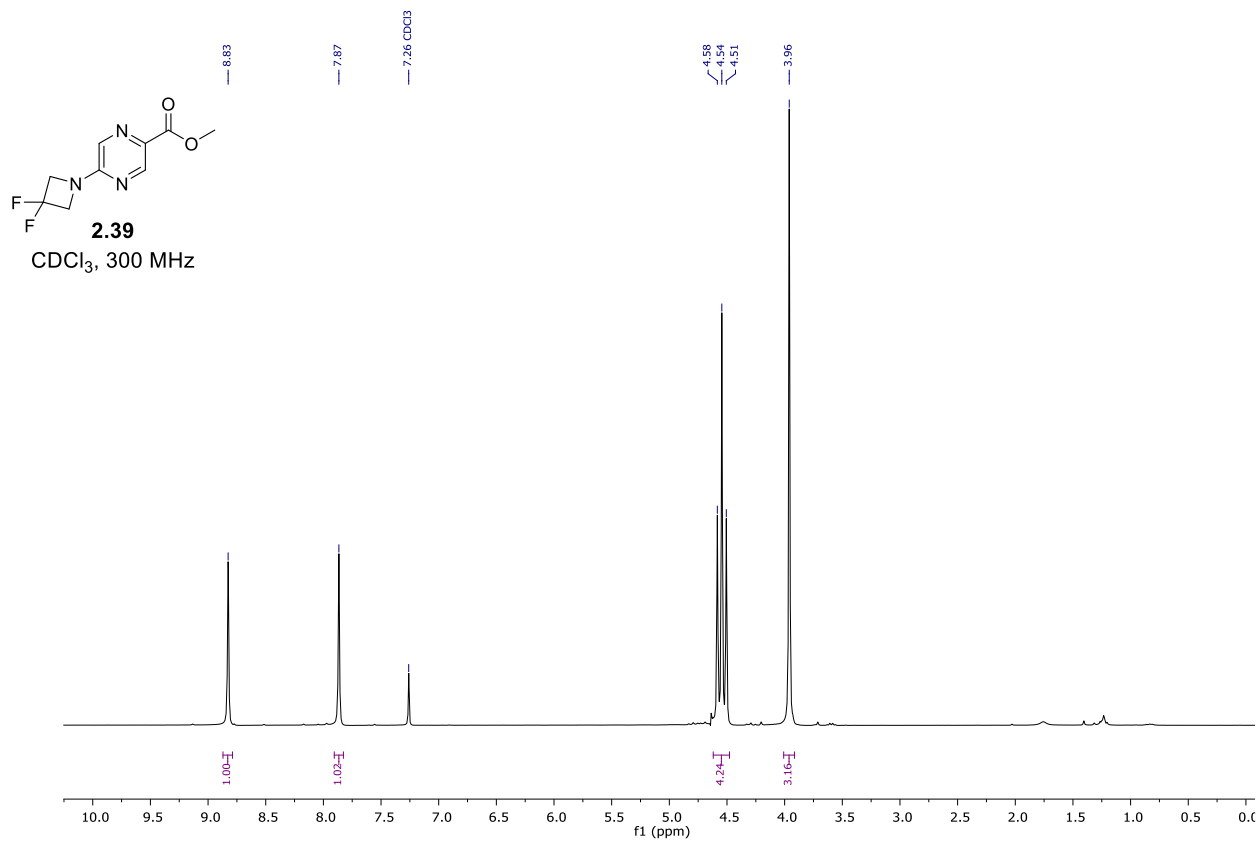
- [268] a) W. Huang, X. Wu, X. Gao, Y. Yu, H. Lei, Z. Zhu, Y. Shi, Y. Chen, M. Qin, W. Wang, Y. Cao, *Nat. Chem.* **2019**, *11*, 310-319; b) J. M. J. M. Ravasco, H. Faustino, A. Trindade, P. M. P. Gois, *Chem. Eur. J.* **2019**, *25*, 43-59.
- [269] C. Wangler, B. Wangler, M. Eisenhut, U. Haberkorn, W. Mier, *Bioorg. Med. Chem.* **2008**, *16*, 2606-2616.
- [270] O. Keller, J. Rudinger, *Helv. Chim. Acta* **1975**, *58*, 531-541.
- [271] a) R. J. Christie, R. Fleming, B. Bezabeh, R. Woods, S. Mao, J. Harper, A. Joseph, Q. Wang, Z.-Q. Xu, H. Wu, C. Gao, N. Dimasi, *J. Controlled Release* **2015**, *220*, 660-670; b) M. Machida, M. I. Machida, Y. Kanaoka, *Chem. Pharm. Bull.* **1977**, *25*, 2739-2743.
- [272] L. A. Carpino, *Acc. Chem. Res.* **1987**, *20*, 401-407.
- [273] a) M. Ueki, N. Nishigaki, H. Aoki, T. Tsurusaki, T. Katoh, *Chem. Lett.* **1993**, *22*, 721-724; b) W. Jiang, J. Wanner, R. J. Lee, P.-Y. Bounaud, D. L. Boger, *J. Am. Chem. Soc.* **2003**, *125*, 1877-1887.
- [274] a) A. K. R. Junker, M. Tropiano, S. Faulkner, T. J. Sørensen, *Inorg. Chem.* **2016**, *55*, 12299-12308; b) T. L. Mindt, C. Müller, F. Stuker, J.-F. Salazar, A. Hohn, T. Mueggler, M. Rudin, R. Schibli, *Bioconjug. Chem.* **2009**, *20*, 1940-1949; c) Z. Cai, B. T. Y. Li, E. H. Wong, G. R. Weisman, C. J. Anderson, *Dalton Trans.* **2015**, *44*, 3945-3948; d) A. Y. Lebedev, J. P. Holland, J. S. Lewis, *Chem. Commun.* **2010**, *46*, 1706-1708; e) I. Dijkgraaf, A. Y. Rijnders, A. Soede, A. C. Dechesne, G. W. van Esse, A. J. Brouwer, F. H. M. Corstens, O. C. Boerman, D. T. S. Rijkers, R. M. J. Liskamp, *Org. Biomol. Chem.* **2007**, *5*, 935-944; f) M. Suchý, M. Milne, A. X. Li, N. McVicar, D. W. Dodd, R. Bartha, R. H. E. Hudson, *Eur. J. Org. Chem.* **2011**, *2011*, 6532-6543; g) J. R. Hanna, C. Allan, C. Lawrence, O. Meyer, N. D. Wilson, A. N. Hulme, *Molecules* **2017**, *22*, 802; h) S. Knör, A. Modlinger, T. Poethko, M. Schottelius, H.-J. Wester, H. Kessler, *Chem. Eur. J.* **2007**, *13*, 6082-6090; i) M. Milne, K. Chicas, A. Li, R. Bartha, R. H. E. Hudson, *Org. Biomol. Chem.* **2012**, *10*, 287-292.
- [275] C. J. Pickens, S. N. Johnson, M. M. Pressnall, M. A. Leon, C. J. Berkland, *Bioconjugate Chem.* **2018**, *29*, 686-701.
- [276] K. Ladomenou, V. Nikolaou, G. Charalambidis, A. G. Coutsolelos, *Coord. Chem. Rev.* **2016**, *306*, 1-42.
- [277] A. J. Sinclair, V. del Amo, D. Philp, *Org. Biomol. Chem.* **2009**, *7*, 3308-3318.
- [278] E. Haldón, M. C. Nicasio, P. J. Pérez, *Org. Biomol. Chem.* **2015**, *13*, 9528-9550.
- [279] a) P. Appukkuttan, W. Dehaen, V. V. Fokin, E. Van der Eycken, *Org. Lett.* **2004**, *6*, 4223-4225; b) C. W. Tornøe, C. Christensen, M. Meldal, *J. Org. Chem.* **2002**, *67*, 3057-3064.
- [280] P. Deschamps, P. P. Kulkarni, M. Gautam-Basak, B. Sarkar, *Coord. Chem. Rev.* **2005**, *249*, 895-909.
- [281] a) K. A. Dave, M. J. Headlam, T. P. Wallis, J. J. Gorman, *Curr. Protoc. Protein Sci.* **2011**, *Chapter 16*, Unit 16.13; b) W. M. Nadler, D. Waidelich, A. Kerner, S. Hanke, R. Berg, A. Trumpp, C. Rösli, *J. Proteome Res.* **2017**, *16*, 1207-1215.
- [282] K. S. Woodin, K. J. Heroux, C. A. Boswell, E. H. Wong, G. R. Weisman, W. Niu, S. A. Tomellini, C. J. Anderson, L. N. Zakharov, A. L. Rheingold, *Eur. J. Inorg. Chem.* **2005**, *2005*, 4829-4833.
- [283] G. Anderegg, A.-N. Francoise, R. Delgado, J. Felcman, K. Popov, *Pure Appl. Chem.* **2004**, *77*, 1445-1495.
- [284] J. A. Thich, D. Mastropaolo, J. Potenza, H. J. Schugar, *J. Am. Chem. Soc.* **1974**, *96*, 726-731.
- [285] R. Ševčík, J. Vaněk, R. Michalíková, P. Lubal, P. Hermann, I. C. Santos, I. Santos, M. P. C. Campello, *Dalton Trans.* **2016**, *45*, 12723-12733.
- [286] A. C. Varas, T. Noël, Q. Wang, V. Hessel, *ChemSusChem* **2012**, *5*, 1703-1707.
- [287] R. Klement, F. Stock, H. Elias, H. Paulus, P. Pelikán, M. Valko, M. Mazúr, *Polyhedron* **1999**, *18*, 3617-3628.
- [288] P. J. M. W. L. Birker, H. C. Freeman, *J. Chem. Soc., Chem. Commun.* **1976**, 312-313.

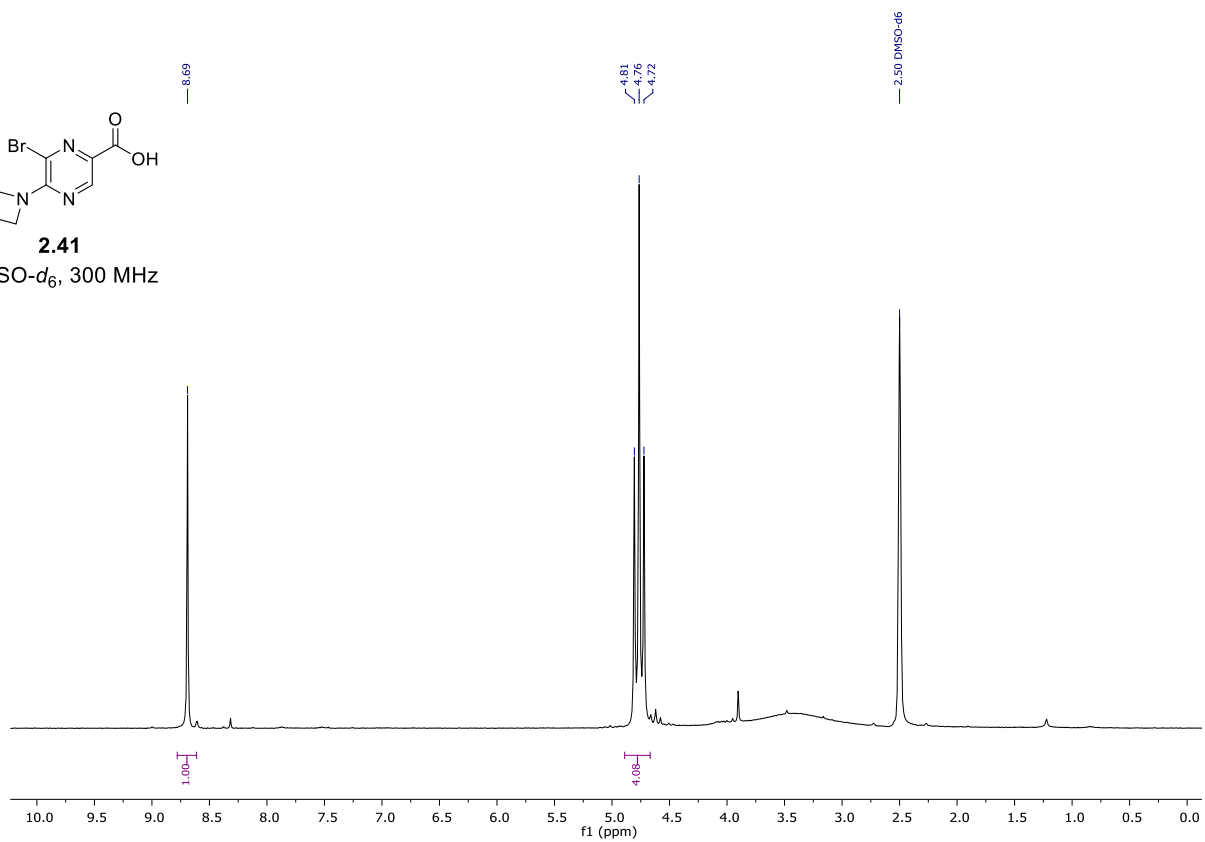
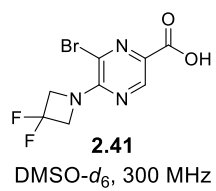
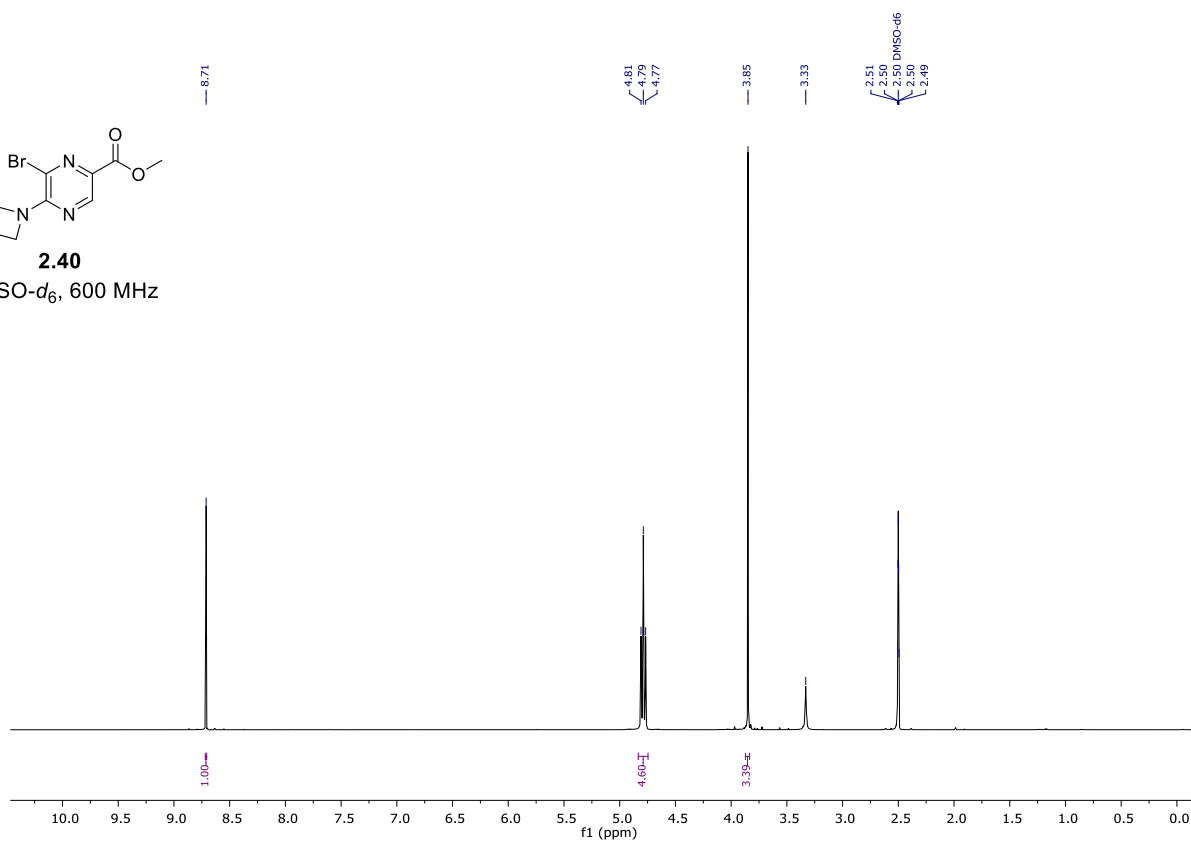
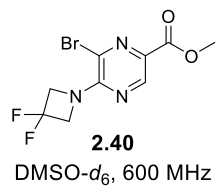
- [289] V. W. Rosso, D. A. Lust, P. J. Bernot, J. A. Grosso, S. P. Modi, A. Rusowicz, T. C. Sedergran, J. H. Simpson, S. K. Srivastava, M. J. Humora, N. G. Anderson, *Org. Process Res. Dev.* **1997**, *1*, 311-314.
- [290] P. Tosatti, A. J. Campbell, D. House, A. Nelson, S. P. Marsden, *J. Org. Chem.* **2011**, *76*, 5495-5501.
- [291] M. C. Bennett, N. O. Schmidt, *Trans. Faraday Soc.* **1955**, *51*, 1412-1418.
- [292] J. Smirnova, E. Kabin, I. Järving, O. Bragina, V. Tõugu, T. Plitz, P. Palumaa, *Sci. Rep.* **2018**, *8*, 1463.
- [293] S. C. Wilschefski, M. R. Baxter, *Clin. Biochem. Rev.* **2019**, *40*, 115-133.
- [294] C.-H. Wong, S. C. Zimmerman, *Chem. Commun.* **2013**, *49*, 1679-1695.
- [295] K. Harpel, R. D. Baker, B. Amirsolaimani, S. Mehravar, J. Vagner, T. O. Matsunaga, B. Banerjee, K. Kieu, *Biomed. Opt. Express* **2016**, *7*, 2849-2860.
- [296] a) L. E. Brieaddy, *Hypolipidemic 1,4-benzothiazepine derivative*, **2002**, WO19965188; b) W. Liu, P. Ray, S. A. Benzra, *J. Chem. Soc., Perkin Trans. 1* **1995**, 553-559.
- [297] B. R. Neustadt, E. M. Smith, T. L. Nechuta, A. A. Bronnenkant, M. F. Haslanger, R. W. Watkins, C. J. Foster, E. J. Sybertz, *J. Med. Chem.* **1994**, *37*, 2461-2476.
- [298] A. Garcia-Rubia, E. Laga, C. Cativiela, E. P. Urriolabeitia, R. Gomez-Arrayas, J. C. Carretero, *J. Org. Chem.* **2015**, *80*, 3321-3331.
- [299] F. Song, Z. Li, J. Li, S. Wu, X. Qiu, Z. Xi, L. Yi, *Organic & biomolecular chemistry* **2016**, *14*, 11117-11124.
- [300] J. Rokka, A. Snellman, C. Zona, B. La Ferla, F. Nicotra, M. Salmona, G. Forloni, M. Haaparanta-Solin, J. O. Rinne, O. Solin, *Bioorg. Med. Chem.* **2014**, *22*, 2753-2762.
- [301] L. Deng, O. Norberg, S. Uppalapati, M. Yan, O. Ramström, *Org. Biomol. Chem.* **2011**, *9*, 3188-3198.
- [302] D. El-Gendy Bel, E. H. Ghazvini Zadeh, A. C. Sotuyo, G. G. Pillai, A. R. Katritzky, *Chem Biol Drug Des* **2013**, *81*, 577-582.
- [303] J. Platzek, H.-J. Weinmann, T. Frenzel, W. Ebert, U. Niedballa, B. Raduechel, *Porphyrin derivatives, pharmaceutical agents that contain the latter, and their use in photodynamic therapy and MRI diagnosis*, **2000**, WO20001698.
- [304] W. Shen, P. G. Schultz, A. Muppidi, A. Cramer, I. Ahmad, P. Yang, *Modified therapeutic agents and compositions thereof*, **2015**, WO201538938.
- [305] C. Hagemeyer, K. Peter, A. P. R. Johnston, D. Owen, *Site-selective modification of proteins*, **2012**, WO2012/142659.
- [306] T. Shoda, M. Kato, T. Fujisato, Y. Demizu, H. Inoue, M. Naito, M. Kurihara, *Medicinal Chemistry* **2017**, *13*, 206-213.
- [307] G. Jones, P. Willett, R. C. Glen, A. R. Leach, R. Taylor, *J. Mol. Biol.* **1997**, *267*, 727-748.
- [308] a) D. R. Lide, *CRC Handbook of Chemistry and Physics, Vol. 131*, 90th ed., American Chemical Society, **2009**; b) G. Greber, *Vogel's textbook of practical organic chemistry, Vol. 29*, 5th ed., John Wiley & Sons Ltd., **1991**.
- [309] C. Klein Herenbrink, D. A. Sykes, P. Donthamsetti, M. Canals, T. Coudrat, J. Shonberg, P. J. Scammells, B. Capuano, P. M. Sexton, S. J. Charlton, J. A. Javitch, A. Christopoulos, J. R. Lane, *Nat. Commun.* **2016**, *7*, 10842.
- [310] H. J. Motulsky, L. C. Mahan, *Mol. Pharmacol.* **1984**, *25*, 1-9.
- [311] C. Yung-Chi, W. H. Prusoff, *Biochem. Pharmacol.* **1973**, *22*, 3099-3108.
- [312] H. Koda, J. A. Brazier, I. Onishi, S. Sasaki, *Biorg. Med. Chem.* **2015**, *23*, 4583-4590.
- [313] L. I. Willems, M. Verdoes, B. I. Florea, G. A. van der Marel, H. S. Overkleeft, *ChemBioChem* **2010**, *11*, 1769-1781.

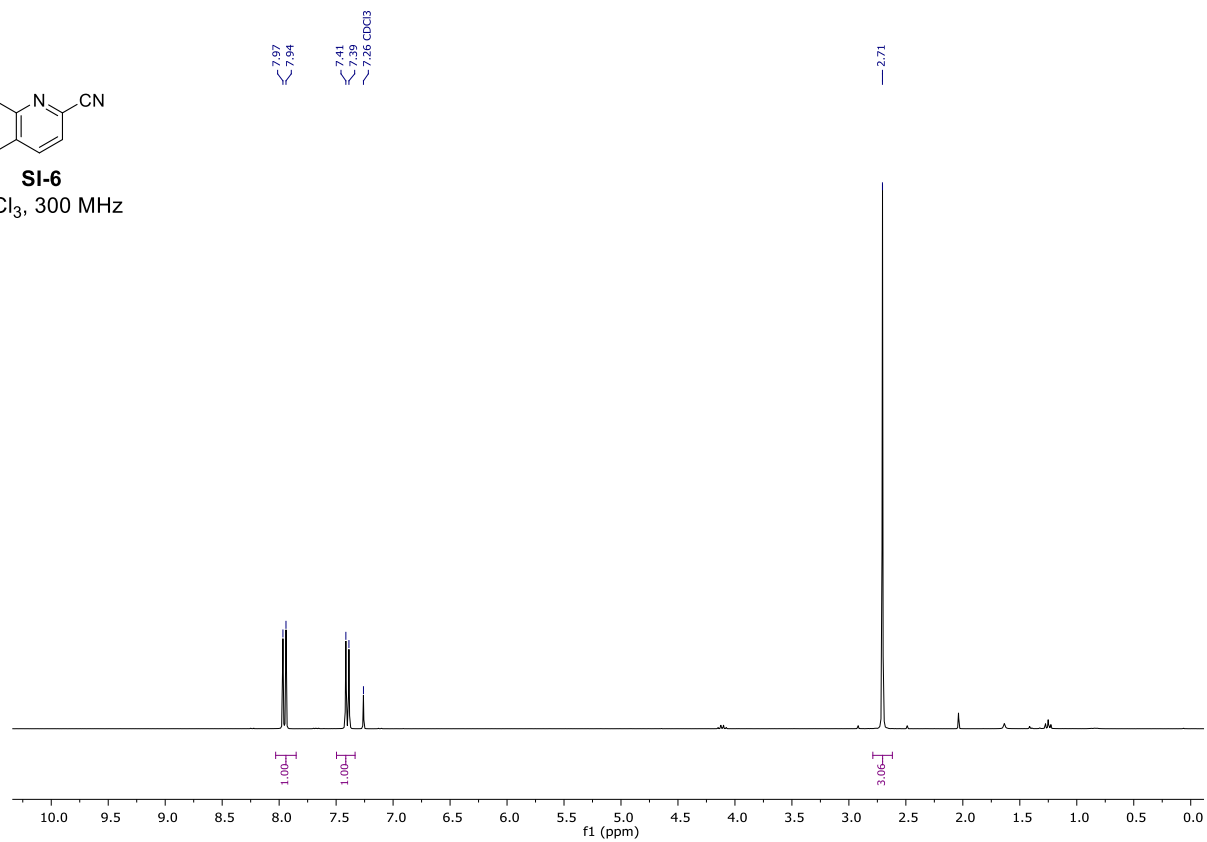
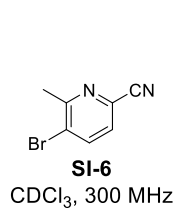
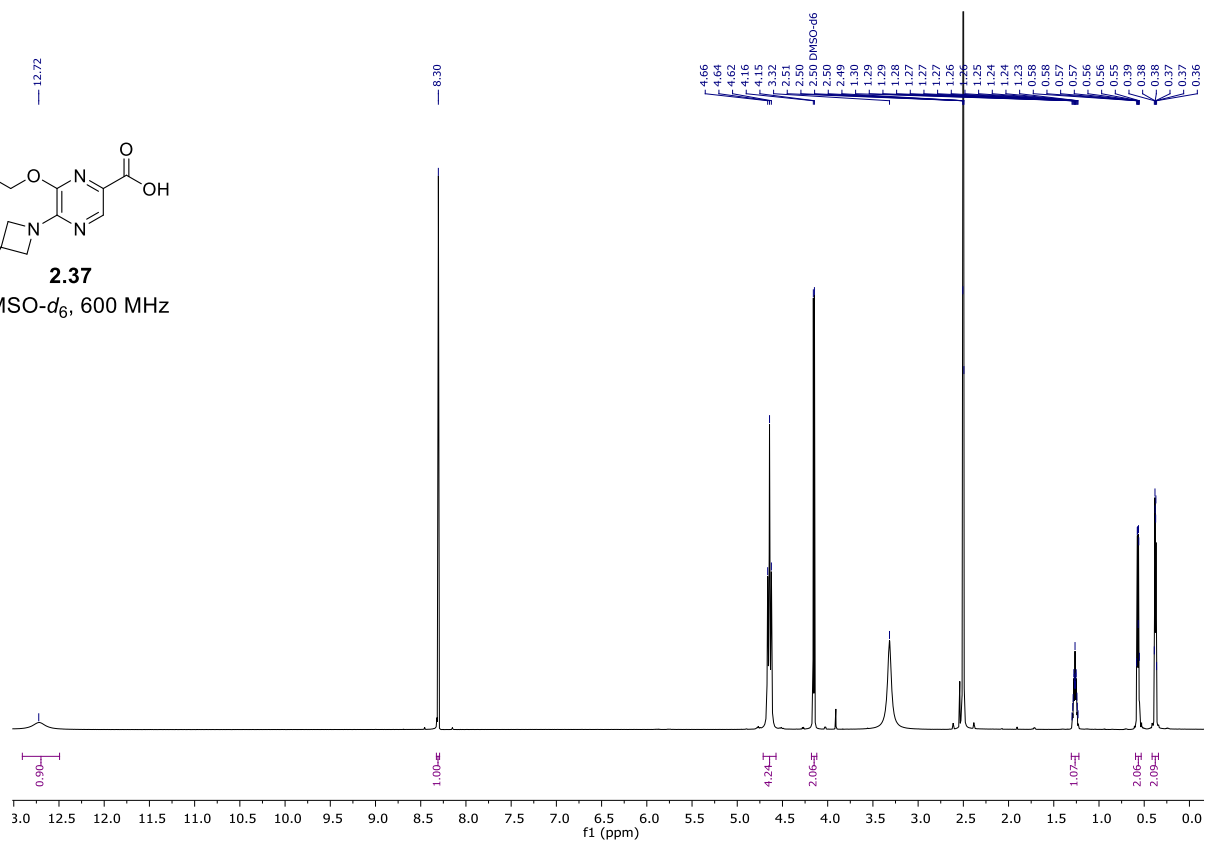
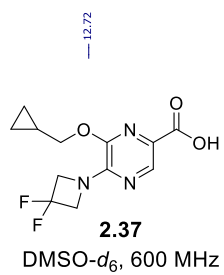
- [314] *International Organization for Standardization, Guide to the expression of uncertainty in measurement*, 1st ed., Joint Committee for Guides in Metrology (JCGM), Geneva, **1993**.
- [315] J. Kragten, *Analyst* **1994**, *119*, 2161-2165.

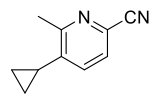


## Appendix: NMR-Spectra

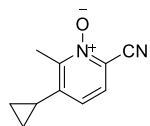
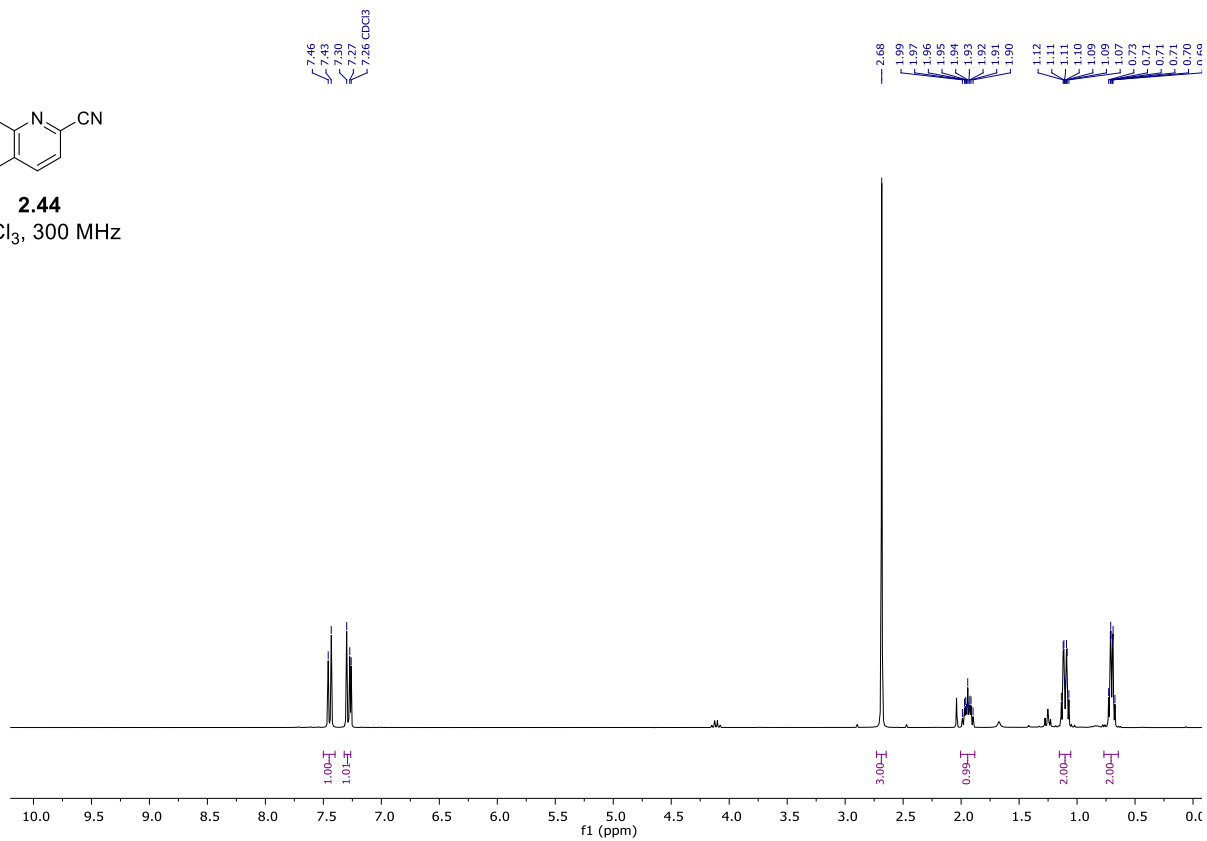




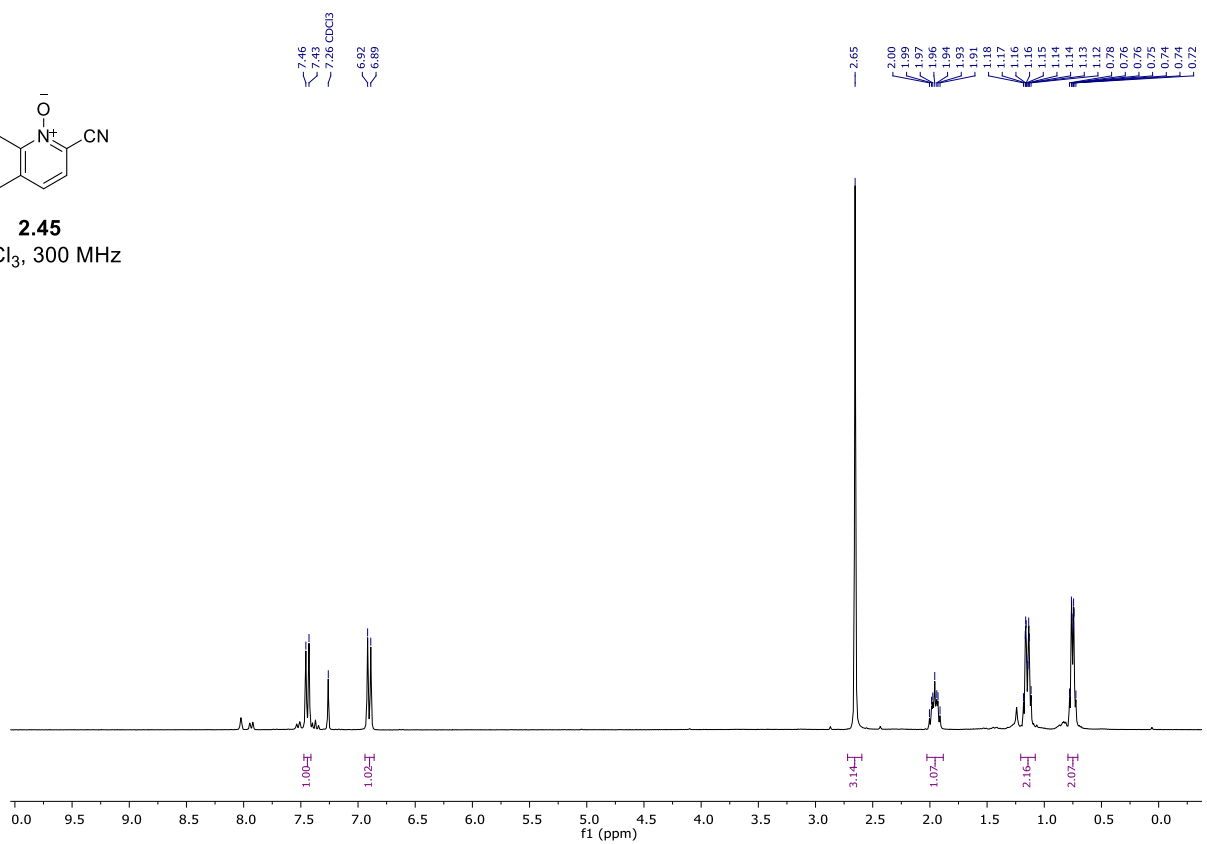


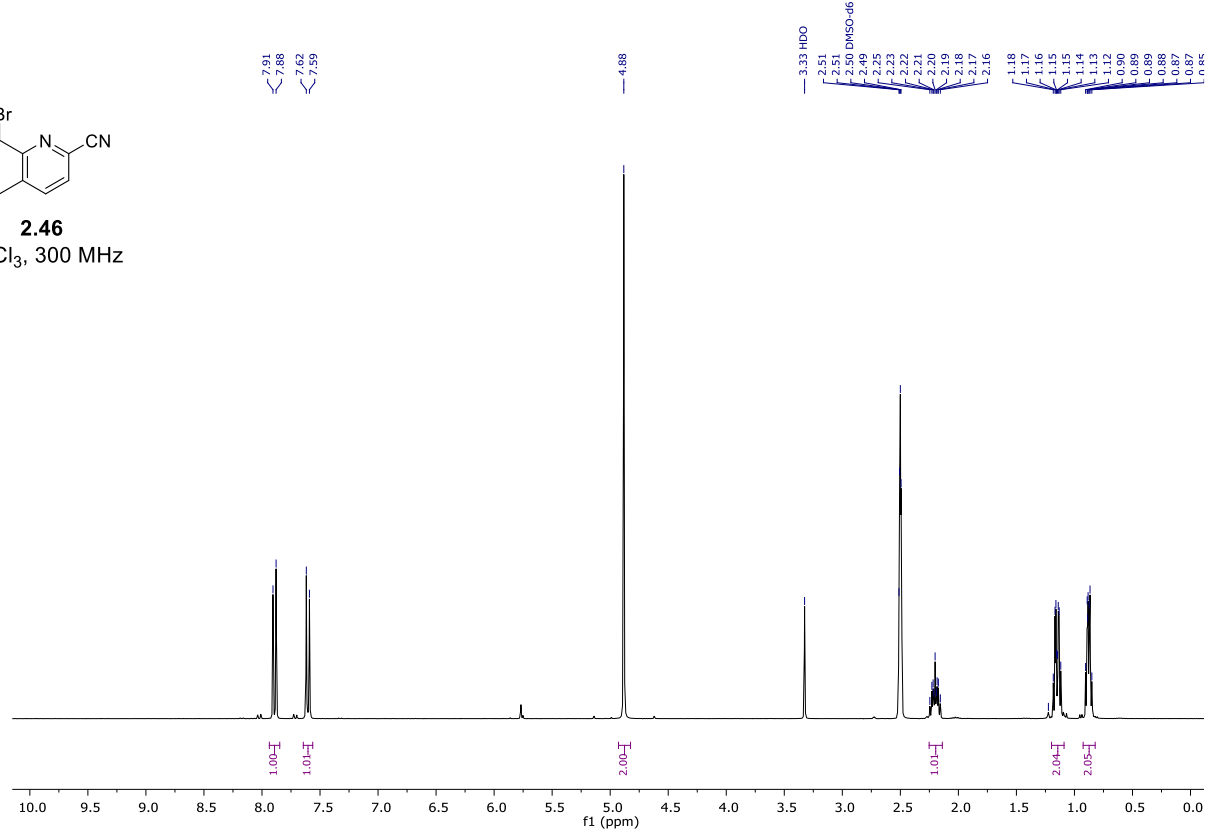
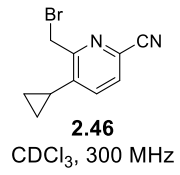
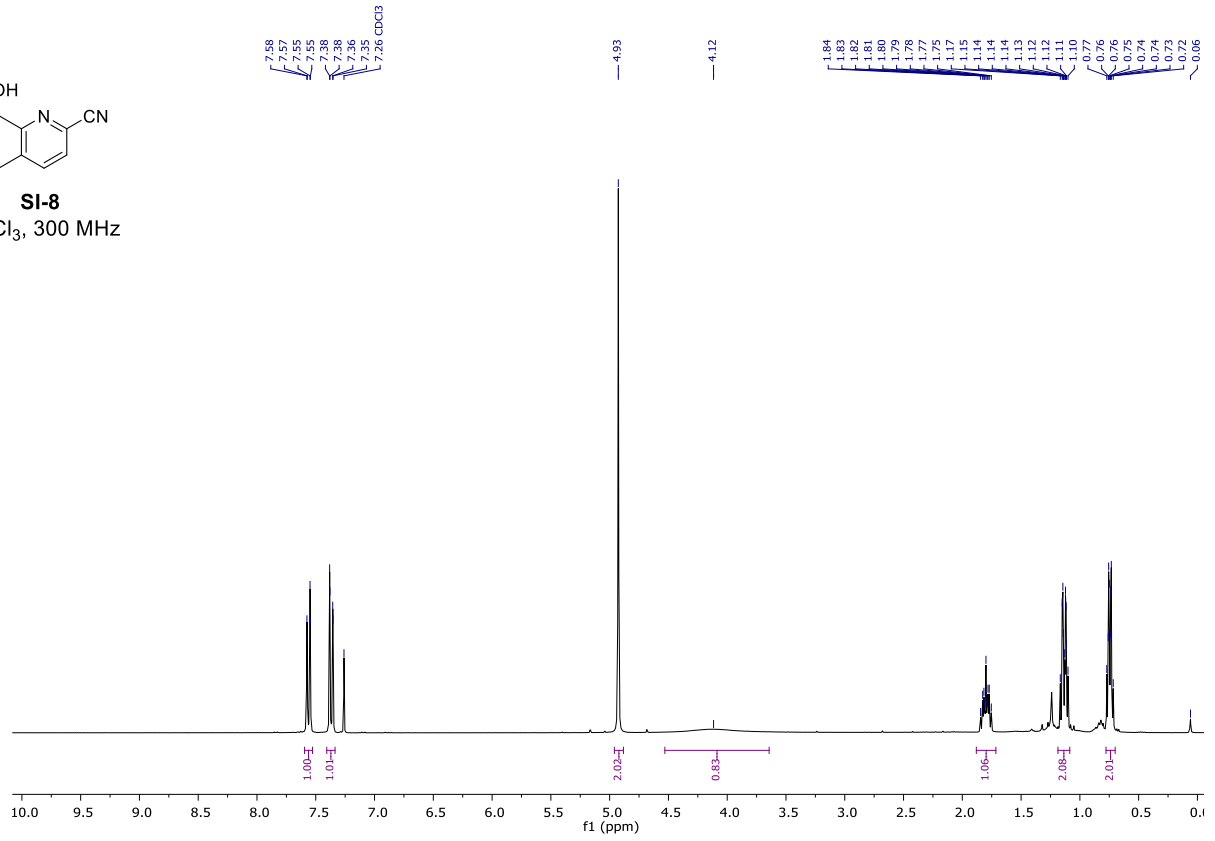


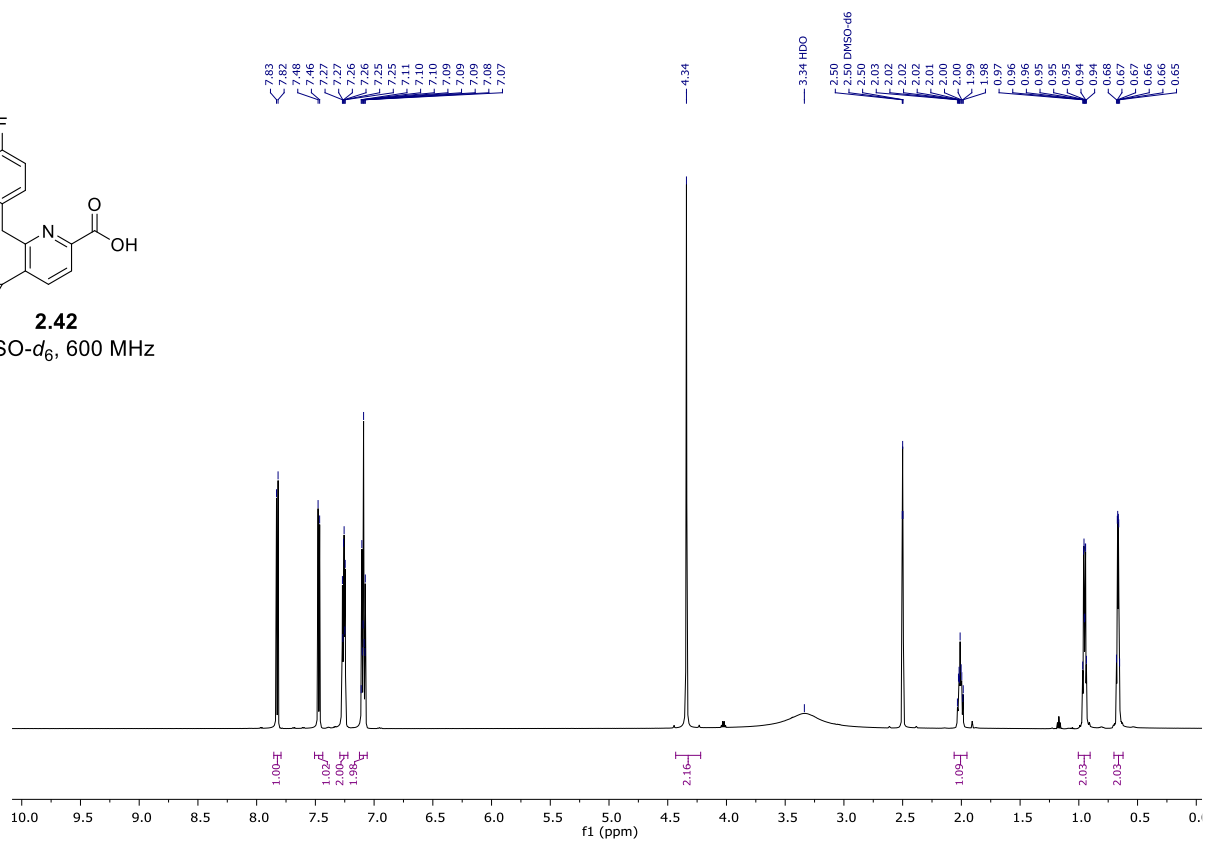
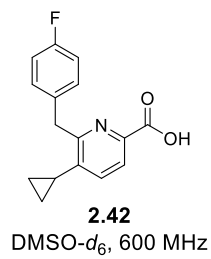
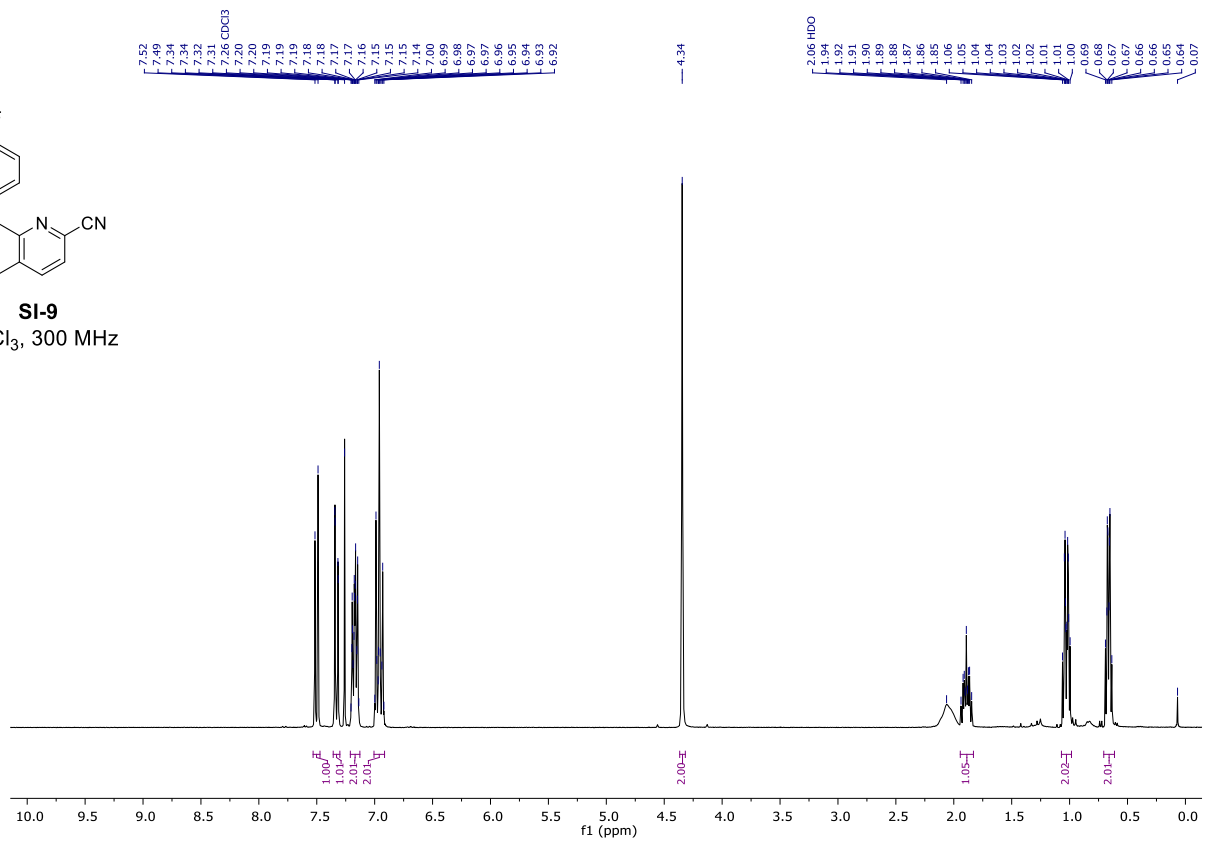
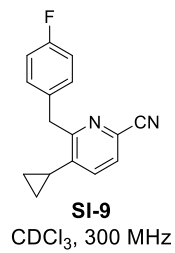
**2.44**  
CDCl<sub>3</sub>, 300 MHz

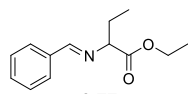


**2.45**  
CDCl<sub>3</sub>, 300 MHz

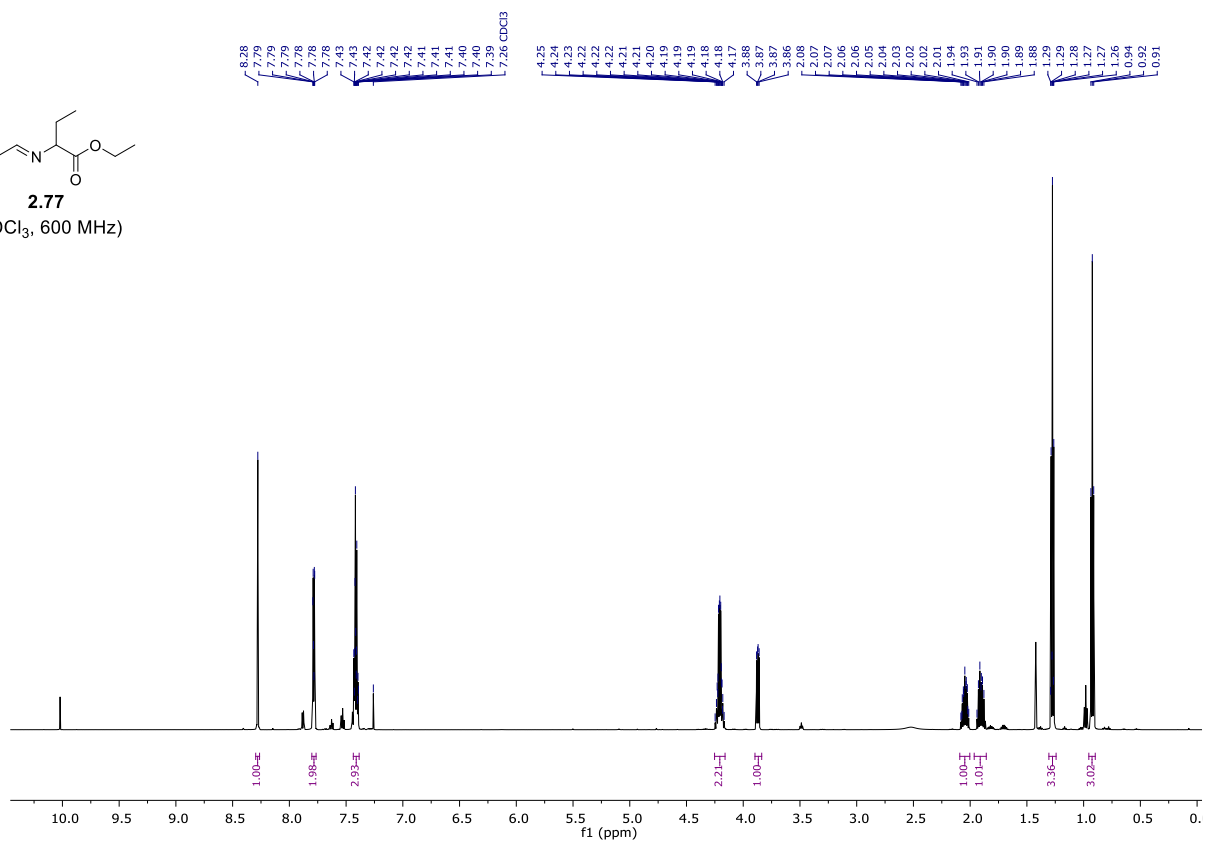


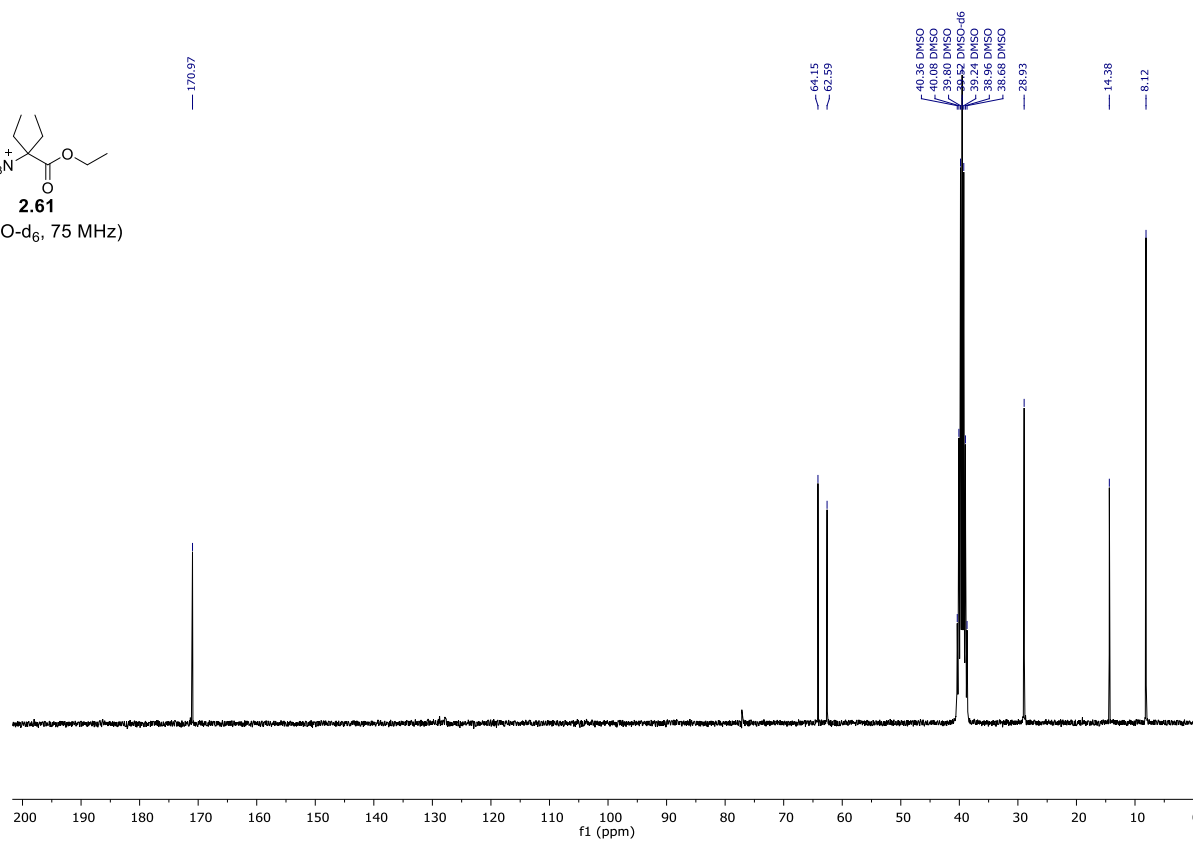
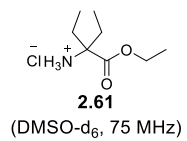
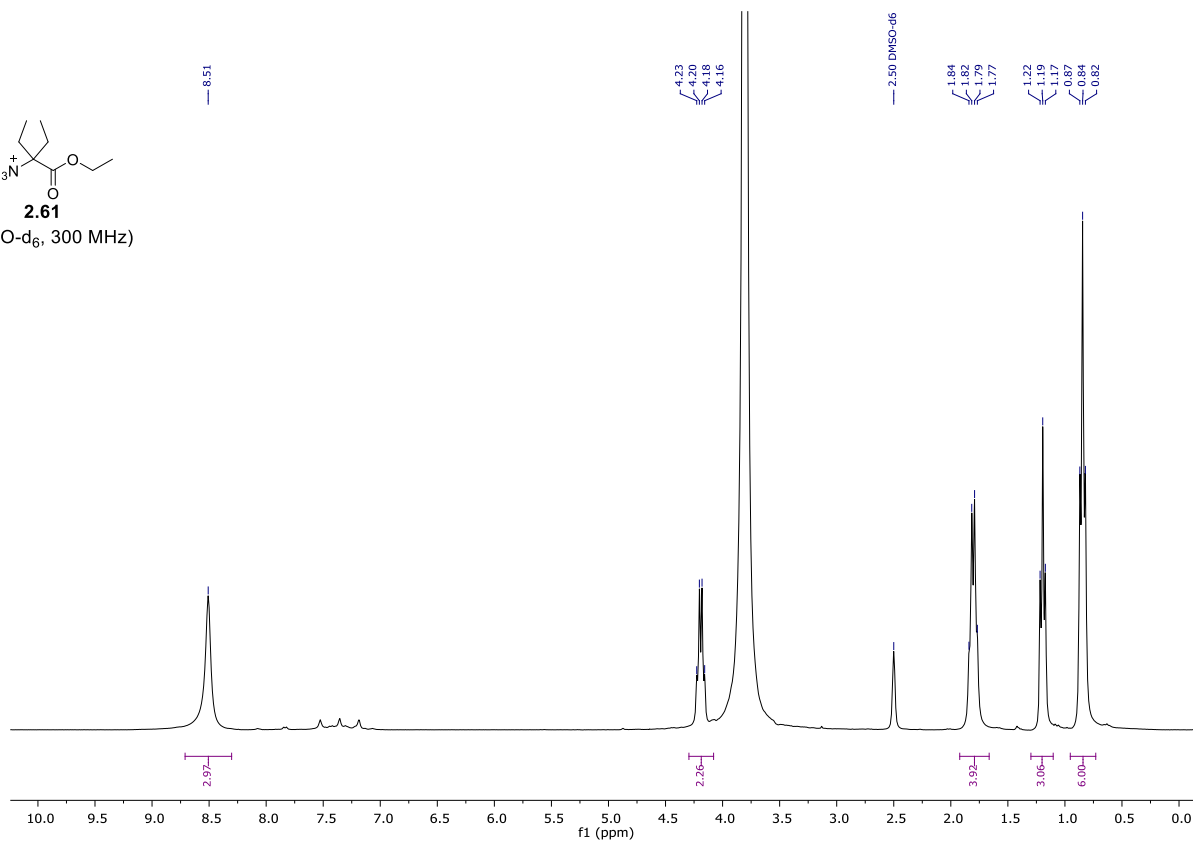
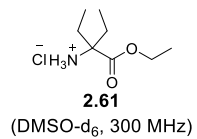




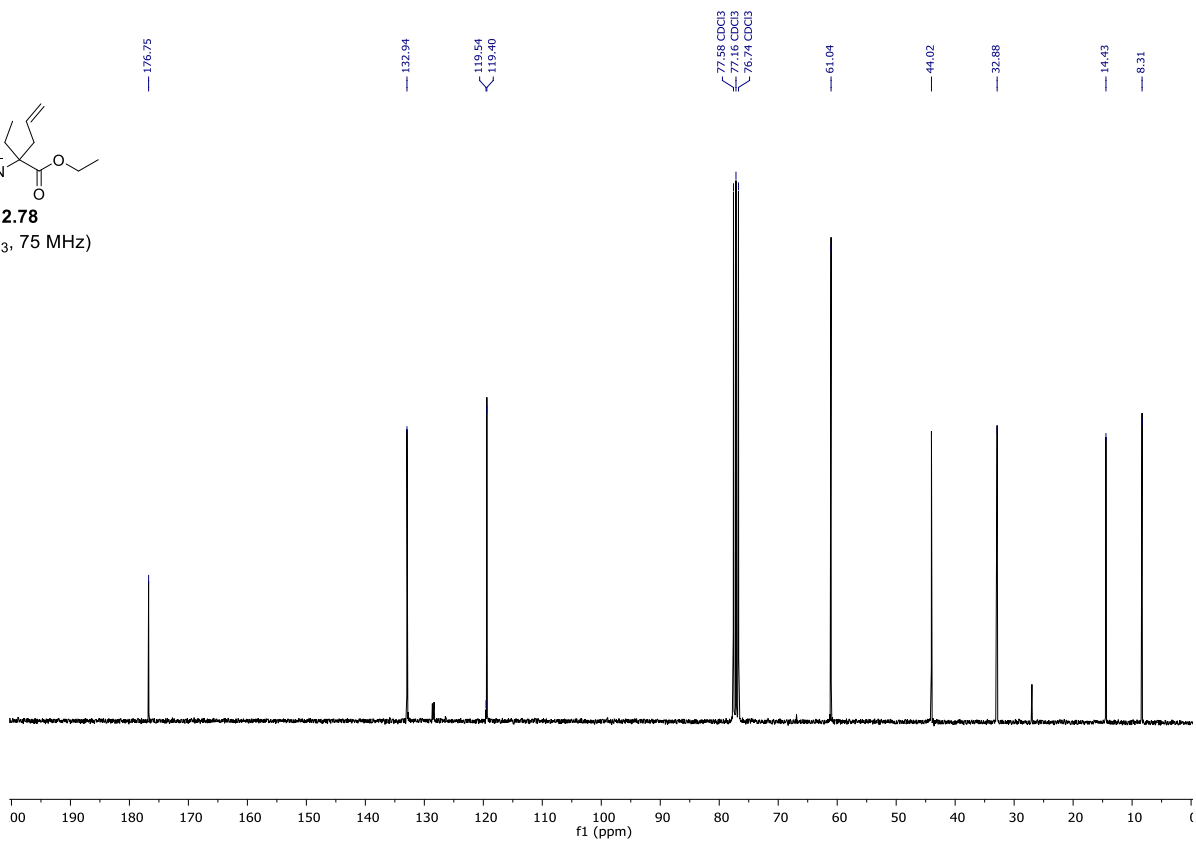
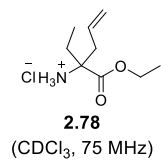
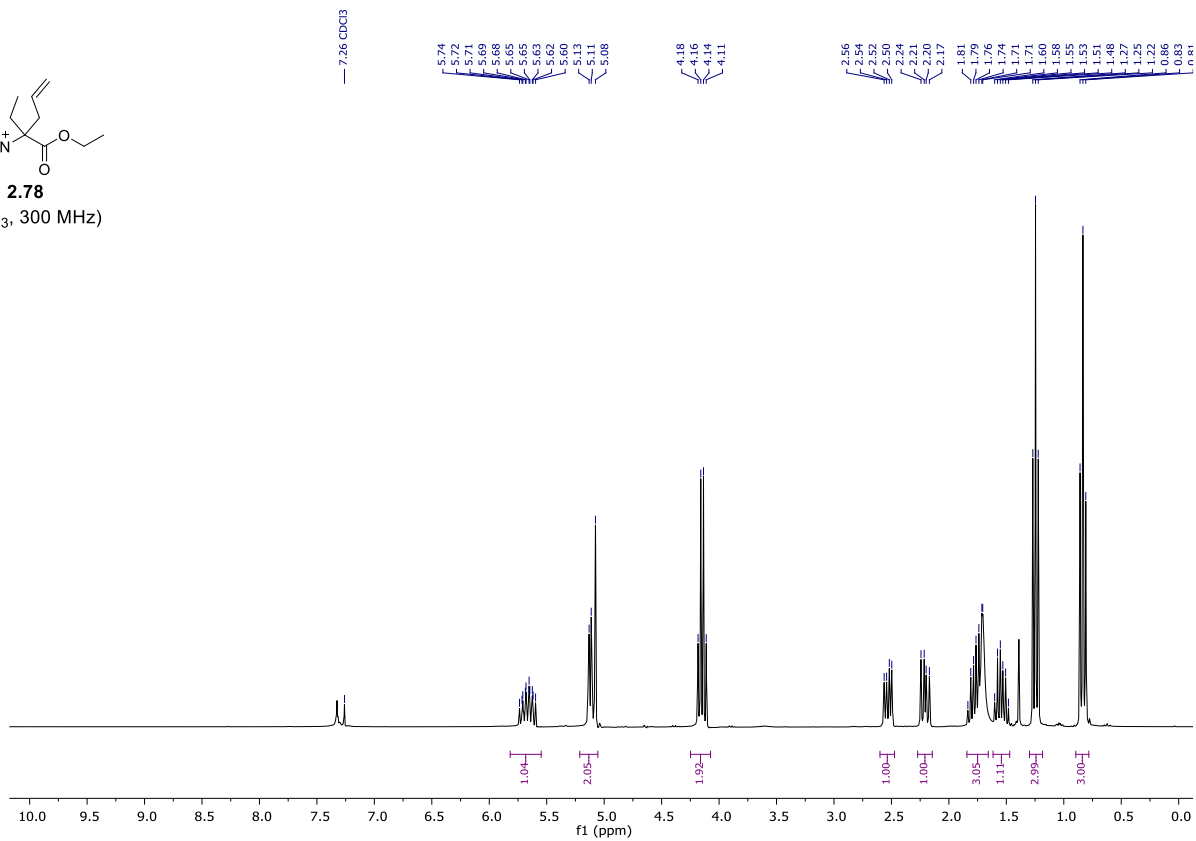
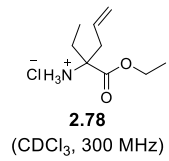


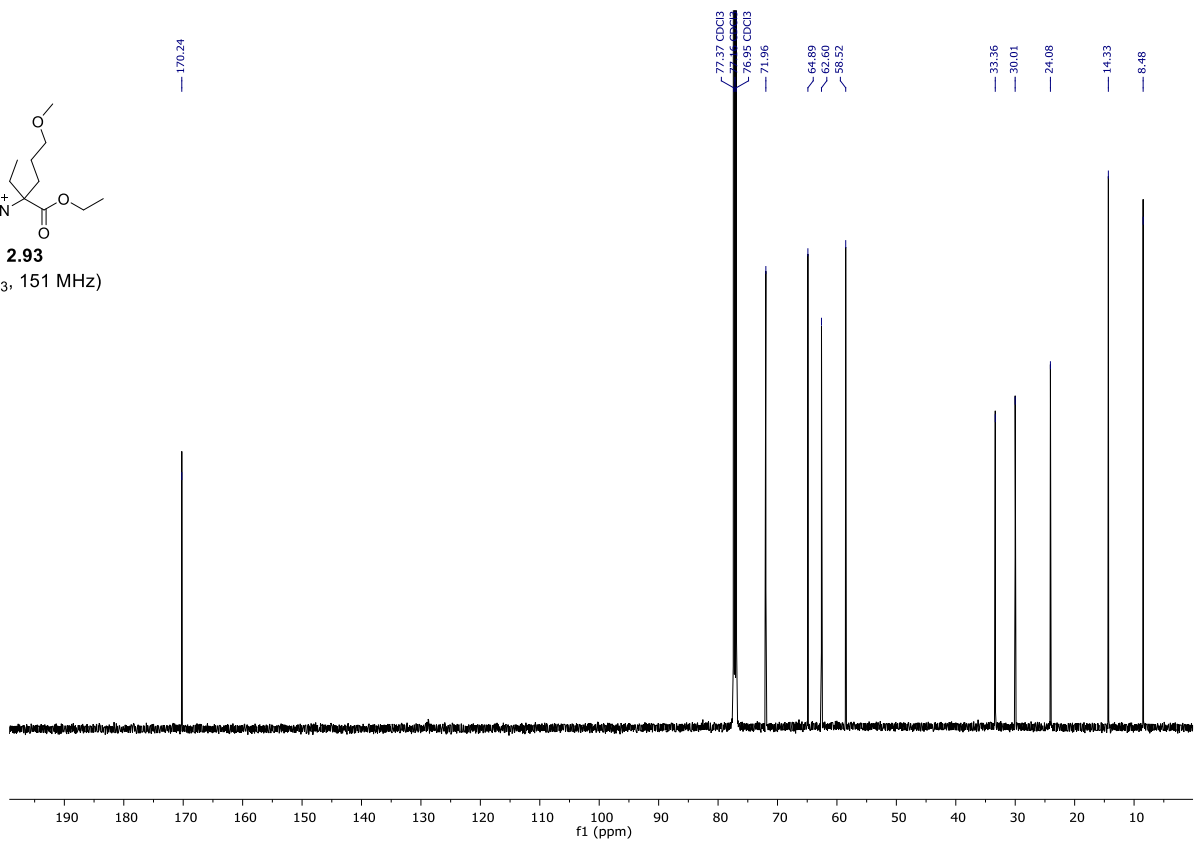
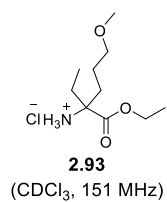
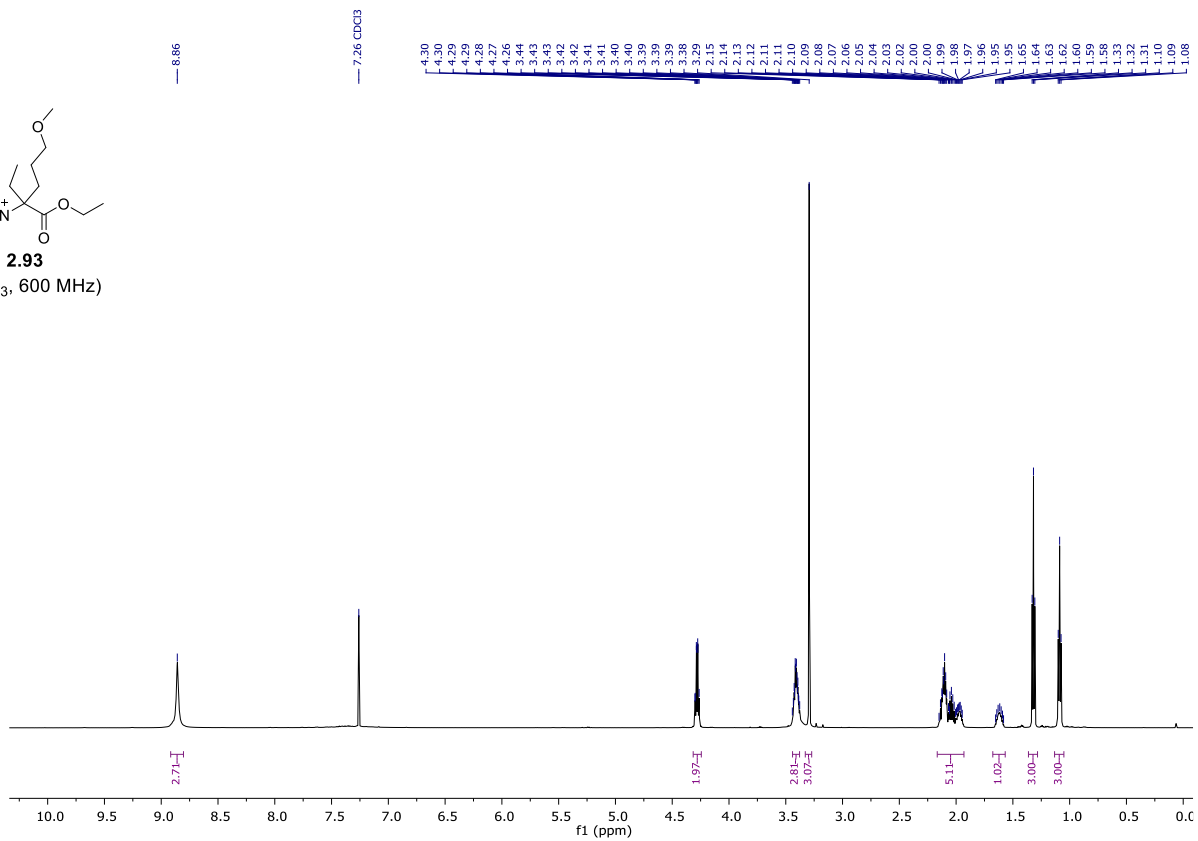
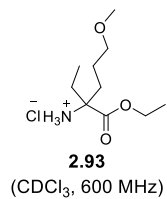
**2.77**  
(CDCl<sub>3</sub>, 600 MHz)

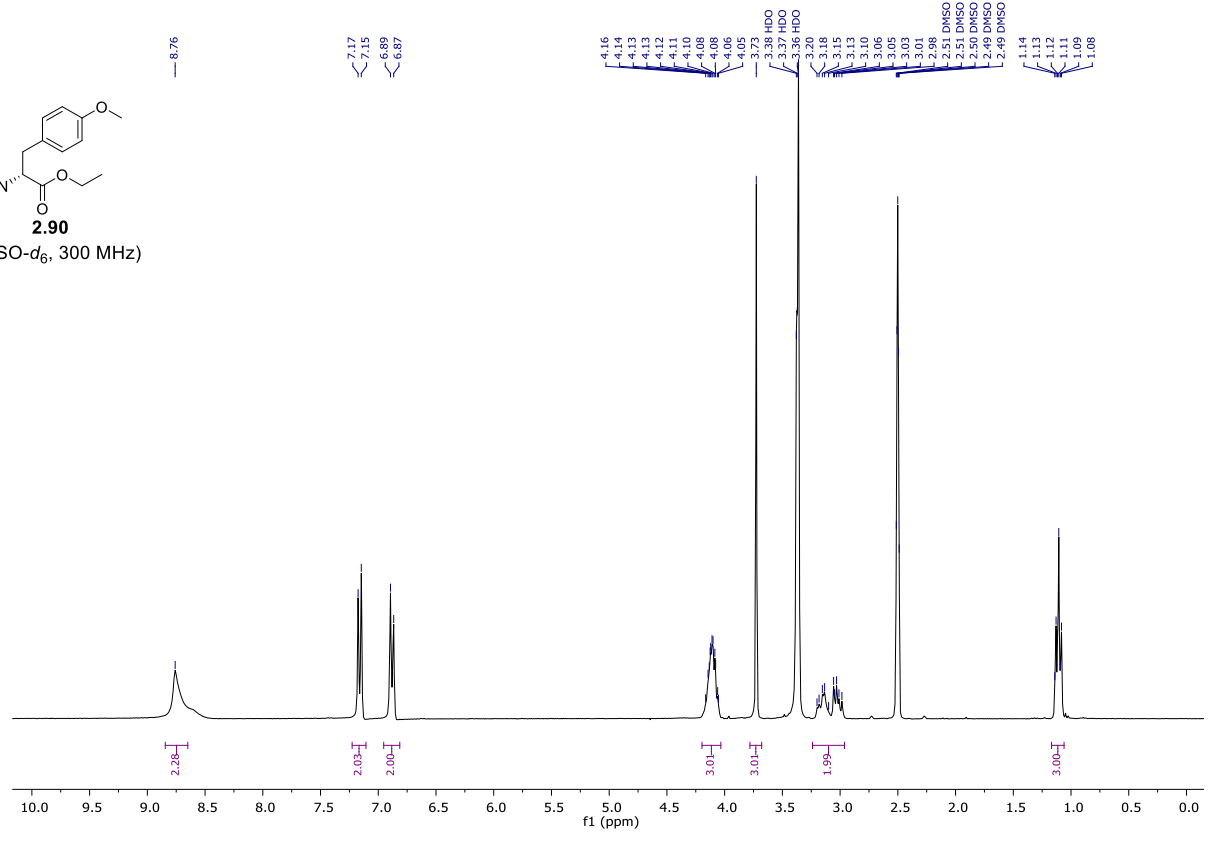
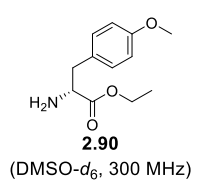
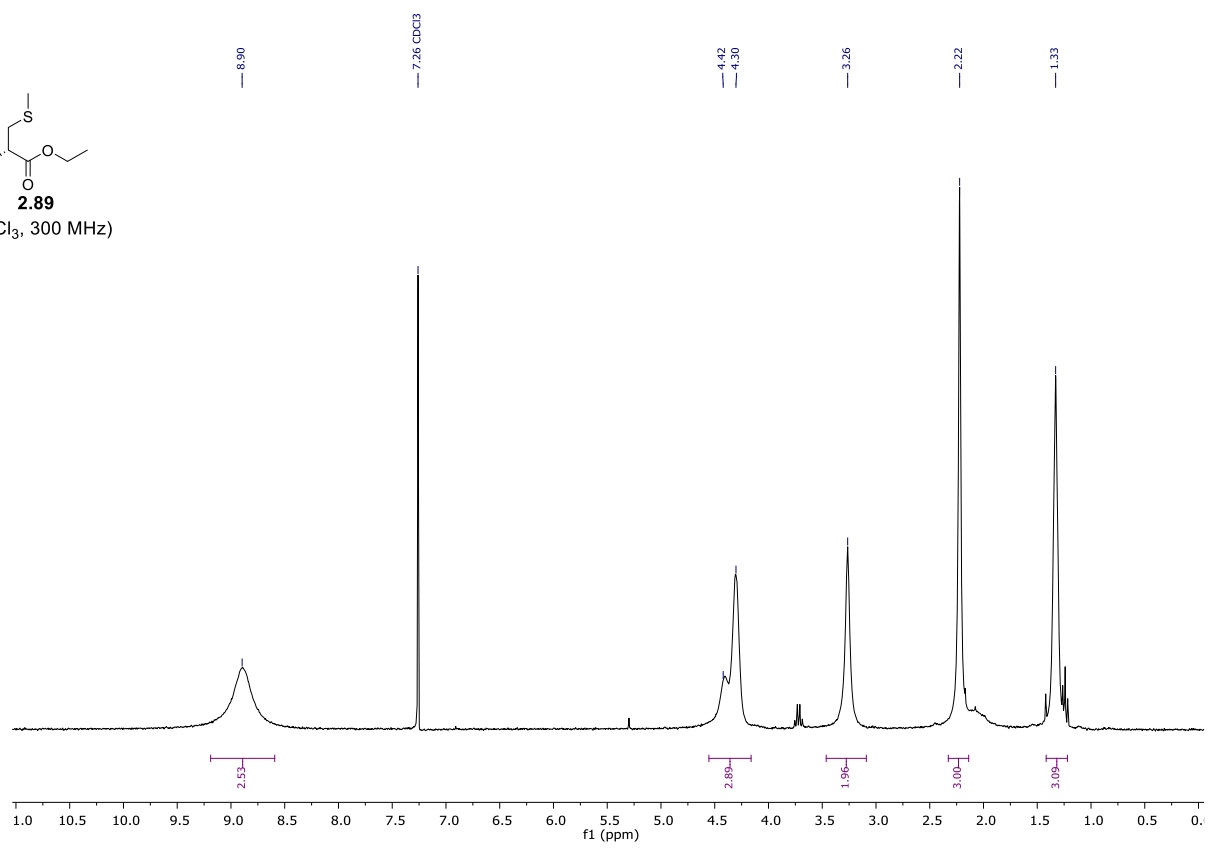
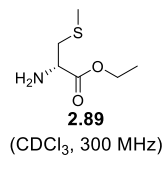


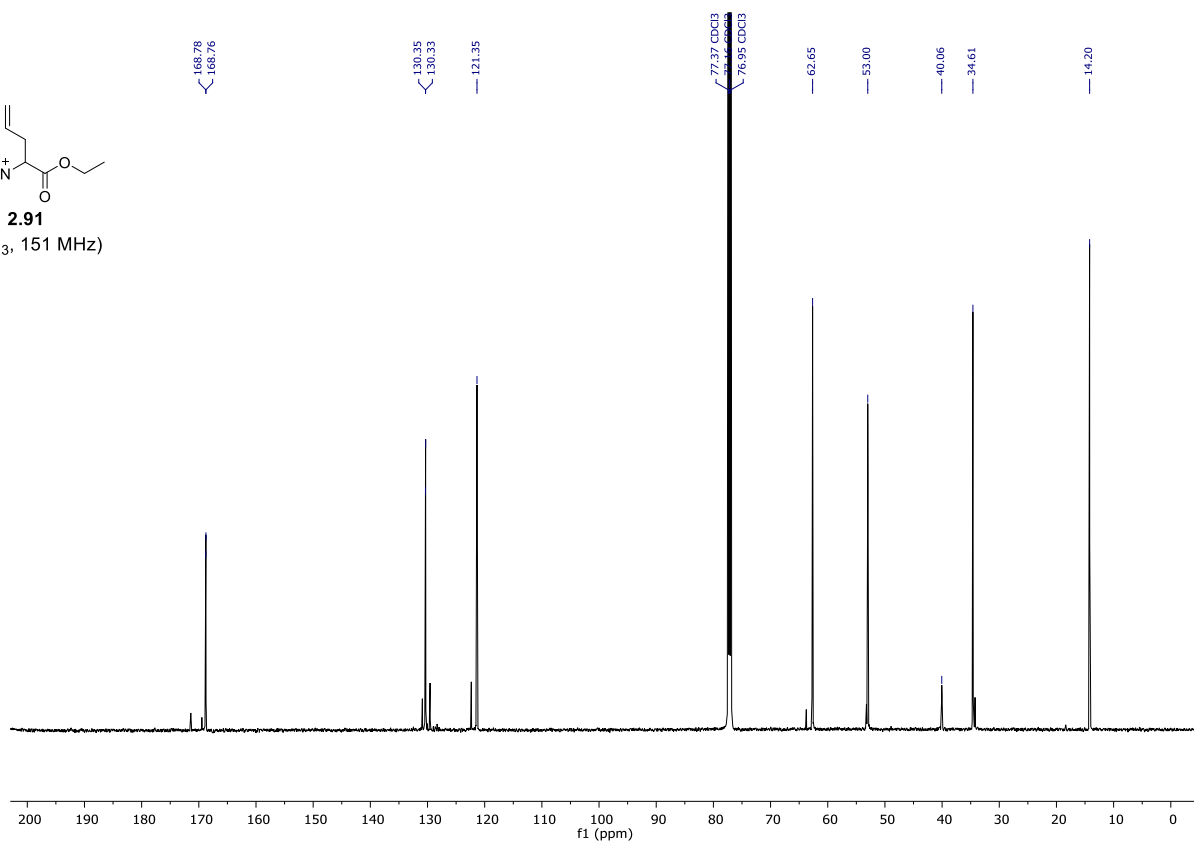
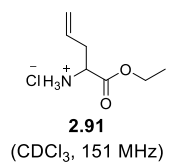
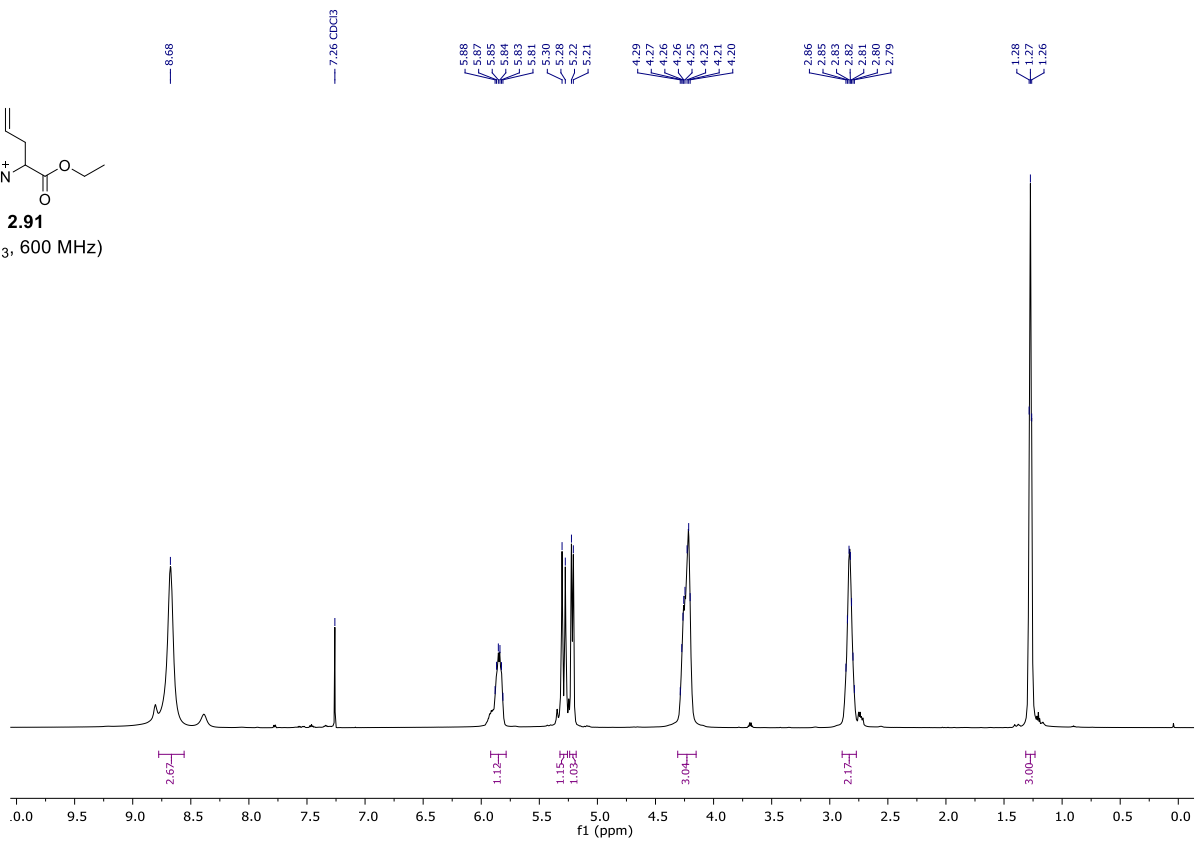
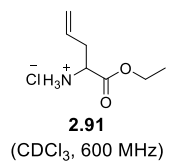


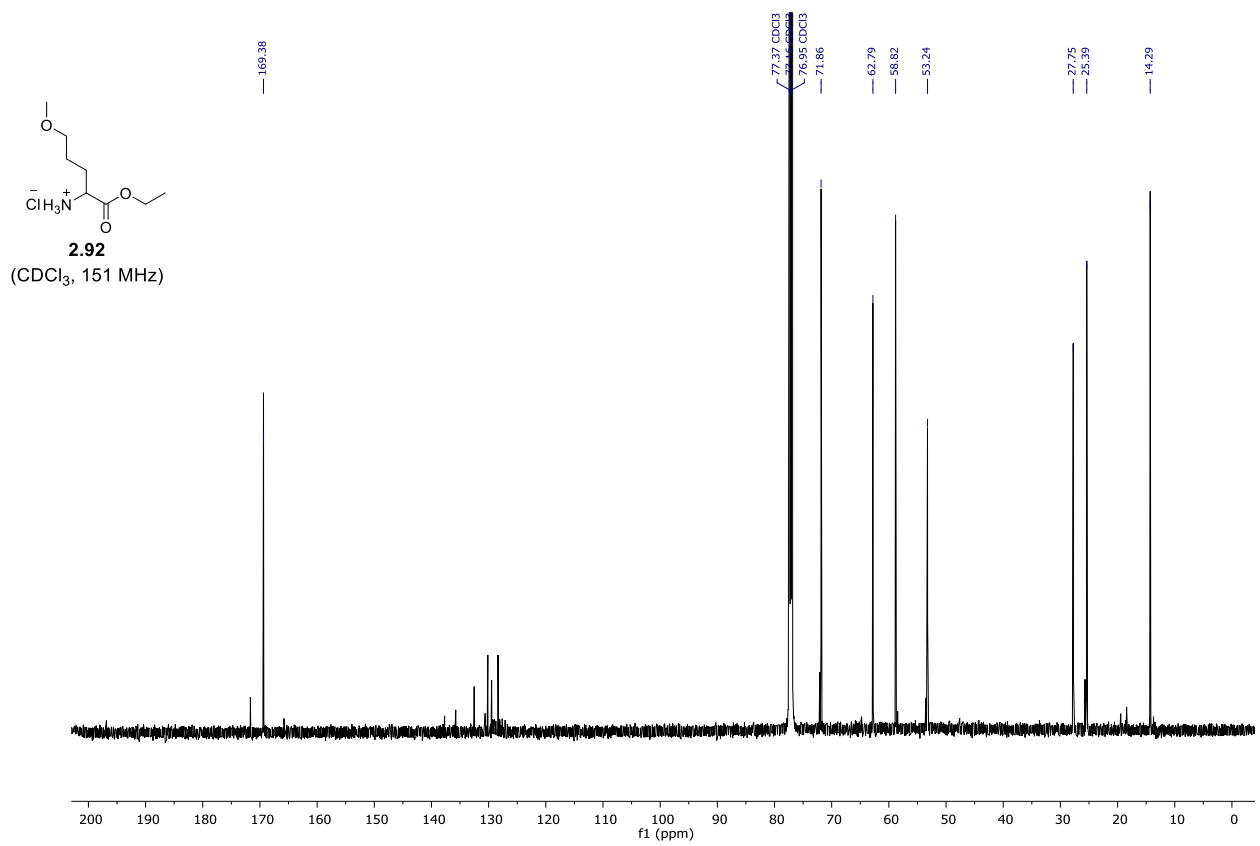
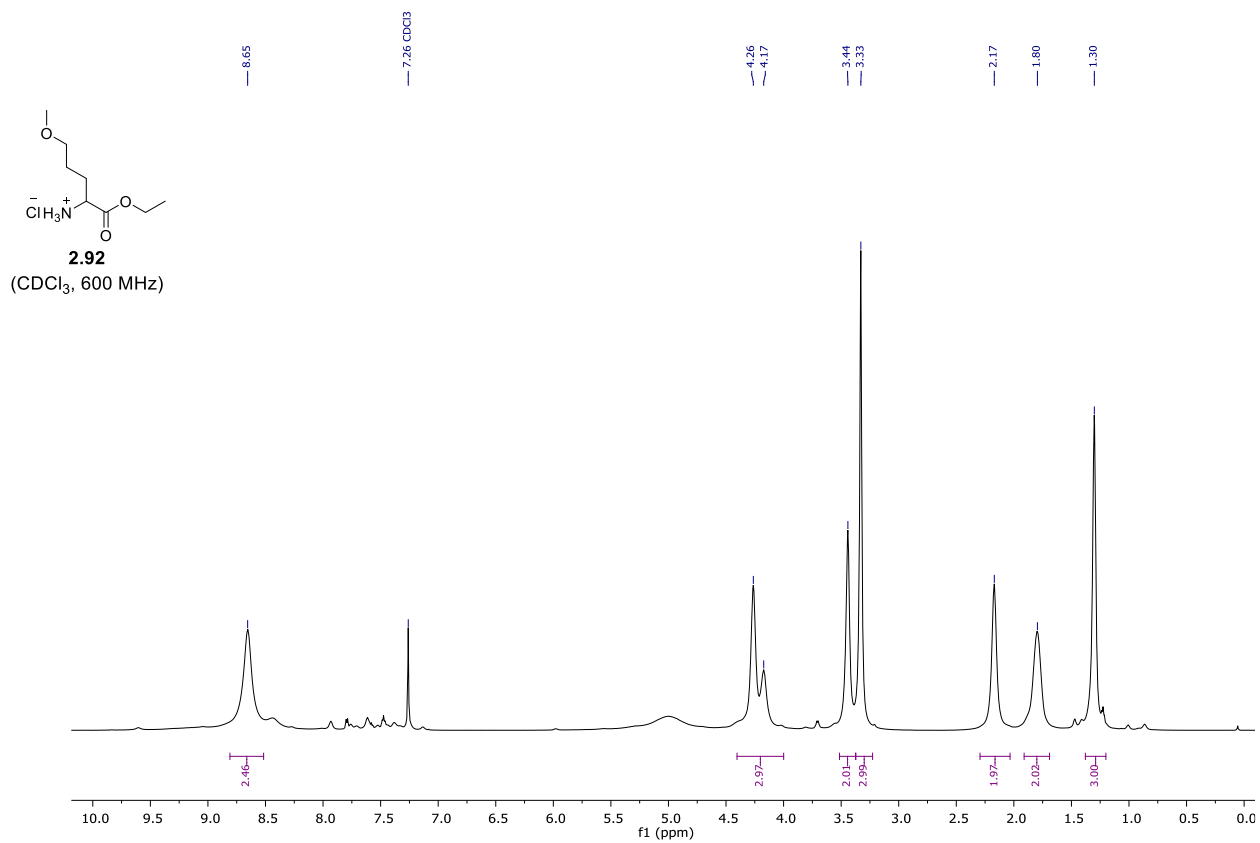


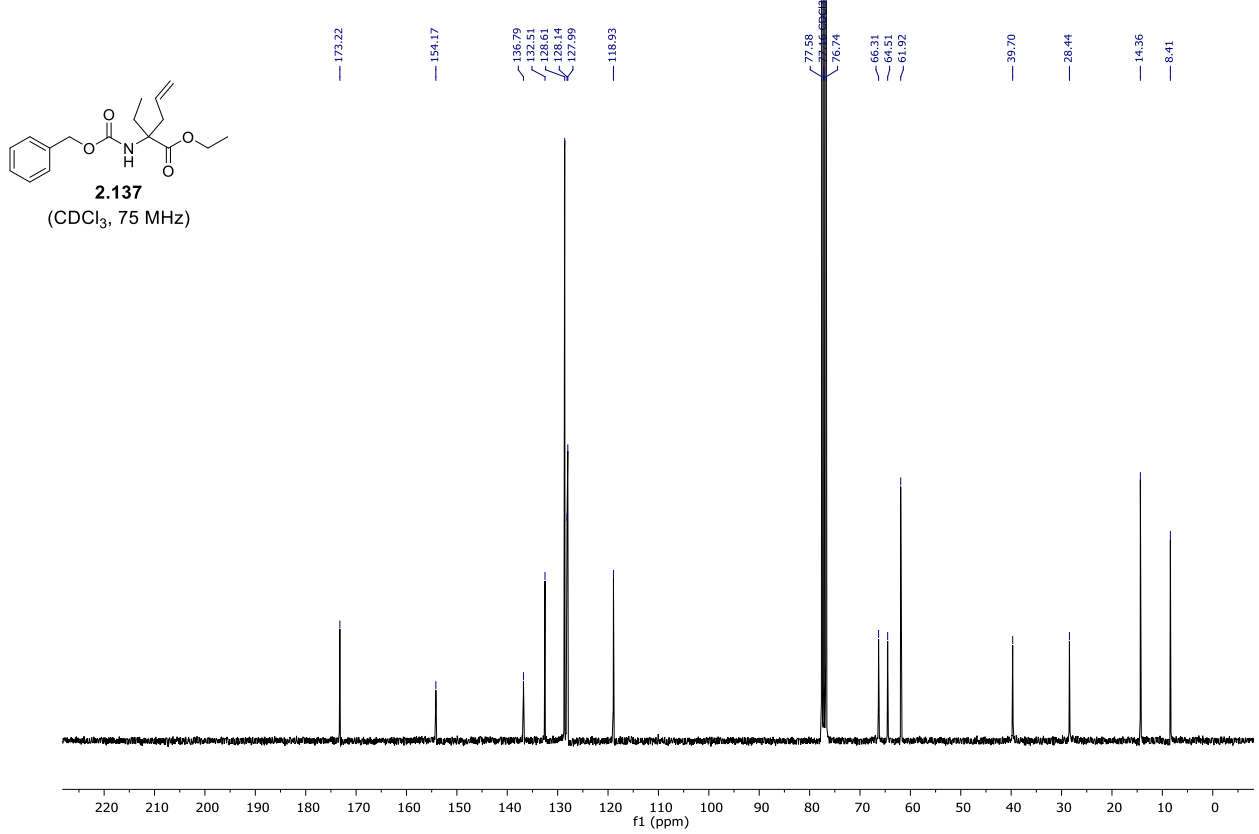
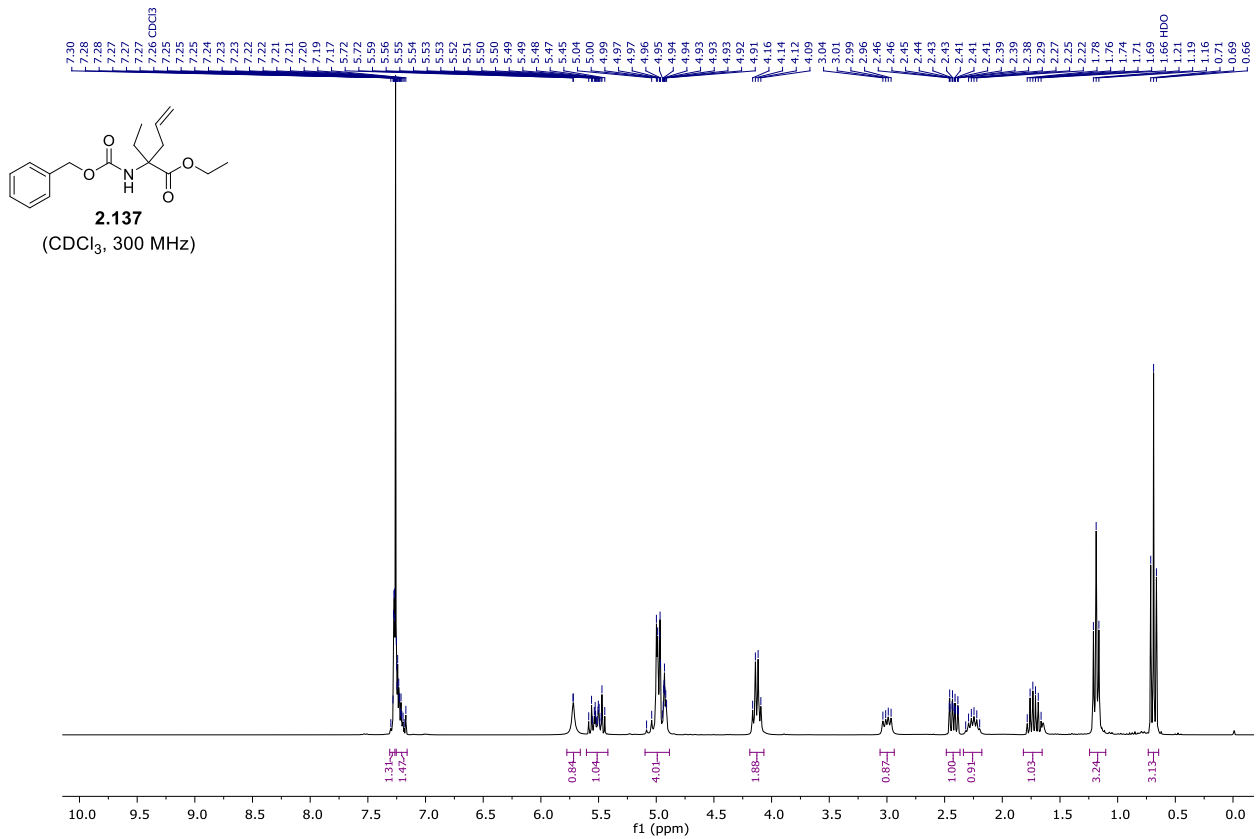


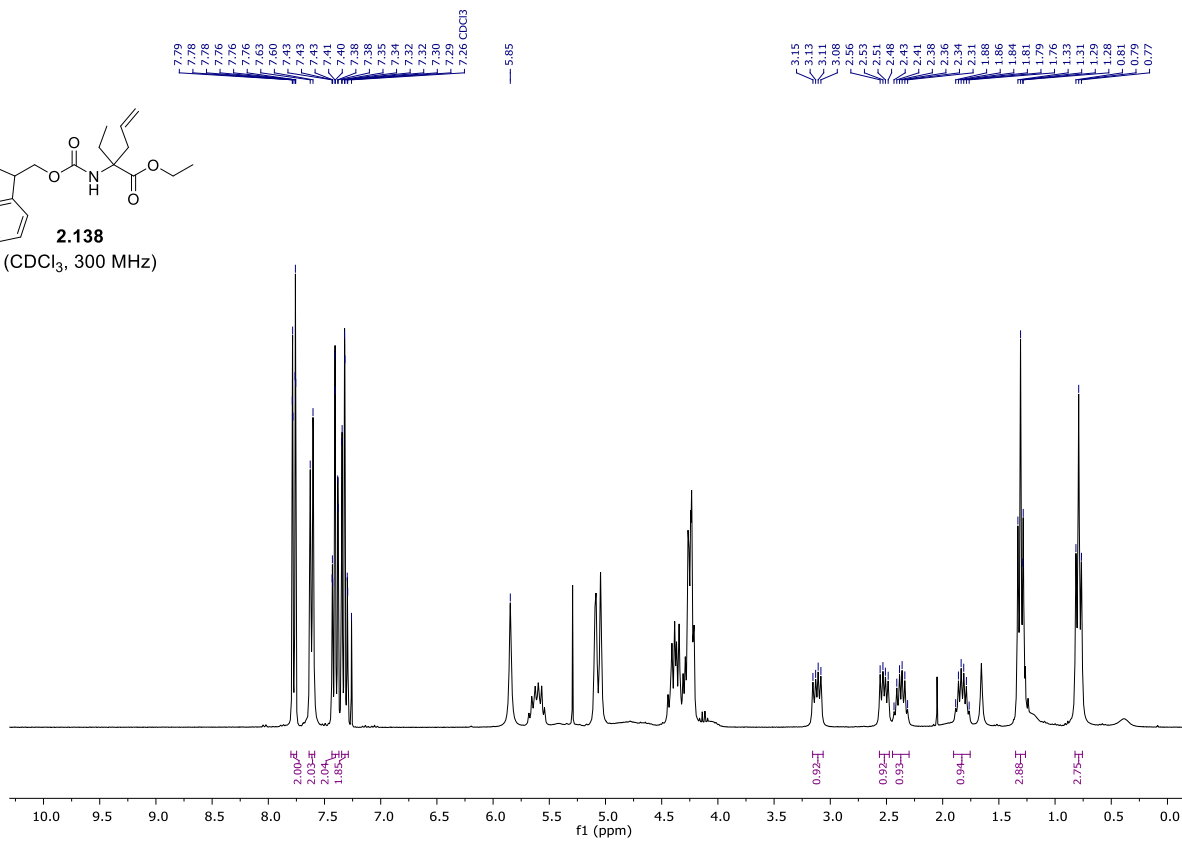
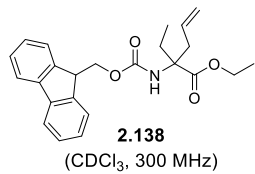


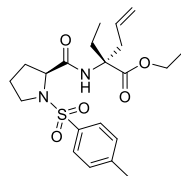




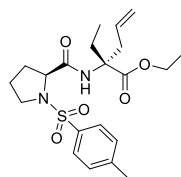
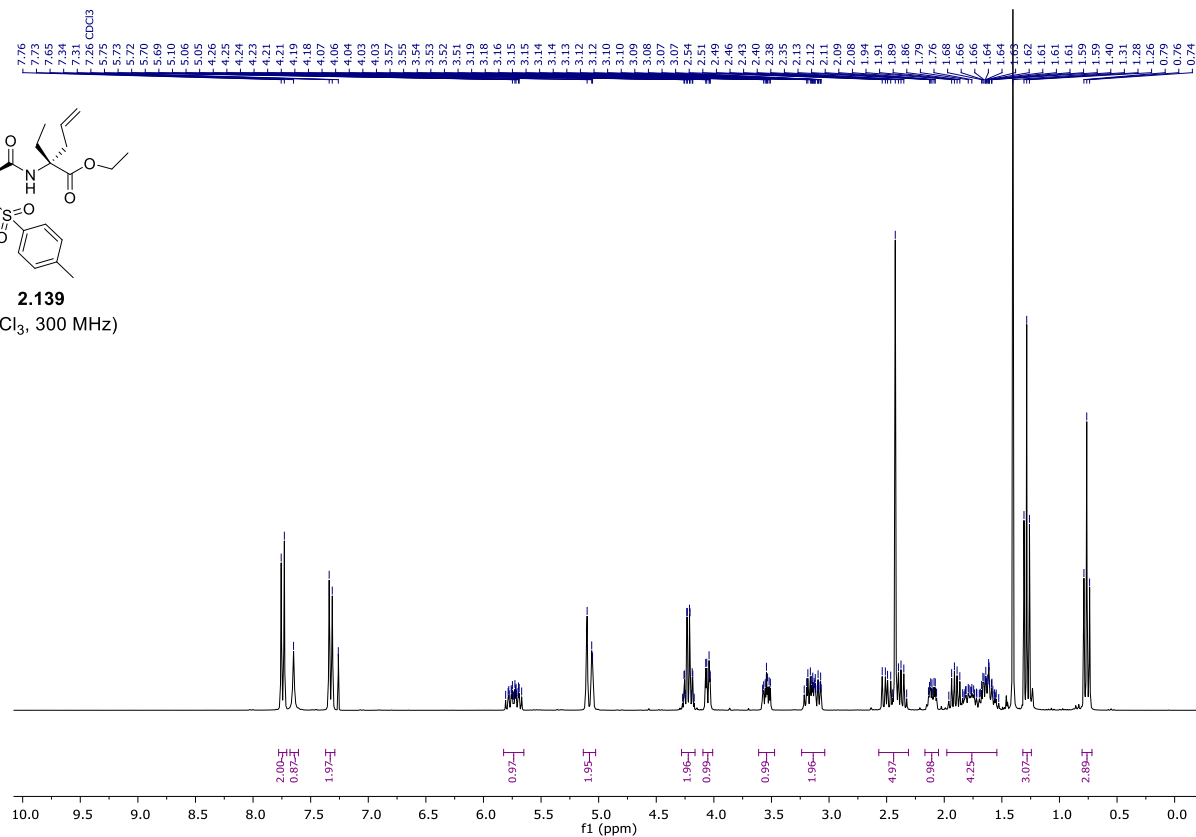




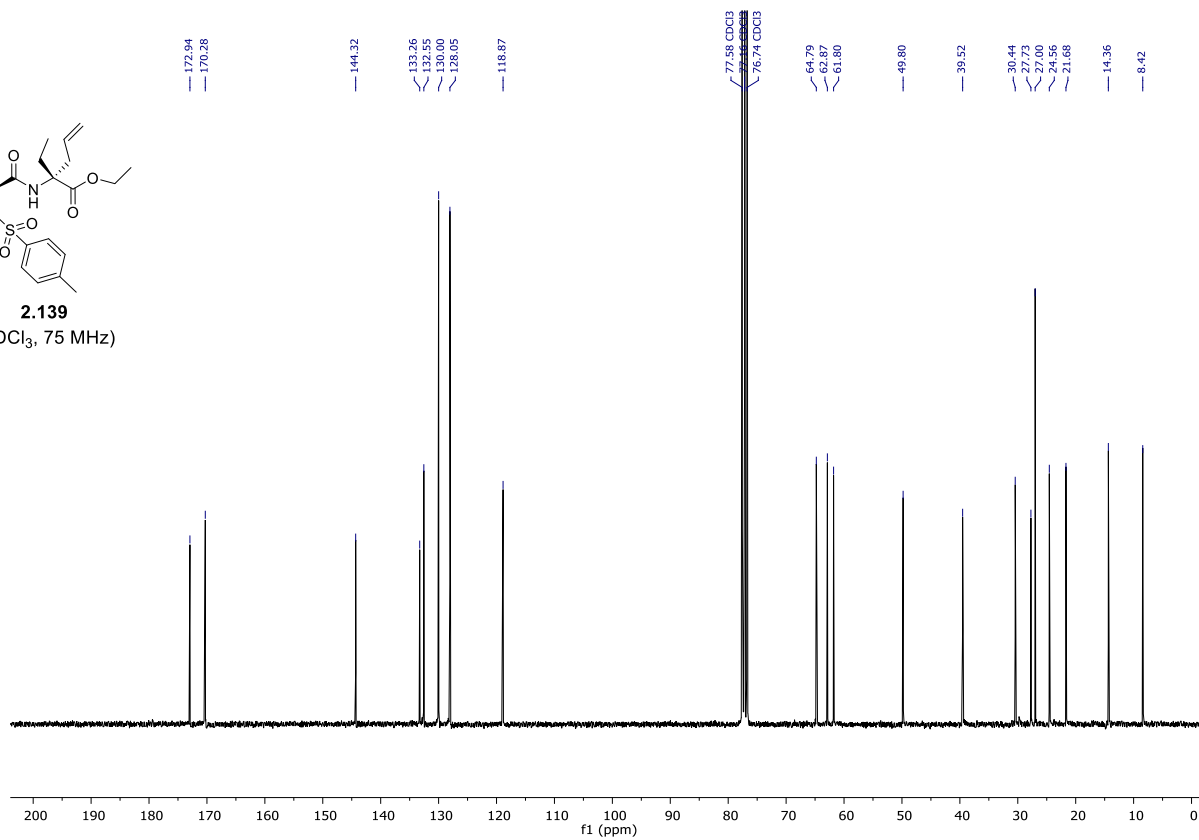




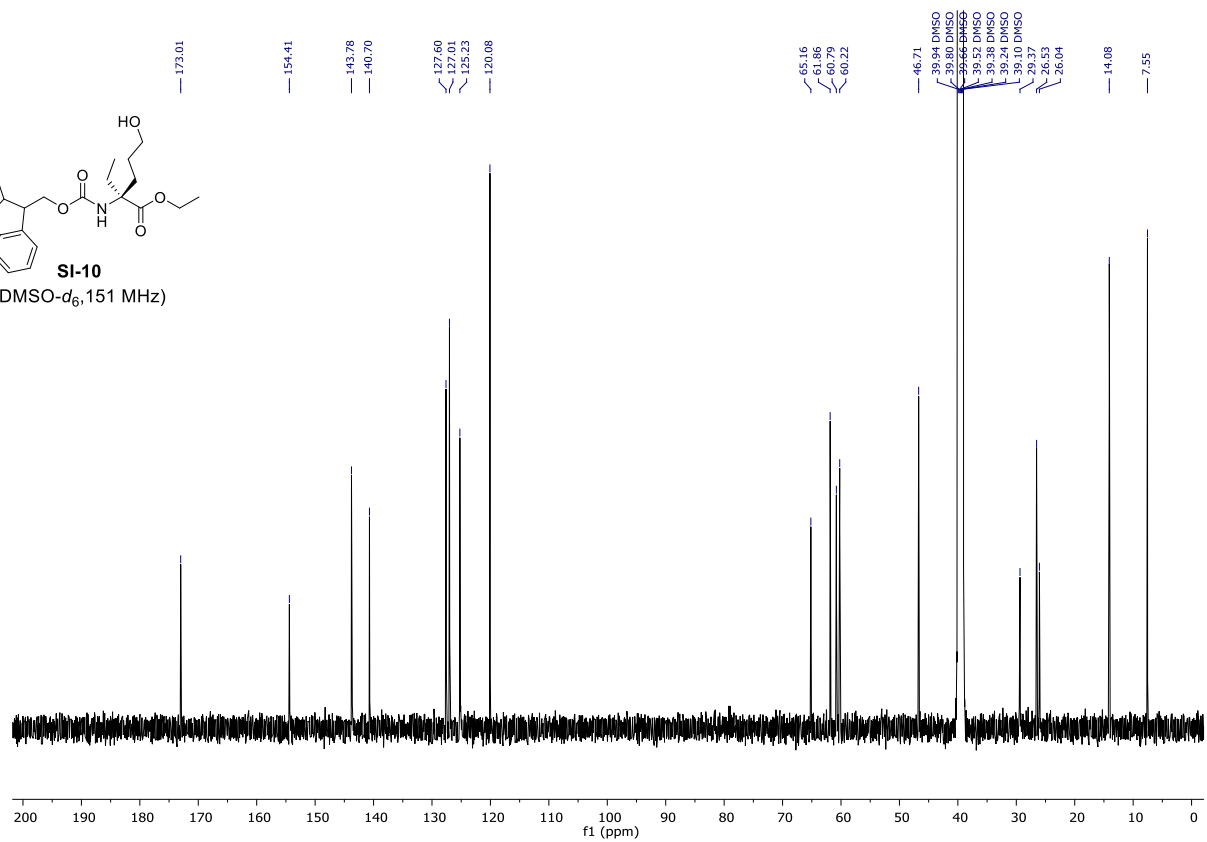
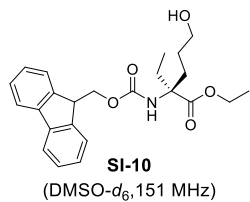
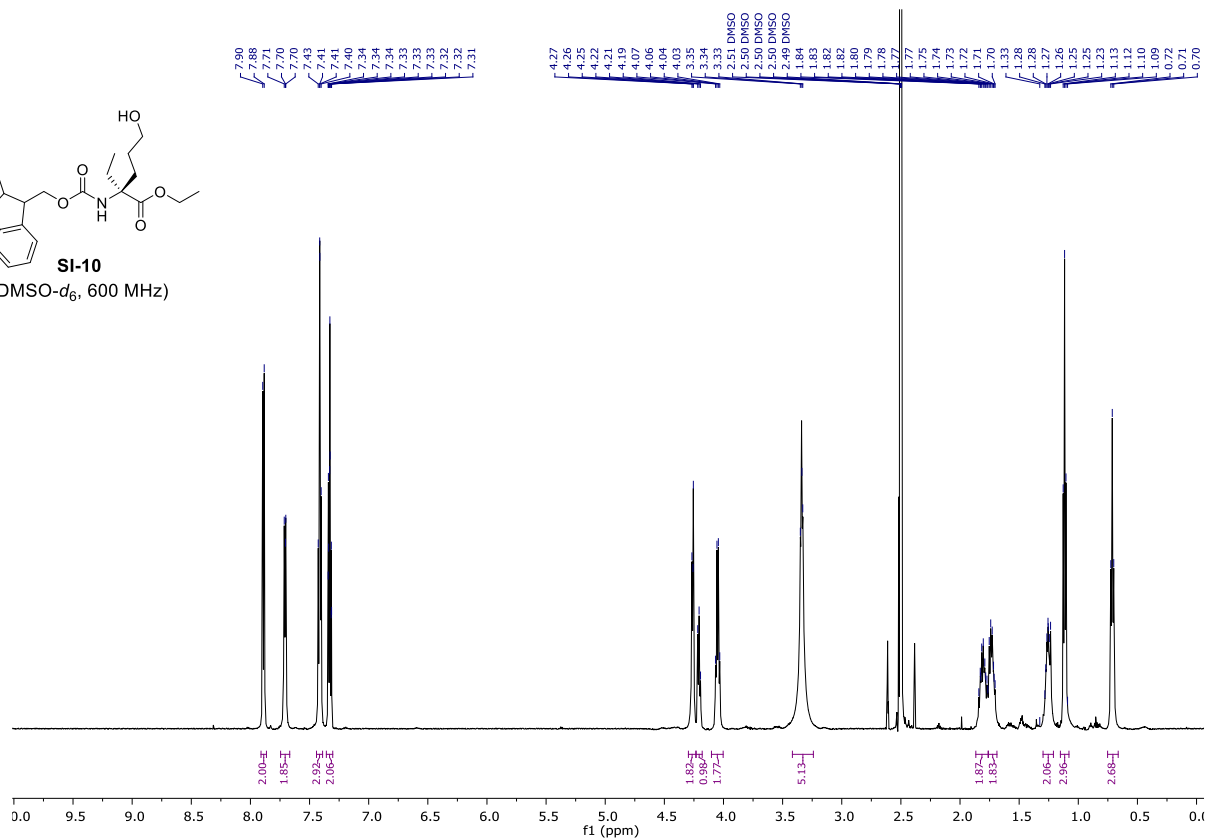
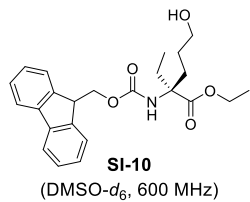
**2.139**  
(CDCl<sub>3</sub>, 300 MHz)

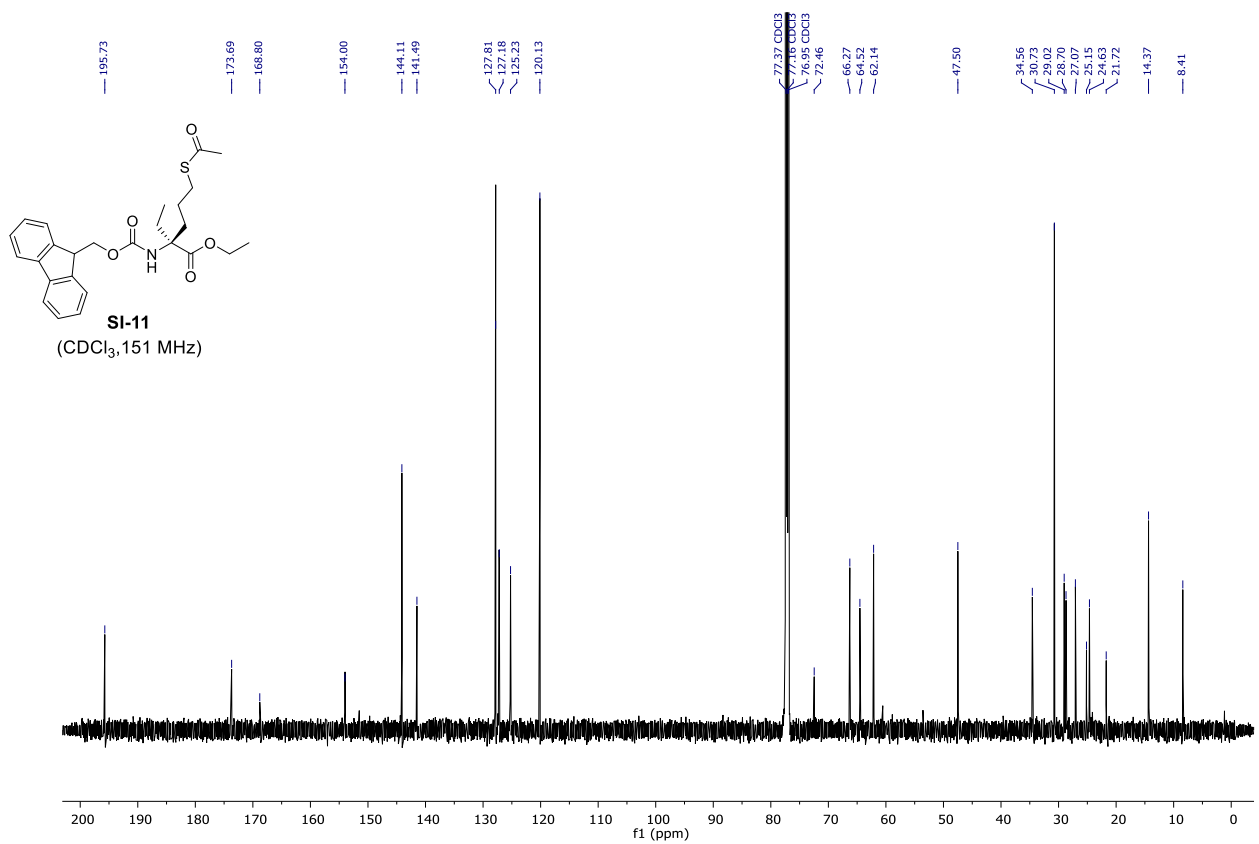
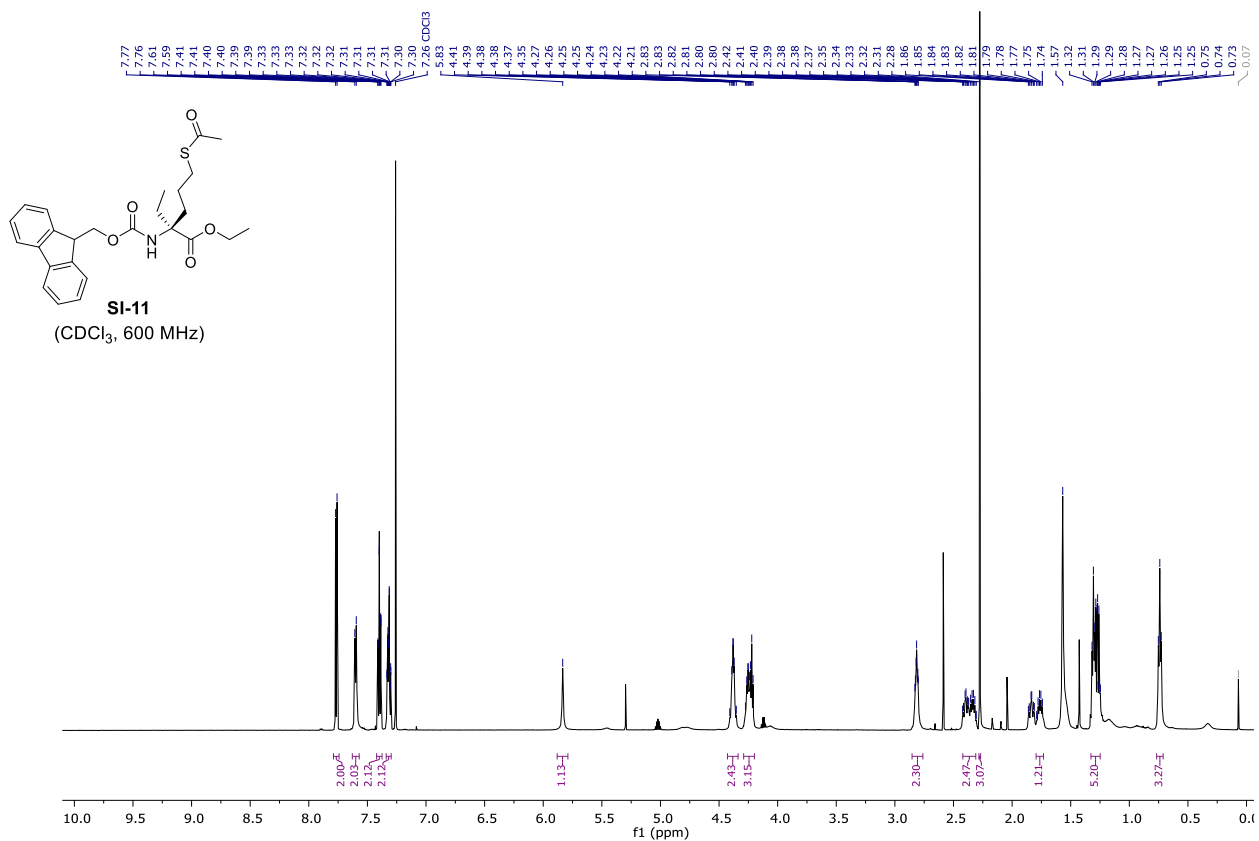


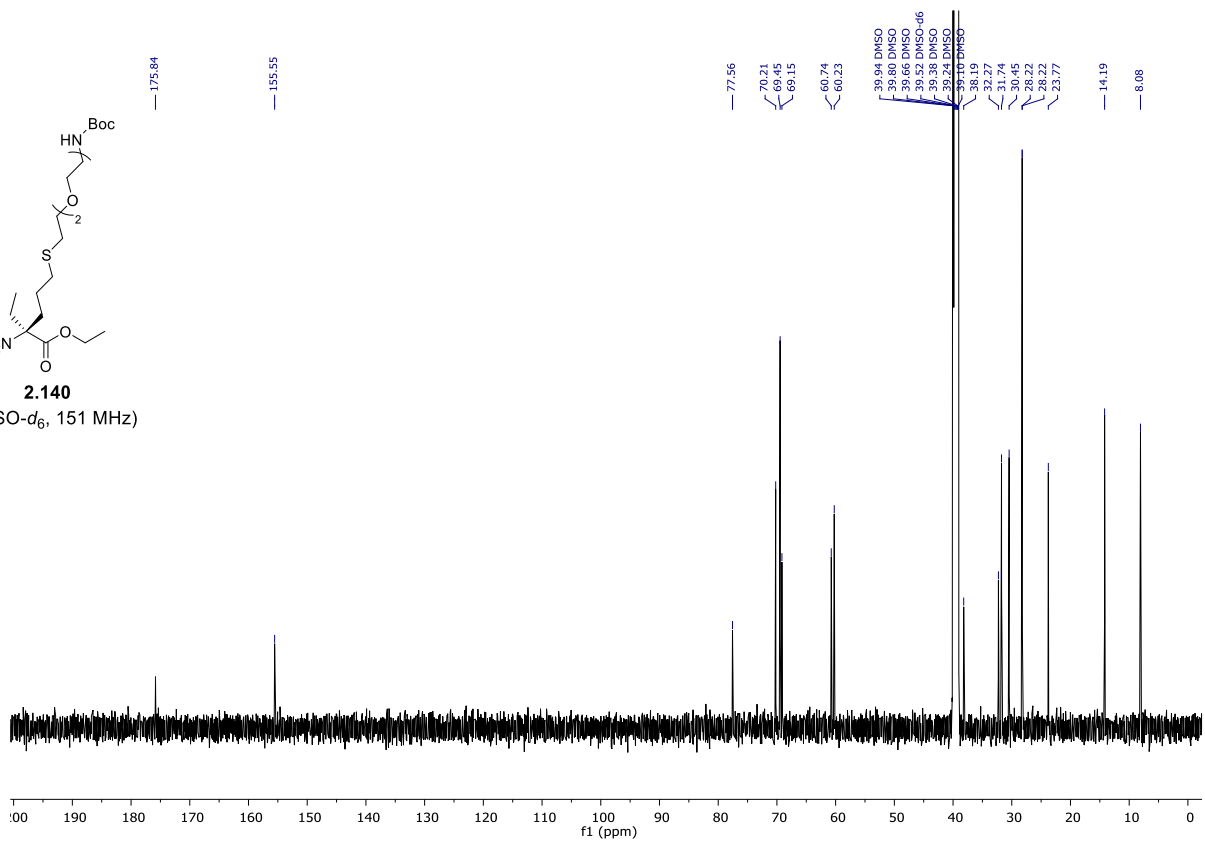
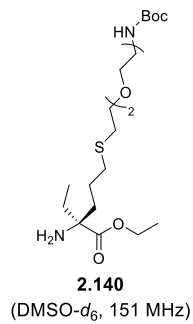
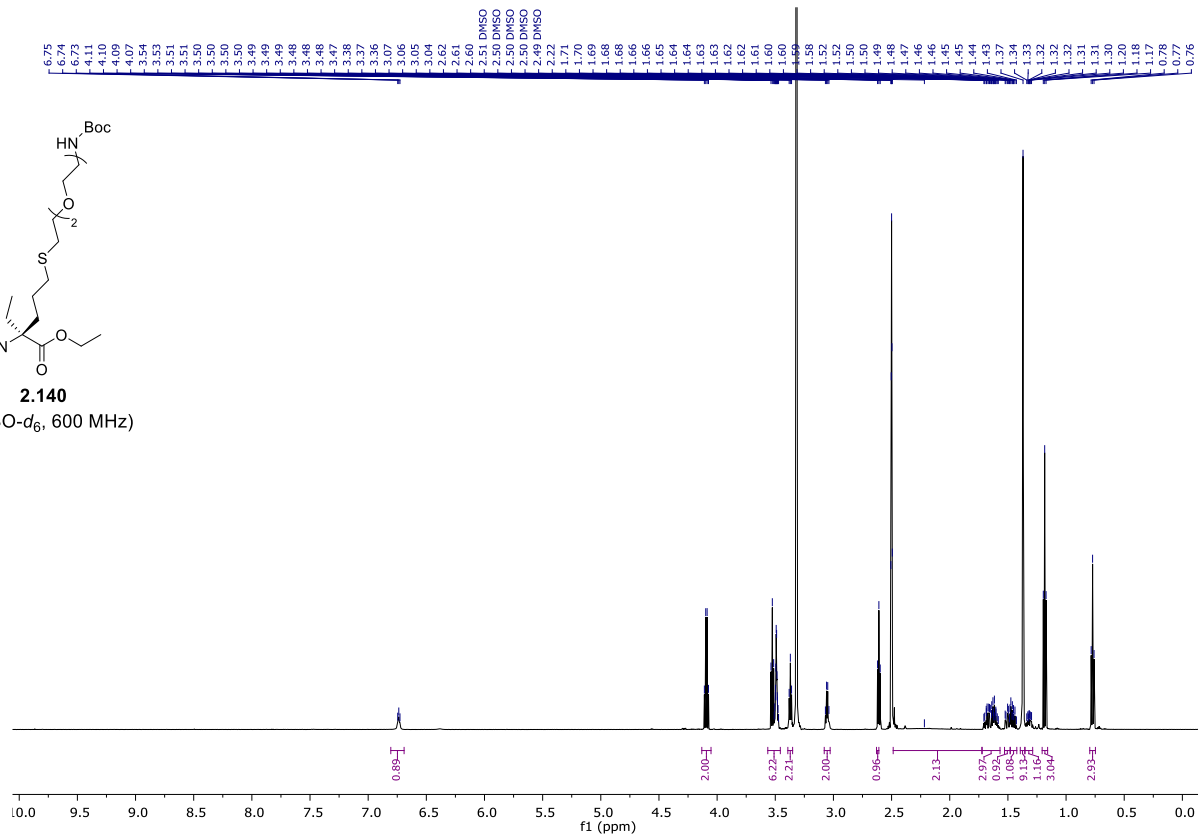
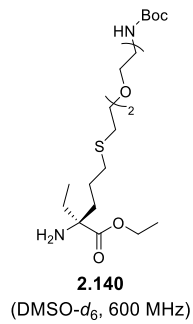
**2.139**  
(CDCl<sub>3</sub>, 75 MHz)

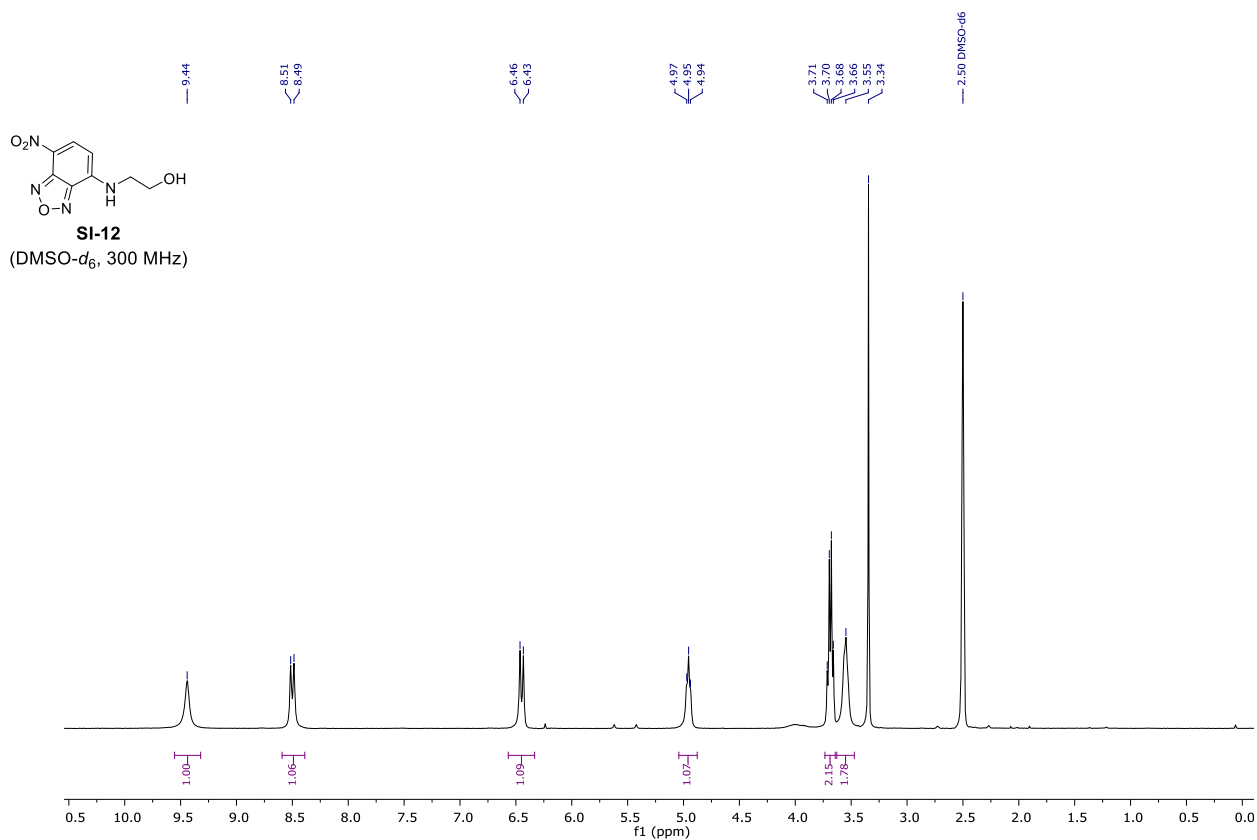
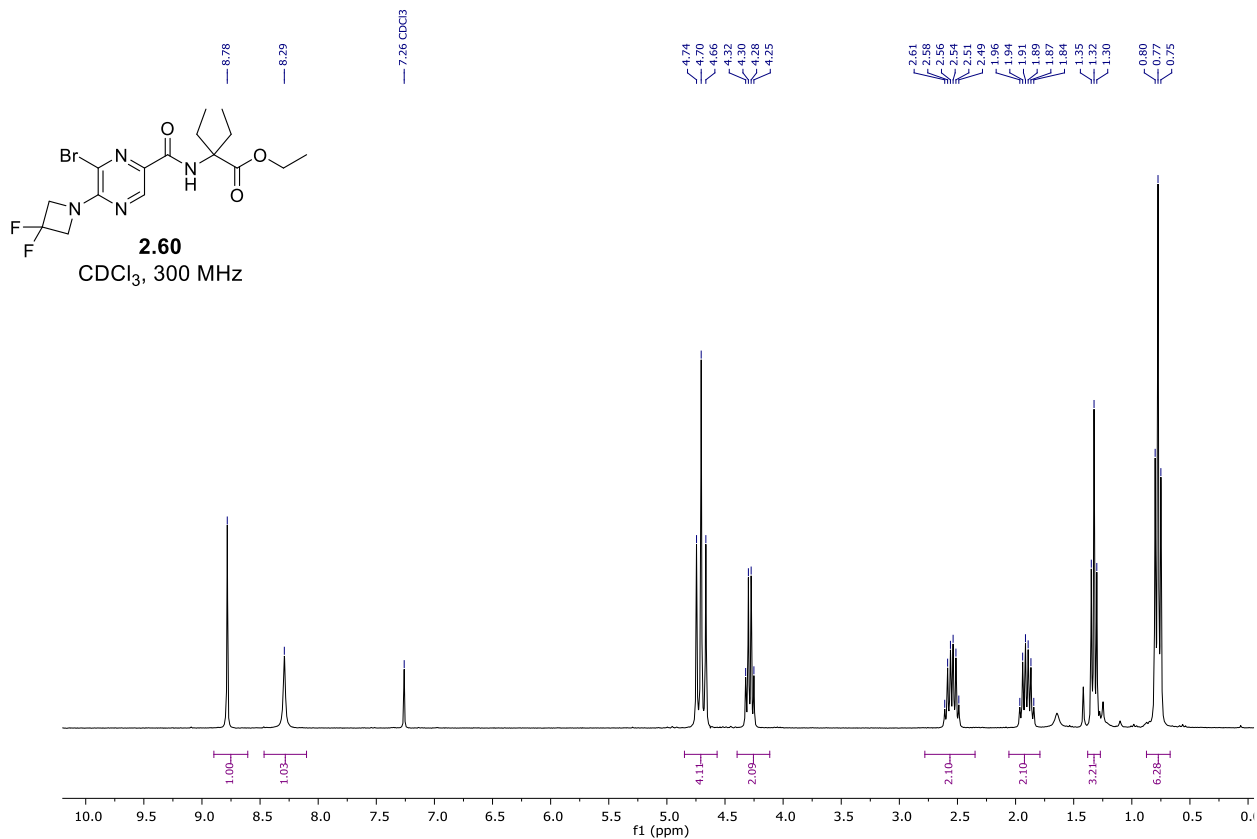


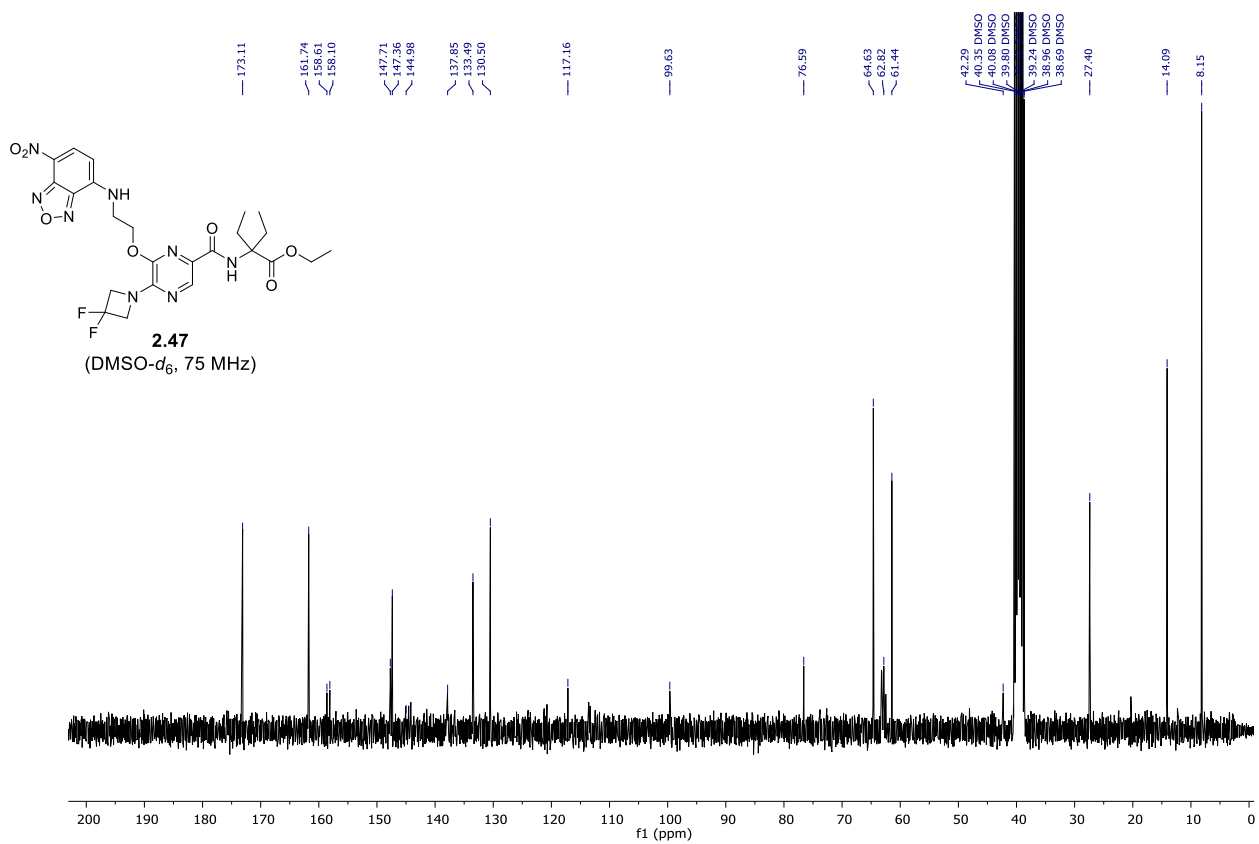
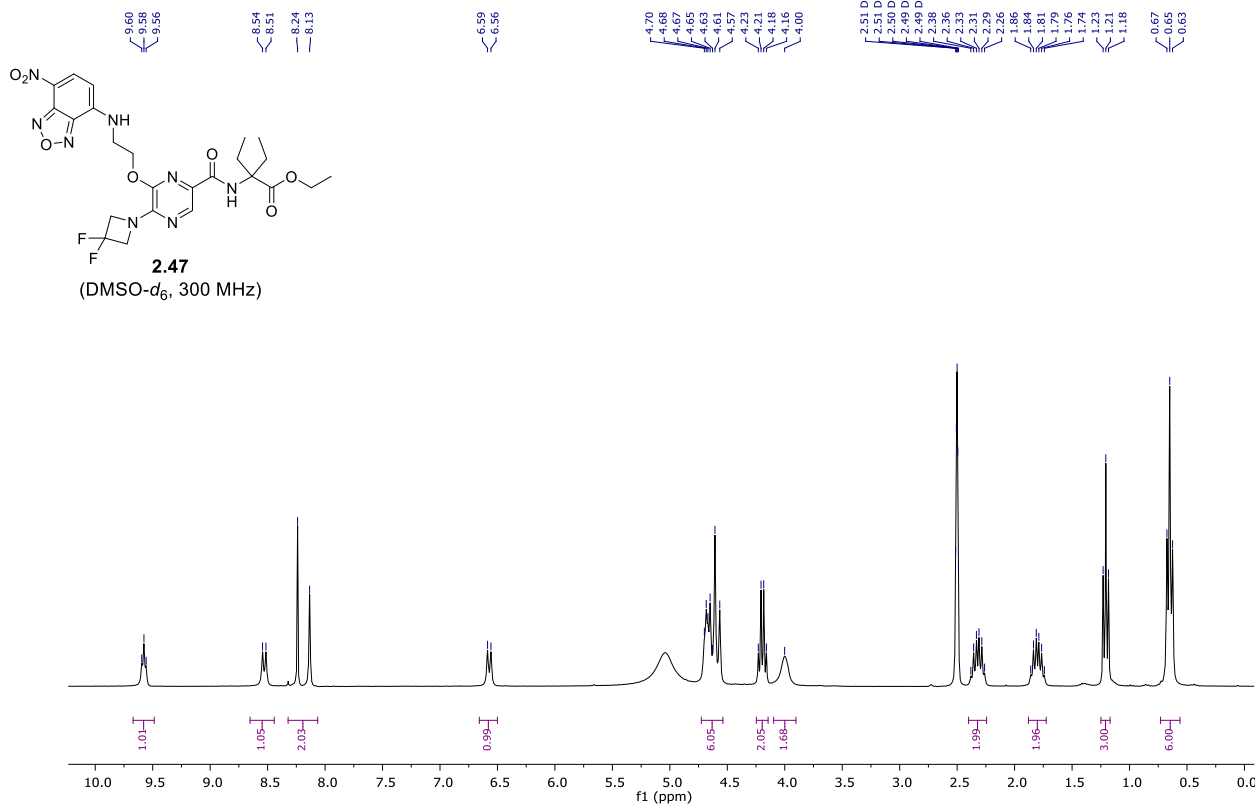


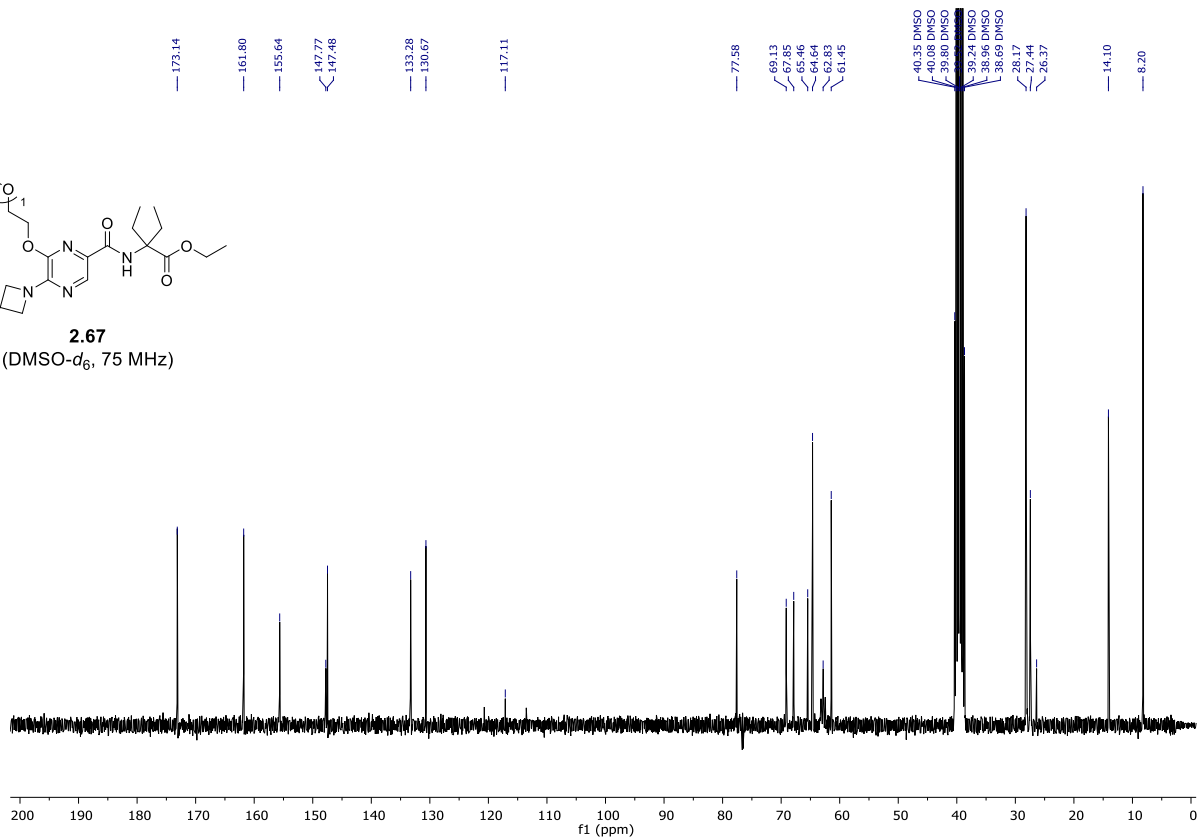
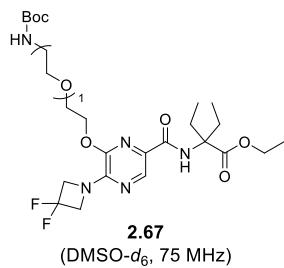
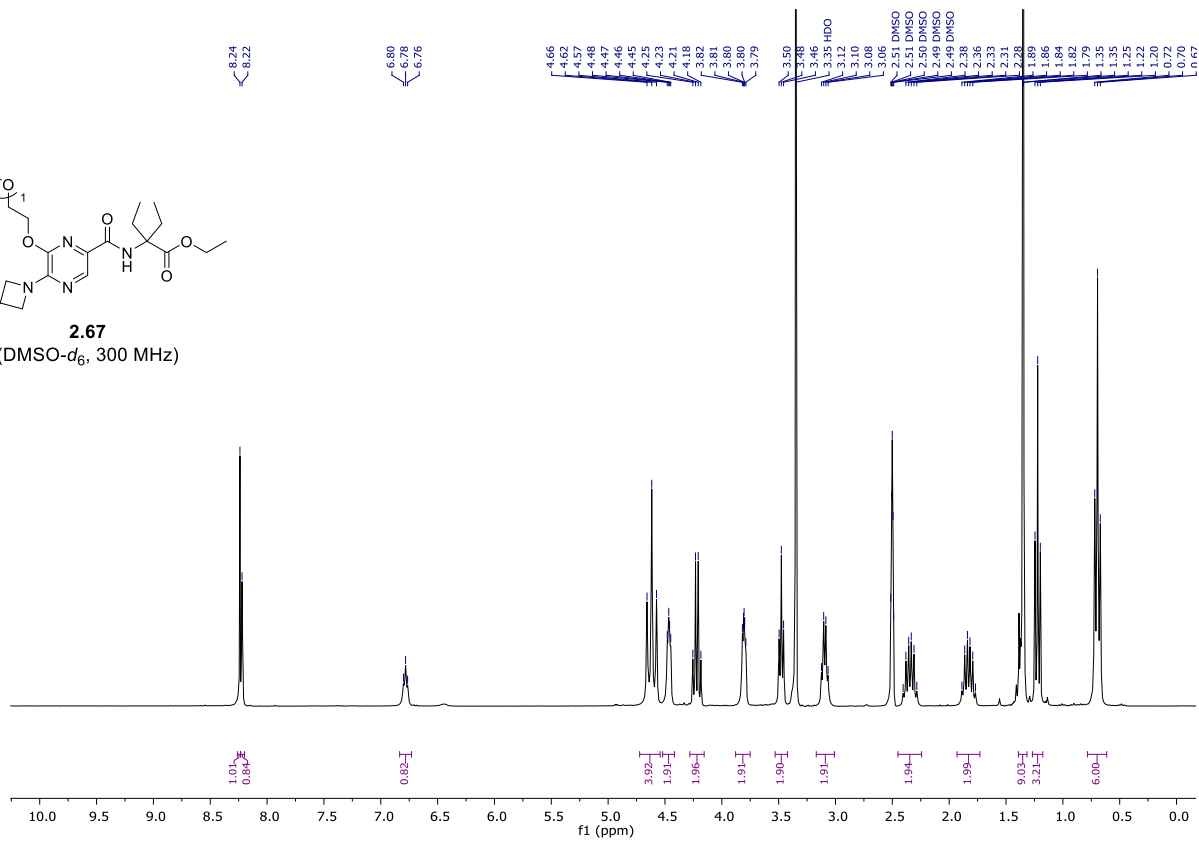
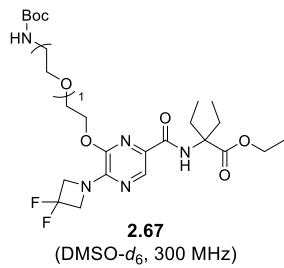


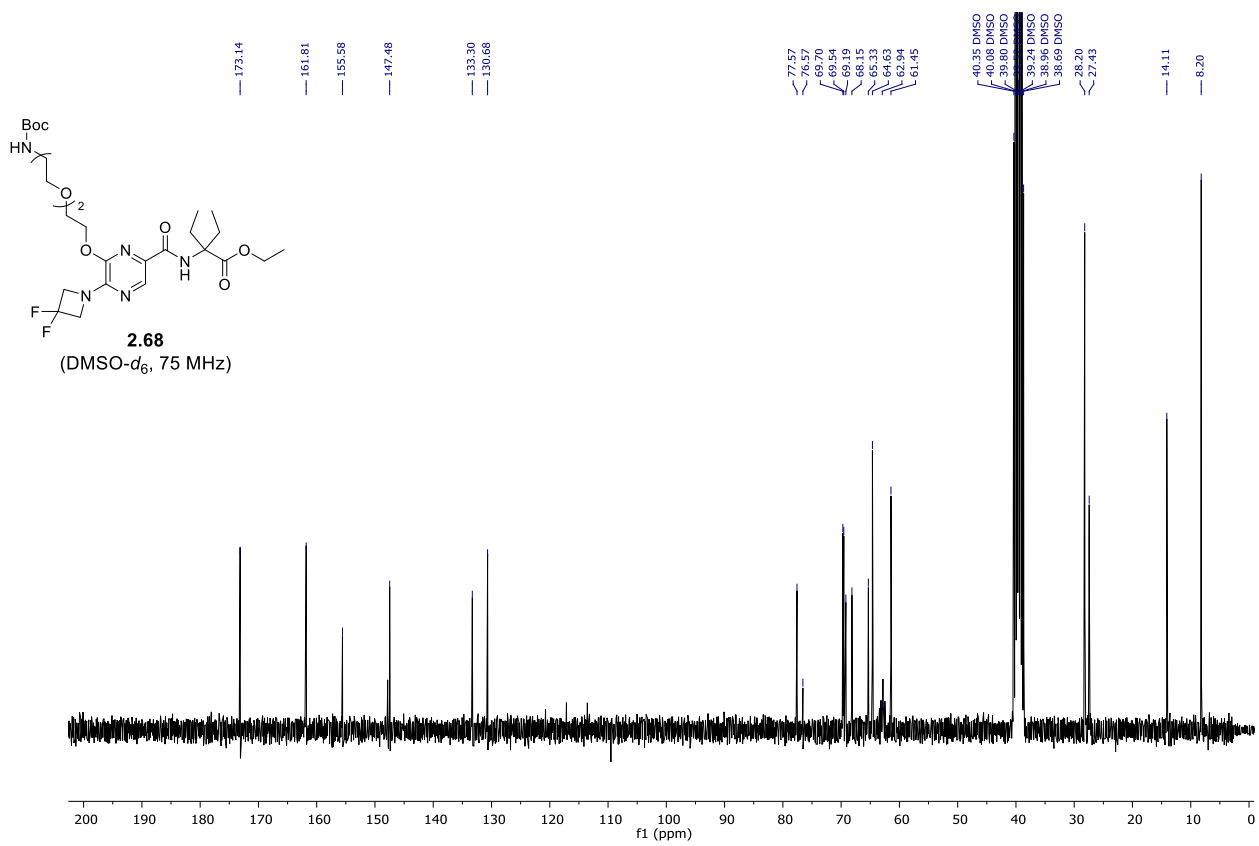
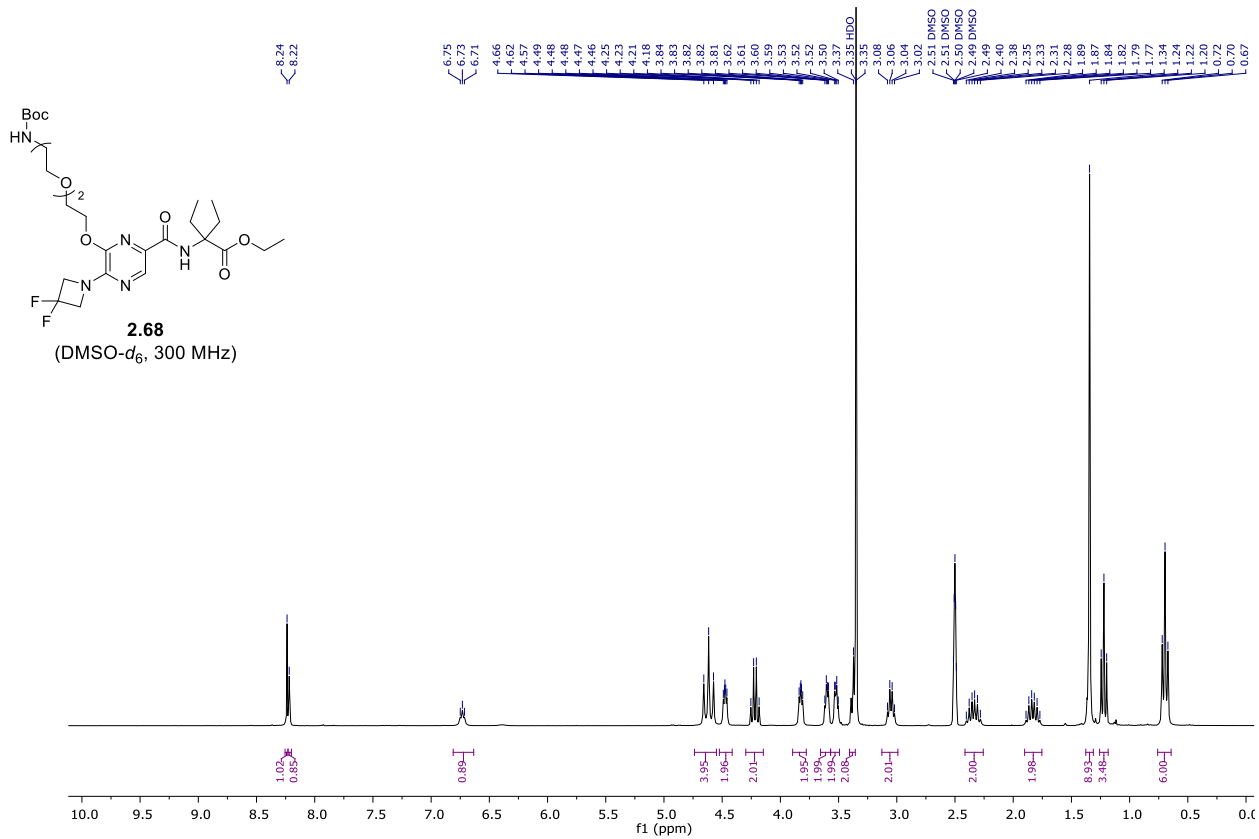


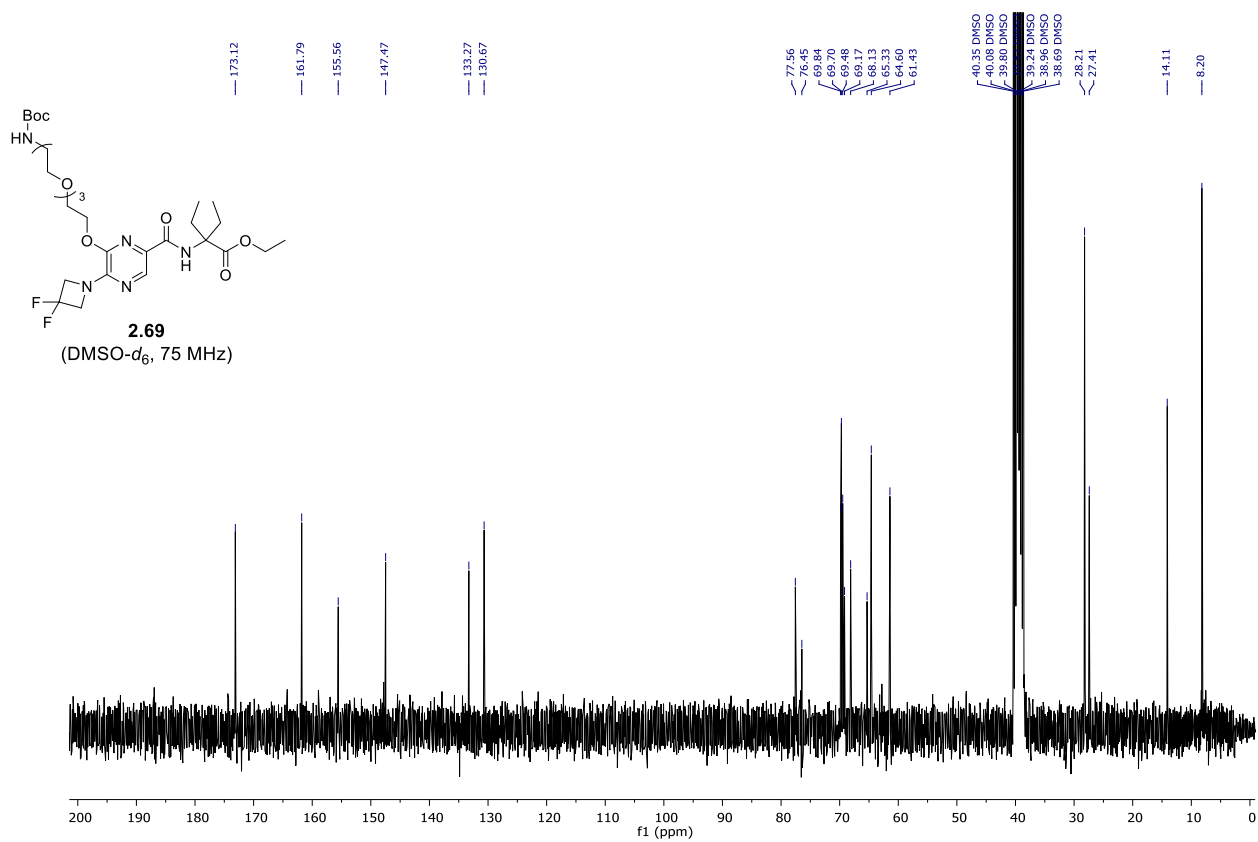
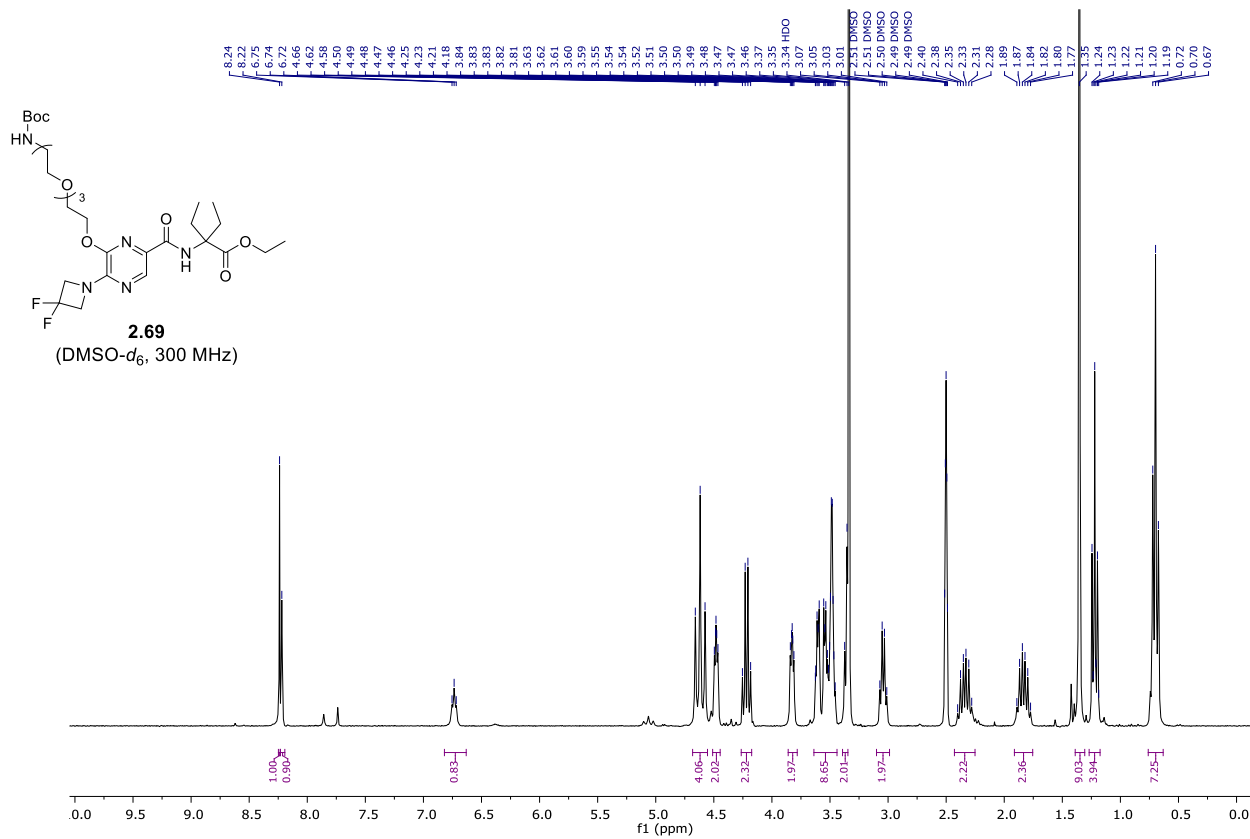




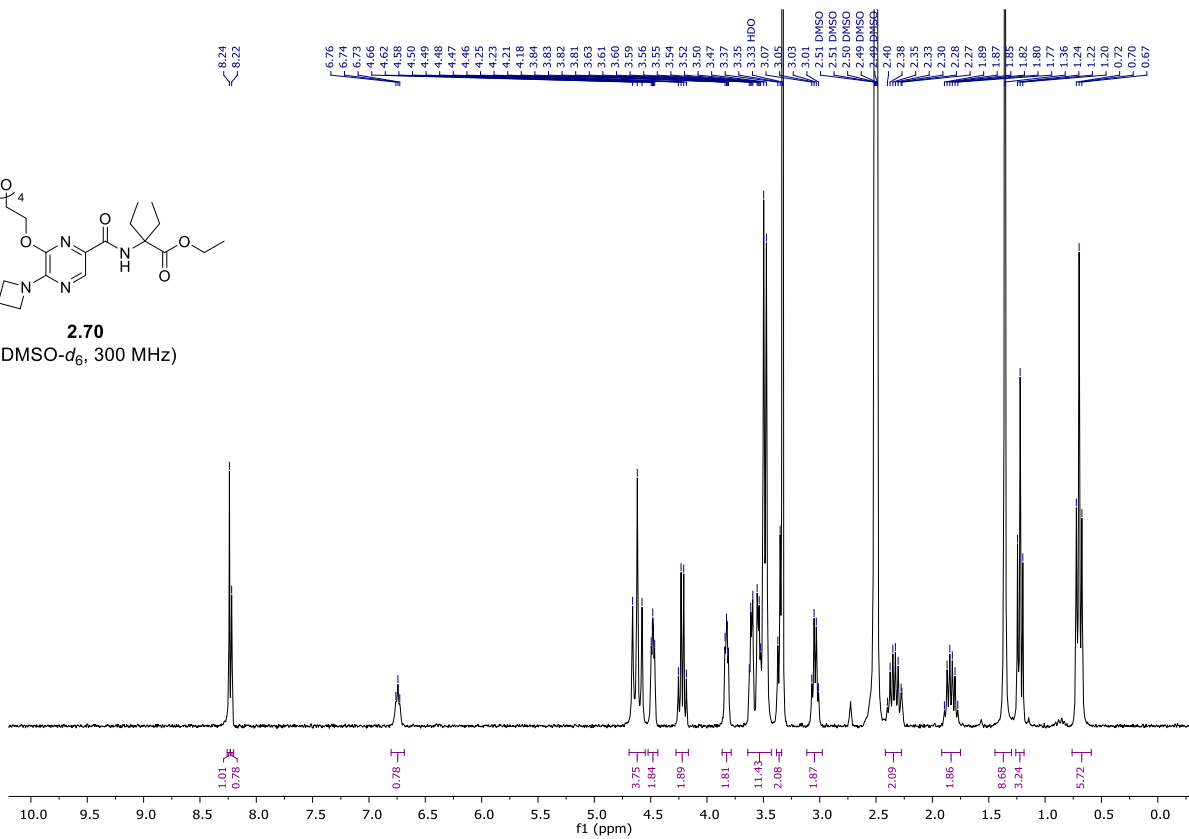
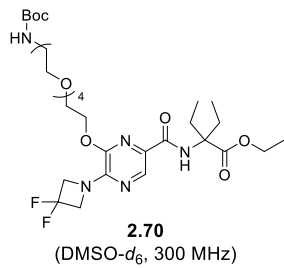


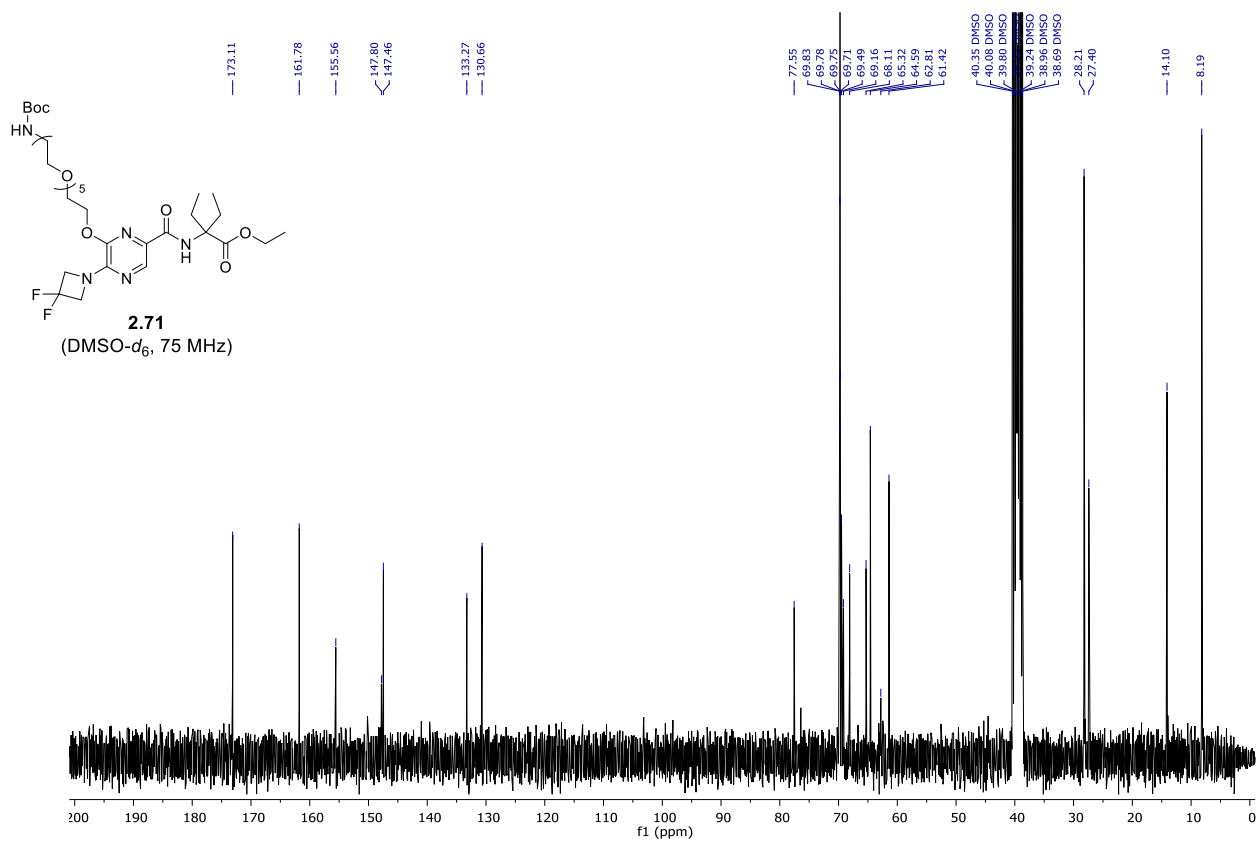
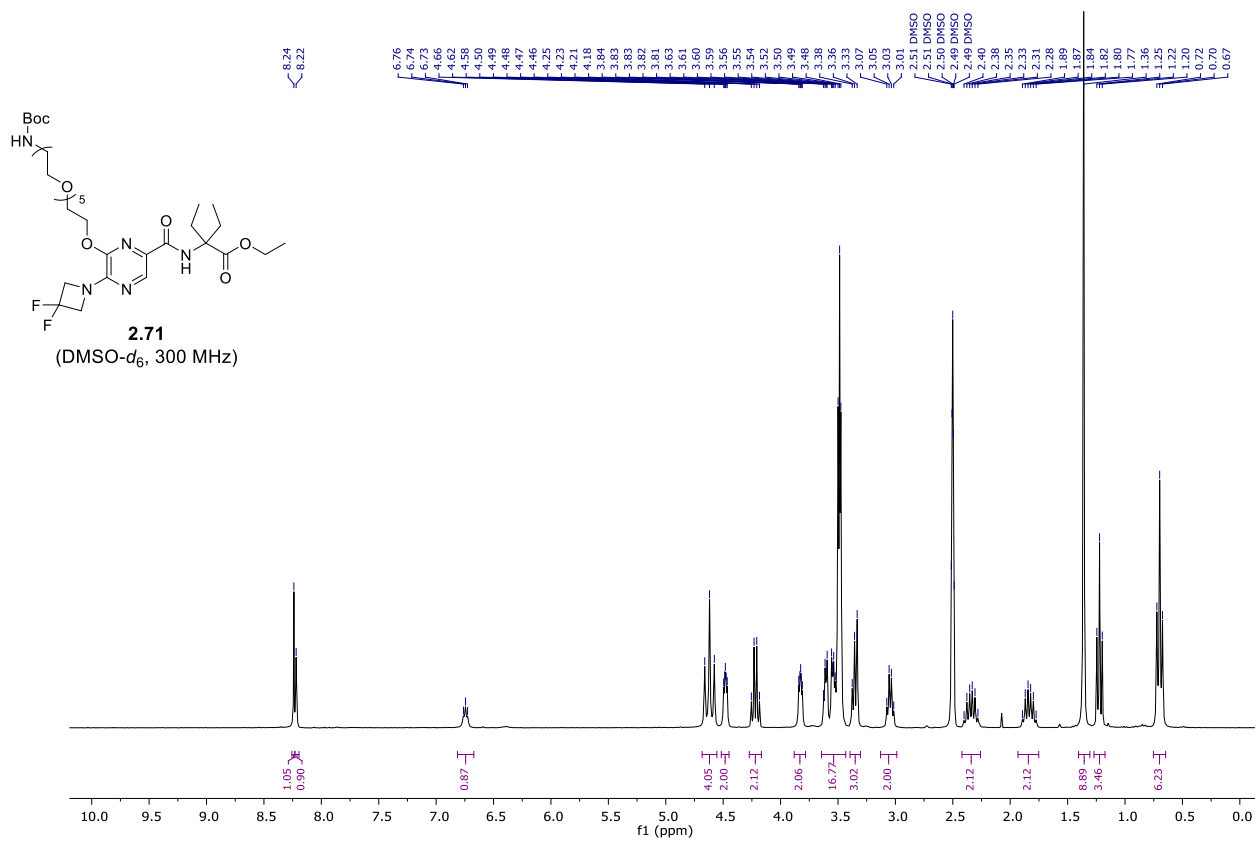


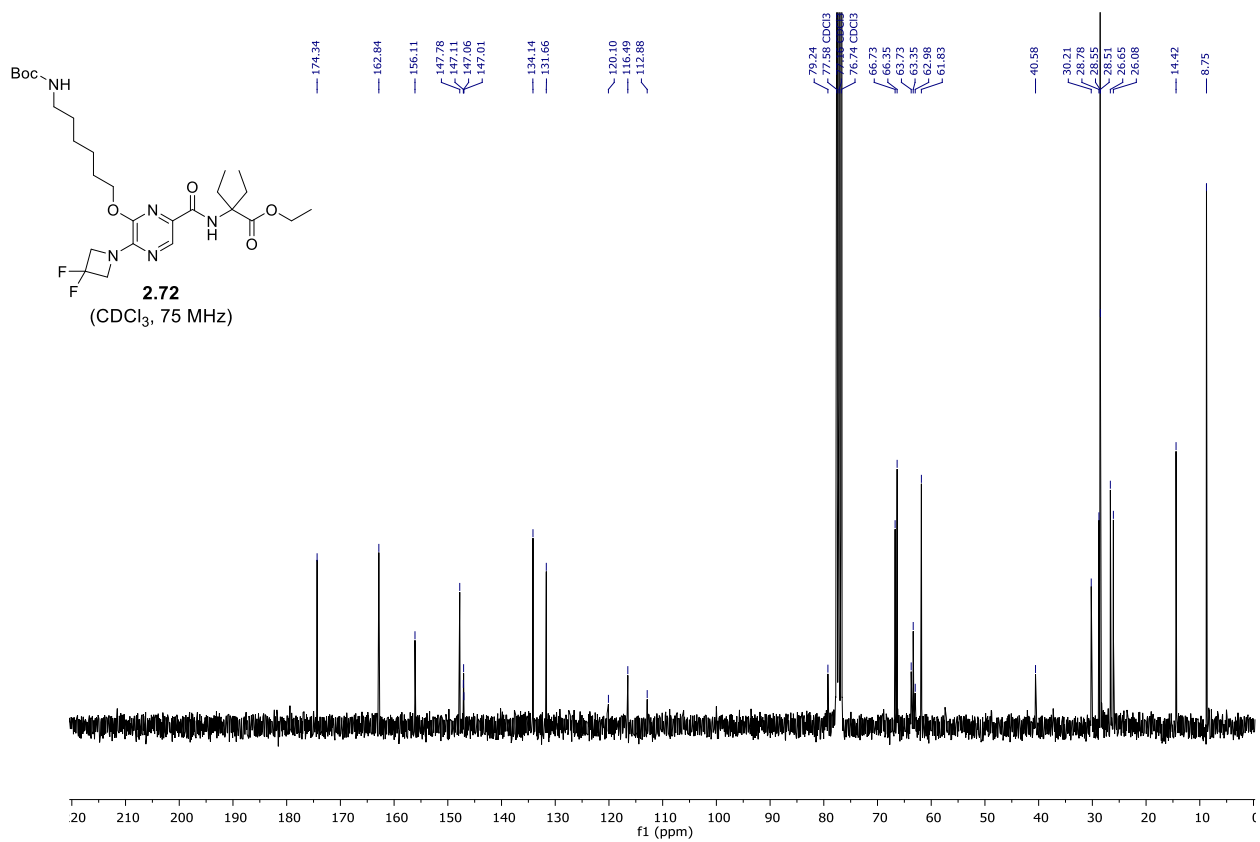
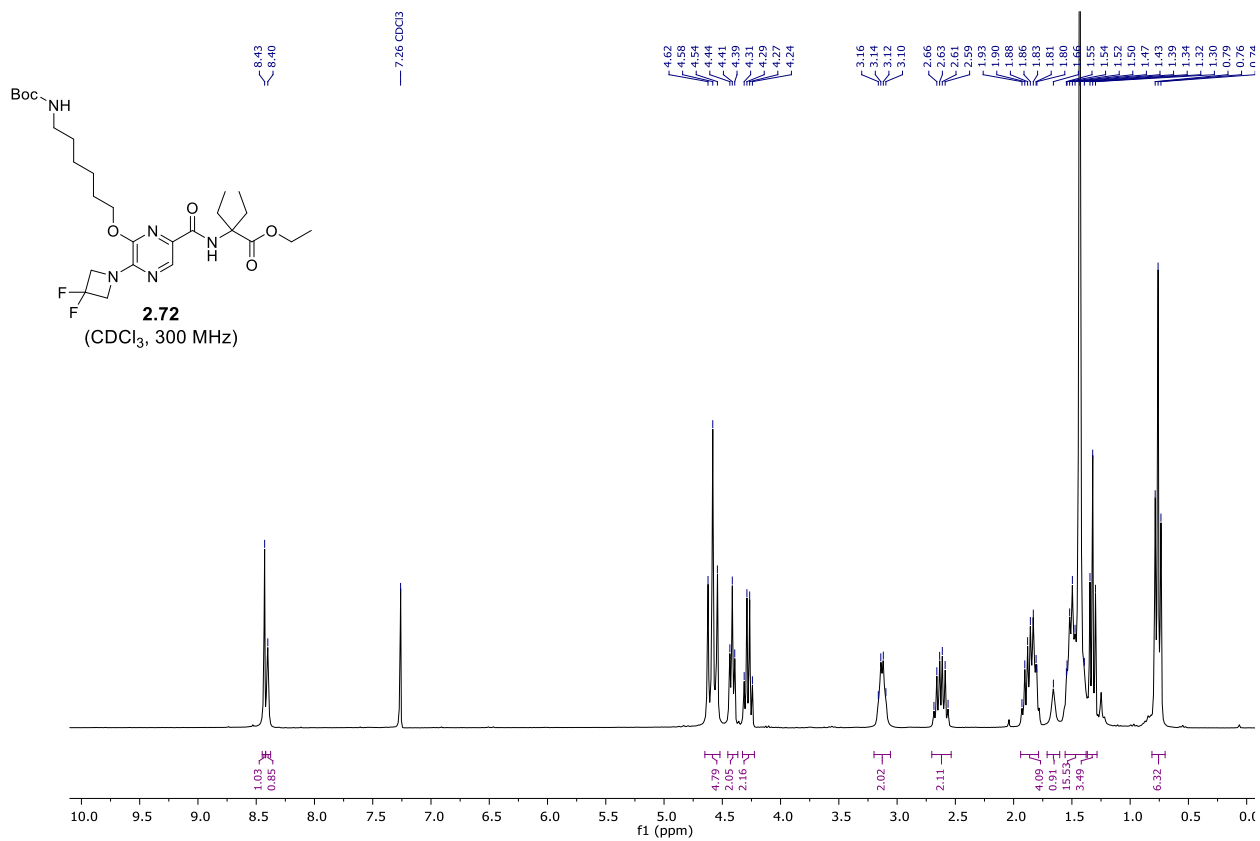


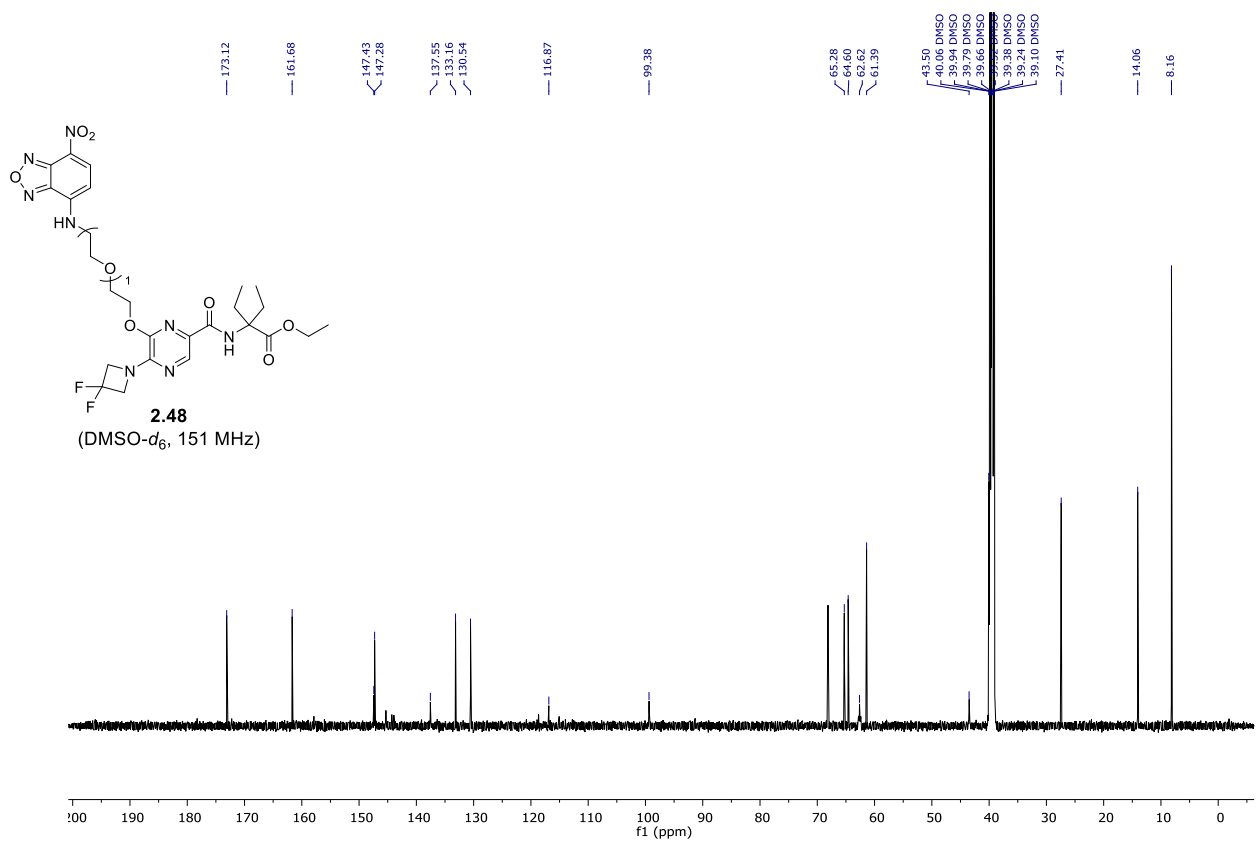
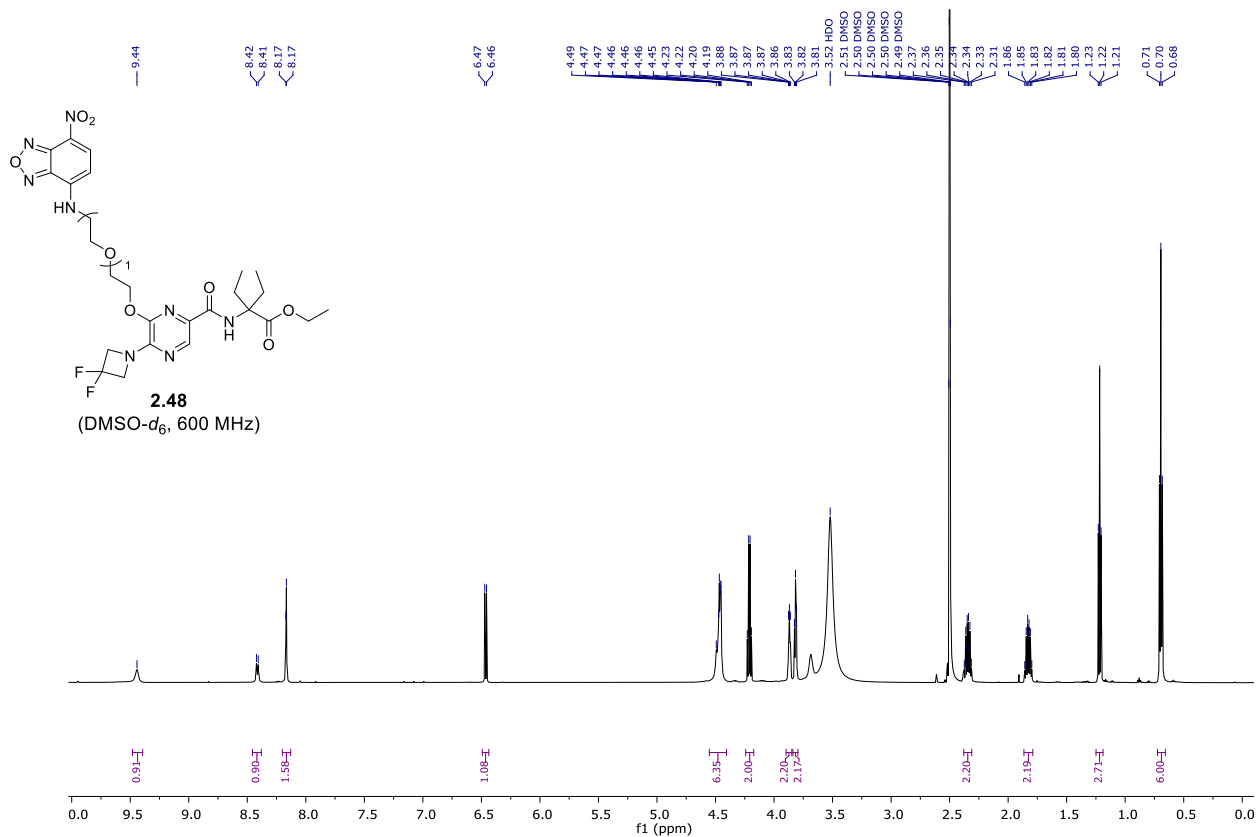


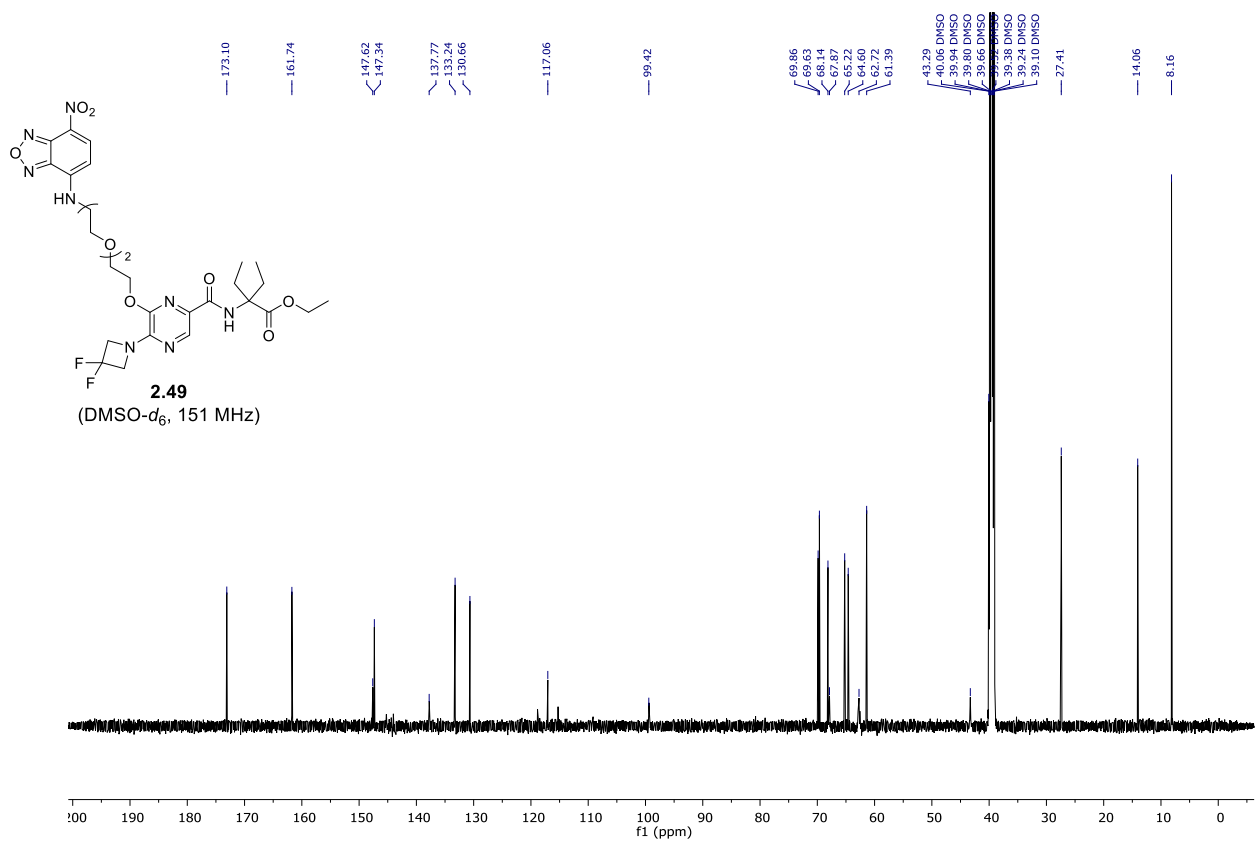
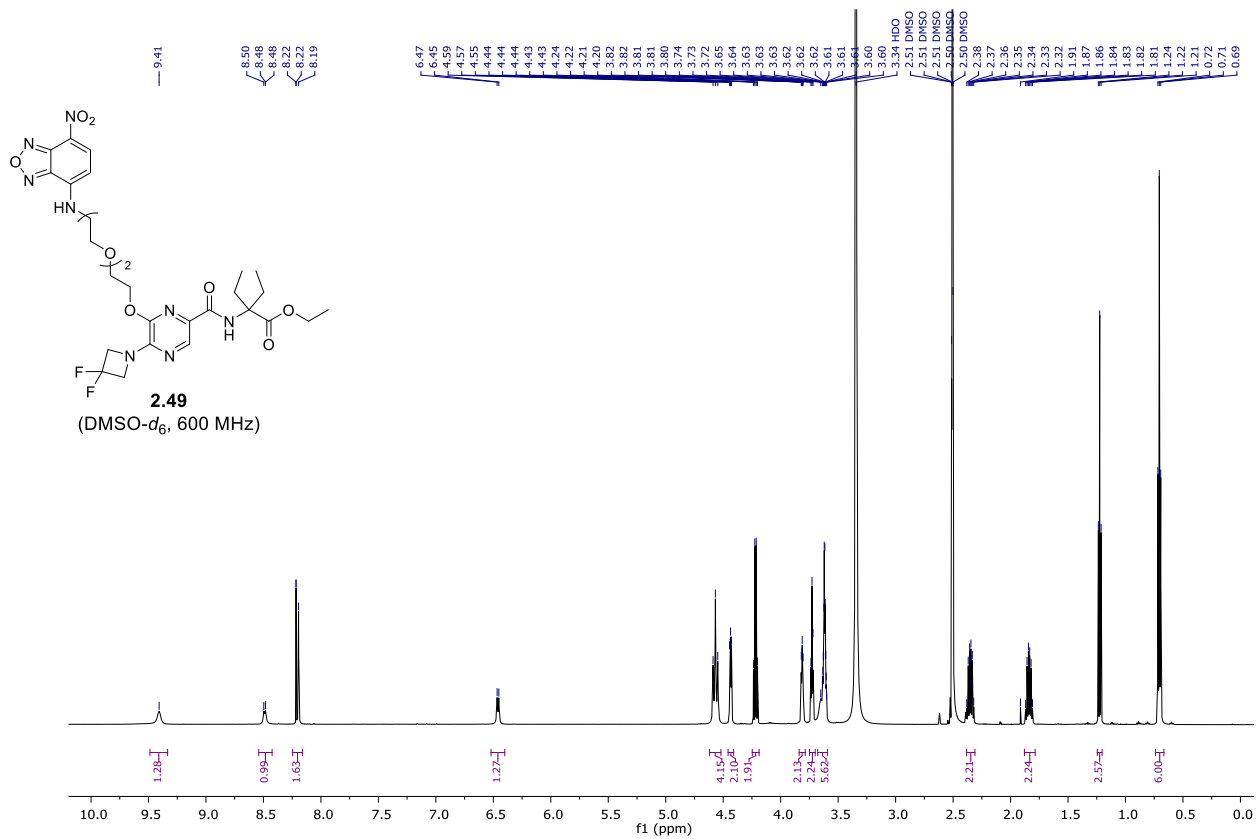


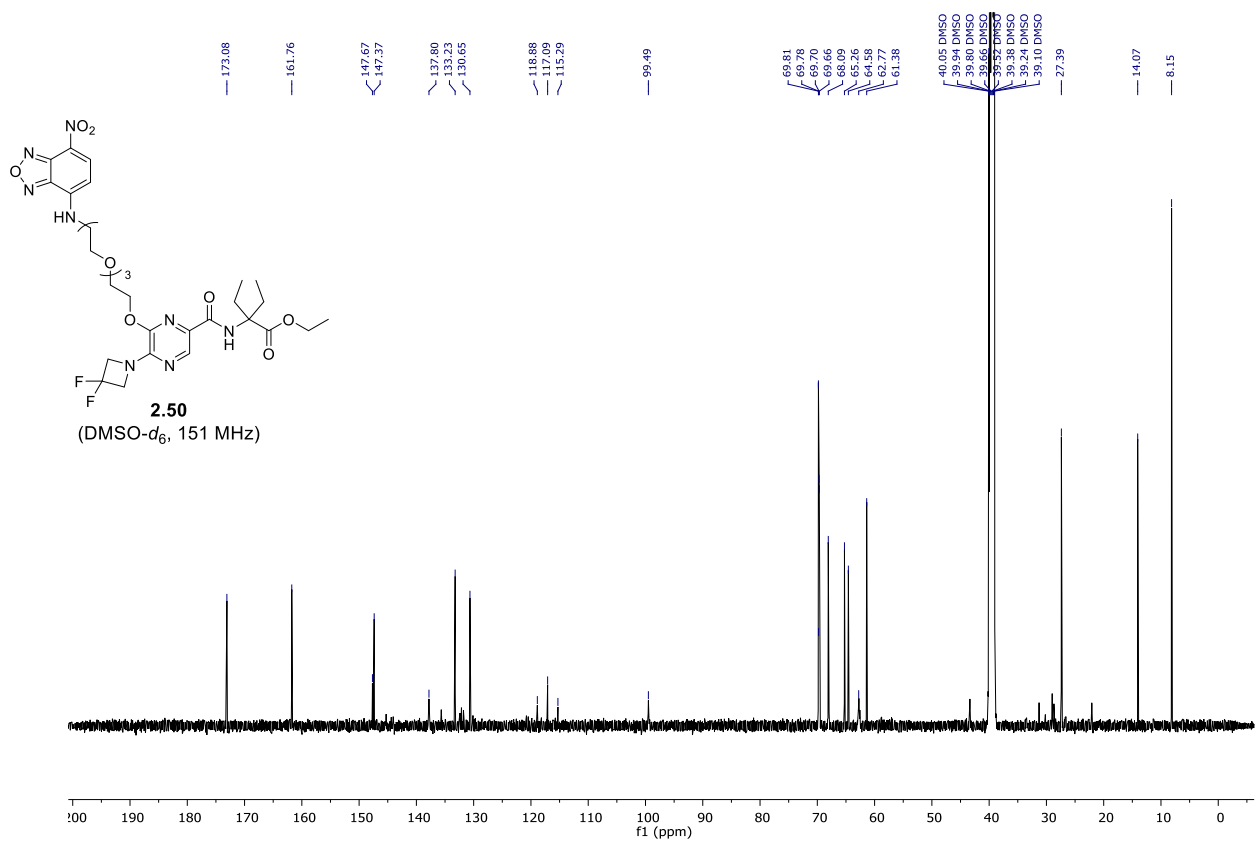
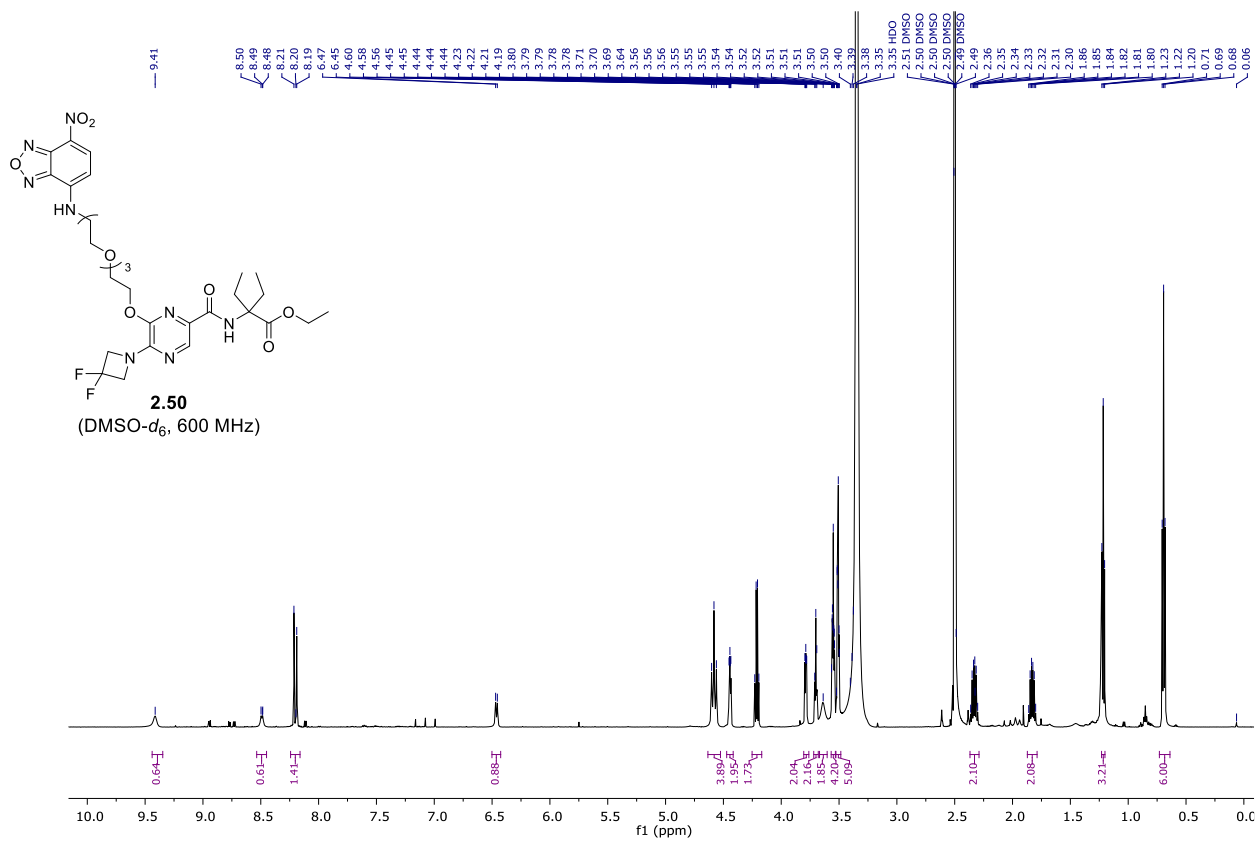


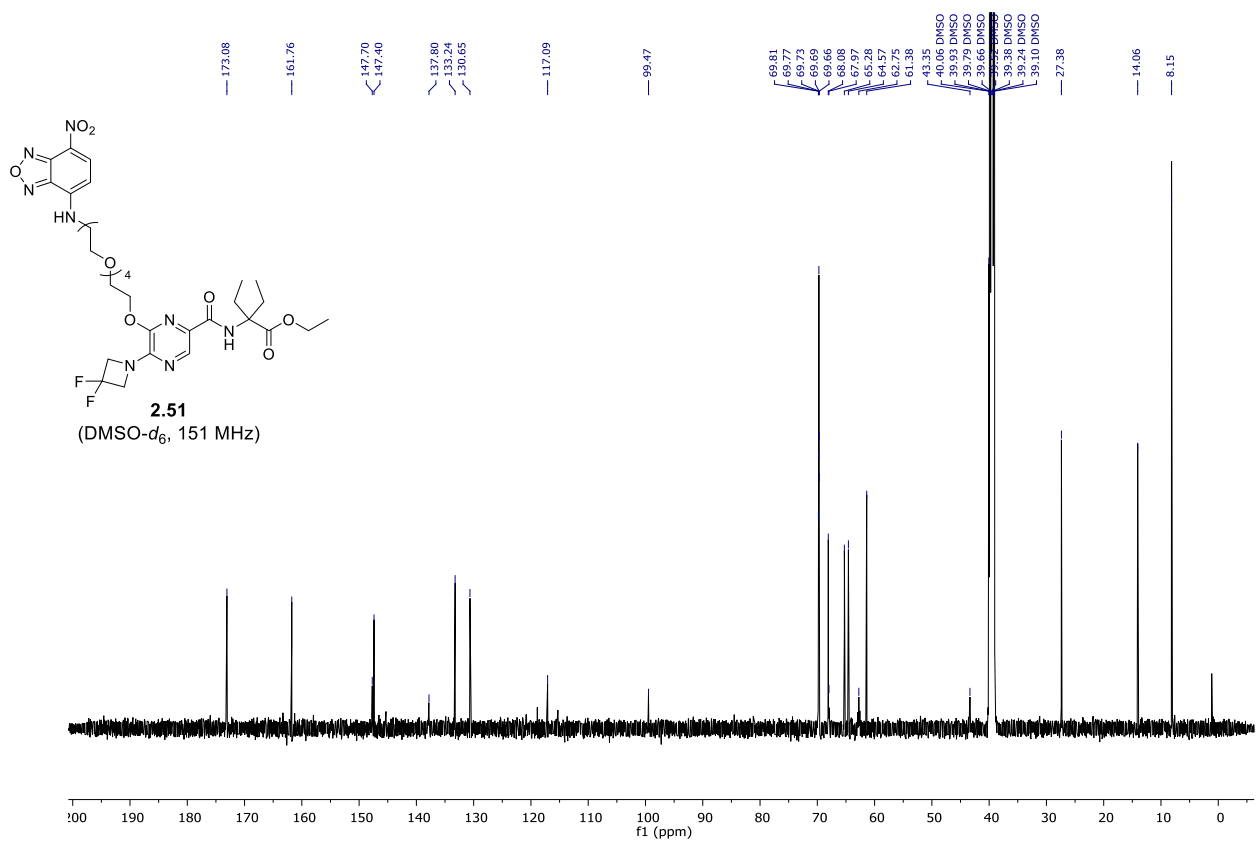
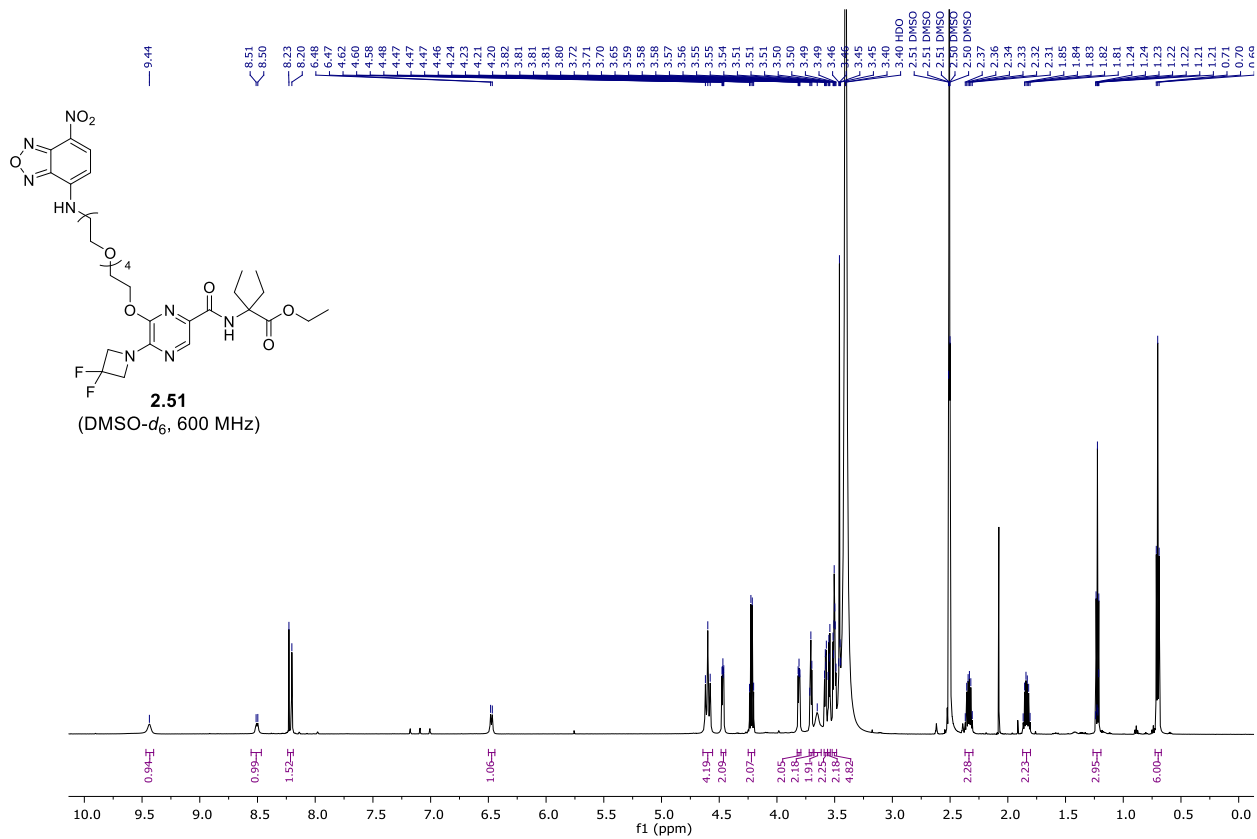


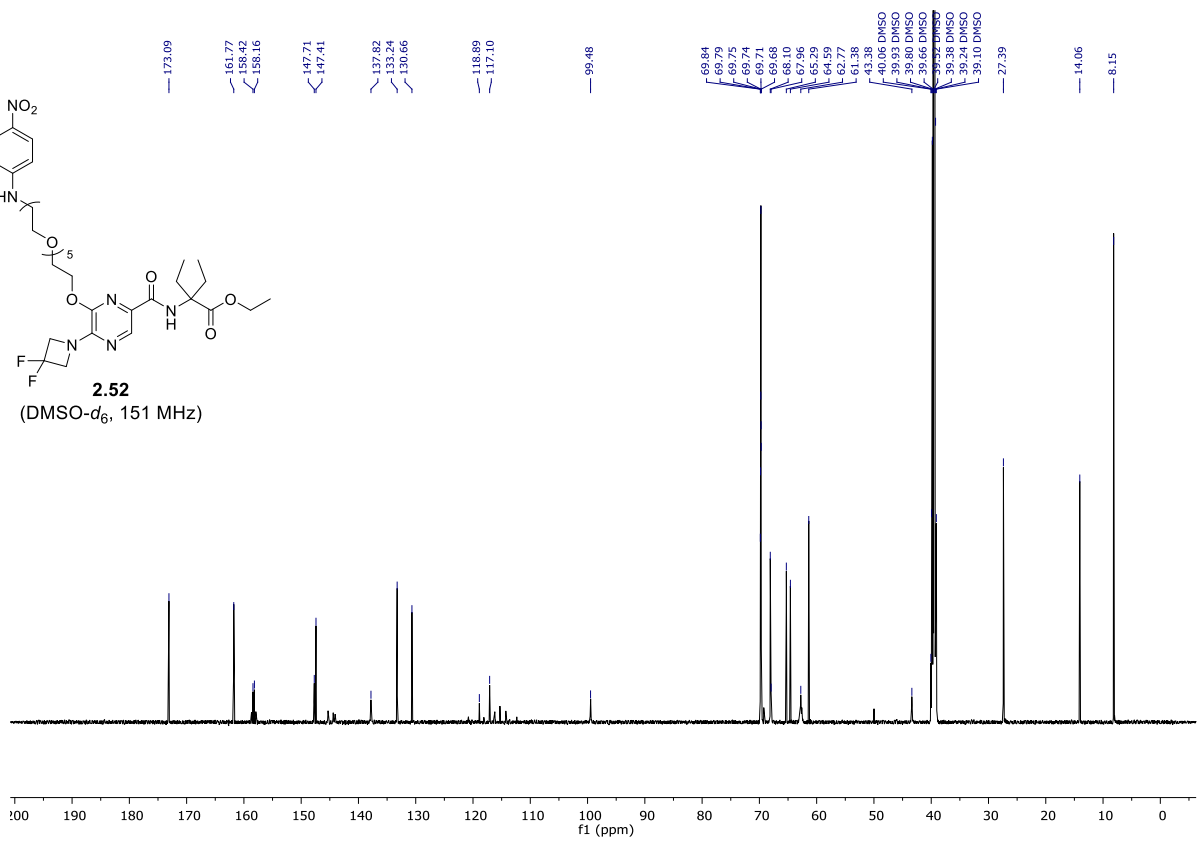
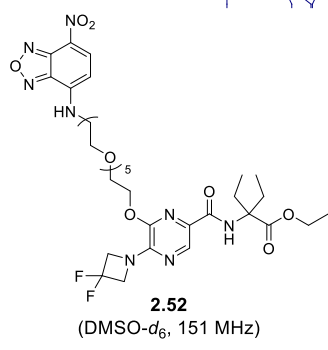
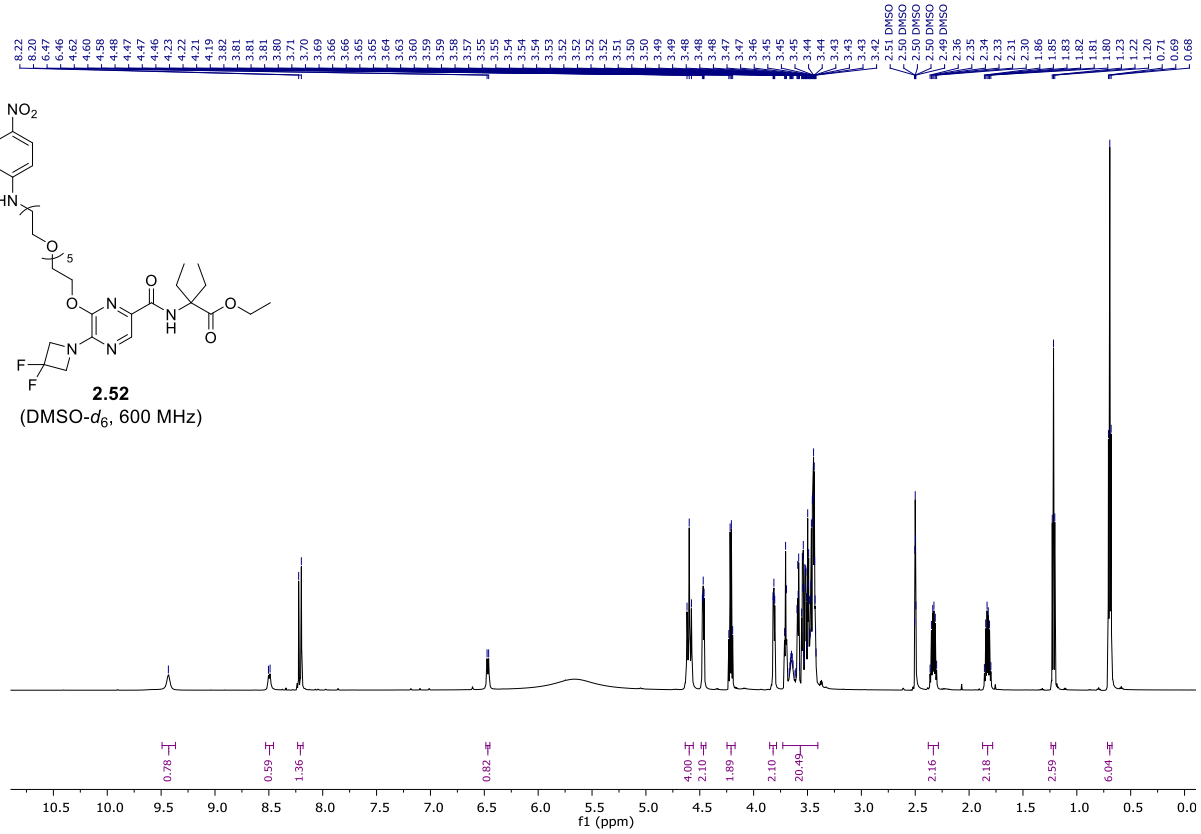
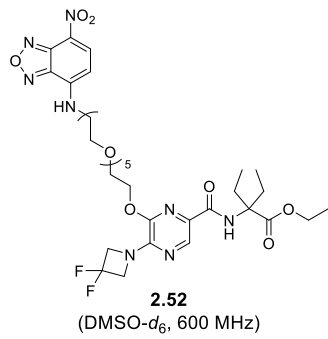




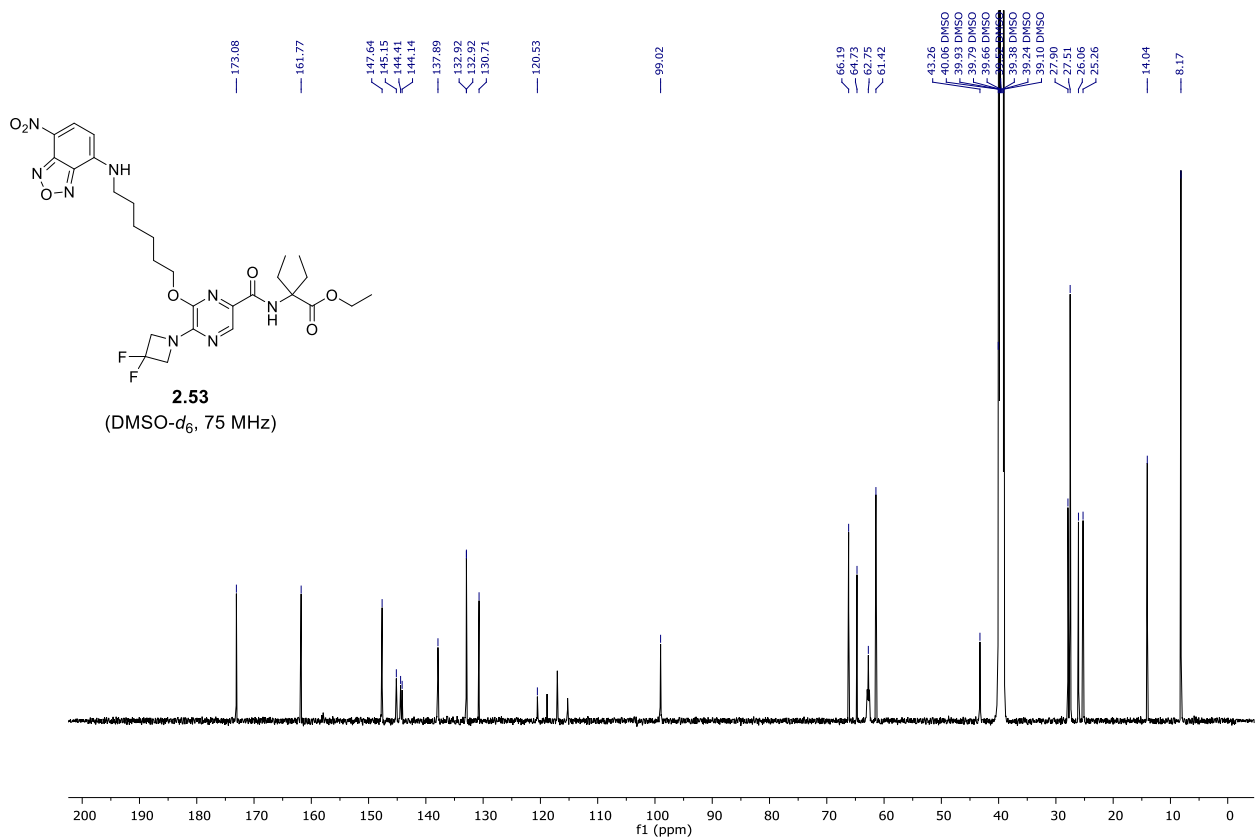
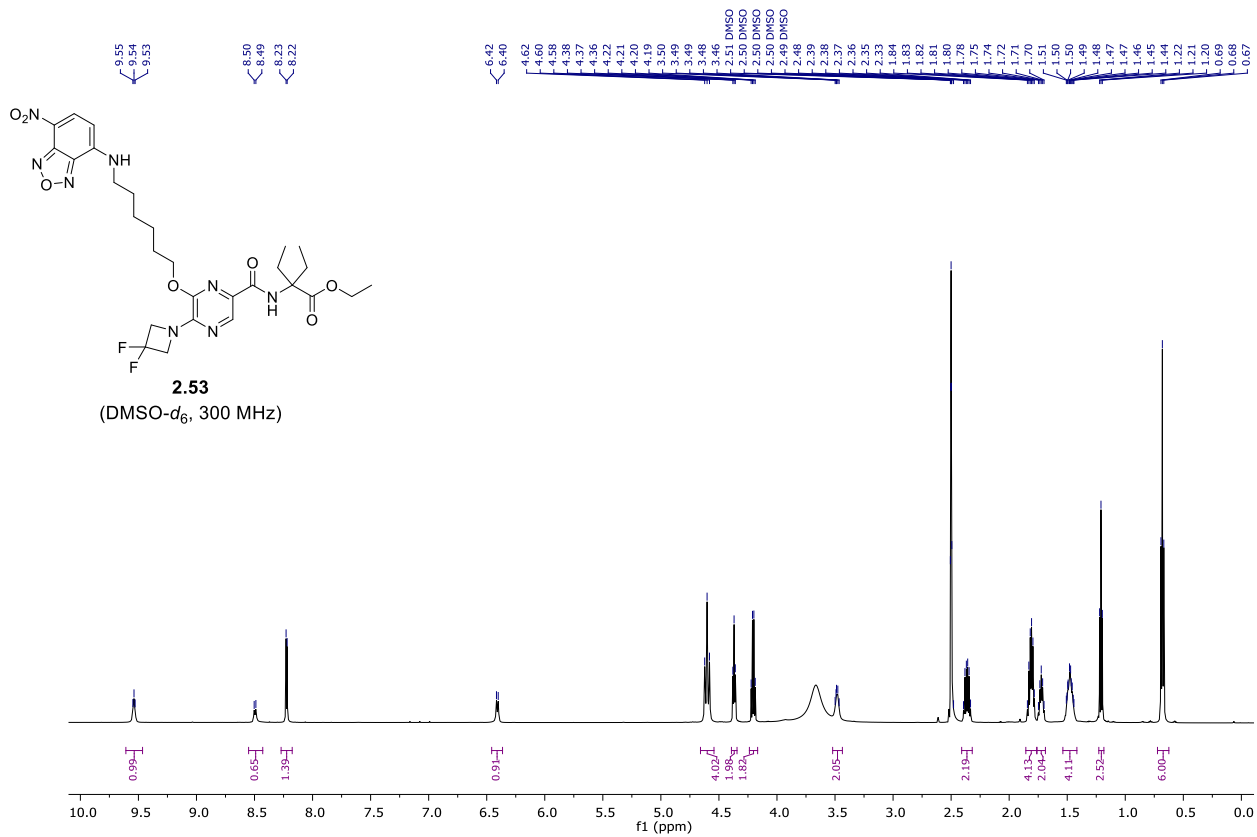


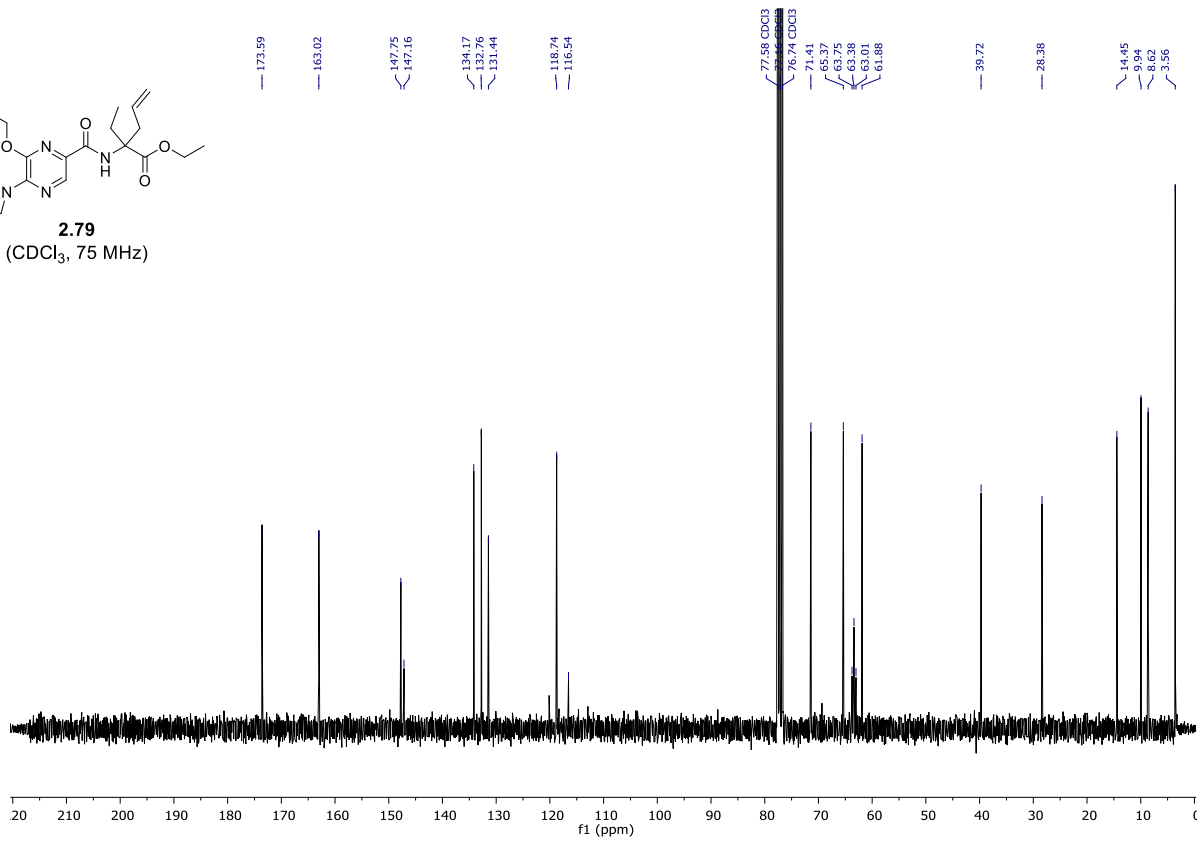
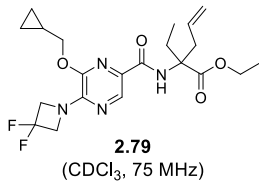
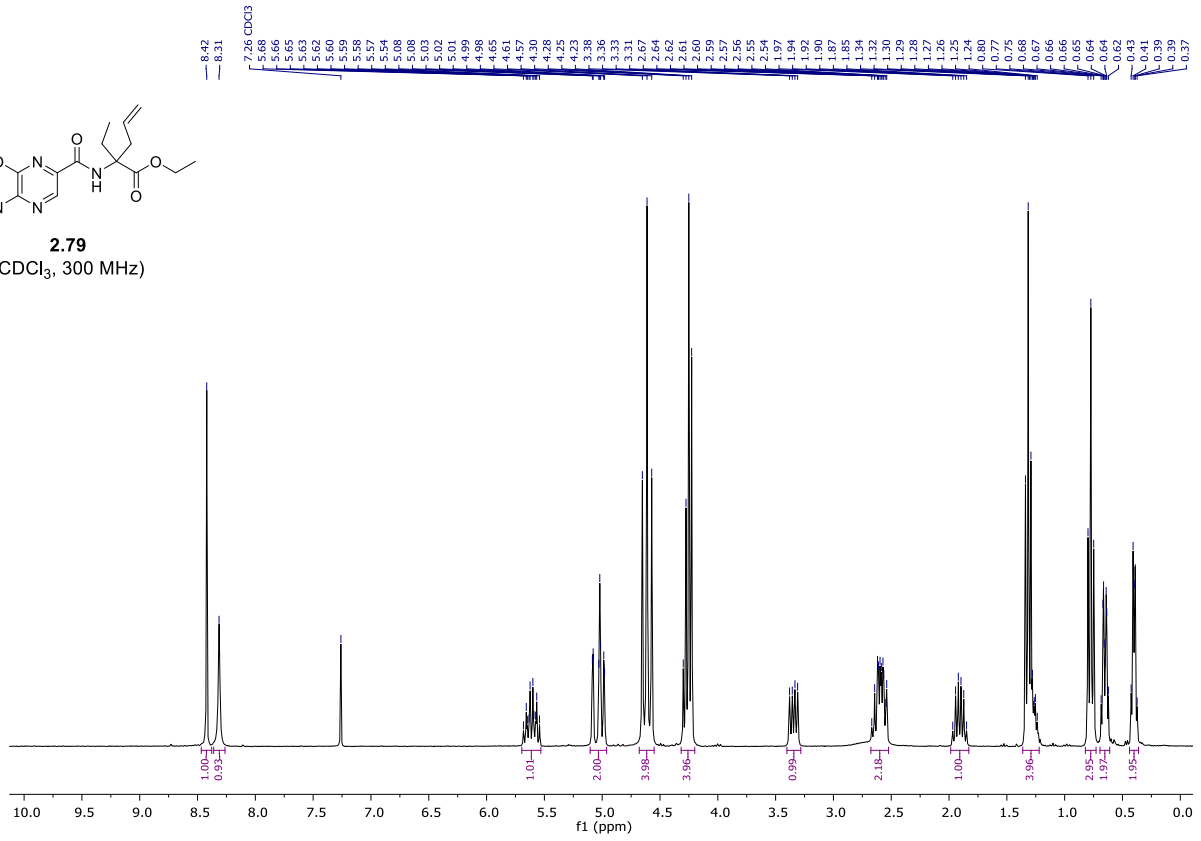
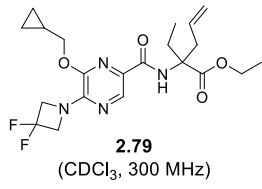


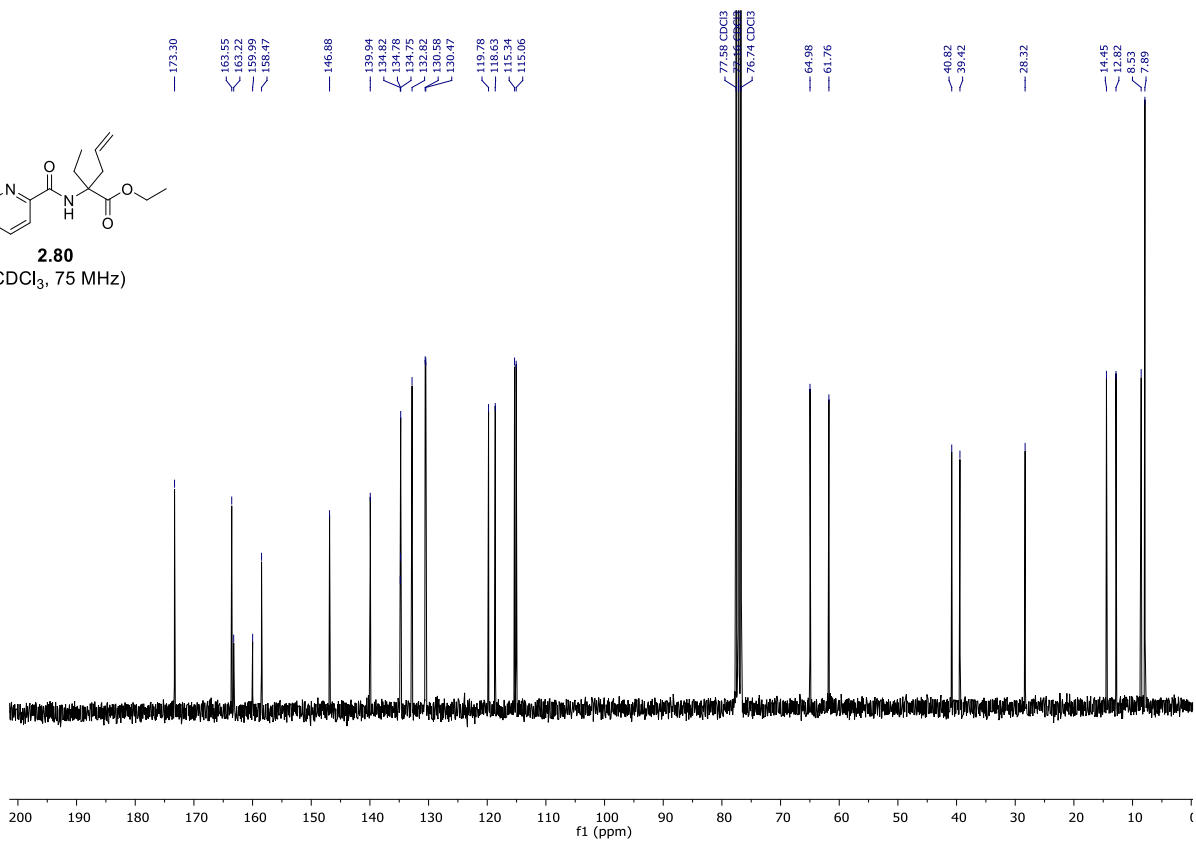
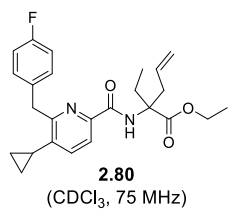
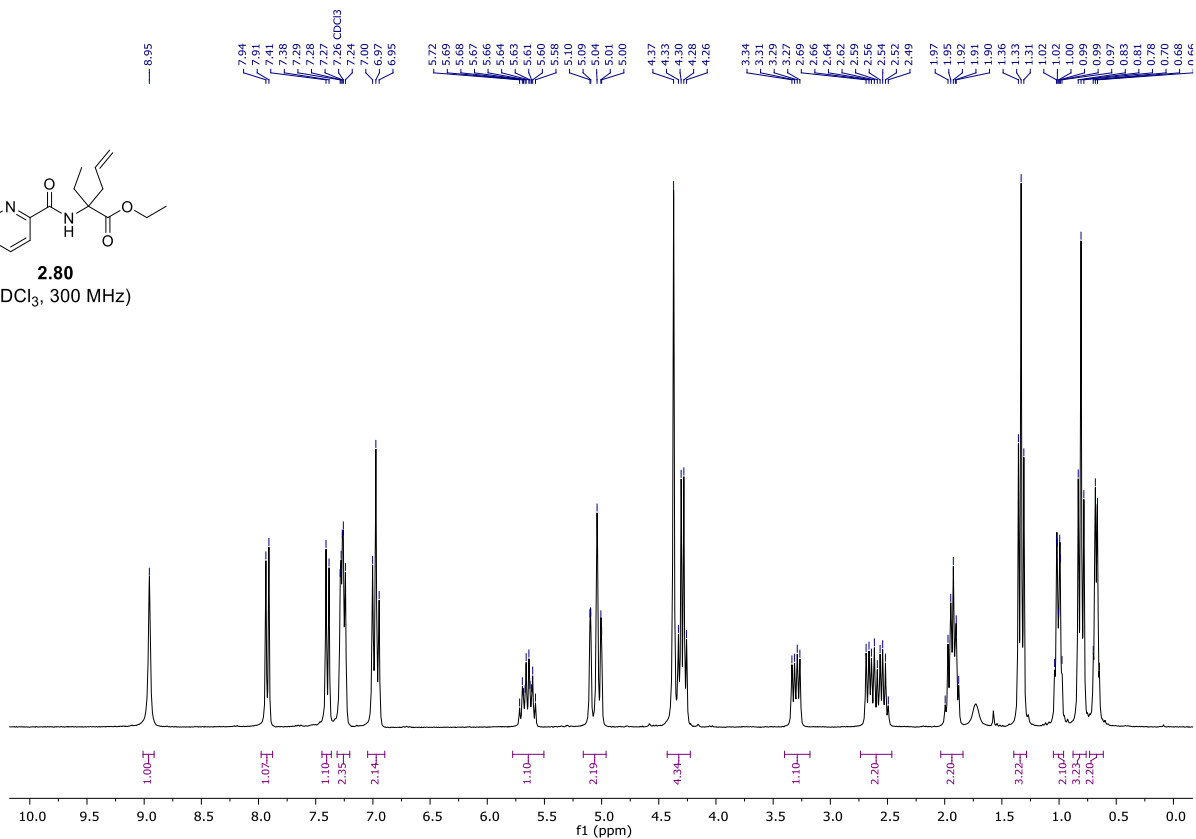
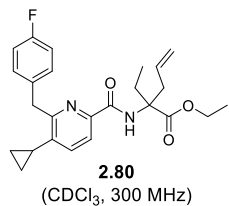


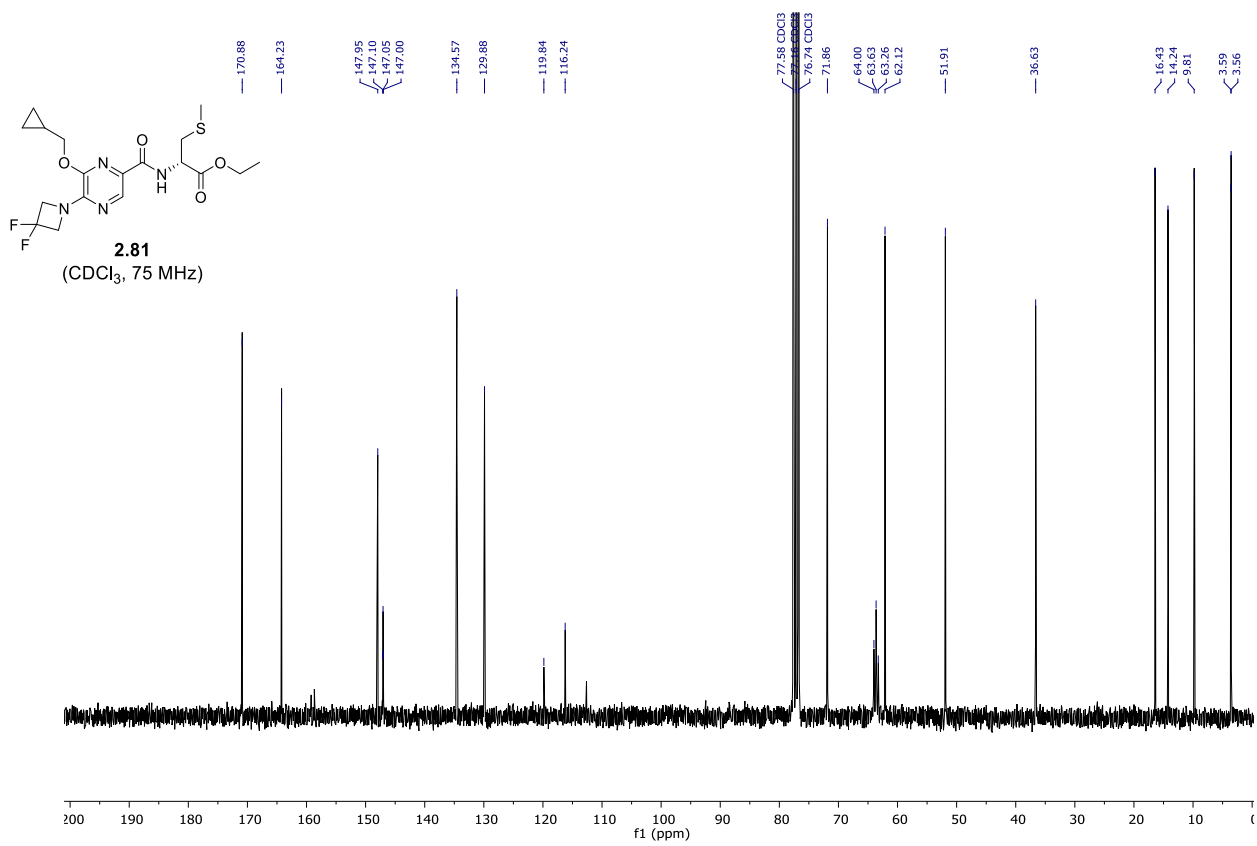
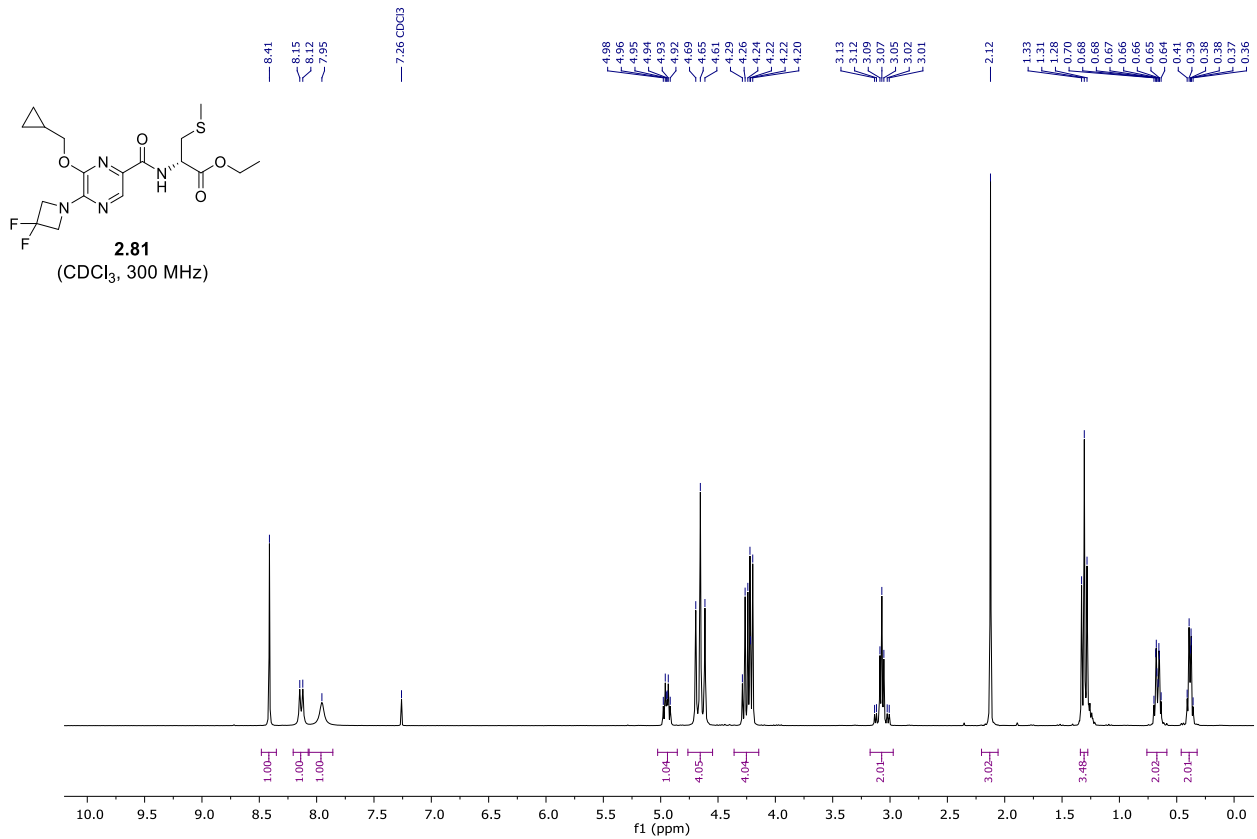


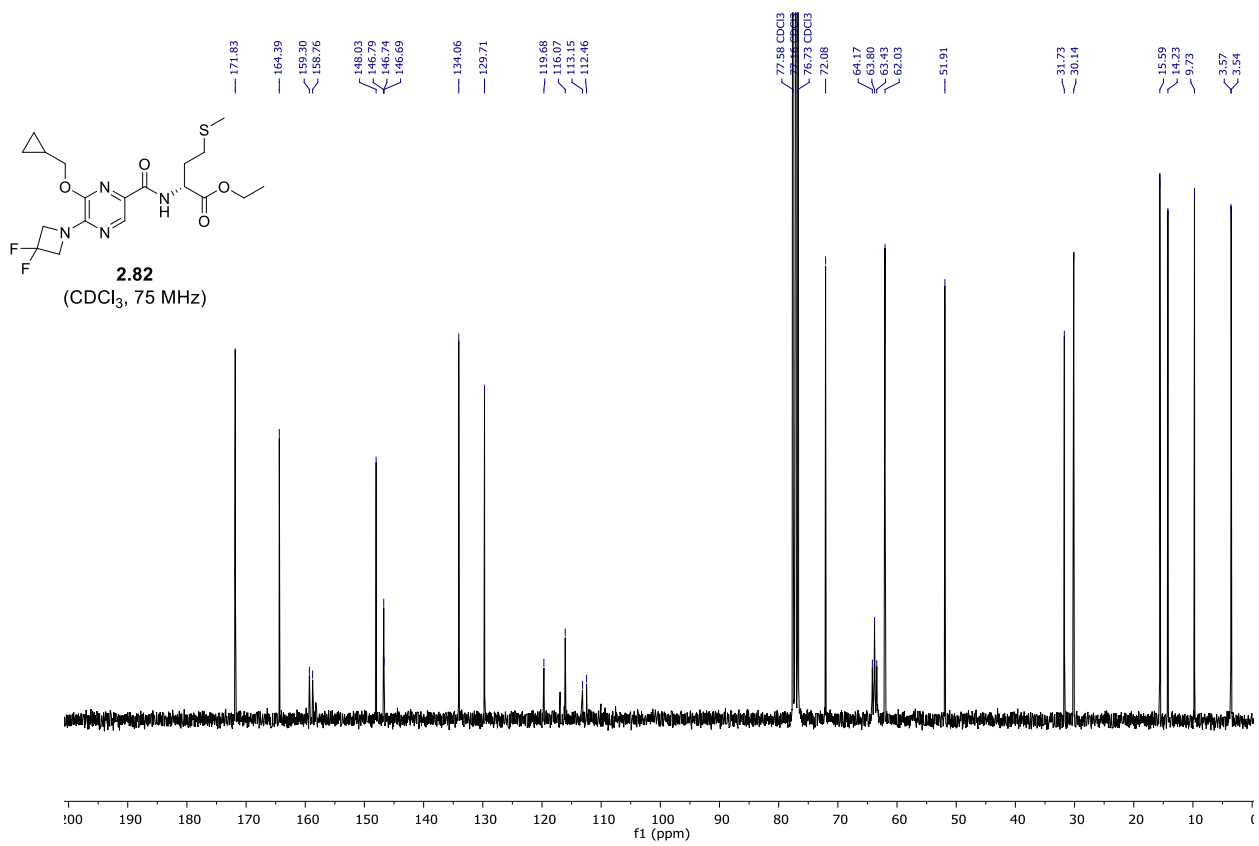
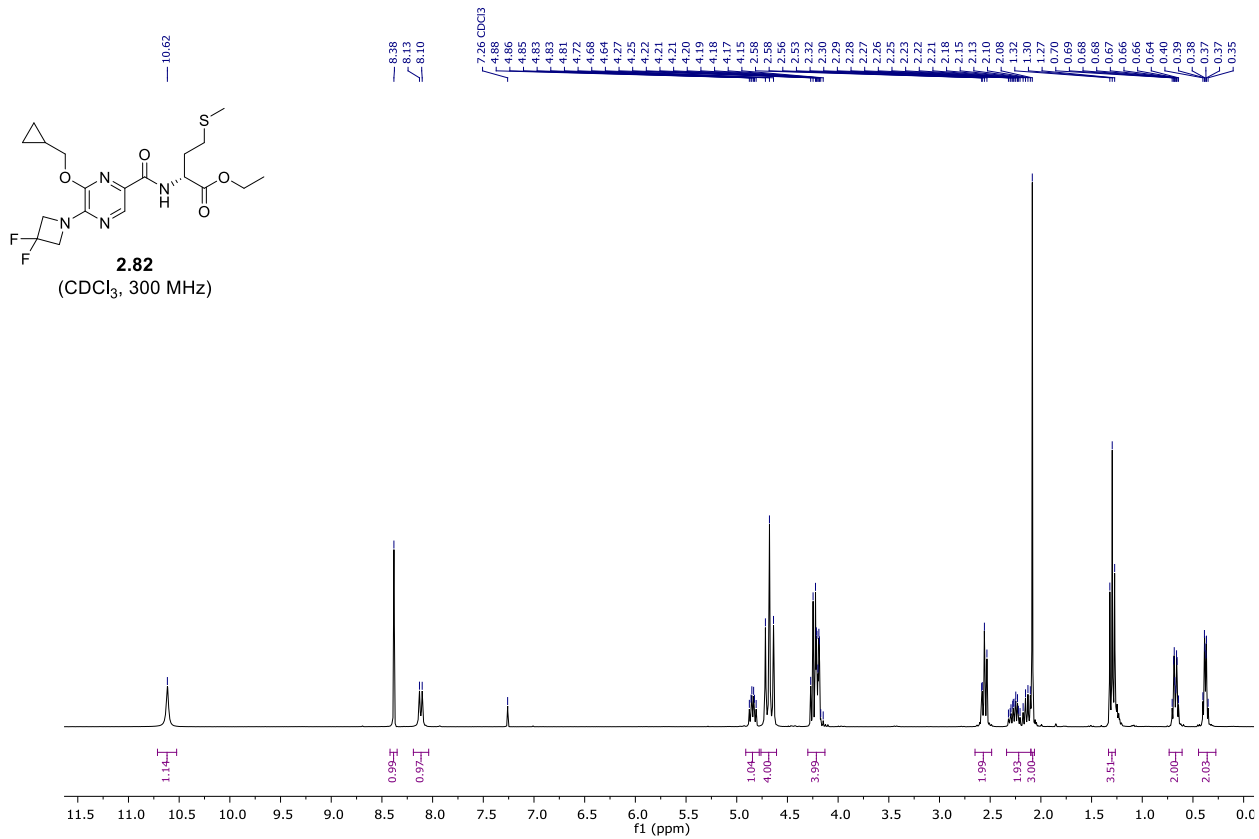


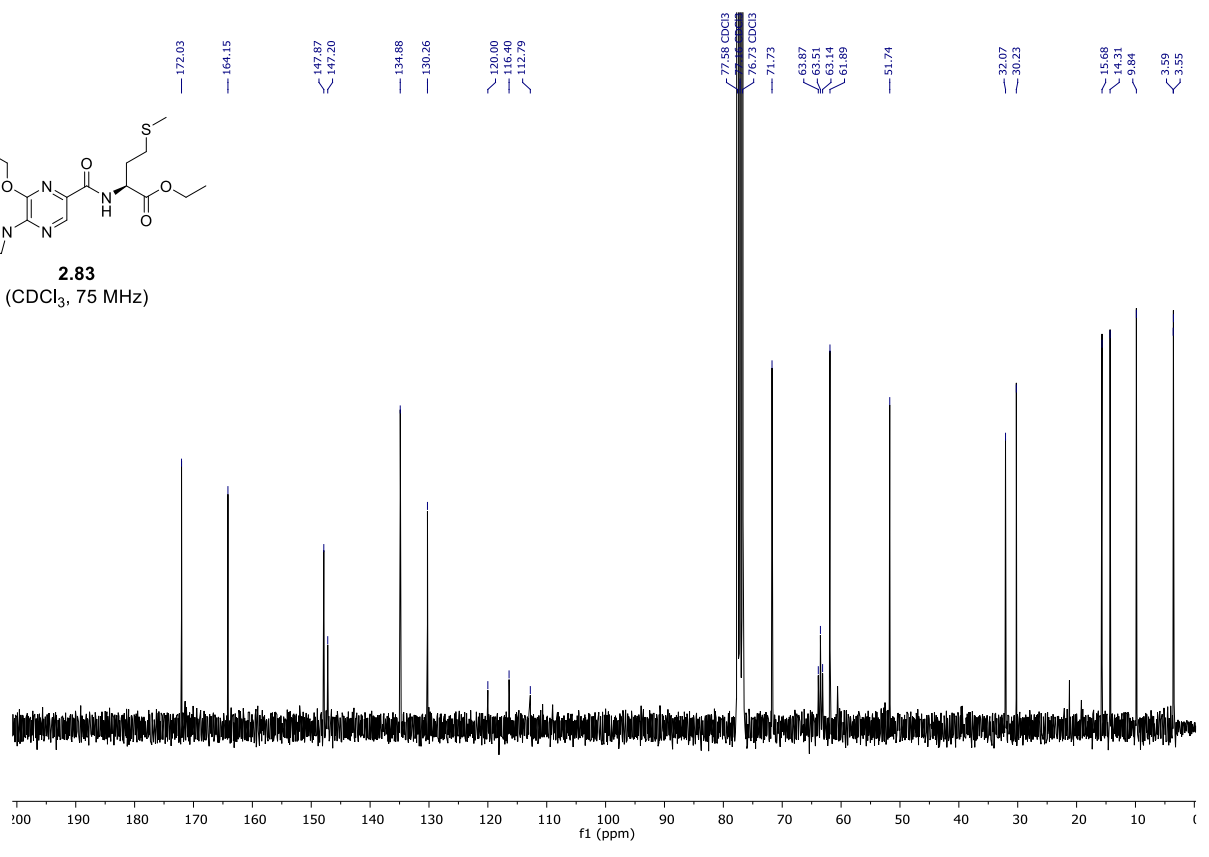
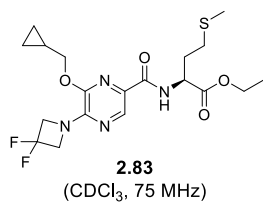
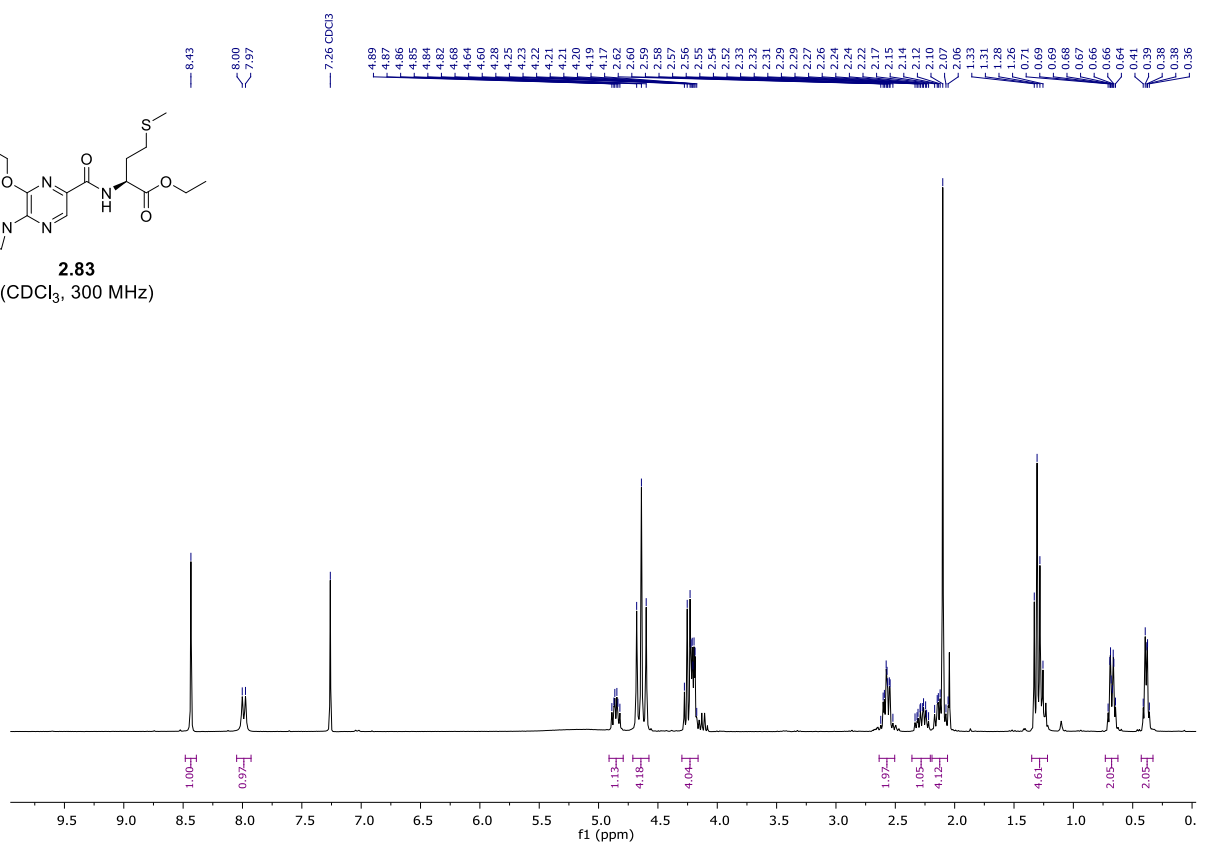
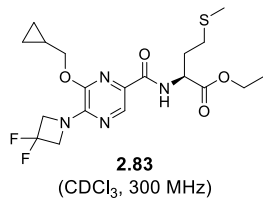


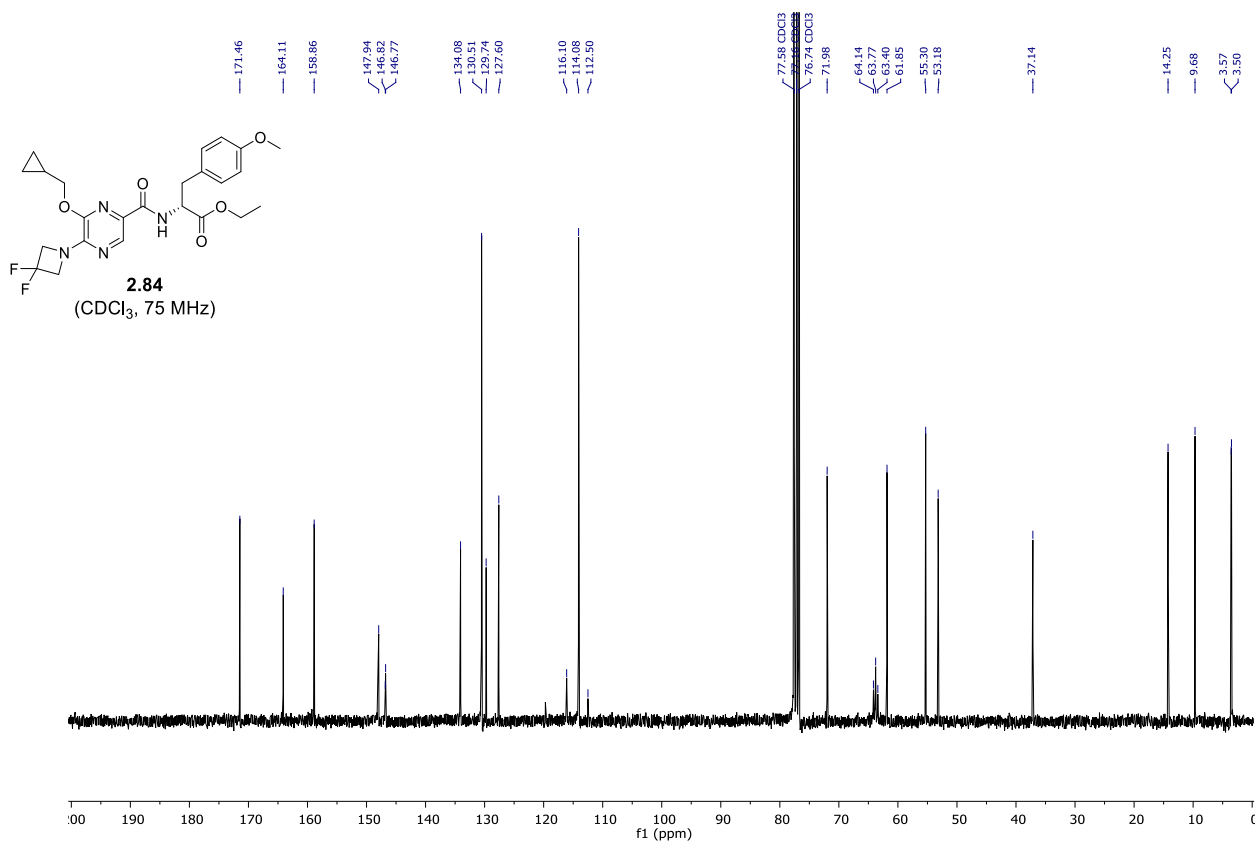
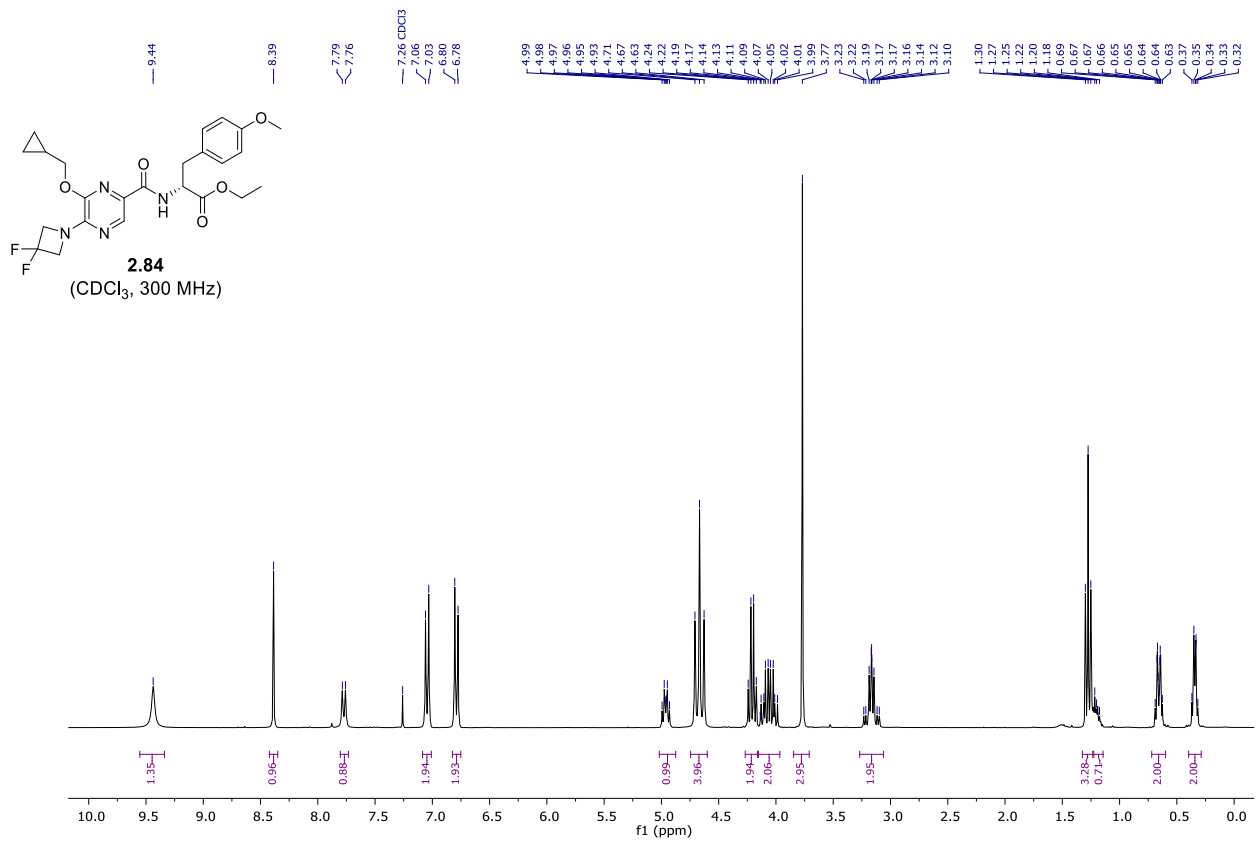


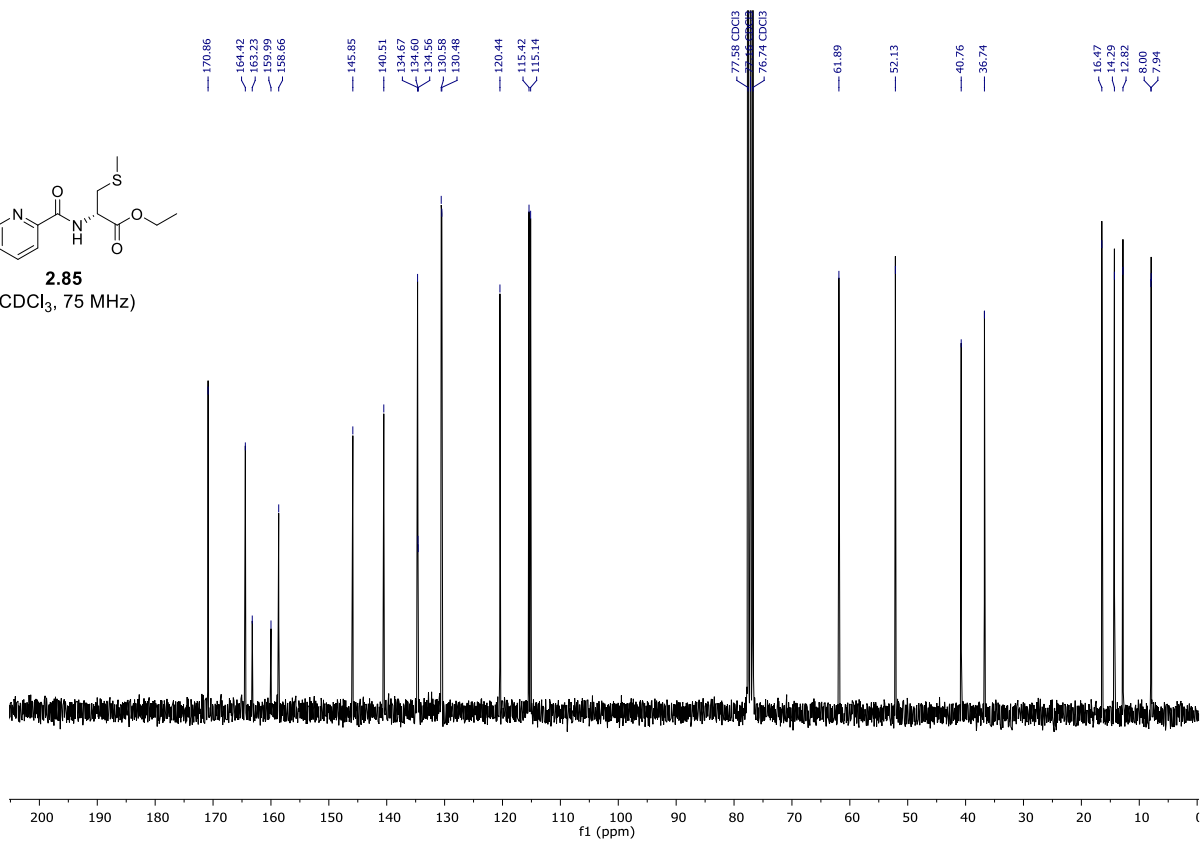
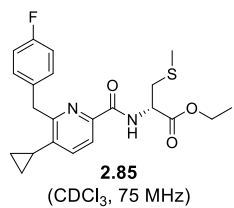
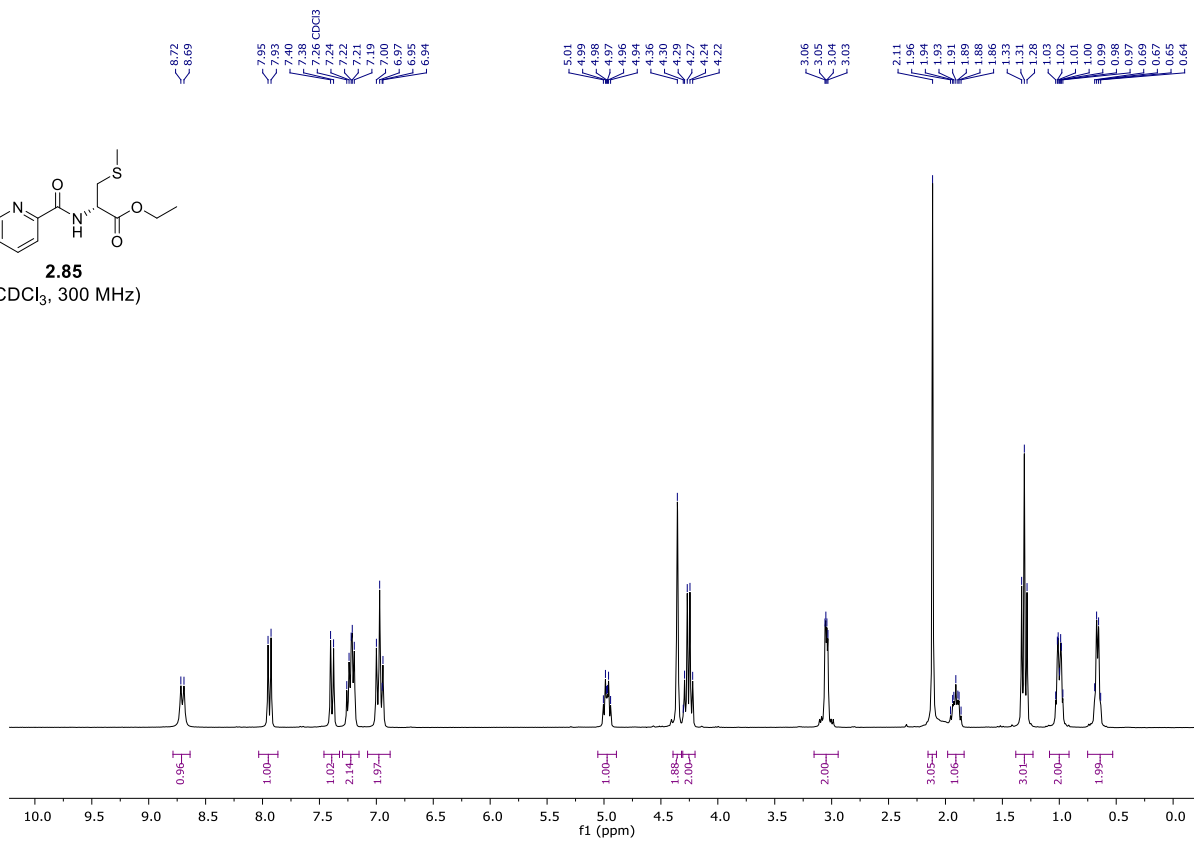
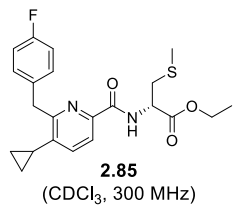




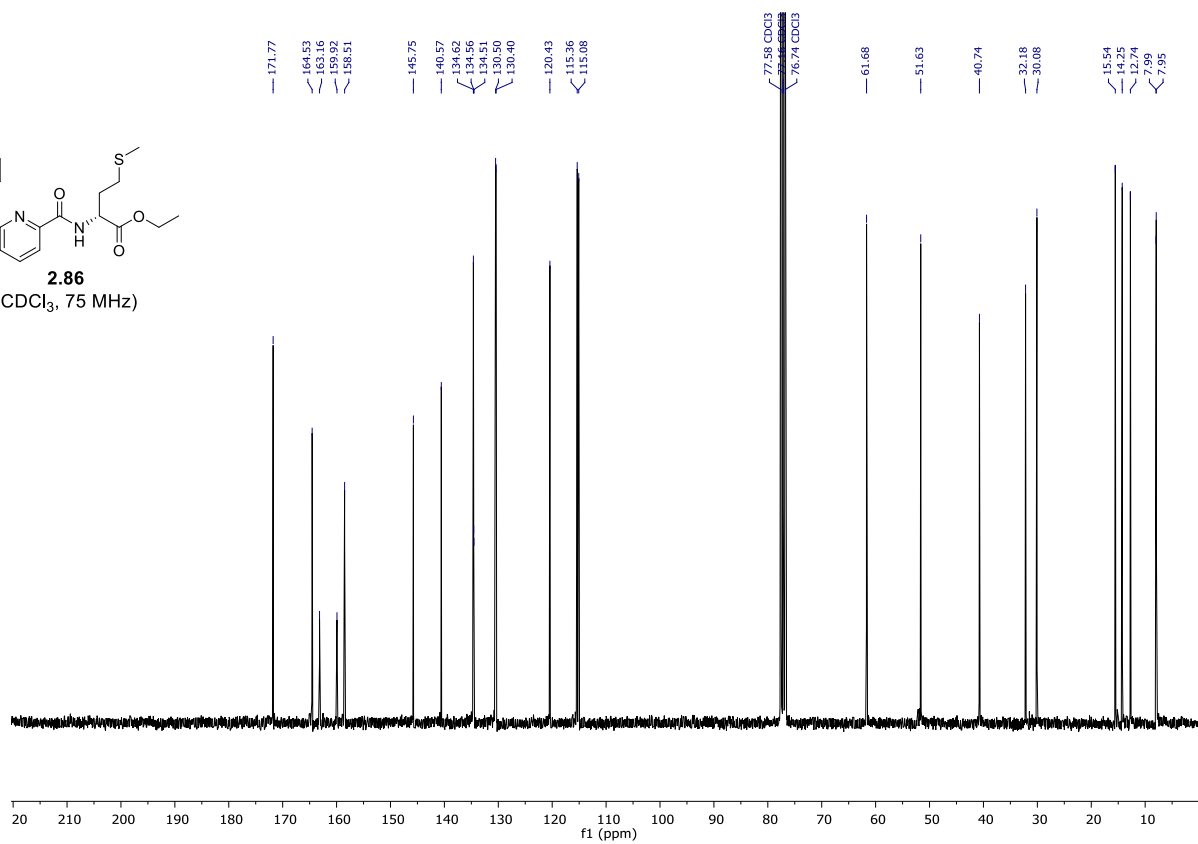
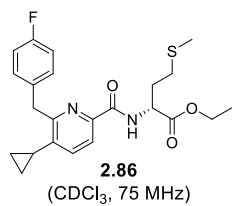
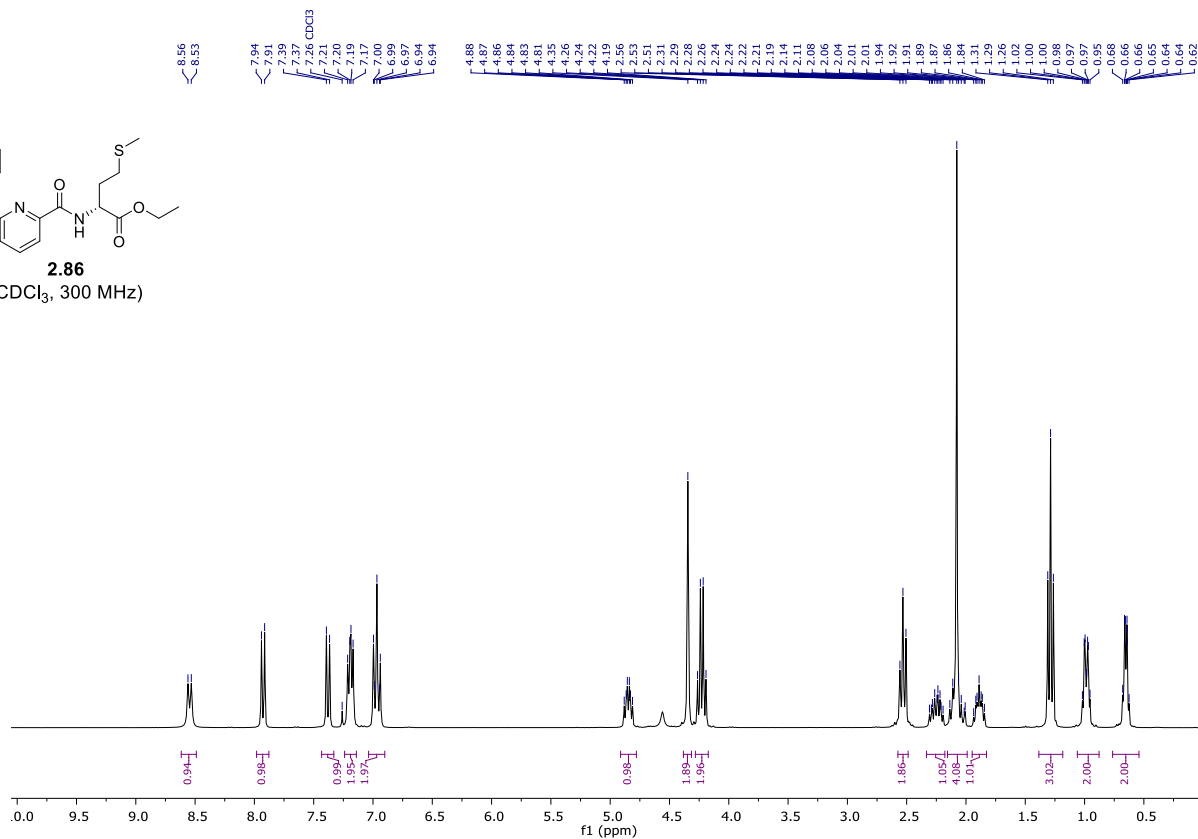
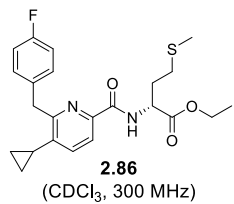


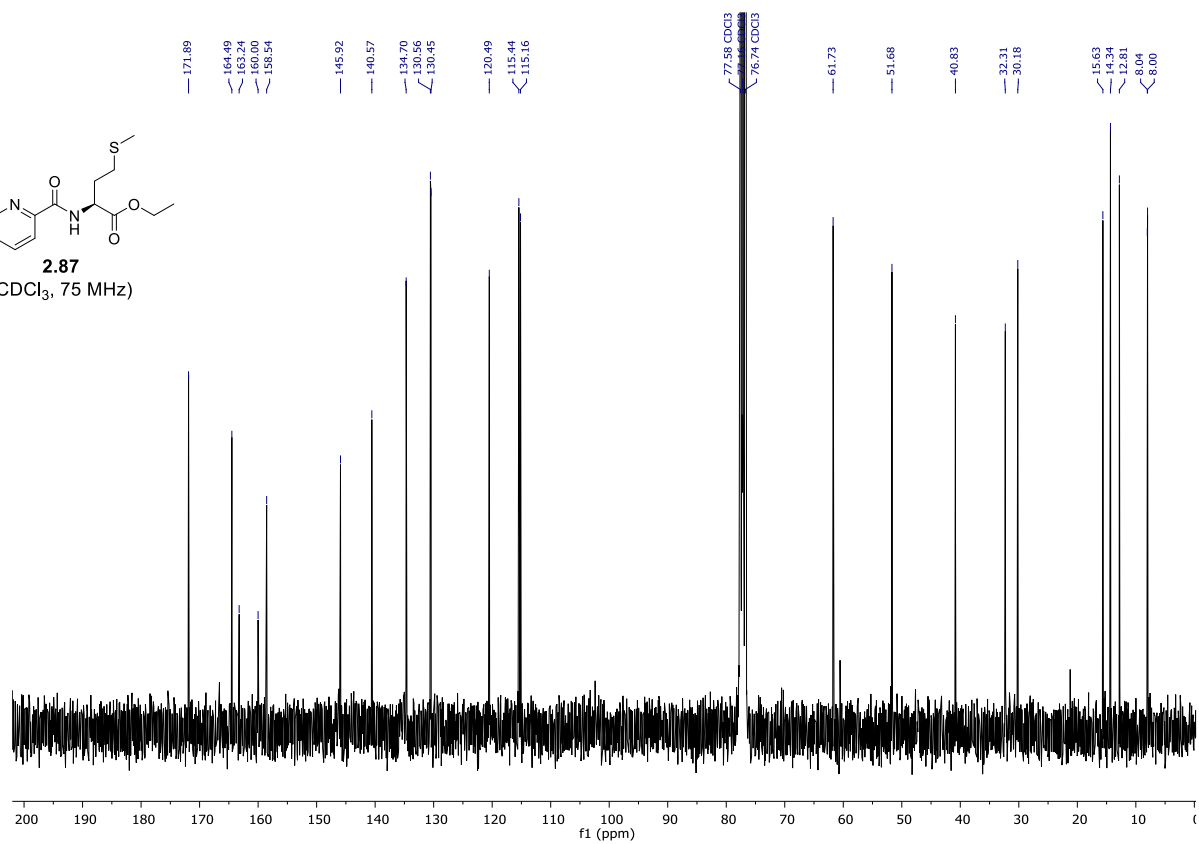
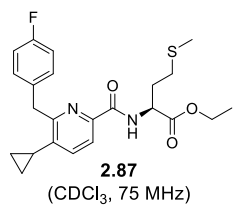
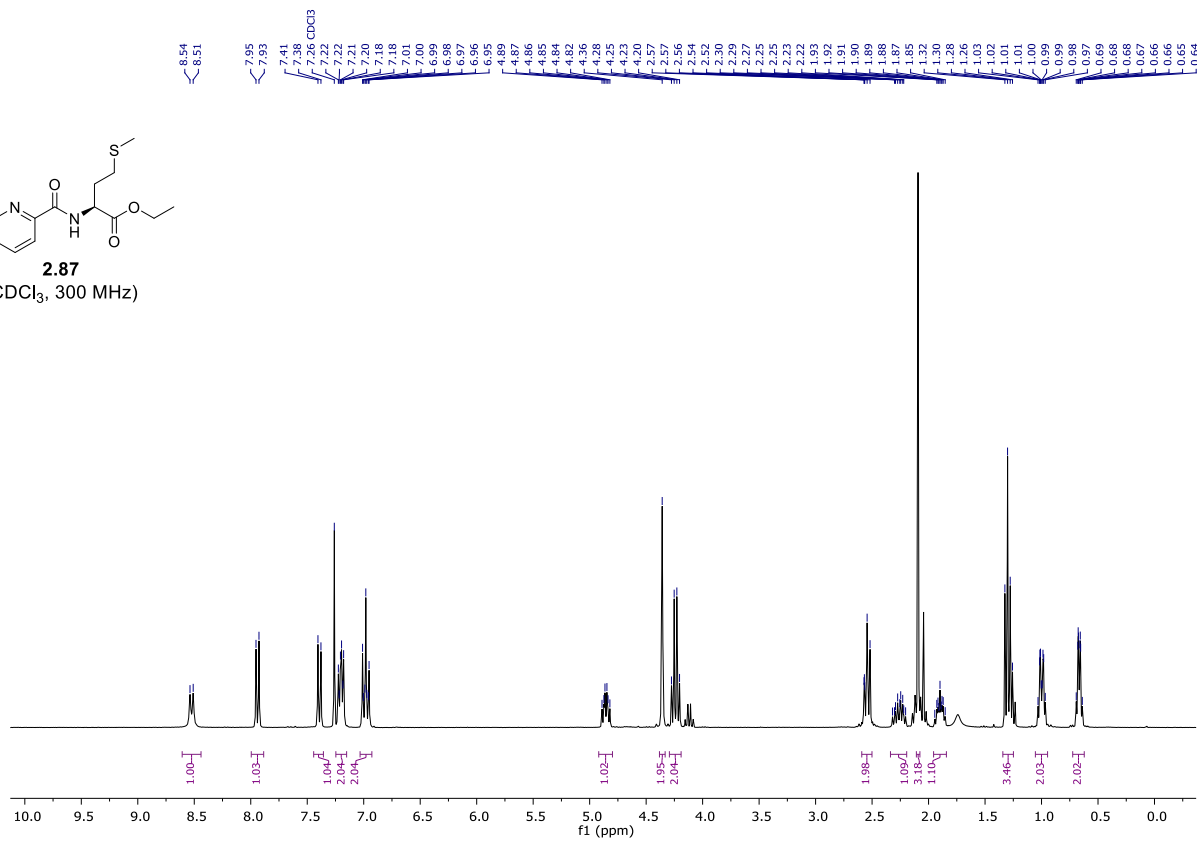
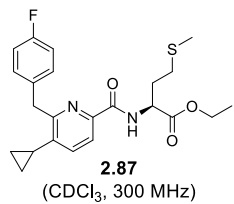


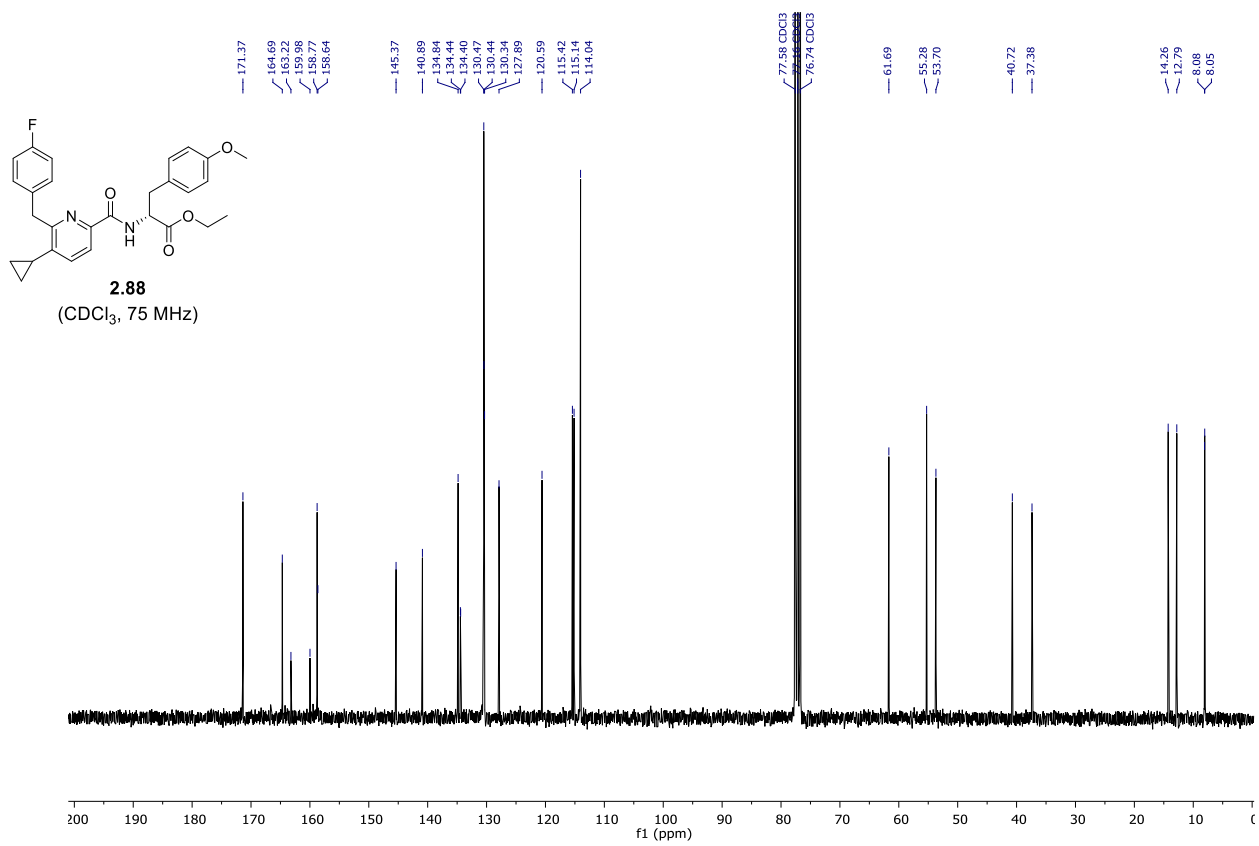
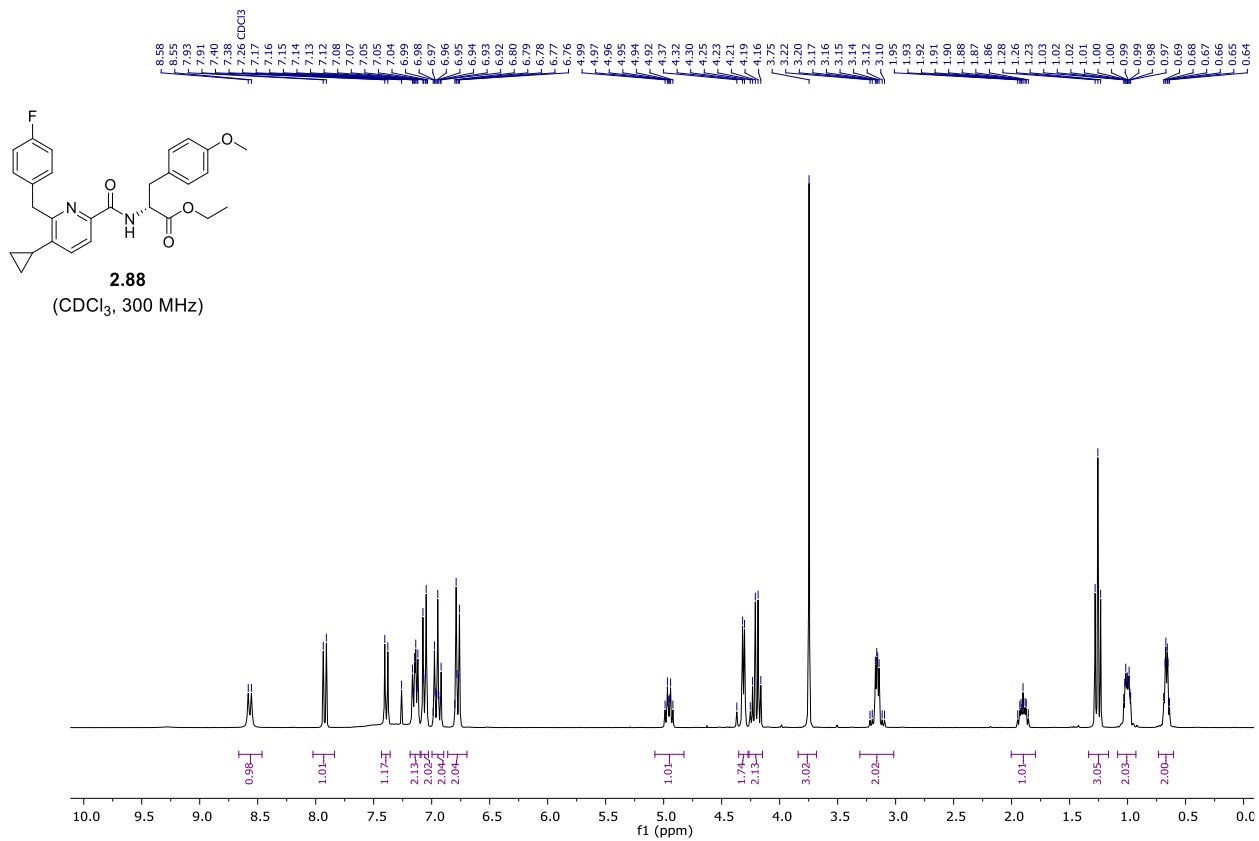


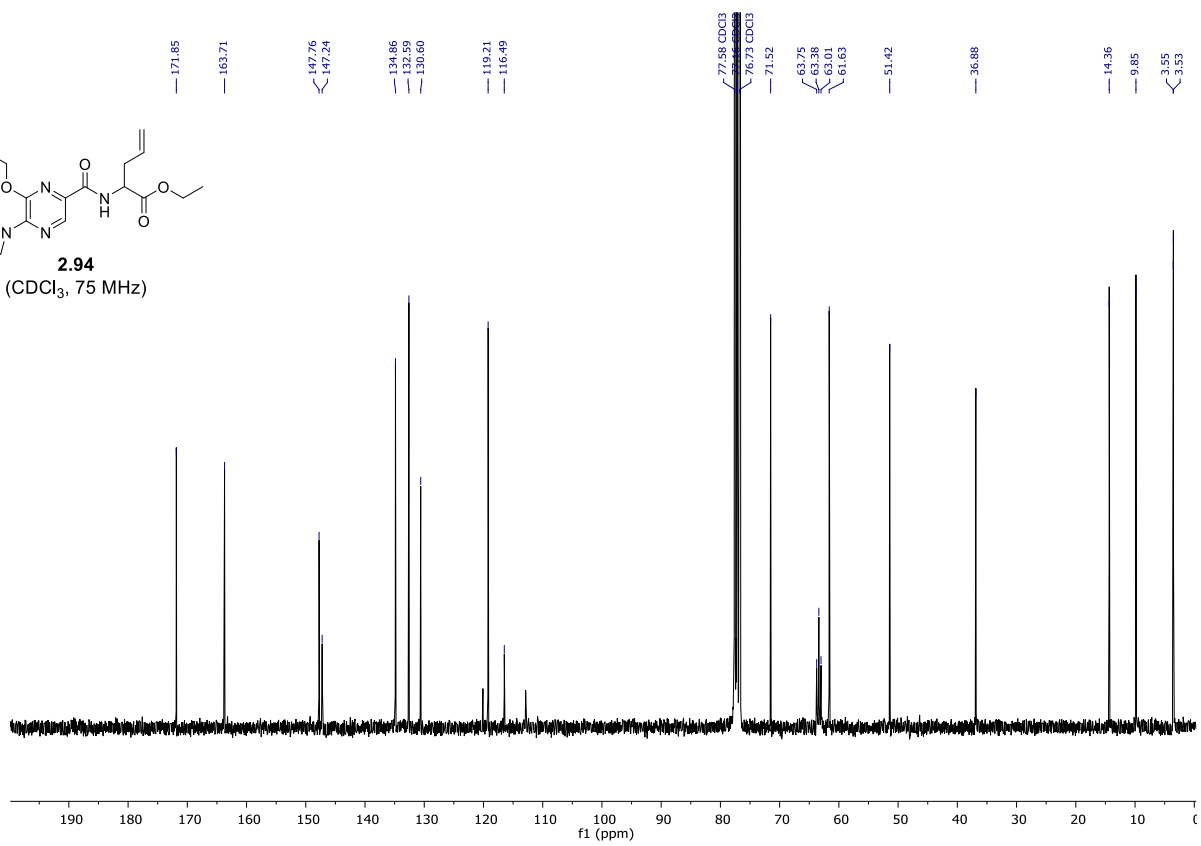
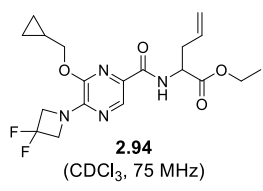
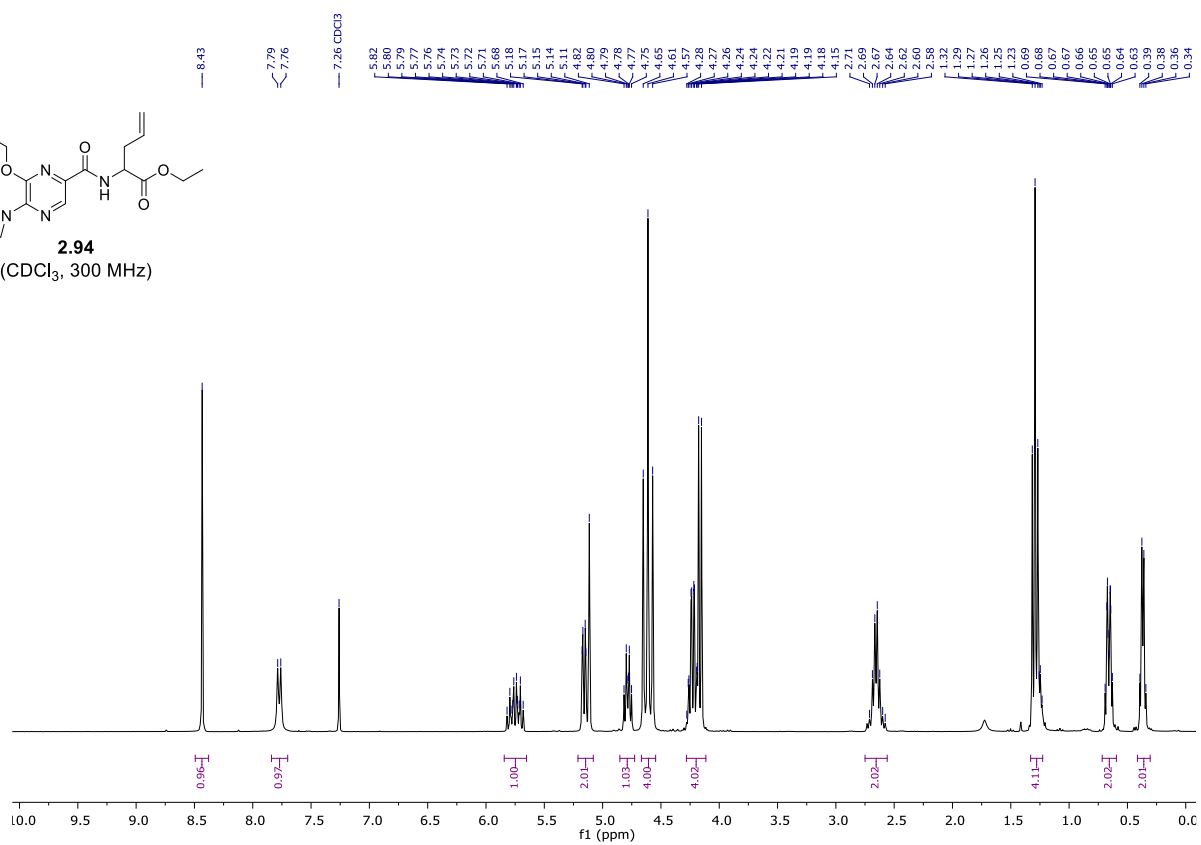
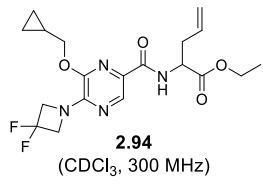


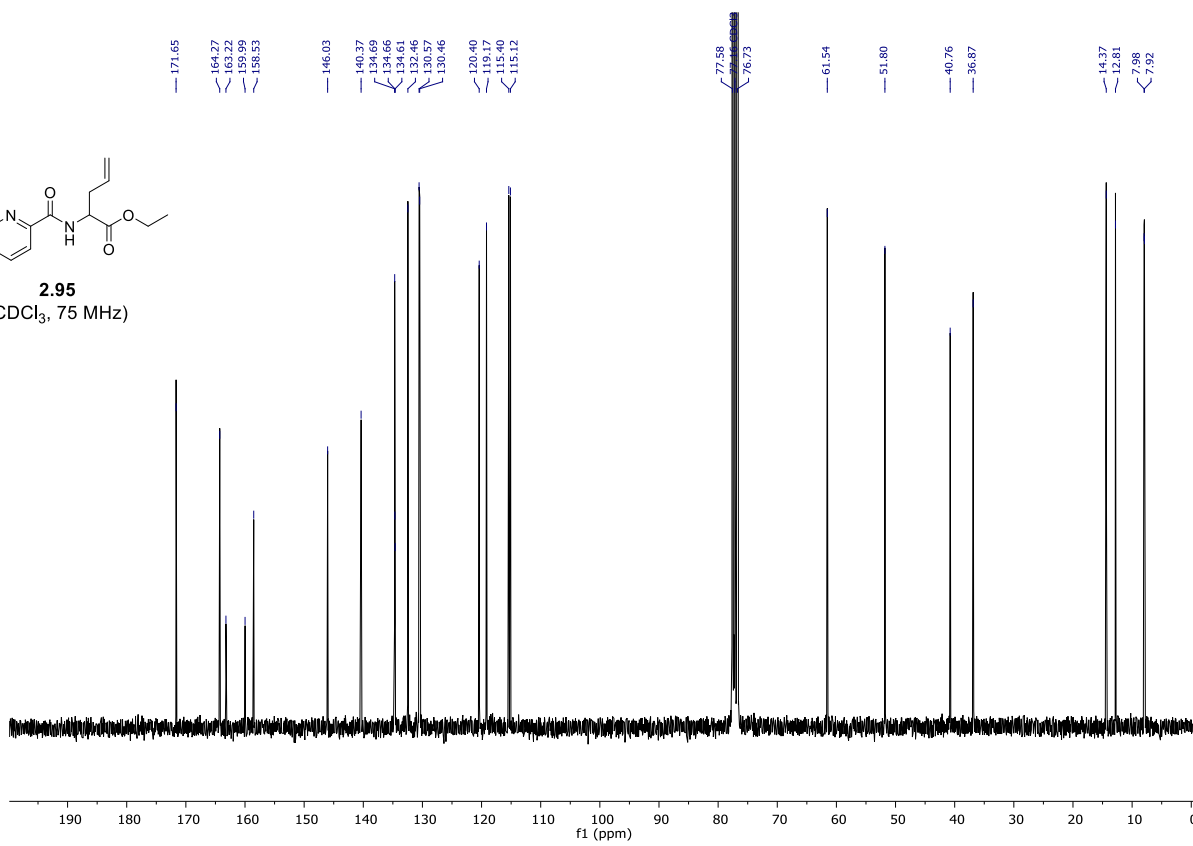
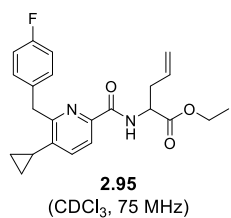
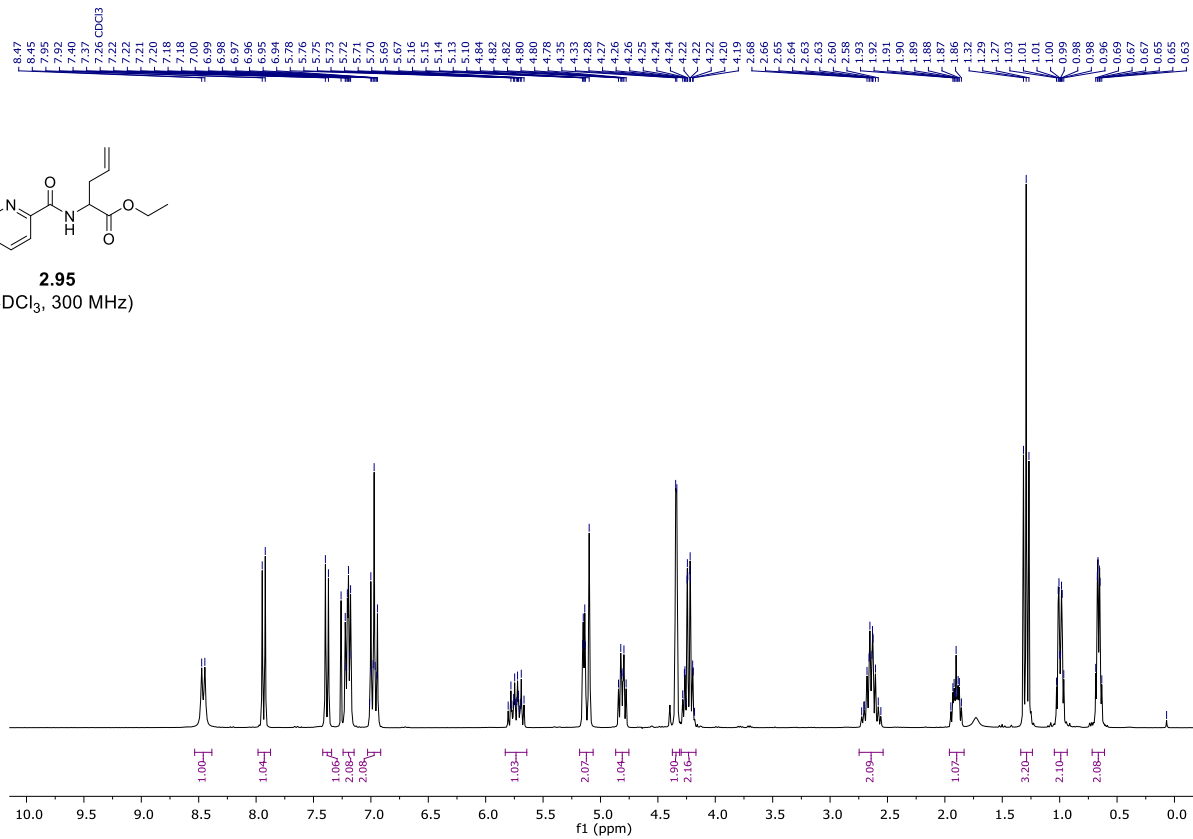
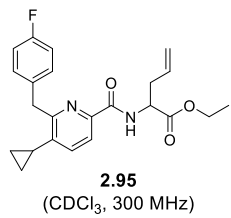


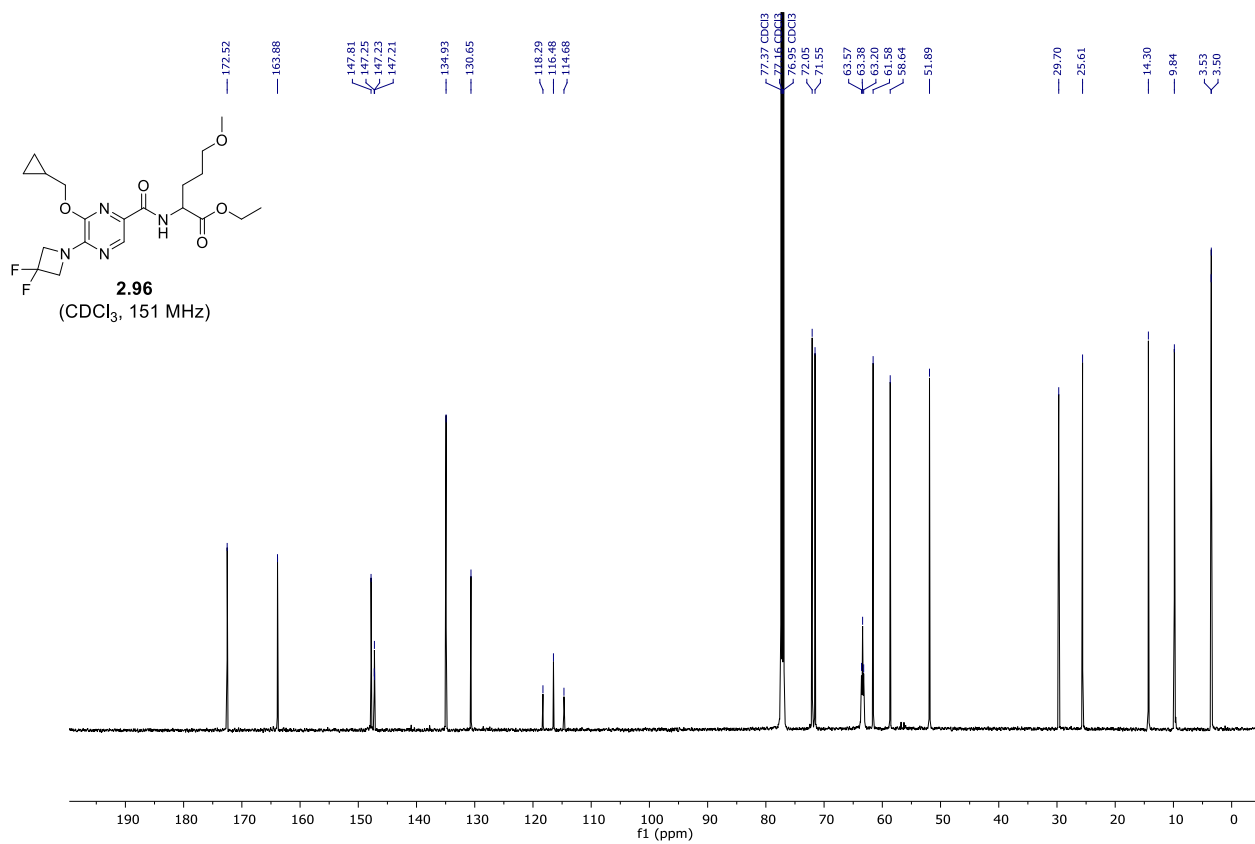
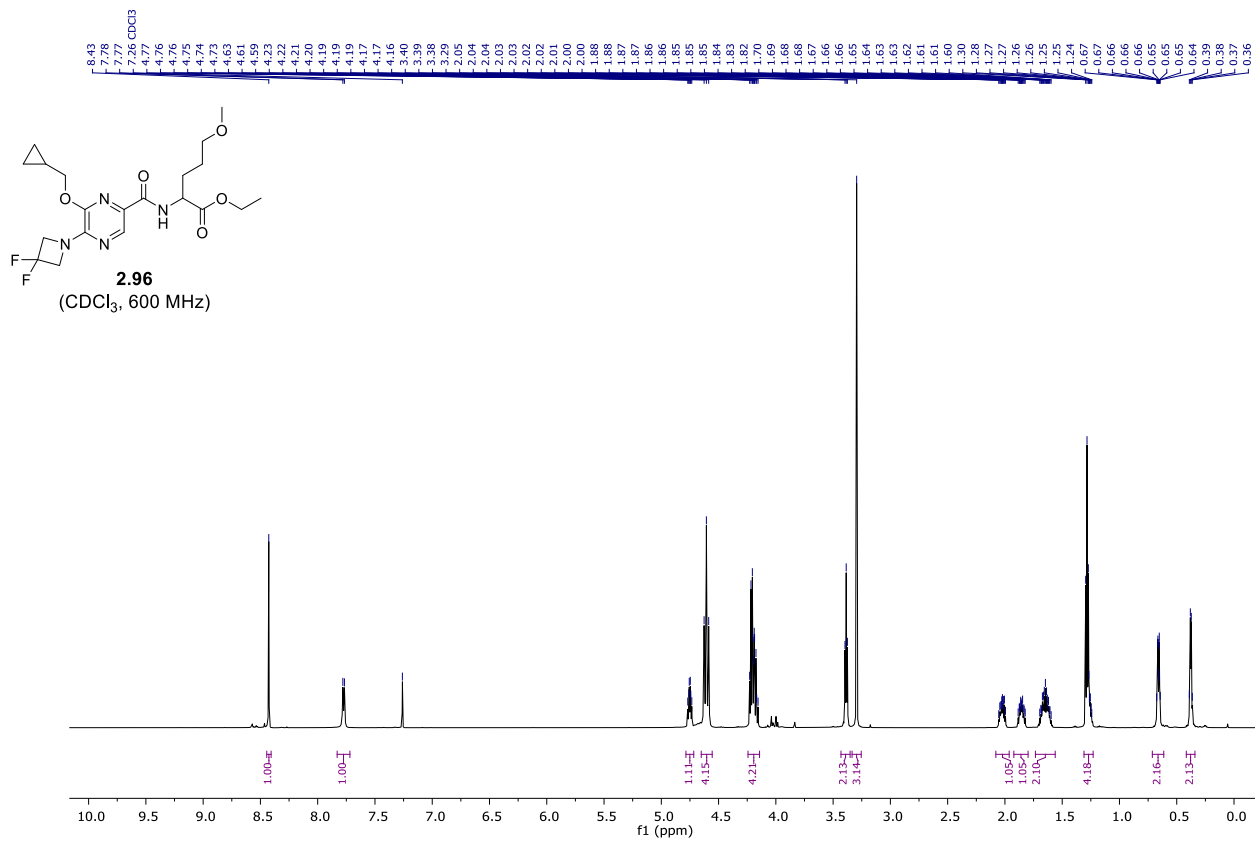


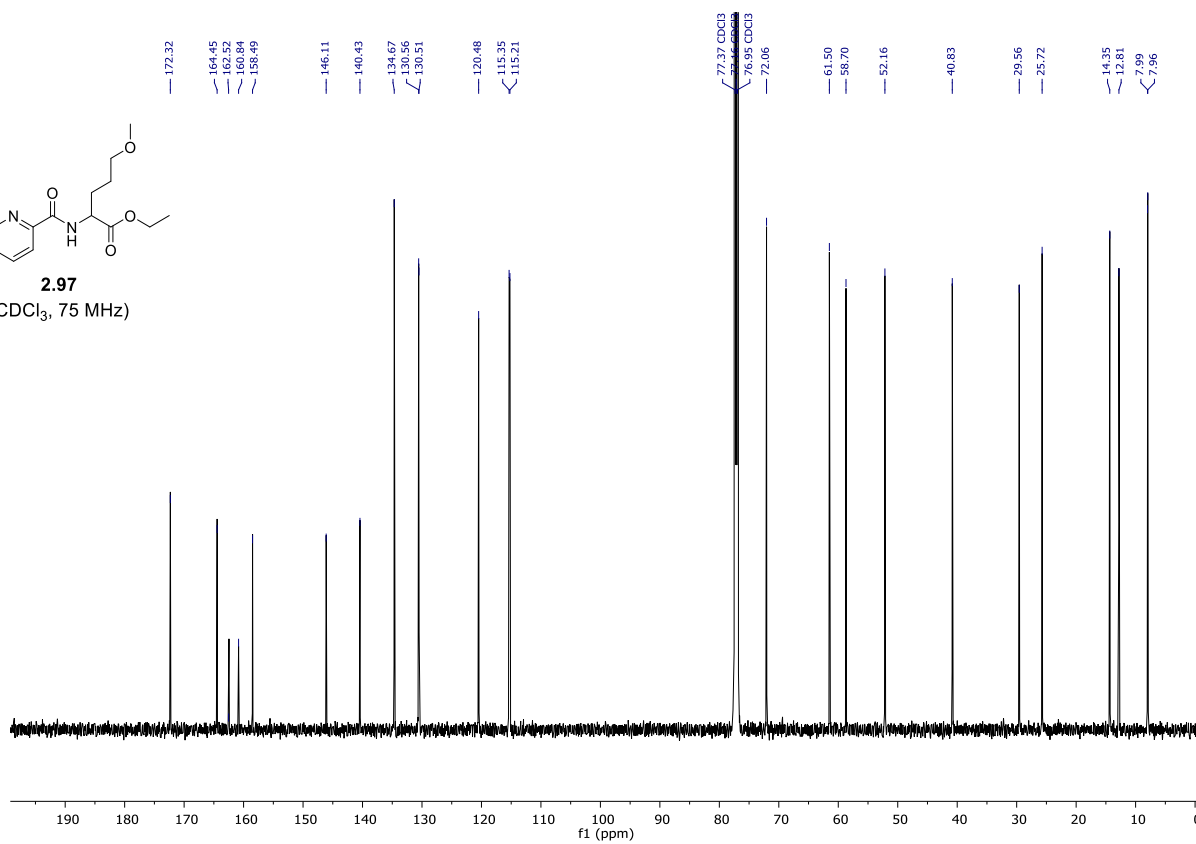
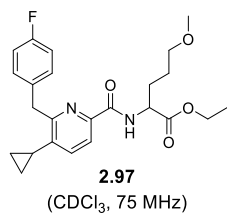
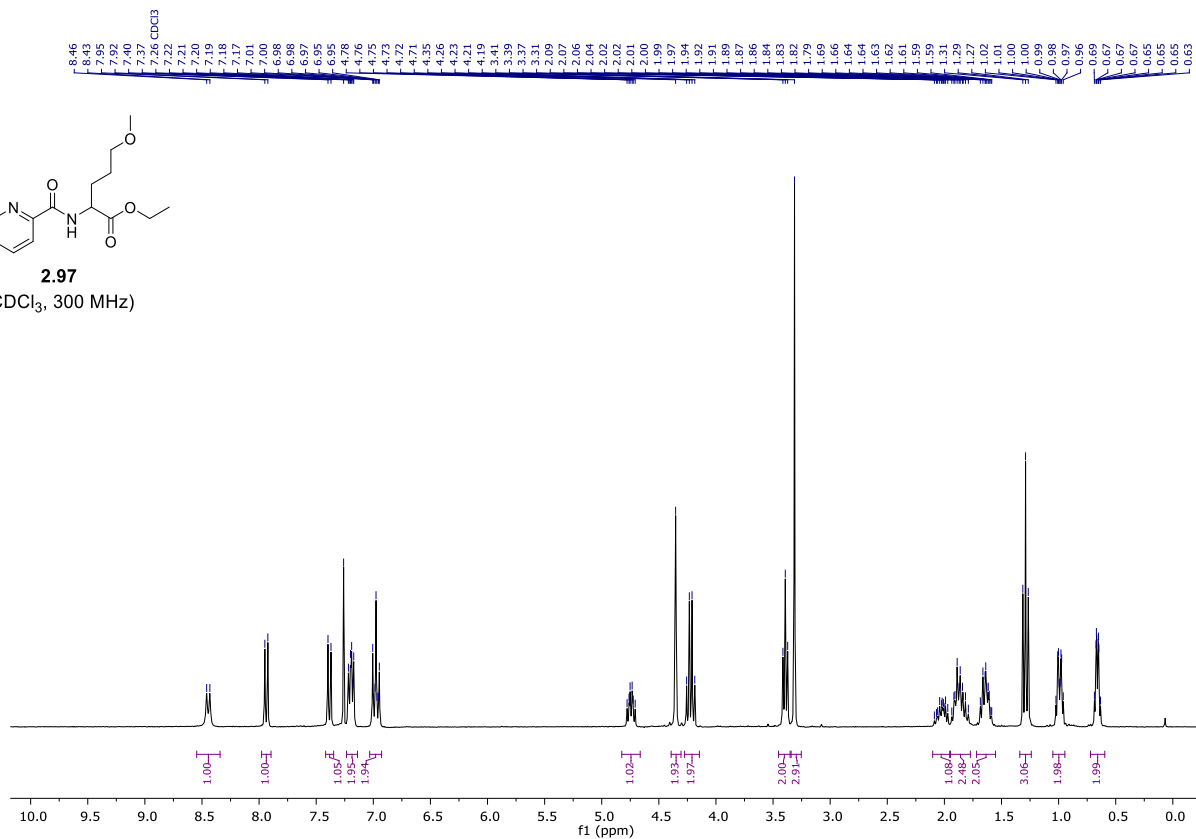
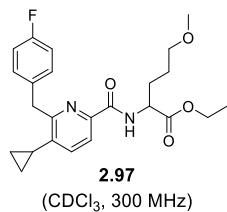






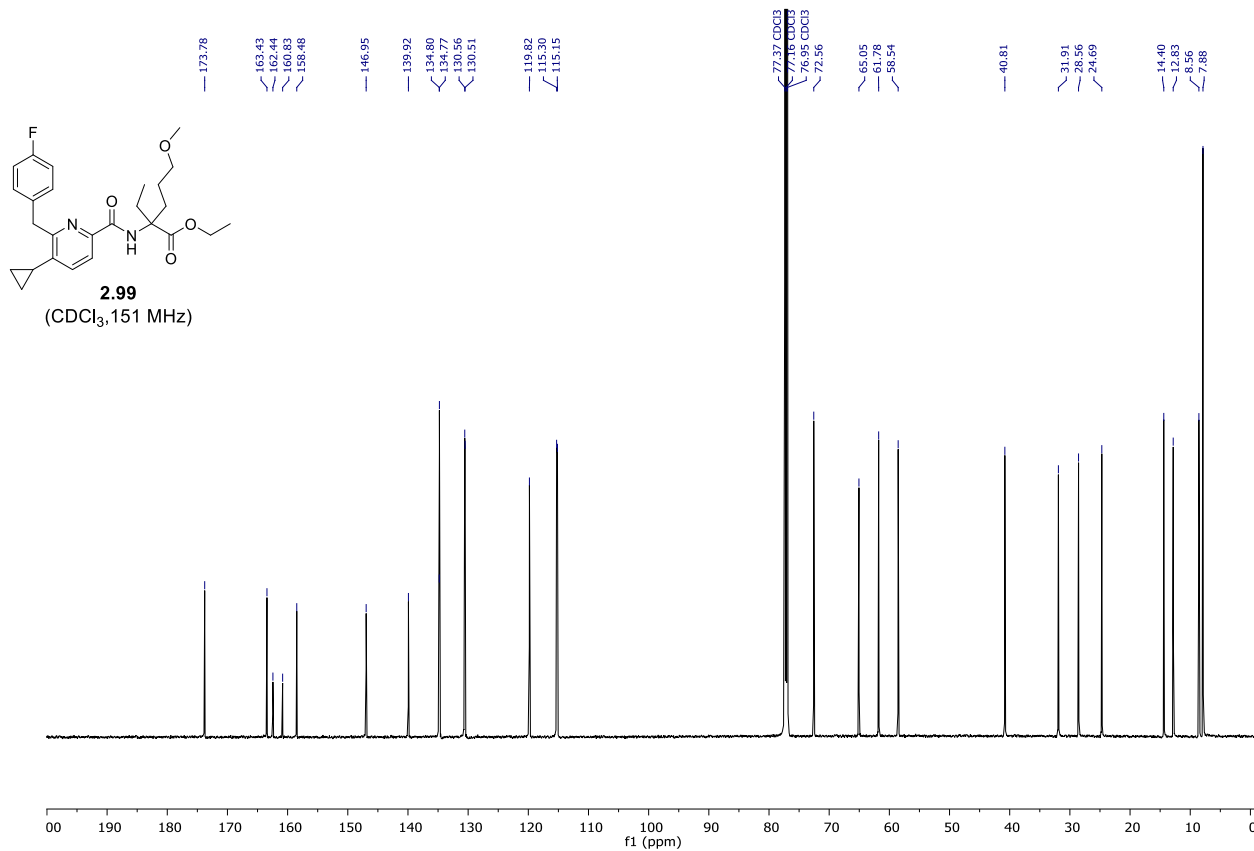
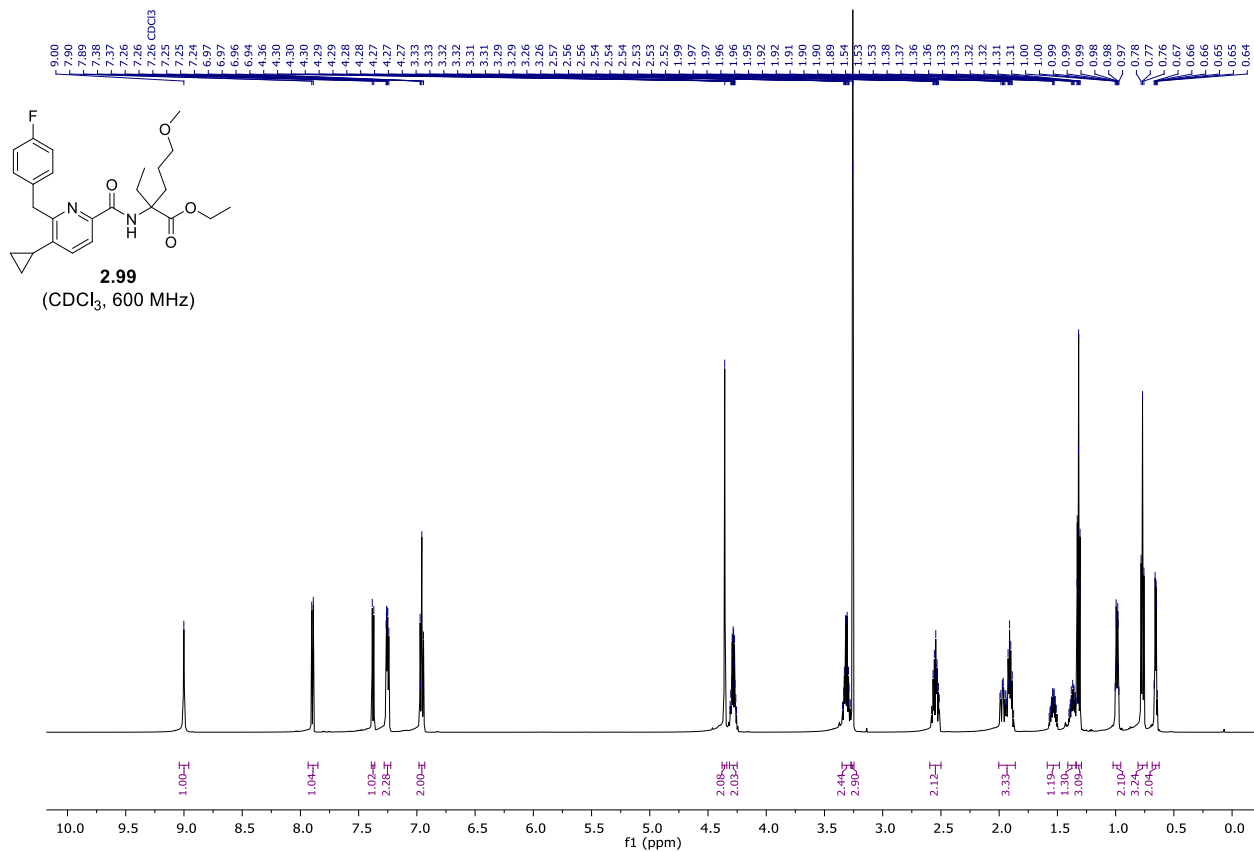


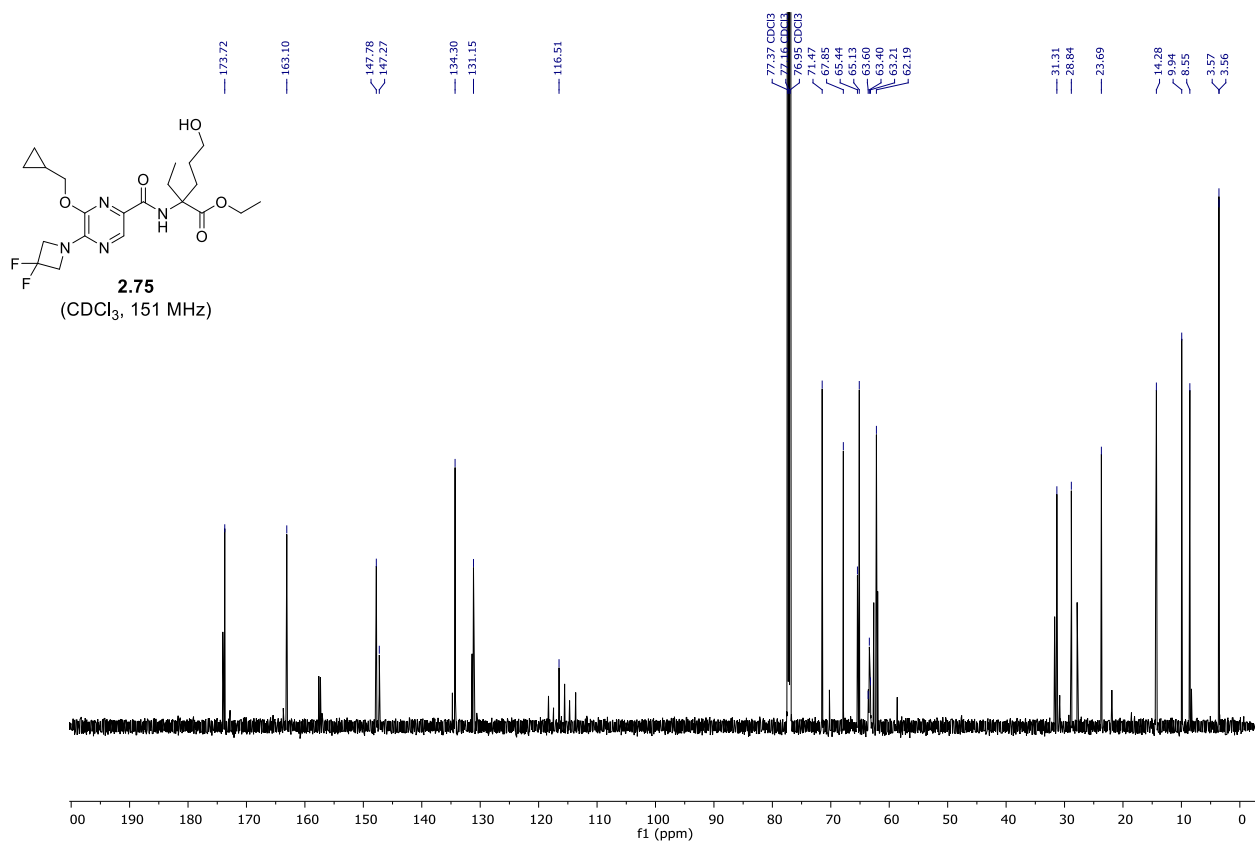
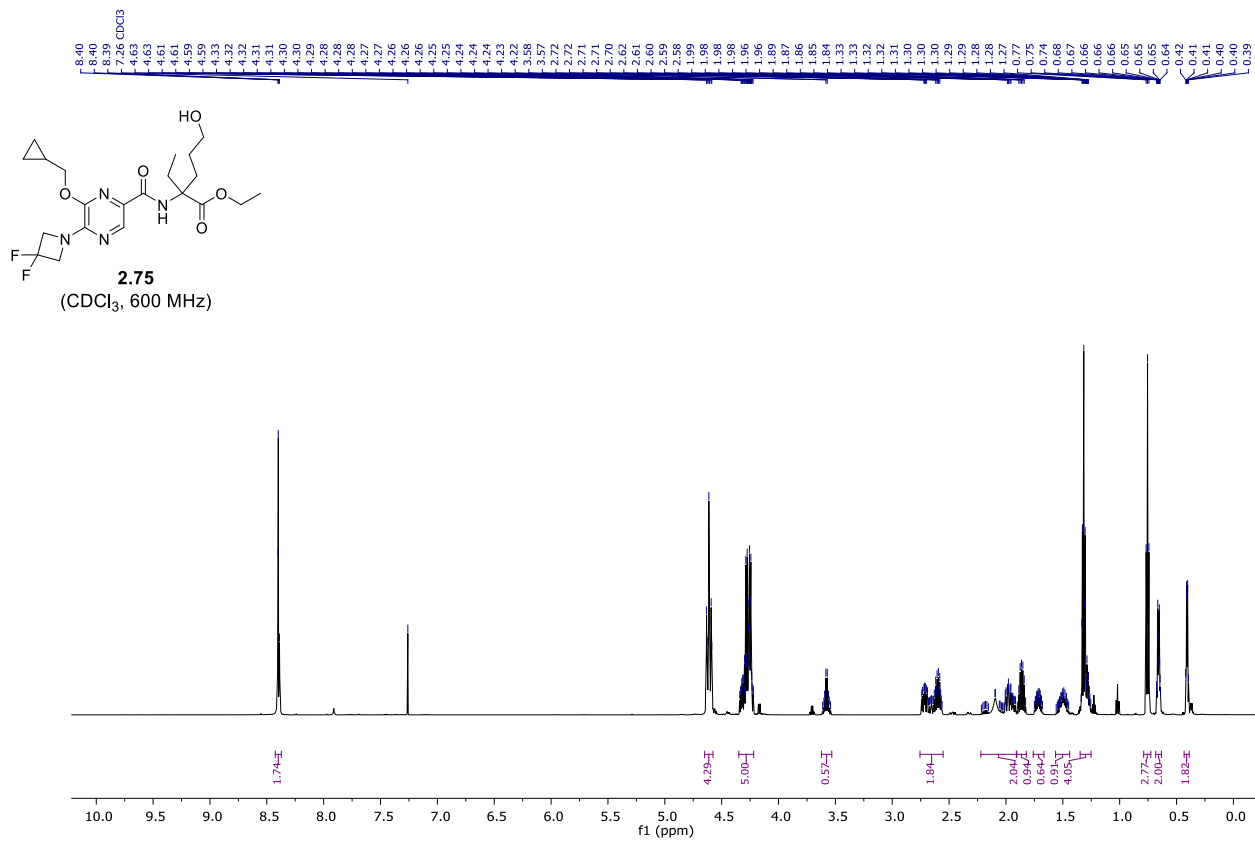


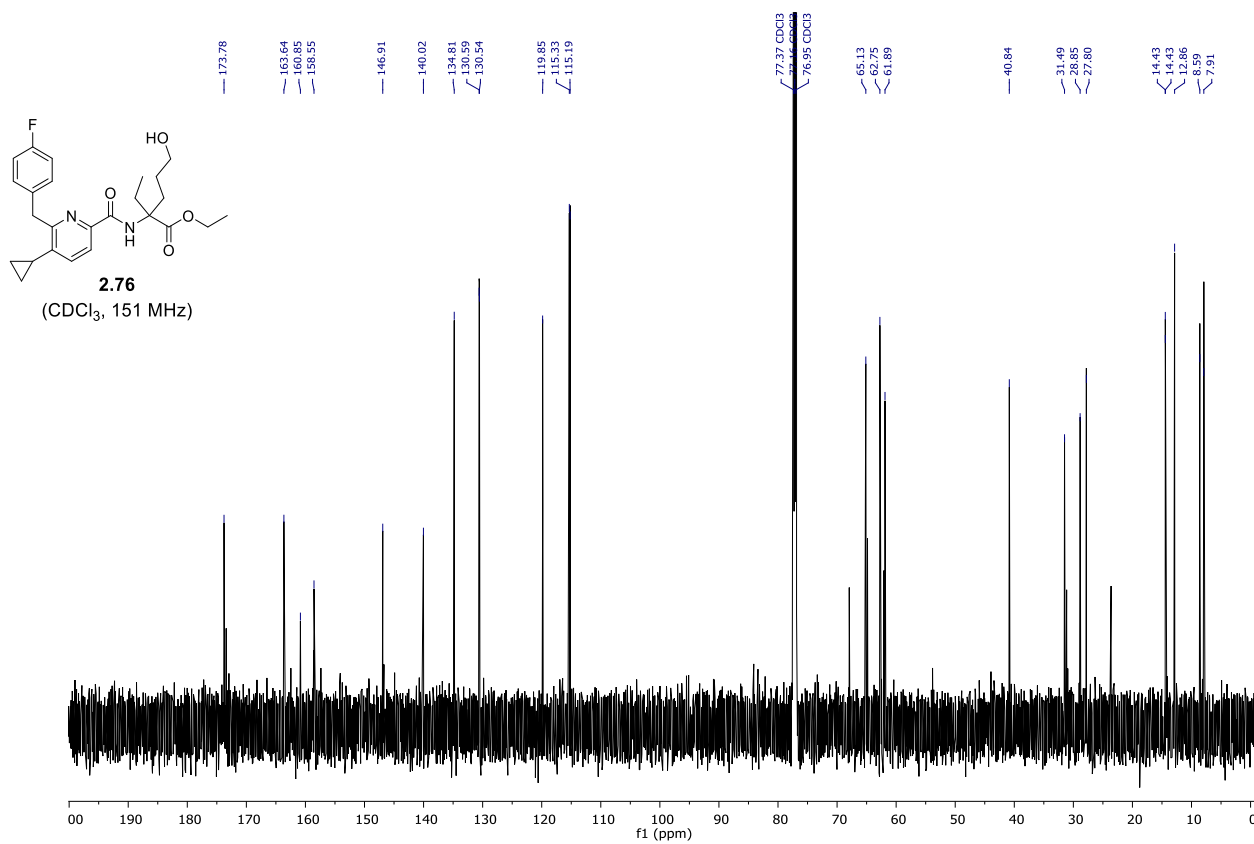
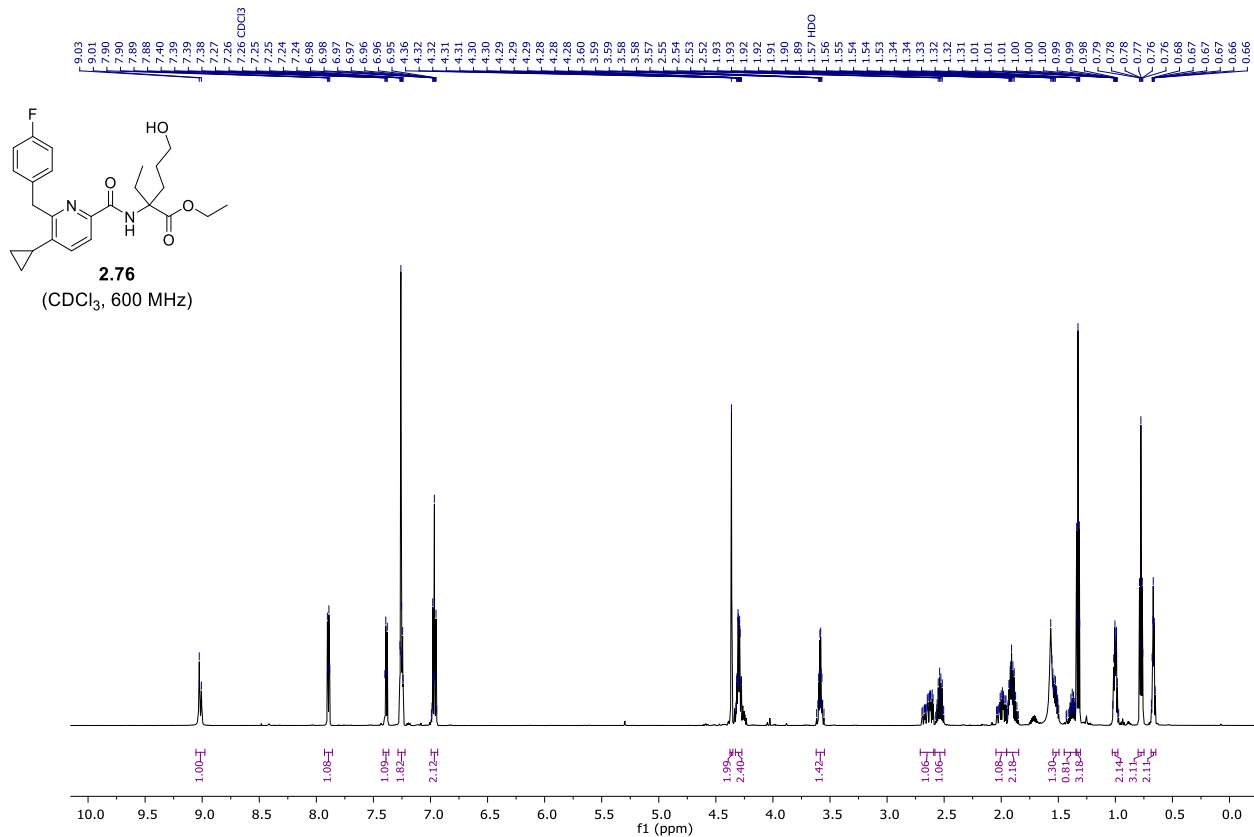


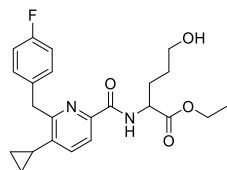




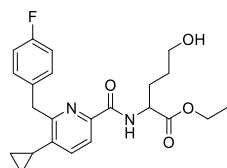
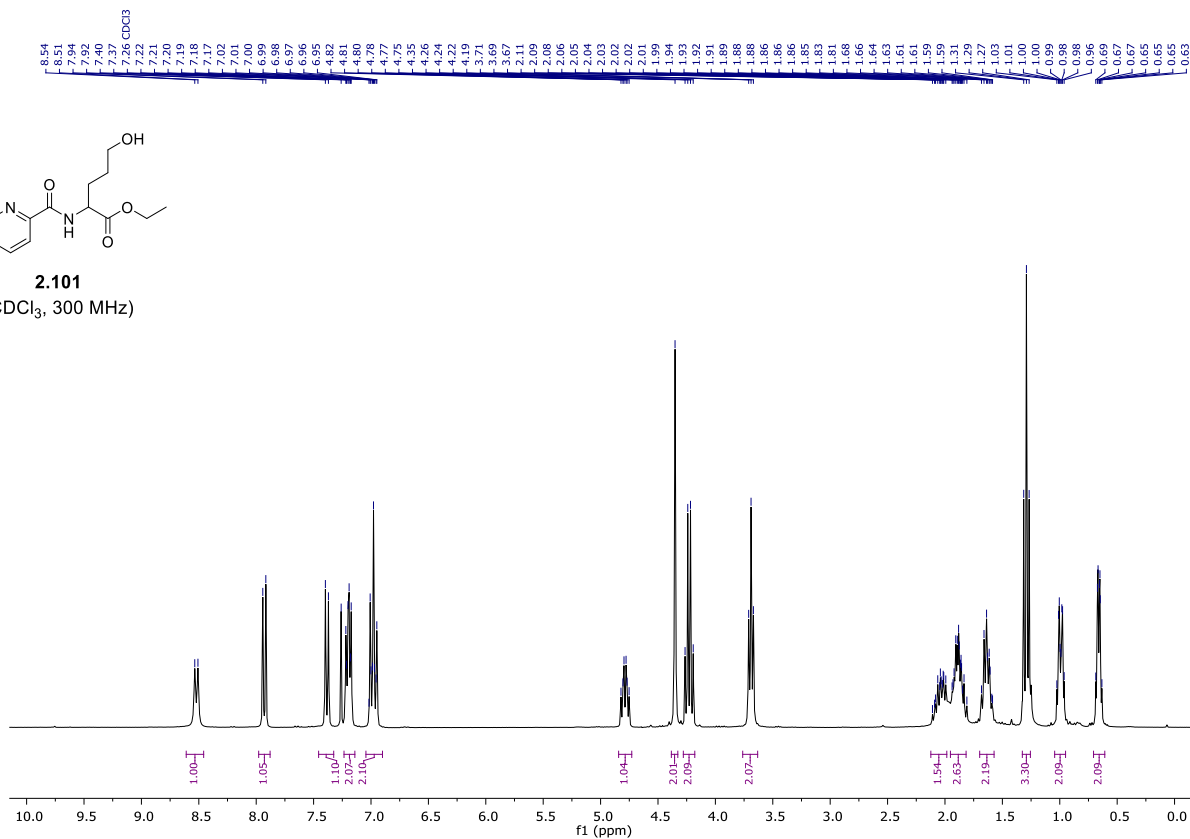




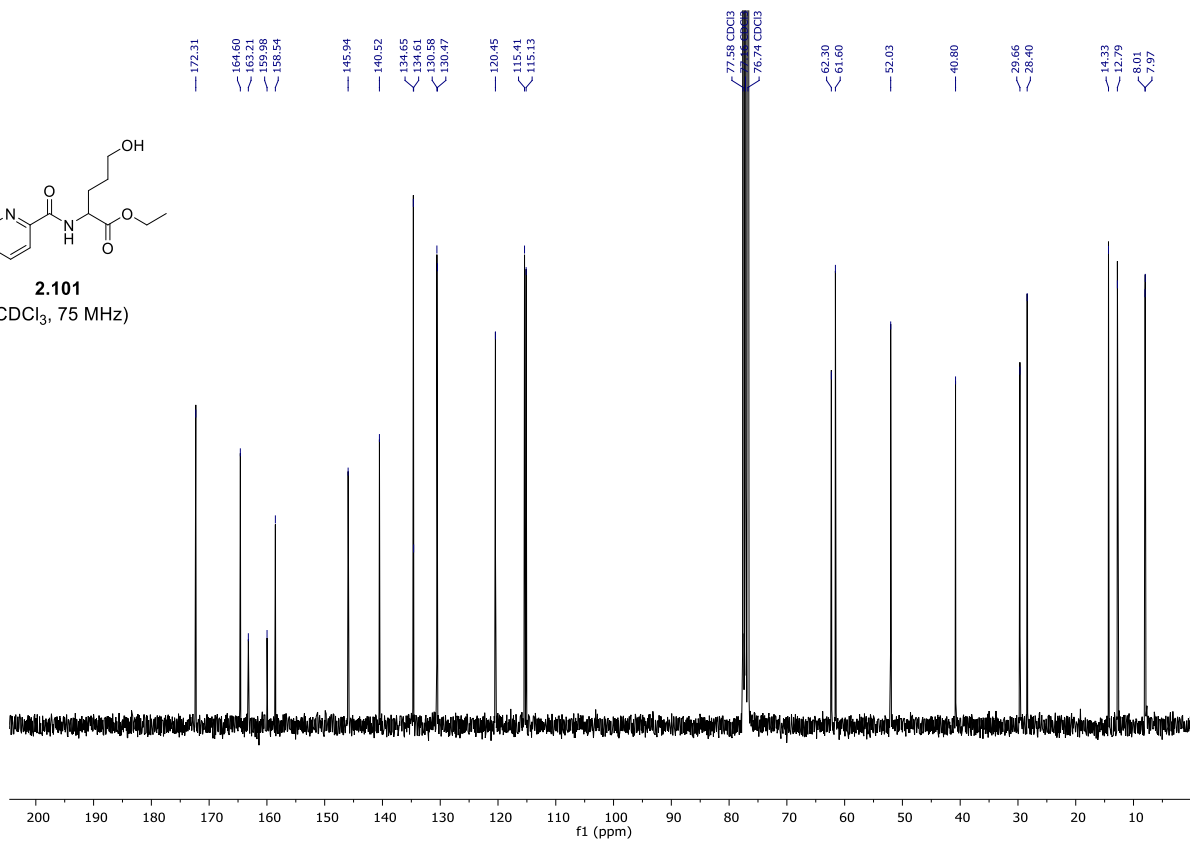




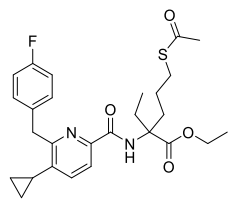
**2.101**  
(CDCl<sub>3</sub>, 300 MHz)



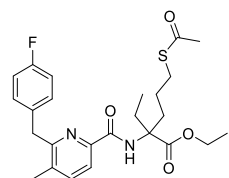
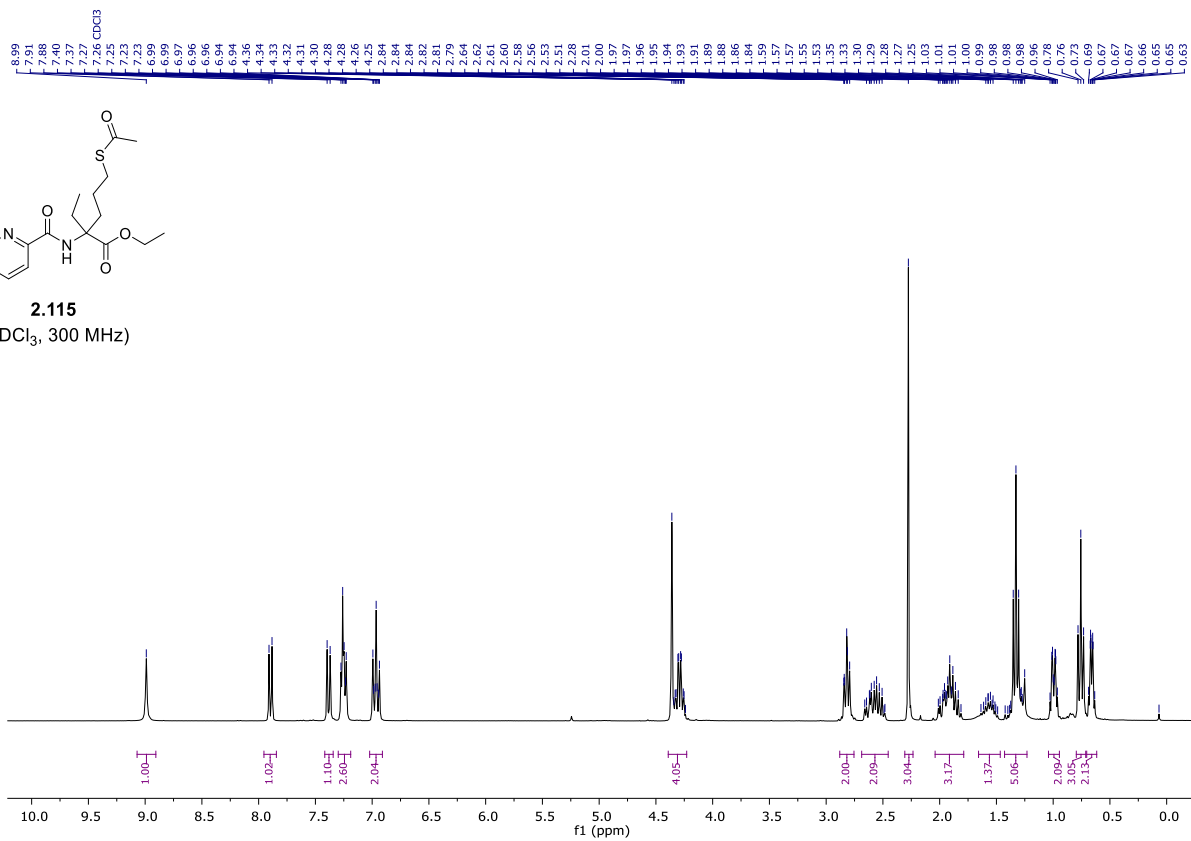
**2.101**  
(CDCl<sub>3</sub>, 75 MHz)



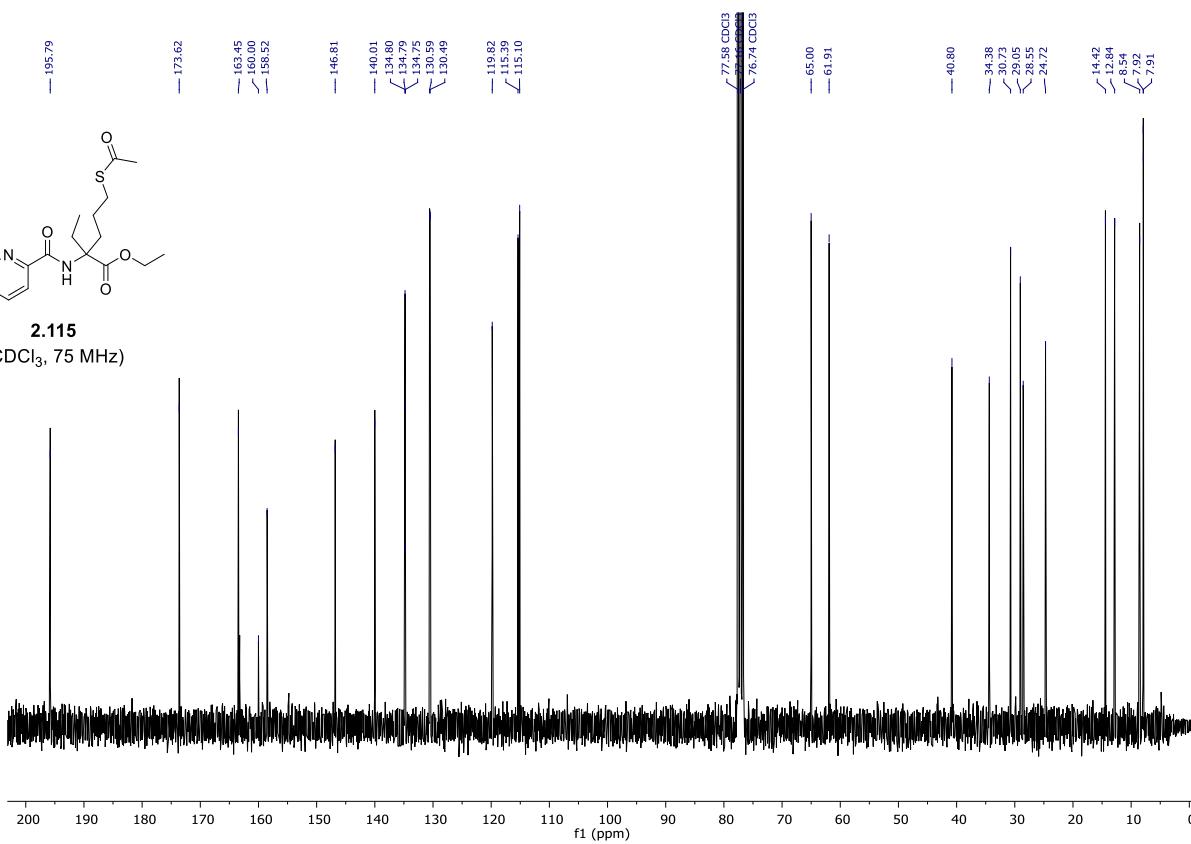


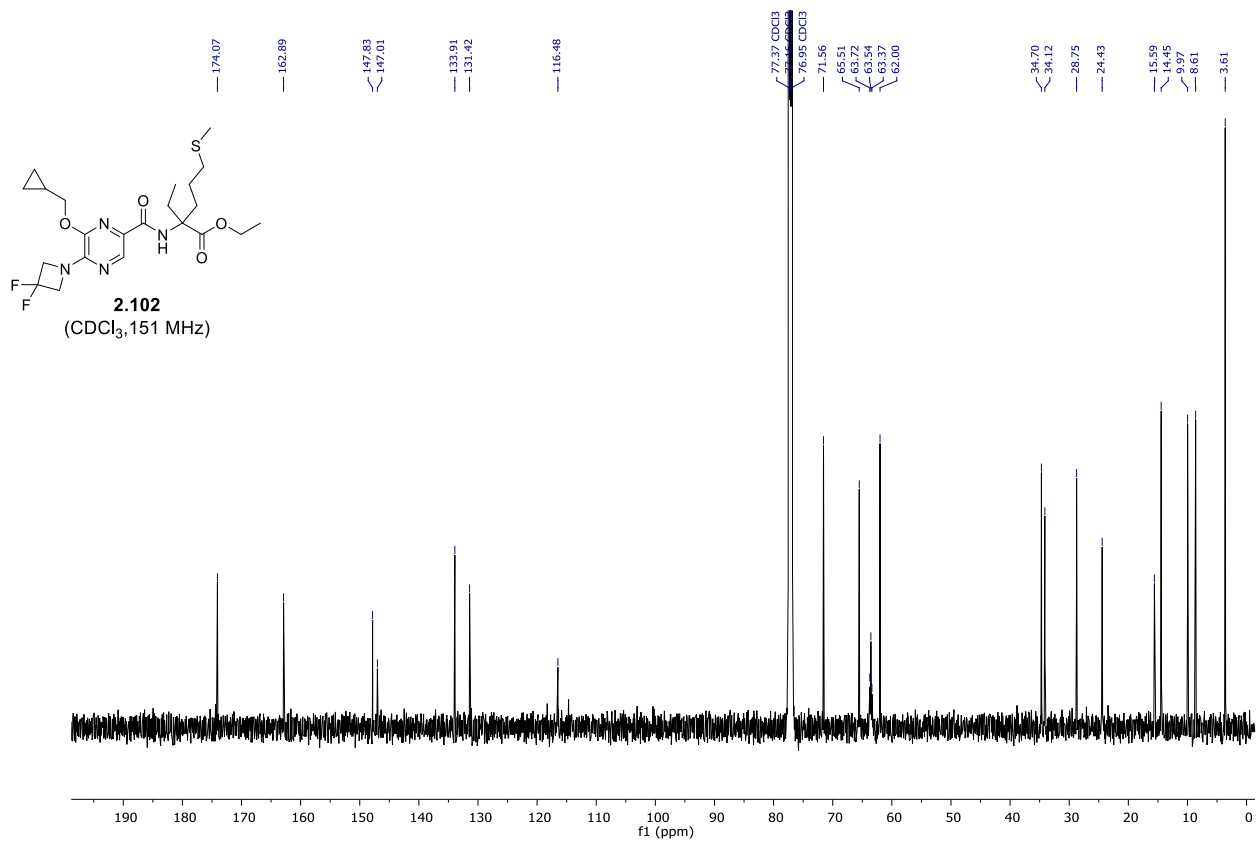
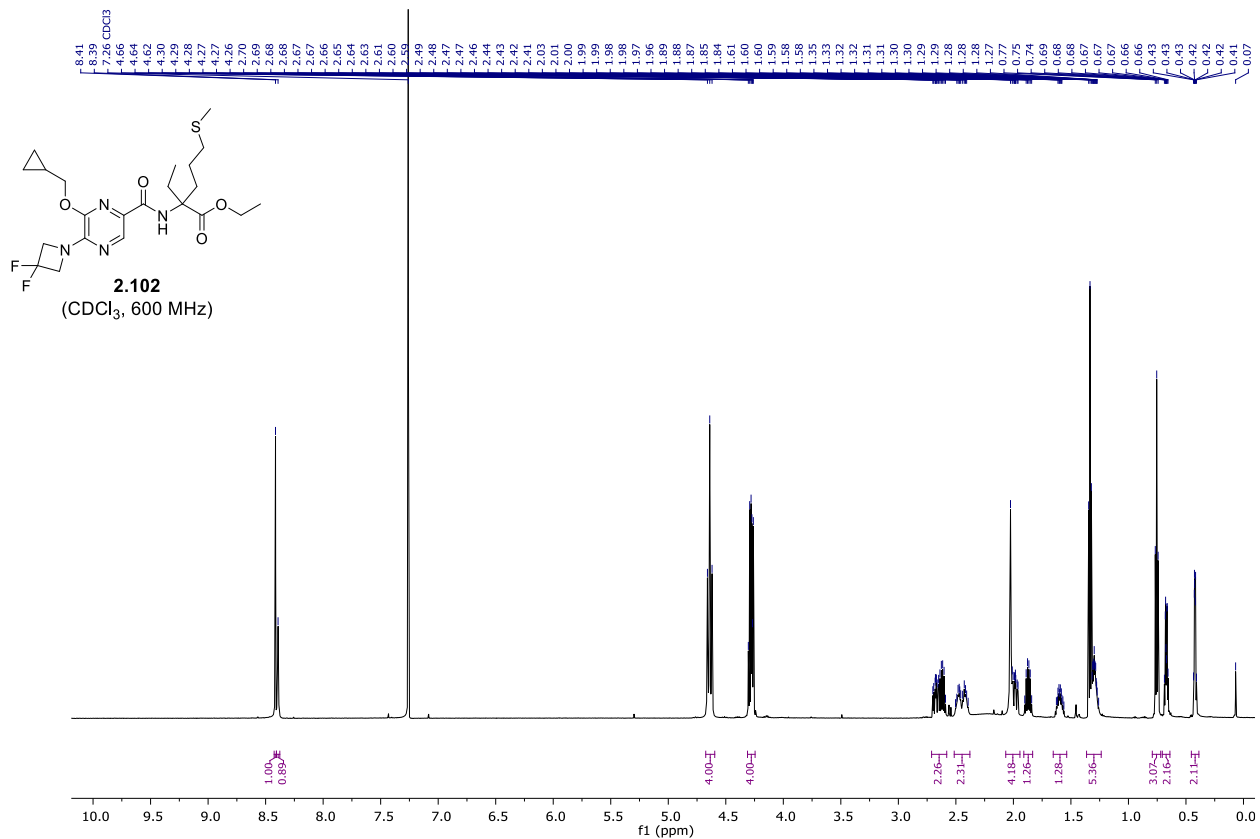


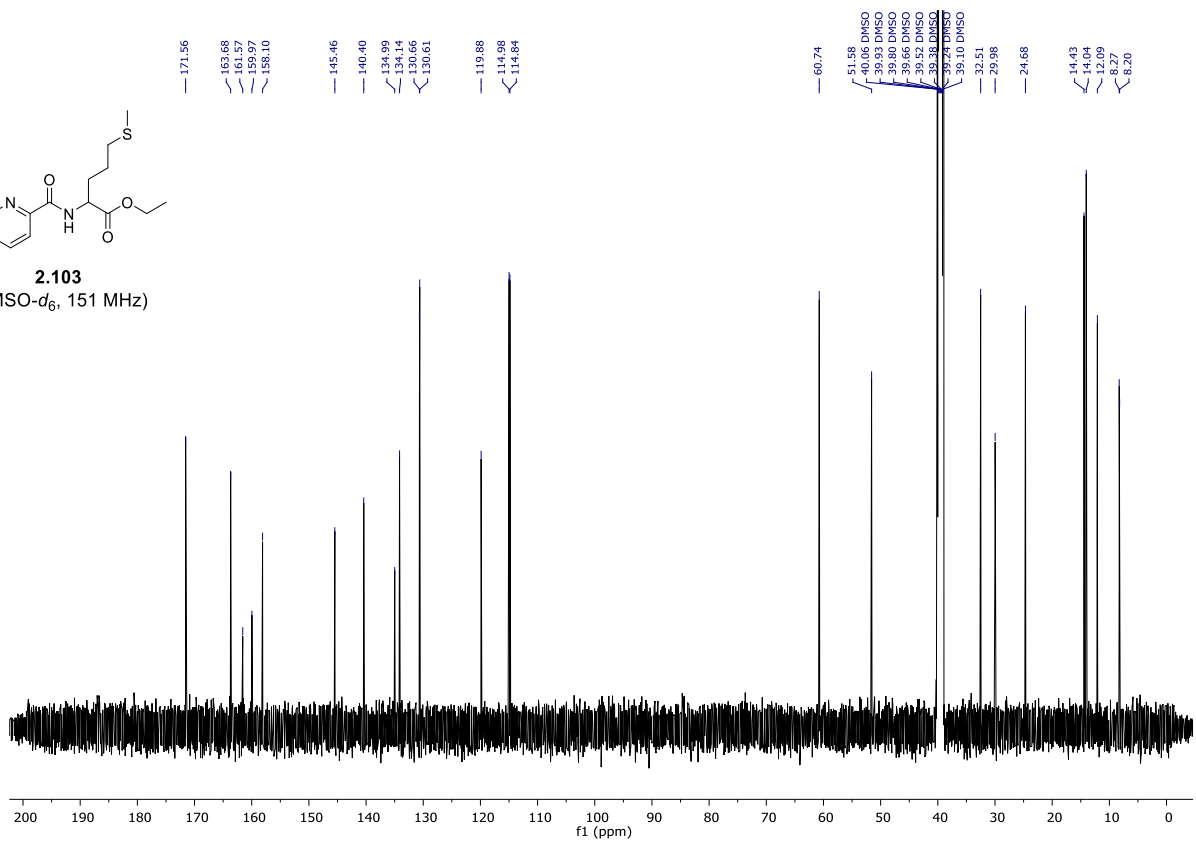
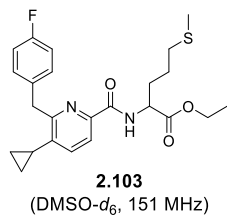
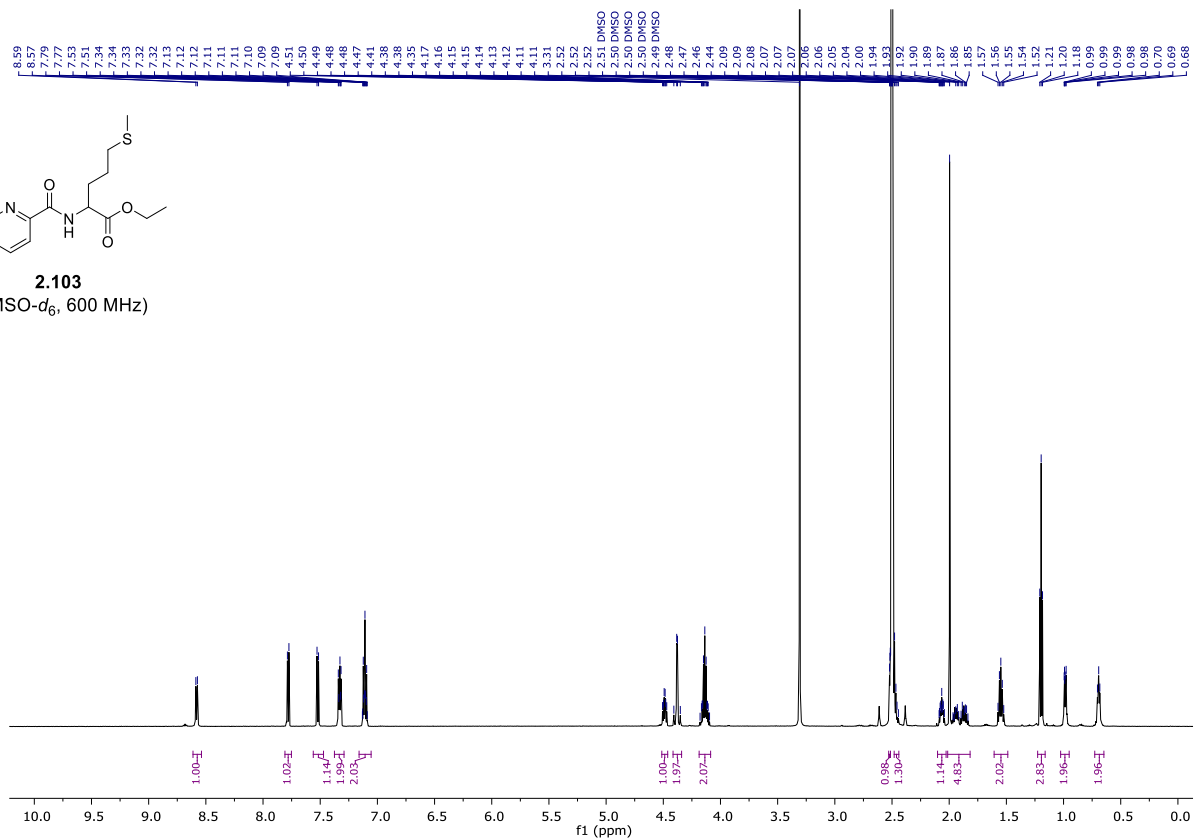
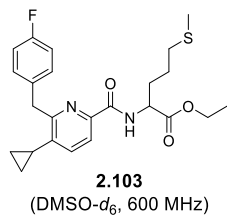
**2.115**  
(CDCl<sub>3</sub>, 300 MHz)



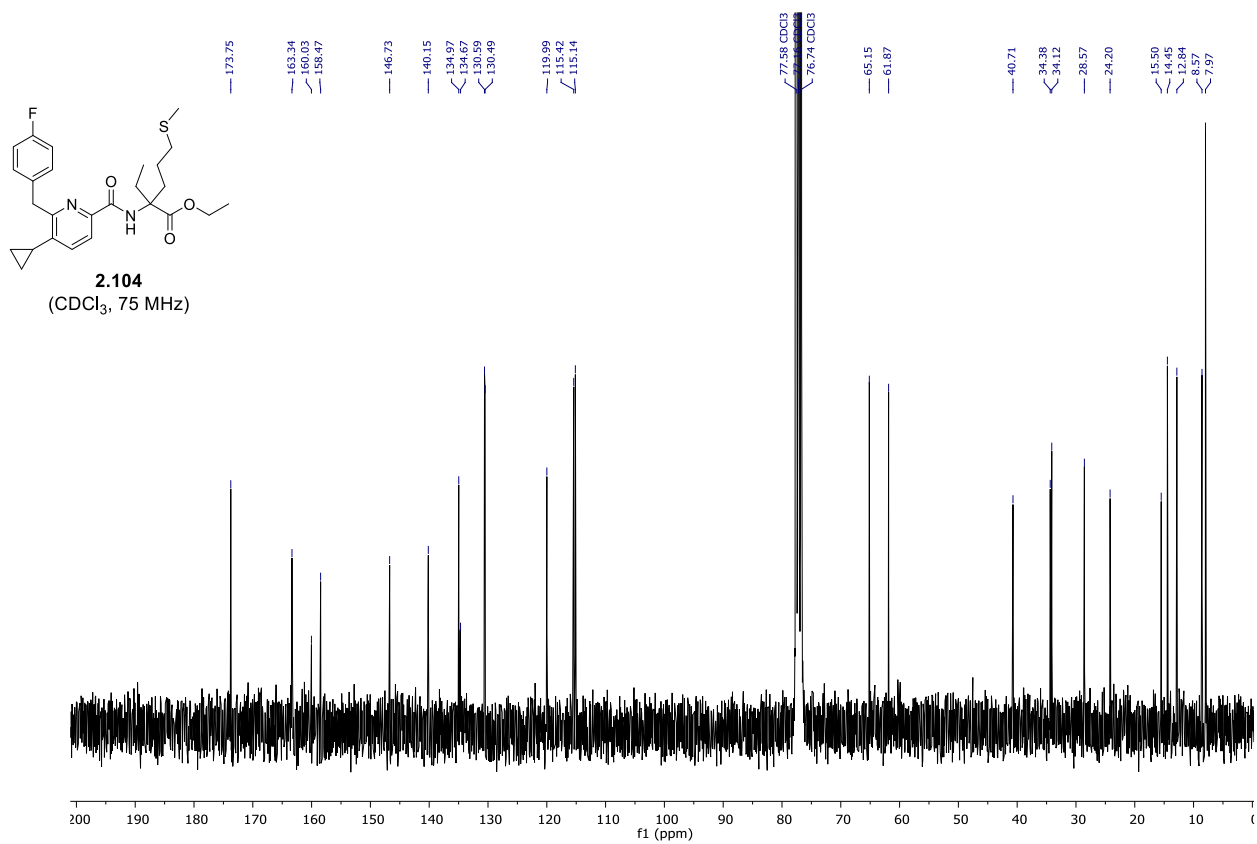
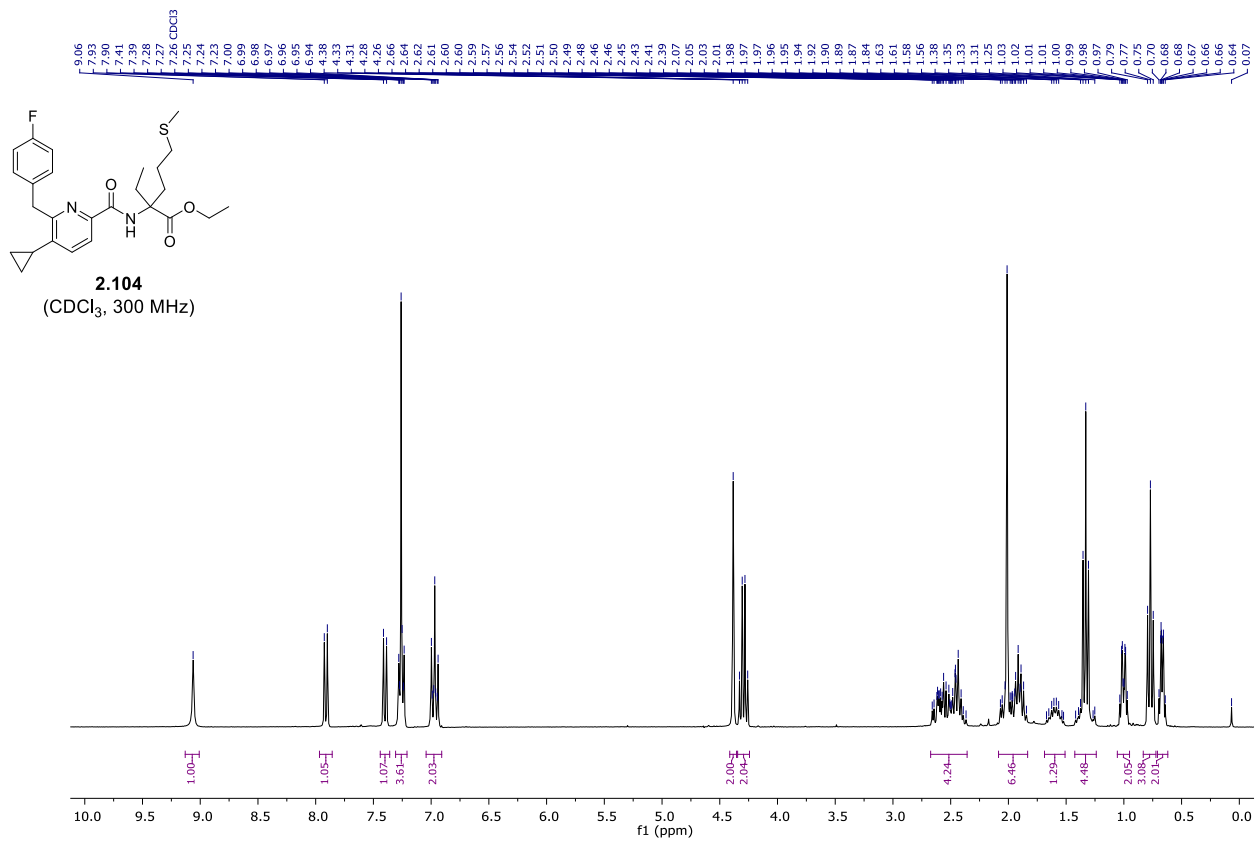
**2.115**  
(CDCl<sub>3</sub>, 75 MHz)

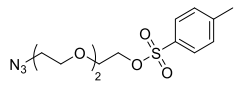




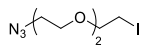
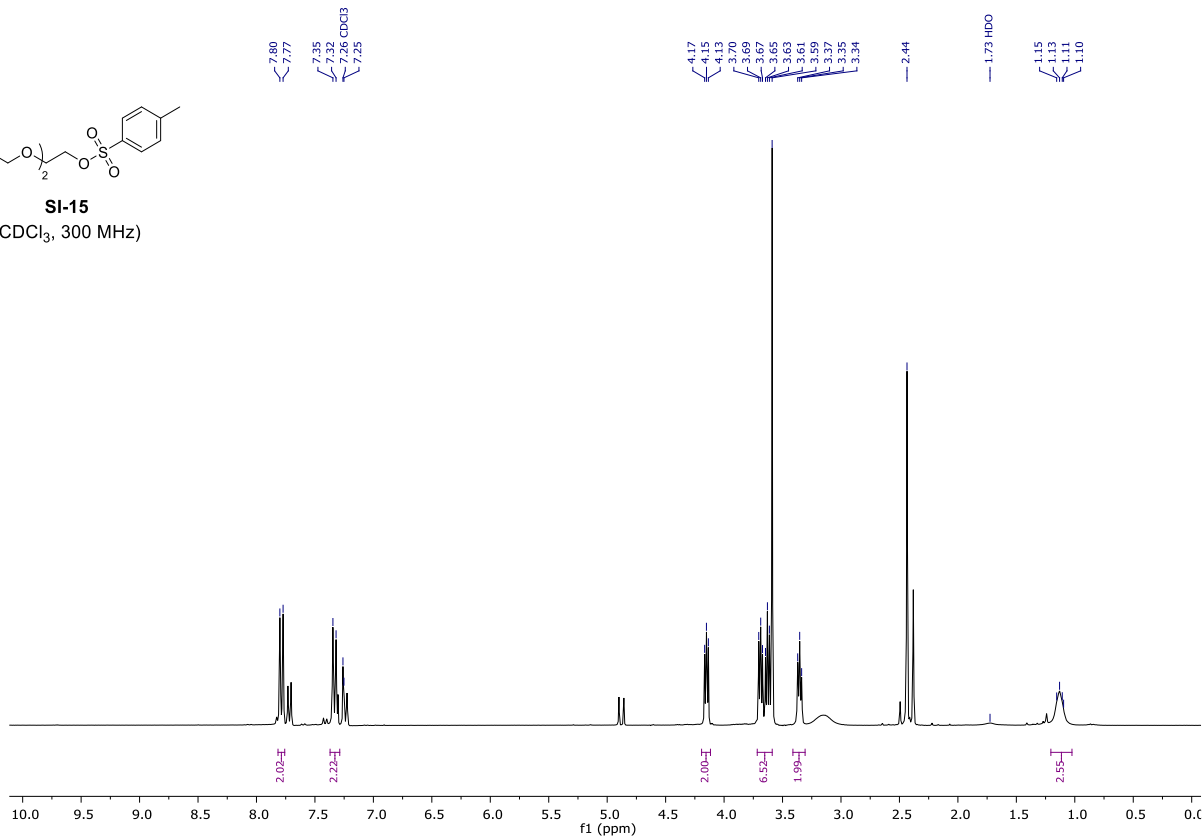




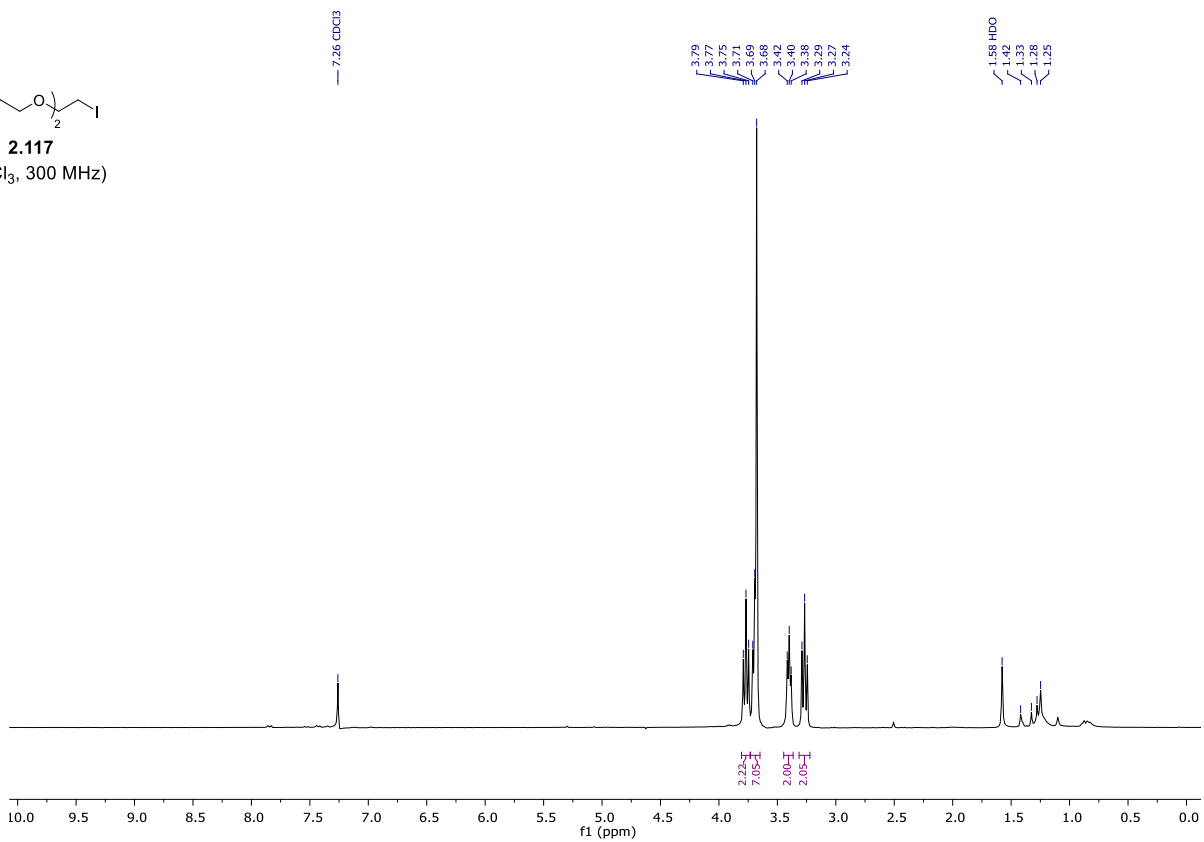


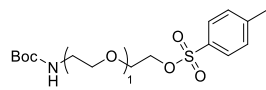


**SI-15**  
(CDCl<sub>3</sub>, 300 MHz)

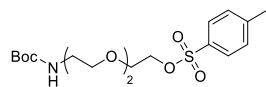
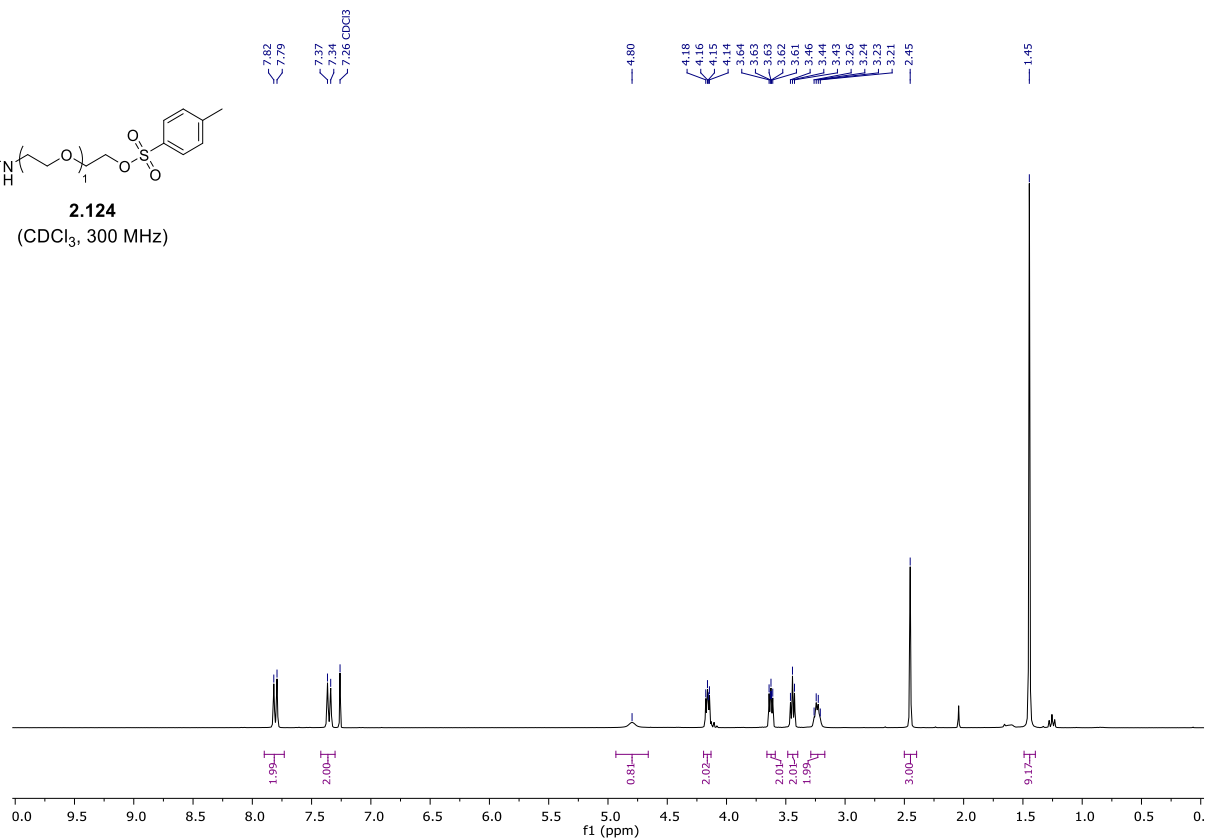


**2.117**  
(CDCl<sub>3</sub>, 300 MHz)

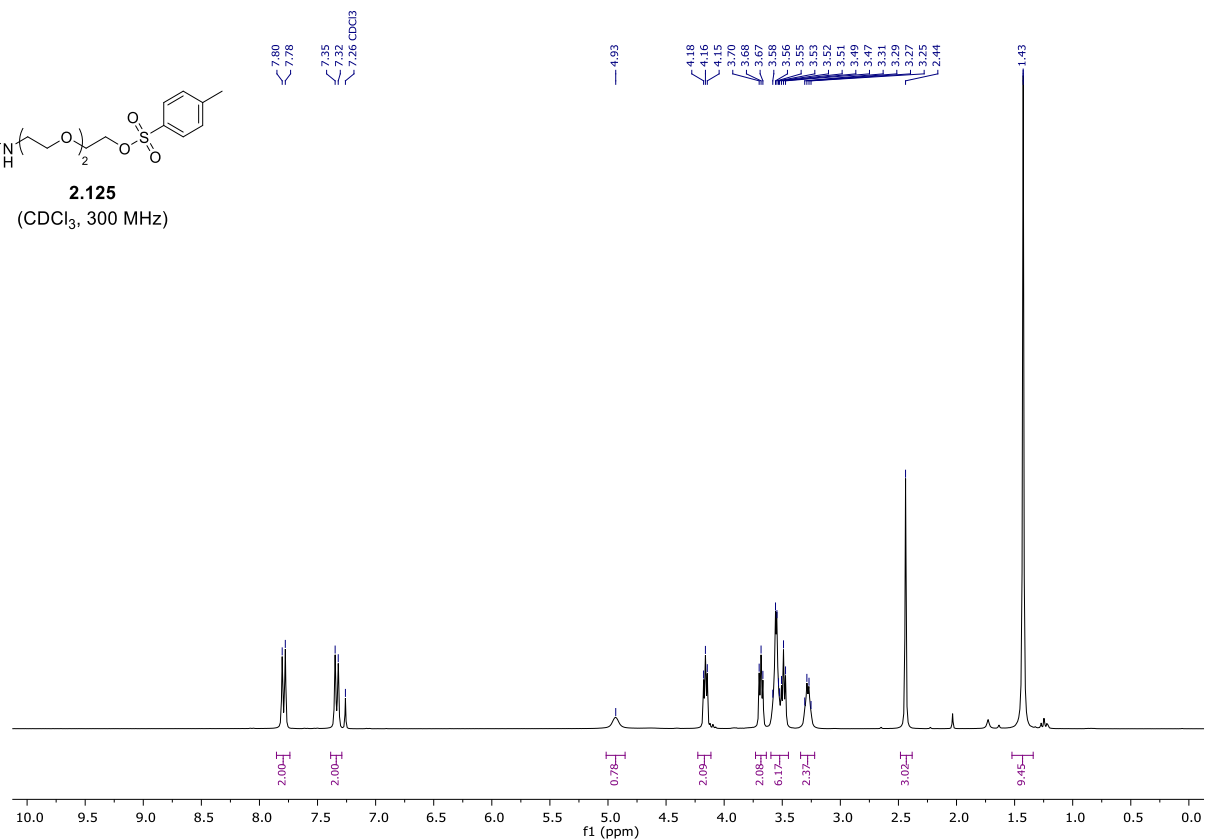


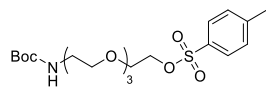


**2.124**  
(CDCl<sub>3</sub>, 300 MHz)

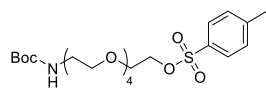
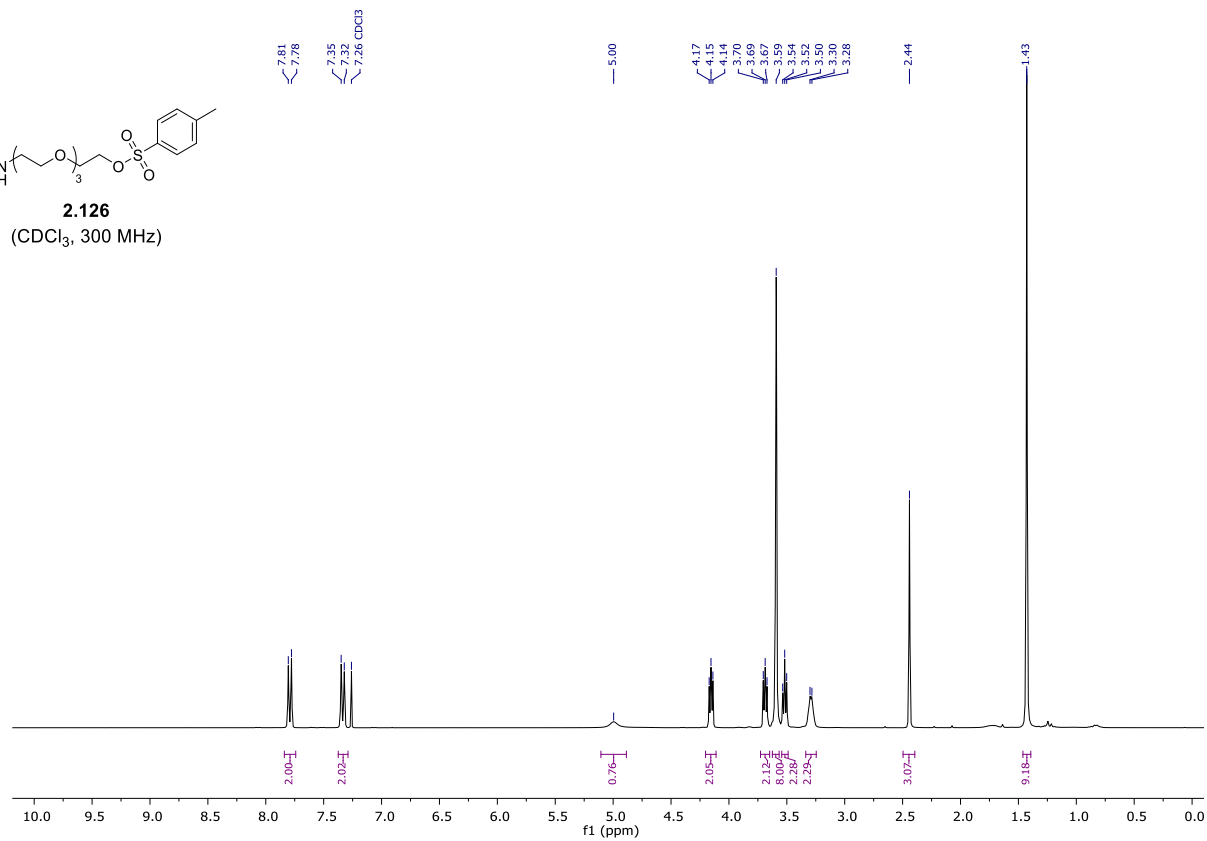


**2.125**  
(CDCl<sub>3</sub>, 300 MHz)

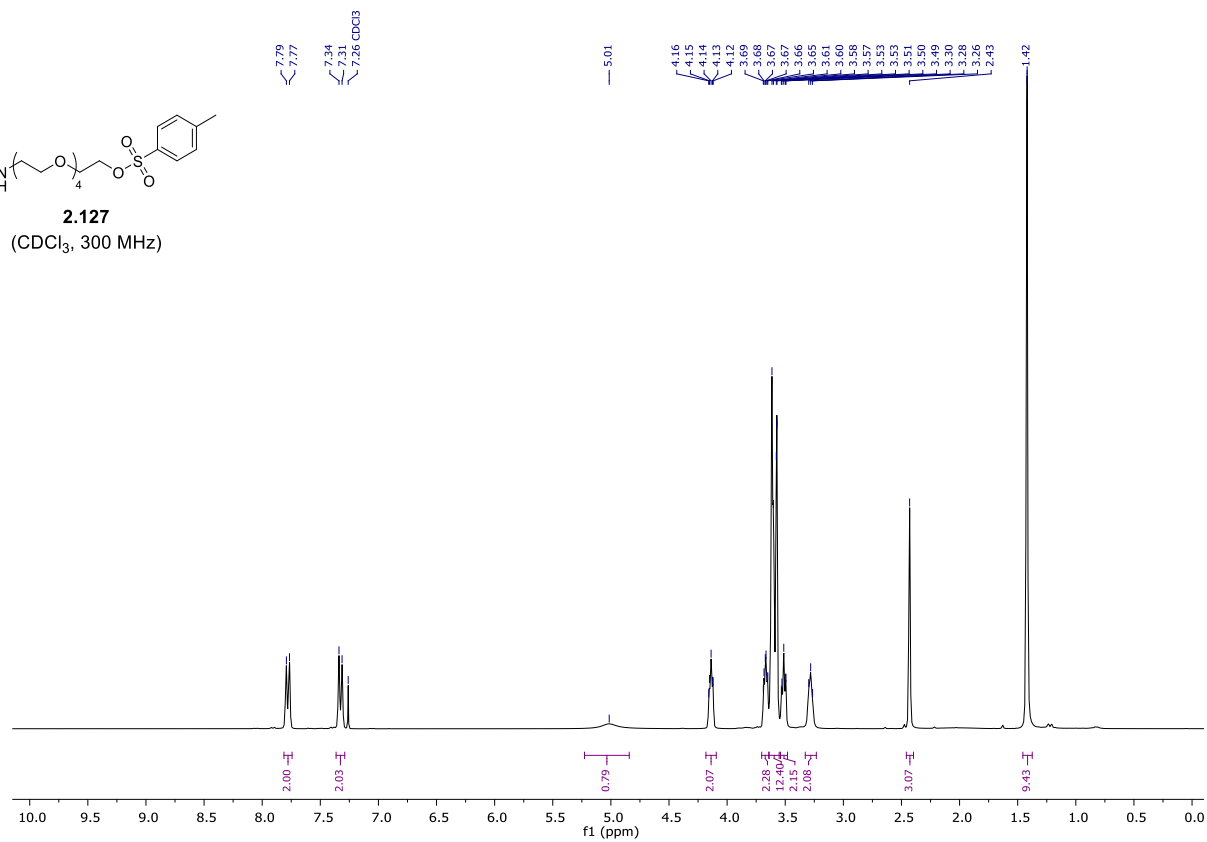


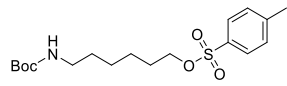


**2.126**  
(CDCl<sub>3</sub>, 300 MHz)

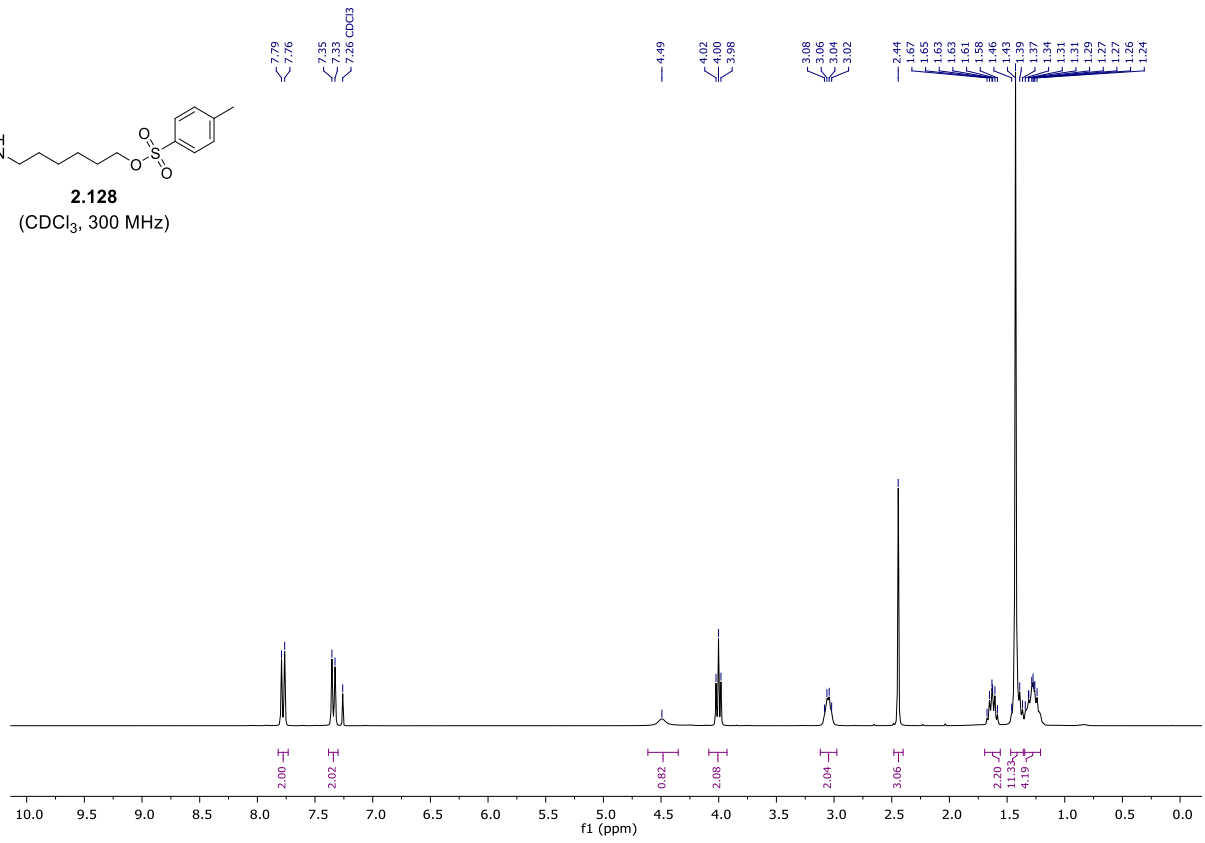


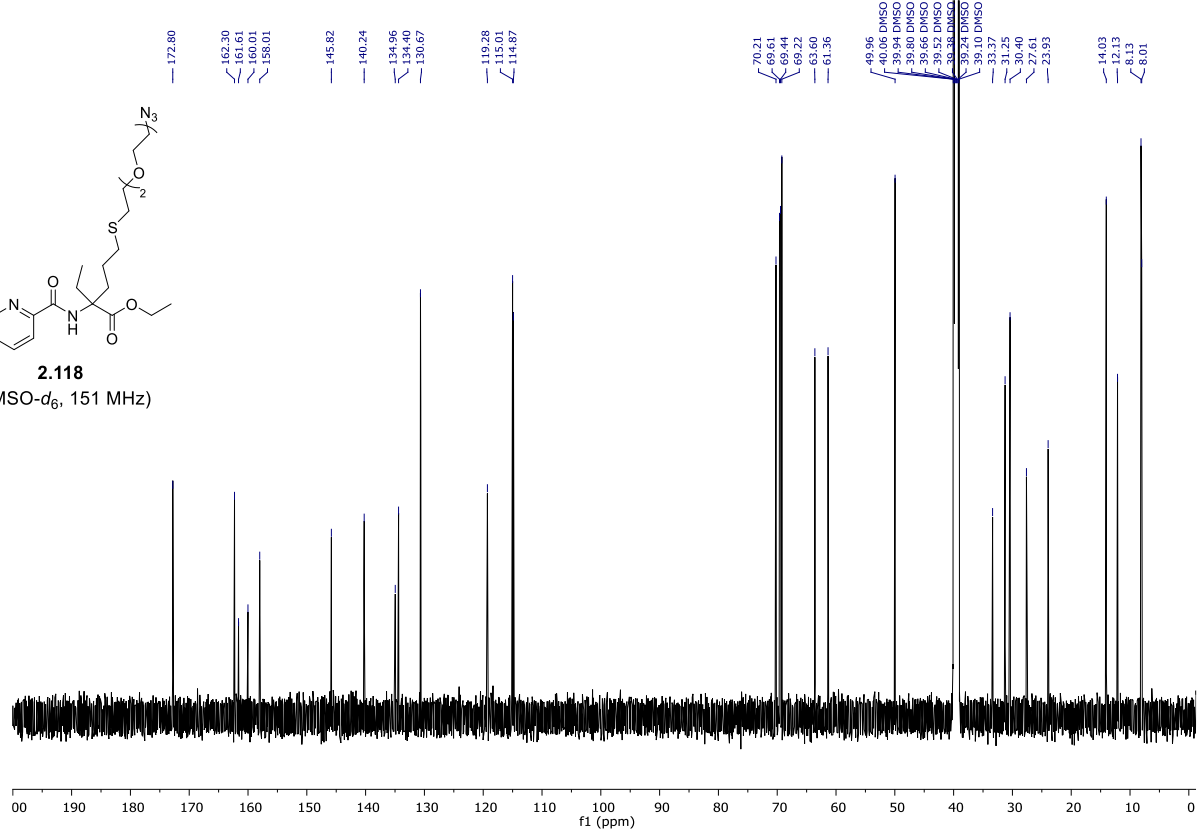
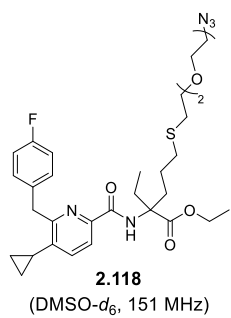
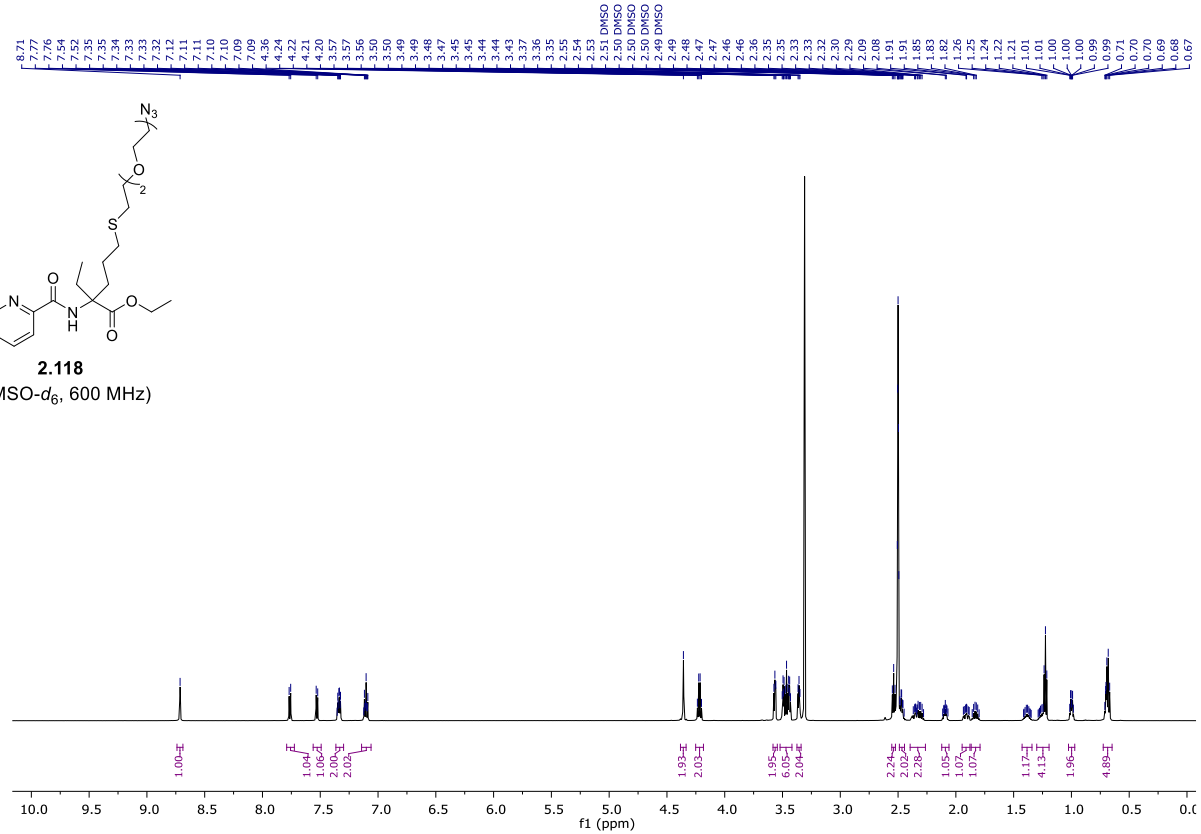
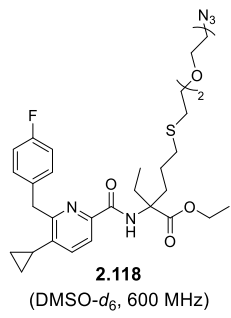
**2.127**  
(CDCl<sub>3</sub>, 300 MHz)

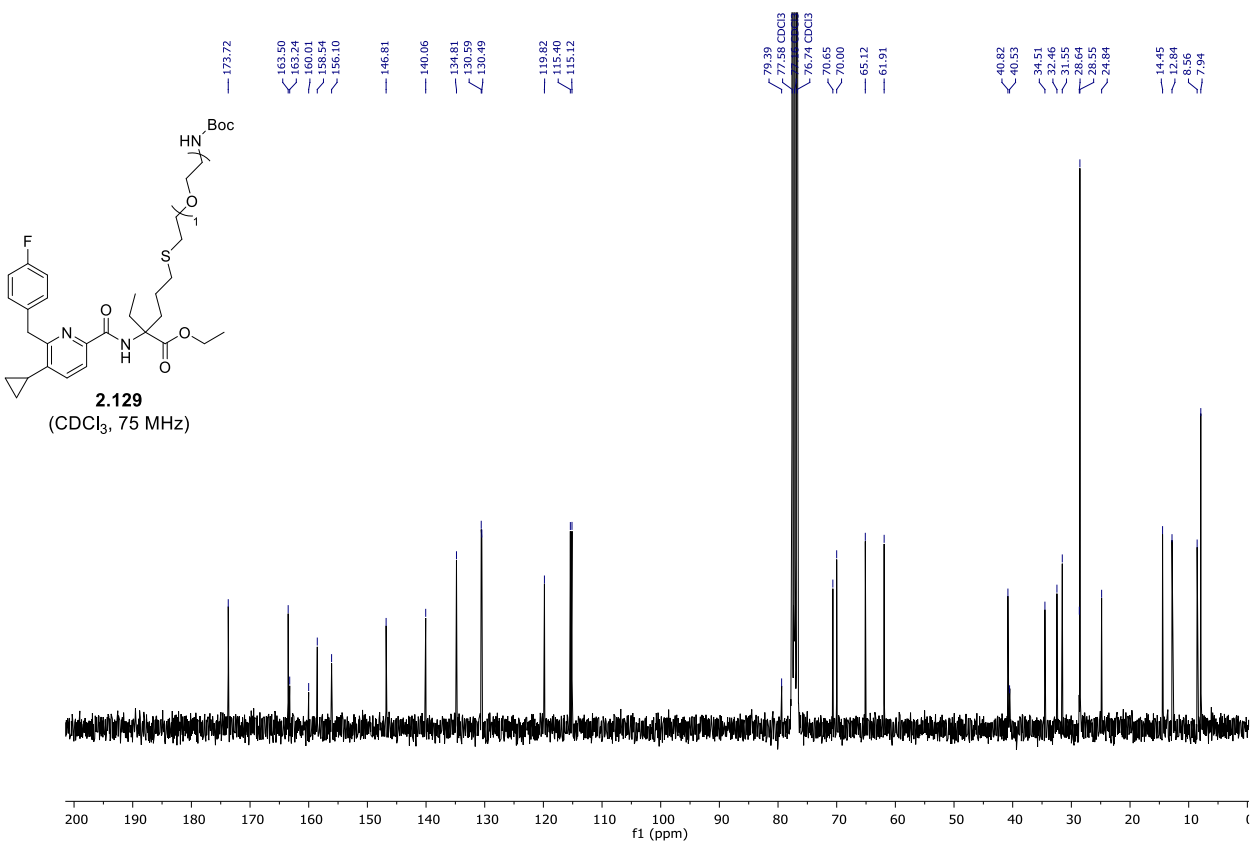
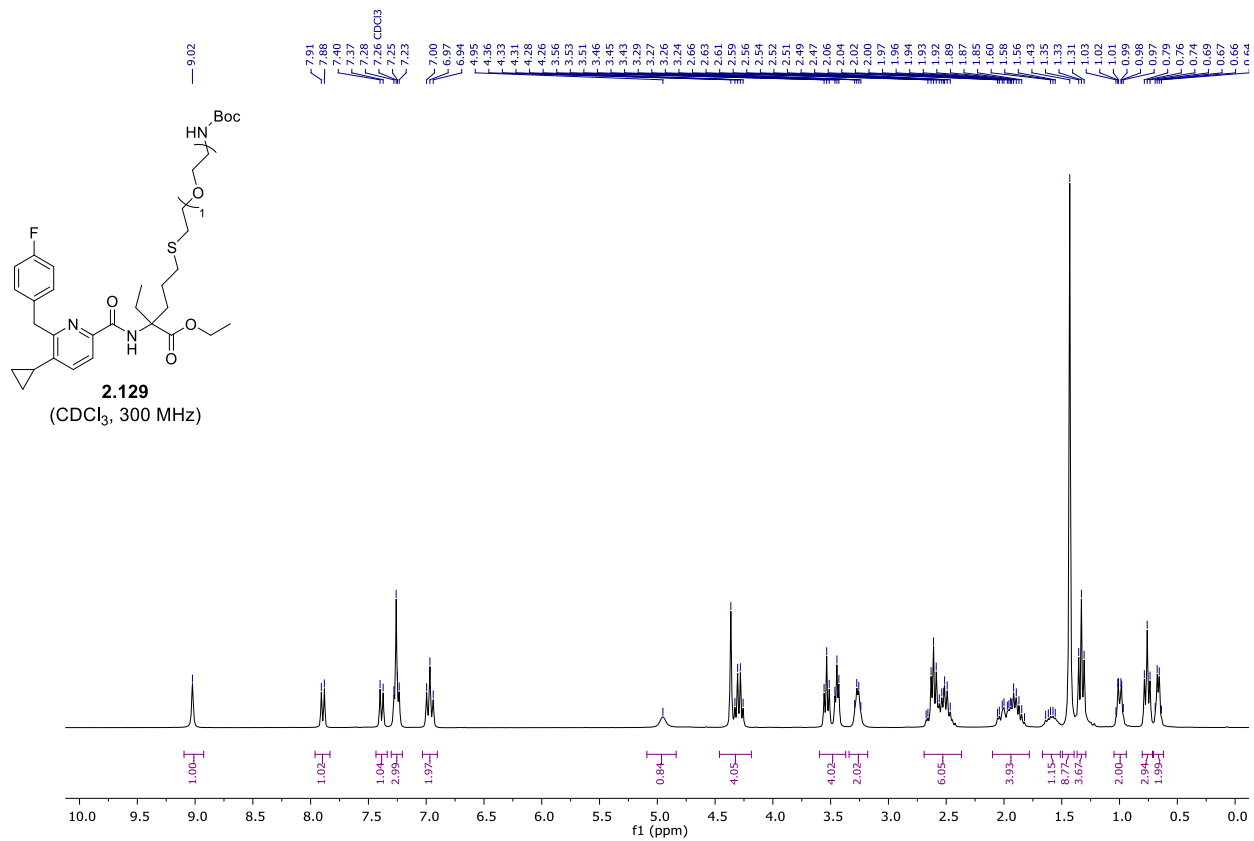


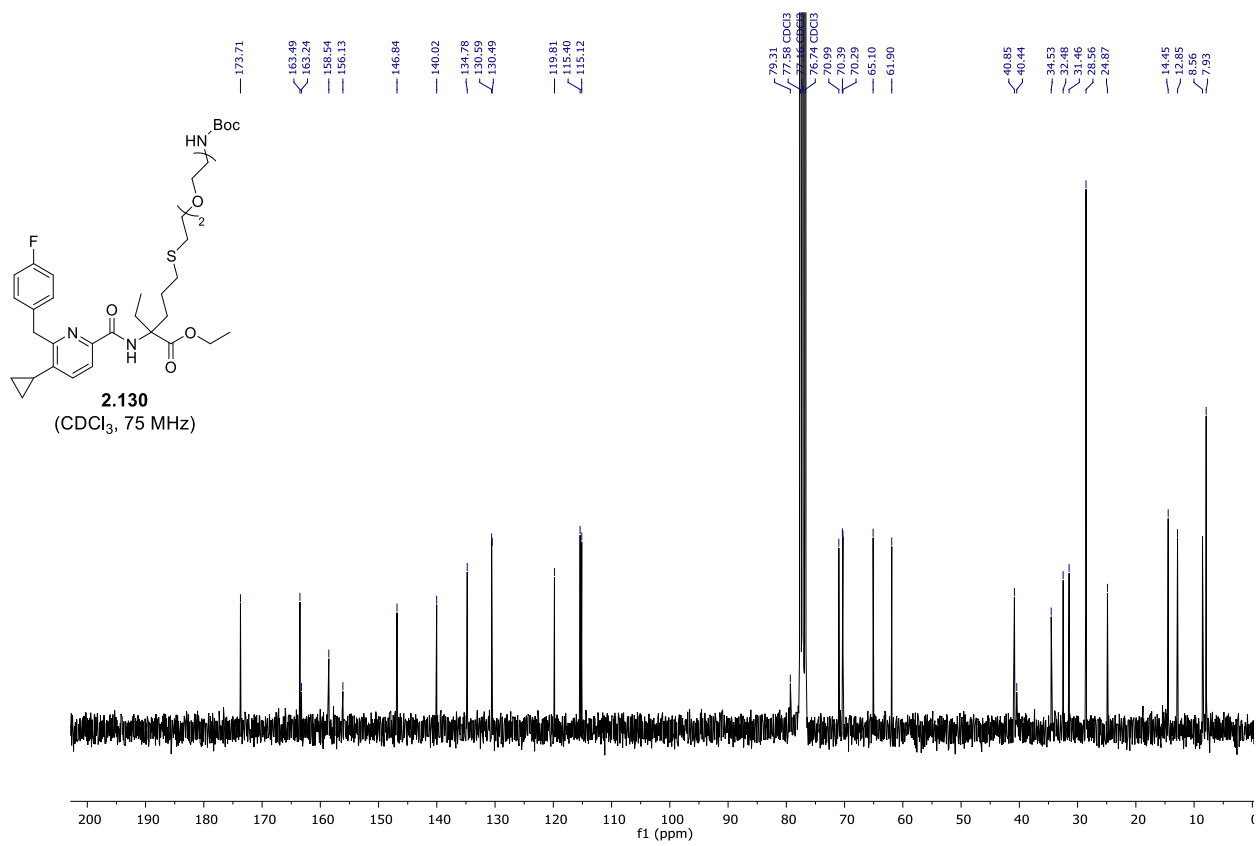
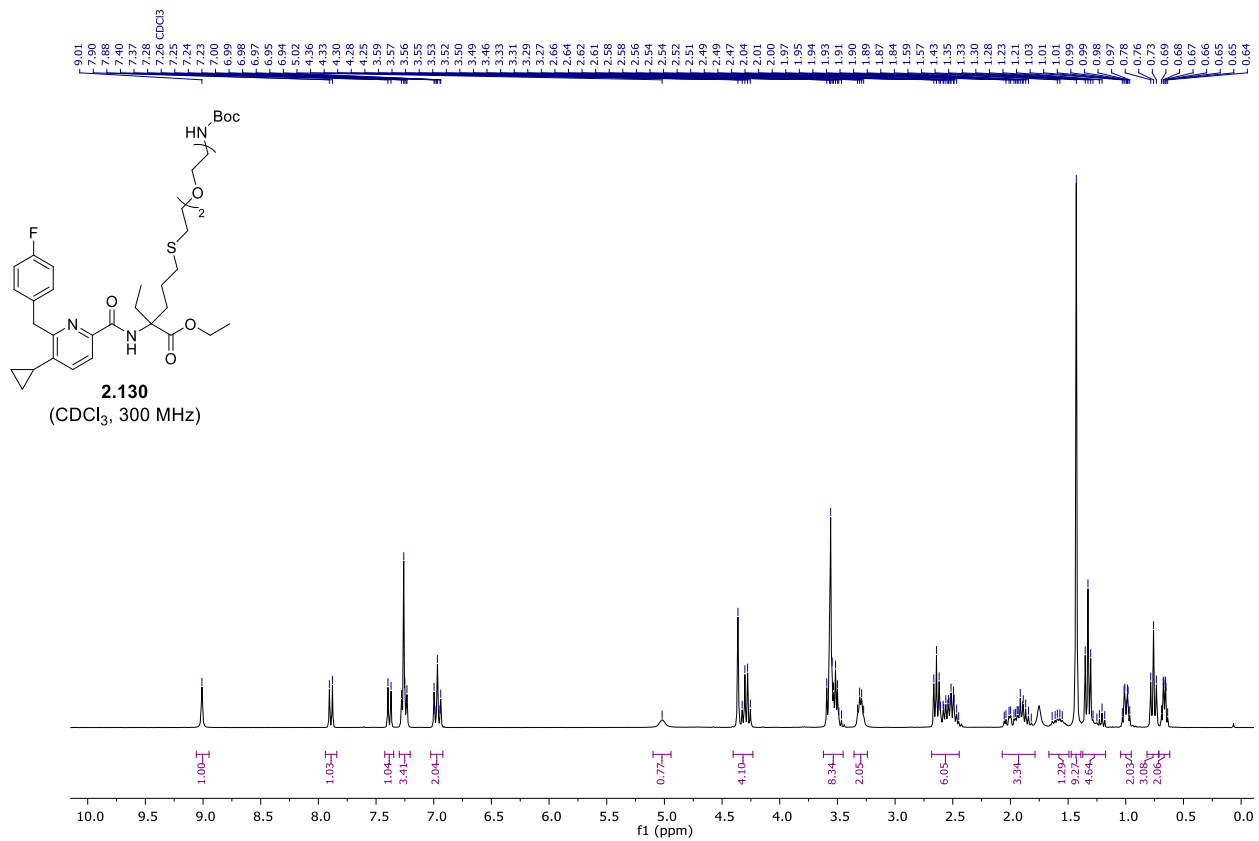


**2.128**  
(CDCl<sub>3</sub>, 300 MHz)

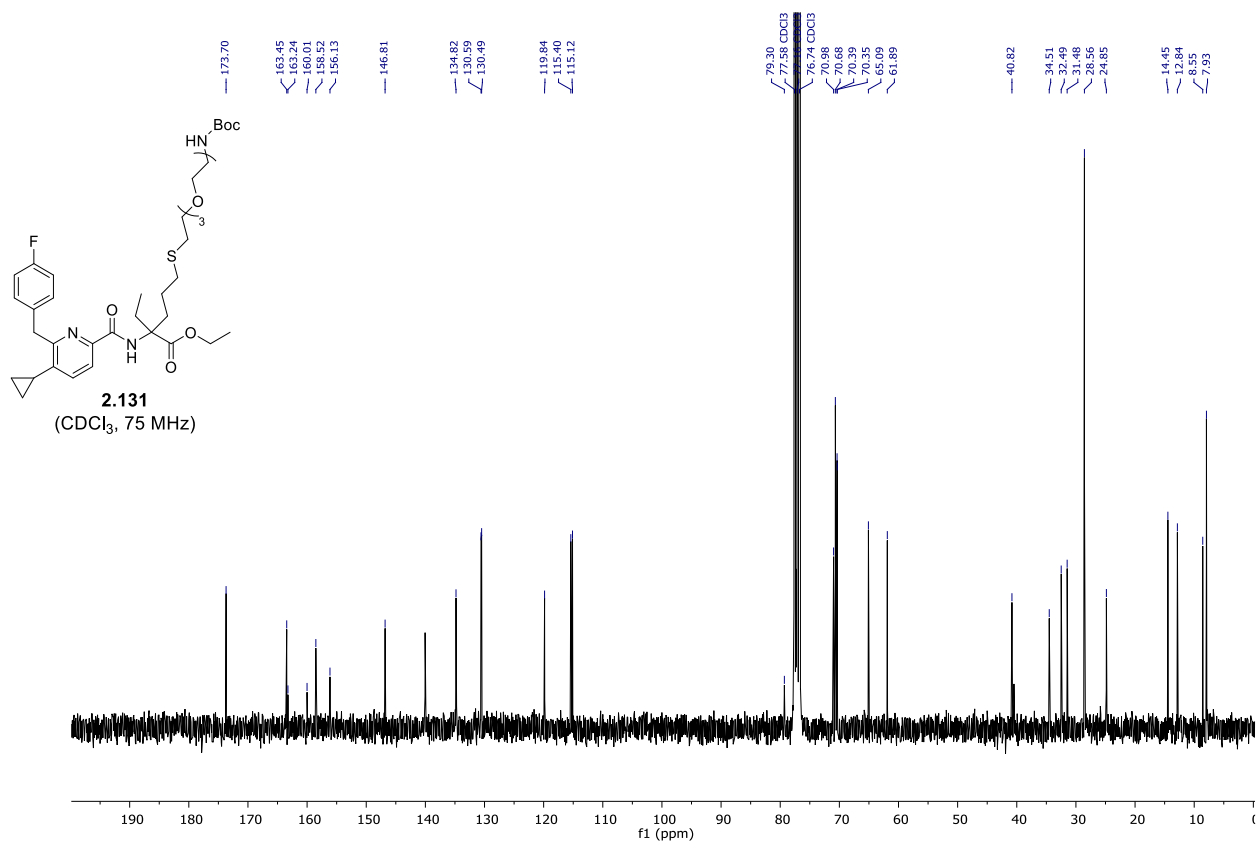
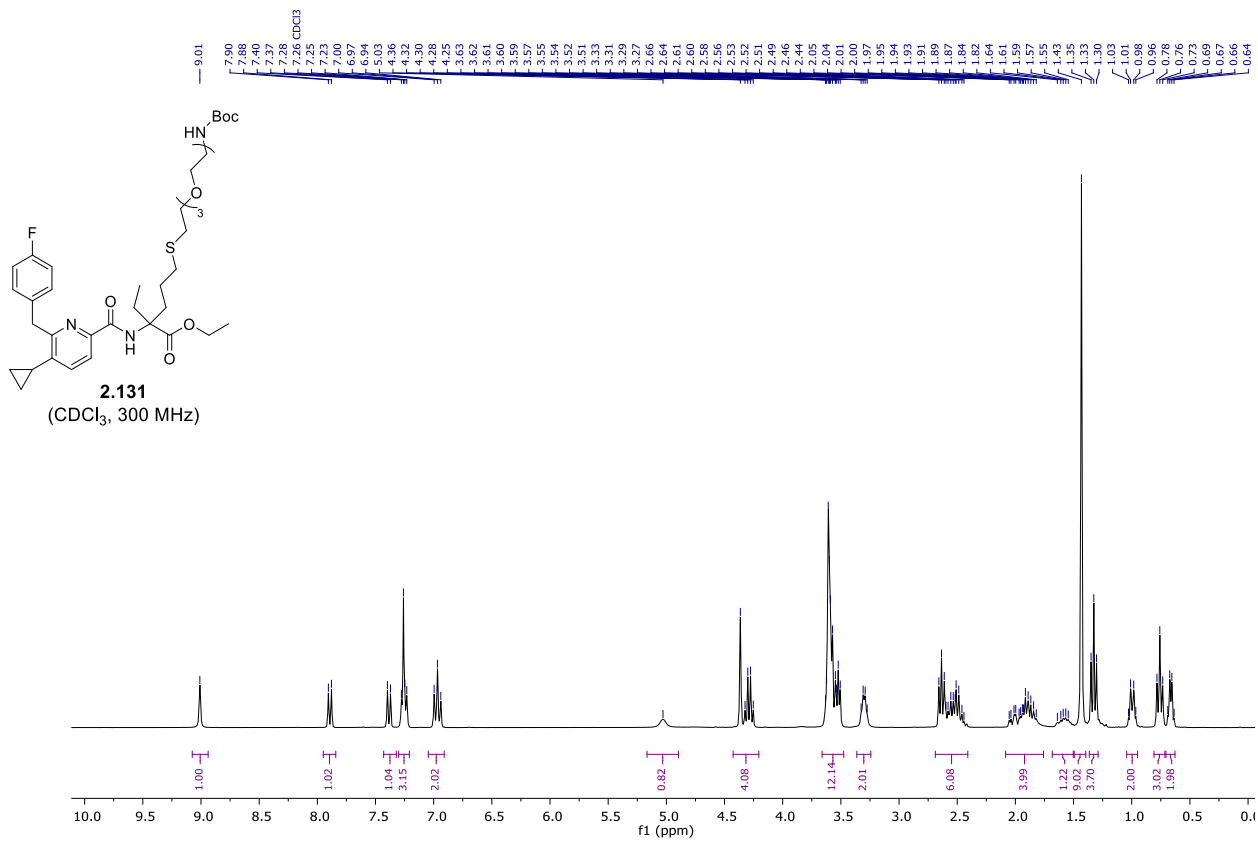


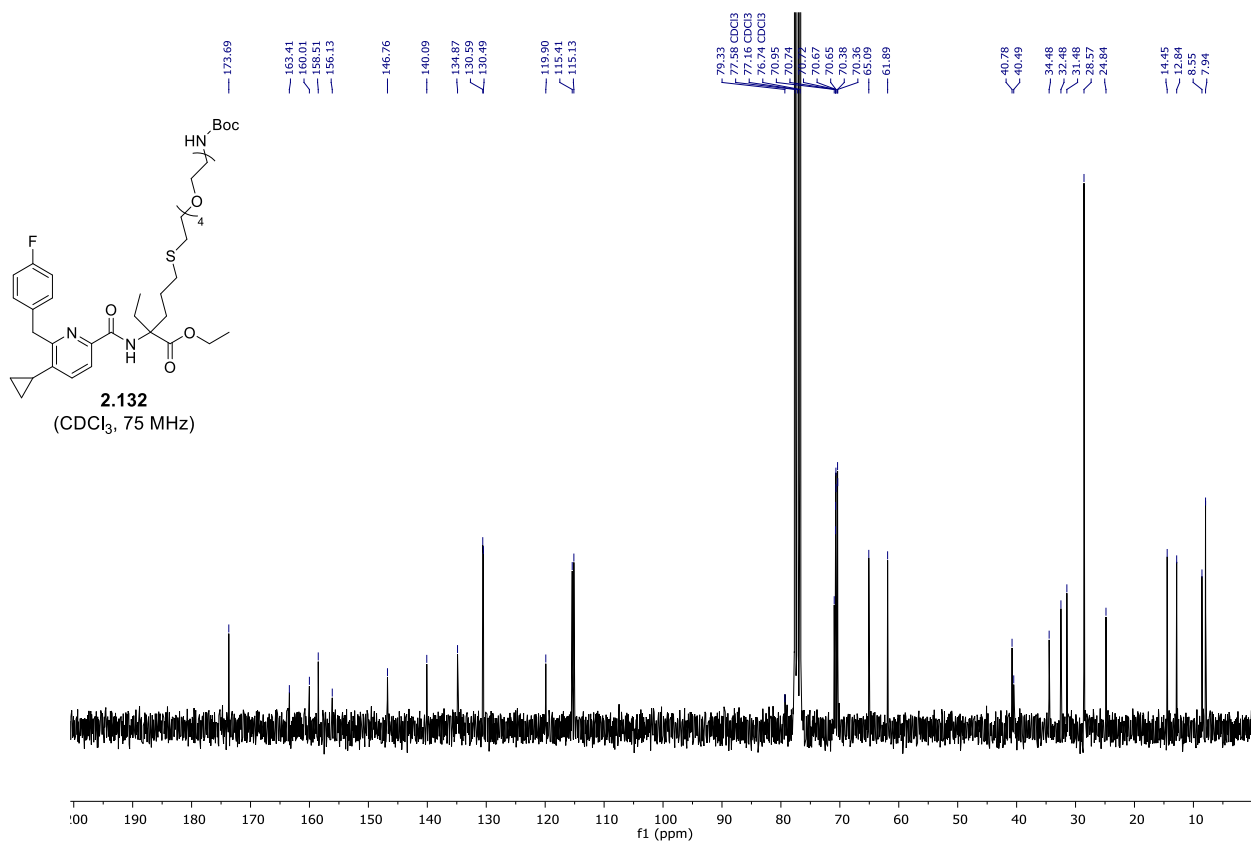
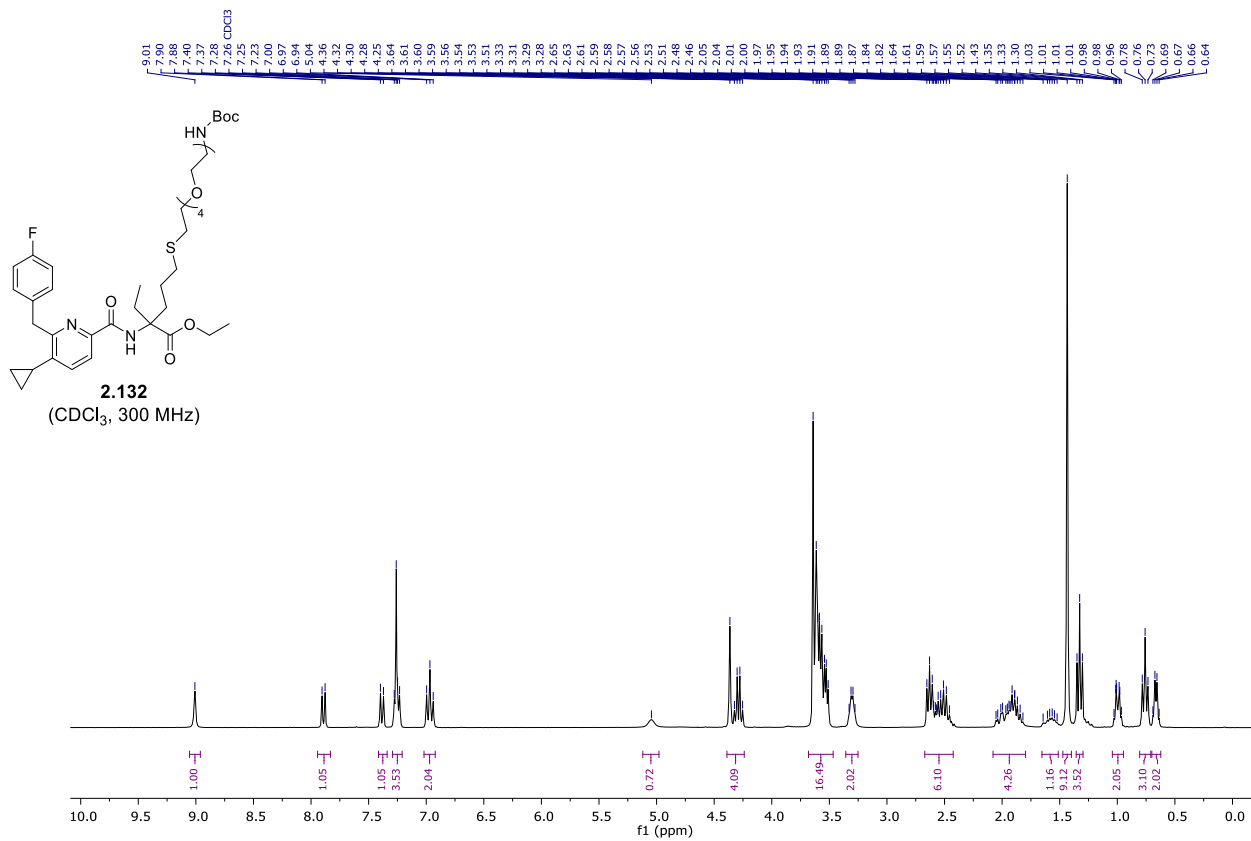


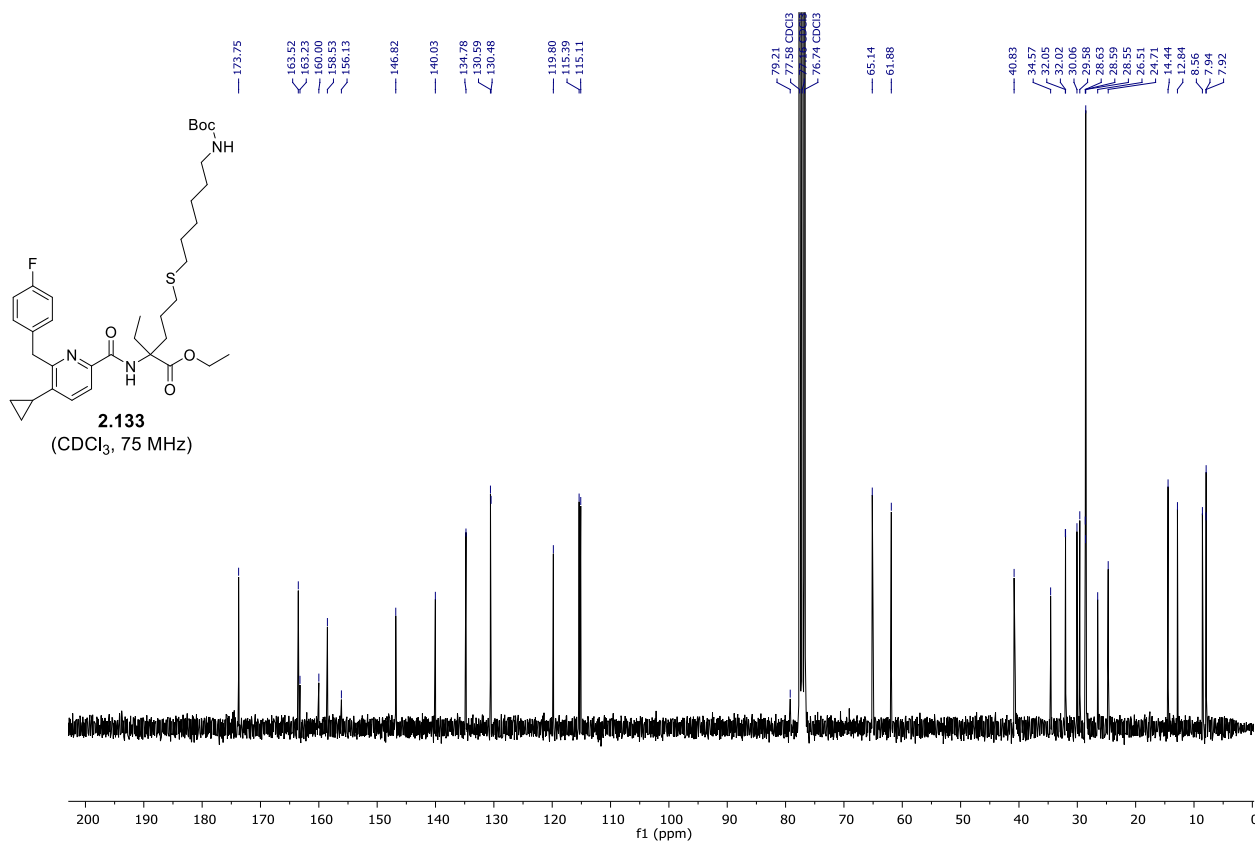
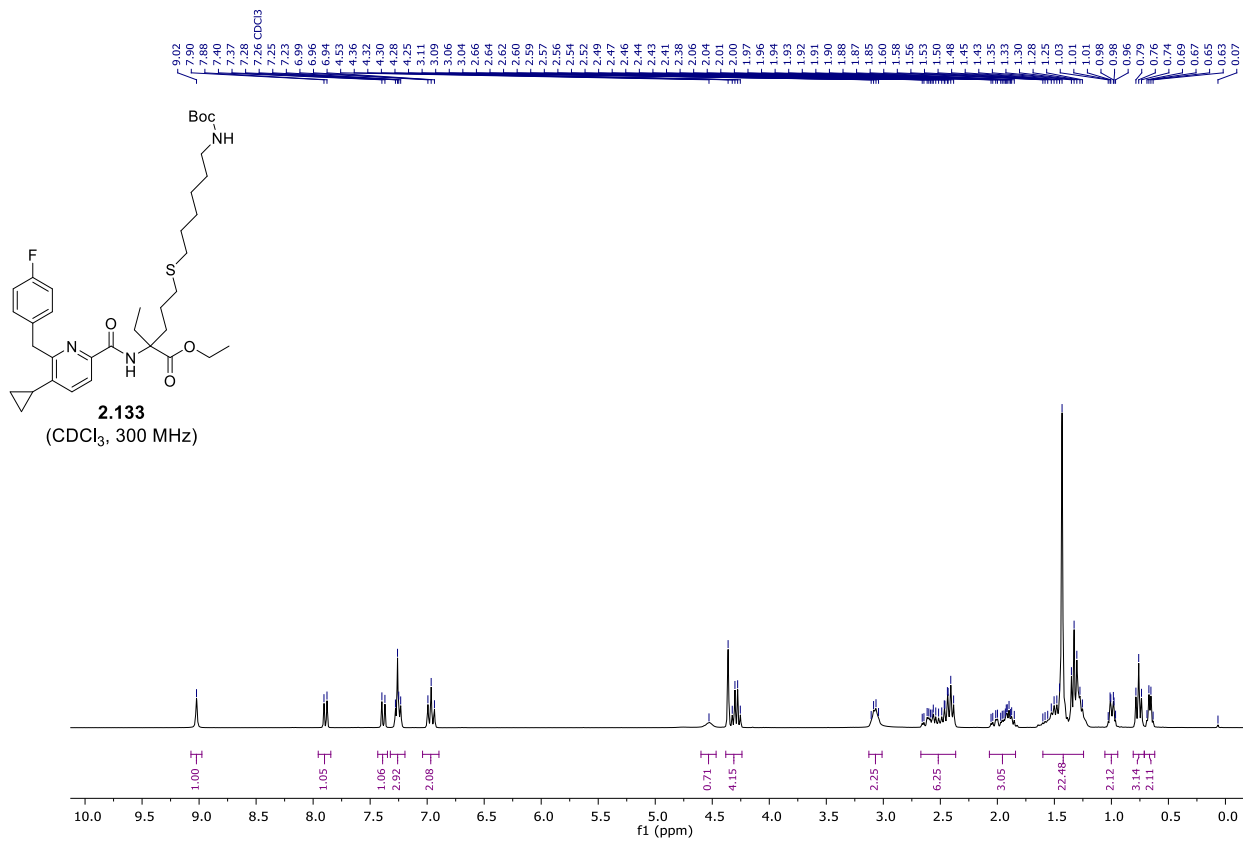


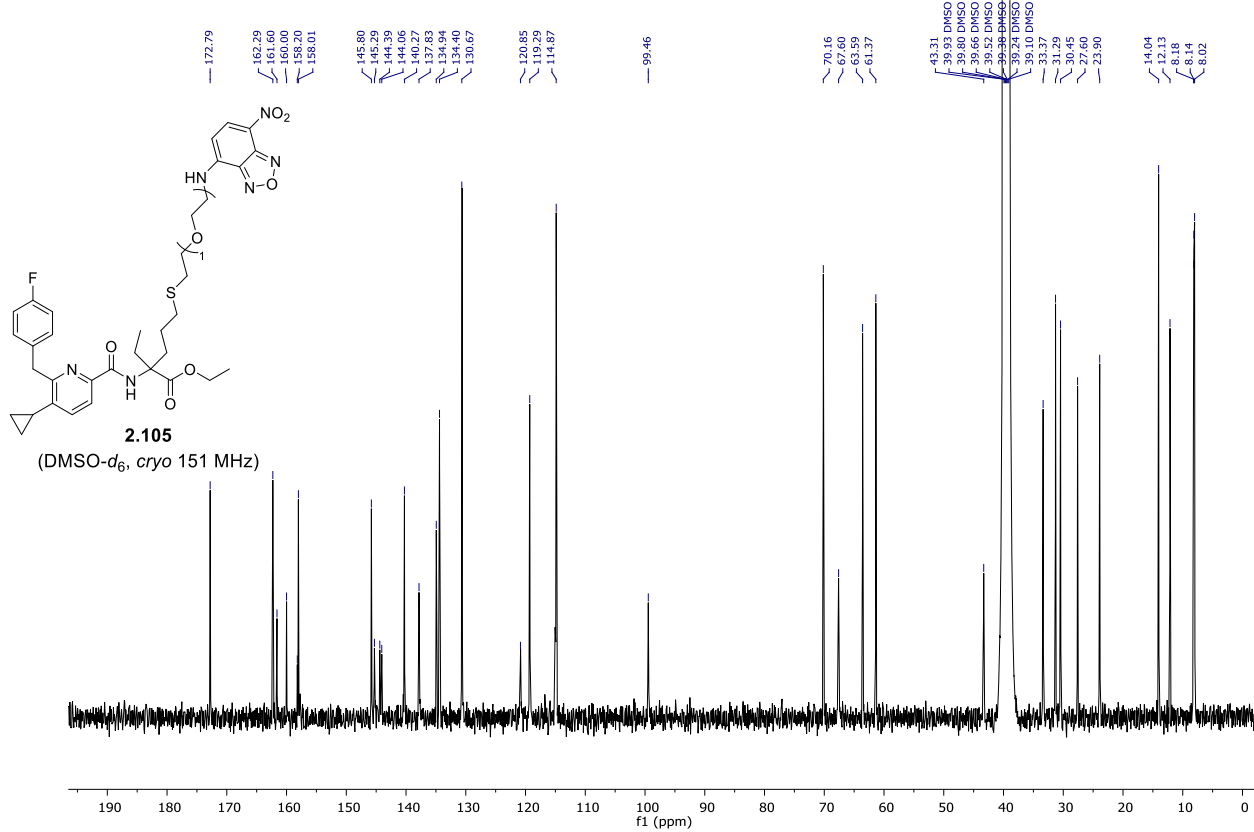
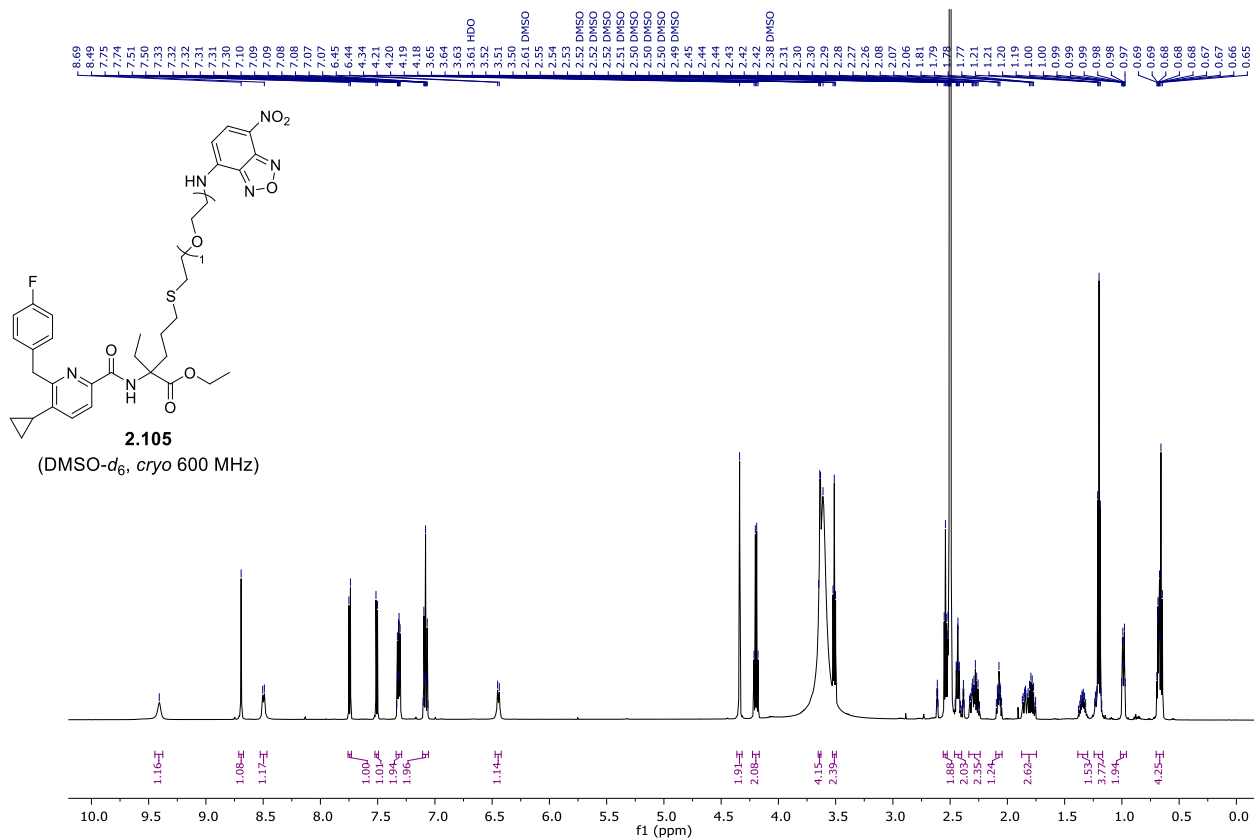


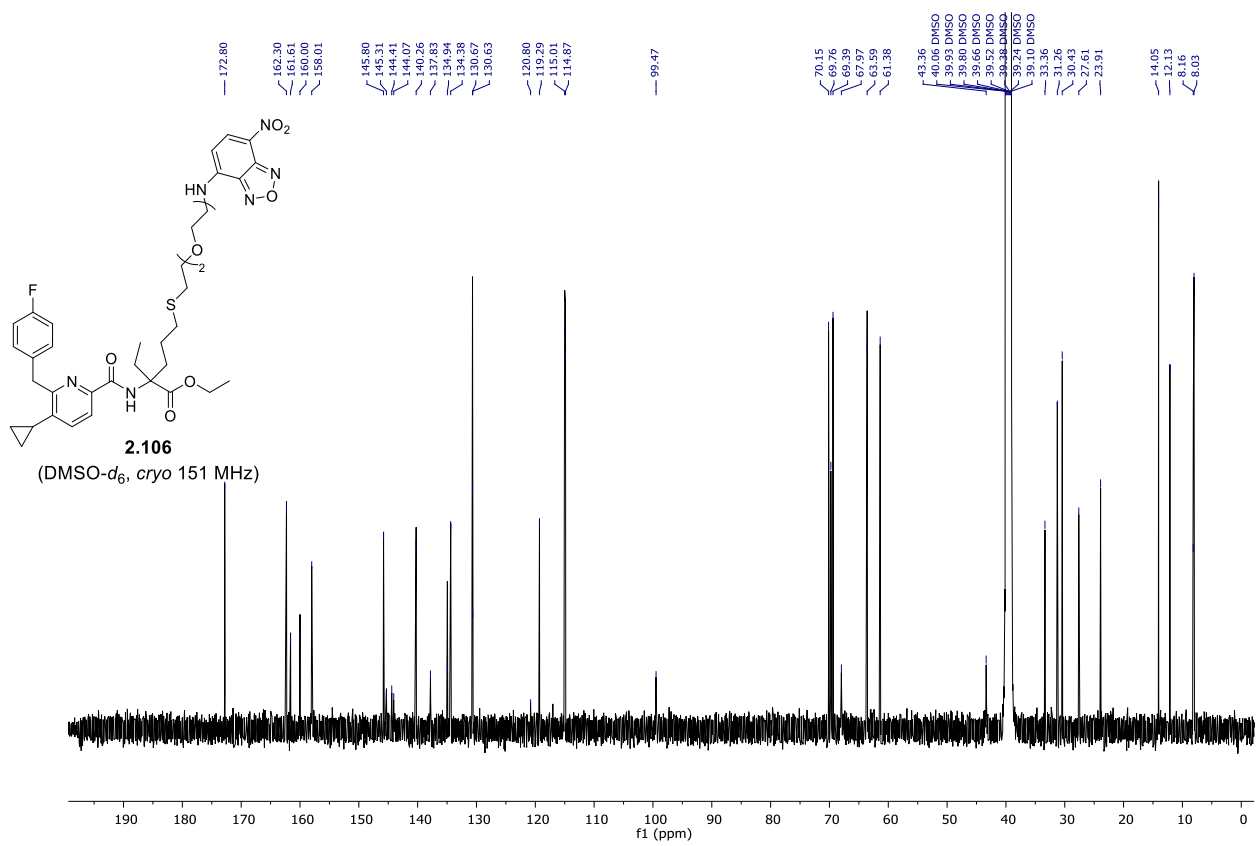
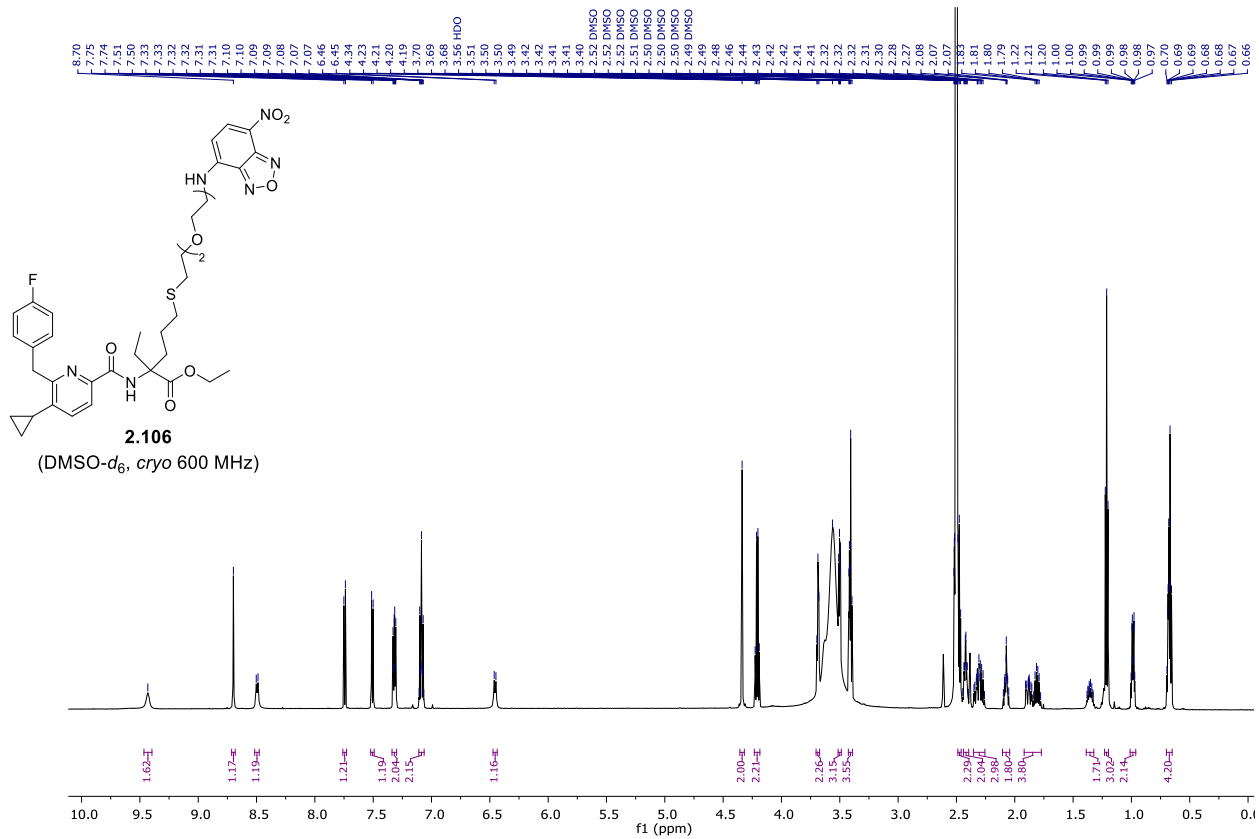


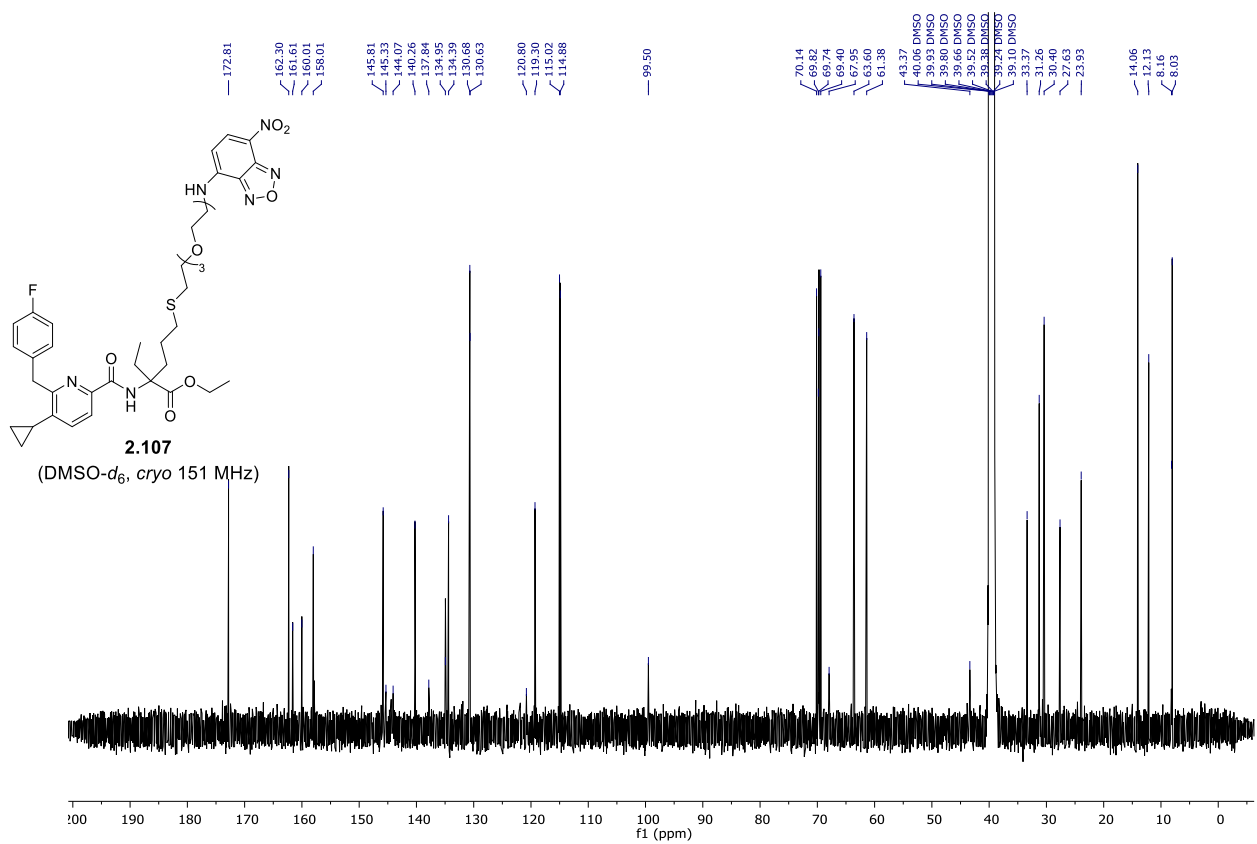
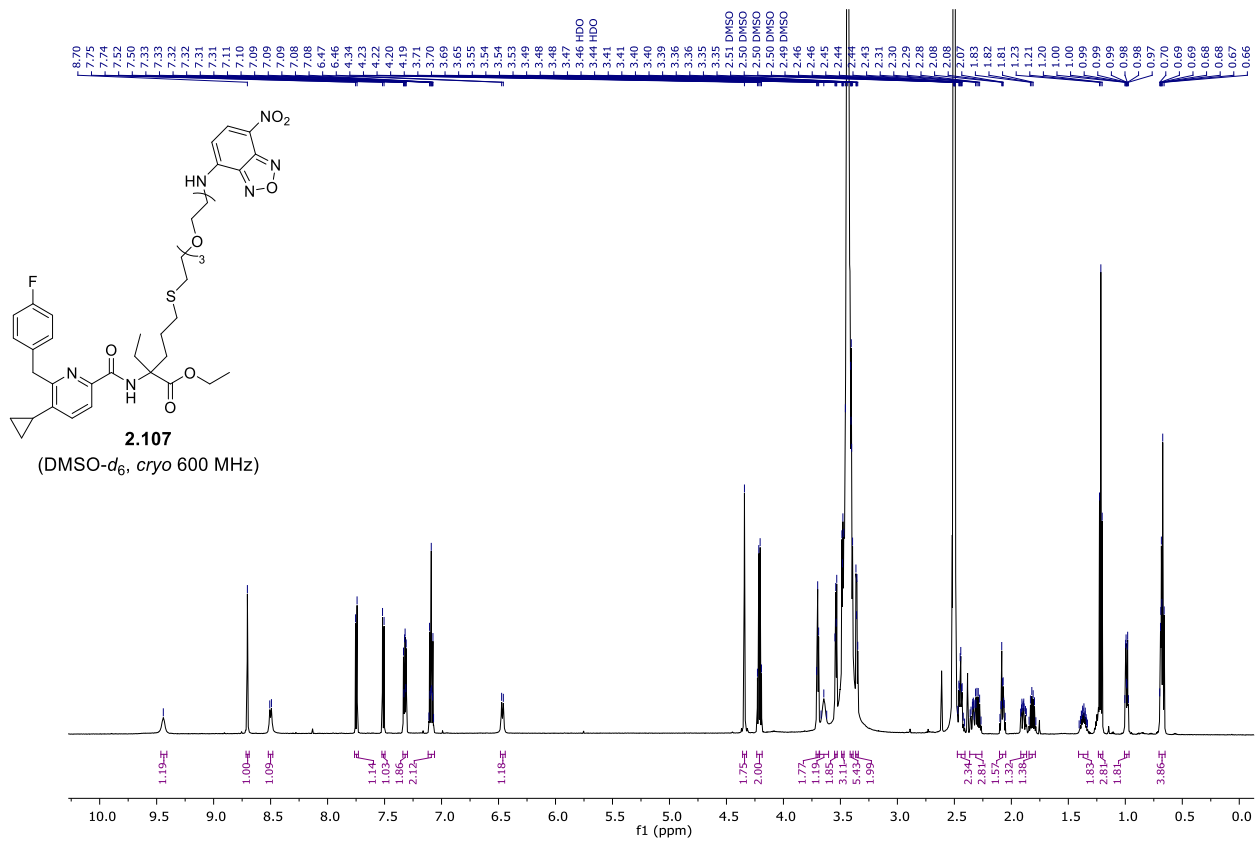


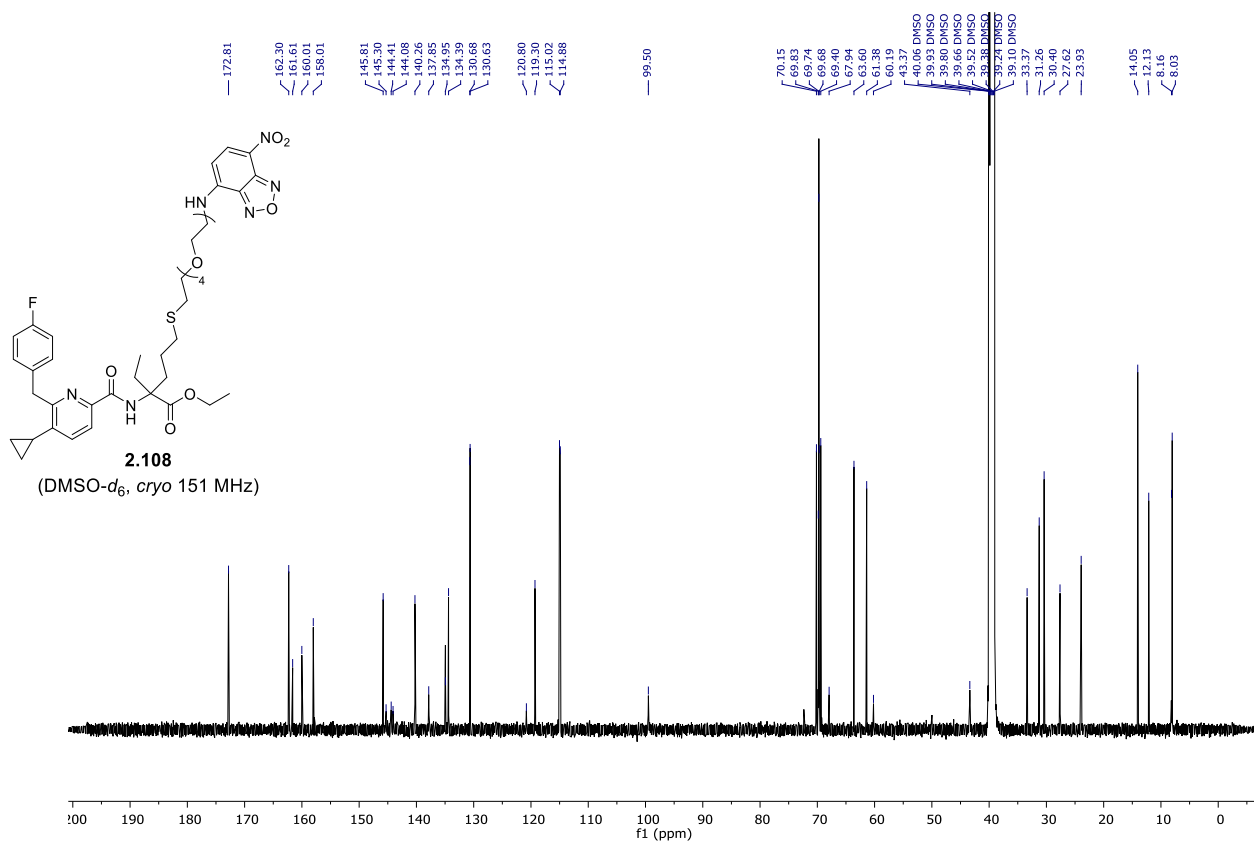
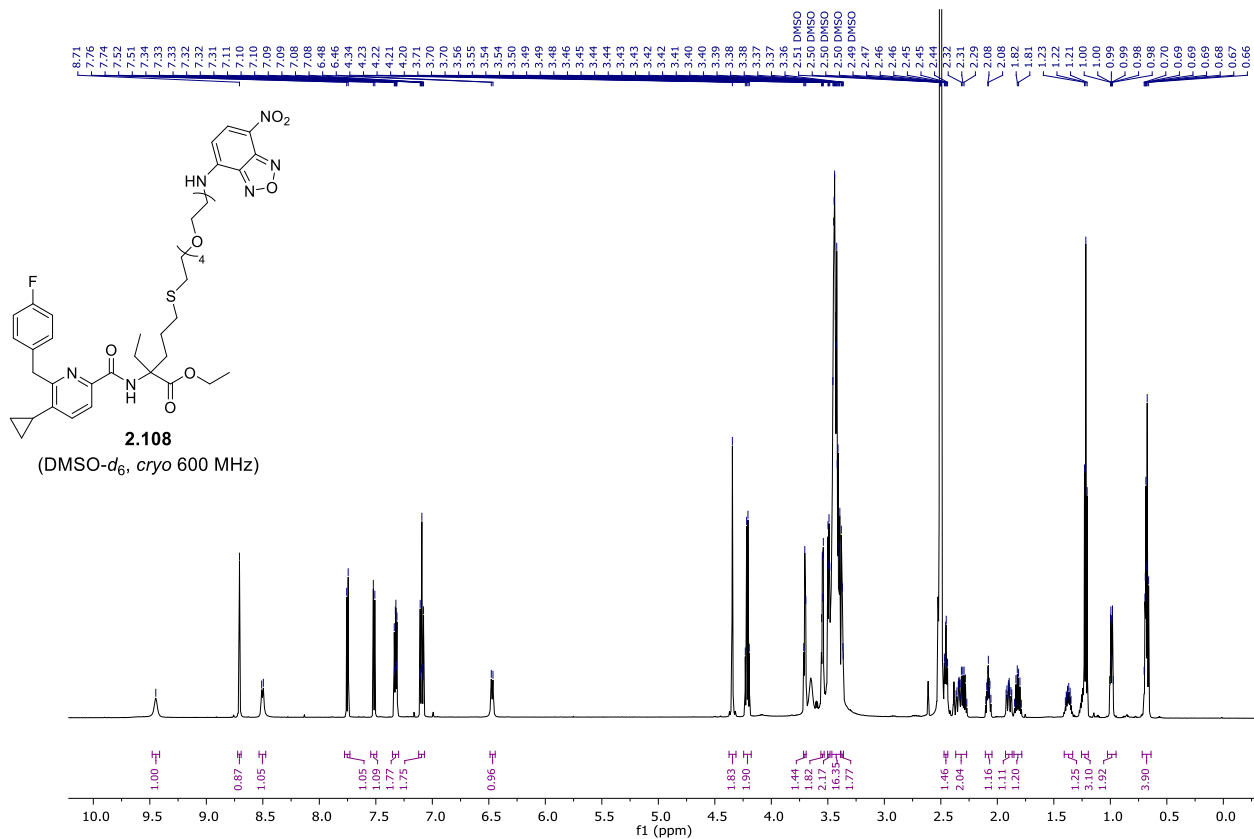


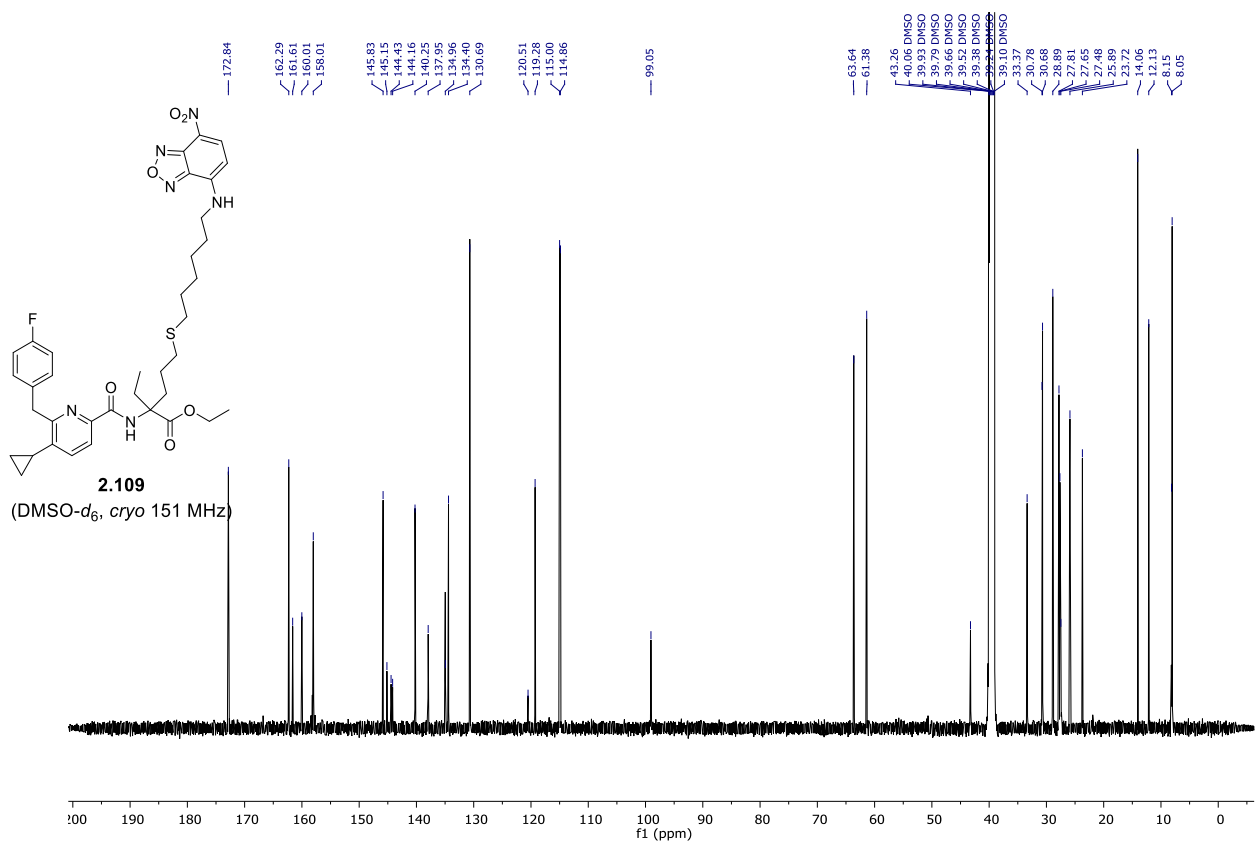
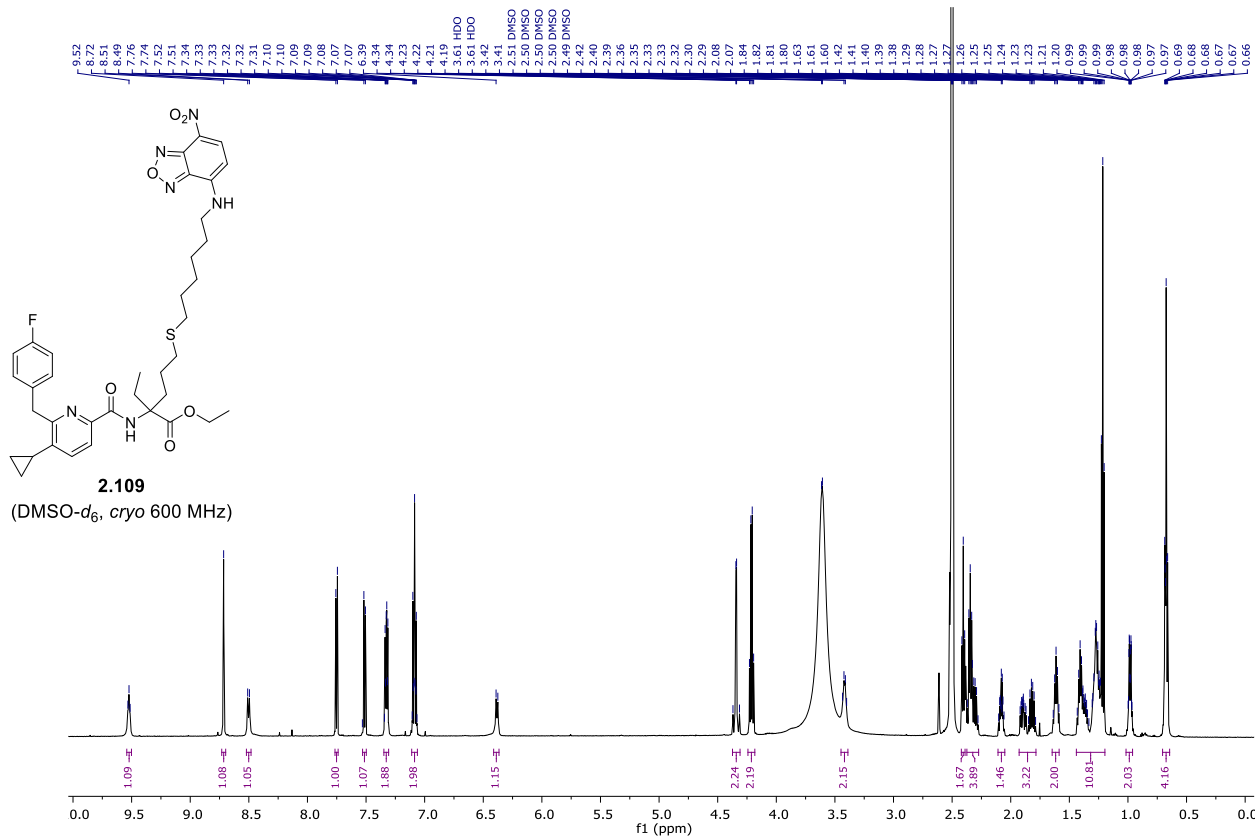




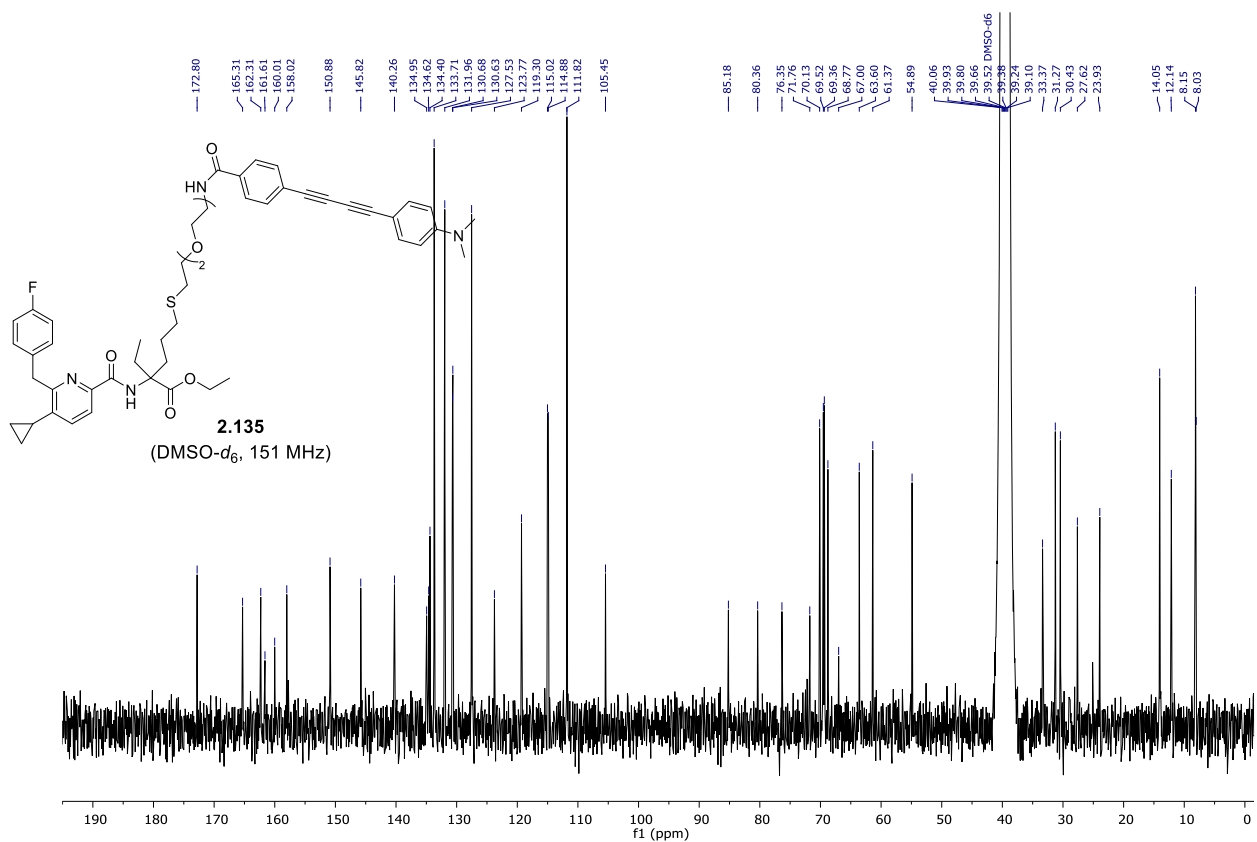
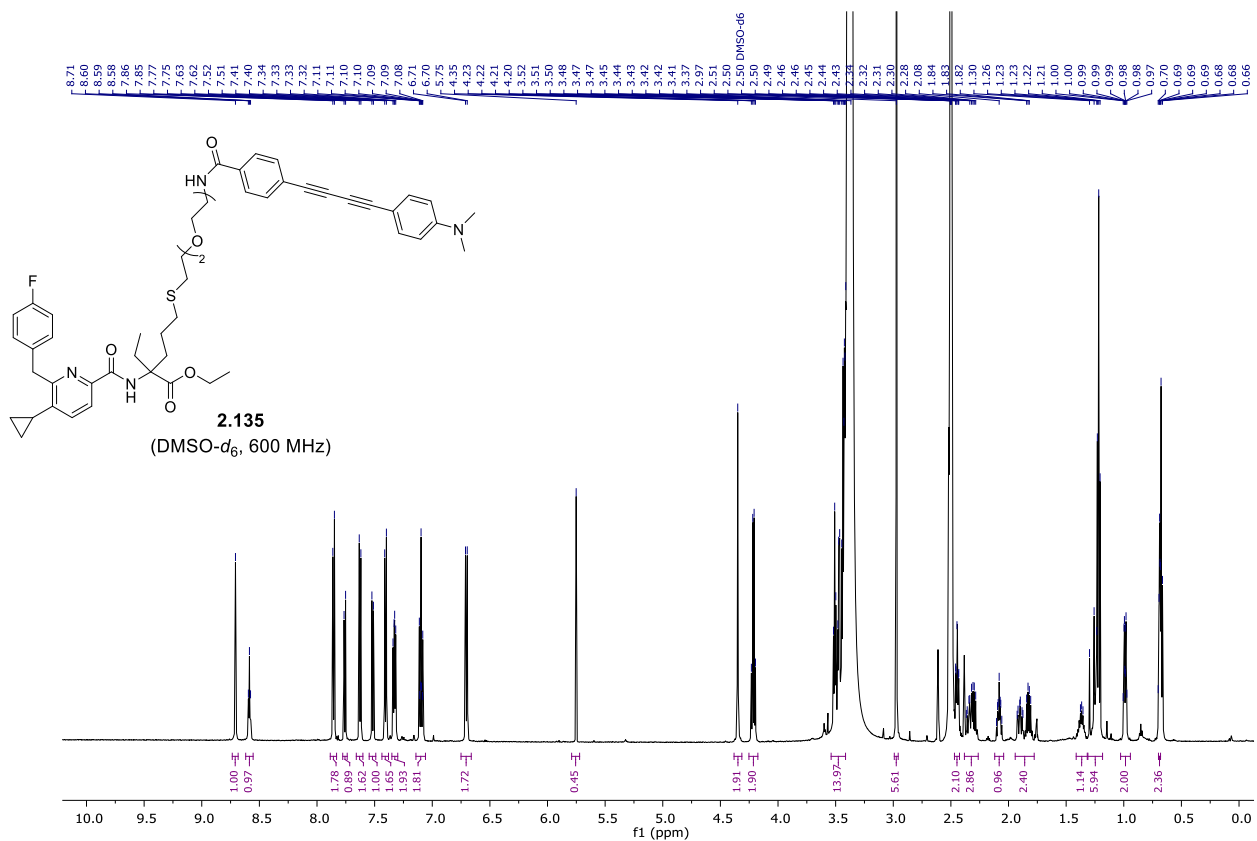




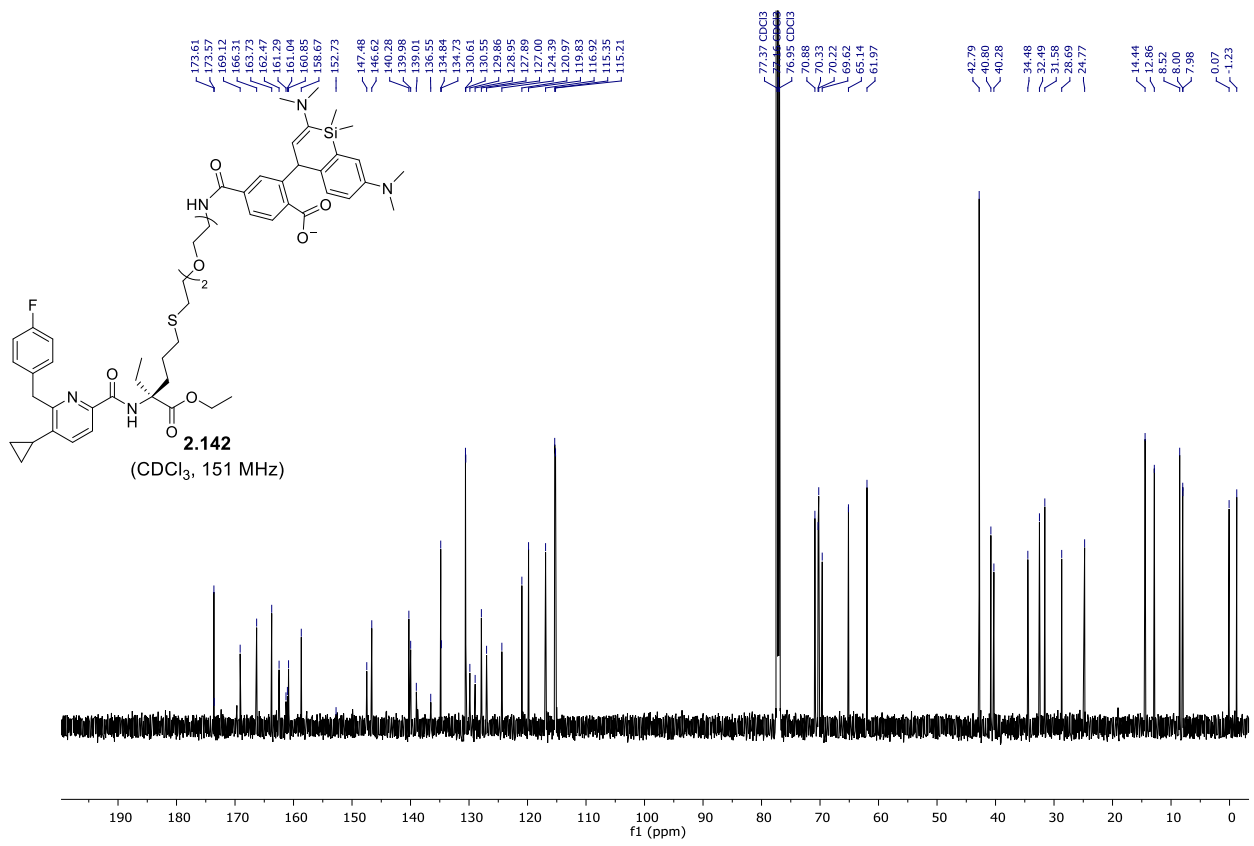
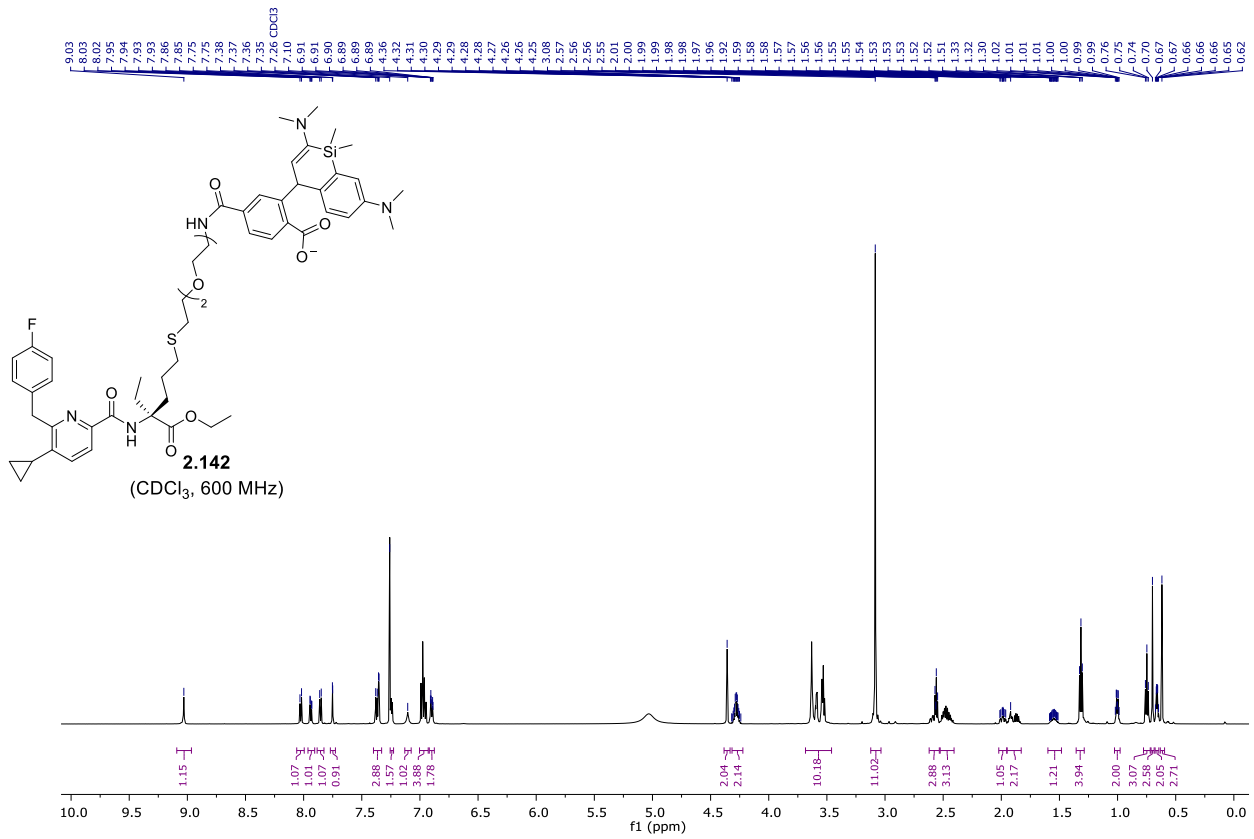


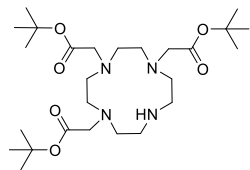




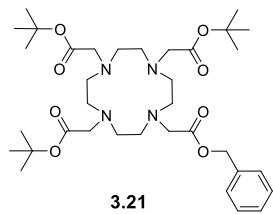
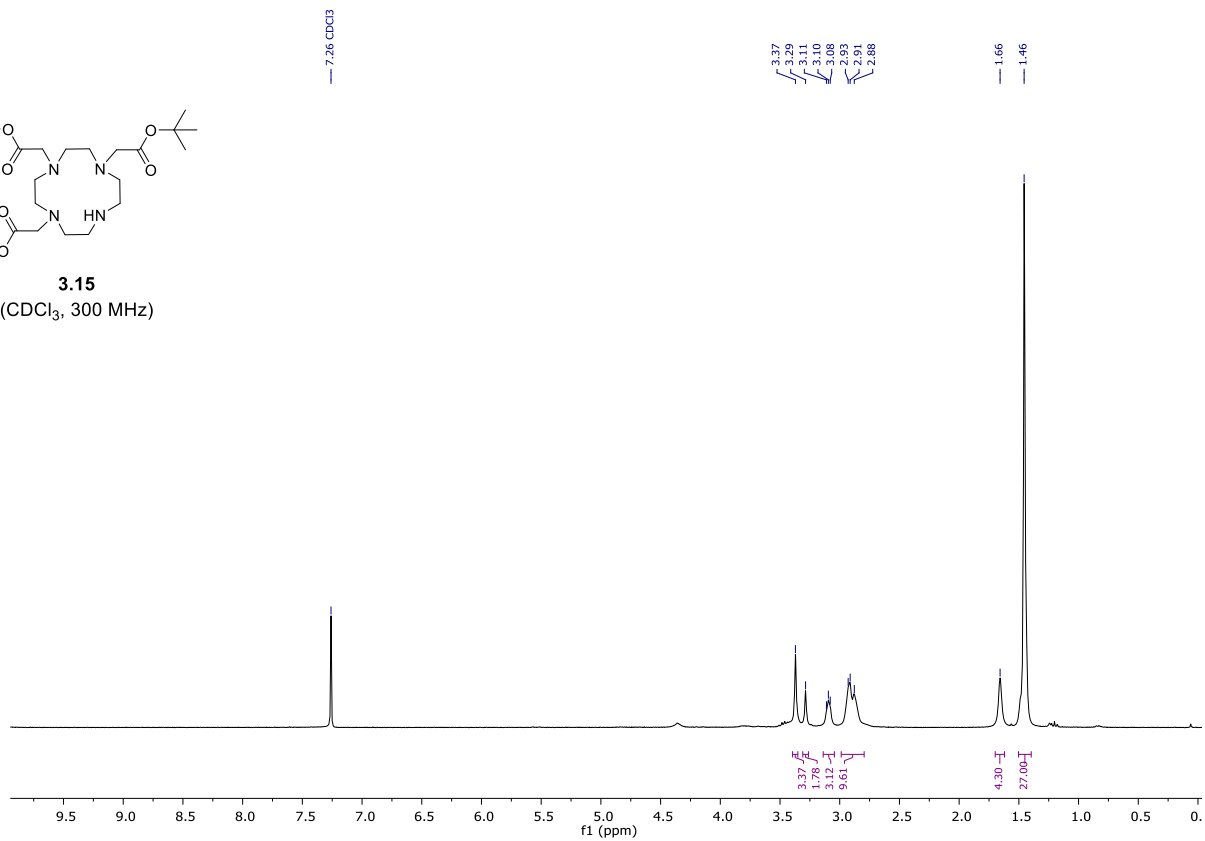




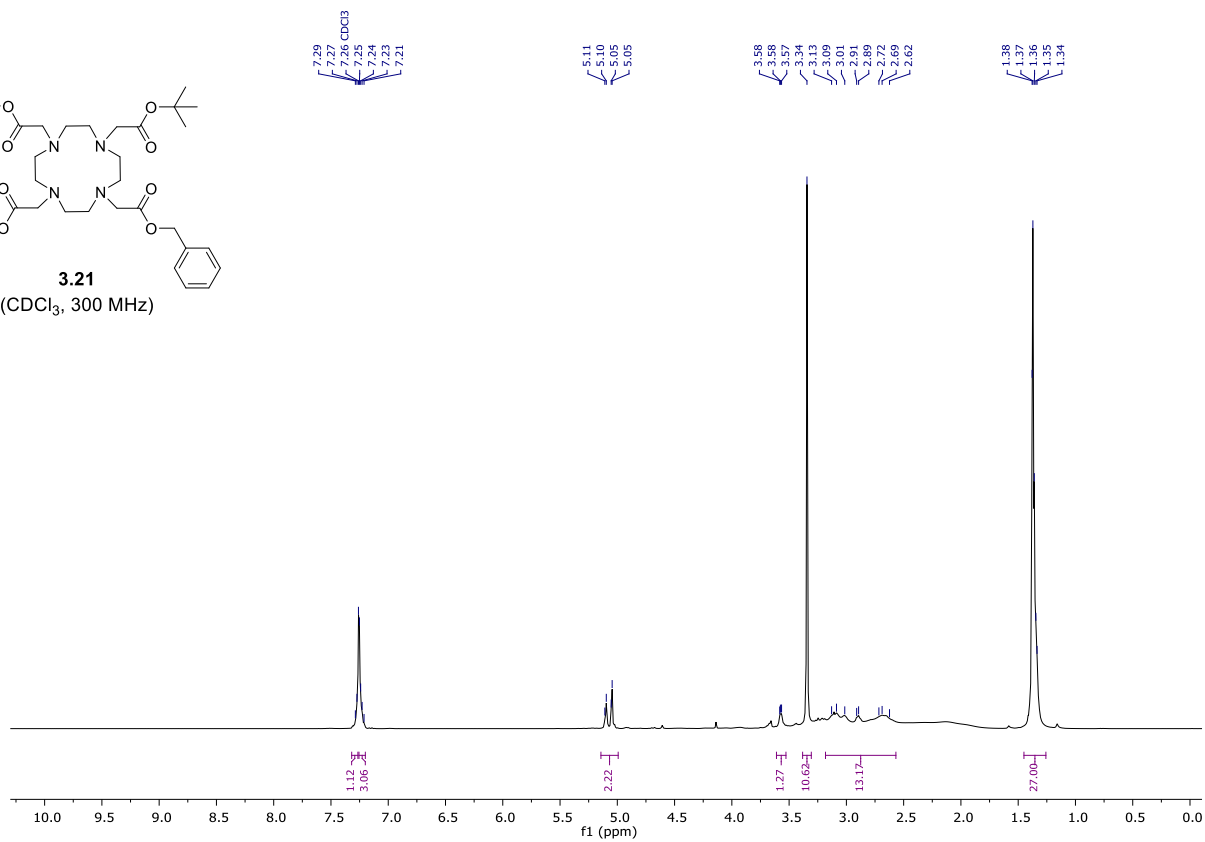


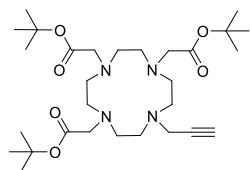


**3.15**  
(CDCl<sub>3</sub>, 300 MHz)

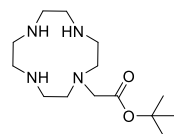
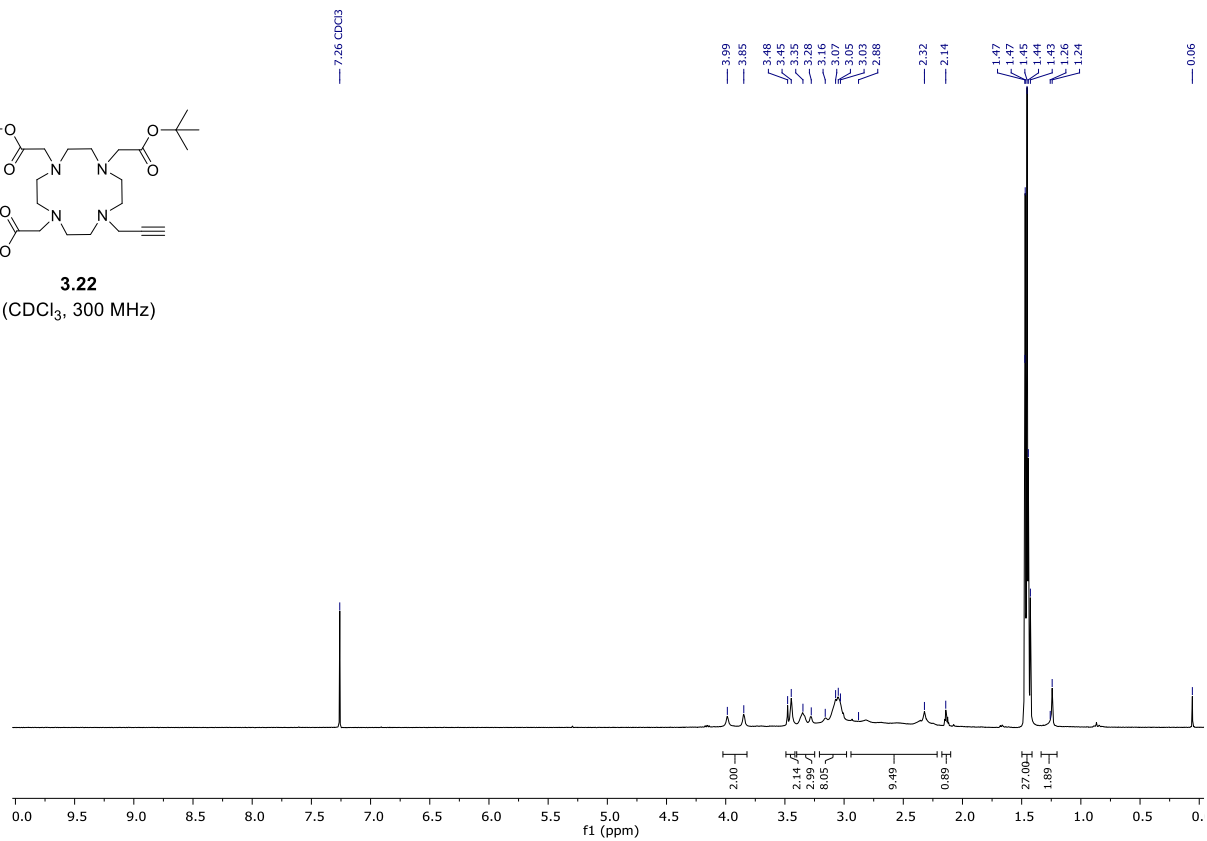


**3.21**  
(CDCl<sub>3</sub>, 300 MHz)

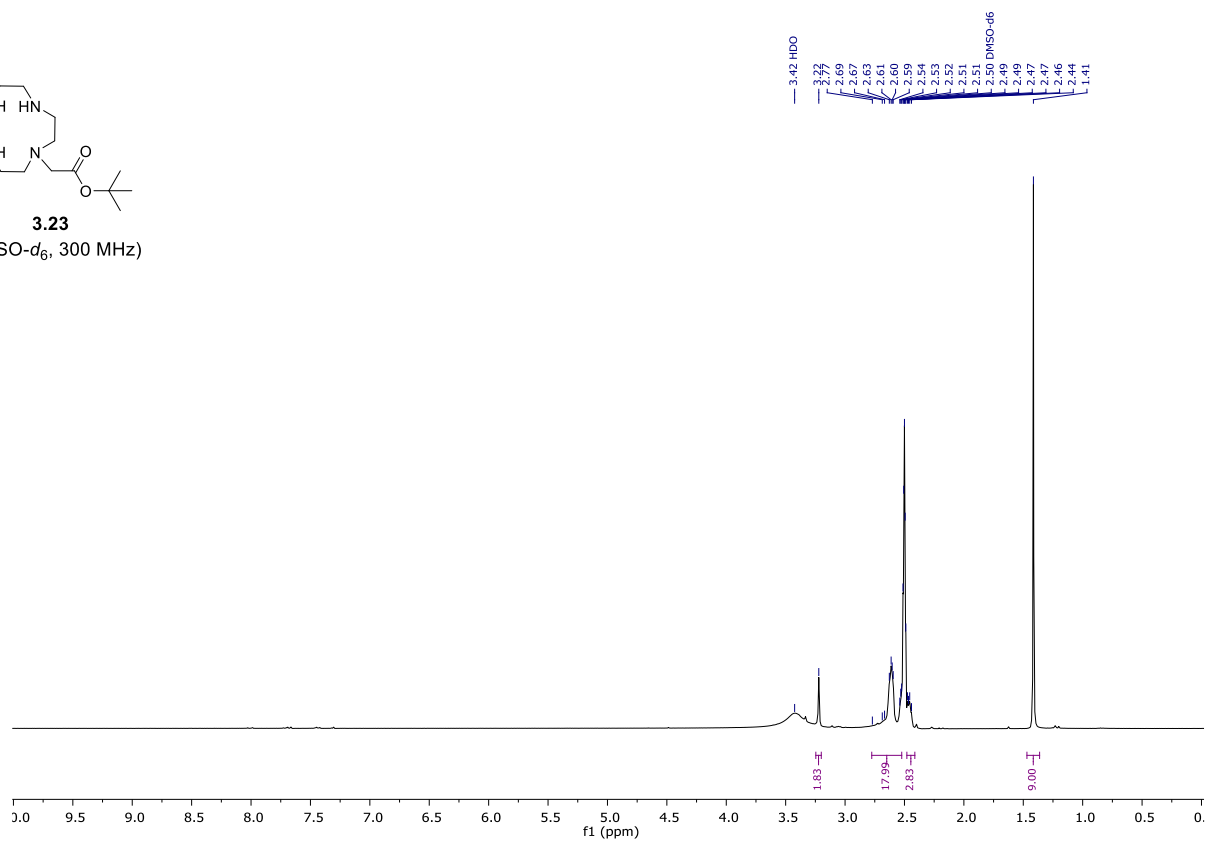


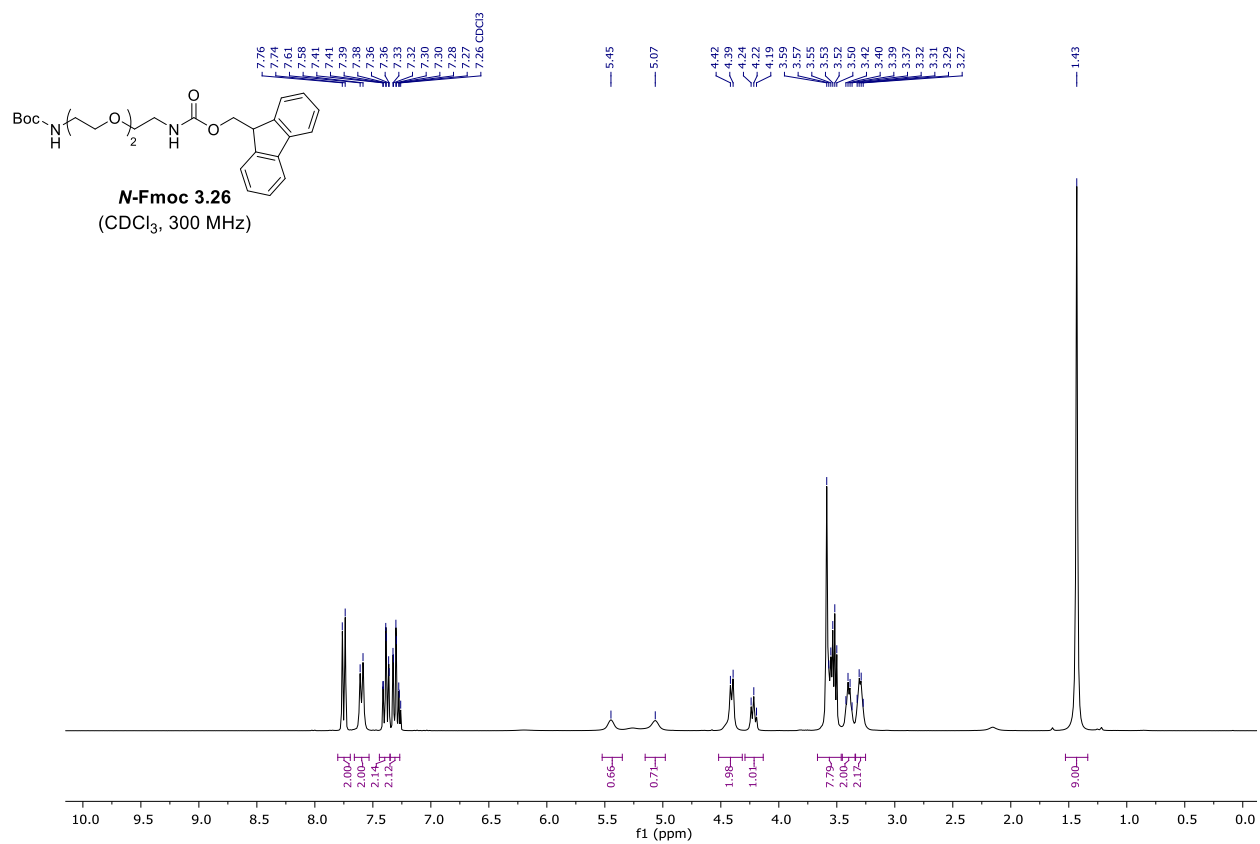
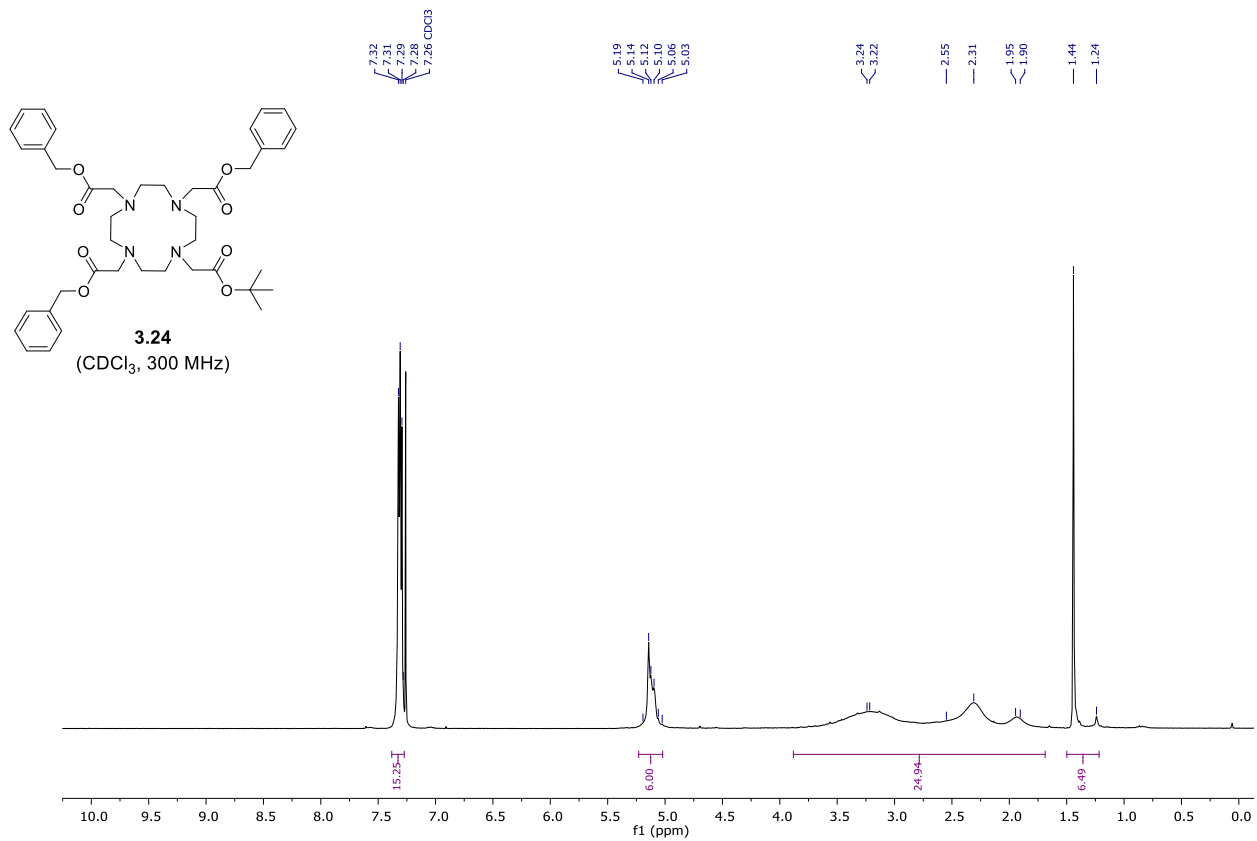


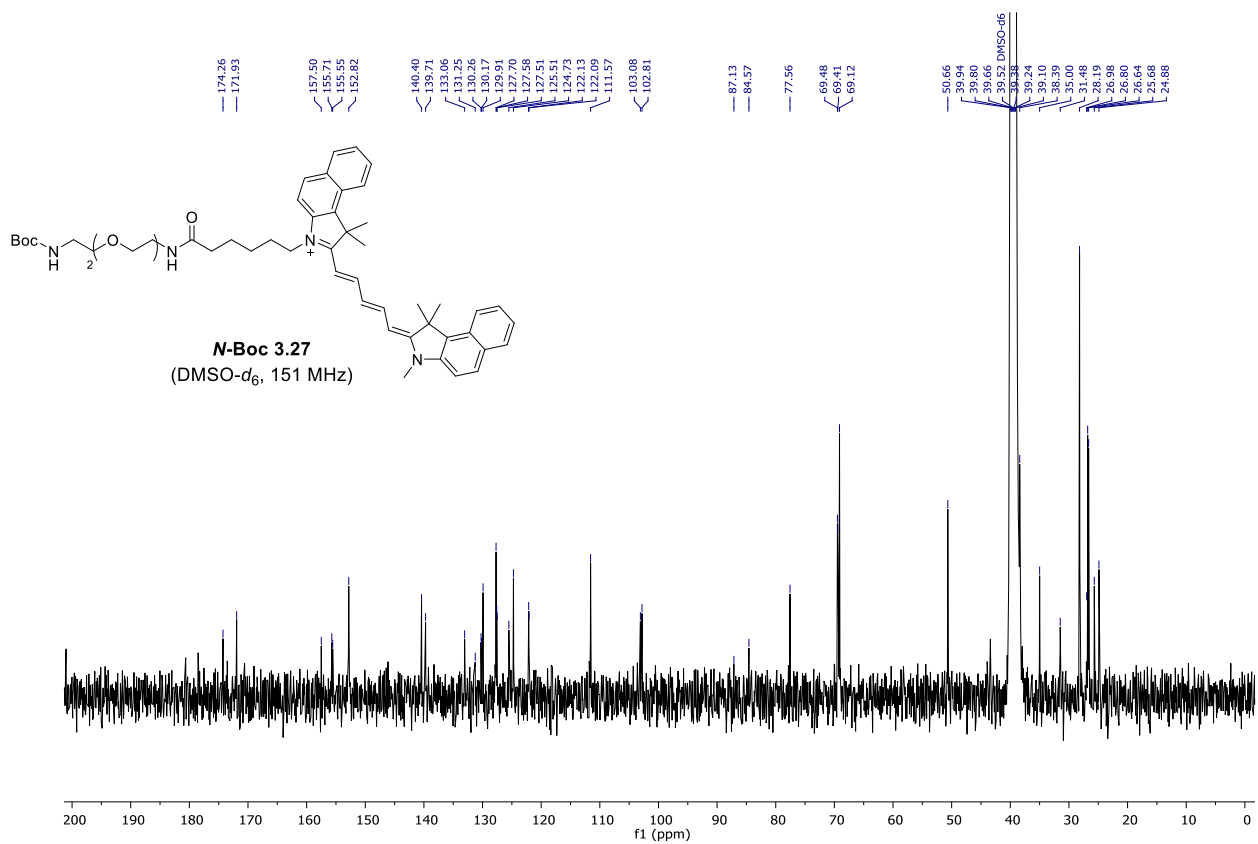
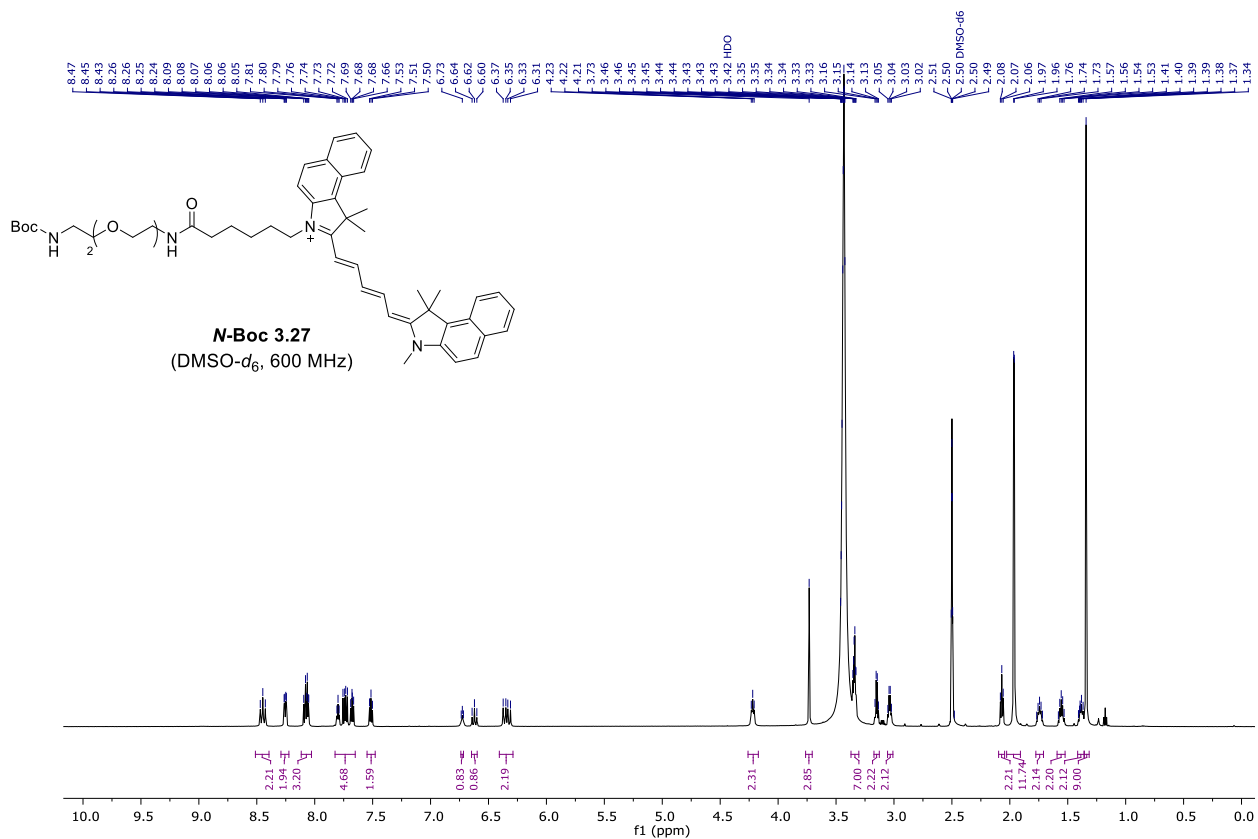
**3.22**  
(CDCl<sub>3</sub>, 300 MHz)

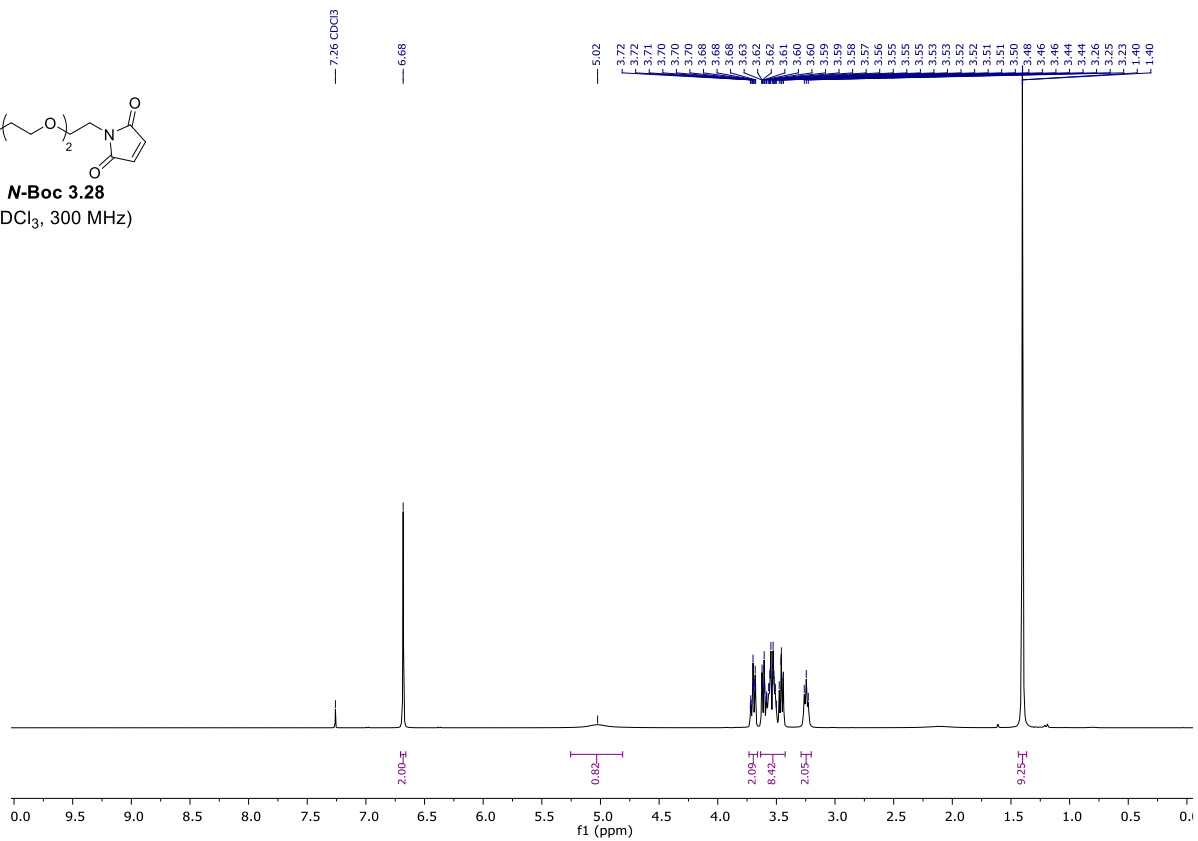
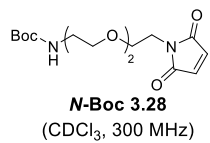


**3.23**  
(DMSO-d<sub>6</sub>, 300 MHz)



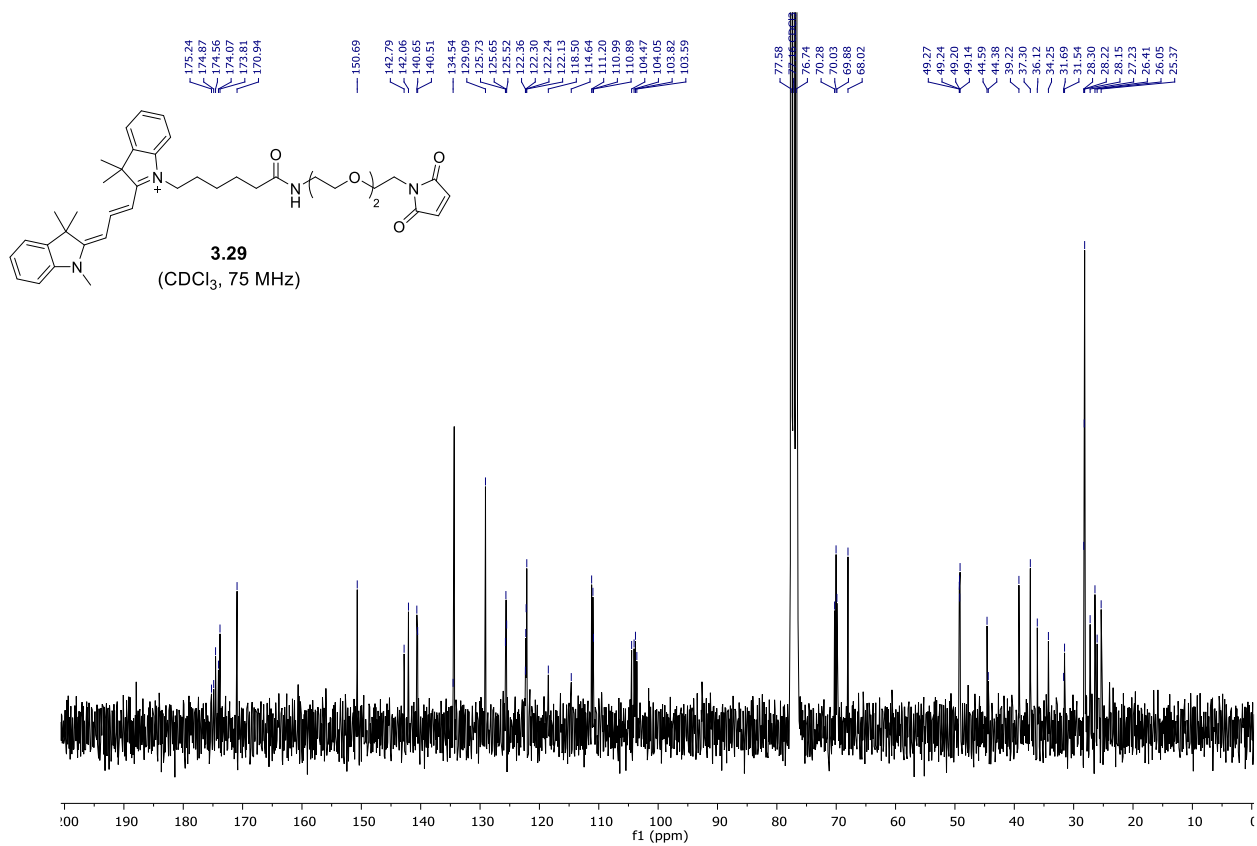
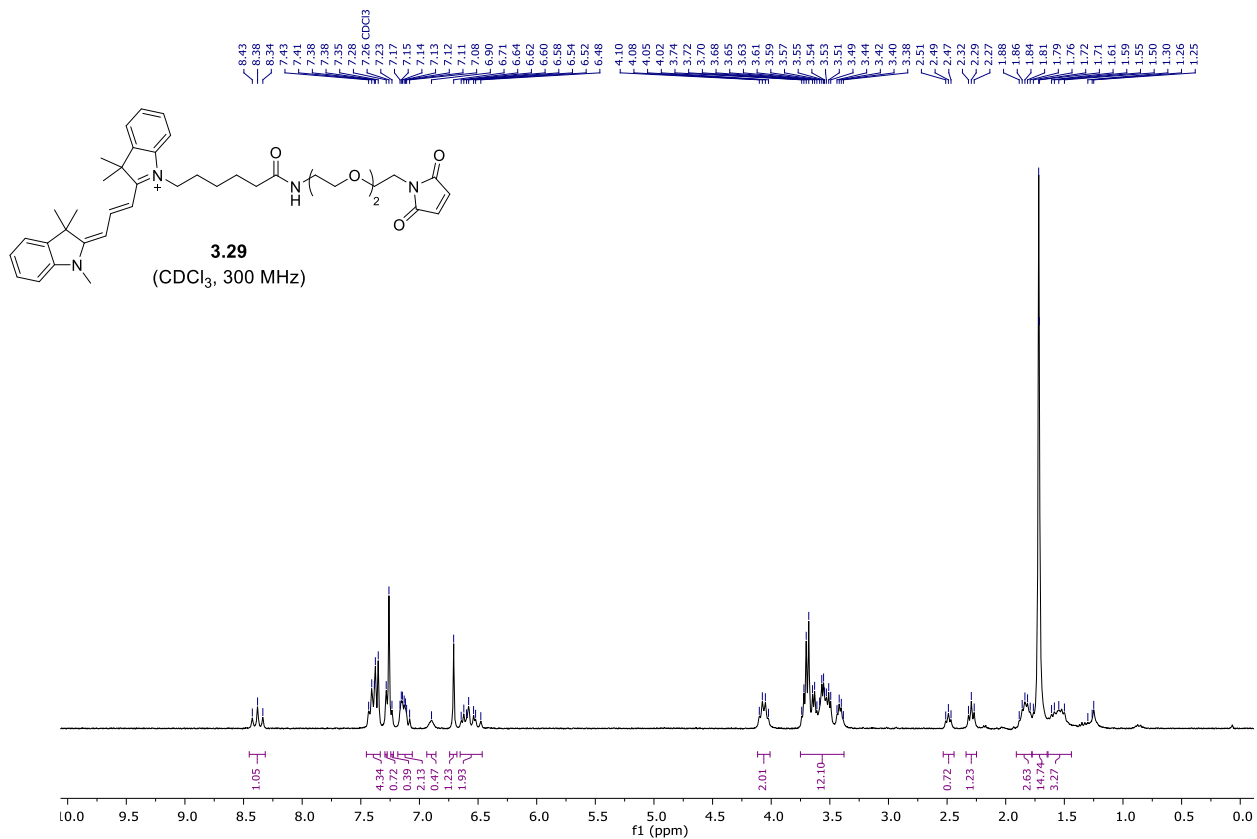


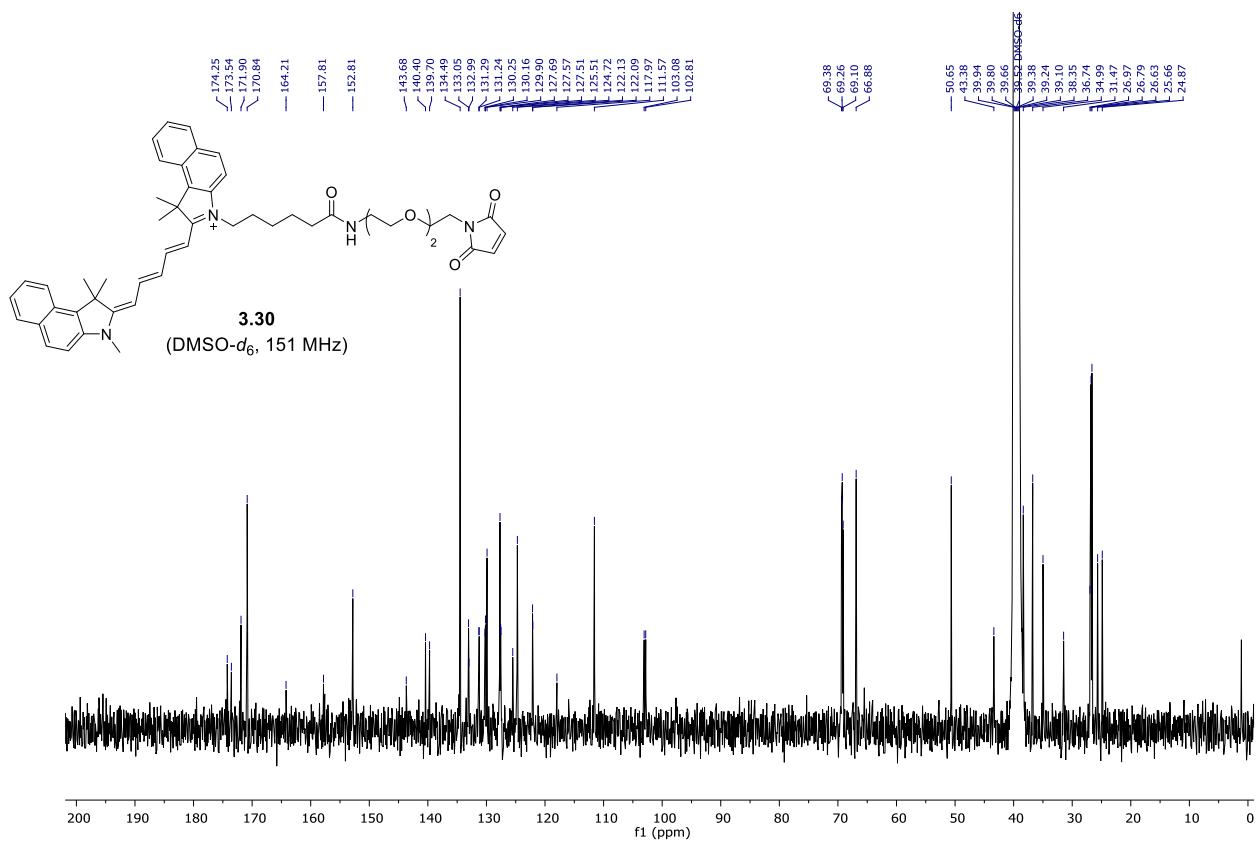
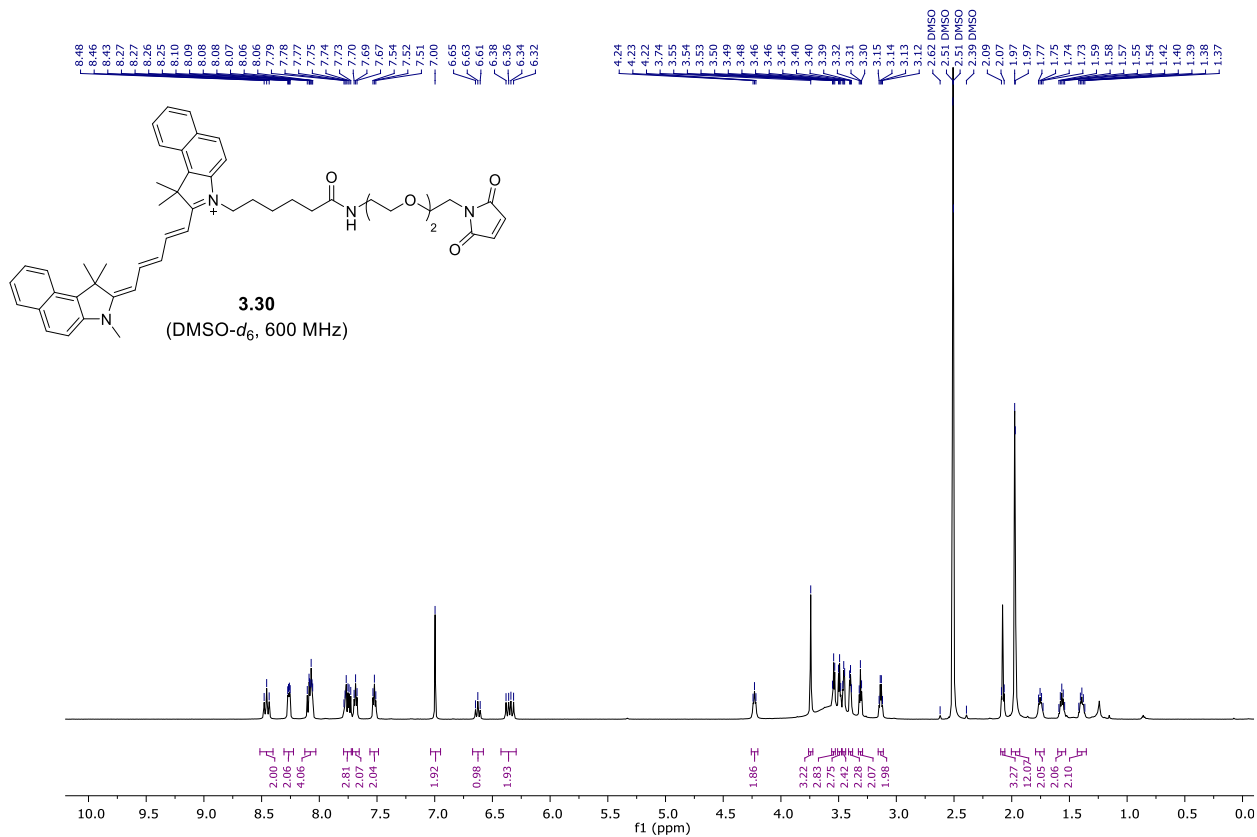


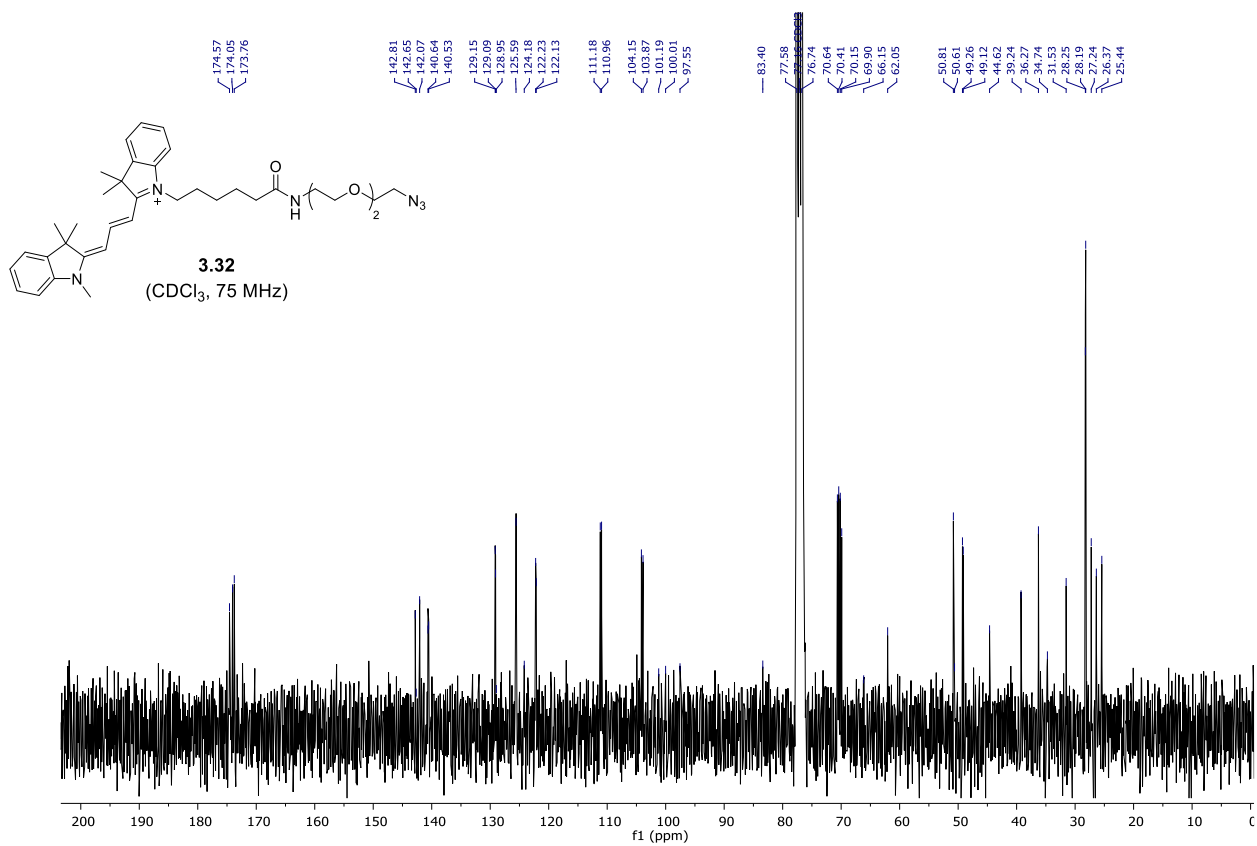
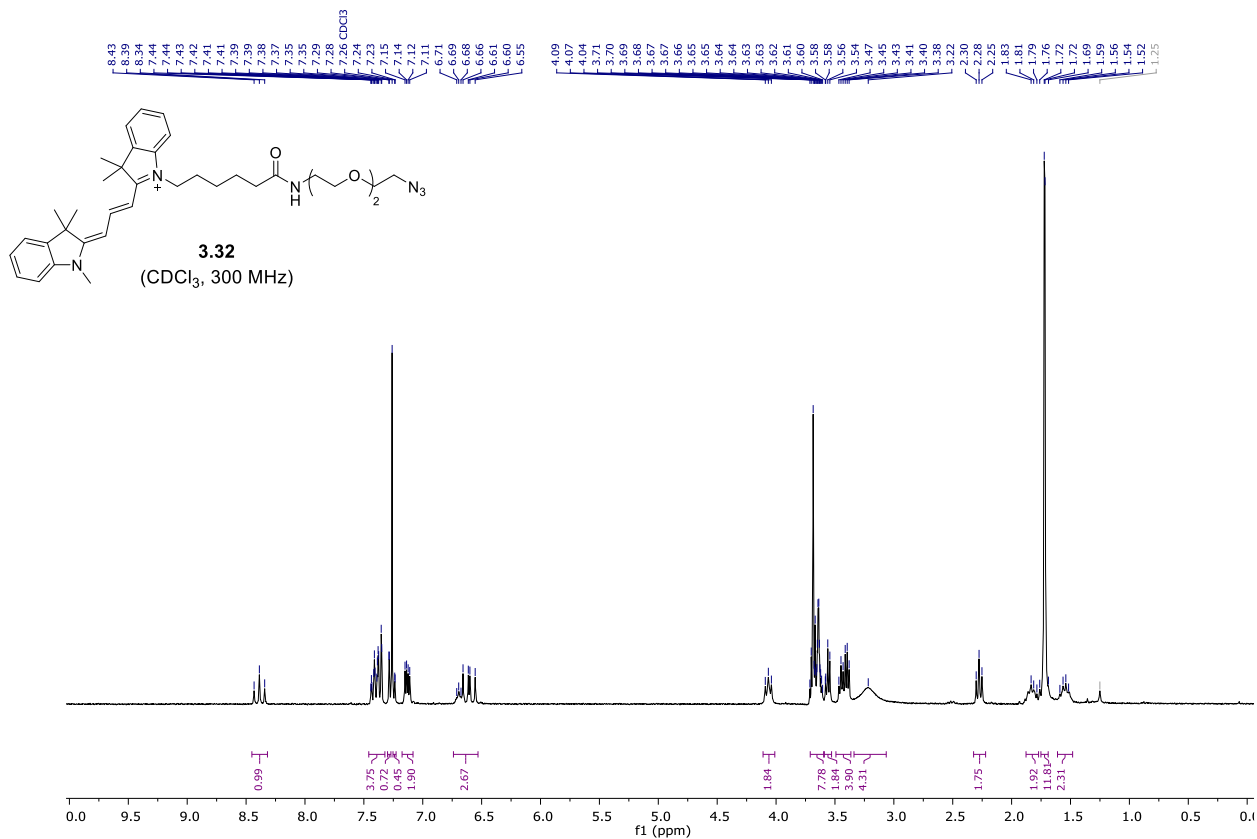


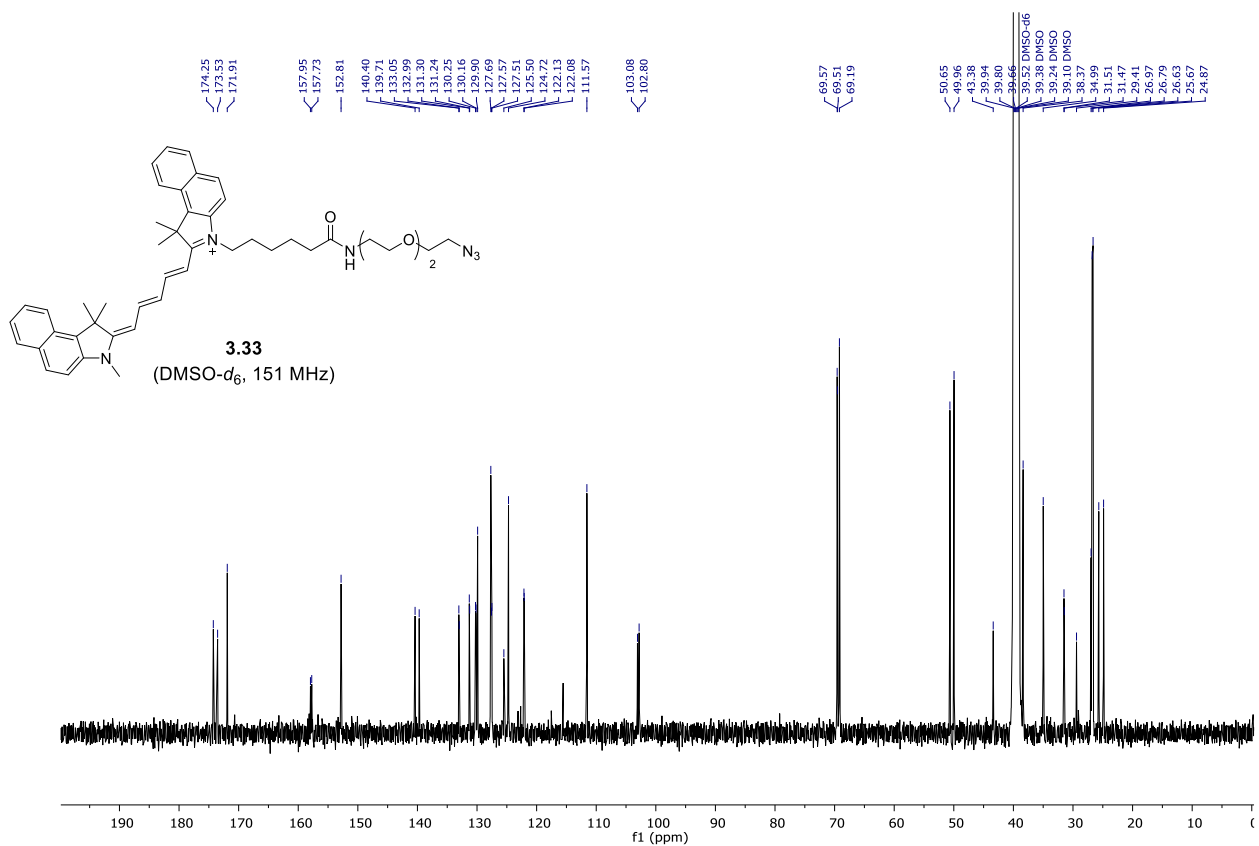
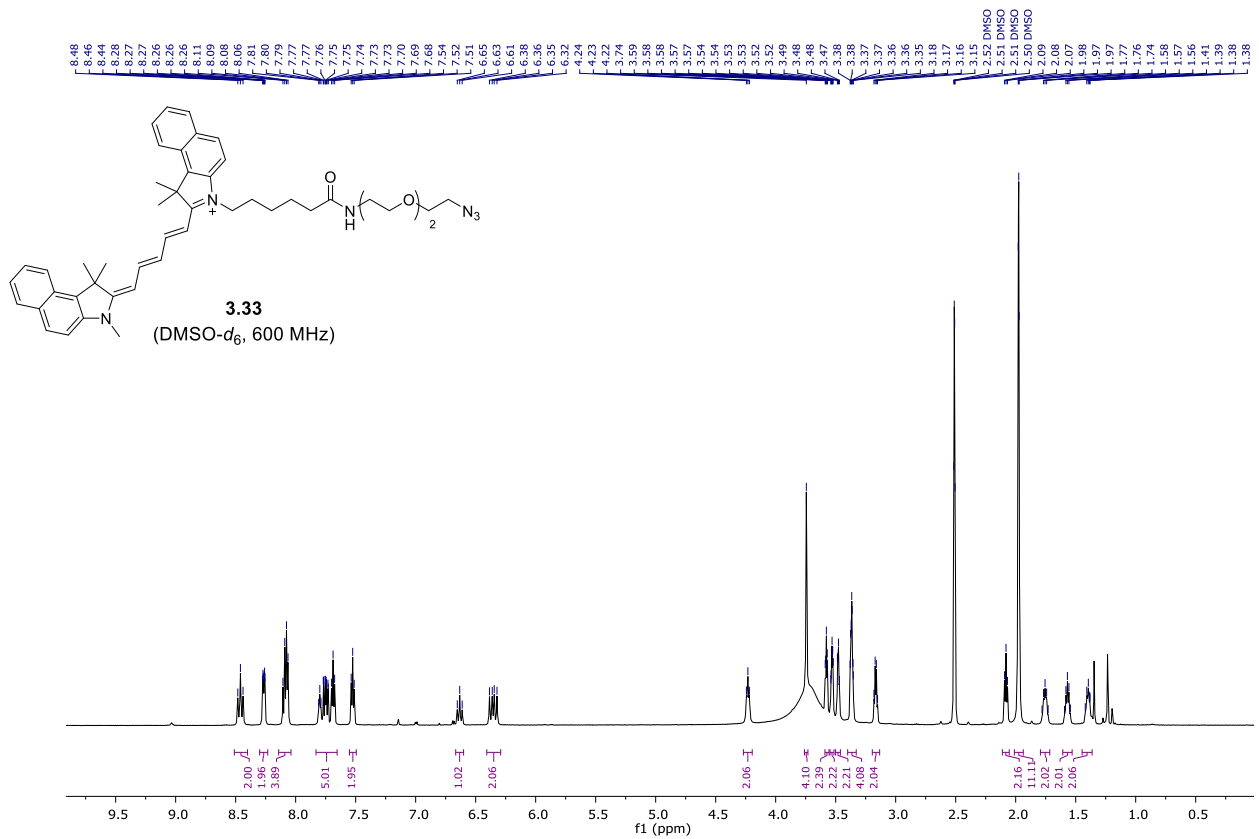


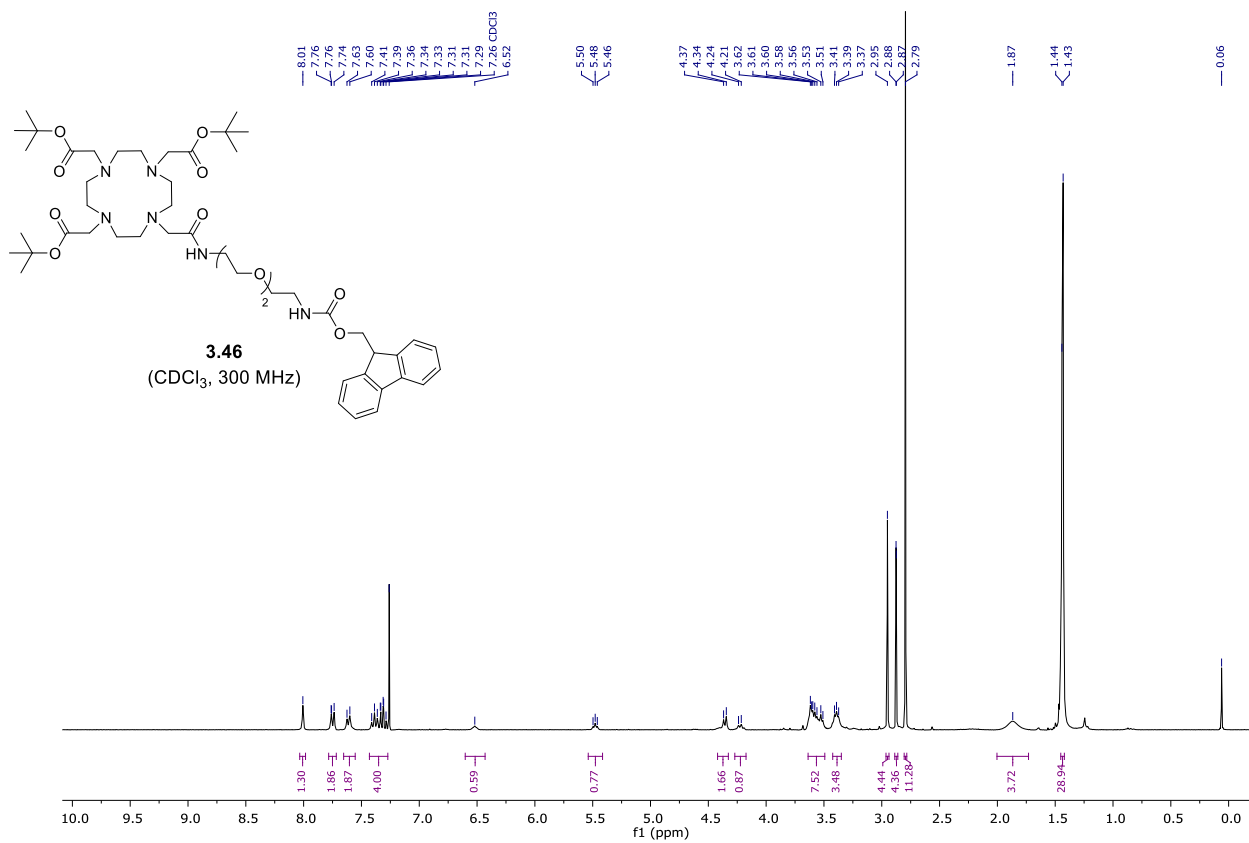


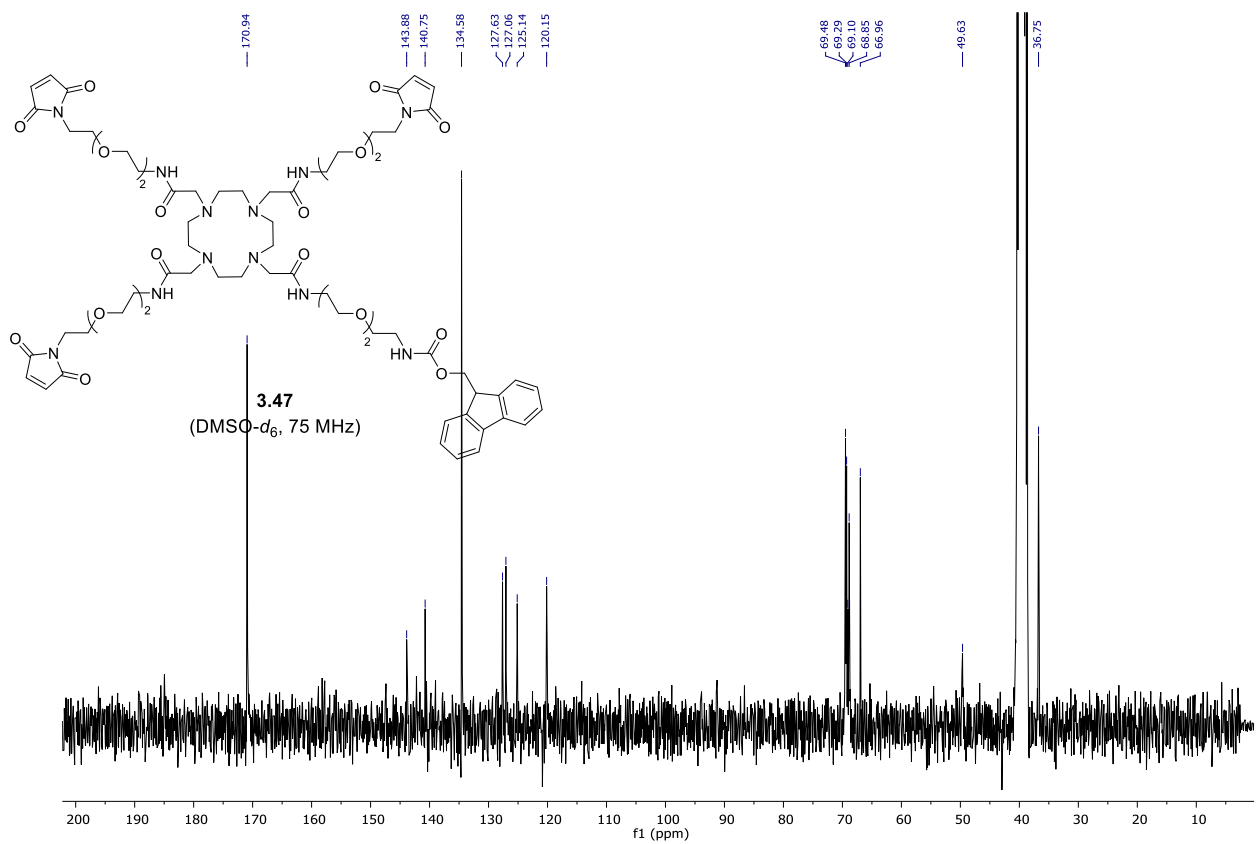
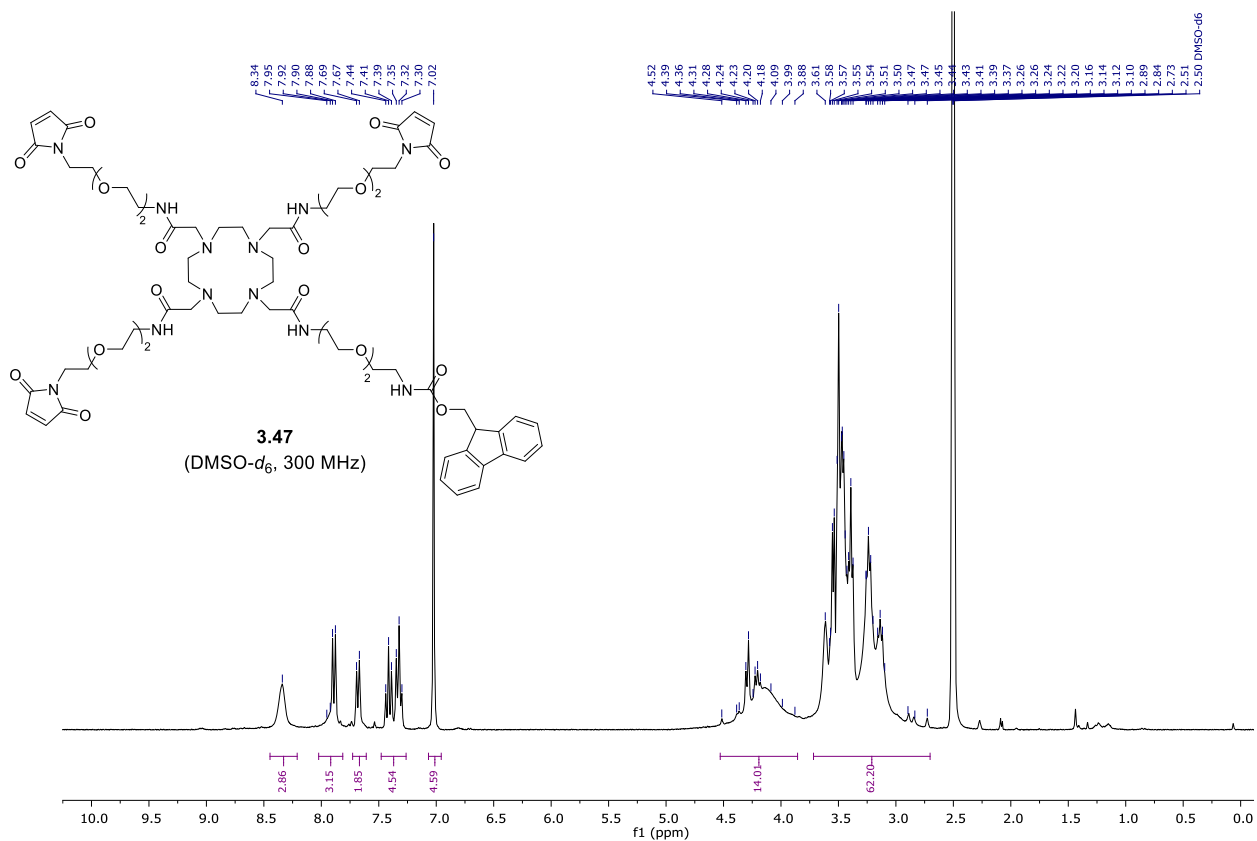


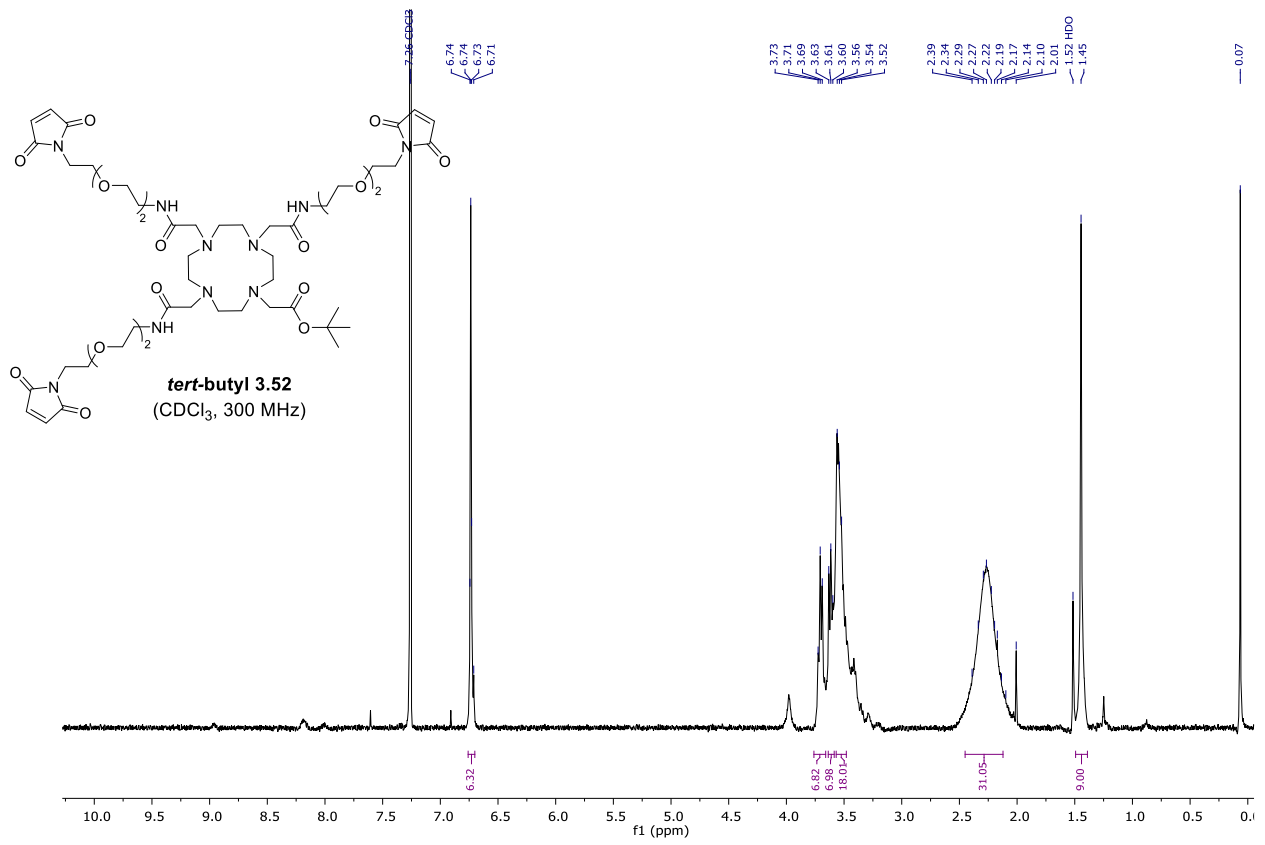




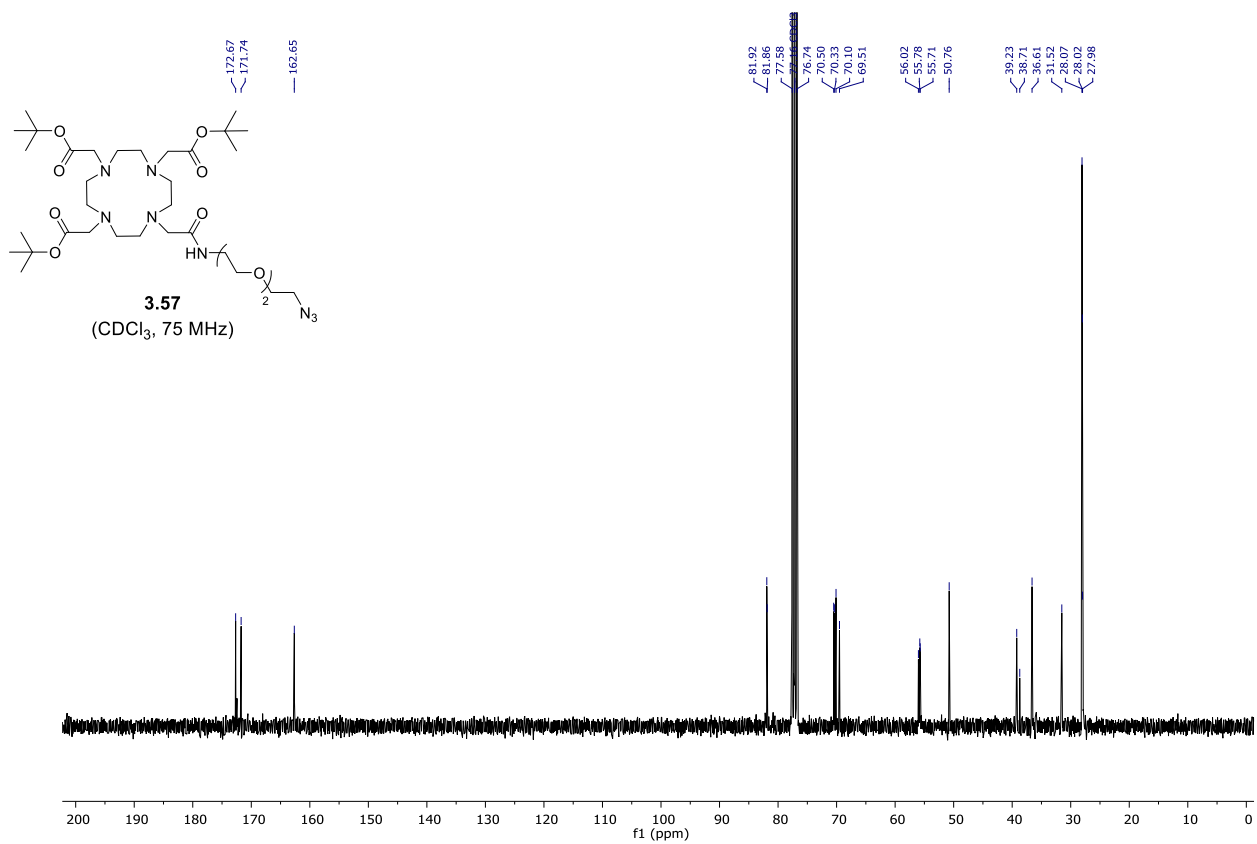
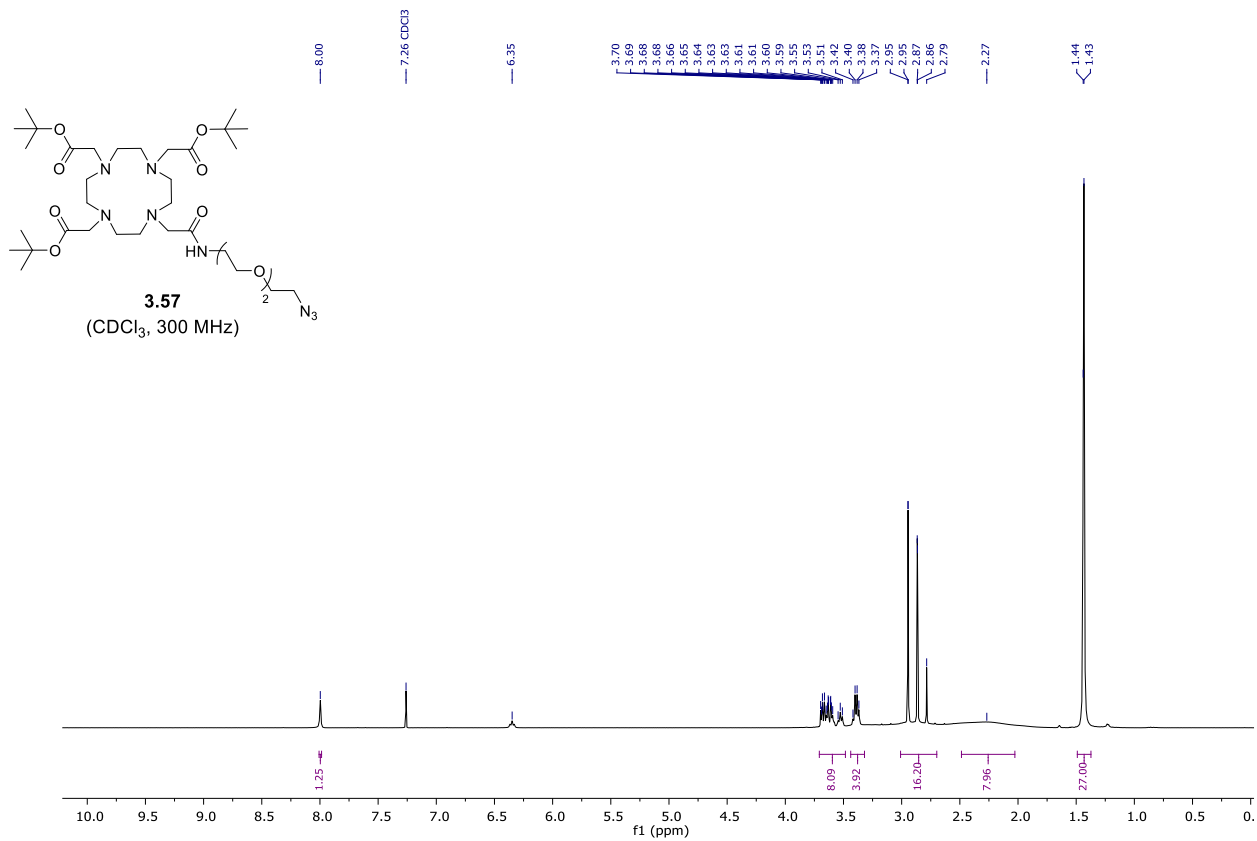


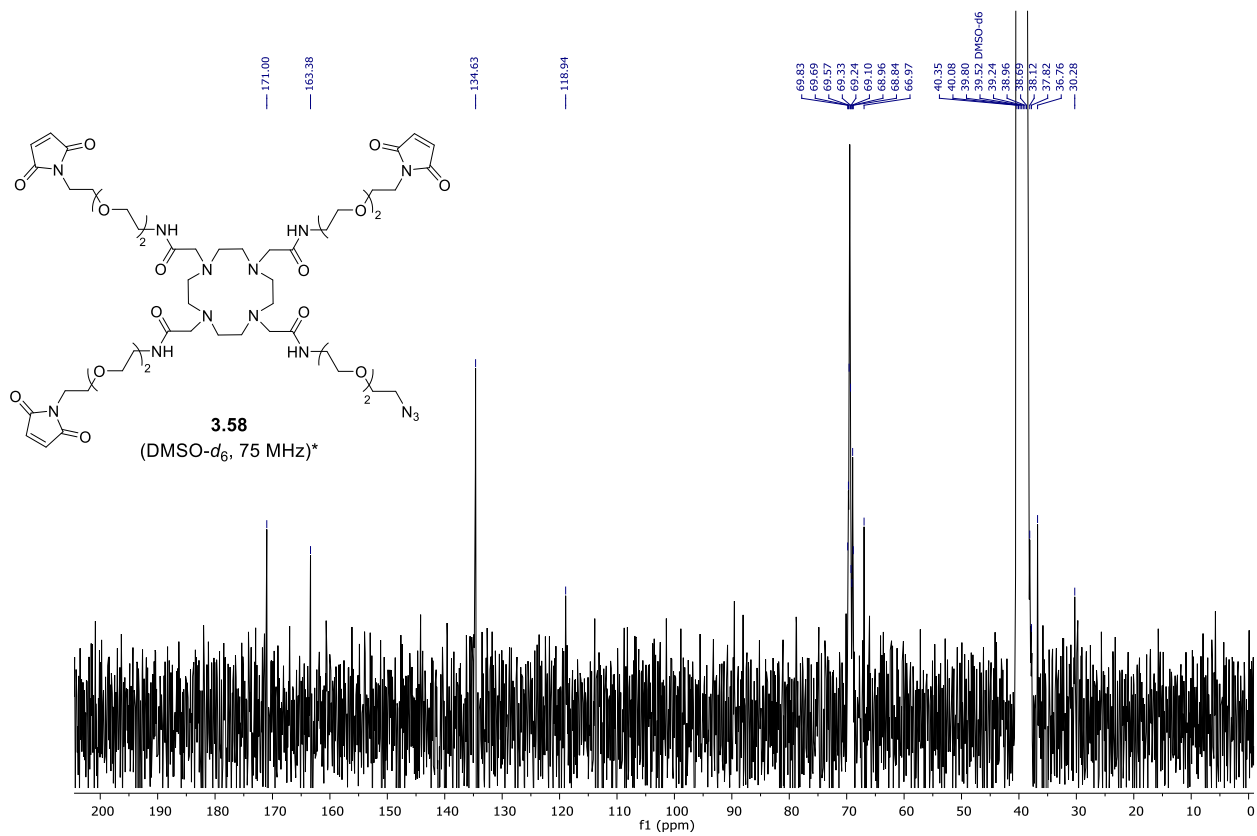
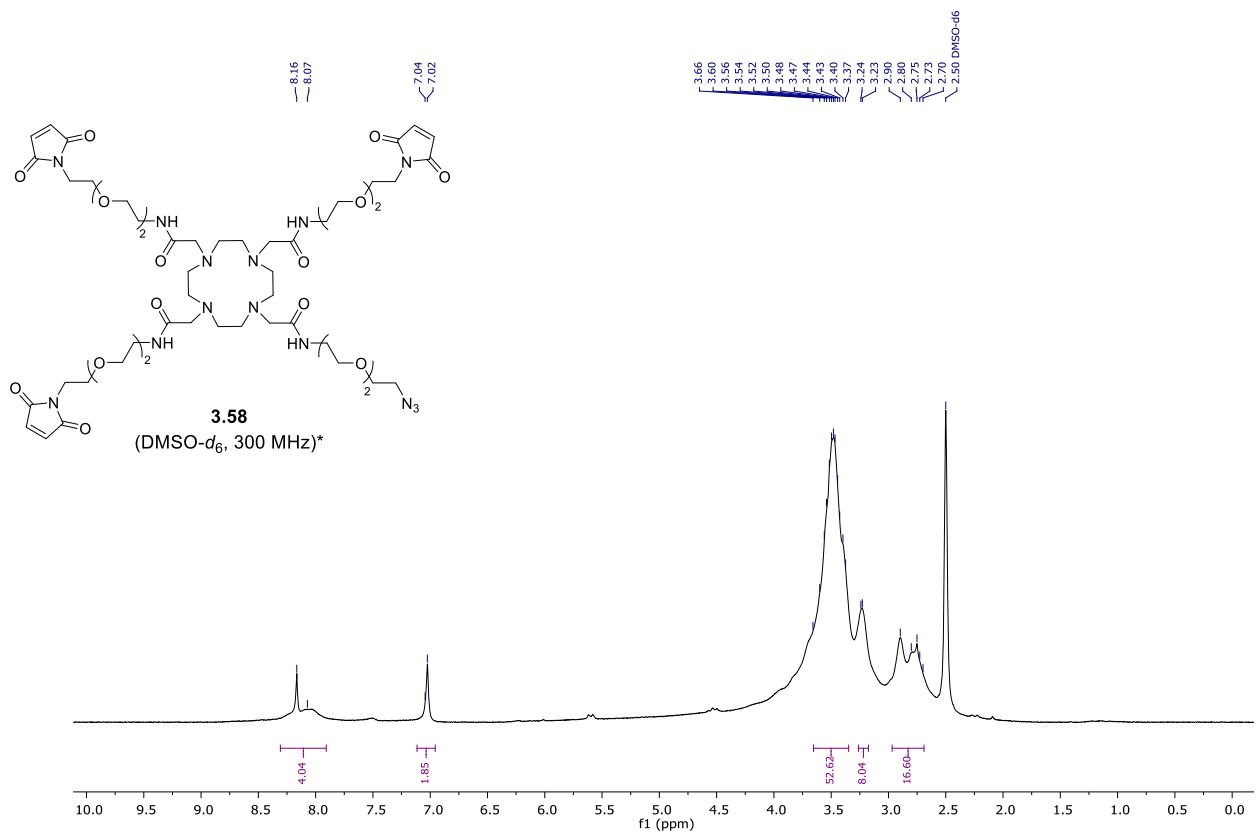












\*Polymerization of this intermediate over time was observed in the range of the NMR measurement.

